Pharmacological studies of aminergic scaffolds and the development of multi-target ligands with focus on the histamine H_3 receptor

Inaugural-Dissertation

zur Erlangung des Doktorgrades
der Mathematisch-Naturwissenschaftlichen Fakultät
der Heinrich-Heine-Universität Düsseldorf

vorgelegt von

Luisa Rosa Leitzbach
aus Sinsheim

Düsseldorf, October 2025

aus dem Institut für Pharmazeutische und Medizinische Chemie
der Heinrich-Heine-Universität Düsseldorf

Gedruckt mit der Genehmigung der
Mathematisch-Naturwissenschaftlichen Fakultät der
Heinrich-Heine-Universität Düsseldorf

Berichterstatter:

1. Univ. Prof. Dr. Dr. h.c. Holger Stark

2. Univ. Prof. Dr. Rainer Kalscheuer

Tag der mündlichen Prüfung:
20.03.2026

Dedicated to Hannes

Table of Contents

Abbreviations

Zusammenfassung

Abstract

1 Introduction 1

1.1 Histamine 1

1.2 Histamine receptors 4

1.3 Histamine H_3 receptor ligands 11

1.4 CNS Disorders Associated with H_3R 17

1.4.1 Sleep disorders 18

1.4.2 Addiction 20

1.4.3 Neuropathic pain 22

1.4.4 Neurodegenerative diseases 25

1.4.5 Psychiatric disorders 29

1.5 Dual- and Multi-targeting directed ligands 35

1.5.1 Targets for combination in DTDLs and MTDLs 38

2 Scope and Objectives 51

3 Publications 53

3.1 Guided rational design with scaffold hopping leading to novel histamine H_3 receptor ligands 53

3.2 Substituted purines as high-affinity histamine H_3 receptor ligands 81

3.3 Aromatic linker variations in novel dopamine D_2 and D_3 receptor ligands 123

3.4 Multitargeting approaches to cognitive impairment: Synthesis of aryl-alkylpiperazines and assessment at cholinesterases, histamine H_3 and dopamine D_3 receptors 177

3.5 Design, synthesis and biological in vitro properties of dual acting ligands as histamine H_3 receptor and L-type Ca^{2+} channel inhibitors 215

3.6 Dual piperidine-based histamine H_3 and sigma-1 receptor ligands in the treatment of nociceptive and neuropathic pain 251

4 Conclusion and Perspectives 315

5 References 321

List of publications 354

Curriculum Vitae 357

Abbreviations

AC	Adenylate cyclase
AChE	Acetylcholinesterase
ACh	Acetylcholine
AD	Alzheimer's disease
ADHD	Attention-deficit hyperactivity disorder
ADP	Adenosine diphosphate
Akt	Proteinkinase B
ASD	Autism spectrum disorder
ATP	Adenosine triphosphate
AUD	Alcohol use disorder
BBB	Blood-brain barrier
BuChE	Butyrylcholinesterase
CNS	Central nervous system
CREB	Cyclic AMP response element binding
CYP	Cytochrome P450 enzyme
DHP	Dihydropyridine
D_xR	Dopamine x receptor (x = 1-5)
DTDL	Dual-target directed ligands
ECLX	Extracellular loop x
EDS	Excessive daytime sleepiness
EMA	European Medicines Agency
FDA	Food and Drug Administration
GABA	γ-aminobutyric acid
GIRK	G-protein inwardly rectifying K^+ channels

GIT	Gastrointestinal tract
cGMP	Cyclic guanosine monophosphate
GPCR	G protein-coupled receptor
HCRT	Hypocretin
HDC	Histidine decarboxylase
hERG	Human ether-à-go-go-related gene
HNMT	Histamine *N*-methyltransferase
HxR	Histamine x receptor (x=1-4)
IL	Interleukin
IP_3	Inositol triphosphate
KO	Knockout
LTCC	L-type calcium channel
MAO B	Monoamine Oxidase B
MTDL	Multi-target directed ligand
M_xR	Muscarinic X receptor
NA	Noradrenaline
NFκB	Nuclear Factor kappa B
NMDA	*N*-Methyl-D-Aspartat
NO	Nitric oxide
NTX	Narcolepsy type x (x=1 or 2)
OSA	Obstructive sleep apnea
PD	Parkinson's disease
PKA	Protein kinase A
PKC	Protein kinase C
PLA_2	Phospholipase A_2

PLC	Phospholipase C
PNS	Peripheral nervous system
RAMH	R-alpha methyl histamine
REM	Rapid eye movement
SN	Substantia nigra
SSRI	Selective serotonin reuptake inhibitor
SSNRI	Selective serotonin noradrenaline reuptake inhibitor
TM	Transmembrane domain
TMN	Tuberomammillary nucleus
TRPMX	Transient receptor potential melastatin X
VPA	Valproic acid

Zusammenfassung

Der weitreichende Einfluss von Histamin-H_3-Rezeptoren (H_3R) im zentralen Nervensystem verdeutlicht das Potenzial inversen Agonisten/Antagonisten in der Therapie neurologischer und neurodegenerativer Erkrankungen. Pitolisant ist der einzige zugelassene selektive inverse H_3R Agonist zur Behandlung von Narkolepsie und exzessiver Tagesschläfrigkeit (EDS). Zusätzlich laufen aktuell weitere klinischen Studien von Pitolisant zur Behandlung von Autismus und Prader-Willi Syndrom Patienten.

Im ersten Teil dieser kumulativen Arbeit ist das Design und die Untersuchung neuer Grundgerüste für H_3R bzw. Dopamin-D_2- und D_3-Rezeptor Liganden beschrieben. Die *in vitro* Evaluierung und das Docking führten zu optimierten Grundgerüsten und zeigen die unterschiedlichen Vorteile der angewandten Design Strategien („Scaffold Hopping“, bioisosterer Austausch und Linker-Variation) als nützliche Instrumente in der Entwicklung neuer Liganden als Grundlage für Struktur-basiertes Wirkstoffdesign.

Die komplexen Mechanismen neurodegenerativer und neurologischer Erkrankungen, wie Morbus Parkinson oder Autismus, erschweren die Entwicklung von Arzneimittel mit ausreichender Wirksamkeit. Multitarget-Liganden (MTDL) bieten mit gezieltem Angriff verschiedener Targets in einem Molekül den Vorteil durch synergistische Effekte eine verbesserte Wirksamkeit erzielen zu können. Der zweite Abschnitt dieser Dissertation betrachtet die Entwicklung neuer Dual-target und MTDL mit dem Fokus auf Kombinationen von H_3R Liganden mit Strukturelementen von Dopamin D_3 Rezeptor (D_3R), Acetycholin- (AChE) und Butyrylcholinesterase (BuChE), L-Typ Ca^{2+}-Kanal oder Sigma Rezeptor Liganden. Die Piperazin-basierten Liganden erzielten ausgewogene Affinitäten an H_3R und D_3R. Piperidin-basierte Liganden in MTDL sind zur Erzielung nanomolarer Affinitäten flexibler einsetzbar. Die Inhibition der entwickelten Dual-target Liganden (H_3R/Ca^{2+}) wurde an spezifischen Ca^{2+}-Kanälen ($Ca_V1.2$ und $Ca_V1.3$) untersucht, angesichts der potenziellen Anwendung in der Therapie bei Morbus Parkinson und Autismus. Die Kombination aus H_3R und Sigma-Rezeptor-Inhibition führte zu einer Leitstruktur mit vielversprechender Wirksamkeit in neuropathischen Schmerzmodellen.

Zusammenfassend präsentiert diese Arbeit durch die optimierten Grundgerüste und die entwickelten MTDL wertvolle Einblicke in die pharmakologischen Eigenschaften und gegenseitigen Einflüsse der Strukturkombinationen mit dem Potential zur Weiterentwicklung von vielseitig einsetzbaren Liganden für die Behandlung neurologischer oder neurodegenerativer Erkrankungen.

Abstract

The broad influence of histamine H_3 receptor (H_3R) in the central nervous system highlights the untapped potential of inverse agonists in the treatment of neurological and neurodegenerative diseases. Pitolisant remains the only approved selective H_3R inverse agonist in the treatment of narcolepsy and excessive daytime sleepiness. In addition, further clinical trials of pitolisant are currently ongoing for the treatment of patients with autism and Prader-Willi syndrome.

The first part of this cumulative thesis describes the design and investigation of new scaffolds for H_3R and dopamine D_2 and D_3 receptor ligands. The *in vitro* evaluation and docking led to optimized scaffolds, demonstrating the distinct advantages of the applied design strategies (scaffold hopping, bioisosteric exchange, and linker variation) as valuable tools in the development of new ligands, providing a basis for structure-based drug design.

The complex mechanisms of neurodegenerative and neurological diseases, such as Parkinson's or autism, make it challenging to develop drugs with sufficient efficacy. Multitarget-directed ligands (MTDLs) offer the advantage of achieving better efficacy through synergistic effects by modulating different targets within a single molecule. The second section of this dissertation examines the development of new dual-target directed ligand (DTDLs) and MTDLs focusing on H_3R ligands in combination with structural elements of dopamine D_3 receptor (D_3R), acetylcholine- (AChE) and butyrylcholinesterase (BuChE), L-type Ca^{2+} channel, and sigma receptor ligands. The piperazine based ligands achieved balanced affinities to the H_3R and D_3R. While the piperidine based ligands are more flexible for application in MTDL achieving nanomolar affinities. Inhibition of the developed DTDLs (H_3R/Ca^{2+}) was investigated on specific Ca^{2+} channels ($Ca_V1.2$ and $Ca_V1.3$), given their potential application in the treatment of Parkinson's disease and autism. The combination of H_3R and sigma receptor inhibition resulted in a lead structure with promising efficacy in neuropathic pain models.

In summary, this work presents valuable insight into the pharmacological properties and mutual influences of the structural combinations through the optimized scaffold and the developed multitarget ligands, with potential for further development of versatile ligands for the treatment of neurological and neurodegenerative diseases.

1 Introduction

A substantial number of approved drugs exert their effects by targeting G protein-coupled receptors (GPCRs). This group of proteins remains a key focus for drug research due to their pharmacological accessibility and broad involvement in pathophysiological pathways. Essentially, aminergic GPCRs lead the list of most approved drugs among other GPCRs, with the dopamine 2 receptor at the top.[8, 9] Second comes the histamine 1 receptor for which the first antihistamines were discovered by Fourneau and Bovet, setting a milestone for further development.[10]

1.1 Histamine

The ubiquitously distributed biogenic amine histamine (2-(1*H*-imidazol-4-yl)ethylamine) is a local mediator that modulates various physiological processes of gastrointestinal, cardiovascular, central, peripheral, and immune system.[11] Versatile effects of histamine include acting as an inflammatory mediator of the immune system, increase acid production in the stomach, local vasodilatation in the skin and lungs, and the role as a neurotransmitter in the central nervous system (CNS).[11, 12] Thereby, it modulates the sleep-wake rhythm, temperature regulation, learning and memory processes, inflammation, gastric acid secretion, and further physiological processes.[7, 11, 13, 14] Early discovery mainly investigated the influence of histamine due to its role in allergic reactions, but the involvement in vast parts of physiological and pathophysiological processes, peripheral and in the CNS, could gradually be uncovered. In the meantime, histamine release from mast cells in the gastrointestinal tract (GIT) is assumed as an immune response against the gut microbiome, which appears as GIT infection, inflammation, and tumor genesis, or lack of histamine 3 receptor (H_3R) in mice impacts autoimmunity and immunomodulation, highlighting the fundamental role of histamine in acquired and innate immunity.[13]

Under physiological conditions, histamine is protonated at the N^{α}-position, but another tautomer exists, in which the imidazole moiety carries the proton at position one ($^{\tau}$).[15] The biosynthesis of histamine from L-histidine is catalyzed by histidine decarboxylase (HDC) to histamine in the tuberomammillary nucleus (TMN), in mast cells and basophils.[7, 16, 17] Therefore, histidine bioavailability, HDC expression, as well as the histamine 3 autoreceptor on somata or axonal varicosities, regulate the rate of histamine biosynthesis and release through a negative feedback mechanism.[18, 19] Additionally, the release of histamine in the CNS is modulated by other transmitters, including muscarinic (M_1R), adrenergic (α_2R), and peptidergic receptors among others.[16]

Peripherally or in the CNS, histamine is stored in mast cells, basophils, other immune cells, enterochromaffin-like cells, cell somata, and axon varicosities.[11, 16, 20] Neuronal, the vesicular monoamine transporter carries histamine into vesicles and release is triggered by different stimuli (e.g., action potential).[21] Degranulation of mast cells with release of histamine and further inflammatory mediators is initiated by binding of specific antigens (e.g., allergens) as immune stimulators, neuropeptides, cytokines, platelet activation factor, and peptides of the complement system.[22, 23] Histamine *N*-methyltransferase (HNMT) and diamine oxidase metabolize histamine mainly intracellular resp. extracellular either to the inactive N^{τ}-methylhistamine or the imidazolyl acetic acid (Figure 1).[24] Monoamine oxidase B (MAO B) further metabolizes N^{τ}-methylhistamine to N^{τ}-methylimidazoyl acetic acid.[25, 26]

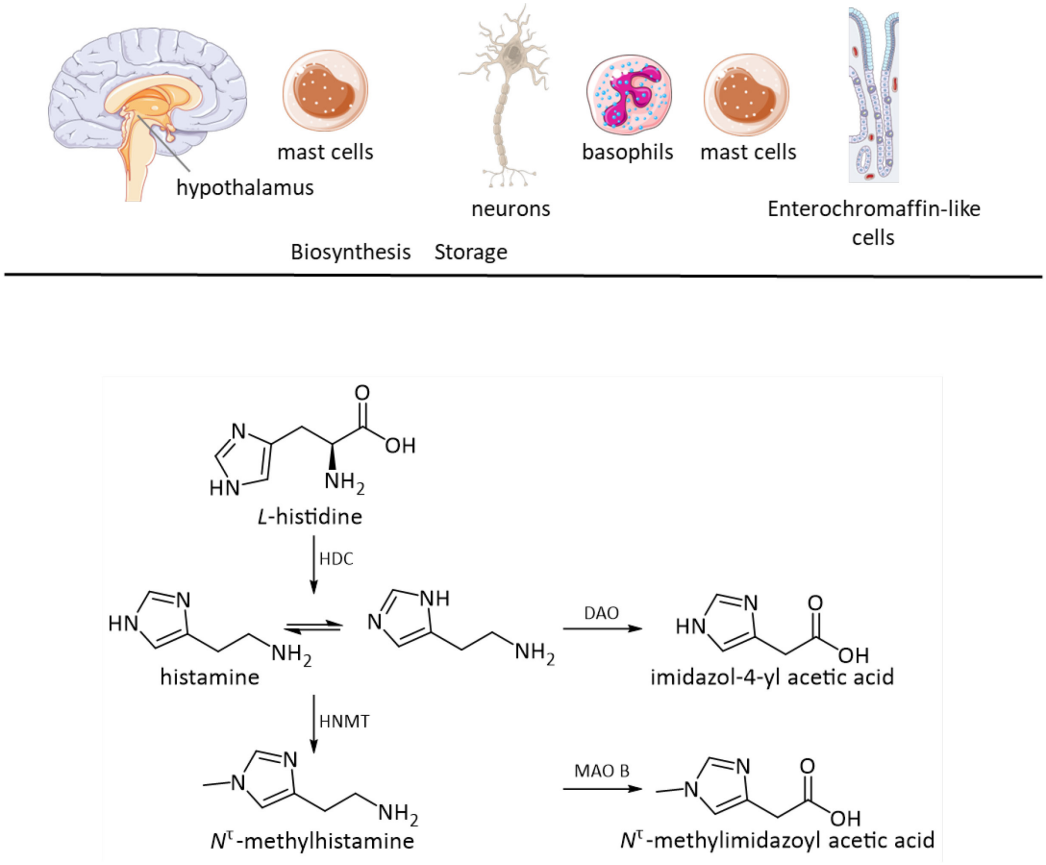


Figure 1: Biosynthesis, metabolism of histamine in histaminergic neurons.[7]

The following section provides a brief overview of the histaminergic neurons and histamine's role in the CNS, accompanied by the histaminergic projections (Figure 2). TMN is located in the posterior hypothalamus and is considered the same nucleus producing histamine besides γ-aminobutyric acid (GABA).[16, 27] Histaminergic neurons spread widely in and surrounding TMN with ascending projections to hypothalamus, hippocampus, thalamus, cortex, basal ganglia, hippocampus and amygdala, and descending projections to spinal cord and brain stem.[16, 28, 29] TMN

network enables fast transition from sleep to wakefulness but concurrently prevents rapid repetitive change of the states whereby histamine release mainly leads to arousal by encouraging wakefulness through activation of basal forebrain cholinergic and raphe serotonergic neurons.[30] Ca^{2+} contributes to repetitive firing of histaminergic neurons, leading to histamine release from dendrites, and N- and P-type currents are sensitive to histamine H_3R activation.[11, 31]

TMN is modulated and regulated by a broad spectrum of signals; for example, in rats, afferent inputs originate from the anterior hypothalamus, prefrontal and subicular cortex, dorsal tegmentum, and the fifth ventricle.[16] Excitatory inputs include glutamate, aminergic neurons (dopamine and serotonin), cholinergic neurons, and nucleotides (e.g., ATP or ADP). Glycine and GABAergic neurons inhibit histaminergic neurons, thereby promoting sleep. In contrast, presynaptic μ receptors excite TMN neurons via the inhibition of GABAergic neurons. Nociceptin is found in fibers near histaminergic somata of the TMN region and inhibits TMN neurons via activation of K^+_{ir} channels. The neuropeptides orexin A and B (hypocretin 1 and 2) arouse histaminergic neurons.[16] Histamine regulates essential elements of metabolism and food intake in hypothalamic areas[13], such as corticotropin-releasing hormone or hypothalamic histamine, which lead to glucagon-like peptide 1 (GLP-1) induced suppression of feeding habits. Thyrotropin-releasing hormone excites most TMN neurons, and endocannabinoids enhance histamine release in the TMN region.[16, 32]

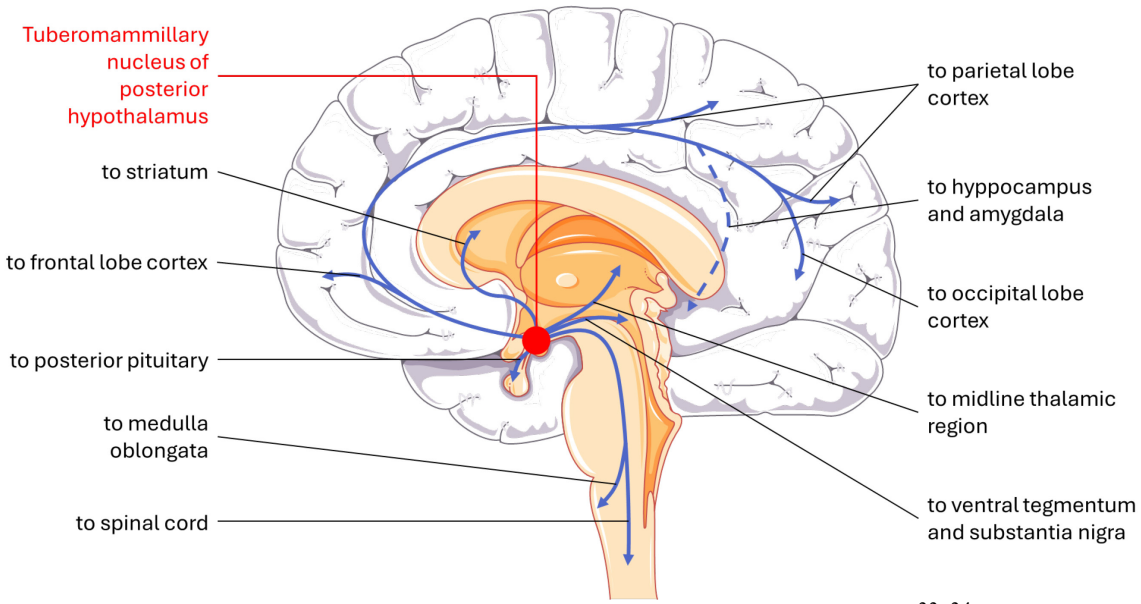


Figure 2: Histaminergic projections from TMN (adapted from reference [33, 34]).

1.2 Histamine receptors

Histamine receptors (H_xR) belong to the rhodopsin class A-like G-protein coupled receptors according to their amino acid sequence.[11] These integral membrane proteins contain an extracellular N terminus, an intracellular C terminus, and seven transmembrane helices interconnected by three intracellular and three extracellular loops (ECL). In general, GPCR ligand binding leads to conformational changes that elicit interactions with intracellular transducers, heterotrimeric G-proteins, GPCR kinases, and β-arrestins. GPCRs are structurally dynamic and comprise different states, namely inactive, transitional, active, or apo state. The transmembrane domain (TM) is highly conserved, forms the ligand-binding pocket, and is essential for transmembrane signal transduction.[35] Some GPCRs activate more than one G protein.[36] Besides ligand-induced signaling, GPCRs have constitutive activity, defined as conformational change from inactive to active state and spontaneous signaling without ligand binding. Therefore, many GPCR antagonists are inverse agonists, stabilizing the inactive state of the receptor.[37, 38] GPCR heterogeneity increases through transcriptional and post-transcriptional diversity, as well as homo- or heterodimerization.[36, 37] Receptor densities are controlled by agonist-induced desensitization, which hampers the receptor from being permanently responsive, or rather, resensitization. Alterations of desensitization and/or resensitization can contribute to pathophysiological conditions.[39-41]

In the case of histamine receptors, four subtypes are classified based on receptor genes and distinct receptor polypeptide sequences: histamine H_1R, H_2R, H_3R, and H_4R.[19, 42-44] The total number of histamine receptor isoforms is significantly higher due to alternative splicing, particularly for the human H_3 and H_4 receptors.[40] Histamine binding is subtype-dependent, with affinities to H_3R and H_4R being higher than to the other subtypes.[45] The section below provides a brief overview of the signal cascades, discovered ligands/drugs, and the structure of the four histamine receptors, along with a summary of their properties in Table 1.

The first discovered histamine receptor subtype is the H_1R, ubiquitously distributed, e.g., in the hypothalamus, cortex, thalamus, aminergic and cholinergic brainstem nuclei, and glia, blood cells, and vessels.[11, 16] The brain regions are neuroendocrine, nutritional state, and behavioral control areas.[46] Human H_1R is generally $G_{q/11}$-coupled, and activation leads to the stimulation of phospholipase C (PLC). PLC cleaves phosphatidylinositol 4,5-bisphosphate into inositol 1,4,5-trisphosphate (IP_3) and diacylglycerol, resulting in the activation of protein kinase C (PKC), which catalyzes Ser/Thr phosphorylation of multiple proteins and release of intracellular Ca^{2+}.[11, 47] Signal transduction was also observed through $G_{i/o}$ coupling activating AMP-kinase, nuclear factor kappa B (NFκB), nitric oxide (NO) synthases and phospholipase A_2 (PLA_2). Activation of effector

molecules results in the release of cyclic guanosine monophosphate (cGMP), NO, and arachidonic acid.[11, 16] Increased intracellular Ca^{2+} induces vasoconstriction of large blood vessels and smooth muscle cells in the lung. Stimulation of NO formation causes dilatation of small blood vessels. H_1Rs are expressed in peripheral tissues, including the skin, lung, GIT, and cardiovascular system, as well as in the CNS.[11, 26] H_1R activation manifests in allergic reactions such as skin redness, swelling of nasal mucous membranes, heavy breathing, and itching.[48] H_1R signaling involves synergistic and bidirectional effects. Depending on the timing and coherence of the receptor activation, H_1Rs can oppose or amplify H_2R functions.[16] H_1R inverse agonists stabilize the inactive state of the receptor and are widely applied as antiallergic treatments for allergic rhinitis and chronic urticaria (e.g., loratadine or cetirizine (Figure 3)). Due to the sedative profile of first generation H_1R inverse agonists, these are primarily used for motion sickness or sleep disorders (e.g., diphenhydramine, doxylamine).[49]

H_1R is evidently expressed as homomeric and oligomeric structures.[11] First crystal structure of the H_1R was reported by Shimamura et al., as a mutant human H_1R complexed with doxepin (3.1 Å resolution).[50] They stabilized the inactive receptor state by replacing the third intracellular loop with T4 lysozyme fusion protein. The resolved crystal structure extended our knowledge of binding properties not only for H_1R but also for other histamine receptors. Strong hydrophobic interactions of the aromatic moieties of doxepin with Trp248 (TM6) have been demonstrated.[50] A recent study by Xia et al. resolved the first cryo-EM structure in G_q complex in active conformation, in which receptor activation by histamine, with residues of TM3 and TM6 compressing the extracellular side of the binding pocket, leading to intracellular G_q signal transduction, was described.[51] Followed by another cryo-EM in the apo state bound to different antihistamines (mepyramine, astemizole, and desloratadine). Wang et al. identified, besides a secondary ligand-binding site (ECL2, TM2, TM3, and TM7), a deep hydrophobic cavity in which the phenyl group of antihistamines inserts, blocking the toggle switch movement of residue Trp428 (TM6). Interestingly, apparent differences to other histamine receptors in the main pocket were reported, e.g., residues Tyr108 (TM3), Asn198 (TM5), and Phe432 (TM6) are in close contact with tested antihistamines.[52]

The histamine H_2R is also expressed ubiquitously and in the CNS, mainly distributed in the amygdala, cortex, basal ganglia, and hippocampus.[11] H_2R is coupled primarily to the G_s-protein activating adenylate cyclase (AC), which results in increased intracellular cAMP. Protein kinase A (PKA) and the transcription factor cyclic AMP response element binding (CREB) are thereby activated, key regulators of neuronal physiology and plasticity. Additionally, cAMP interacts directly with the hyperpolarization-activated cyclic nucleotide-gated channel 2. The calcium-

activated K^+ conductance is blocked by PKA-dependent phosphorylation. H_2R inhibits PLA_2 and the release of arachidonic acid.[11, 17] Additionally, $G_{q/11}$ coupling is for H_2R, resulting in increased intracellular Ca^{2+} and IP_3. Currently, the therapeutic use of H_2R is limited to inverse agonists (e.g., famotidine (Figure 3), ranitidine) in the treatment of gastric and duodenal ulcers, gastroesophageal reflux disease, and dyspepsia.[11, 17] However, some studies have demonstrated the efficacy of famotidine in schizophrenia patients[53], implicating a potential new therapeutic area. In mice with deficient H_2Rs, the appearance of cognitive deficits, impaired hippocampal long-term potentiation, nociception, gastric, and immune functions indicates that dysfunctional H_2Rs are involved in further pathophysiological processes.[16] Lack of histamine leads to downregulation of H_2R expression in a tissue-specific manner. H_1R and H_2R may be arranged as heterodimers, presenting functional cross-talk such as cross-desensitization and modulation through complex signaling networks.[54] Köck et al. disclosed cryo-EM of H_2R in active conformation bound to histamine with G_s protein (3.4 Å) in a nanodisc approach, which presents new insights into histamine interactions with the receptor and critical residues for selectivity.[55]

H_4R is a G_i-coupled receptor with structural similarities to the H_3R, but its expression pattern differs, with more peripheral expression, particularly on eosinophilic granulocytes.[11, 56, 57] H_4R is expressed on mast cells, monocytes, dendritic cells, basophils, and natural killer cells.[11, 58] H_4Rs are associated with inflammatory responses, including cell recruitment, chemotaxis, upregulated adhesion molecule expression, chemokine release, and cytokine modulation.[59, 60] The therapeutic potential of H_4R ligands in inflammatory and allergic diseases is still to be explored.[58] However, preclinical and clinical data support that H_4R plays a role in atopic skin disease and pruritus.[61] H_4R-deficient mice revealed H_4R modulation of various neurophysiological processes, namely locomotor activity, nociception, anxiety, and feeding behavior.[62] H_4R agonists resulted in the upregulation of interleukin 31 (IL-31) and AP-1 *in vitro*.[63] To date, no H_4R ligand has made it a registered drug. JNJ-7777120 (Figure 3) was the first selective H_4R antagonist[64], and many compounds entered clinical trials, but lack of efficacy is the main reason for failure in clinical trials.[65]

In patients with atopic dermatitis, high H_4R expression indicates involvement in the pathophysiology, and histamine plays a role in the upregulation of IL-18 and activation of eosinophils.[66] Cryo-EM structure of H_4R-G_i complexes with histamine and further agonists (clozapine, VUF6884, clobenpropit) demonstrates different binding modes of histamine in H_4R compared to that of H_1R. Whereas histamine occupies TM3 and TM5 in H_1R binding, in H_4R, histamine binds only on the TM7 side (π-π network). Larger ligands (clobenpropit and clozapine) also occupy the TM3 and TM5 sides. Presumably, E182 (TM5) is a regulator for receptor activation

that may facilitate the design of H_4R ligands.[67] At the same time, histamine and agonist imetit bound to H_4R in complex with G_q was reported.[68] This recently gained insights into ligand binding in various states and interactions with the receptor facilitate the development of selective ligands for each receptor subtype.

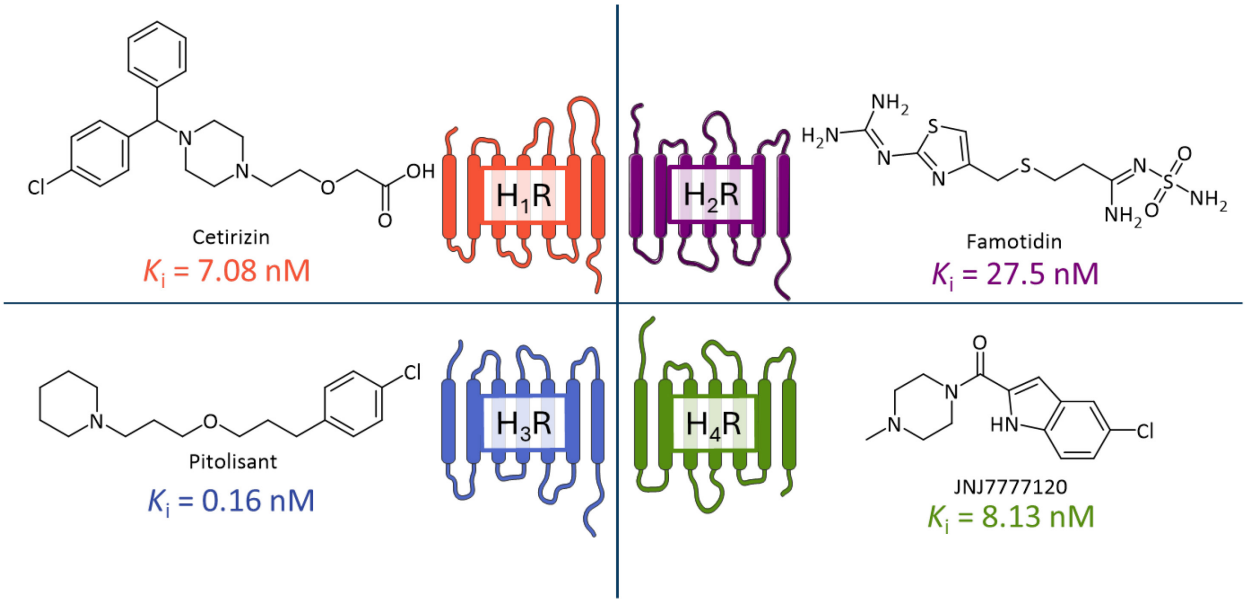


Figure 3: Examples of inverse agonists/antagonists to the histamine receptors and their binding affinities to the respective receptor.[11]

The H_3R was discovered by J.-C. Schwartz's group in 1983.[19] The 70-kDa protein consists of 445 amino acids, and its gene is located on chromosome 20q13.33, comprising either two introns and three exons or three introns and four exons.[69-71] The most prominent signaling pathways of H_3R are shown in Figure 4. H_3R is negatively coupled to $G_{i/o}$ proteins, inhibiting N- and P/Q-type voltage-gated Ca^{2+} channels and AC.[72-75] H_3R activation induces increased intracellular Ca^{2+} by PLC activation and IP_3 formation.[71, 76, 77] In contrast, H_3R decreases depolarization-induced Ca^{2+} in histaminergic neurons of the hypothalamus and in striatal neurons. Modulation of neurotransmitter release through the $G_{\beta/\gamma}$ subunit activating G-protein inwardly rectifying K^+ channels (GIRK) may lead to inhibition of synaptic transmission.[78] H_3R activation is crucial for presynaptic autoinhibition as a negative feedback mechanism. Through crosstalk with other GPCRs, $G_{q/11}$ signaling and activation of PLA_2, Akt/GSK-3β, and MAP kinase pathways are involved in axonal and synaptic plasticity.[71, 79, 80] In sympathetic nerve terminals, Na^+/H^+ exchanger activity is attenuated, resulting in inhibition of noradrenaline (NA) release.[81, 82] High constitutive activity of H_3R was demonstrated both *in vivo* and *in vitro,* with the suggestion that a short amino acid sequence in the sixth TM is responsible.[83]

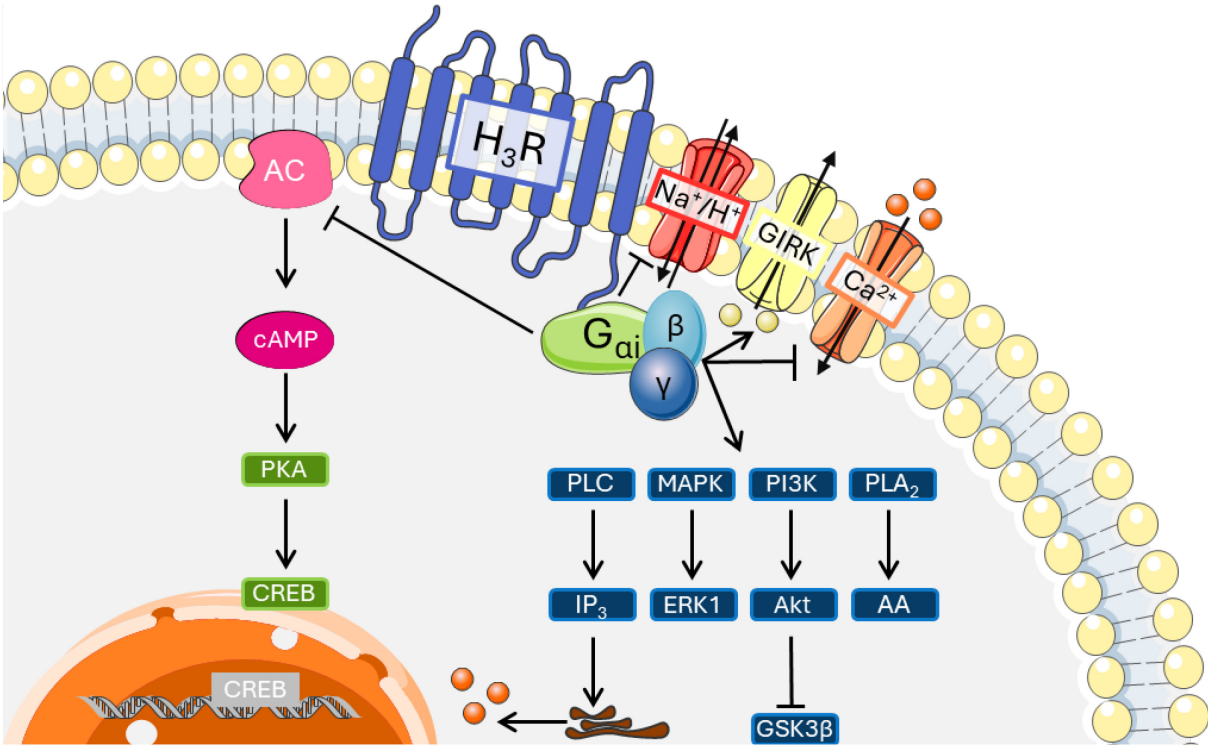


Figure 4: Main signaling cascades of H_3R.[11, 84]
Abbreviations: AA – arachidonic acid, AC – Adenylatcyclase, Akt – protein kinase B, cAMP - cyclic adenosine monophosphate, CREB – cAMP response element binding protein, PKA – protein kinase A, PLC – phospholipase C, IP_3 – Inositoltriphosphate, ERK1 – GSK3β – glycogen synthase kinase 3β, GIRK – G-protein gated inwardly rectifying K^+ channel

RNA sequencing data have revealed the expression of multiple H_3R isoforms in the brain and tissue-specific distribution; however, the functional significance of H_3R isoforms remains poorly explored. H_3R splicing across species reveals evolutionary dissonance and conservation, indicating that species-specific control mechanisms and isoform-specific interactions and effects are feasible. Twenty-four human isoforms identified by cloning and/or RNA sequencing, including canonical isoform hH_3R-445, extended hH_3R-453 (C-terminal tail), and shorter hH_3R-365.[40] Interestingly, Gao et al. found that the short hH_3R is constitutively more active and binding properties of agonist and antagonist/inverse agonist differ between hH_3R-445 and hH_3R-365 isoforms namely binding affinities of agonists are lower to the short isoform in contrast to binding affinities of inverse agonists which are lower at the canonical isoform.[85] Complexity of isoforms and their expression have rendered it challenging to explore the importance of all H_3R isoforms.[11] Insight into isoform functionality may pave the way for precise pharmacological treatment and targeted therapeutics.

As previously described, H_3R acts either as an autoreceptor on axons of TMN neurons, dendrites, and somata, resulting in the inhibition of histamine biosynthesis and release from varicosities, and thus inhibiting signal transmission, or as a heteroreceptor.[16, 86] High densities of H_3R are found in

the amygdala, striatum, nucleus accumbens, hippocampus, cerebral cortex, cerebellum, substantia nigra (SN), and brain stem. H_3 heteroreceptors regulate the release of various transmitters, including biogenic amines, acetylcholine (ACh), glutamate, GABA, and peptides.[11, 16] Genetic linkage studies in knockout (KO) mice suggest that the loss of H_3R function is linked to reduced locomotion, metabolic syndrome, late-onset obesity, behavioral disorders, increased leptin and insulin levels, and neuroinflammatory diseases.[16] Recently, a crystal structure of H_3R was revealed, unleashing new possibilities for ligand design and discovery of ligand-receptor interactions.[87] Interestingly, homo- and heterodimers are shown, e.g., with D_1R and D_2R.[13, 88, 89]

Table 1: Overview of the properties, distribution, ligands and effects from the four histamine receptors*.[11, 16, 47, 50, 90]

	H_1R	H_2R	H_3R	H_4R
G-protein coupling	$G\alpha_{q/11}$	$G_{\alpha s}$	$G_{i/o}$	$G_{i/o}$
Location	Smooth muscle, vascular cells, neuronal and glial cells (thalamus, hypothalamus, septum, hippocampus, olfactory bulb, amygdala, cortex), epithelial cells	Smooth muscle vascular cells, immune system, parietal cells, CNS (basal ganglia, hippocampus, amygdala, cerebral cortex)	Striatum, basal ganglia, nucleus accumbens, cerebral cortex, hippocampus	Hematopoietic cells, CNS in discussion (amygdala, thalamus, cortex, hippocampus, spinal cord)
Agonists	Histamine Histaprofiden	Impromidine Amtamine UR-AK 24	N_α-Methyl histamine, Imepip, Imetite	4-Methylhistamine, VUF-8430, ST-1006
Antagonists	Doxepin, Levocetirizine, Loratadine	Ranitidine, Cimetidine, Famotidine,	Pitolisant, ABT-239, DL-77	JNJ-7777120, SENS-1111, JNJ-3975879,
Cellular effects	cAMP↑, cGMP, phospholipase C↑, phospholipase D, phospholipase A_2, NF-κB, Ca^{2+}↑	cAMP↑, AC, c-fos, C-Jun, PKC, p70S6K	cAMP↓, Ca^{2+}↑, MAP kinase↑	cAMP↓, Ca^{2+}↑, MAP kinase↑
Pathophysiological effect	Sleep-wake disorders, allergic reactions, emesis	Gastric ulcer	Sleep-wake disorders, schizophrenia, pain, epilepsy, depression	Inflammatory diseases, e.g., asthma, pain, allergy
Histamine affinity pK_i	4.6	5.1	8.2	8.1

*↑ increase, ↓ decrease, CNS – central nervous system, cAMP – cyclic Adenosine monophosphate, cGMP – cyclic Guanosine monophosphate, AC – adenylylcyclase, MAP – Mitogen-activated protein

1.3 Histamine H_3 receptor ligands

At the beginning of H_3R ligand discovery, structures were imidazole-based, oriented on histamine itself yielded in the antagonist thioperamide and agonist R^{α}-methylhistamine (RAMH) as selective ligands over H_1R and H_2R.[91] Despite the selectivity of these ligands, thioperamide revealed to be hepatotoxic, and the first-pass metabolism of RAMH is extensive, but the tritiated agonist proved to be a good radioligand.[92] Ciproxifan was very potent *in vivo,* but performed poorly in toxicity tests.[93] Extensive development led to many promising imidazole-based ligands, among other imetit, methimepip, immethridine, BP2-94 (FUB94), [^{125}I]iodoproxyfan[94], clobenpropit[95], imoproxifan[96], and FUB-407[97]. For some imidazole-based agonists, low selectivity over H_4R was detected after the discovery of H_4R in the early 2000s.[98] BP2-94 (FUB94), and SCH50971 increased sleep time and/or sedation in preclinical animal models.[99] Cipralisant, also known as GT-2331[100], was one of the first H_3R ligands in phase II clinical trials for ADHD.[101]

Cloning and functional expression of the human H_3R enabled the simplified screening of new compounds at the human target.[72] The discovery of various isoforms by alternative mRNA splicing[83] and sequence differences in the transmembrane domains, including pharmacological variations in animal species[102], complicates the interpretation of preclinical data and highlights translational hurdles in the development of novel drug candidates.

Simultaneously, a crucial step in the development of H_3R antagonists/inverse agonists was the replacement of imidazole with nitrogen-containing heterocycles. Thereby, major drawbacks of imidazole-containing compounds, such as poor brain penetration and interaction with cytochrome P450 enzymes (CYP), including drug-drug interactions, liver toxicity, extrapyramidal symptoms, and inhibition of adrenal steroid synthesis, and selectivity over H_4R, were improved and/or avoided.[11, 103, 104] Ganellin et al. described one of the first potent nonimidazole derivatives containing pyrrolidine, with the lead compound UCL 1972[105], followed by numerous potent nonimidazole H_3R inverse agonists/antagonists comprising different structural elements as replacements for imidazole. The benzofuran ABT-239 with basic amide methylpyrrolidine is a potent H_3R antagonist with promising results in preclinical studies for schizophrenia and cognitive disorders, but an unfavorable toxicity profile due to human ether-à-go-go-related gene (hERG) affinity and consequently QT prolongation.[106] Cardiovascular side effects caused by the antitarget hERG are one of the main reasons for failure in drug development or even withdrawal from the market after approval.[107] Cardiac hERG encodes a voltage-gated K^+ channel contributing to cardiac repolarization and QT intervals. Inhibition of hERG leads to QT prolongation, and consequently, arrhythmias and cardiotoxic effects. Therefore, avoiding hERG interactions and employing design-

out strategies for structural optimization are highly recommended.[108] Point out the importance of early toxicological screening in drug development to modify structural elements responsible for adverse events in the early research stages. The design of H_3R agonist without imidazole is more difficult, and only a few are described yet, e.g, VUF 16839.[4]

On account of H_3Rs' localization in the CNS, a key property of ligands targeting H_3R is blood-brain barrier (BBB) permeability.[109] The BBB is a tight membrane that allows only low molecular weight molecules (<400-600 Da) to enter by passive diffusion. Increased lipophilicity enhances BBB permeability, with the limitation that high lipophilicity may result in substantial side effects due to longer retention times and drug accumulation.[110, 111] Furthermore, P-gp, multidrug resistance-associated membrane proteins, transport drugs from the CNS back into the blood by ATP-dependent efflux pumps[112] and thus represent an additional protection mechanism between the periphery and the CNS. Therefore, ligands should not only be BBB-permeable but also non-P-gp substrates to obtain clinical efficacy by systemic administration.

The approval of Pitolisant (FUB649, BF2.649, or tiprolisant) by the European Medicines Agency (EMA) and the U.S. Food and Drug Administration (FDA) was a milestone in the development of H_3R ligands.[113, 114] The *N*-piperidyl derivative (Figure 3) is still the only approved H_3R antagonist/inverse agonist on the market, showing high selectivity (nearly hundred various human receptors or channels at 100 nM (K_i (hH_3R) = 0.3-1.0 nM).[115] The application for narcolepsy with or without cataplexy was extended by EMA with the approval for the treatment of excessive daytime sleepiness (EDS) in obstructive sleep apnea (OSA).[116] In practice, gradual dosing to max. 18 mg/day (EDS in OSA) resp. 36 mg/day (narcolepsy). While preclinical and clinical safety found single doses up to 120 mg acceptable without severe adverse events. Toxic properties were only seen at very high doses (several orders of magnitude higher than necessary to saturate cerebral H_3Rs) and present as behavioral manifestations, mainly convulsive episodes. It is of great importance that plasma levels alleviate at the end of the day to avoid disturbing sleep at night due to waking effects. Pharmacokinetic decay is mainly driven by CYP3A4 and 2D6 hydroxylation, followed by opening of the piperidine ring as a soluble major metabolite inactive at H_3R and principal elimination pathway through urine.[1]

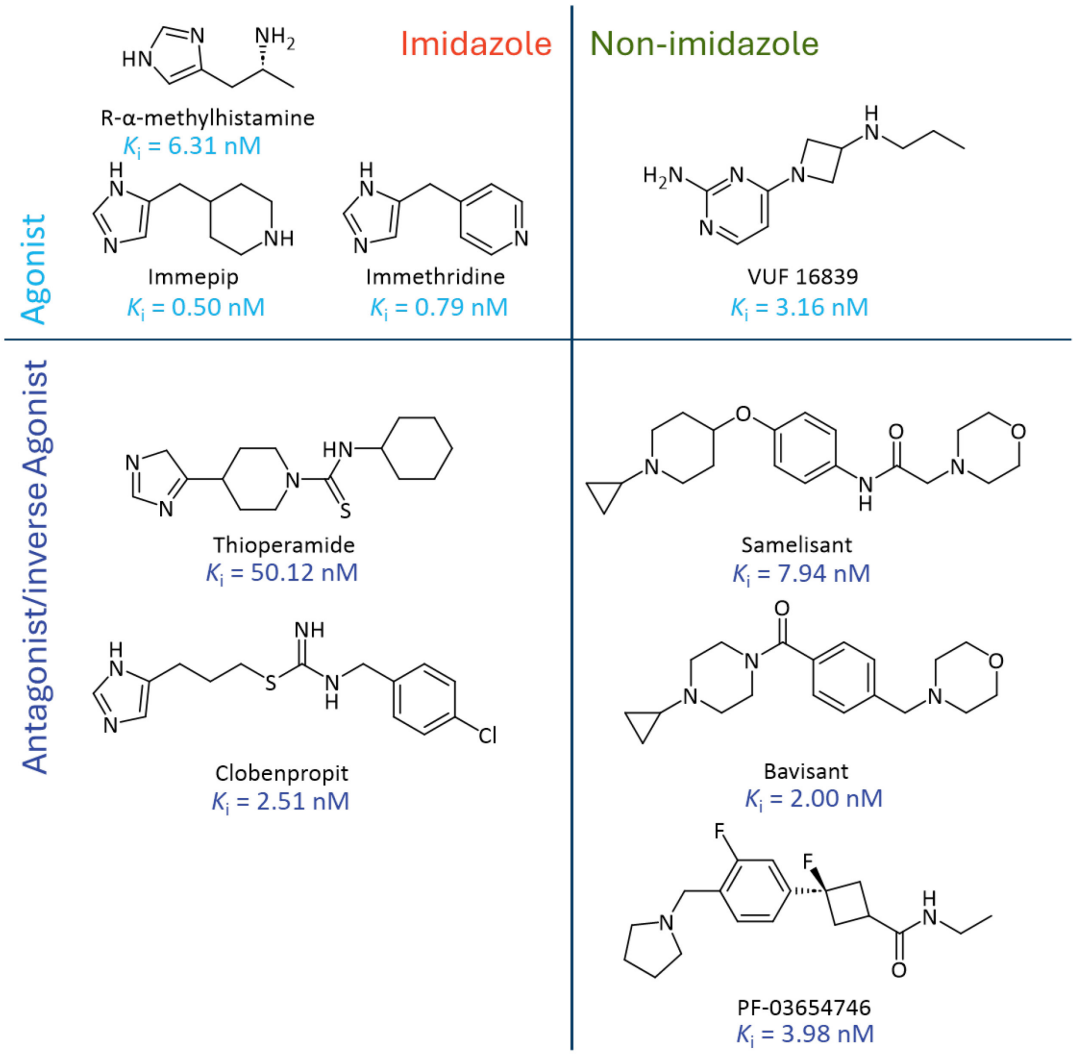


Figure 5: Structures and affinity values of imidazole and non-imidazole based H_3R agonist and antagonist.[1-6]

Among others, the most common motifs for bioisosteric exchange are pyrrolidine (e.g., UCL-2190[117]), piperidine (e.g., FUB-833[118]), and piperazine (e.g., Bavisant[3] (Figure 5)). Extensive structure-activity relationship studies disclosed a blueprint for H_3R antagonists/inverse agonists (Figure 6). The basic amine moiety is separated from the eastern part by a linker to the central core, which is primarily hydrophobic and connected to the eastern region. The eastern region is more flexible, permitting basic amines, polar or non-basic moieties.[103, 119]

Pitolisant (Figure 3) binding site is located within the transmembrane below the extracellular loop, where Glu206 (TM5) forms a salt bridge with the piperidine, the hydroxyl of Tyr374 (TM6) is H-bonded with the central oxygen of the ligand, Phe198 and/or Tyr189 make π-stacking interactions with the para-chlorophenyl group.[120]

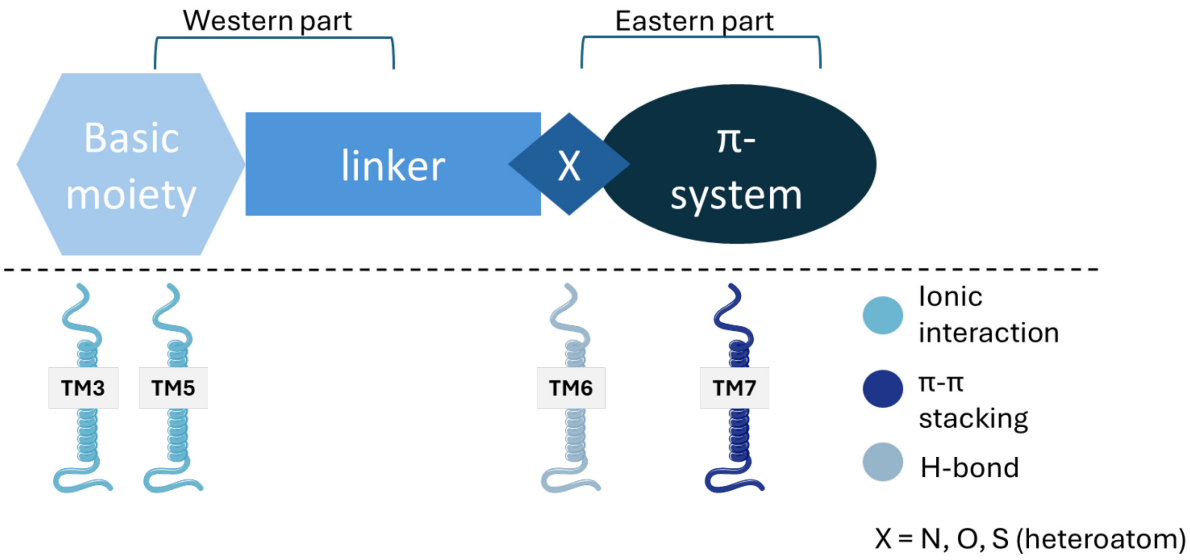


Figure 6: Blueprint for H_3R pharmacophores and common protein-target interaction with the H_3R TMs.[87, 119, 121]

Abbreviation: TM – transmembrane domain

The crystal structure of H_3R bound to PF-03654746 (Figure *5*) was resolved in an inactive state at 2.6 Å resolution by Peng et al. in 2022. In this study, hydrogen bonds between *N*-ethylcarboxamide and carbonyl residues with Glu395 (TM7), and hydrophobic interactions with Tyr91 (TM2), were identified. Moreover, a cholesterol-binding site was identified with the potential for allosteric modulation. In molecular docking studies, the binding modes of various H_3R antagonist/inverse agonists (Pitolisant (Figure 3), GSK189254A (Figure 7), LML134, Clobenpropit (Figure 5), JNJ5207852, GSK334429 (Figure 7), MK-0249, PF-03654746 (Figure 5), Bavisant (Figure 5), Thioperamide (Figure 5)) were investigated; however, it should be noted that docking scores were lower than the experimental K_i values. Conserved salt bridges with Asp114 (TM3) and protonated nitrogen atoms, and strong hydrophobic contacts at the bottom of the pocket were established.[87] Common interactions with the H_3R are ionic interaction of basic moieties with Asp114 (TM3), π-stacking with the aromatic cluster of TM6, TM5 determines the functional selectivity and Trp402 (TM7) is a conserved residue.[87, 121]

In a recent study, cryo-EM structures of Zhang et al., all four histamine receptors in complex with their main G protein bound to histamine, determined important conserved residues for histamine recognition in H_3R: Asp114 (TM3) for the recognition of histamine by a hydrogen bond with the delta nitrogen of the imidazole, Asp114 (TM3)-Tyr115 (TM3)-Tyr374 (TM6) as critical motif for histamine recognition, as well as Phe398 (TM7) and Trp402 (TM7) π-π stacking with imidazole.[122]

In this study, distinct binding orientations of histamine were identified in H_1R and H_2R compared to H_3R and H_4R, with approximately a 180° rotation. In addition, Leu401 (TM7) of H_3R and Gln347 (TM7) of H_4R were identified for the selectivity of the piperidine ligand immethridine (Figure 5).[122] Conserved residues and ligand recognition of H_3R facilitate the design of specific ligands and pave the way for agonist and inverse agonist development.

1.4 CNS Disorders Associated with H_3R

The H_3R has been implicated in various neurological and neurodevelopmental disorders, including Alzheimer's disease (AD) and Parkinson's disease (PD), schizophrenia, sleep disorders, attention deficit hyperactivity disorder (ADHD), autism spectrum disorder (ASD), and depression.[11, 123] However, the breakthrough to marketed pharmaceuticals is still limited to Pitolisant for the treatment of narcolepsy and EDS in obstructive sleep apnea. The reasons for the failure of H_3R ligands in clinical trials are heterogeneous, inter alia, insufficient efficacy, lack of separation between side effects and efficacy, and strategic decisions of sponsors.[123] Ongoing clinical trials of Pitolisant for additional indications such as ASD in children and adolescents (phase II in active status)[124] and prader willi syndrome (phase III in recruiting status)[125] underline unexploited capabilities of H_3R ligands to date. Recently, promising results of a phase II clinical trial for EDS in patients with prader willi syndrome were published.[126] Furthermore, the safety profile of Pitolisant has been demonstrated since its approval, and an investigation into a pregnancy registry is recruiting [127] and for children [128], highlighting its tolerability.

The following chapter discusses the potential therapeutic applications and the underlying pathophysiological mechanisms of H_3R ligands, as well as the verified and potential effects of H_3R modulation in diseases.

1.4.1 Sleep disorders

Sleep impairment leads to deficits in attention, executive function, and processing speed, promoting impulsivity, emotional lability, and depression. Sleep disorders in neurodegenerative diseases are common and may contribute to the progression and severity of neurodegeneration. Furthermore, the glymphatic pathway is predominantly active during sleep and is proposed to play a critical role in the clearance of extracellular neurotoxic waste. Lack of sleep promotes the propagation of tau and neuroinflammation. Therefore, addressing sleep disorders in neurodegenerative diseases is inevitable. Sleep disorders vary from increased arousal, loss of rapid eye movement (REM) sleep, or increased time to REM sleep initiation.[129]

Narcolepsy is a chronic sleep disorder with onset in adolescence and characterized by EDS.[130] Genetic and environmental factors cause immune-mediated selective loss or malfunction of orexin neurons in the lateral hypothalamus. Consequently, patients suffer from reduced quality of life and socioeconomic impact. A distinction is made between narcolepsy type 1 (NT1) and type 2 (NT2), with similar clinical profiles, with the exception that cataplexy is only present in NT1. The symptoms are sleep paralysis, disturbed sleep, impaired wakefulness, abnormal REM sleep, and hallucinations. Narcolepsy may also be a comorbidity, e.g., in Parkinson's disease.[131] In NT1 patients, approximately 90% of the wake-promoting neuropeptide hypocretin (HCRT or orexin) signal is lost, which is in contrast to NT2. The hypothesis of NT1 pathogenesis involves the autoimmune destruction of orexin-producing neurons in the hypothalamus, and immune-related genetic and environmental factors. The clinical spectrum and mechanism leading to orexin loss are not entirely clarified. Symptomatic treatment has shown good efficacy and safety, encompassing a broad spectrum of substance classes, including modafinil, sodium oxybate, solriamfetol, methylphenidate, and the already described H_3R antagonist Pitolisant.[130] Neither a drug combats the cause of the disease, nor an approved drug modulates orexin receptors directly. However, orexin agonists are in the development for narcolepsy to directly reduce the orexin deficiency and manage multiple aspects of the syndromic condition of narcolepsy.[132] Although the oral orexin 2 receptor agonist TAK-994 showed good efficacy, hepatotoxic effects in clinical trials led to no further consideration as a potential treatment[133], several other candidates are in development, such as ALKS 2680, a selective orexin 2 agonist[134, 135] in phase 2 and 3 clinical trials for NT1 and NT2 or TAK-861 in clinical trial for the treatment of NT1.[136, 137]

H_3R inverse agonists, such as Pitolisant, activate histaminergic neurons with a wake-promoting effect. This drug has fewer limitations compared to other narcolepsy treatments, e.g., low abuse potential and fewer side effects. Increased numbers of histamine neurons and decreased histamine

release have been observed in patients with narcolepsy.[138-140] Furthermore, the interplay between HCRT and histamine plays a role in maintaining wakefulness and arousal throughout the day. Enhancement of wake-promoting neurons by histaminergic neurons suppresses sleep-promoting neurons.[131] Samelisant (SUVN-G3931 (Figure 5)) is a novel morpholine-based H_3R inverse antagonist under investigation for the treatment of NT1 and NT2. Phase 2 clinical trials resulted in an improvement in daytime sleepiness, as determined by ESS score, and phase 3 clinical trials are planned.[6] These clinical trials found fewer side effects and improved cardiovascular safety compared to that of Pitolisant; however, the study's duration limits its validity. Phase 3 clinical trials will show whether samelisant has a favorable safety profile and whether its efficacy can be demonstrated in larger patient groups.

Furthermore, Pitolisant reduced daytime sleepiness in patients with obstructive sleep apnea. Obstructive sleep apnea is associated with multiple comorbidities such as EDS, fatigue, stroke, arrhythmia, coronary heart disease, and metabolic dysfunction.[141]

1.4.2 Addiction

Alcohol use disorder (AUD) is a major health risk with high mortality. Pharmacological treatment plays a crucial role as a counterpart to psychological interventions.[142] Pharmacological interventions in the therapy of AUD focus on the prevention of relapses and complete avoidance or reduction of alcohol intake. Currently, approved drugs for AUD have versatile mechanisms of action. Disulfiram inhibits the enzyme responsible for alcohol decay, acetaldehyde dehydrogenase, leading to an increased concentration of acetaldehyde in the blood. Consequently, unpleasant effects of alcohol intake are initiated, including nausea, flushing, vomiting, sweating, and even cardiovascular effects. Due to its mechanism, it only acts in a preventive manner by deterring the consequences of a relapse. Acamprosate is generally considered safe, although its mechanism of action is not fully understood. It conceivably restores the imbalance between neuronal excitation and inhibition, presumably through *N*-methyl-D-aspartic acid (NMDA) receptor action and metabotropic glutamate receptor 5.[143] However, it failed in the COMBINE study to be useful for relapse prevention, with different outcomes of studies attributed to genetic factors or study design, notably in detoxified patients, alcohol abstinence was maintained. Naltrexone is a μ-, κ-, and δ-opioid receptor antagonist and decreases dopamine release in the nucleus accumbens. It reduces the quantity of alcohol intake and recurrence to heavy drinking in consequence to the contrast desirable alcohol effects.[142] Similar is nalmefene, an opioid modulator at μ, δ (antagonist), and κ (partial agonist) that decreases alcohol consumption and heavy drinking days in patients with high drinking risks with moderate adverse events.[143]

H_3R is expressed in many brain areas involved in alcohol drinking and reward, as the mesocorticostriatal system and amygdala.[11] Alcohol affects GABA, glycine, and glutamatergic NMDA receptors.[144, 145] H_3R inverse agonists may be beneficial in the treatment of AUD, and some H_3R antagonists (thioperamide (Figure 5), clobenpropit (Figure 5), ciproxifan, JNJ-39220675, JNJ-10181475, DL77, ST-1283) demonstrated reduced alcohol intake *in vivo* in mice or rats.[146] The clinical trial of Pitolisant for AUD was terminated due to strategic reasons of the sponsor.[147] A phase 2 clinical trial of the H_3R inverse agonist BP1. 3656 with low daily doses (30 to 90 μg) from Bioprojet for AUD is completed.[148] This compound was removed from the website pipeline of Bioprojet and will presumably not be pursued [149] presumably due to insufficient efficacy as indicated by the results of the primary outcome on EudraCT.[150] The question remains open whether other H_3R ligands may be beneficial in AUD therapy.

Besides the possible application in AUD, H_3R is also indicated as a pharmacotherapeutic target in other addictive disorders. Upregulation of H_3R expression in opioid use disorder patients due to

chronic opioid use is presumably induced by modulation of histaminergic neurotransmission. This adaptive mechanism may modulate opioid tolerance and analgesia. In animal models, the opioid fentanyl combined with H_3R agonists and RAMH showed synergistic effects. Whether the upregulation is a compensatory mechanism for opioid analgesia tolerance and whether H_3R ligands could serve as a therapeutic intervention needs to be elucidated.[151]

1.4.3 Neuropathic pain

Neuropathic pain is defined as pain initiated or directly caused by primary lesions or dysfunction of the somatosensory system. This complex condition can be differentiated between peripheral (Aβ, Aδ, and C fibers) and central neuropathic pain, depending on the anatomical location of the lesion or disease.[152] The pathophysiological mechanisms of neuropathic pain are multidimensional and not completely understood. Symptoms include allodynia, hyper-, and hypoalgesia occurring as spontaneous pain, among others, induced, for example, by trauma, vascular disease, nerve compression, neurological diseases, metabolic syndrome, drugs, or infectious diseases.[153] Despite pharmacological treatment, for most patients, freedom from pain cannot be achieved. Prevalence lies between 7 and 10%, and a realistic therapeutic goal is pain reduction by more than 30%.[154] Due to the lack of freedom from pain, essential goals in treatment are improvement of sleep quality, quality of life, functionality, maintaining the ability to work, and social activities. Pharmacotherapy remains necessary for neuropathic pain treatment.[152] Monotherapy with currently available drugs is associated with limited efficacy and dose-related side effects. The combination of two or more analgesic drugs may improve efficacy, e.g., combination of opioid and gabapentin, but side effects increase and are dose-limiting.[155] Opioids combined with antidepressants or gabapentinoids and gabapentinoids with antidepressants are applied, demonstrating synergistic effects but not outstanding efficacy.[156] The already available drugs applied in the therapy of neuropathic pain either by registration or in off-label use (Table 2).

Neuropathic pain models in the development of novel drugs have some limitations: reliable and objective measures of behavioral response, adequacy of outcome measures, and a multimodal mechanism underlying the development of neuropathic pain.[157]

The lack of effective pharmacotherapeutic treatment comprising low side effects and long-term efficacy confirms a definite demand for new therapeutic strategies in neuropathic pain management.

Histamine is a key molecule for the transmission of nociceptive signals, being antinociceptive in the CNS and nociceptive in the peripheral nervous system (PNS). While excitatory histamine signaling in nociceptive pathways is associated with increased pain, inhibition of histamine receptors is neuroprotective, exhibiting antinociceptive effects. All histamine receptors may be involved in nociception and, consequently, neuropathic pain, but the exact role of each receptor and whether mutual influences exist need further elucidation.[7]

Table 2: Drugs, their mechanism of action, side effects and applications in the treatment of neuropathic pain.[158-163]

Drug	Mechanism of action/ effect	Side effects	Application
Amitriptyline (tricyclic antidepressant)	NA and 5-HT transporters, activation	anticholinergic and neurologic effects	Neuropathic pain fibromyalgia
Duloxetine (SSNRI)	SSNRI Diabetic peripheral neuropathic pain	Nausea, raised blood pressure/administration, restricted authorization, diabetic polyneuropathy	Painful diabetic neuropathy
Venlafaxine (SSNRI)	SSNRI	Not authorized, but medication of choice in other guidelines	Symptomatic treatment of neuropathic pain
Gabapentin	GABA Decreases release of glutamate, norepinephrine and substance P	Neurological symptoms as fatigue, dizziness,	Postherpetic neuralgia
Pregabalin	GABA, $\alpha_2\delta$ subunit of calcium channel neurons	Neurological symptoms as fatigue, dizziness	Postherpetic neuralgia painful diabetic peripheral neuropathy
Tramadol	μR agonist and NA and 5-HT reuptake inhibitor	Nausea/vomiting, constipation, dizziness	Postherpetic neuralgia, peripheral diabetic neuropathy, spinal cord injury, polyneuropathy
Morphine	μR agonist	Substance abuse, suicide risk and driving impairment	Rapid onset of analgesic effect
Oxycodone	μR agonist and κR antagonist	Substance abuse, suicide risk and driving impairment	Rapid onset of analgesic effect
Lidocain	Block of sodium channels	Skin reaction (erythema or rash)	Postherpetic neuralgia

Abbreviation: GABA – γ-aminobutyric acid, μR – μ opioid receptor, κR – κ opioid receptor, 5-HT – 5-Hydroxytryptamine, NA – Noradrenaline, SSNRI – selective serotonin and noradrenaline reuptake inhibitor

H_3R is distributed in the spinal cord, primary sensory neurons, dermal tissue, dorsal root ganglia, periaqueductal gray area, and superior cervical ganglia regions, modulating pain transmission.[79, 164, 165] H_3R has been found in both the ascending nociceptive pathway and the descending pain control pathway, both of which are critical for the transmission of nociception. Studies on H_3R inverse agonists and agonists in neuropathic pain models have presented contradictory results. Indeed, the various animal models, dosages, administration routes, and outcome measures contribute to the complexity of result interpretation and the difficulty in drawing the correct conclusions by clearly

proving the influences of H_3R ligands in the modulation of neuropathic pain. The study findings of thioperamide (an H_3R and H_4R inverse agonist) are controversial due to a lack of selectivity and different effects depending on the route of administration and dose.[166-168] However, several selective H_3R antagonists (e.g., GSK189254, A-960656) have demonstrated analgesic effects in animal models of neuropathic pain, which are listed along with their respective H_3R affinity in Figure 7. Mechanical and cold hypersensitivity were reduced to a comparable extent to the clinically relevant drugs pregabalin and gabapentin.[164, 169, 170] The analgesic effect appears to involve histamine release in the locus coeruleus, modulation of descending noradrenergic pathways, and α_2R desensitization.[171, 172] Despite the low affinity of S38093, chronic administration led to antihyperalgesia in two neuropathic pain models, and other effects cannot be excluded.[169] Efficacy against mechanical hypersensitivity, but not thermal, proves the modality-specific action presumably due to selective effect on H_3R expressing A-fibers rather than C-fibers. Co-expression of H_3R and transient receptor potential melastatin 8 (TRPM8) on Aδ fibers may contribute to cold hypersensitivity. Popiolek-Barczyk et al. (2018) investigated E-162, a selective H_3R antagonist, in mouse pain models, demonstrating analgesic effects and the contribution of spinal H_1R, as evidenced by the lower analgesic outcome observed when H_1R inhibition using pyrilamine resulted in a lower analgesic effect.[173]

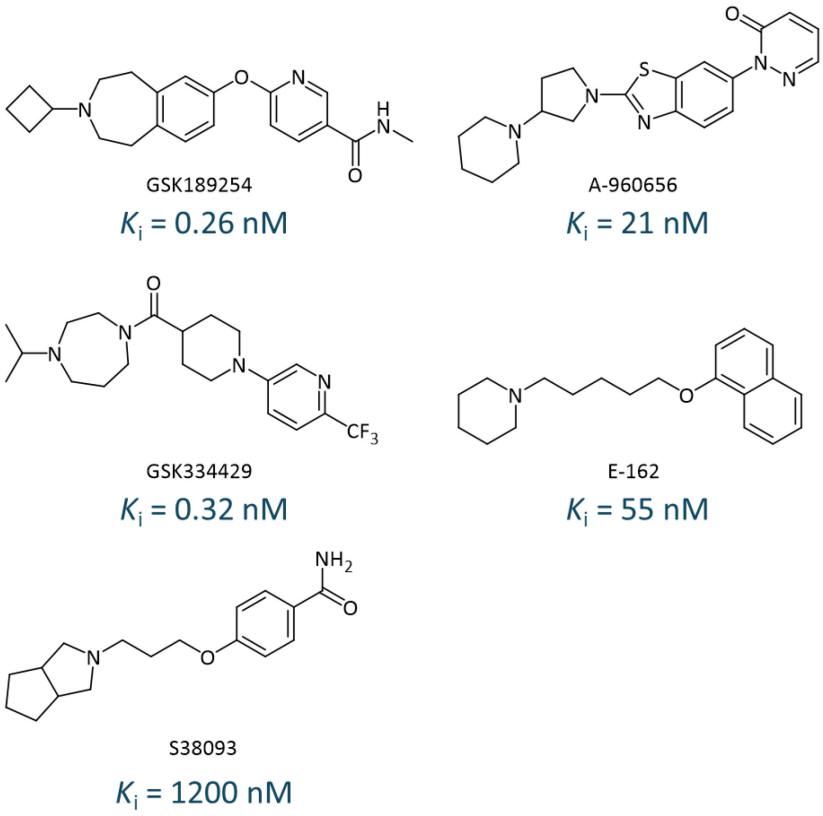


Figure 7: H_3R ligands and their binding properties tested in neuropathic pain models.[170, 173-176]

1.4.4 Neurodegenerative diseases

Parkinson's Disease

PD is a neurodegenerative condition characterized by the presence of bradykinesia with rigidity, rest tremor, or both, provoked by multiple causes (e.g., genetically or sporadic) that are not fully known.[177] Some gene mutations (SNCA, LRRK2, PRKN, PINK1, and GBA) are involved in PD development, and environmental factors such as toxins, head injuries, and pesticide exposure are associated with PD.[177] Besides the primary symptoms, various non-motor symptoms, including mental and emotional manifestations, constipation, urinary, skin, and sleep problems, cognitive symptoms and dementia, muscle cramps and dystonia, pain, fatigue, and loss of energy, difficulties in swallowing and chewing, also occur in PD patients.[177, 178] This clinical syndrome is multifaceted and comprises individual characteristics. The non-motor effects are substantially involved in the progression of PD, and no disease-modifying therapy is available to date.[178] The pathophysiology of PD is complex, and individual manifestations seem that treatment of the disease cause for all disease forms by a single pharmacological intervention is unlikely. Processes differ from prodromal and early to later stages of the disease.[179] Pathophysiology interplay of aberrant α-synuclein aggregation, dysfunction of mitochondria, lysosomes, vesicle and synaptic transport, and neuroinflammation. Neuronal death of dopaminergic neurons in the SN pars compacta is characteristic of PD and accelerates during the progression of the disease. Loss of nigrostriatal dopamine cells causes a gradient of striatal dopamine depletion, resulting in an imbalance between the direct (dopamine D_1 receptor) and indirect (dopamine D_2 receptor) pathways through the basal ganglia, which leads to bradykinesia. New insights assume compensatory alterations of brain activity in areas that are initially unaffected by the pathology of PD, leading to a shift toward more anterior corticostriatal circuits and recruitment of cortical regions less connected to the basal ganglia.[177]

Currently, pharmacotherapy focuses on the symptomatic treatment of disabilities. Symptoms of individual PD patients and treatment goals vary from patient to patient, emphasizing the need for personalized therapeutic options.[177, 178] First-line treatment focuses on the improvement of motor symptoms by increasing dopamine in the SN either with dopamine agonists (e.g., pramipexole) and/or levodopa (a precursor of dopamine), MAO-B inhibitors (e.g., safinamide, rasagiline), and COMT inhibitors (e.g., entacapone).[179, 180] Co-medication is used to treat non-motor symptoms with emphasis on behavioral and psychological symptoms to maintain independence in daily life activities, improve quality of life, prevent dopaminergic side effects, and avoid care dependency. For example, adjunctive therapies are cholinergic AChE inhibitors (rivastigmine) for mild to

moderate dementia in PD and the atypical antipsychotic clozapine for PD-related psychosis.[179, 181, 182] Despite the reasonable control of motor symptoms in the early stages of PD with levodopa, efficacy decreases in later stages, accompanied by motor fluctuations, e.g., dyskinesia.[183, 184] Tavapadone is a selective dopamine D_1/D_5 receptor partial agonist (D_1R $K_i = 9$ nM, D_5R $K_i = 13$ nM) with promising results in phase III clinical trials as an adjunctive treatment for PD with motor fluctuations. Besides, the first of its class ligand is also under investigation in clinical trials as monotherapy for PD.[185, 186]

H_3Rs are co-expressed on dopaminergic and glutamatergic neurons in the striatum and SN, brain regions directly involved in PD.[187, 188] H_3Rs are present on glutamatergic and dopaminergic afferents from SN pars compacta and cerebral cortex, modulating the release of other neurotransmitters within the basal ganglia.[187, 189] H_3R potentiates D_2R but inhibits D_1R action, among others, by functional heterodimers with D_1R and D_2R can form on spiny projection neurons.[88, 89] In PD, alterations in the histaminergic system, including elevated brain histamine, increased H_3R mRNA levels, morphology, and density changes of histaminergic fibers, indicate a possible contribution to disease pathophysiology.[190, 191] Despite this, the number of histaminergic neurons in TMN and expression of HDC do not appear to be altered in PD.[192, 193]

H_3Rs modulate dopaminergic signaling through indirect mechanisms in rodent models. Histamine can increase the dopaminergic inhibitory effects of D_2R in medium spiny neurons and mitigate D_1R effects. Additionally, presynaptic H_3Rs result in the inhibition of cortical and thalamic excitatory projections in medium spiny neurons.[21]

6-OHDA rats, as a PD model treated with HDC inhibitor (α-fluoromethylhistidine), exhibit a significant decrease in rotation behavior induced by apomorphine.[194, 195] Thioperamide increases histamine in the brain and alleviates apomorphin-induced behavioral responses in rats and may also rescue memory impairment in the mouse model of PD.[196] In summary, these observations emphasize the role of the dysregulated histaminergic system in PD and the potential benefits of H_3R modulation.

Alzheimer's Disease

AD is a progressive neurodegenerative disorder with advanced deterioration of quality of life for patients and a primary health issue with increasing prevalence.[197] Cognitive impairment is often accompanied by neurobehavioral symptoms (e.g., apathy, anxiety, and depression).[198] Loss of cholinergic neurons and diminished ACh, as well as elevated activity of NMDA receptors on

glutamatergic neurons, appear in AD patients.[199] Aggregated amyloid β-peptides (Aβ) and intracellular neurofibrillary tangles (NFTs) containing phosphorylated tau (τ) accumulate leading to progressive synaptic and neuronal loss.[200] Despite the immense efforts, disease cause remains uncovered to date, and besides the amyloid cascade hypothesis, non-amyloid hypotheses including neuroinflammation, τ, and neuroprotection are under discussion.[198] The multifaceted characteristics require complex pharmacological and non-pharmacological treatment and interventions, depending on the state of disease.[201] Therapeutic goals are delaying the course of the disease, alleviation of symptoms, delayed admission to nursing homes, improvement of quality of life, and relief for relatives. Cognitive enhancing pharmacological management focuses on symptomatic treatment, and cognitive enhancing drugs include acetylcholinesterase (AChE) inhibitors (e.g., rivastigmine) and the NMDA antagonist memantine.[197]

In the last decade, several biological drugs have been approved as AD treatments, including Aducanumab (Aduhelm™) by the FDA in 2021. The antibody reduces amyloid β-plaques in mild cognitive impairment and AD, but the clinical benefits are limited, and approval was controversial.[202, 203] Two further antibodies against amyloid plaques for the treatment of mild cognitive impairment and mild dementia were approved by the FDA, namely Lecanemab-irmb (Leqembi™) and Donanemab-azbt (Kisunla™). The latter is an amyloid β-directed antibody that binds only to insoluble amyloid-β.[204, 205] However, the application of these antibodies for AD is debatable in terms of patient benefits. The EMA declined to approve donanemab, concluding that the benefits do not outweigh the serious adverse events, including brain swelling and bleeding.[206] Despite progress in approving biological treatments for AD, the disease-modifying effect has not been ensured. The costs of development and manufacturing of daily doses are significantly higher compared to those of small molecules.

Histamine receptors are highly expressed in brain areas responsible for cognition, and the neurotransmitter is assumed to be a key modulator in cognition. Higher mRNA levels of H_3R splice variants were observed in the brains of patients with AD symptoms, but H_3R densities in the prefrontal cortex of AD patients appear to be unchanged.[207, 208] The number of histaminergic neurons and the activity of HDC in AD patients remain unaltered. However, mRNA fluctuations are lost in some patients with AD.[32, 209] H_3R KO mice perform similarly to wild-type mice in novel object recognition and passive avoidance learning, and interestingly, the performance is better in spatial learning task suggesting task depending role of histamine in rodents.[210] Several studies investigated properties of H_3R antagonists in cognitive models with emerging positive effects on cognitive decline.[33] Procognitive properties suggest potential utility in dementia, and some H_3R

ligands (GSK-239512, ABT-288, and S38093 (Figure 7)) made it to phase 2 clinical trials. However, cognitive improvement remained modest or was not clinically meaningful compared to placebo.[211-213] Further studies suggest the neuroprotective effect of the H_3R antagonist via CREB and GSK3β pathways[214, 215] and in a recent study of Pitolisant, restoration of cognitive deficits was demonstrated in mice linked to the lysosomal system rather than the neuronal activity of histamine.[216] Clinical trials are limited by the number of H_3R antagonists investigated, however, the mechanism for the discrepancy between preclinical observations and clinical trials remains unclear.

1.4.5 Psychiatric disorders

Schizophrenia

Schizophrenia is a neurological disorder with episodic progression and clinically apparent positive and negative symptoms. People with schizophrenia can be affected by the disorder for a lifetime, with generally lower life expectancy.[217] Positive symptoms are mainly present in acute, psychotic episodes, including delusions, hallucinations, and disorganized speech, and at least one of these symptoms has to be present. In contrast, the negative symptoms are persistent, such as psychomotor, drive disorder, and affectivity. Moreover, disorganization, cognitive, and affective disorders, and comorbidities such as substance abuse, post-traumatic stress disorder, depression, and suicidality are common in schizophrenia patients. The onset of schizophrenia is usually in early adulthood, and somewhat earlier in men than in women.[218] Multiple pharmacotherapeutic options are available with different modes of action, mainly affecting dopamine transmission, among other neurotransmitter systems. Antipsychotics are grouped into the typical class (first generation), like haloperidol, and the atypical class, clozapine (second generation), aripiprazole, and cariprazine (third generation), which are shown in Figure 8. Even though the second and third generation of antipsychotics led to reduced extrapyramidal side effects, the available treatments mainly show good improvement of positive symptoms, and efficacy on negative domains is limited.[219, 220] Furthermore, multiple side effects, such as weight gain or extrapyramidal effects, alleviate patient compliance.[221, 222]

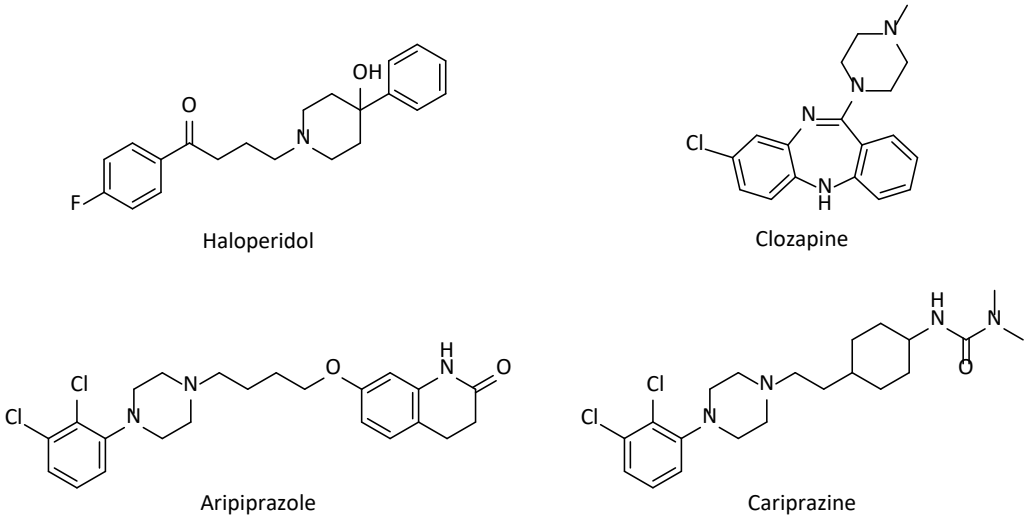


Figure 8: Structures of first, second, and third generation antipsychotics in the treatment of schizophrenia.[223]

Recently, a new approval of Cobenfy® that contains xanomeline and trospium chloride for the treatment of schizophrenia in adults as the first antipsychotic drug that targets cholinergic receptors.

Xanomeline is a muscarinic receptor agonist (M_1R and M_4R) with a secondary effect on dopaminergic alterations. Trospium is an antimuscarinic molecule that counteracts the peripheral adverse effects of xanomeline.[224]

The role of H_3R in schizophrenia has been implicated in several studies, with the principal focus on cognitive impairment.[174, 225, 226] However, the procognitive effects of H_3R antagonist demonstrated in rodents were not verified in controlled, double-blind trials of Pitolisant and other H_3R inverse agonists given in addition to antipsychotics.[175] Upregulated H_3R expression was observed in the prefrontal cortex of individuals with schizophrenia postmortem.[226] H_3R is present presynaptically on glutamate, dopamine, ACh, serotonin, NA, and GABAergic neurons.[11] Clozapine is an antipsychotic drug that acts as a potent H_1R partial inverse agonist, weak H_2R full inverse agonist, and as a moderate H_3R and H_4R agonist. These binding properties may contribute to the antipsychotic, but also the sedative profile of the drug.[227] Recent PET studies of schizophrenia patients implicate that H_3R levels are not altered but potentially disrupted histaminergic modulation of executive function.[228] In summary, further studies are necessary investigating H_3R antagonist influence in schizophrenia patients to prove H_3R modulation in schizophrenia patients.

Depression

The prevalence of major depressive disorder is 15-20% and is often accompanied by comorbidities, higher mortality, and increased risk of suicide.[229, 230] It is a central public health issue worldwide with high heritability. Bidirectional relationships of comorbidities such as bipolar disorder, schizophrenia, substance use disorder, anxiety, and neurodegenerative diseases hamper confirmed diagnosis.[231] Predominant and persistent symptoms are cognitive, affective, and behavioral disorders, depressed mood, anhedonia, weight changes, and loss of interest.[232] Several hypotheses are discussed for the pathological mechanism of major depressive disorder, namely, hypothalamic-pituitary-adrenal axis dysfunction, monoamine, inflammatory, genetic, and epigenetic anomalies, and structural as well as functional brain remodeling hypothesis. However, none of the hypotheses provides a complete explanation of the pathological mechanism. The complexity of the disease not only limits accurate diagnostics, but the choice and possibilities of pharmacological strategies are also limited.[233] Even though antidepressants improve symptoms of some patients, recurrence after discontinuation of antidepressants and insufficient effect are major issues.[229, 233, 234]

Neuropathology and molecular mechanisms of major depressive disorder remain to be elucidated, but stress is an etiology proposed to play a fundamental role, especially by chronic activation of

stress response pathways.[235, 236] Imbalances of monoamines such as dopamine, norepinephrine, and serotonin are also implicated in the pathology of major depressive disorder.[233] These monoamines synergistically regulate different aspects of mood and are dysregulated in depression. For example, extracellular serotonin levels in blood, urine, and cerebrospinal fluid are lower than in healthy humans. Moreover, the noradrenergic system in the locus coeruleus is impaired, with decreases in norepinephrine transporters and increased α_2-adrenergic receptors.[237] Dopamine plays a role in motivation, concentration, pleasure, reward, emotions, and psychomotor speed. Chronic stress induces neuroadaptation that attenuates dopamine-mediated reward pathways following depression and fatigue associated with changes in dopamine function. Serotonin is involved in cognition, sleep, circadian rhythms, motor activity, and other biological functions, and selective serotonin reuptake inhibitors (SSRIs) such as fluoxetine are widely used in depression. Drawbacks of these therapeutic options are partial lack of clinical efficacy, adverse events, and patient compliance.[237] Delayed effects of SSRIs may be attributable to long-term neuroplasticity deficits and restorage needs chronic treatment. Chronic treatment with antidepressants is associated with increased transmission of serotonin in the locus coeruleus and neuroplasticity in specific brain regions.[233, 238] Some antidepressants show high affinity to σ_1R, like the SSRIs fluvoxamine and sertraline. The antidepressant like effects of σ_1R agonists are demonstrated in several preclinical and clinical studies, however, the clinical outcome is indecisive, and none are approved for the treatment of depression yet.[239, 240] Recently, the widely applied anesthetic drug ketamine was repurposed and approved as a nasal spray in combination with SSRI or SNRI for treatment resistant depression and major depressive disorder by the FDA and EMA. The FDA extended the use of the rapidly acting drug as a standalone therapy in 2025. Esketamine mitigates symptoms of depression rapidly, but NMDAR antagonists can lead to serious side effects, e.g., abuse and cognitive impairment.[241, 242]

Several studies have postulated a convergence between H_3R antagonists and antidepressant resp. anxiolytic effects in rodents. It is suggested that precognitive and antidepressant effects are induced by H_3R modulation of glutamatergic transmission.[237] For example, clobenpropit increased hippocampal plasticity and decreased immobility in forced swim test by H_3R inhibition and thereby disinhibition of H_1R and H_2R in the hippocampus.[243] Ciproxifan alleviates depression-like behavior.[244] ST-1283 demonstrated anxiolytic effects and alleviates depression-like behaviors in mice in multiple tests (open field test, elevated plus maze, depression, forced swim test, tail suspension test, novelty suppressed feeding test).[245] JNJ10181457 improves depression-like behavior in mice in the tail suspension test and release of proinflammatory cytokines.[246] Compound 3h (3,5-dimethyl-*N*-(2-methyl-4-((2*S*,3'*S*)-2-methyl-[1,3'-bipyrrolidin]-1'-yl)phenyl)isoxazole-4-carboxamide), an inverse agonist of H_3R with a favorable safety profile, displayed antidepressant-

like effects in the forced swimming test in rats.[247] However, clear evidence of the association between depression and H_3R is still missing and needs further elucidation.

Autism spectrum disorder

Patients with ASD exhibit social deficits and repetitive sensory-motor behaviors. Due to the versatile characteristics, no reliable biomarkers are available, and diagnosis is currently based solely on behavior. According to the DSM-5, the following aspects must be fulfilled: social communication and/or interaction impairment, sensory anomalies, and repetitive behavior (e.g., restricted interests and hyper/hyposensitivity). The symptoms must be present in early development and cause impairment in current functioning without another explanation. Various levels of intellectual disability are possible.[248]

Pathophysiological differences include functional brain and subtle anatomical changes, e.g., evident in electroencephalography. More than 100 genes and genomic regions are associated with ASD, but the knowledge of genetic components has not shown clear benefits yet. Presumably, complex interactions in the development of children's brain activity and behavior cause altered synaptic signaling and gene expression. Treatment aims to interfere with specific behaviors, joint attention, language, and social engagement through psychosocial interventions. In contrast, pharmacological treatment should improve associated symptoms such as irritability and comorbidities, including anxiety, Tourette syndrome, ADHD, and depression.[249-251] Genetic risk factors of Tourette syndrome match those of ASD, and both neurodevelopmental disorders may be associated with the upregulated microglia activation, neuroinflammation, and dysfunction of basal ganglia circuits. Furthermore, a family association study has shown that nonsense mutations in the HDC gene are associated with TS.[252] ASD can be classified into syndromic and nonsyndromic based on apparent clinical criteria.[253] Although some pharmacological treatment options are available, the improvement of social interaction is only a secondary effect. Currently applied medicinal products and the respective treated symptoms are displayed in Table 3.

Due to the heterogeneity of ASD with varying principal symptoms, several therapeutic options are required. Furthermore, only associated symptoms or comorbidities such as ADHD or anxiety are treated with the available drugs to date.[248] Prescriptions are mostly off-label, bearing the risk of overmedication and insufficient effect due to interindividual differences. Furthermore, side effects of these drugs, such as weight gain from atypical antipsychotics, aggression from stimulants, or emotional flattening with SSRIs, deteriorate patient compliance.[248, 254] Hence, a preferable safety profile needs to be considered for novel drug discovery. Treatments targeting the cause of the disease and focusing on improving social and communication skills are still in development.

Table 3: Drugs in use for specific symptoms of ASD.[248, 254, 255]

Drug or drug class	Symptoms
Methylphenidate	ADHD
Atomoxetine	
Guanfacine	
Risperidone	Agitation, irritability, aggression, self-injury, severe tantrums
Aripiprazole	
Atypical antipsychotics	Aggression, self-injury, tantrum
SSRI	Anxiety, repetitive behaviors
Psychostimulants	Hyperactivity
Opioid antagonists (e.g., naltrexone)	

Abbreviations: ADHD – attention deficit hyperactivity disorder, SSRI – selective serotonin reuptake inhibitor

De novo deletions in HNMT suggest a possible influence of the histaminergic system in ASD, the comorbidity with Tourette syndrome, and their similar pathophysiological mechanism indicates that the histaminergic system may be involved in repetitive behavior.[252] In particular, increased H_3R activity in the striatum might contribute to repetitive behavior in ASD patients. H_3R antagonist alleviates repetitive behaviors in BTBR mice.[256] H_3R blockade improved social deficits in phencyclidine (PCP) exposed mice.[257] Ciproxifan improved sociability and decreased stereotypy in valproic acid (VPA) induced ASD.[258, 259] E169 demonstrated memory-enhancing capabilities with efficacy in modulating cognitive impairment and enhancing short-term recognition memory in mice.[260] ST-2223 with H_3R and D_2/D_3R properties improved anxiety.[256] The H_3R antagonist and AChE inhibitor E100 alleviated VPA-induced autistic, stereotypic, and repetitive behaviors in mice model of ASD.[261] DL77 mitigates autistic behavior in the VPA-induced mouse model but failed to restore anxiety and hyperactivity.[259] These preclinical studies indicate the benefits of H_3R antagonists in ASD patients, but clinical trials are needed to unravel the effect of H_3R antagonists in ASD patients.

1.5 Dual- and Multi-targeting directed ligands

In the field of drug discovery, the paradigm of 'one molecule, one target' dominated for many years. Nevertheless, highly selective ligands targeting individual proteins often fail to provide adequate therapeutic efficacy. In diseases with simple pathophysiological mechanisms and clear disease causes, traditional single-target drugs are feasible. Nevertheless, the influence of multiple receptors, enzymes, and signaling pathways in the pathophysiology of complex diseases demands sophisticated solutions.[123, 262]

Polypharmacology is frequently applied in multifactorial diseases, either as a drug cocktail or coformulation. For example, the dopamine agonist pramipexole is combined with the catechol-O-methyltransferase inhibitor entacapone or the MAO-B inhibitor safinamide with COMT inhibitors for the treatment of PD.[180] The applications of drug cocktails are versatile, but the main goal is increased efficacy and/or prevention of adverse events, e.g., a non-steroidal anti-inflammatory drug with proton pump inhibitors to reduce heartburn.[263] Administration of drug cocktails is accompanied by poor patient compliance, different pharmacokinetics, and may result in severe adverse events.[264, 265]

Coformulations such as tablets containing multiple active pharmaceutical ingredients improve patient compliance and efficacy. Technologically developed formulations are challenging in a physicochemical and pharmacokinetic manner. Especially if the combined active pharmaceutical ingredients have different technological requirements and a mutual influence on pharmacokinetics. The flexibility of dosing is limited, for example, with non-separable tablets or if only a specific strength is manufactured.[266] However, Corbilta® is a successful example of a coated tablet with levodopa, carbidopa, and entacapone for the treatment of PD.[266, 267]

The development of new drug candidates with high efficacy and preferable toxicological properties, lacking severe adverse events, is becoming increasingly complex due to stricter regulatory requirements. Moreover, the lack of definite targets involved in pathophysiology or the cause of disease hinders drug discovery. Multitarget-directed ligand (MTDL) development has moved into the spotlight of CNS disease recently.[123] Formerly, the main reason for MTDL discovery was by serendipity, such as the antipsychotic haloperidol (see Figure 8) or imipramine, a tricyclic antidepressant, found by serendipity acting as a potent SSRI with NA reuptake inhibition and acting as a H_1R and mAChR antagonist.[268]

The opportunities of MTDL and dual-target directed ligands (DTDL) include synergistic effects, higher efficacy and safety, and a simplified dose schedule.[262] Taking antipsychotic drugs as an

example, the atypical antipsychotic drug clozapine (Figure *8*) acts as a dopamine D_2R agonist, 5-$HT_{2A}R$ and mAChR antagonist. This target combination leads to antipsychotic effects (D_2R), reduction of side effects (5-$HT_{2A}R$, mAChR), and an overall improvement of positive and negative symptoms in schizophrenia. Moreover, the antipsychotic drug Cariprazine (Figure *8*) acts as dopamine D_3R and D_2R partial agonist (pK_i=10.07, 9.31), 5-$HT_{1A}R$ partial agonist (pK_i=8.59), 5-$HT_{2A}R$ antagonist (pK_i= 7.73), and 5-$HT_{2B}R$ (pK_i= 9.24), and H_1R (pK_i =7.63). The interplay of several targets improves cognitive and negative symptoms (D_3 and D_2R), acts as an anxiolytic and mood stabilizing agent (5-$HT_{1A}R$), and reduces extrapyramidal side effects (5-$HT_{2A}R$).[269, 270]

Challenges in the development of MTDL include its large molecular weight due to combined pharmacophores, the selection of targets for combination, and the fact that higher drug promiscuity may result in unforeseen side effects.[262]

The identification of target combinations can be realized with several strategies. Rational combinations can be based on clinical observations, such as aripiprazole or cariprazine (Figure *8*). Moreover, phenotypic screening in cell systems and animal models, as well as in silico techniques, such as network pharmacological methods or machine learning, are valuable tools for target selection.[267] In-silico techniques require wet lab validation. High-throughput screening of effective compounds for another target is indeed time-consuming, but it can still result in hit identification. Thereafter, affinities and selectivity are improved during lead optimization. The lead ligand's physicochemical and pharmacokinetic properties, and biological activities are improved. The challenges of MTDLs improvement are conserving activities on all targets and reducing activities at off-targets.[262]

MTDLs are classified into linked, fused, or merged ligands depending on the structural overlap of the pharmacophores. In contrast, for the linked MTDLs, known pharmacophores are linked to one molecule via stable or biodegradable linkers, the fused ligands do not contain a linker, and the pharmacophores of the desired targets are fused. The merged approach has the highest overlap of pharmacophores. Linked pharmacophores are the most straightforward approach to generating MTDLs, eliminating the need for excessive structural optimization. This strategy is of great interest for target delivery, e.g., antibody-drug conjugates in cancer therapy, imaging purposes, and modulation of pharmacokinetic properties. However, this approach often results in large molecules, hindrance of the linker, and bioavailability issues.[262, 271] One example, among others, is the dual-targeting fluorescent ligand UR-NR266 with a polyethylenglycol linker.[272] Linker chemistry is decisive as it can either support the properties of the MTDL, e.g., polarity and solubility, or impact biological activities towards selected targets, e.g., with steric hindrance. Non-cleavable or cleavable

linkers, such as hydrazone or disulfide linkers, can be applied depending on the purpose of the MTDL. In the fused class, two or more molecules are fused without the necessity of a linker, and the merged class composite ligands with similar core structural elements interact with two or multiple targets. The main pitfall of this class is promiscuity without selectivity to the intended targets.[262, 267, 271]

A holistic and rational approach to target and ligand selection, balancing desired activities, is necessary to accomplish selectivity, in addition to biological activity at multiple targets. The validation of target combinations and elucidation of tolerant positions of structural elements are helpful in achieving this. The strategy of lead generation depends on the type of MTDL, and the knowledge-based approach focuses on known pharmacophores of selective ligands for multiple targets combined into a single compound. An alternative strategy is design-in, in which potent and selective compounds that modulate the two targets are employed for MTDL development. The first pharmacophore is designed into the second and subsequently modified for dual or multiple potency. Similarity of structural features is essential for achieving potency on the selected targets. In an optimal scenario, the central building block of both ligands is the same, and only the configuration of substituents differs. This approach is beneficial for known selective ligands with detailed structure-activity relationships. This helps identify adaptable positions and determine whether scaffold hopping might be applicable. In comparison, the design-out approach starts with an unselective ligand that modulates multiple targets of interest. The development focuses on structural adaptation toward selectivity and reducing the potency of unintended targets.[262, 267]

1.5.1 Targets for combination in DTDLs and MTDLs

The last decades have seen a growing trend towards MTDLs in the field of H_3R.[123] Selective ligands were in the focus of the area, although dual target properties of some H_3R antagonists were already described more than 20 years ago, e.g., H_3R and H_1R for allergy and inflammation, NO donor properties with guanidine derivatives (neuromodulator), and H_3R antagonist with inhibition of HNMT.[273] Renewed interest in MTDLs has developed in recent years, with several concepts of target combinations.[123] Targets of interest include other GPCRs such as dopamine D_2R and D_3R, adenosine A_1 and A_{2A} receptors, e.g., ST-1992[274], serotonin receptors, e.g., ST-2300[275], and/or enzymes such as cholinesterases and monoamine oxidases, e.g., contilisant[109]. Understanding the causes of disease leads to the best target combinations, and this chapter presents specific combinatory targets (Figure 9) focusing on their impact on disease pathophysiology and case studies of already described MTDLs.

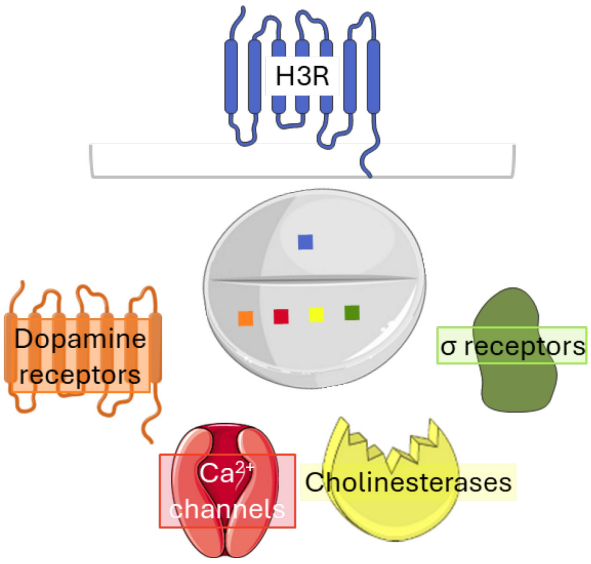


Figure 9: Schematic representation of dual- and multi-target directed ligand combinations described in this thesis (adapted from reference [276]).

Dopamine Receptors

Dopamine receptors are GPCRs distinguished into five receptor subtypes, D_1-D_5R. The receptors are grouped into D_1/D_5 (D1-like) that are mainly G_s-coupled receptors, and $D_2/D_3/D_4$ (D2-like) which are mainly $G_{i/o}$-coupled receptors.[277-279] Dopamine is a neurotransmitter involved in multiple CNS circuits, influencing, among others, motivation, cognition, emotions, and motor function. An imbalanced dopamine system in the CNS is associated with mood disorders, schizophrenia, and PD. Dopaminergic innervations are present in the nigrostriatal, mesocortical, mesolimbic, and tuberoinfundibular regions[280, 281] with D1-like receptors postsynaptically and D2-like receptors pre- and postsynaptically.[282] Affinity of dopamine to the receptor subtypes varies, and higher sensitivity of presynaptic receptors may induce biphasic effects of these receptors, which means suppression at low and stimulation at high doses.[283] D_2R is located pre- and postsynaptically, with two main splicing variants, the short D_{2S} (mainly presynaptic) and long D_{2L} (mainly postsynaptic) elicit distinct functions.[284-287] While presynaptic inhibition of dopamine release initiates neuromodulation leading to reduced locomotion, postsynaptic inhibition of D_2R improves motor activity. For D_3R and D_4R, splicing variants were also found, but their functional characteristics are less well characterized.[288, 289]

Antipsychotics mainly affect dopamine receptors, and the occurrence of extrapyramidal side effects, namely akathisia, parkinsonism, dystonia, and tardive dyskinesia, is caused by the inhibition of striatal dopamine receptors.[290] Even though the antipsychotic effect is an interplay of several neurotransmitters, the main part is the inhibition of dopamine receptors in the mesolimbic area. The dopaminergic system is associated with depression, and some dopaminergic agonists have shown antidepressant effects in preclinical studies.[291] Dopamine agonists and DA reuptake inhibitors may have therapeutic effects on depression.[292] As already mentioned in section 1.4.4, dopamine D_2R agonists such as pramipexol or ropinirole are used in the treatment of PD. Moreover, MAO B and COMT inhibitors increase dopamine by inhibiting dopamine decay.[293] D_1R is involved in cognitive processes such as learning, attention, and memory, motor functions, and reward, indicating it is a potential target in PD, but to date, no selective ligand is available.[283]

H_3R antagonist alone or as MTDL with MAO-B inhibition increases dopamine concentration and achieves improvements in cognitive impairment [109]. Some examples are displayed in Figure 10. The dual ligand AG-0029 (Figure *10*), featuring a merged D_2R/D_3R partial agonistic and H_3R antagonistic pharmacophore, ameliorates motor symptoms and improves cognition *in vivo* (in rats). Receptor occupancy study implies that higher doses are required for therapeutic effect at H_3R *in vivo* compared to the dopaminergic occupancy, with the emphasis on the balanced activity at both

targets.[294] ST-2223 (Figure 10) is a merged MTDL with H_3R pharmacophore and part of the D_3R selective inverse agonist BP-897 with H_3 and D_2/D_3R affinity and demonstrating improvement of autism-like behavior.[256] LINS01 compounds are dihydrobenzofuranyl-piperazine derivates with H_3R and moderate to weak D_2/D_3 affinities.[295, 296] ST-713 (Figure *10*) comprising chlorpromazine and H_3R pharmacophore showed high affinity at H_3R and D_2/D_3R with additional moderate affinity to H_1R, H_4R, D_1R and D_5R. In mice, ST-713 ameliorates autism-like behavior.[297] Compound 11 (Figure 10) combines H_3R pharmacophore and the neuroleptic amitriptyline (H_3R, H_1, moderate D_2, D_3, D_1, and D_5).[298]

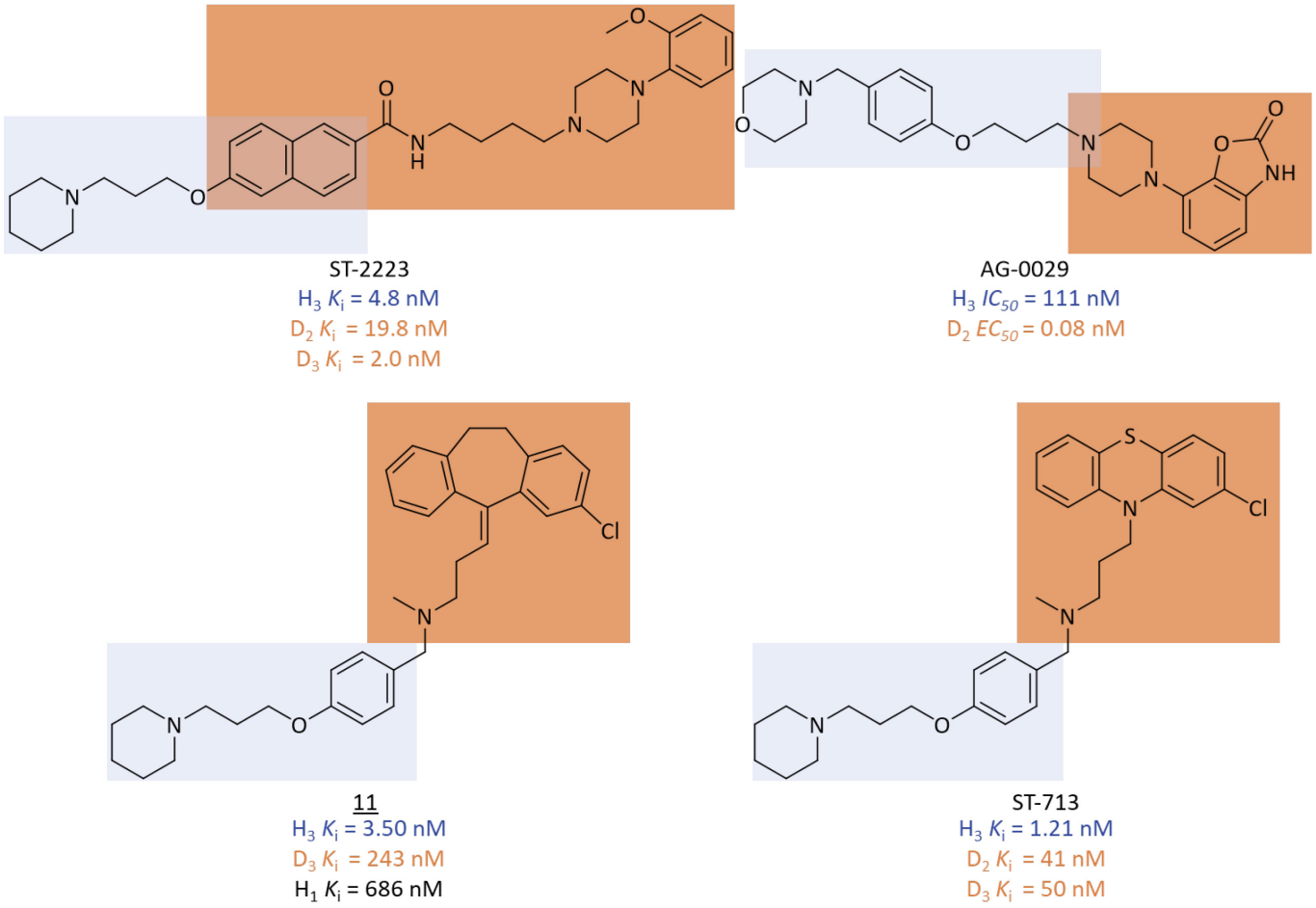


Figure 10: MTDLs comprising dopamine (orange) and H_3 (blue) receptor pharmacophores and their respective activity at the targets.[256, 294, 297, 298]

Cholinesterases

Acetylcholinesterase (EC 3.1.1.7, AChE) and Butyrylcholinesterase (EC 3.1.1.8, BuChE) are enzymes responsible for the hydrolysis of the neurotransmitter ACh in the synaptic cleft.[299] The difference between cholinesterase enzymes is their substrate specificity, kinetics, expression pattern, and activity in different brain regions, e.g., BuChE affinity for ACh is lower.[300-302] AChE inhibitors increase ACh levels in synapses and elevate central excitability with neuroprotective effects on the stimulation of nicotinic and muscarinic ACh receptors, which improve cognitive functions in AD patients.[303-305] The AchE inhibitors donepezil, rivastigmine, and galantamine are still the first-line treatment of AD but lack long-term effect in progressed AD.[306] During the progression of AD, AChE levels decrease, and drug efficacy deteriorates, but BuChE levels can increase, presumably as a compensatory mechanism.[307] BuChE inhibitors may be a possible strategy in advanced AD, and selective ligands are assumed to be neuroprotective.[301, 308]

Many structurally diverse MTDLs that combine cholinesterase inhibition and H_3R antagonism have already been described (Figure 11). The most prominent is contilisant (Figure 11), combining good affinity to H_3R, good MAO B, and MAO A inhibition, as well as moderate cholinesterase inhibitory activity and antioxidative properties demonstrated restorage of cognitive deficit *in vivo*.[109] Later moderate affinity to σ_1R of contilisant (Figure 11) was established.[309] Isoflavones with H_3R and AChE inhibition.[310, 311] The tacrine derivative FUB 833 (Figure 11) has additional HNMT inhibition (IC_{50}=48 nM) .[118] The merged ligand UW-DM-71 (Figure 11) combines balanced H_3R affinity and AChE inhibition with moderate BuChE.[312] Compound 23 (Figure 11) is a xanthone derivative comprising a merged H_3R and AChE pharmacophore, which showed an enhancing effect on drug-induced amnesia in rats and analgesic effects in neuropathic pain models in mice and rats.[313]

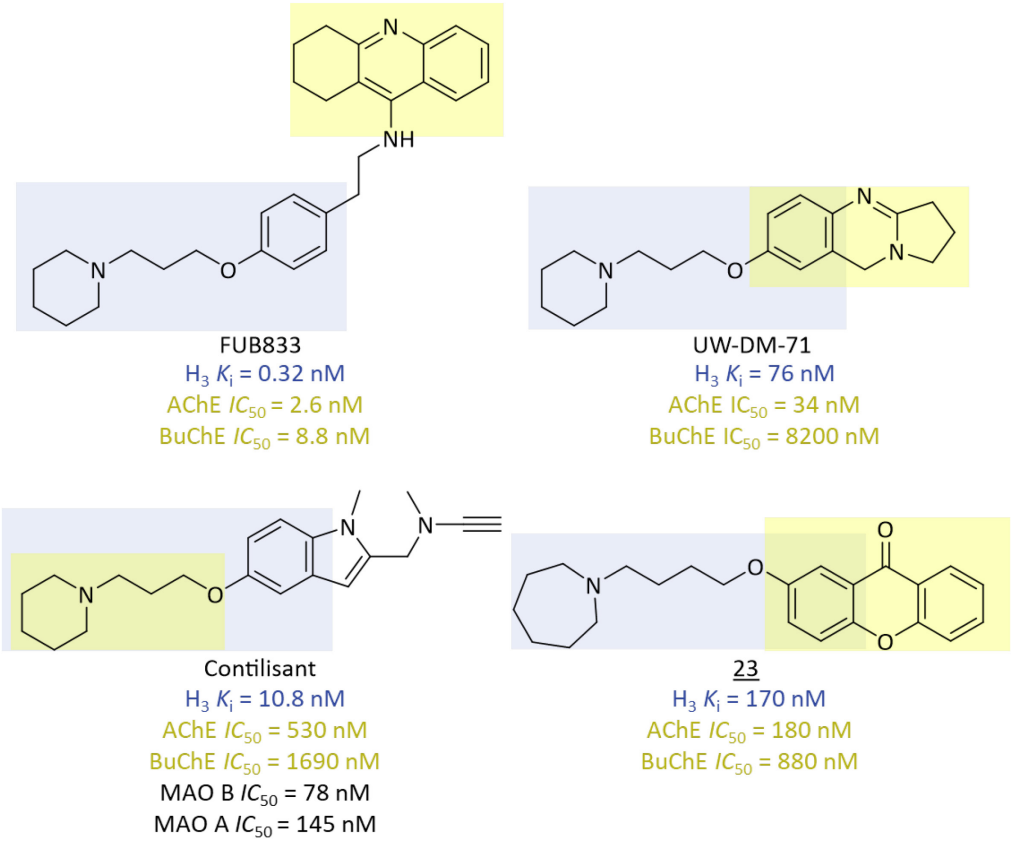


Figure 11: MTDL with H_3R (blue) and AChE and/or BuChE pharmacophore (yellow) and their respective activity at the targets.[109, 118, 312, 313]

L-type calcium channels

Intracellular Ca^{2+} signals control Ca^{2+}-dependent cellular processes, and Ca^{2+} ion inward current drives membrane depolarization, contributing to the electrical activity of cells.[314] Ca^{2+} channels contribute to transmitter secretion, endocrine system, learning, memory, muscle contraction, heart pacemaker activity, and sensory functions.[314, 315] Voltage-gated Ca^{2+} channels are classified in L-type (LTCCs), P/Q-, N-, R-, and T-type calcium channels.[316] LTCCs are divided into four channel subtypes, namely Cav1.1 (CACNA1S), 1.2 (CACNA1C), 1.3 (CACNA1D) and 1.4 (CACNA1F).[317-319] LTCCs consist of five subunits either α_1, α_2, β, δ and γ component.[315] The pore-forming α_1-subunit is highly conserved and depicts mutation sensitive region.[314] In the CNS, primarily $Ca_V1.2$ and 1.3 are expressed [320], but these are also located peripheral on the sinoatrial node, atrial myocytes, or chromaffin cells with impact on heart, brain, and endocrine cells (see Figure 12).[321, 322]

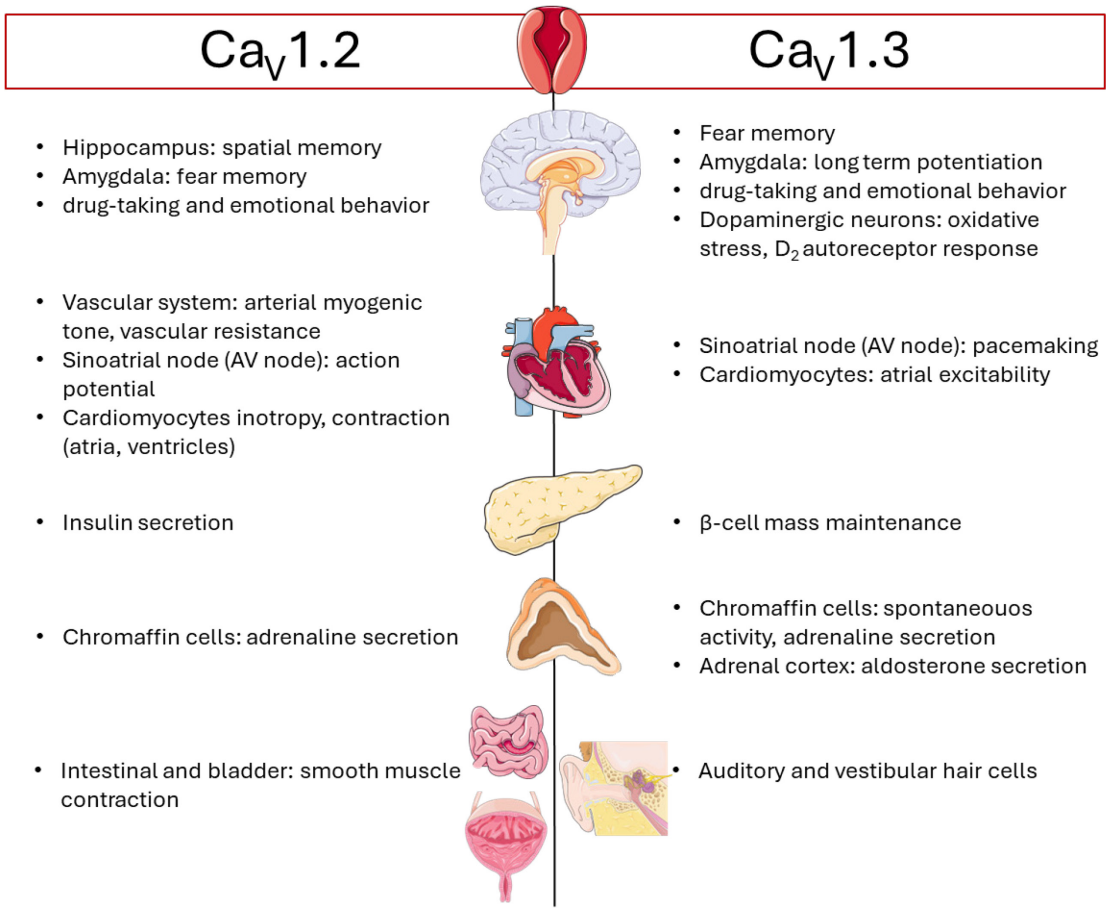


Figure 12: Main functions of $Ca_V1.2$ and $Ca_V1.3$ (adapted from [322]).

The section below focuses on these two LTCCs due to their localization in the brain, their role in CNS disease pathophysiology, possible therapeutic applications, and previous studies of MTDLs.

In the brain, both channels are primarily located postsynaptically, modulating neuronal firing with an impact on multiple pathways. $Ca_V1.2$ is involved in spatial memory, long-term potentiation, emotional behavior, and addiction, while $Ca_V1.3$ regulates both short- and long-term potentiation and is associated with memory learning and emotional behavior. The calcium channels activate at different voltages, namely $Ca_V1.3$ at more negative voltages (9-15 mV), and the proportion of $Ca_V1.2$ in the brain was detected nine times higher.[314, 315, 323]

Calcium channel blockers like isradipine (Figure 13) and amlodipine are widely applied in the treatment of cardiac diseases and as antihypertensives.[315] The tolerability of these drugs is proved during many years of application therefore repurposing of calcium channel blockers was extensively studied in recent years.[324] Isradipine (Figure 13) was investigated in clinical trials for PD, adjunctive for bipolar depression, cognitive improvement in schizophrenia and schizoaffective disorder, but efficacy was not persuasive [325-328] or the trial was terminated due to insufficient recruitment and study delay[329]. The disease modifying effect was evaluated in the clinical trial for PD, and it was considered that the dose (10 mg/day) may be insufficient to achieve neuroprotective effects and questioned whether the timing of administration post diagnosis was too late.[330] The influences of dihydropyridines (DHP) on brain functions in humans at therapeutic doses were found to be low, however, alterations of metaplasticity have been demonstrated.[315, 331] It has to be noted that interpretation of experimental results is complex, for example differentiation between current components of different calcium channels (e.g. Ca_V1 and Ca_V2) in native tissue or *in vivo* experiments is challenging due to the contribution of several calcium channels to total Ca^{2+} current and complexity increases even more due to the possible association of α_1 subunit with all β subunits, alternative splicing and interaction with various modulatory proteins.[314, 315] Moreover, a major issue in several *in vivo* experiments concerned the use of supratherapeutic doses leading to cardiovascular effects.[315] Multiple Ca^{2+} channelopathies of these LTCC subtypes are discovered, and these genetic variations are associated with multiple human diseases.[314] Symptoms of the rare genetic disease Timothy syndrome are ASD like behavior, such as repetitive and social behavior, and ADHD. This syndrome is caused by a mutation of the pore-forming α_1 subunit of $Ca_V1.2$ and suggests that enhanced $Ca_V1.2$ may also contribute to other neuropsychological disorders like ASD.[321, 332] Single nucleotide polymorphism of $Ca_V1.2$ is associated with ASD, schizophrenia, and major depressive disorder in genome-wide association studies.[333] Furthermore, $Ca_V1.3$ dysfunction is associated with a neurodevelopmental disorder showing symptoms such as hyperactivity, autistic behavior, and intellectual disability.[322]

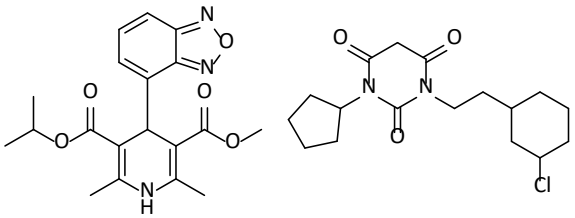


Figure 13: The structures of exemplary LTCC modulators.

Both Ca^{2+} channels modulate pain sensitization in dorsal spinal neurons, suggesting their involvement and potential therapeutic benefit in neuropathic pain. For example, it is assumed that $Ca_V1.3$ inhibition might be beneficial for spasticity treatment in spinal cord injury patients.[322]

Increased intracellular Ca^{2+} levels are correlated with mitochondrial dysfunction, oxidative stress, or even cellular death and are associated with neurodegenerative disorders, including AD and PD.[178] LTCCs have been reported to play a part in dopaminergic neuron vulnerability in SN by contributing to oxidative stress and thereby may be involved in PD progression.[321] Even though both Ca^{2+} channels are expressed in SN dopaminergic neurons, it is believed that especially $Ca_V1.3$ selective blockers allow therapeutic targeting of these neurons. Dose-limiting side effects of DHPs could be avoided, which are caused by $Ca_V1.2$ inhibition in blood vessels.[321, 322] The pyrimidine-2,4,6-trione cp-PYT (Figure 13) was first described as a selective $Ca_V1.3$ modulator with low potency, but following evaluation in another lab showed inconclusive results.[334-336] Dopamine receptors modulate $Ca_V1.3$ on medium spiny neurons, namely, D_1R amplifies and D_2R diminishes channel opening. Loss of dopaminergic neurons in the SN pars compacta in PD consecutively results in degeneration of dendritic spines on striatal medium spiny neurons. Dysregulated Ca^{2+} influx via $Ca_V1.3$ is involved in the degeneration, and this is presumably triggered by lower modulation of $Ca_V1.3$ by dopaminergic receptors.[337] Interestingly, downregulation and genetic silencing of $Ca_V1.3$ in the striatum decreased dyskinesia in rats.[338, 339]

Recently, the first MTDLs with the combination of H_3R pharmacophore and calcium channel inhibition were reported by Malek et al. as a potential treatment for AD.[340, 341] In their studies, MTDLs were designed to exhibit calcium channel inhibition, H_3R antagonism, and ChE inhibition. Both lead compounds, 3p and 3e (Figure 14), restored cognitive impairment *in vivo,* despite their differing properties at the desired targets. While the DHP 3p (Figure 14) showed a more balanced but less potent activity profile (H_3R K_i = 565 nM, BuChE IC_{50} = 7.83 µM, Ca^{2+} channel blockade IC_{50} = 21 µM), the dihydropyrimidine 3e (Figure 14) is more potent at H_3R and AChE inhibition but weaker calcium channel inhibition.[340, 341] These studies indicate that these target combinations

may be beneficial in neurodegenerative disease. However, activity on specific Ca^{2+} channels was not explored, and further studies are necessary to achieve balanced activity on all targets.

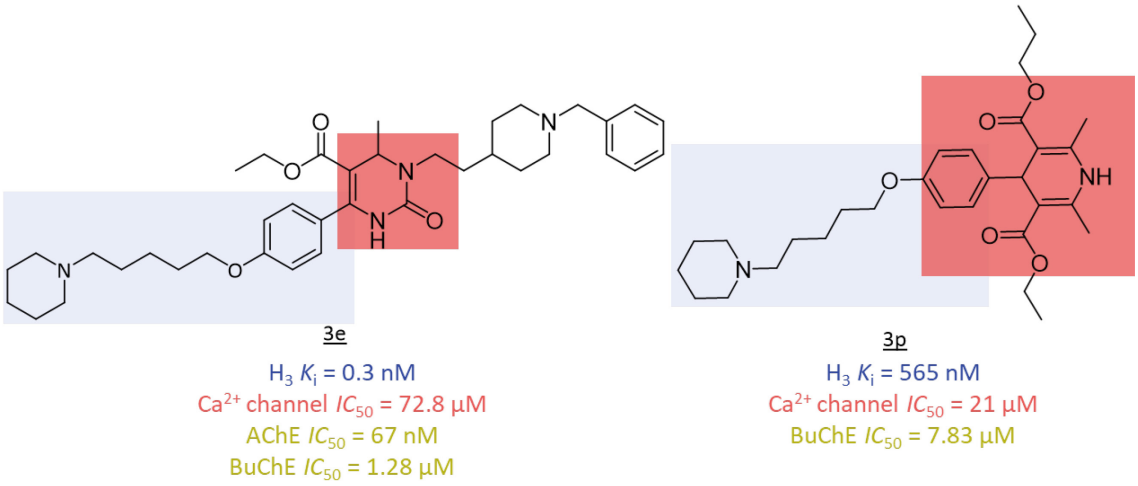


Figure 14: MTDL with H_3R (blue) and calcium channel (red) pharmacophore and their respective activity at the targets.[340, 341]

Sigma receptors

Sigma receptors (σ_1 and σ_2 receptors) are structurally and genetically unrelated endoplasmic reticulum membrane proteins that are located in lipid raft-containing cholesterol and sphingolipids of the plasma membrane.[342, 343] Despite the structural and genetic differences, the binding pockets of the two proteins are remarkably similar, and they modulate closely related cellular activities. Both targets are involved in neurological and neurodevelopmental disorders, namely AD, PD, pain, depression, and Huntington's disease.[343] σ_1R Consists of four transmembrane helices and is primarily expressed in the CNS, breast, colon, stomach, esophagus, and lung. In addition, σ_1R is highly expressed in cancer cells. σ_1R is an endoplasmic reticulum-associated molecular chaperone protein that can translocate to the plasma membrane, interact, and modulate the activity of other proteins such as IP_3R, ion channels, and small molecule G-protein (Rac1). Regulation and modulation of voltage-regulated and ligand-gated ion channels (Ca^{2+}, K^+, Na^+, Cl^-, and SK channels, NMDA and IP_3 receptors) by σ_1R inhibits voltage-gated ion channels and potentiates ligand-gated channels.[344]

σ_1R Agonists have neuroprotective, mood-modifying, analgesic, or cognitive effects. Activation of σ_1R has been suggested to be involved in the development of neuropathic pain and upregulation of spinal cord σ_1R during the induction phase of neuropathic pain. KO mice failed to develop mechanical allodynia, implicating σ_1R antagonist as a potential analgesic strategy.[342] Clinical studies in healthy and neuropathic pain patients of the selective σ_1R antagonist E-52862 alleviated diabetic neuropathy and chronic pain with a good safety profile.[345, 346] The neuroprotective effect of σ_1 receptor ligands is linked to regulation of intracellular calcium homeostasis. In PET experiments, downregulation of σ_1R was observed in early-stage PD patients.[347] PRE-084 stimulates σ_1R and demonstrates an improvement of spontaneous forelimb use in 6-OHDA-lesioned mice. Furthermore, increased density of dopaminergic fibers, modest recovery of dopamine levels, and upregulation of neurotrophic factors (brain-derived neurotrophic factor and glial cell line derived neurotrophic factor) indicate involvement of σ_1R in PD.[348]

σ_1R is highly expressed in the CNS and research has primarily focused on pain and neurotransmission.[343] Some σ_1R variants (G-241T/C-240T (rs.1799729) and A61C (rs.1800866)) may be involved in AD development.[349] In early stages of AD, σ_1R decreases in the brain [350, 351] possibly associated with higher vulnerability of neuronal cells to amyloid β-mediated toxicity and cell death.[352] σ_1R controls τ-phosphorylation by encouraging p35 turnover, as supported by KO and overexpression experiments[353], and KO in hippocampal neurons leads to decreased dendritic spine formation.[354-356] Blacarmesine, an σ_1R activator, demonstrated promising results in an early AD

phase IIb/III clinical trial.[357] CT1812 is a σ_2R antagonist in phase 2 clinical trials for AD with positive outcomes and clear benefits. The compound could also be a potential cure-modifying therapy, not only for symptomatic relief.[358] In addition to the influence of σ_1R on pain, the σ_2R has recently emerged as a target for the treatment of pain. Several ligands demonstrated antinociceptive properties in neuropathic pain models, but the understanding of the mechanism of action is limited to date.[346]

For several H_3R inverse agonists (JNJ-5207852, PF-3654746 (Figure 5), GSK189254 (Figure 7), ABT-239, Pitolisant (Figure 3), S 38093-2), σ_1R affinity was shown recently, suggesting σ_1 modulation should be considered interpreting the effects of these compounds.[359] Furthermore, for the already described contilisant, later σ_1R agonism was demonstrated with the implication to restore cognitive impairment induced by LPS *in vivo*.[309] The piperazine derivative KSK94 (Figure 15) with high affinity for H_3R and preference for σ_2R over σ_1R was studied *in vivo* in an obesity model, reducing the development of obesity in rats.[360, 361] The activity in neuropathic pain models was only evaluated for the piperidine-based dual H_3R and σ_1R antagonists, e.g., KSK68 (Figure 15). These dual target ligands demonstrated promising antinociceptive activity in several *in vivo* pain models.[360]

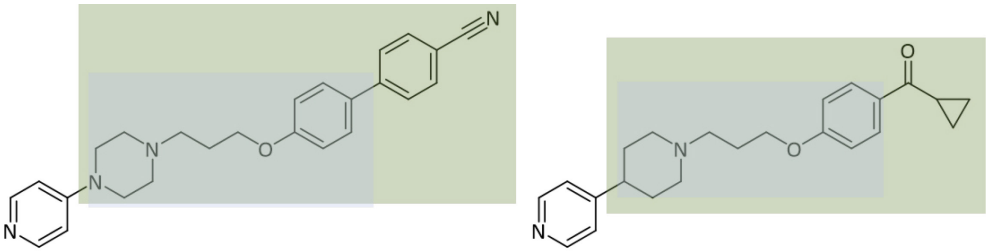


Figure 15: MTDL with H_3R (blue) and sigma receptor (green) pharmacophore and their respective activity at the targets.[360]
Abbreviation: n.d.

2 Scope and Objectives

This dissertation aims to develop, evaluate biologically, and optimize novel multi-target directed ligands, with special emphasis on the histamine H_3 receptor. Almost a decade after the approval of Pitolisant, it remains the only approved drug targeting H_3R in the treatment of the orphan disease narcolepsy and obstructive sleep apnea. Multi-target directed ligands offer the possibility, through synergistic effects, to pave the way for further therapeutic areas of H_3R antagonists/inverse agonists in neurological and neurodegenerative diseases.

Structure-based drug design requires detailed knowledge of structure-activity relationships and pharmacokinetic properties. Therefore, the first part of this work aims to design, identify, and evaluate novel scaffolds targeting histamine and dopamine receptors utilizing scaffold hopping, isosteric replacement, and linker variation. The design strategies are complemented by *in vitro* studies, pharmacokinetic property calculations, and molecular docking, which provide early drug-target evaluation and safety profiling to guide future applications and lead generation.

The second part of this thesis aims to explore novel multi-targeted ligands with a key focus on the histamine H_3 receptor, in combination with complementary CNS targets involved in neurological and neurodegenerative diseases. Three sets of target combinations will include GPCRs (D_3R), σ receptors, enzymes (AChE/BuChE), and ion channels ($Ca_V1.2$ and $Ca_V1.3$) to explore and compare various co-targets. The first set of ligands will be piperazine-based, while the second and third sets are piperidine-based dual-targeting ligands. The focus lies on early pharmacological evaluation for the identification and mutual influences of key structural aspects of these multi-target ligands. Extensive pharmacological and pharmacokinetic screening of the sigma receptor-MTDLs will be conducted to achieve an in-depth analysis of these ligands. The study of the barely investigated combination with calcium channels will focus on the pharmacological characterization of these dual target ligands on specific Ca^{2+} channels

3 Publications

3.1 Guided rational design with scaffold hopping leading to novel histamine H_3 receptor ligands

Nakisa Ghamari[1,2], Saeed Kouhi Hargelan[2], Aleksandra Zivkovic[3], Luisa Leitzbach[3], Siavoush Dastmalchi[1,2], Holger Stark[3*], Maryam Hamzeh-Mivehroud[1,2*]

[1] Biotechnology Research Center, Tabriz University of Medical Sciences, Tabriz, Iran, [2] School of Pharmacy, Tabriz University of Medical Sciences, Tabriz, Iran, [3] Heinrich Heine University Düsseldorf, Institute of Pharmaceutical and Medicinal Chemistry, Universitätsstr. 1, D 40225 Düsseldorf, Germany

Published in: Bioorganic Chemistry, 2021, 105411, Vol. 117,
https://doi.org/10.1016/j.bioorg.2021.105411

Impact Factor: 4.7 (2024)

Contribution: L.L. designed and conducted the *in vitro* experiments, explored and interpreted the *in vitro* data and reviewed the manuscript.

Bioorganic Chemistry 117 (2021) 105411

Contents lists available at ScienceDirect

Bioorganic Chemistry

journal homepage: www.elsevier.com/locate/bioorg

Guided rational design with scaffold hopping leading to novel histamine H_3 receptor ligands

Nakisa Ghamari [a,b], Saeed Kouhi Hargelan [b], Aleksandra Zivkovic [c], Luisa Leitzbach [c], Siavoush Dastmalchi [a,b], Holger Stark [c,*], Maryam Hamzeh-Mivehroud [a,b,*]

[a] Biotechnology Research Center, Tabriz University of Medical Sciences, Tabriz, Iran
[b] School of Pharmacy, Tabriz University of Medical Sciences, Tabriz, Iran
[c] Heinrich Heine University Düsseldorf, Institute of Pharmaceutical and Medicinal Chemistry, Universitaetsstr. 1, D-40225 Duesseldorf, Germany

ARTICLE INFO

Keywords:
Histamine H_3 receptor
Scaffold hopping
Molecular docking
Molecular dynamics simulation
H_3R antagonist
Synthesis

ABSTRACT

During the past decades, histamine H_3 receptors have received widespread attention in pharmaceutical research due to their involvement in pathophysiology of several diseases such as neurodegenerative disorders. In this context, blocking of these receptors is of paramount importance in progression of such diseases. In the current investigation, novel histamine H_3 receptor ligands were designed by exploiting scaffold-hopping drug-design strategy. We inspected the designed molecules in terms of ADME properties, drug-likeness, as well as toxicity profiles. Additionally molecular docking and dynamics simulation studies were performed to predict binding mode and binding free energy calculations, respectively. Among the designed structures, we selected compound **d2** and its demethylated derivative as examples for synthesis and affinity measurement. *In vitro* binding assays of the synthesized molecules demonstrated that **d2** has lower binding affinity (K_i = 2.61 μM) in radioligand displacement assay to hH_3R than that of demethylated form (K_i = 12.53 μM). The newly designed compounds avoid of any toxicity predictors resulted from extended in silico and experimental studies, can offer another scaffold for histamine H_3R antagonists for further structure–activity relationship studies.

1. Introduction

Histamine as biogenic multifunctional amine is involved in wide variety of physiological processes via four distinct subtypes of G-protein coupled histamine receptors (H_1, H_2, H_3, and H_4). Since the identification of H_3 receptors over the nearly four decades, versatile potential of this receptor in physiological processes have been elucidated [1]. This receptor is located pre-synaptically as auto- and heteroreceptor in central nervous system (CNS) responsible for modulating the release of histamine and other neurotransmitters such as acetylcholine, γ-aminobutyric acid (GABA), dopamine, serotonin, and noradrenaline via a negative feedback mechanism [2]. For the past decades of research, the importance of H_3R in neurological disorders has been well explored and hence it can be considered as a therapeutic potential target in such diseases. Attention deficit hyperactivity disorder (ADHD), Alzheimer's disease, schizophrenia, learning and memory disorders, Parkinson's disease and sleep disorders, and epilepsy are examples of neuronal abnormalities and impairments that can be treated by H_3R antagonists and inverse agonists [3]. Based on ever growing number of H_3R related candidate molecules in different phases of clinical trials [4], it is anticipated that these types of agents might become drugs of future in neurodegenerative diseases beneficial especially for elderly population.

Launching a therapeutic agent from idea to market necessitates considerable amounts of time and cost in a process known as drug design and discovery. Shortening this process is a high priority for scientists working in this field. Undoubtedly, integration of computational approaches and experimental methods synergistically fulfill this task in a timely and cost effective manner. The main objectives followed in computer-aided drug design (CADD) are: *i)* filtering the large libraries against target of interest in a procedure called "virtual screening" to reach the bioactive lead compounds, *ii)* lead optimization step in order to achieve favorable compounds in terms of developmental potential [5].

The key elements in the context of lead optimization are scaffold hopping and bioisosteric replacement aiming to improve potency, drug-like properties and safety profiles of the lead compounds. Scaffold

* Corresponding authors at: Biotechnology Research Center, Tabriz University of Medical Sciences, Tabriz, Iran (M. Hamzeh-Mivehroud) and Heinrich Heine University Düsseldorf, Institute of Pharmaceutical and Medicinal Chemistry, Duesseldorf, Germany (H. Stark).
E-mail addresses: stark@hhu.de (H. Stark), hamzehm@tbzmed.ac.ir (M. Hamzeh-Mivehroud).

https://doi.org/10.1016/j.bioorg.2021.105411
Received 9 September 2021; Received in revised form 3 October 2021; Accepted 4 October 2021
Available online 8 October 2021
0045-2068/© 2021 Elsevier Inc. All rights reserved.

hopping (or lead hopping) is defined as structural decoration of a given molecule by replacing the available scaffolds for introducing new chemotypes with improved properties. Indeed, the main emphasis of scaffold hopping has been put on altering the properties of the molecule by moving it into novel chemical space while retaining the biological activity. This approach is routinely employed for a number of reasons such as prohibited structural motifs responsible for toxicity, unwanted side effects, metabolic liabilities, and undesirable physicochemical properties. Evidently, chemical synthesizability of the designed compounds should be taken into account in rational drug design. The most principal approaches in scaffold hopping are shape matching, pharmacophore searching, fragment replacement and similarity search [6–8].

The only marketed histamine H_3R antagonist/inverse agonist is pitolisant (Wakix®) approved by the European Medicines Agency available in the European Union for treatment of narcolepsy with or without cataplexy [9,10]. However, there is ongoing interest in identification of novel histamine H_3R antagonists/inverse agonists for treatment of neurological impairments and still some of them are in clinical trials for a range of indications [11–21]. Previously, we have identified two compounds capable of binding to H_3R in the submicromolar K_i range using radioligand displacement studies [22]. The introduced lead compounds were also functional in terms of antagonist activity [23]. The aim of the present study was structural optimization of these computationally identified lead compounds in order to improve physicochemical properties useful in neurological disorders.

2. Results

2.1. Scaffold-hopping analysis

In the current study, scaffold-hopping analysis was used on previously identified H_3R antagonists (Fig. 1) aiming to improve biological activity and eliminate potential toxicophores. The procedure was started with exhaustive fragmentation of these molecules along the single non-ring bonds followed by selection of each portion serving as a query for database search using bioisosteric replacement tool implemented in Spark program. To this end, the resulting fragments were subjected to iterative seeking procedure for finding similar bioisosters and fragments to that of original entity in terms of shape and electronic properties in the region of interest. Based on the calculated field point patterns, the fragments were derived from ChEMBL and Zinc database available in Spark program. Upon the generation of virtual library, a diverse array of ligands with novel chemotypes were sorted out based on a scaled score called bioisostere factor (BIF%). The greater positive value of BIF score is indicative of favorable bioisostere with higher similarity to the starter molecule from geometrical viewpoint. Likewise, the negative BIF value reflects that the fragment is not appropriate for the replaced moiety. Finally, top-scoring entities were carefully inspected according to the features associated with field and shape scores, radial plots, and unstable/reactive functionality.

2.2. ADME, Drug-Likeness and toxicity property analysis

The retrieved compounds from scaffold-hopping analysis were filtered on the basis of pharmacokinetic and drug-likeness parameters calculated by SwissADME online webserver. Fig. 2 and Supplementary Table S1 represent the structure of top-ranked candidates with desirable physicochemical parameters, pharmacokinetics, drug-likeness, and medicinal chemistry friendliness. The selected compounds were predicted to be of orally bioavailable inferred from their optimal physicochemical properties fall within desired range. Furthermore, it was predicted that the compounds were expected to have the ability for gastrointestinal absorption and blood–brain barrier (BBB) permeability. Moreover, all the selected candidates encompassed the different drug-likeness properties proposed by Lipinski [24], Ghose [25], Egan [26], Muegge [27], and Veber [28]. Additionally, the molecules were free from potentially problematic fragments reported in promiscuous compounds using pan-assay interference compounds (PAINS) [29] and Brenk [30] filters. The tendency of the selected compounds for being substrate of P-glycoprotein (P-gp) and cytochrome P450 enzymes were also investigated and shown in Supplementary Table S1. The other critical factor considered in the filtering process was synthetic

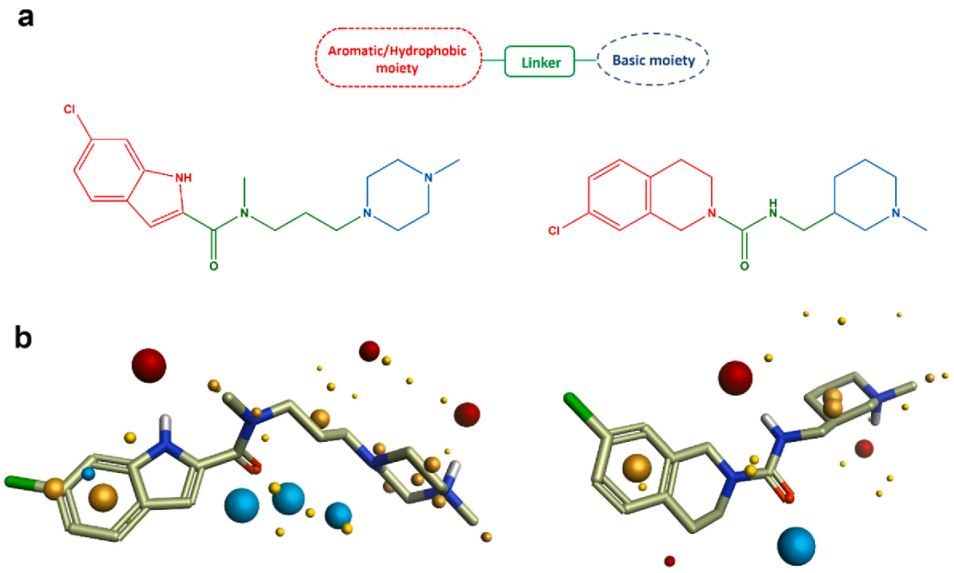


Fig. 1. **(a)** Schematic representation of the pharmacophore model proposed for H_3R antagonists along with structure of previously identified compounds as starter molecules for scaffold hopping analysis **(b)** Calculated field point patterns represented for the query molecules. Negatively charged field points are shown in blue; positively charged field points are red; van der Waals/shape field points are displayed in yellow; centers of hydrophobicity are shown in orange. (For interpretation of the references to colour in this figure legend, the reader is referred to the web version of this article.)

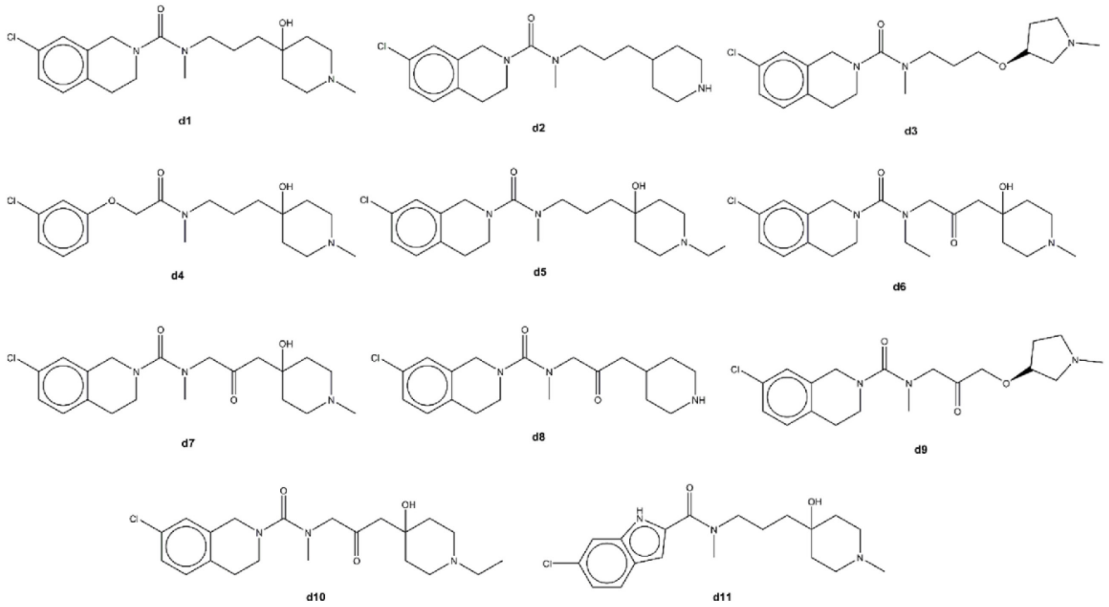


Fig. 2. Chemical structures of designed compounds as H_3R antagonists.

tractability of the designed molecules. The analysis demonstrated that the chemical synthesis of all the proposed molecules is feasible deduced from low synthetic accessibility score shown in Supplementary Table S1. The candidate molecules were also investigated according to their possible binding affinity towards H_3R using SwissTargetPrediction webserver and those compounds with highest probability of affinity to H_3R were progressed to the next steps of analyses. To gain insight into CNS drug likeness of the candidates, MPO analysis was performed across a range of physicochemical property space determining CNS permeability. The result of MPO analysis for the selected compounds presented in Supplementary Table S2 showed that all molecules passed the threshold of MPO score considered for marketed CNS drugs (MPO desirability score ≥ 4 in a scale of 0–6). For toxicological profile analysis of the selected compounds, OpenVirtualToxLab platform was used. Based on predicted TP values for the selected compounds shown in Supplementary Table S3, most of them are categorized in class 0 in the scale of toxicity alert suggesting the possible safety of the candidate molecules.

2.3. *Molecular docking and calculation of binding free energy for ligand-receptor complex*

Following applying different filtering criteria on the designed compounds, molecular docking calculations were used to determine the binding mode of the selected candidate molecules towards H_3R using GOLD program. Fig. 3 provides 2D and 3D illustrations for **d2** compound

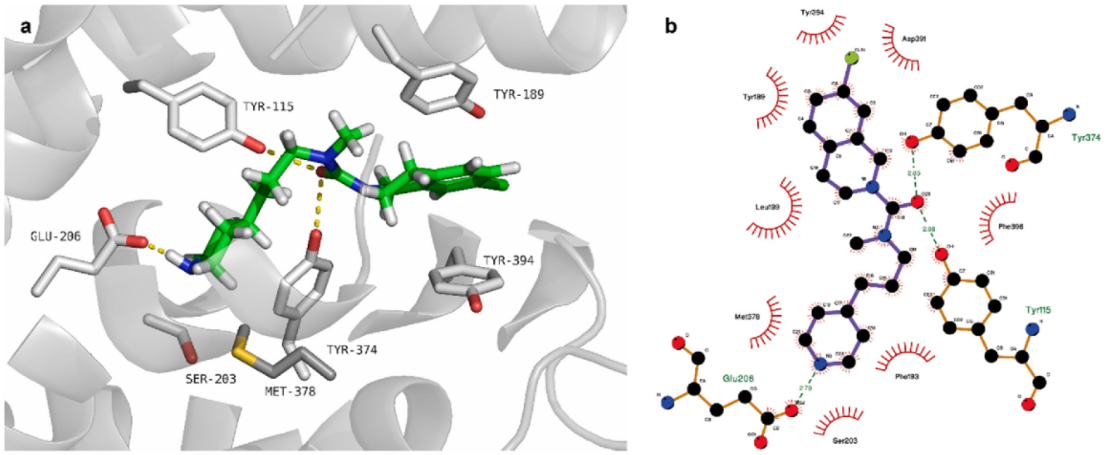


Fig. 3. **(a)** 3D representation of compound **d2** docked into the binding site of H_3R generated by PyMol program (version 1.7.x). The ligands and the main interacting residues are displayed as sticks. Only the side chains of the interacting residues from receptor are shown for further clarity. **(b)** 2D illustration of the interactions between compound **d2** and H_3R generated by LigPlot program.

as representative of all compounds docked into the binding site of H_3R. Analysis the docking results showed that the most important amino acids interact with H_3R are: Tyr^{115}, Tyr^{189}, Glu^{206}, Tyr^{374}, Met^{378}, Tyr^{394}. The predominant interactions observed for the selected molecules are: π-π stacking, ionic, and hydrogen bond interactions. The phenyl ring in hydrophobic/aromatic moiety of the compounds is engaged in π-π stacking with Tyr^{189} and Tyr^{394}. The ionic interaction is established between Glu^{206} and nitrogen of basic moiety. Tyr^{115} and Tyr^{374} make H-bonds with the linker (cf. Supplementary Fig. S4).

The best docked solution in complex with H_3R was subjected to a 50 ns molecular dynamics studies using AMBER package. Prior to proceed to binding free energy calculations, the stability of each system was evaluated based on conformational and energy analyses. Analysis of MD trajectory throughout the production period revealed that all the systems were adequately equilibrated and stable judged from calculated potential energy and root mean square deviation (RMSD) for each system (Supplementary Fig. S5). During the simulation period, the snapshots were extracted every 100 ps from the MD trajectory to be used for calculation of binding free energies using MM-PBSA/GBSA methodologies. The results of free energy values (ΔG) for ligand-receptor complexes can be found as Supplementary Table S6 online.

2.4. Chemistry

The synthesis has been performed by straight forward procedure from the *boc*-protected amine **1**, which alcohol functionality was transformed into amine **3** via Mitsonobu reaction and hydrazinolysis. The amine was transformed into isocyanate **4** by reaction with triphosgene, and then this isocyanate was taken for a convenient coupling to the 7-chlorinated 1,2,3,4-tetrahydroisochinoline derivative. Deprotection, or methylation and then deprotection led to the proposed lead structures **7** and **9** (**d2**), respectively (Fig. 4).

3. Human histamine H_3 receptor *in-vitro* assay

The result of human H_3R *in-vitro* assay using [^{3}H]-N^{α}-methylhistamine revealed affinity of the selected compound **d2** to hH_3R in low micromolar range. The demethylated **d2** showed lower affinity to hH_3R. Displacement curves of normalized data and determined K_i-values of **d2**, demethylated **d2** and pitolisant (as reference) are shown in Fig. 5. In comparison to pitolisant affinity estimates of **d2** are about 2 log units lower.

4. Materials and methods

4.1. Molecular field-based scaffold hopping

Computationally guided fragment and bioisosteric replacement tool implemented in Spark program (version 10.5.6; Cresset®, Cambridgeshire, UK) [32,33] was employed for performing scaffold hopping analysis on two previously identified potential lead compounds [22]. To accomplish this purpose, the starting compounds were fragmented in different portions followed by iterative experiments for finding similar fragments in terms of shape, pharmacophoric features, hydrophobicity, and electronic properties in region of interest. Following the creation of

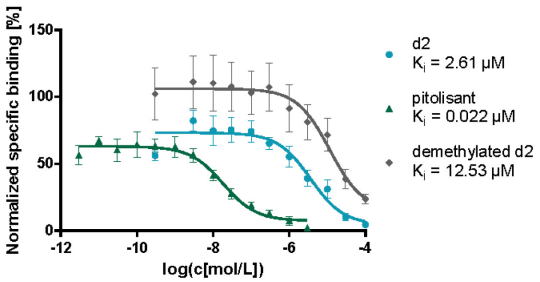


Fig. 5. Displacement of [^{3}H]-N^{α}-methylhistamine (**c** 2 nM, K_d 3.08 nM) by **d2** (K_i 2.61 [1.19–5.72] μM), demethylated **d2** (**7**) (K_i 12.53 [4.79–32.76] μM) and pitolisant (K_i 0.022 [0.002–0.250] μM). The assay were performed on HEK-293 cell membranes expressing the hH_3R. Data are expressed as mean values ± SEM (three independent experiments, each performed in duplicates).

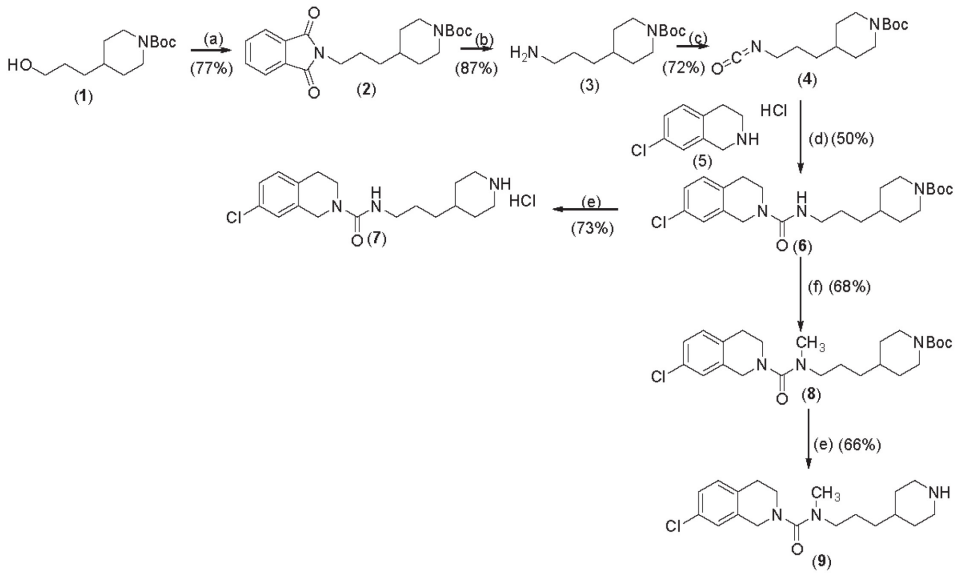


Fig. 4. Synthesis of compounds. Reagents and Conditions: (a) phthalimide, DEAD, PPh_3, THF; (b) hydrazine, EtOH; (c) triphosgene, sat. $NaHCO_3$, DCM; (d) DIPEA, DCM; (e) HCl sat. in dioxane; (f) NaH, MeI, THF;

the virtual library, the newly designed molecules were scored based on similarity of calculated fields to that of original compound.

4.2. In silico ADME and drug-likeness properties and toxicity assessment

The resulting compounds were comprehensively scrutinized according to the drug-likeness, ADME, and toxicity profiles. SwissADME web server (http://www.swissadme.ch) was used to compute physicochemical properties and predict pharmacokinetic and drug-likeness, and medicinal chemistry parameters [34]. Compounds fulfilled all the drug-likeness filtering criteria with desired ADME properties were selected for further evaluations. In addition, for predicting the potential target for the designed compounds in a chemical-pharmacological space, SwissTargetPrediction web server was employed [35]. In order to predict blood–brain barrier (BBB) permeability for the selected compounds, a drug-likeness central nervous system multiparameter optimization (CNS MPO) algorithm [31] proposed by Pfizer was applied. The CNS MPO score is calculated using the physiochemical parameters important for CNS drugs including: molecular weight (MW); lipophilicity as calculated partition coefficient (Clog P); calculated distribution coefficient at pH 7.4 (Clog D); ionization constant of the most basic center (pK_a) (ACD/Labs, version 6.00); topological polar surface area (TPSA) and number of hydrogen bond donors (HBDs). For calculation of ClogP, Bio-Loom program (version 5, Biobyte®) and for computing Clog D and pK_a, ACD/Labs software (version 6.00) were utilized. For toxicity assessment, off-target binding affinity profile of the candidate molecules were evaluated using OpenVirtualToxLab platform (version 5.8) [36,37]. In this platform, a thermodynamic-dependent parameter known as toxic potential (TP) is determined based on the flexible docking of a given query to 16 validated off-target proteins using 4D Boltzmann scoring criterion calculated for ligand-receptor complexes. The target proteins consist of nuclear receptors (androgen receptor (AR), estrogen receptor α (ERα), ERβ, glucocorticoid receptor (GR), mineralocorticoid receptor (MR), progesterone receptor (PR), liver X receptor (LXR), peroxisome proliferator-activated receptor γ (PPARγ), thyroid receptor α (TRα), and TRβ, cytochrome P450 enzyme family (1A2, 2C9, 2D6, 3A4), cytosolic transcription factor (aryl hydrocarbon receptor (AhR)) and potassium ion channel (hERG).

4.3. Molecular docking and binding free energy calculation studies

Following inspection of the designed compounds in terms of drug-likeness, ADME, CNS penetrability properties, and toxicity assessment, the candidate molecules were subjected to molecular docking experiment according to the procedure described previously [22]. Briefly, molecular docking of the retrieved compounds into the previously modeled structure of the H_3R [22] was conducted on a LINUX operating environment using GOLD program (version 5.0; CCDC Inc., Cambridge, UK) [38,39]. For defining the binding site, a geometric center was assigned based on the important amino acids involved in the binding pocket and all atoms in a 10 Å radius around the geometric center was set as the binding site of molecular docking. Moreover, two sets of distance constraints (1.5–3.5 Å) consisting of Tyr^{189} and Glu^{206} residues in H_3R model were applied in order to simulate the π-π stacking and ionic interactions observed for pitolisant structure [22]. For π-π stacking, phenyl groups of Tyr^{189} and designed compounds are considered whereas in the case of ionic interaction, electrostatic interaction between oppositely charged oxygen atom from Glu^{206} and nitrogen atom of piperidine/pyrrolidine ring from the designed molecules were imposed. During the semi-flexible protein–ligand docking calculations, the residues side chains engaged in the calculations were permitted to be flexible whereas the backbone atoms were considered rigid. Finally, the best docking pose among the solutions was selected on the basis of GoldScore fitness function and processed for molecular dynamics (MD) simulation analysis.

All the MD calculations were executed by Assisted Model Building with Energy Refinement (AMBER) package (version 14) [40,41] operating on a Linux-based (CentOS-6.8) GPU workstation consisting of four NvidiaK40M (each has 12 GB RAM and 2880 cuda cores), 2X Intel Xeon E5–2697 v2, 2.7 GHz (total of 48 cores), total RAM = 128 GB. The coordinate files for all ligands, protein, as well as ligand–protein complexes were generated by antechamber and LEaP module of AMBER. The FF14SB and GAFF force fields were applied for parameterization of protein and ligand, respectively. Then, the appropriate number of counter ions was added to electrostatically neutralize the total charge of the system. The neutralized complex was solvated using a rectangular box of explicit TIP3P water with buffering distance of 12 Å from the periphery of complex. Prior to MD simulation, different steps of minimization, heating, and equilibration were performed using Sander module of AMBER. Initially, energy minimization of solvated system was performed using 500 steps of steepest descent method followed by 500 steps of conjugate gradient algorithm. Afterwards, the system was gradually heated up from 0 to 300 K for 50 ps with subsequent 50 ps density equilibration at 300 K. The final equilibration of the system was conducted under constant pressure at 300 K for 500 ps using a 2 fs time step.

By applying SHAKE algorithm, all bonds involving hydrogen atoms were constrained. The SHAKE algorithm was employed to constrain all the bond lengths involving hydrogen atoms. Furthermore, a final 50 ns MD production was carried out by applying Particle Mesh Ewald (PME) method to treat long-range electrostatics interactions using GPU version of the PMEMD program. Periodic boundary conditions were used for all MD calculations without utilizing any constraint to either the ligand or the protein molecules. The simulation trajectory was obtained by capturing the coordinates every 10 ps during 50 ns of production period. Following the MD simulation, postprocessing of the trajectory was conducted using CPPTRAJ module implemented in AMBER. Moreover, the trajectory was also analyzed for calculation of binding free energy using Molecular Mechanics Poisson-Boltzmann Surface Area (MM-PBSA)/Generalized-Born Surface Area (GBSA) available in AMBER package [40,42]. Binding free energy for ligand–protein complexes was determined by summing up molecular mechanics energies, solvation-free energies, and entropic terms followed by averaging over the extracted equilibrated snapshots derived from MD simulation trajectory and presented as the average value. During the calculation of interaction energy, water molecules and counter ions were excluded. The interior and exterior dielectric constant was set to 1.0 and 80 for solute and the surrounding solvent, respectively.

Binding free energy ($\Delta G_{binding}$) is calculated according to the following equation:

$$\Delta G_{binding} = G_{water(complex)} - [G_{water(protein)} + G_{water(ligand)}] \quad (1)$$

where the terms denoted by $G_{water(complex)}$, $G_{water(protein)}$ and $G_{water(ligand)}$ refer to free energies of complex, protein, and ligand, respectively. Free energy for each species is obtained based on the following equations:

$$G = E_{gas} + G_{solvation} - TS \quad (2)$$

$$E_{gas} = E_{int} + E_{vdw} + E_{elec} \quad (3)$$

$$E_{int} = E_{bond} + E_{angle} + E_{torsion} \quad (4)$$

$$G_{solvation} = G_{polar} + G_{non-polar} \quad (5)$$

In the above equations, G demonstrates the calculated average free energy, E_{gas} shows the standard force-field energy, $G_{solvation}$ indicates solvation free energy and TS is vibrational entropy term. E_{gas} consists of internal strain energy (E_{int}) in the gas phase, non-covalent van der Waals (E_{vdw}) and electrostatic (E_{elec}) energies. The E_{int} consists of strain energies caused by deviation of the bonds (E_{bond}), angle (E_{angle}), and torsion angles (E_{tors}) from their equilibrium values. G_{polar} and $G_{non\text{-}polar}$ represent the polar and non-polar contributions to the solvation free

energy. The polar contribution is obtained from Poisson-Boltzmann or Generalized Born model whereas the non-polar contributions are determined by the calculation of solvent accessible surface area (SASA) based on the linear combinations of pairwise overlaps (LCPO) method [43]. In this work, the entropy contribution of the solute was ignored by considering similar solute entropy contribution on binding free energy for all the complexes.

4.4. Synthesis procedure

All starting materials have been obtained from Acros Organics (Geel, Belgium), Apollo Scientific (Cheshire,UK), Sigma Aldrich (part of Merck KGa Group, Darmdstadt, Germany), VWR (Darmstadt, Germany), and were used without further purification. Sorbent: Kieselgel 60 (0.04–0.063 mm) for column chromatography (Macherey-Nagel, Düren, Deutschland, Acros Organics, Geel, Belgien). Flash chromatography: Biotage Isolera™ Spektra Systems with *ACI*™ and Assist (Biotage, Uppsala, Sweden Stationary phase: Sfaer Silica D (Biotage, Uppsala, Sweden). Column capacity: 10 g, 25 g, 50 g, 100 g. Mass spectra have been determined using Advion Mass Express (Advion, Ithaca, USA). The expression CMS uses Edwards RV12 rotary vane pump and The CETAC ASX-7000 auto-sampler platform. Atmospheric-pressure chemical ionization (APCI) (constant current 0 – 15 μA) and electrospray ionization (ESI) (constant voltage 0 – 5 kV) were used as a method of ionization, operating in both positive and negative mode. Data have been shown as $[M + H^+]^+$. And $[M-H^+]^-$ Footprint - Width: 27 cm (10.6 in); Depth: 54.9 cm (21.6 in) rate range: Expression CMS :10 μL/min to 0.5 mL/min (ESI), 10 μL/min to 1.0 mL/min (APCI), nebulization gas: 0.5 L/mi, heated desolvation/APCI gas: 1 to 10 L/min. Mass calibration stability of ± 0.1 Da over the defined mass range (10 – 1200 for S systems and 10–2000 for L systems) over 12 h. Linear dynamic range of 5×10^3 The abundance of naturally occurring isotopes is accurately produced from the full-scan mass spectra. The expression CMS system Voltage: 100–240 VA, Frequency: 50–60 Hz CMS Fuse: 6 Amps, Max Power Consumption: 600 VA. NMR Spectroscopy: ^1H and ^{13}C NMR spectra of compounds of interest were measured at Bruker Avance III – 300 (Year 2010) and Bruker Avance III – 600 (Year 2011) Bruker, Germany. As NMR solvents were used $CDCl_3$ and DMSO-d_6 and tetramethylsylane was used as a standard.. Chemical shifts are given as parts per million (ppm) and been reported as: s (singlet), brs (broaden singulet), d (doublet), dd (double of doublets), ddd (double of double of doublets), dt (double of triplets), t (triplet), q(quartet), quint(quintet) or m (multiplet), Coupling constant (*J*) were given in Hertz (Hz).

Compounds purity was determined by liquid chromatography-mass spectrometry (LC-MS) Elute SP (HPG 700) Bruker Daltronics and amaZon speed ion Trap LC/MSn System (ESI-MS), Method: Alternating ion-Polarity :on; Scan Range: *m/z*: 80–1200; Nebulizer: Nitrogen, 15 Psi; Dry Gas: Nitrogen, 8 L/min, 200 °C; Massrange Mode: UltraScan; Column: Intensity Solo 2 C18 (100 mm * 2.1 mm); Temperature: 50 °C; Mobile phase: A. water hypergrade for LC-MS with 0.1 % formic acid (v/v) (Merck); B. Acetonitrile hypergrade for LC-MS (for LC-MS); Method of Analysis: 0–4 min 98 % A, 4–5 min gradient 95% A, 5–9 min 95 % A, 9–16 min gradient 5% A, 16–17 min. gradient to 0% A, reconditioning: 17–18 min. gradient to 98 % A, 18–21 min 98 % A.

Synthetic route started using Mitsunobu reaction of compound (1) and phtalimide . Resulting compound (2) was deprotected to amine with hydrazine under reflux in ethanol [44]. Free amine, after derivatisation to isocyanate (4) [45] reacted with compound (5) in THF to form urea compound (6). Methylation of (6) afforded after deprotection of Boc compound **d2** (**9**). Deprotection of compound (**6**) afforded demethylated compound **d2** (**7**) [46].

4.4.1. *tert*-Butyl 4-(3-(1,3-dioxoisoindolin-2-yl)propyl)piperidine-1-carboxylate (2) [44]

To a solution of *tert*-butyl 4-(3-hydroxypropyl)piperidine-1-carboxylate (1) (1.2 g, 4.9 mmol) and phthalimide (1.2 eq., 880 mg, 6.0 mmol) in THF (20 mL) was added PPh_3 (1.5 eq., 1.9 g, 7.3 mmol) and DEAD (1.5 eq. 1.27 g, 7.3 mmol) at RT. The resulting mixture was stirred at RT overnight and diluted with EtOAc (100 mL) . The organic layer was washed with brine (20 mL × 2) and dried over anhydrous $MgSO_4$. The organic phase was concentrated and the residue was purified by flash chromatography (hexane/EtOAc 3/1) to afford *tert*-butyl 4- (3- (1, 3-dioxoisoindolin-2-yl) propyl) piperidine-1-carboxylate (1.41 g, 77 %) ; APCI *m/z* (-): 372,6 ($[M-H^+]^-$); ^1H NMR: δ [ppm] (300 MHz, DMSO-d_6) δ 8.00–7.70 (m, 4H), 3.90 (d, $J = 13.1$ Hz, 2H), 3.55 (t, $J = 7.1$ Hz, 2H), 2.64 (m, 2H), 1,70–1,50 (m, 4H), 1,37 (s, 9H), 1.25–1.05 (m, 3H), 0.92 (qd, $J = 12.5$ Hz, 4.3 Hz, 2H);

4.4.2. *tert*-Butyl 4- (3-aminopropyl) piperidine-1-carboxylate (3) [44]

To a solution of *tert*-butyl 4- (3- (1, 3-dioxoisoindolin-2-yl) propyl) piperidine-1-carboxylate (2) (1.41 g, 3.8 mmol) in 25 mL EtOH was added 60 % hydrazine hydrate (3 mL) . The mixture was stirred at reflux for 3 h and then the solid was filtered off. The filtrate was concentrated under reduced pressure and the residue was suspended in DCM (50 mL) and filtered. The filtrate was concentrated to give the crude *tert*-butyl 4-(3-aminopropyl) piperidine-1-carboxylate (800 mg, 95) which was used in next step directly. Yield (800 mg, 87 %); APCI *m/z*(+): $[(M + H^+)]^+$ 243.3; ^1H NMR: δ [ppm] (300 MHz, DMSO-d_6) δ 3.90 (d, $J = 13.1$ Hz, 2H), 3.40 (bs, 2H), 2.65 (m, 2H), 2.50 (m, 2H), 1,60(m, 2H), 1,37 (m, 12H), 1.25–1.05 (m, 2H), 0.92 (qd, $J = 12.5$ Hz, 4.3 Hz, 2H);

4.4.3. *tert*-Butyl 4-(3-isocyanatopropyl)piperidine-1-carboxylate (4) [45]

To a vigorously stirred mixture of *tert*-butyl 4- (3-aminopropyl) piperidine-1-carboxylate (3) (400 mg, 1.65 mmol) in DCM (6 mL) and saturated $NaHCO_3$ (6 mL), cooled at 0 °C was added triphosgene (490 mg, 1.65 mmol). After 1 h at 0 °C the mixture was diluted with DCM and the layers were separated. Organic layer was dried over $MgSO_4$ and evaporated to dryness. Yield (320 mg, 72 %); APCI *m/z*(+): $[(M + H^+)]^+$ 269.3; ^1H NMR: δ [ppm] (300 MHz, DMSO-d_6) δ 3.98 (d, $J = 13.0$ Hz, 2H), 2.74 (m, 2H), 1.63 (m, 4H), 1.45 (s, 10*H*), 1.37 – 1.20 (m, 2H), 1.01 (qd, $J = 12.4$, 4.3 Hz, 2H).

4.4.4. *tert*-Butyl 4-(3-(7-chloro-1,2,3,4-tetrahydroisoquinoline-2-carboxamido)propyl)piperidine-1-carboxylate (6) [46,47]

tert-Butyl 4-(3-isocyanatopropyl)piperidine-1-carboxylate (4) (180 mg, 0.7 mmol), DIPEA (1.2 eq, 1.1 mmol, 188 μL) and 7-chloro-1,2,3,4-tetrahydroisoquinoline hydrochloride (5) (0.9 mmol, 150 mg) were dissolved in 20 mL of THF and stirred at RT over 48 h. The reaction mixture was evaporated to dryness and portioned between DCM (50 mL) and water (30 mL). Water layer was extracted with DCM twice more. Collected organic layers were dried over MgSO4 and the residue was purified by silica gel chromatography (hexane/EtOAc 1/3) to afford *tert*-butyl 4-(3-(7-chloro-1,2,3,4-tetrahydroisoquinoline-2-carboxamido) propyl)piperidine-1-carboxylate (146 mg, 50 %); APCI *m/z*(+): $[(M + H^+)]^+$ 437.1; ^1H NMR:δ [ppm] (300 MHz, DMSO-d_6) δ 7.28–6.97 (m, 3H), 6.53 (t, $J = 5.4$ Hz, 1H), 4.44 (s, 2H), 3.88 (d, $J = 13.1$ Hz, 2H), 3.49 (t, $J = 5.9$ Hz, 2H), 2.99 (q, $J = 6.8$ Hz, 2H), 2.78–2.52 (m, 4H), 1.97 (s, 2H), 1.59 (s, 2H), 1.36 (s, 12H), 1.01–0.77 (m, 2H);

4.4.5. 7-Chloro-N-(3-(piperidin-4-yl)propyl)-3,4-dihydroisoquinoline-2[1H]-carboxamide hydrochloride (7)

tert-Butyl-4-(3-(7-chloro-1,2,3,4-tetrahydroisoquinoline-2-carboxamido)propyl)piperidine-1-carboxylate (**6**) (140 mg, 0.33 mmol) was dissolved in 2 mL of saturated HCl solution in dioxane and left stirring for 1 h. Reaction mixture was coevaporated a three times with dioxane. The crude product was washed with Et_2O to afford pure 7-chloro-*N*-(3-(piperidin-4-yl)propyl)-3,4-dihydroisoquinoline-2[1*H*]-carboxamide hydrochloride (90 mg, 73 %); APCI *m/z*(+): $[(M + H^+)]^+$ 336.2; ^1H NMR: δ [ppm] (300 MHz, DMSO-d_6) δ 8.95 (bs, 2H), 7.31–7.05 (m, 3H), 6.64 (s, 1H), 4.47 (s, 2H), 3.49 (t, $J = 7.1$ Hz, 2H), 3.29–3.10(m, 2H), 3.01 (t, $J = 7.1$ Hz, 2H), 2.88–2.66 (m, 4H), 1.89–1.65 (m, 2H), 1,54–1.05 (m, 7H);); 13C NMR (75 MHz, DMSO-d_6) δ 157.23, 136.68,

133.80, 130.41, 130.22,126.04, 125.82, 60.68, 45.03, 43.03, 40.85, 40.16, 39.05, 32.78, 29.16, 28.30, 27.48; LC-MS (ESI-(+)): 95.3 % 336.09 $[M + H^+]^+$;

4.4.6. *tert*-Butyl-4-(3-(7-chloro-*N*-methyl-1,2,3,4-tetrahydroisoquinoline-2-carboxamido)propyl)piperidine-1-carboxylate (8) [46]

tert-Butyl 4-(3-(7-chloro-1,2,3,4-tetrahydroisoquinoline-2-carboxamido)propyl)piperidine-1-carboxylate (**6**) (250 mg, 0.57 mmol) was dissolved in 30 mL of THF and excess of NaH (60 % on oil, 100 mg) was added). The reaction mixture was allowed to stir at RT for 3 h. After three hours an excess of methyl iodide (5.0 mL) was added and the stirring was continued over night). Reaction mixture was evaporated to dryness and purified by flash chromatography (hexane/EtOAc, 1/3) to afford *tert*-butyl 4-(3-(7-chloro-*N*-methyl-1,2,3,4-tetrahydroisoquinoline-2-carboxamido)propyl)piperidine-1-carboxylate (173 mg, 68 %). APCI *m/z*(+): $[(M + H^+)]^+$ 450.3; ^{1}H NMR: δ [ppm] (300 MHz, DMSO-d_6) δ 7.30–7.12 (m, 3H), 4.27 (s, 2H), 3.89 (d, $J = 13.1$ Hz, 2H), 3.40–3.32 (m, 2H),3.11 (t, $J = 7.3$ Hz, 2H), 2.80 (m, 5H), 2.61 (m, 2H), 1.54 (m, 3H), 1.38 (s, 9H), 1.24 (s, 2H) , 1.13 (m, 2H), 1.01–0.79 (m, 2H);

4.4.7. 7-Chloro-*N*-methyl-*N*-(3-(piperidin-4-yl)propyl)-3,4-dihydroisoquinoline-2[1H]-carboxamide (9)

tert-Butyl-4-(3-(7-chloro-*N*-methyl-1,2,3,4-tetrahydroisoquinoline-2-carboxamido)propyl)piperidine-1-carboxylate (**8**) (200 mg, 0.44 mmol) was dissolved in 4 mL of saturated HCl solution in dioxane and left stirring for 1 h. Reaction mixture was coevaporated a three times with dioxane. The crude product was purified by column chromatography (DCM/MeOH (sat·NH_3) 95/5) to afford (9): (102 mg, 66 %). APCI *m/z*(+): $[(M + H^+)]^+$ 351.0; ^{1}H NMR: δ [ppm] (300 MHz, $CDCl_3$) δ 7.17–6.84 (m, 3H), 4.26 (s, 2H), 3.37 (t, $J = 5.8$ Hz, 2H), 3.11 (t, $J = 7.5$ Hz, 2H), 2.93 (d, $J = 10.4$ Hz, 2H), 2.79 (d, $J = 2,4$ Hz, 6H), 2.05–1.71 (m, 2H), 1.65–0.98 (m, 9H); ^{13}C NMR (75 MHz, $CDCl_3$) δ 164.65, 135.82, 133.01, 131.62, 130.17, 126.54, 126.21, 53.44, 50.34, 48.61, 44.87, 44.41, 36.51, 36.26, 35.63, 33.50, 31.90, 28.14, 24.24 ; LC-MS (ESI-(+)): 95.1 % 336.09 $[M + H^+]^+$;

4.5. Human histamine H_3 receptor in-vitro assay

Compounds were tested in H_3R binding studies *in-vitro* as reported previously [48] Click or tap here to enter text.. Briefly summarized, crude hH_3R membrane extracts from HEK-293 cells stably expressing the hH_3R were incubated with several concentrations of test compounds and [^{3}H]-N^{α}-methylhistamine (2 nM, $K_D = 3.08$ nM). The cell line was kind gift from Prof. J.-C. Schwartz, Bioprojet Pharma, France. Non-specific binding was determined using pitolisant (10 μM final concentration). Obtained data in duplicates from at least three independent experiments were analyzed with GraphPad Prism 7 (San Diego, CA, USA) using non-linear regression. K_i values were transformed from IC_{50} according to Cheng-Prusoff [49]. Statistical analysis of pK_i values was performed and converted to mean K_i values and 95% confidence intervals.

5. Discussion

According to the profound impact of histamine H_3 receptors in modulating the release of histamine and other important neurotransmitters in central nervous system, these receptors deserve much consideration as an important target in neurological disorders. Since neurotransmitter deficiency in CNS has been implicated in several neurological disorders, developing histamine H_3R antagonists/inverse agonists is of paramount importance in this line of research. Drug design and discovery pipeline is a multiobjective optimization process necessitates contribution of various disciplines. In view of this, computational approaches are inevitable part of pharmaceutical research accelerating the identification of novel therapeutic agents in early stages of rational drug design. Scaffold hopping technique as structural optimization strategy in medicinal chemistry aims to improve the key parameters of any bioactive compound in terms of safety and efficacy. In the current study, scaffold-hopping analysis was performed on previously identified compounds [22] to find potentially bioisosteric substructures with similar shape and electronic properties in order to develop novel molecules with improved pharmacokinetic and physicochemical attributes while simultaneously lacking of any potentially toxic fragments. For this purpose, a variety of scaffolds are shuffled based on the calculated field points. This replacement was noticeable especially for compound 3 containing indole and piperazine moieties reported as structural elements frequently observed in promiscuous compounds [50].

The newly designed molecules containing favorable bioisosteres with high similarity to the starter molecule were carefully scrutinized on the basis of BIF scores, radial plots, and unstable/reactive functional groups. The obtained candidate molecules were inspected in terms of drug-likeness, ADME, selectivity towards H_3R, and toxicity. The designed molecules were predicted to have high intestinal absorption. The majority of the candidates showed no inhibition of drug metabolizing isoforms of CYP450 enzymes. Moreover, no violation of rules determining drug-likeness were observed for the selected compounds. Since CNS penetration is essential for H_3R ligands, the calculated MPO score demonstrated the possible brain permeability for the designed compounds within the defined threshold. The off-target activity prediction for the selected compounds revealed lower potential of candidate molecules to be toxic. To predict the mode of interaction of the selected molecules with H_3R, molecular docking was conducted. Analysis the results indicate the key residues interact with different moieties of the candidate molecules are: Tyr^{189} (TM5) and Tyr^{394} (TM7) involved in hydrophobic interaction in hydrophobic/aromatic moiety, Tyr^{115} (TM3) and Tyr^{374} (TM6) interact with the linker, and Glu^{206} (TM5) in ionic interaction with basic moiety. The results are in agreement with the other investigations reported previously [51–58]. The results of binding free energy values (ΔG) for the designed molecules presented (cf. Supplementary Table S6) revealed that the binding affinity for the majority of them are lower compared to pitolisant implying the suitable predicted affinity of the designed compounds towards H_3R.

In the next step, compound **d2** was considered as a representative for the designed compounds for synthesis and affinity measurement. This compound has a high synthetically feasible structure associated with the necessary features considered for screening and is lacking any stereocenters. Moreover, among the compounds it is the only one that passed all the lead-likeness criteria. In addition, it possess the lowest TPSA in this set of compound proving the potential new lead structure.

In accordance with the results of binding free energy values, **d2** showed lower binding affinity in radioligand displacement assay to hH_3R than that of pitolisant. Demethylation into compound **7** led to decreased affinity. Although, experimental determined affinity of **d2** is not in the submicromolar K_i-range as previously identified compounds [22], binding affinities are in good agreement with molecular docking simulations and offer another scaffold for histamine H_3R antagonists [4,59,60].

6. Conclusion

Substantial progress in developing histamine H_3R antagonists/inverse agonists has been made in the past decades owing to the significant role of H_3 receptors in neurological diseases. In this investigation, we sought to identify novel H_3R antagonists by applying computational approaches integrated with experimental validation. For this purpose, scaffold-hopping technique was utilized to design novel compounds based on calculated field point patterns on previously identified H_3 antagonists using ChEMBL and Zinc database. Following the filtering the compounds on the basis of pharmacokinetic, drug-likeness and toxicity parameters, the selected compounds were subjected to molecular docking and dynamics simulation studies in order to predict the binding

mode and binding free energy estimation, respectively. Considering the predicted features as well as synthetic tractability of the designed compounds, **d2** compound was selected for synthesis. The biological evaluation using radioligand displacement study revealed micromolar K_i values for **d2** and its demethylated derivative. The presented novel histamine H_3 ligands with the new 1,2,3,4-tetrahydroisoquinoline element can provide a safe and promising framework for further optimization through medicinal chemistry oriented strategies.

Declaration of Competing Interest

The authors declare that they have no known competing financial interests or personal relationships that could have appeared to influence the work reported in this paper.

Acknowledgements

The authors thank to Biotechnology Research Center and School of Pharmacy, Tabriz university of Medical Sciences for providing computational resources (Grant No: 64123). Support by the EU COST Actions CA15135, CA18133, and CA18240 is greatly acknowledged (to HS).

Author contributions

NS and SKH carried out the computational simulations. AZ and LL performed the chemical synthesis and in vitro evaluations. SD helped in analyzing the results. MHM and HS designed the study, analyzed the data, supervised the project, and prepared the manuscript. All authors have read the manuscript and approved the final version.

Appendix A. Supplementary material

Supplementary data to this article can be found online at https://doi.org/10.1016/j.bioorg.2021.105411.

References

[1] G. Nieto-Alamilla, R. Márquez-Gómez, A.-M. García-Gálvez, G.-E. Morales-Figueroa, J.-A. Arias-Montaño, The Histamine H3 Receptor: Structure, Pharmacology, and Function, Mol. Pharmacol. 90 (5) (2016) 649–673, https://doi.org/10.1124/mol.116.104752.
[2] M.J. Gemkow, A.J. Davenport, S. Harich, B.A. Ellenbroek, A. Cesura, D. Hallett, The histamine H3 receptor as a therapeutic drug target for CNS disorders, Drug Discov. Today. 14 (9–10) (2009) 509–515, https://doi.org/10.1016/j.drudis.2009.02.011.
[3] M. Berlin, C.W. Boyce, M. de Lera Ruiz, Histamine H3 receptor as a drug discovery target, J. Med. Chem. 54 (1) (2011) 26–53, https://doi.org/10.1021/jm100064d.
[4] N. Ghamari, O. Zarei, J.-A. Arias-Montaño, D. Reiner, S. Dastmalchi, H. Stark, M. Hamzeh-Mivehroud, Histamine H3 receptor antagonists/inverse agonists: Where do they go? Pharmacol. Ther. 200 (2019) 69–84, https://doi.org/10.1016/j.pharmthera.2019.04.007.
[5] G. Sliwoski, S. Kothiwale, J. Meiler, E.W. Lowe, E.L. Barker, Computational methods in drug discovery, Pharmacol. Rev. 66 (1) (2014) 334–395, https://doi.org/10.1124/pr.112.007336.
[6] G. Schneider, P. Schneider, S. Renner, Scaffold-Hopping: How Far Can You Jump? QSAR Comb. Sci. 25 (12) (2006) 1162–1171, https://doi.org/10.1002/(ISSN)1611-021810.1002/qsar.v25:1210.1002/qsar.200610091.
[7] S.R. Langdon, P. Ertl, N. Brown, Bioisosteric Replacement and Scaffold Hopping in Lead Generation and Optimization, Mol. Inform. 29 (5) (2010) 366–385, https://doi.org/10.1002/minf.201000019.
[8] H.-J. Böhm, A. Flohr, M. Stahl, Scaffold hopping, Drug Discov. Today Technol. 1 (3) (2004) 217–224, https://doi.org/10.1016/j.ddtec.2004.10.009.
[9] Y.Y. Syed, Y. Pitolisant: First Global Approval, Drugs. 76 (13) (2016) 1313–1318, https://doi.org/10.1007/s40265-016-0620-1.
[10] M. Kollb-Sielecka, P. Demolis, J. Emmerich, G. Markey, T. Salmonson, M. Haas, The European Medicines Agency review of pitolisant for treatment of narcolepsy: summary of the scientific assessment by the Committee for Medicinal Products for Human Use, Sleep Med. 33 (2017) 125–129, https://doi.org/10.1016/j.sleep.2017.01.002.
[11] Z. Szakacs, Y. Dauvilliers, V. Mikhaylov, I. Poverennova, S. Krylov, S. Jankovic, K. Sonka, P. Lehert, I. Lecomte, J.-M. Lecomte, J.-C. Schwartz, M. Poluektov, E. Yakupov, A. Kalinkin, M. Aksu, H. Yilmaz, G. Benbir, D. Wolynczyk-Gmaj, W. Jernajczyk, I. Staykov, A.N. Tavarari, Safety and efficacy of pitolisant on cataplexy in patients with narcolepsy: a randomised, double-blind, placebo-controlled trial, Lancet Neurol. 16 (3) (2017) 200–207, https://doi.org/10.1016/S1474-4422(16)30333-7.
[12] H. Sun, C. MacLeod, K. Mostoller, C. Mahon, L. Han, J.J. Renger, J. Ma, K. R. Brown, V. Schulz, G.G. Kay, W.J. Herring, C. Lines, L.B. Rosen, M.G. Murphy, J. A. Wagner, Early-stage comparative effectiveness: randomized controlled trial with histamine inverse agonist MK-7288 in excessive daytime sleepiness patients, J. Clin. Pharmacol. 53 (12) (2013) 1294–1302, https://doi.org/10.1002/jcph.v53.1210.1002/jcph.182.
[13] J.R. Stokes, F.A. Romero, R.J. Allan, P.G. Phillips, F. Hackman, J. Misfeldt, T. B. Casale, The effects of an H3 receptor antagonist (PF-03654746) with fexofenadine on reducing allergic rhinitis symptoms, J. Allergy Clin. Immunol. 129 (2) (2012) 409–412.e2, https://doi.org/10.1016/j.jaci.2011.11.026.
[14] O. Spiegelstein, et al., Pharmacokinetics, pharmacodynamics and safety of CEP-26401, a high-affinity histamine-3 receptor antagonist, following single and multiple dosing in healthy subjects, J. Psychopharmacol. 30 (2016) 983–993.
[15] C.J. Schwartzbach, et al., Lesion remyelinating activity of GSK239512 versus placebo in patients with relapsing-remitting multiple sclerosis: a randomised, single-blind, phase II study, J. Neurol. 264 (2017) 304–315.
[16] A.A. Othman, et al., The H3 antagonist ABT-288 is tolerated at significantly higher exposures in subjects with schizophrenia than in healthy volunteers, Br. J. Clin. Pharmacol. 77 (2014) 965–974.
[17] P.J. Nathan, et al., The safety, tolerability, pharmacokinetics and cognitive effects of GSK239512, a selective histamine H(3) receptor antagonist in patients with mild to moderate Alzheimer's disease: a preliminary investigation, Curr. Alzheimer Res. 10 (2013) 240–251.
[18] Jucaite, A. et al. AZD5213: a novel histamine H3 receptor antagonist permitting high daytime and low nocturnal H3 receptor occupancy, a PET study in human subjects. Int. J. Neuropsychopharmacol. 16, 1231-1239, 10.1017/s1461145712001411 (2013).
[19] Dauvilliers, Y. et al. Pitolisant versus placebo or modafinil in patients with narcolepsy: a double-blind, randomised trial. Lancet Neurol. 12, 1068-1075, 10.1016/S1474-4422(13)70225-4 (2013).
[20] P. Daley-Yates, et al., The efficacy and tolerability of two novel H(1)/H(3) receptor antagonists in seasonal allergic rhinitis, Int. Arch. Allergy Immunol. 158 (2012) 84–98, https://doi.org/10.1159/000329738.
[21] S. Ashworth, A. Berges, E.A. Rabiner, A.A. Wilson, R.A. Comley, R.Y.K. Lai, R. Boardley, G. Searle, R.N. Gunn, M. Laruelle, V.J. Cunningham, Unexpectedly high affinity of a novel histamine H3 receptor antagonist, GSK239512, in vivo in human brain, determined using PET, Br. J. Pharmacol. 171 (5) (2014) 1241–1249, https://doi.org/10.1111/bph.12505.
[22] N. Ghamari, O. Zarei, D. Reiner, S. Dastmalchi, H. Stark, M. Hamzeh-Mivehroud, Histamine H3 receptor ligands by hybrid virtual screening, docking, molecular dynamics simulations, and investigation of their biological effects, Chem. Biol. Drug Des. 93 (5) (2019) 832–843, https://doi.org/10.1111/cbdd.2019.93.issue-510.1111/cbdd.13471.
[23] N. Ghamari, S. Dastmalchi, O. Zarei, J.-A. Arias-Montaño, D. Reiner, F. Ustun-Alkan, H. Stark, M. Hamzeh-Mivehroud, In silico and in vitro studies of two non-imidazole multiple targeting agents at histamine H3 receptors and cholinesterase enzymes, Chem. Biol. Drug Des. 95 (2) (2020) 279–290, https://doi.org/10.1111/cbdd.v95.210.1111/cbdd.13642.
[24] C.A. Lipinski, F. Lombardo, B.W. Dominy, P.J. Feeney, Experimental and computational approaches to estimate solubility and permeability in drug discovery and development settings, Adv. Drug Deliv. Rev. 46 (2001) 3–26.
[25] A.K. Ghose, V.N. Viswanadhan, J.J. Wendoloski, A Knowledge-Based Approach in Designing Combinatorial or Medicinal Chemistry Libraries for Drug Discovery. 1. A Qualitative and Quantitative Characterization of Known Drug Databases, J. Comb. Chem. 1 (1999) 55–68.
[26] W.J. Egan, K.M. Merz Jr., J.J. Baldwin, Prediction of drug absorption using multivariate statistics, J. Med. Chem. 43 (2000) 3867–3877.
[27] I. Muegge, S.L. Heald, D. Brittelli, Simple Selection Criteria for Drug-like Chemical Matter, J. Med. Chem. 44 (2001) 1841–1846.
[28] D.F. Veber, et al., Molecular properties that influence the oral bioavailability of drug candidates, J. Med. Chem. 45 (2002) 2615–2623.
[29] J.B. Baell, G.A. Holloway, New Substructure Filters for Removal of Pan Assay Interference Compounds (PAINS) from Screening Libraries and for Their Exclusion in Bioassays, J. Med. Chem. 53 (7) (2010) 2719–2740, https://doi.org/10.1021/jm901137j.
[30] R. Brenk, A. Schipani, D. James, A. Krasowski, I. Gilbert, J. Frearson, P. Wyatt, Lessons Learnt from Assembling Screening Libraries for Drug Discovery for Neglected Diseases, ChemMedChem. 3 (3) (2008) 435–444, https://doi.org/10.1002/(ISSN)1860-718710.1002/cmdc.v3:310.1002/cmdc.200700139.
[31] T.T. Wager, X. Hou, P.R. Verhoest, A. Villalobos, Moving beyond rules: the development of a central nervous system multiparameter optimization (CNS MPO) approach to enable alignment of druglike properties, ACS Chem. Neurosci. 1 (6) (2010) 435–449, https://doi.org/10.1021/cn100008c.
[32] T. Cheeseright, M. Mackey, S. Rose, A. Vinter, Molecular Field Extrema as Descriptors of Biological Activity: Definition and Validation, J. Chem. Inf. Model. 46 (2006) 665–676, https://doi.org/10.1021/ci050357s.
[33] P.H. Olesen, The use of bioisosteric groups in lead optimization, Curr. Opin. Drug Discov. Devel. 4 (2001) 471–478.
[34] A. Daina, O. Michielin, V. Zoete, SwissADME: a free web tool to evaluate pharmacokinetics, drug-likeness and medicinal chemistry friendliness of small molecules, Sci. Rep. 7 (2017) 42717, https://doi.org/10.1038/srep42717.
[35] A. Daina, O. Michielin, V. Zoete, SwissTargetPrediction: updated data and new features for efficient prediction of protein targets of small molecules, Nucleic Acids Res. 47 (2019) W357–W364, https://doi.org/10.1093/nar/gkz382.

[36] A. Vedani, M. Dobler, Z. Hu, M. Smieško, OpenVirtualToxLab–a platform for generating and exchanging in silico toxicity data, Toxicol. Lett. 232 (2) (2015) 519–532, https://doi.org/10.1016/j.toxlet.2014.09.004.

[37] A. Vedani, M. Dobler, M. Smiesko, VirtualToxLab - a platform for estimating the toxic potential of drugs, chemicals and natural products, Toxicol. Appl. Pharmacol. 261 (2012) 142–153.

[38] G. Jones, P. Willett, R.C. Glen, Molecular recognition of receptor sites using a genetic algorithm with a description of desolvation, J. Mol. Biol. 245 (1995) 43–53.

[39] G. Jones, P. Willett, R.C. Glen, A.R. Leach, R. Taylor, Development and validation of a genetic algorithm for flexible docking, J. Mol. Biol. 267 (1997) 727–748, https://doi.org/10.1006/jmbi.1996.0897.

[40] D.A. Case, et al., The Amber biomolecular simulation programs, J. Comput. Chem. 26 (2005) 1668–1688.

[41] D.A. Pearlman, D.A. Case, J.W. Caldwell, W.S. Ross, T.E. Cheatham, S. DeBolt, D. Ferguson, G. Seibel, P. Kollman, AMBER, a package of computer programs for applying molecular mechanics, normal mode analysis, molecular dynamics and free energy calculations to simulate the structural and energetic properties of molecules, Comput. Phys. Commun. 91 (1-3) (1995) 1–41, https://doi.org/10.1016/0010-4655(95)00041-D.

[42] P.A. Kollman, et al., Calculating structures and free energies of complex molecules: combining molecular mechanics and continuum models, Acc. Chem. Res. 33 (2000) 889–897, https://doi.org/10.1021/ar000033j.

[43] J. Weiser, S. Shenkin Peter, W.C. Still, Approximate atomic surfaces from linear combinations of pairwise overlaps (LCPO), J. Comput. Chem. 20 (1999) 217–230, https://doi.org/10.1002/(SICI)1096-987X(19990130)20:2<217::AID-JCC4>3.0.CO;2-A.

[44] Rudd, M. T. et al. N-Aryl and N-Heteroaryl Piperidine Derivatives As Liver X Receptor B Agonists, Compositions, and Their Use. WO2018/68297 (2018).

[45] P. Trivedi, N. Adhikari, S.A. Amin, Y. Bobde, R. Ganesh, T. Jha, B. Ghosh, Design, synthesis, biological evaluation and molecular docking study of arylcarboxamido piperidine and piperazine-based hydroxamates as potential HDAC8 inhibitors with promising anticancer activity, Eur. J. Pharm. Sci. 138 (2019) 105046, https://doi.org/10.1016/j.ejps.2019.105046.

[46] R. Bach, J. Clayden, U. Hennecke, A-Arylation of Cyclic Amines by Aryl Transfer in Lithiated Ureas, SYNLETT 03 (2009) 421–424.

[47] S. Del Prete, V. De Luca, C. Capasso, C.T. Supuran, V. Carginale, Recombinant thermoactive phosphoenolpyruvate carboxylase (PEPC) from Thermosynechococcus elongatus and its coupling with mesophilic/thermophilic bacterial carbonic anhydrases (CAs) for the conversion of CO2 to oxaloacetate, Bioorg. Med. Chem. 24 (2) (2016) 220–225, https://doi.org/10.1016/j.bmc.2015.12.005.

[48] M.A. Khanfar, D. Reiner, S. Hagenow, H. Stark, Design, synthesis, and biological evaluation of novel oxadiazole- and thiazole-based histamine H(3)R ligands, Bioorg. Med. Chem. 26 (14) (2018) 4034–4046, https://doi.org/10.1016/j.bmc.2018.06.028.

[49] C. Yung-Chi, W.H. Prusoff, Relationship between the inhibition constant (KI) and the concentration of inhibitor which causes 50 per cent inhibition (I50) of an enzymatic reaction, Biochem. Pharmacol. 22 (23) (1973) 3099–3108, https://doi.org/10.1016/0006-2952(73)90196-2.

[50] N.A. Meanwell, Improving drug candidates by design: a focus on physicochemical properties as a means of improving compound disposition and safety, Chem. Res. Toxicol. 24 (9) (2011) 1420–1456, https://doi.org/10.1021/tx200211v.

[51] F.U. Axe, S.D. Bembenek, S. Szalma, Three-dimensional models of histamine H3 receptor antagonist complexes and their pharmacophore, J. Mol. Graph. Model. 24 (2006) 456–464.

[52] M. Bajda, K.J. Kuder, D. Łażewska, K. Kieć-Kononowicz, A. Więckowska, M. Ignasik, N. Guzior, J. Jończyk, B. Malawska, Dual-acting diether derivatives of piperidine and homopiperidine with histamine H(3) receptor antagonistic and anticholinesterase activity, Arch. Pharm. (Weinheim) 345 (8) (2012) 591–597, https://doi.org/10.1002/ardp.v345.810.1002/ardp.201200018.

[53] S. Harusawa, K. Sawada, T. Magata, H. Yoneyama, L. Araki, Y. Usami, K. Hatano, K. Yamamoto, D. Yamamoto, A. Yamatodani, Synthesis and evaluation of N-alkyl-S-[3-(piperidin-1-yl)propyl]isothioureas: high affinity and human/rat species-selective histamine H(3) receptor antagonists, Bioorg. Med. Chem. Lett. 23 (23) (2013) 6415–6420, https://doi.org/10.1016/j.bmcl.2013.09.052.

[54] K. Kuder, D. Łażewska, G. Latacz, J.S. Schwed, T. Karcz, H. Stark, J. Karolak-Wojciechowska, K. Kieć-Kononowicz, Chlorophenoxy aminoalkyl derivatives as histamine H(3)R ligands and antiseizure agents, Bioorg. Med. Chem. 24 (2) (2016) 53–72, https://doi.org/10.1016/j.bmc.2015.11.021.

[55] D. Łażewska, J. Jończyk, M. Bajda, N. Szałaj, A. Więckowska, D. Panek, C. Moore, K. Kuder, B. Malawska, K. Kieć-Kononowicz, Cholinesterase inhibitory activity of chlorophenoxy derivatives-Histamine H3 receptor ligands, Bioorg. Med. Chem. Lett. 26 (16) (2016) 4140–4145, https://doi.org/10.1016/j.bmcl.2016.04.054.

[56] N. Levoin, et al., Determination of the binding mode and interacting amino-acids for dibasic H3 receptor antagonists, Bioorg. Med. Chem. 21 (2013) 4526–4529.

[57] R. Sheng, et al., Novel 1-phenyl-3-hydroxy-4-pyridinone derivatives as multifunctional agents for the therapy of Alzheimer's disease, ACS Chem. Neurosci. 7 (2015) 69–81.

[58] G. Wen, Q. Liu, H. Hu, D. Wang, S. Wu, Design, synthesis, biological evaluation, and molecular docking of novel flavones as H3 R inhibitors, Chem. Biol. Drug Des. 90 (4) (2017) 580–589, https://doi.org/10.1111/cbdd.2017.90.issue-410.1111/cbdd.12981.

[59] P. Panula, P.L. Chazot, M. Cowart, R. Gutzmer, R. Leurs, W.L.S. Liu, H. Stark, R. L. Thurmond, H.L. Haas, E.H. Ohlstein, International Union of Basic and Clinical Pharmacology, XCVIII. Histamine Receptors. *Pharmacol. Rev.* 67 (3) (2015) 601–655, https://doi.org/10.1124/pr.114.010249.

[60] K. Wingen, H. Stark, Scaffold variations in amine warhead of histamine H(3) receptor antagonists, Drug Discov. Today Technol. 10 (4) (2013) e483–e489, https://doi.org/10.1016/j.ddtec.2013.07.001.

Supplemental Information

Guided rational design with scaffold hopping leading to novel histamine H_3 receptor ligands

Nakisa Ghamari[1,2], Saeed Kouhi Hargelan[2], Aleksandra Zivkovic[3], Luisa Leitzbach[3], Siavoush Dastmalchi[1,2], Holger Stark[3,*], and Maryam Hamzeh-Mivehroud[1,2,*]

[1] Biotechnology Research Center, Tabriz University of Medical Sciences, Tabriz, Iran
[2] School of Pharmacy, Tabriz University of Medical Sciences, Tabriz, Iran
[3] Heinrich Heine University Düsseldorf, Institute of Pharmaceutical and Medicinal Chemistry, Universitaetsstr. 1, D-40225 Duesseldorf, Germany

[*] **Corresponding Authors:**

Maryam Hamzeh-Mivehroud and Holger Stark

Full address: Biotechnology Research Center and School of Pharmacy, Tabriz University of Medical Sciences, Tabriz, Iran. Tel:+98 (41) 3336 4038, Fax: +98 (41) 3337 9420, E-mail: hamzehm@tbzmed.ac.ir, maryam_h_7860@yahoo.com.

Full address: Heinrich Heine University Düsseldorf, Institute of Pharmaceutical and Medicinal Chemistry, Universitaetsstr. 1, D-40225 Duesseldorf, Germany. Tel:+49 211 81-10478, Fax: +49 211 81-13359, Email: stark@hhu.de.

Supplementary Table S1. Calculated physicochemical, pharmacokinetic, drug-likeness, and medicinal chemistry properties of lead compounds

Molecular Descriptor	d1	d2	d3	d4	d5	d6
Physicochemical Properties						
Formula	$C_{20}H_{30}ClN_3O_2$	$C_{19}H_{28}ClN_3O$	$C_{19}H_{28}ClN_3O_2$	$C_{18}H_{27}ClN_2O_3$	$C_{21}H_{32}ClN_3O_2$	$C_{21}H_{30}ClN_3O_3$
Molecular weight	379.92 g/mol	349.90 g/mol	365.9 g/mol	354.87 g/mol	393.95 g/mol	407.93 g/mol
Num. rotatable bonds	6	6	7	8	7	7
Num. H-bond acceptors	3	2	3	4	3	4
Num. H-bond donors	1	1	0	1	1	1
Molar Refractivity	113.15	107.05	108.22	99.81	117.95	118.15
TPSA	47.02 Å²	35.58 Å²	36.02 Å²	53.01 Å²	47.02 Å²	64.09 Å²
Pharmacokinetic properties						
GI absorption	High	High	High	High	High	High
BBB permeant	Yes	Yes	Yes	Yes	Yes	Yes
P-gp substrate	Yes	Yes	Yes	No	Yes	Yes
CYP1A2 inhibitor	No	No	No	No	No	No
CYP2C19 inhibitor	No	No	No	No	No	No
CYP2C9 inhibitor	No	No	No	No	No	No
CYP2D6 inhibitor	Yes	Yes	Yes	Yes	Yes	Yes
CYP3A4 inhibitor	No	No	Yes	No	No	No
Log K_p (skin permeation)	-6.96 cm/s	-6.36 cm/s	-6.87 cm/s	-6.70 cm/s	-6.79 cm/s	-7.21 cm/s
Druglikeness						
Lipinski	Yes	Yes	Yes	Yes	Yes	Yes
Ghose[a]	Yes	Yes	Yes	Yes	Yes	Yes
Veber[b]	Yes	Yes	Yes	Yes	Yes	Yes
Egan[c]	Yes	Yes	Yes	Yes	Yes	Yes
Muegge[d]	Yes	Yes	Yes	Yes	Yes	Yes
Bioavailability Score	0.55	0.55	0.55	0.55	0.55	0.55
Medicinal Chemistry properties						
Lead-likeness[e]	No; 1 violation: MW>350	Yes	No; 1 violation: MW>350	No; 2 violations: MW>350, Rotors>7	No; 1 violation: MW>350	No; 1 violation: MW>350
Synthetic accessibility	2.96	2.78	3.43	2.62	3.08	3.06

2

Molecular Descriptor	d7	d8	d9	d10	d11
Physicochemical Properties					
Formula	$C_{20}H_{28}ClN_3O_3$	$C_{19}H_{26}ClN_3O_2$	$C_{19}H_{26}ClN_3O_3$	$C_{21}H_{30}ClN_3O_3$	$C_{19}H_{26}ClN_3O_2$
Molecular weight	393.91 g/mol	363.88 g/mol	379.88 g/mol	407.93 g/mol	363.88 g/mol
Num. rotatable bonds	6	6	7	7	6
Num. H-bond acceptors	4	3	4	4	3
Num. H-bond donors	1	1	0	1	2
Molar Refractivity	113.35	107.25	108.42	118.15	105.56
TPSA	64.09 Å²	52.65 Å²	53.09 Å²	64.09 Å²	59.57 Å²
Pharmacokinetic properties					
GI absorption	High	High	High	High	High
BBB permeant	Yes	Yes	Yes	Yes	Yes
P-gp substrate	Yes	Yes	Yes	Yes	Yes
CYP1A2 inhibitor	No	No	No	No	No
CYP2C19 inhibitor	No	No	No	No	No
CYP2C9 inhibitor	No	No	No	No	No
CYP2D6 inhibitor	Yes	Yes	Yes	Yes	Yes
CYP3A4 inhibitor	No	No	Yes	No	No
Log K_p (skin permeation)	-7.39 cm/s	-7.18 cm/s	-7.37 cm/s	-7.21 cm/s	-6.45 cm/s
Druglikeness					
Lipinski	Yes	Yes	Yes	Yes	Yes
Ghose[a]	Yes	Yes	Yes	Yes	Yes
Veber[b]	Yes	Yes	Yes	Yes	Yes
Egan[c]	Yes	Yes	Yes	Yes	Yes
Muegge[d]	Yes	Yes	Yes	Yes	Yes
Bioavailability Score	0.55	0.55	0.55	0.55	0.55
Medicinal Chemistry properties					
Lead-likeness[e]	No; 1 violation: MW>350	No; 1 violation: MW>350	No; 1 violation: MW>350	No; 1 violation: MW>350	No; 1 violation: MW>350
Synthetic accessibility	2.94	2.74	3.43	3.06	2.48

[a]Ghose filter: $160 \leq MW \leq 480$; $-0.4 \leq WLOGP \leq 5.6$; $40 \leq MR \leq 130$; $20 \leq atoms \leq 70$.
[b]Veber filter: Rotatable bonds ≤ 10; TPSA ≤ 140.
[c]Egan filter: $WLOGP \leq 5.88$; TPSA ≤ 131.6.
[d]Muegge: $200 \leq MW \leq 600$; $-2 \leq XLOGP \leq 5$; TPSA ≤ 150; Num. rings ≤ 7; No of carbons > 4; Num. heteroatoms > 1; Num. rotatable bonds ≤ 15; Num. H-bond acceptors ≤ 10; and Num. H-bond donors ≤ 5
[e]Lead-likeness: $250 \leq MW \leq 350$; $XLOGP \leq 3.5$; and Rotatable bonds ≤ 7.

3

Supplementary Table S2. Physicochemical attributes of selected compounds used for calculation of MPO score

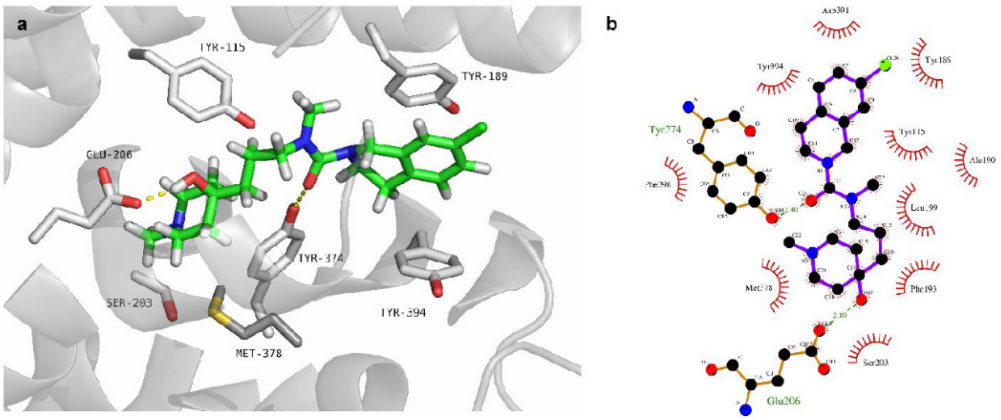
Compound	MW	cLogP	cLogD	TPSA	pK_a	HBD	MPO score[a]
d1	379.92	2.23	0.91	47.02	14.86	1	4.69
d2	349.90	3.87	0.85	35.58	11.23	1	4.18
d3	365.90	3.58	0.92	36.02	9.31	0	4.81
d4	354.87	1.75	-0.3	53.01	14.77	1	4.83
d5	393.95	2.76	1.37	47.02	14.87	1	4.59
d6	407.93	2.57	1.33	64.09	14.02	1	4.49
d7	393.91	2.29	0.80	64.09	14.02	1	4.59
d8	363.88	3.03	-0.02	52.65	10.84	1	4.79
d9	379.88	2.98	1.02	53.09	9.06	0	5.33
d10	407.93	2.82	1.26	64.09	14.03	1	4.49
d11	363.88	1.81	-1.15	59.57	14.87	2	4.47

Supplementary Table S3. *In silico* toxicity evaluation of candidate molecules. The calculated binding affinities (IC_{50}, Molar) for selected candidates against all 16 target proteins as well as toxic potential using VirtualToxLab are shown.

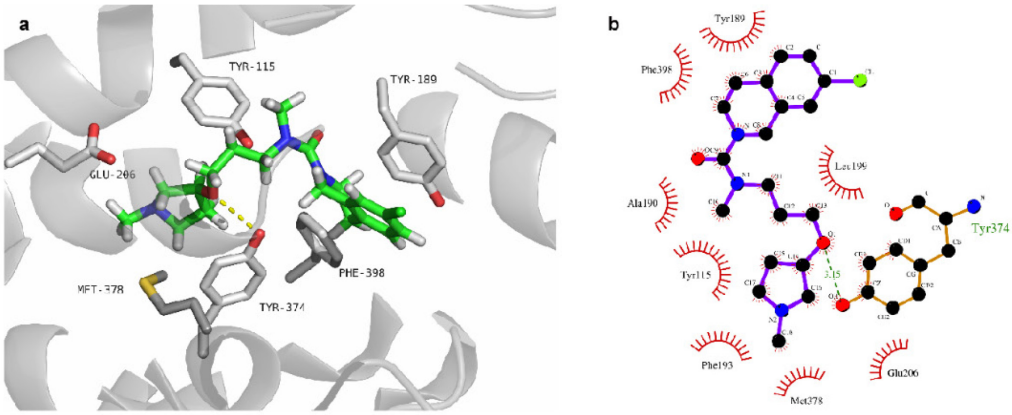
Molecule	TP	AR	AhR	CYP1A2	CYP2C9	CYP2D6	CYP3A4	ERα	ERβ	GR	hERG	LXR	MR	PPARγ	PR	TRα	TRβ
d1	0.52	2.32E-06	NB	NB	NB	1.64E-05	7.92E-05	3.12E-05	5.67E-06	4.98E-08	6.44E-07	3.75E-05	2.03E-05	3.05E-07	1.31E-05	4.62E-05	NB
d2	0.51	2.24E-05	2.77E-05	NB	9.44E-05	6.59E-05	NB	7.61E-08	1.18E-06	6.33E-07	8.37E-08	3.04E-05	5.07E-05	4.85E-06	9.62E-06	1.90E-06	1.53E-06
d3	0.44	NB	NB	NB	NB	6.31E-05	8.33E-05	8.52E-07	7.30E-07	4.77E-06	3.56E-07	NB	8.39E-05	2.46E-05	2.18E-05	NB	1.51E-05
d4	0.39	1.01E-06	NB	NB	NB	NB	NB	2.12E-05	1.05E-05	1.21E-06	3.24E-06	NB	NB	7.35E-06	6.08E-05	NB	6.38E-06
d5	0.52	1.17E-06	NB	NB	NB	NB	NB	2.66E-05	9.46E-07	4.89E-07	4.19E-08	NB	9.37E-06	3.29E-05	NB	NB	NB
d6	0.47	1.64E-07	NB	NB	NB	NB	NB	1.93E-05	5.00E-05	1.04E-05	1.56E-06	4.49E-05	NB	8.42E-05	1.55E-05	NB	6.83E-05
d7	0.39	7.85E-06	NB	NB	NB	NB	NB	8.97E-07	1.95E-06	1.57E-06	1.87E-06	NB	2.72E-06	1.00E-05	3.03E-05	7.27E-05	NB
d8	0.66	1.51E-06	NB	3.99E-05	1.60E-05	5.50E-05	6.06E-05	2.09E-06	6.71E-07	2.43E-05	2.42E-09	1.05E-05	5.41E-05	3.65E-05	2.10E-06	5.15E-05	2.04E-05
d9	0.41	NB	2.74E-06	NB	NB	NB	NB	8.07E-06	1.12E-05	NB	6.60E-07	NB	9.80E-05	9.14E-05	2.85E-05	NB	NB
d10	0.46	4.09E-07	NB	NB	NB	NB	NB	1.02E-05	8.18E-05	4.35E-06	1.89E-07	NB	8.03E-06	3.58E-06	NB	NB	NB
d11	0.43	3.35E-07	NB	NB	NB	NB	NB	5.02E-07	7.98E-05	6.80E-06	5.49E-07	NB	NB	2.40E-05	7.42E-05	NB	NB

AR: Androgen receptor; AhR: Aryl hydrocarbon receptor; ERα: Estrogen receptor α; ERβ: Estrogen receptor β; GR: Glucocorticoid receptor; hERG: LXR: Liver X receptor; MR: Mineralocorticoid receptor; PR: Progesterone receptor, TRα: Thyroid receptor α; TRβ: Thyroid receptor β; NB:not binding. TP is a measure of toxic potential derived from normalized binding affinities in respect to series of proteins with known adverse effects. Toxic alerts are defined as:
Class 0: TP ≤ 0.3(none); 0.3 < TP ≤ 0.4 (low); 0.4 < TP ≤ 0.5 (moderate)
Class I: 0.5 < TP ≤ 0.6 (elevated)
Class II: 0.6 < TP ≤ 0.7 (high)
Class III: 0.7 < TP ≤ 0.8 (Very high)
Class IV: > 0.8 (Extreme)

d1

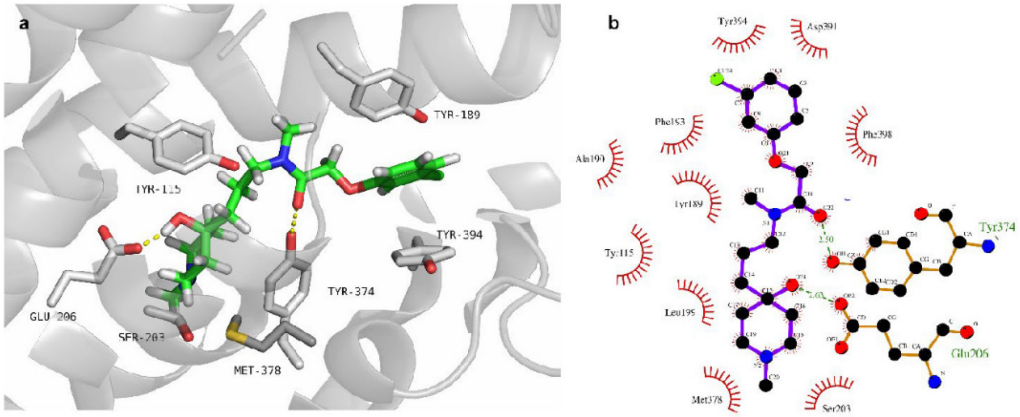

a
TYR-115
TYR-189
GLU-206
TYR-374
SER-203
TYR-394
MET-378
b
Asn391
Tyr394
Tyr185
Tyr374
Tyr115
Ala190
Leu99
Met78
Phe193
Ser203
Glu206

d3

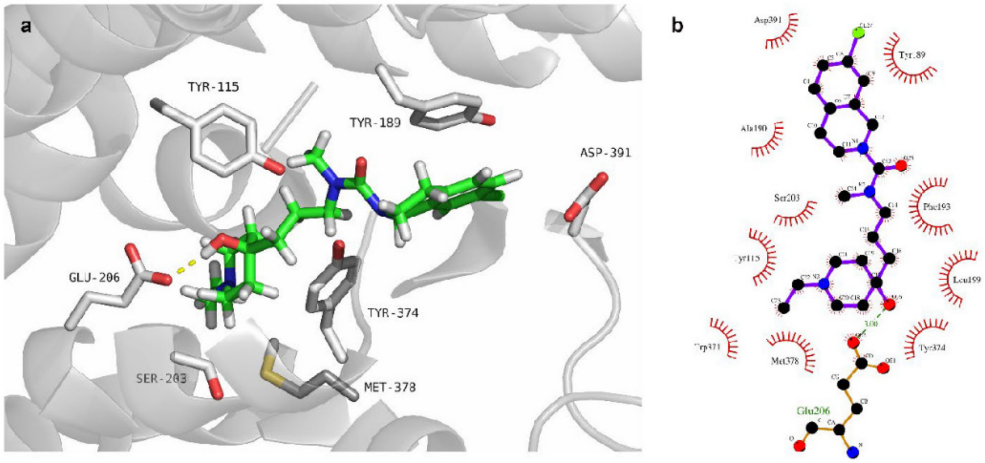

a
TYR-115
TYR-189
GLU-206
PHE-398
MET-378
TYR-374
b
Tyr189
Phe398
Leu199
Ala190
Tyr374
Tyr115
Phe193
Glu206
Met378

6

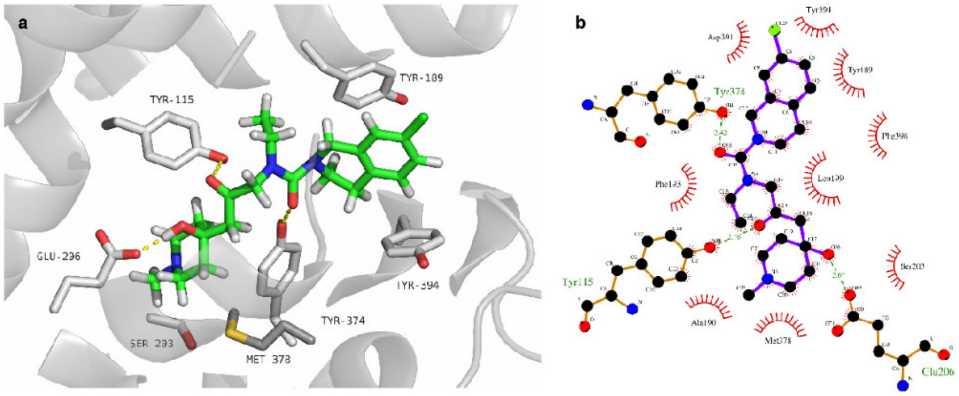
d4


a
TYR-189
TYR-115
TYR-394
TYR-374
GLU-206
SER-203
MET-378
b
Tyr394
Asp391
Phe153
Phe398
Ala190
Tyr189
Tyr115
Tyr374
Leu195
Glu206
Met378
Ser203

d5

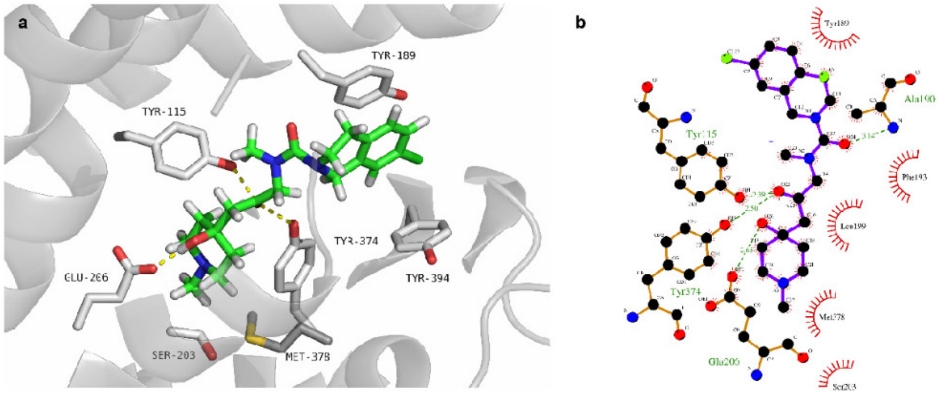

a
TYR-115
TYR-189
ASP-391
GLU-206
TYR-374
SER-203
MET-378
b
Asp391
Tyr.89
Ala190
Ser203
Phe193
Tyr115
Leu159
Met378
Tyr374
Glu206

d6

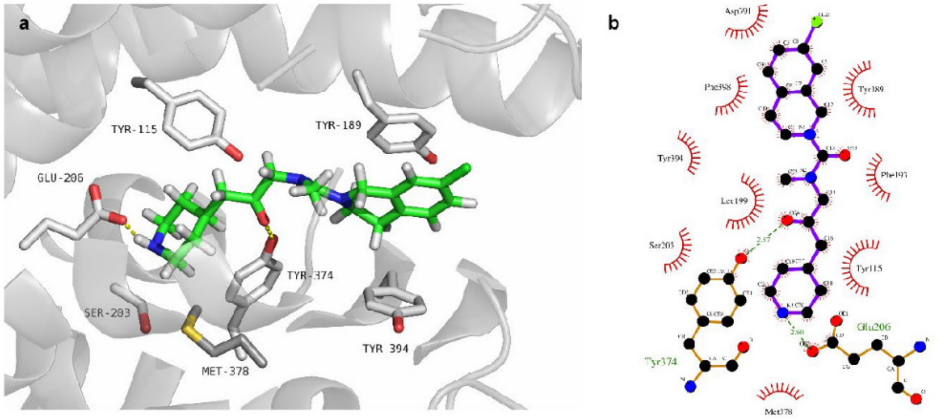

a
TYR-189
TYR-115
GLU-206
TYR-394
TYR-374
SER-203
MET-378
b
Tyr394
Asp391
Tyr189
Tyr374
Phe398
Phe153
Leu159
Tyr115
Ser203
Ala190
Met378
Glu206

7

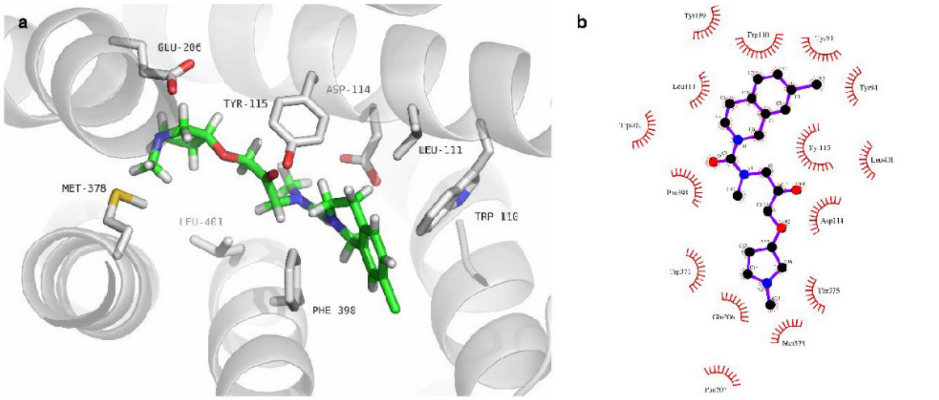
d7


a
TYR-189
TYR-115
TYR-374
TYR-394
GLU-206
SER-203
MET-378
b
Tyr189
Ala190
Tyr115
Phe193
Leu199
Tyr374
Met378
Glu206
Ser203

d8

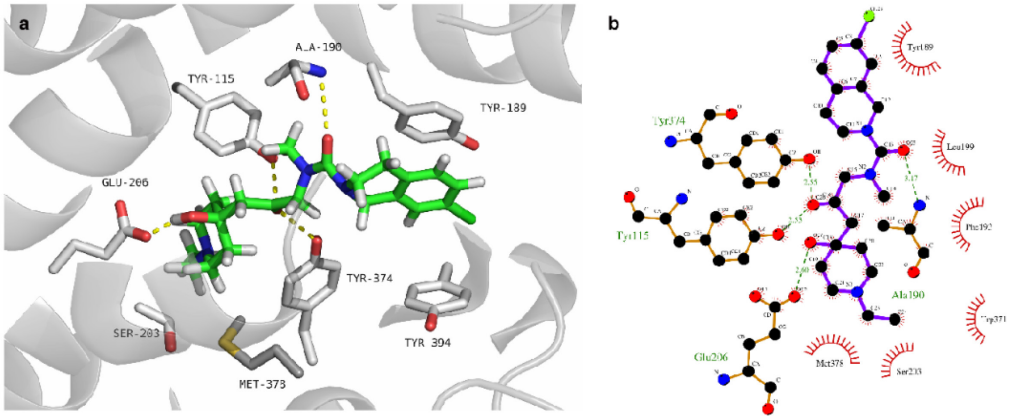

a
TYR-115
TYR-189
GLU-206
TYR-374
SER-203
TYR 394
MET-378
b
Asp391
Phe398
Tyr189
Tyr394
Phe193
Leu199
Ser203
Tyr115
Glu206
Tyr374
Met378

d9

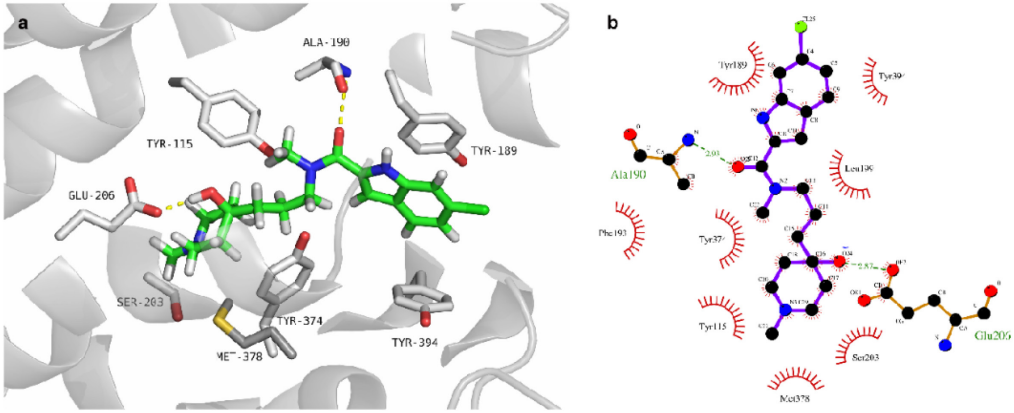

a
GLU-206
TYR-115
ASP-114
LEU-111
MET-378
TRP 110
PHE 398
b
Tyr189
Tyr110
Leu111
Tyr94
Phe193
Asp114
Phe398
Glu206
Met378

8

d10

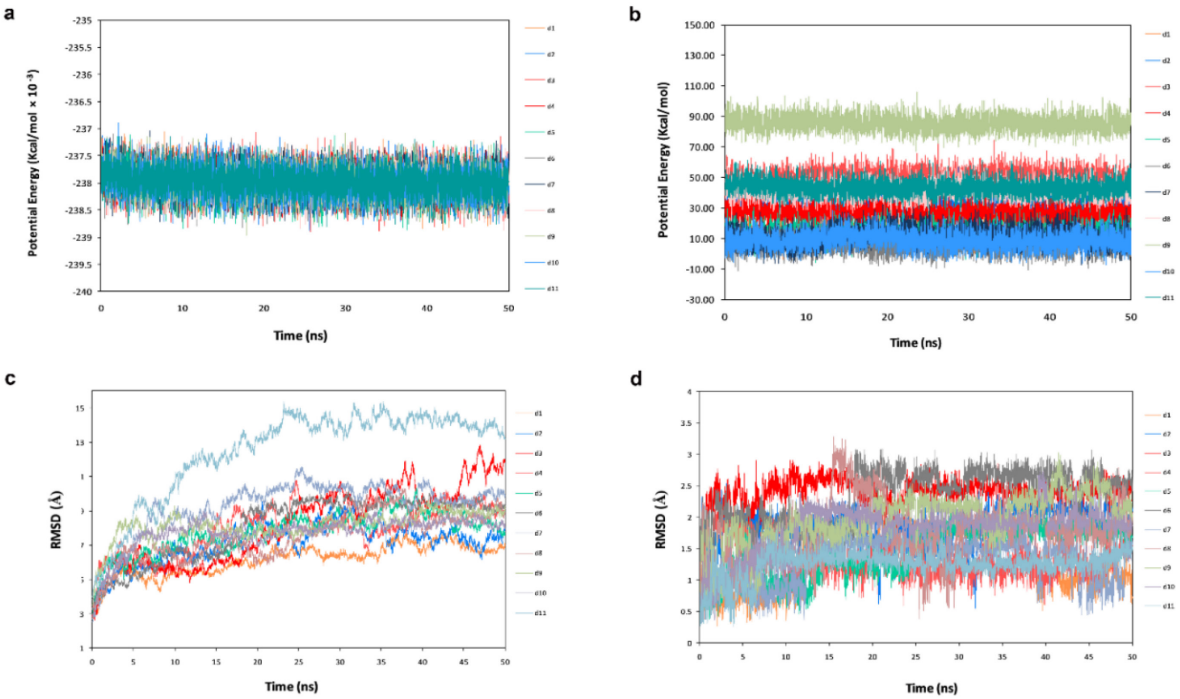


d11



Supplementary Fig. S4. (a) 3D representation of designed **d1** – **d11** docked into the binding site of H_3R generated by PyMol program (version 1.7.x). The ligands and the main interacting residues are displayed as sticks. Only the side chains of the interacting residues from receptor are shown for further clarity. **(b)** 2D illustration of the interactions between compounds **d1** – **d11** and H_3R generated by LigPlot program.

9



Supplementary Fig. S5. The results of molecular dynamics simulation analyses on ligand-H_3R complexes. Panels **a** and **b** show the plot of root mean square deviation (RMSD) fluctuation in a 1 to 50 ns molecular dynamics simulation for ligand-H_3R complexes and ligands, respectively. Panels **c** and **d** indicate potential energies for the ligand-H_3 complexes and designed compounds during 50 ns molecular dynamics simulation, respectively.

10

Supplementary Table S6. Calculated mean values of binding free energies for the complex of docked candidate molecules and H_3R using Generalized-Born, $\Delta G_{Binding\ (GB)}$ and Poisson–Boltzmann, $\Delta G_{Binding\ (PB)}$ method for 50 ns MD simulation. Standard deviations are shown in parentheses.

Compound	$\Delta G_{Binding\ (GB)}$	$\Delta G_{Binding\ (PB)}$
d1	-42.90(±3.35)	-34.21(±3.61)
d2	-39.84(±4.20)	-34.20(±4.12)
d3	-46.94(±3.55)	-41.37(±4.67)
d4	-37.05(±3.98)	-29.74(±3.99)
d5	-41.84(±2.93)	-33.36(±3.86)
d6	-43.87(±4.90)	-36.02(±5.54)
d7	-46.53(±4.82)	-39.34(±4.90)
d8	-32.19(±3.97)	-26.98(±5.34)
d9	-44.17(±6.00)	-35.03(±6.44)
d10	-41.93(±4.18)	-35.01(±4.50)
d11	-36.12(±4.15)	-28.62(±4.49)
Pitolisant	-36.96(±3.48)	-31.47(±3.66)

11

Supplementary Table S7. Spectral and LC-MS Data for Compounds **7** (AZ1147) and **9** (AZ1161B).

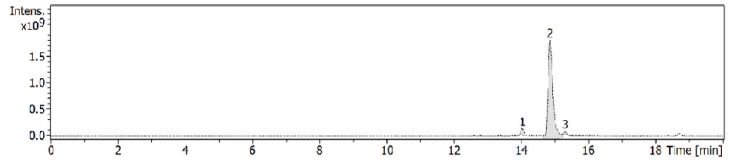
Compound Spectrum List Report

Analysis Info

Analysis Name	D:\Data\Reinheit\2020\new software\03112020\AZ I147_2_1_339 — Blank_1_1_331.d	Acquisition Date	11/3/2020 6:46:57 PM
Method	new2ab2bis100 50 loop pasa wasch5eq3min_339.m	Operator	demo
Sample Name	AZ I147	Instrument	amaZon speed ETD
Comment	Original analysis: 'AZ I147_2_1_339.d', Subtracted analysis: 'Blank_1_1_331.d' (Xpose, 0.5s, 5)		

Acquisition Parameter

Ion Source Type	ESI	Ion Polarity	Negative	Alternating Ion Polarity	on
Mass Range Mode	UltraScan	Scan Begin	80 m/z	Scan End	1200 m/z
Accumulation Time	2000 µs	RF Level	59 %	Trap Drive	44.8
SPS Target Mass	350 m/z	Averages	5 Spectra		



#	RT [min]	Area	S/N	Area Frac. %	Max. m/z
1	14.0	701908160	1937.7	3.4	252.52
2	14.9	19485216768	29146.8	95.3	336.10
3	15.3	264919472	860.2	1.3	350.07

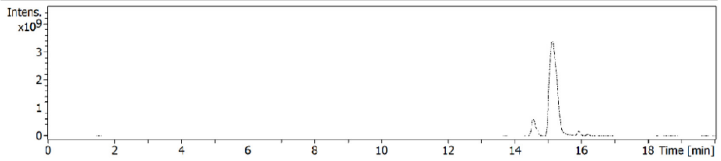
Compound Spectrum List Report

Analysis Info

Analysis Name	D:\Data\Reinheit\2021\23022021\AZ I161B_2_1_106 — Blank_1_1_79.d	Acquisition Date	2/23/2021 6:22:50 PM
Method	ab2bis100 50 loop pasa wasch5eq3min_106.m	Operator	demo
Sample Name	AZ I161B	Instrument	amaZon speed ETD
Comment	Original analysis: 'AZ I161B_2_1_106.d', Subtracted analysis: 'Blank_1_1_79.d' (Xpose, 0.5s, 5)		

Acquisition Parameter

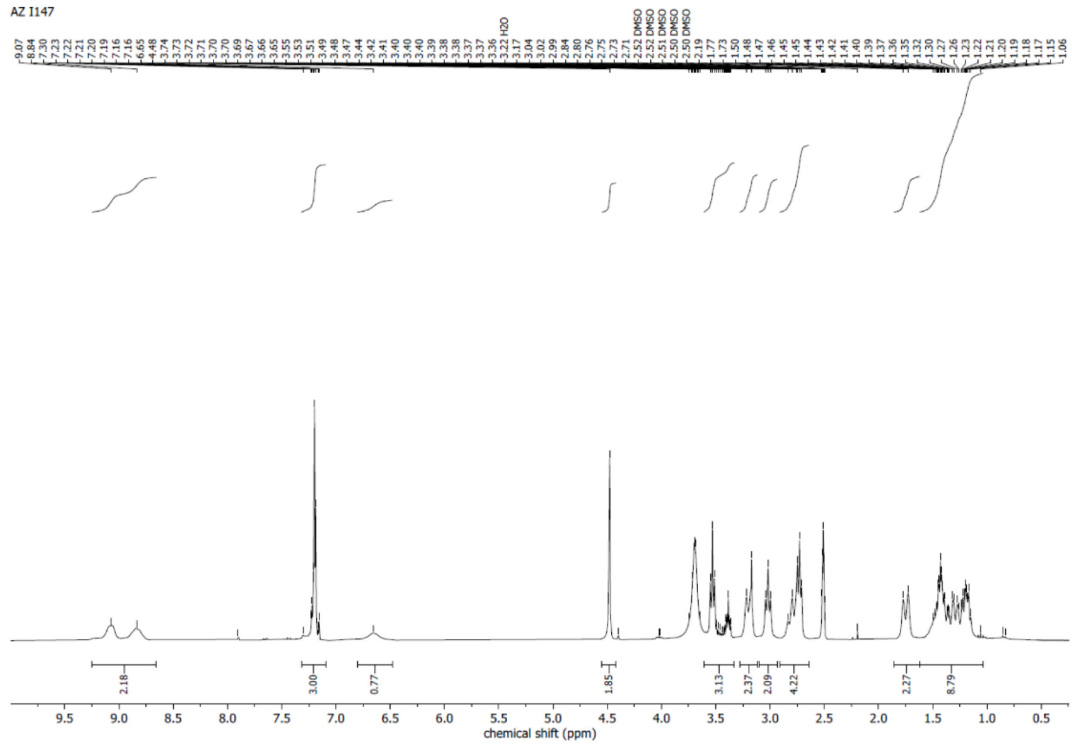
Ion Source Type	ESI	Ion Polarity	Negative	Alternating Ion Polarity	on
Mass Range Mode	UltraScan	Scan Begin	80 m/z	Scan End	1200 m/z
Accumulation Time	2000 µs	RF Level	59 %	Trap Drive	44.8
SPS Target Mass	350 m/z	Averages	5 Spectra		



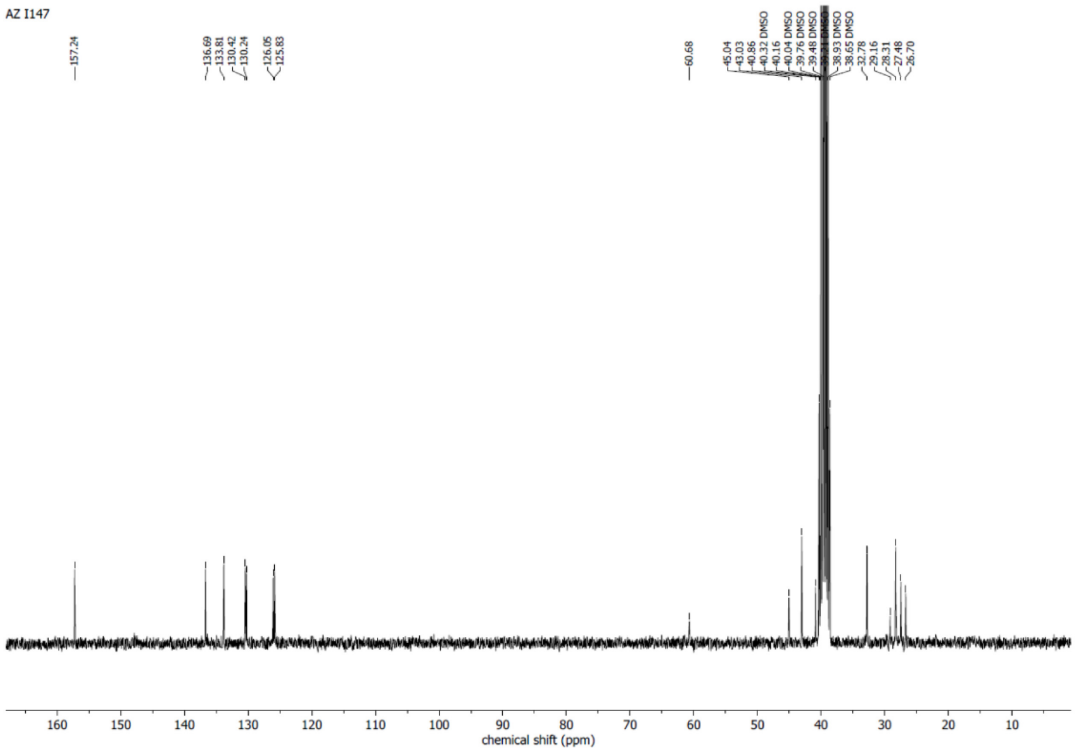
#	RT [min]	Area	S/N	Area Frac. %	Max. m/z
1	14.6	2785553152	7742.3	4.9	366.13
2	15.1	54154067968	59003.3	95.1	350.13

12

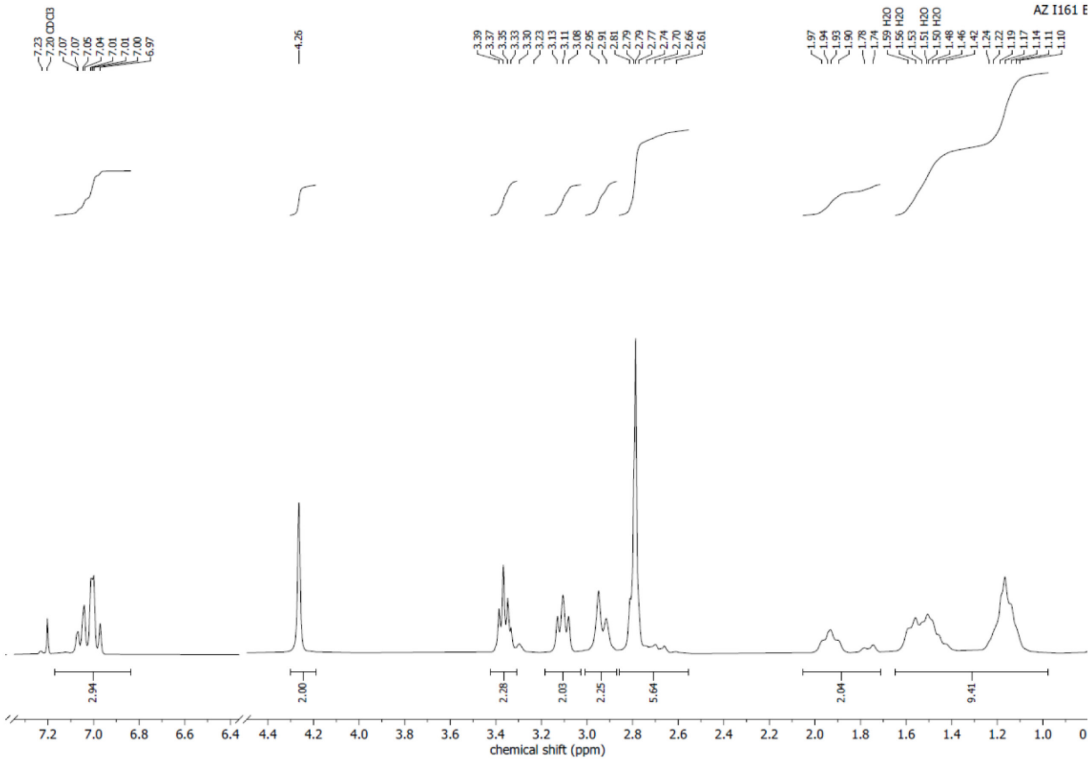
Supplementary Table S8. ^{1}H-NMR and ^{13}C-NMR Spectra for Compounds **7** (AZ1147) and **9** (AZ1161B).



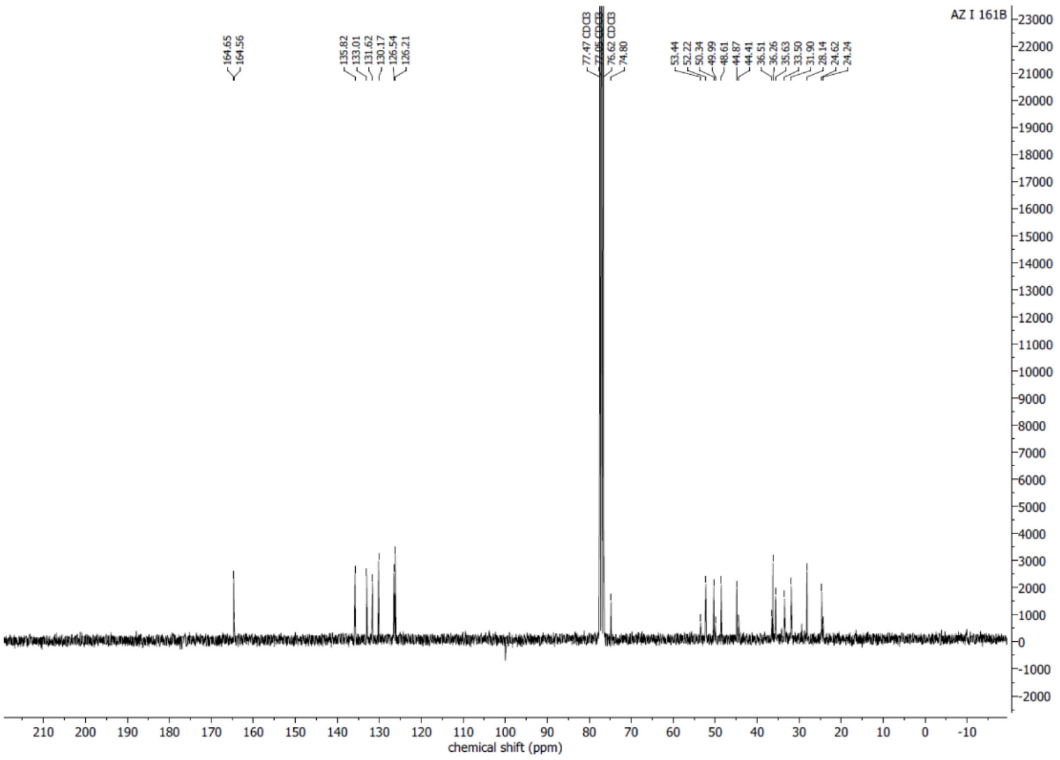
13


AZ I147
157.24
136.69
133.81
130.42
130.24
126.05
125.83
60.68
45.04
43.03
40.86
40.32 DMSO
40.16
40.04 DMSO
39.76 DMSO
39.48 DMSO
38.93 DMSO
38.65 DMSO
32.78
29.16
28.31
27.48
26.70
160
150
140
130
120
110
100
90
80
70
60
50
40
30
20
10
chemical shift (ppm)

14



15


AZ I 161B
164.65
164.56
135.82
133.01
131.62
130.17
126.54
126.21
77.47 CDCl3
76.62 CDCl3
74.80
53.44
52.22
50.34
49.99
48.61
44.87
44.41
36.51
36.26
35.63
33.90
31.66
28.14
24.62
24.24
chemical shift (ppm)

16

3.2 Substituted purines as high-affinity histamine H_3 receptor ligands

Christian Espinosa-Bustos[1], Luisa Leitzbach[2], Tito Añazco[1], María J. Silva[1], Andrea del Campo[1], Alejandro Castro-Alvarez[3], Holger Stark[2] and Cristian O. Salas[4]

[1] Departmento de Farmacia, Facultad de Quimica y de Farmacia, Pontificia Universidad Catolica de Chile, Santiago 7820436, Chile, [2] Institute of Pharmaceutical and Medicinal Chemistry, Heinrich Heine University Düsseldorf, Universitaetsstraße 1, 40225 Duesseldorf, Germany, [3] Laboratorio de Bioproductos Farmaceuticos y Cosmeticos, Centro de Excelencia en Medicina Traslacional, Facultad de Medicina, Universidad de La Frontera, Temuco 4780000, Chile, [4] Departamento de Quimica Organica, Facultad de Quimica y de Farmacia, Pontificia Universidad Catolica de Chile, Santiago 7820436, Chile

Published in: Pharmaceuticals, 2022, 573, Vol. 15, https://doi.org/10.3390/ph15050573

Impact Factor: 4.8 (5 year, 2024)

Contribution: L.L. designed and performed the H_3R binding studies, evaluated the data and reviewed the manuscript.

pharmaceuticals

MDPI

Article

Substituted Purines as High-Affinity Histamine H_3 Receptor Ligands

Christian Espinosa-Bustos [1,*], Luisa Leitzbach [2], Tito Añazco [1], María J. Silva [1], Andrea del Campo [1], Alejandro Castro-Alvarez [3], Holger Stark [2] and Cristian O. Salas [4,*]

1 Departamento de Farmacia, Facultad de Química y de Farmacia, Pontificia Universidad Católica de Chile, Santiago 7820436, Chile; tanazco@uc.cl (T.A.); mjsilva15@uc.cl (M.J.S.); andrea.delcampo@uc.cl (A.d.C.)
2 Institute of Pharmaceutical and Medicinal Chemistry, Heinrich Heine University Düsseldorf, Universitaetsstr. 1, 40225 Duesseldorf, Germany; luisa.leitzbach@hhu.de (L.L.); stark@hhu.de (H.S.)
3 Laboratorio de Bioproductos Farmacéuticos y Cosméticos, Centro de Excelencia en Medicina Traslacional, Facultad de Medicina, Universidad de La Frontera, Temuco 4780000, Chile; qf.alec.astro@gmail.com
4 Departamento de Química Orgánica, Facultad de Química y de Farmacia, Pontificia Universidad Católica de Chile, Santiago 7820436, Chile
* Correspondence: ccespino@uc.cl (C.E.-B.); cosalas@uc.cl (C.O.S.)

Abstract: Continuing with our program to obtain new histamine H_3 receptor (H_3R) ligands, in this work we present the synthesis, H_3R affinity and in silico studies of a series of eight new synthetically accessible purine derivatives. These compounds are designed from the isosteric replacement of the scaffold presented in our previous ligand, pyrrolo[2,3-*d*]pyrimidine ring, by a purine core. This design also considers maintaining the fragment of bipiperidine at C-4 and aromatic rings with electron-withdrawing groups at N-9, as these fragments are part of the proposed pharmacophore. The in vitro screening results show that two purine derivatives, **3d** and **3h**, elicit high affinities to the H_3R (Ki values of 2.91 and 5.51 nM, respectively). Both compounds are more potent than the reference drug pitolisant (K_i 6.09 nM) and show low toxicity with in vitro models (IC_{50} > 30 μM on HEK-293, SH-SY5Y and HepG2 cell lines). Subsequently, binding modes of these ligands are obtained using a model of H_3R by docking and molecular dynamics studies, thus determining the importance of the purine ring in enhancing affinity due to the hydrogen bonding of Tyr374 to the N-7 of this heterocycle. Finally, in silico ADME properties are predicted, which indicate a promising future for these molecules in terms of their physical–chemical properties, absorption, oral bioavailability and penetration in the CNS.

Keywords: histamine H_3 receptor; H_3R ligands; purines; in silico studies; ADME prediction

check for updates

Citation: Espinosa-Bustos, C.; Leitzbach, L.; Añazco, T.; Silva, M.J.; Campo, A.d.; Castro-Alvarez, A.; Stark, H.; Salas, C.O. Substituted Purines as High-Affinity Histamine H_3 Receptor Ligands. *Pharmaceuticals* **2022**, *15*, 573. https://doi.org/10.3390/ph15050573

Academic Editors: Thierry Besson and Pascal Marchand

Received: 7 April 2022
Accepted: 2 May 2022
Published: 4 May 2022

Publisher's Note: MDPI stays neutral with regard to jurisdictional claims in published maps and institutional affiliations.

Copyright: © 2022 by the authors. Licensee MDPI, Basel, Switzerland. This article is an open access article distributed under the terms and conditions of the Creative Commons Attribution (CC BY) license (https://creativecommons.org/licenses/by/4.0/).

1. Introduction

The histamine 3 receptor (H_3R) belongs to a superfamily of G protein-coupled receptors (GPCRs) and has received great interest in recent years due to its distribution, mainly in the central nervous system, acting as an auto- and heteroreceptor and regulating the release of histamine itself and other neurotransmitters, such as acetylcholine and dopamine, among others [1–3]. Antagonists or inverse agonists of this receptor prevent the activation of the H_3R and therefore, due to negative feedback, increase the concentration of histamine and the other neurotransmitters mentioned above. Therefore, these are being investigated as therapeutic alternatives in neurodegenerative diseases such as Alzheimer's and Parkinson's, as well as in disorders such as narcolepsy and attention deficit hyperactivity disorder. In present times, the H_3R inverse agonist pitolisant (Wakix, Figure 1) is the only drug approved by the EMA for the treatment of narcolepsy with or without cataplexy and for obstructive sleep apnea, which has increased interest in the clinical applications of novel H_3R inverse agonists or antagonists [4,5].

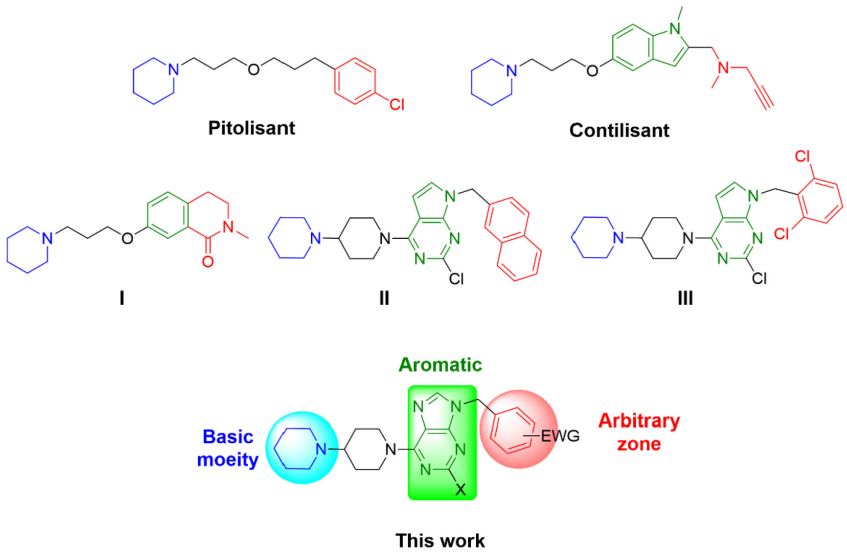


Figure 1. Chemical structures of H_3R ligands containing piperidine moiety, and the proposed structures in this work.

In this regard, many series of compounds with great structural diversity have been synthesized [6]. However, there is a common pharmacophore consisting of a basic moiety, separated by a linker (often saturated alkyl chains) from an aromatic zone attached to an arbitrary scaffold that is generally hydrophobic [7]. First generation H_3R ligands usually contain imidazole-based scaffolds, with regard to histamine structure [8]. Otherwise, the second generation of H_3R ligands, the imidazole heterocycle, is replaced by piperidine moieties [9].

In recent years, several H_3R ligands that contain the piperidine heterocycle in their structure have been reported. Contilisant (Figure 1) was reported to display H_3R antagonism as well as cholinesterase and MAO-B inhibition [10]. Zhang et al. published a series of lactams that contain several basic scaffolds in their structure, in which compound **I** shows great affinity for the H_3R and selectivity against the H_1R [11]. On the other hand, our research group has reported several pyrrolo[2,3-*d*]pyrimidines substituted in position C-4 with the bipiperidine moiety, obtaining affinities for H_3R in the nanomolar range and highlighting compounds **II** and **III**, which show K_i values of 126 and 6.0 nM, respectively [12,13]. Our previous antecedents suggest that derivatives with a higher affinity for H_3Rs are obtained using bipiperidine as a basic moiety, whereas in the arbitrary zone, the best results have used aromatic rings with electron-withdrawing groups (EWG).

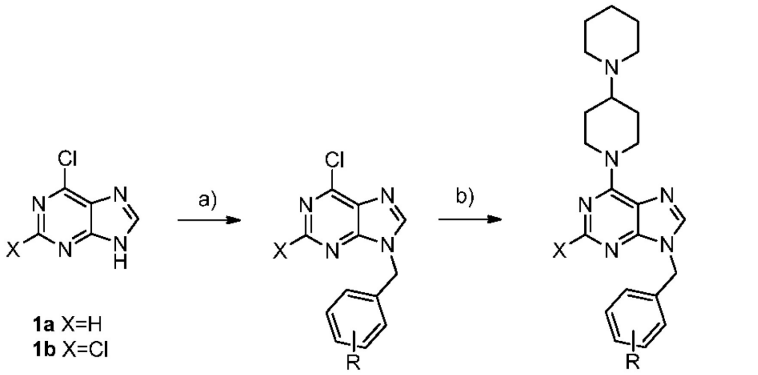
In order to improve affinity to the H_3R, in this work we propose the use of purine heterocycle as a pyrrolo[2,3-*d*]pyrimidine bioisostere while maintaining the aforementioned substitution patterns present in **III** (Figure 1). Purine heterocycle is selected because this scaffold is part of several compounds with diverse biological activities [14–17]. Moreover, this heterocycle significantly improves pharmacological activities and physicochemical properties [18]. In addition, the effects of EWG on the aromatic ring at N-9 are considered as well as the replacement of a hydrogen atom at the C-2 position by a chlorine atom. Later, the synthesized purine derivatives are evaluated for their affinity to the human H_3R and the most promising compounds are evaluated for their cytotoxicity on cell lines. Finally, docking and molecular dynamic studies are carried out to understand the effects of chemical modifications on affinity to the H_3R. Considering the great need to find new therapeutic alternatives for the treatment of neurodegenerative diseases, this work contributes to medicinal chemistry through the discovery of easily accessible compounds with high

affinity to the H_3R, with low toxicity in the cell lines evaluated and with a promising ADME profile.

2. Results and Discussion

2.1. Chemistry

The general synthetic procedures to obtain 6-([1,4′-bipiperidin]-1′-yl)-9-aryl-9*H*-purines **3a–d** and 6-([1,4′-bipiperidin]-1′-yl)-9-aryl-2-halo-9*H*-purines **3e–h** are summarized in Scheme 1. The derivatives **2a–h** were synthesized by nucleophilic substitution among the commercially available 6-chloro-9*H*-purine derivatives **1a–b** and the respective benzyl halide, in low to moderate yields. In this first step, a mixture of N-9 and N-7-alkylated purines were obtained in a proportion of 4:1, respectively. In a second step, a nucleophilic substitution (S_NAr) reaction was achieved with N-9 substituted purines, using bipiperidine, providing the target compounds **3a–h**, with good yields (>60%). The chemical structures of the purine derivatives were established based on their spectral properties (IR, ^1H NMR, ^{13}C NMR and HRMS, see experimental section and Supplementary Materials).



Scheme 1. Synthesis of purine derivatives **3a–h**. Reagents and conditions: (a) Benzyl halides, K_2CO_3, CH_3CN, reflux, 2–4 h, 19–48%. (b) Bipiperidine, DIPEA, ethanol, reflux, 1–2 h, 41–66%.

2.2. H_3R Affinity

Compounds **3a–h** were screened for their affinities to the human H_3R by performing competitive radioligand binding assays using [^{3}H]N^{α}-methylhistamine as a radioligand (Table 1). All compounds presented K_i values in the nanomolar range, confirming that the purine heterocycle provides derivatives with a high affinity to the receptor and that some substitution patterns are important in structure–activity relationships. Firstly, the presence of a chlorine atom at the C-2 position maintains or slightly decreases affinity to H_3R, as observed in **3a–d** versus **3e–h** compounds. In the arbitrary zone, the presence of the *p*-fluorophenyl portion yields the derivatives with the lowest affinity (**3a** and **3e**), and this is an interesting result that correlates with our previous works [13]. Finally, the substitution in N-9 with 2,6-dichlorobenzyl provides the most active derivatives of this series, **3d** and **3h**, which present K_i values of 2.91 nM and 5.51 nM, respectively, being even better than those presented by pitolisant (Figure 2). In this case, a purine scaffold appears

to increase affinity to H_3R compared to derivatives with pyrrolo[2,3-*d*]pyrimidine [13], but this observation is not decisive, since this tendency is not observed in other derivatives.

Table 1. Affinities to the H_3R of compounds **3a-h** and reference ligand pitolisant.

Compound	Substitution Pattern		K_i (nM) [a] [95% CI nM]
	X	R	
3a	H	4-F	105 [79.6–140]
3b	H	4-Cl	39.4 [8.78–177]
3c	H	4-CN	28.8 [9.90–83.7]
3d	H	2,6-diCl	2.91[1.31–6.44]
3e	Cl	4-F	94.6 [47.5–189]
3f	Cl	4-Cl	44.6 [14.2–141]
3g	Cl	4-CN	77.8 [29.2–207]
3h	Cl	2,6-diCl	5.51 [1.17–25.9]
Pitolisant			6.09 [2.28–16.3]

[a] K_i values were determined by [^{3}H]N^{α}-methylhistamine binding assay at the human histamine H_3R. Values represent affinity as mean values and as corresponding confidence intervals (CI 95%) of at least three independent experiments in duplicate.

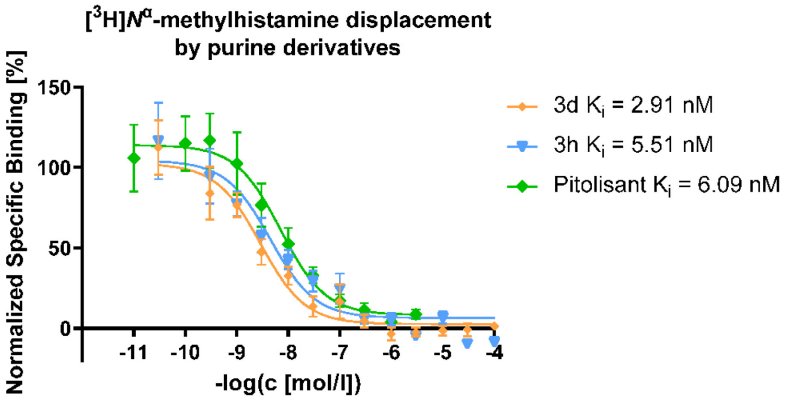


Figure 2. Displacement of [^{3}H]N^{α}-methylhistamine (c = 2 nM, K_d = 3.08 nM by **3d** (K_i = 2.91 nM), **3h** (K_i = 5.51 nM) and pitolisant (K_i = 6.09 nM). The assay was performed on HEK-293 cell membranes stably expressing the human H_3R. Data are expressed as mean values ± SEM (at least three independent experiments, each performed in duplicate).

2.3. Cytotoxicity Assays

The potential general nephrotoxic, neurotoxic and hepatotoxic effects of selected H_3R ligands **3d** and **3h** were investigated to determine their influence on the viability of normal HEK-293, neuroblastoma SH-SY5Y and hepatoma HepG2 cell lines by a colorimetric MTT reduction assay (Table 2). Tested compounds showed similar and weak influences on the viability of all examined cell lines, which may indicate that both compounds would not be potentially cytotoxic in future in vivo studies.

Table 2. Cytotoxicity of selected compounds **3d** and **3h**.

Cell line	IC_{50} (μM) [a]	
	3d	3h
HEK-293	69.14 ± 13.95	54.31 ± 3.54
SH-SY5Y	>100	32.38 ± 4.75
HepG2	57.57 ± 12.02	33.76 ± 4.29

[a] IC_{50} values were determined in three independent experiments in triplicate in the range 0.1 to 100 μM.

2.4. Docking Studies

Although the crystal structure of the H_3R receptor is not yet available, the inactive H_3R model was downloaded from the GPCRdb website (https://gpcrdb.org, accessed on 1 November 2021), which comes from homology modelling using the crystal of the histamine H_1 receptor (PDB ID: 3RZE) as a template [19]. Subsequently, an energetic minimization of the residues was performed to adjust the dihedral angles of each amino acid. According to the literature, the critical residues of the orthosteric binding pocket are Asp114 and Glu206. Both residues assist in recognizing the endogenous ligand (Figure S1), forming salt bridges of the carboxylates of these residues with the cationic amines of the synthesized ligands [20].

Molecular docking studies were carried out to understand the binding mode of the most active compound, **3d**, within the H_3R binding site. A standard protocol was used to perform induced-fit docking, which generated four binding poses for **3d**. The four best poses were analyzed based on their docking scores and polar and non-polar interactions. The best poses showed docking scores of −10.23 kcal/mol with interaction with Asp114 and of −9.18 kcal/mol with Glu206 (Figure S2). Therefore, the lowest energy pose was selected, and the other synthesized compounds were screened. Once the pose was obtained for each ligand, an MM-GBSA calculation was performed, energetically minimizing the residues composing the binding site at about 6 Å from the center of mass of the ligands. Finally, the binding free energy was calculated for each of them (Table 3). With an R^2 of 0.71, the correlation between the estimated affinity energy and the experimental data (-logK_i) was reached, indicating that the resulting posture is the best representative of biological activity and affinity with this receptor (Figure 3).

Table 3. Biological activity in K_i values and binding free energy calculated with MM-GBSA.

	Biological Activity		Binding Free Energy
	K_i (nM)	−logK_i	kcal/mol
3a	105.0	6.98	−59.21
3b	39.4	7.40	−57.72
3c	28.8	7.54	−64.10
3d	2.9	8.54	−76.98
3e	94.5	7.02	−66.08
3f	44.6	7.35	−64.97
3g	77.8	7.11	−64.56
3h	5.5	8.26	−75.10

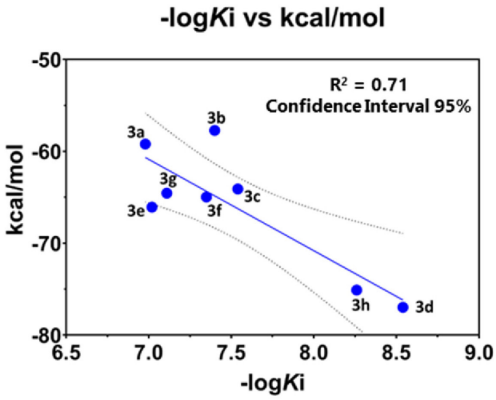


Figure 3. Correlation graph for binding free energy predicted activity (kcal/mol) and -logK_i values.

Ligand–receptor interactions can be divided into three regions constituting the synthesized ligands (Figure 4), where the basic moiety interacts firstly with a hydrophobic pocket

(hydrophobic pocket 1, HP1) composed of three aromatic rings of residues Tyr91, Phe398 and Trp402. In addition, there is an electrostatic interaction between the cationic amine of piperidine with Asp114. Next, the aromatic region of purine forms a π-stacking interaction with Tyr115 and a hydrogen bond with the N-7 of purine core with the hydroxyl of Tyr374. Finally, the halogenated aromatic region interacts with a second hydrophobic pocket (HP2) consisting of Tyr374, Trp371, Phe207 and Phe367. This region interacts favorably with the electron-deficient ring of the synthesized ligands, and halogen substitution has a direct impact on the favorable hydrophobic interaction, with the *para*-position being the least favorable due to a steric hindrance it causes with Phe207, which coincides with substitutions in the *ortho*-position being the most active, as is the case for compounds **3d** and **3h**.

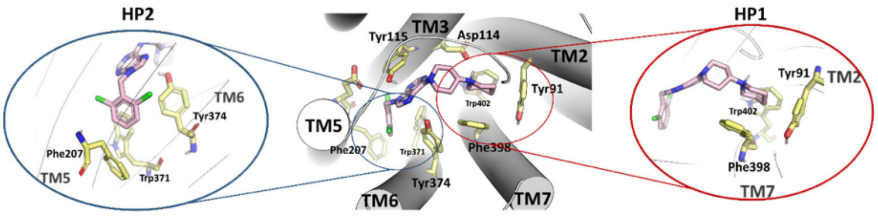


Figure 4. Binding mode of **3d** in the H_3R model.

The same protocol was repeated to obtain the best poses with pitolisant, considering the interaction of protonated piperidine with Asp114 and Glu206. However, the difference in affinity energy between both poses was not so vast (Figure 5). Additionally, apart from an electrostatic interaction of the carboxylate with Asp114 or Glu206 (regardless of what the case may be), the ether oxygen interacts, forming a hydrogen bond with Tyr374, thus highlighting the importance of this residue for the affinity for the binding site.

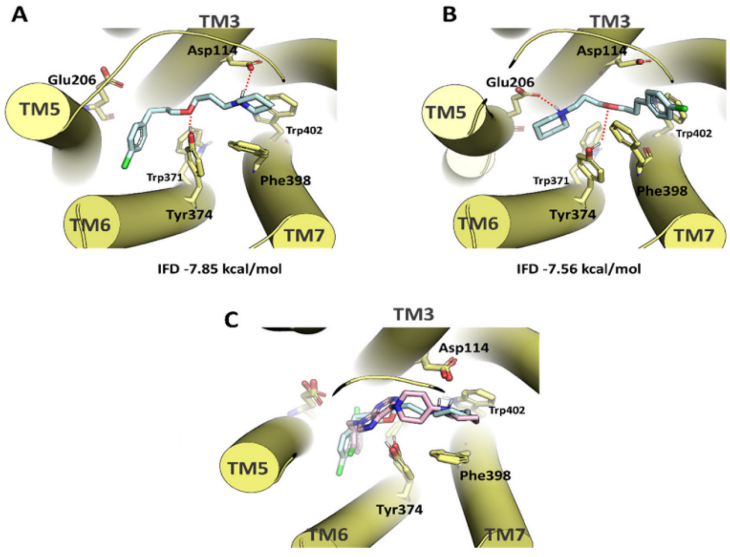


Figure 5. (**A**) The best pose of pitolisant interacting with Asp114; (**B**) The best pose of pitolisant interacting with Glu206; (**C**) The overlap between the best pose achieved for **3d** and pitolisant.

2.5. Molecular Dynamic Studies

To understand the affinity differences between the most active compound and the less active compound, molecular dynamics of 50 ns were performed with the ligand–receptor

complexes of compound **3d** (most active compound) and **3a** (least active compound). We considered the phospholipids that constitute the lipid membrane and a solvated system (water), and we obtained a transmembrane system.

The trajectories were analyzed with the Simulation Interaction Diagram module of the Schrodinger Suite. The ligand–protein interactions revealed the residues that persist the most during molecular dynamics. The **H_3R–3d** complex interacts with Asp114 with almost 99% during the whole trajectory, with an average distance of 2.06 Å between the amine proton of the piperidine and the carboxylate, whereas **3a** has an interaction with 88% of the molecular dynamics with an average distance of 2.22 Å (Figure 6). Another important aspect is the presence of hydrogen bonding of Tyr374 with the N-7 of purine in compound **3d** with a presence of 36%, which, in turn, caused an enhanced π-stacking interaction with Trp371 with 45% during molecular dynamics.

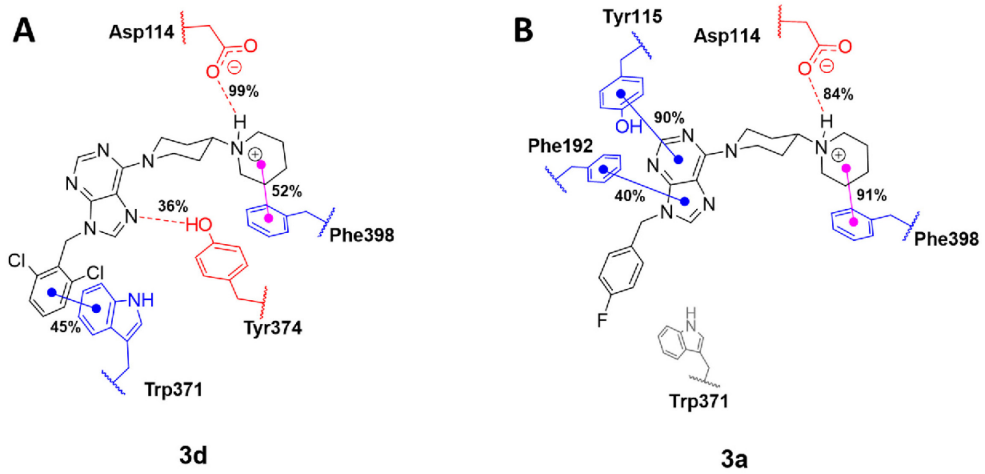


Figure 6. Binding modes of **3d** (**A**) and **3a** (**B**) during the 50 ns MD simulations at H_3R. Red dotted lines represent hydrogen bonds, blue lines represent hydrophobic interactions and violet lines represent π-cation interactions. Percentages represent specific interactions during the simulation.

The molecular dynamics of the **H_3R–3a** system demonstrates the importance of the halogen atom in the *para* position of the aromatic ring and its low biological activity, which responds to the steric hindrance generated by the halogen with the Phe207 residue, causing a very poor interaction with Tyr374 and Trp371 but improving hydrophobic interactions with Tyr115 and Phe192.

Considering the molecular dynamics results, both systems, **H_3R–3d** and **H_3R–3a**, reveal positive interactions at the binding site. However, **3d** interacts preferentially with TM6 domain residues (Trp371 and Tyr374). In contrast, **3a** interacts with Tyr115, a residue belonging to TM3, and with Phe192, an amino acid residue belonging to the extracellular loop (Figure 6). Therefore, the inverse agonist action of the most active compound (**3d**) may be explained by the interaction between the TM3 (Asp114) and TM6 (Trp371 and Tyr374) domains, similar to that which occurs with other synthesized ligands that have a similar mechanism of action [21,22].

2.6. In Silico ADME and Drug-Likeness Properties

Employing the SwissADME online webserver [23], compounds **3a–h** were analyzed to predict their physicochemical properties, in relation to absorption, bioavailability and blood–brain barrier (BBB) permeability. Lipinski's rule establishes that an orally bioavailable drug should not violate the following criteria: ≤5 hydrogen bond donors (HBD); ≤10 hydrogen bond acceptors (HBA); a MW of <500 g/mol; and a log *p* value of <5 [24]. Moreover,

Veber et al. described the magnitude of PSA and the number of rotatable bonds as criteria to rate oral bioavailability. Veber's rule states that, to be orally bioavailable, a molecule should have either a PSA $\leq$ 140 Å and $\leq$10 rotatable bonds (NRB) or $\leq$12 HBD and HBA in total and $\leq$10 rotatable bonds [25]. As shown in Table 4, compounds **3a–h** accomplished the drug-likeness criteria described by Lipinski and Veber; hence, they are expected to have good oral bioavailability. Moreover, according to the brain or intestinal estimated permeation method (BOILED-Egg), all compounds should have good gastrointestinal absorption and should cross the blood–brain barrier [26], and this is an important result considering the CNS distribution of the H_3R. Furthermore, the SwissADME server resolved that compounds **3a–h** should have no pan-assay interference liability (PAINS). In addition, the SwissADME server indicated that the bioavailability radar chart for **3d** was within the desired range (pink region) for six parameters used for oral absorption prediction: flexibility (FLEX), lipophilicity (LIPO), solubility (INSOLU), size and polarity (POLAR) and saturation (INSATU) (Figure 7), which can foresee their predicted good oral bioavailability.

Table 4. In silico ADME and drug-likeness properties of compounds **3a–h**.

Compound	MW (g/mol)	NRB	HBA	HBD	TPSA	cLogP	GI Absorption	BBB Permeant
3a	394.49	4	5	0	50.08	3.26	High	Yes
3b	410.94	4	4	0	50.08	3.48	High	Yes
3c	401.51	4	5	0	73.87	2.76	High	Yes
3d	445.39	4	4	0	50.08	3.91	High	Yes
3e	428.93	4	5	0	50.08	3.82	High	Yes
3f	445.39	4	4	0	50.08	4.04	High	Yes
3g	435.95	4	5	0	73.87	3.30	High	Yes
3h	479.83	4	4	0	50.08	4.58	High	Yes

MW: molecular weight; NRB: number of rotatable bonds; HBA: number of hydrogen bond acceptors; HBD: number of hydrogen bond donors; cLogP: consensus Log *p* value; TPSA: topological polar surface.

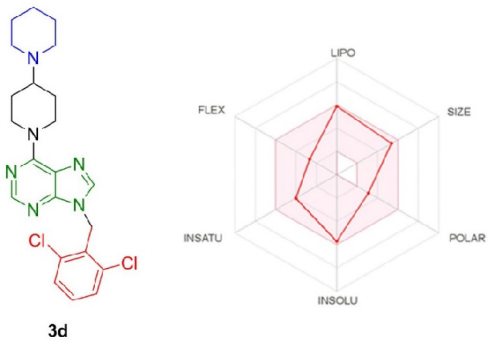


Figure 7. The bioavailability radar chart of **3d**. The pink area indicates the range of the values of the optimal oral bioavailability property, and the predicted properties are shown as red lines. The radar was generated by SwissADME (http://www.swissadme.ch/index.php, accessed on 30 March 2021).

3. Materials and Methods

3.1. Chemistry

Melting points were determined on a Thermogeräte Kofler apparatus (Reichert, Werke A.G., Wien, Austria) and were uncorrected. All reagents were purchased from Sigma-Aldrich (St. Louis, MO, USA) unless otherwise specified. The NMR spectra were recorded at NMR Bruker AV 400 or 200 MHz. Chemical shifts were given in parts per million relative to TMS [^{1}H and ^{13}C, δ ($SiMe_4$) = 0]. Most NMR assignments were supported by additional 2D experiments. HRMS-ESI-MS experiments were carried out using a high-resolution mass spectrometer, Exactive™ Plus Orbitrap, ThermoFisher Scientific (Bremen, Germany). Thin layer chromatography (TLC) was performed using Merck GF-254 type 60 silica gel. Column

chromatography was carried out using Merck silica gel 60 (70–230 mesh). Compound purity ≥ 95% was determined by HPLC Shimadzu 10-ADvp (Shimadzu, Kioto, Japón) with a C18 column (Kinetex 5u XB-C18), an acetonitrile/water (0.1% formic acid) mobile phase and a flow rate of 1 mL/min for 15 min.

3.1.1. General Procedure for the Synthesis of **2a–h** Derivatives

A mixture of purines **1a-b** (1.0 mmol), the respective benzyl halide (1.2 mmol) and potassium carbonate (3.0 mmol) in acetonitrile (5 mL) were stirred for 3 h, and then the mixture was filtered and evaporated under vacuum. The products were separated by flash chromatography on silica gel eluted with dichloromethane.

6-Chloro-9-(4-fluorobenzyl)-9*H*-purine **2a**. White solid, yield 37%, m.p. 135–138 °C. (lit. 129–131 °C) [27]. ^{1}H NMR (400 MHz, $CDCl_3$) δ 8.95 (s, 1H), 8.30 (s, 1H), 7.51 (dd, *J* = 8.5, 5.2 Hz, 2H), 7.23 (t, *J* = 8.5 Hz, 2H), 5.61 (s, 2H). ^{13}C NMR (101 MHz, $CDCl_3$) δ 164.10–161.63 (d, $^1J_{CF}$ = 248.6 Hz), 152.23, 151.77, 151.20, 144.78, 131.49, 130.44–130.41 (d, $^4J_{CF}$ = 3.4 Hz), 129.97–129.89 (d, $^3J_{CF}$ = 8.4 Hz), 116.40–116.18 (d, $^2J_{CF}$ = 21.8 Hz), 47.24. ^{19}F NMR (376 MHz, $CDCl_3$) δ −112.32 (1F).

6-Chloro-9-(4-chlorobenzyl)-9*H*-purine **2b**. White solid, yield 34%, m.p. 134–136 °C. (lit. 130–133 °C) [27]. ^{1}H NMR (200 MHz, $CDCl_3$) δ 8.77 (s, 1H), 8.14 (s, 1H), 7.30 (q, *J* = 8.5 Hz, 4H), 5.43 (s, 2H). ^{13}C NMR (50 MHz, $CDCl_3$) δ 152.27, 151.74, 151.23, 144.77, 134.94, 133.00, 131.42, 129.46 (2C), 129.32 (2C), 47.25.

4-((6-Chloro-9*H*-purin-9-yl)methyl)benzonitrile **2c**. White solid, yield 38%, m.p. 205–207 °C. ^{1}H NMR (200 MHz, $CDCl_3$) δ 8.77 (s, 1H), 8.18 (s, 1H), 7.67 (d, *J* = 7.8 Hz, 2H), 7.42 (d, *J* = 8.0 Hz, 2H), 5.54 (s, 2H). ^{13}C NMR (50 MHz, $CDCl_3$) δ 152.44, 151.75, 151.51, 144.71, 139.66, 133.02 (2C), 131.48, 128.41 (2C), 117.97, 112.95, 47.34.

6-Chloro-9-(2,6-dichlorobenzyl)-9*H*-purine **2d**. White solid, yield 36%, m.p. 188–191 °C. (lit. 186–188 °C) [27]. ^{1}H NMR (400 MHz, $CDCl_3$) δ 8.79 (s, 1H), 7.93 (s, 1H), 7.43 (d, *J* = 8.2 Hz, 2H), 7.38–7.29 (m, 1H), 5.73 (s, 2H). ^{13}C NMR (101 MHz, $CDCl_3$) δ 152.11, 151.81, 151.06, 144.31, 136.78, 131.37, 131.26, 129.87, 129.06 (3C), 43.13.

2,6-Dichloro-9-(4-fluorobenzyl)-9*H*-purine **2e**. White solid, yield 43%, m.p. 133–136 °C. (lit. 120–122 °C) [27]. ^{1}H NMR (200 MHz, $CDCl_3$) δ 8.07 (s, 1H), 7.33 (dd, *J* = 8.3, 5.2 Hz, 2H), 7.08 (t, *J* = 8.4 Hz, 2H), 5.39 (s, 2H). ^{13}C NMR (50 MHz, $CDCl_3$) δ 165.44–160.49 (d, $^1J_{CF}$ = 249.0 Hz), 153.26, 153.06, 151.96, 145.35, 130.66, 130.16–129.99 (d, $^3J_{CF}$ = 8.4 Hz, 2C), 129.93–129.87 (d, $^4J_{CF}$ = 3.4 Hz), 116.63–116.20 (d, $^2J_{CF}$ = 21.9 Hz, 2C), 47.36.

2,6-Dichloro-9-(4-chlorobenzyl)-9*H*-purine **2f**. White solid, yield 48%, m.p. 158–160 °C (lit. 162–164 °C) [27]. ^{1}H NMR (200 MHz, $CDCl_3$) δ 8.08 (s, 1H), 7.36 (d, *J* = 8.5 Hz, 2H), 7.26 (d, *J* = 8.5 Hz, 2H), 5.39 (s, 2H). ^{13}C NMR (50 MHz, $CDCl_3$) δ 153.31, 153.06, 152.00, 145.31, 135.17, 132.49, 130.62, 129.58 (2C), 129.43 (2C), 47.35.

4-((2,6-Dichloro-9*H*-purin-9-yl)methyl)benzonitrile **2g**. White solid, yield 19%, m.p. 199–202 °C. ^{1}H NMR (200 MHz, $CDCl_3$) δ 8.12 (s, 1H), 7.70 (d, *J* = 7.9 Hz, 2H), 7.42 (d, *J* = 8.0 Hz, 2H), 5.50 (s, 2H). ^{13}C NMR (50 MHz, $CDCl_3$) δ 153.59, 153.05, 152.36, 145.18, 139.11, 133.13 (2C), 130.65, 128.47 (2C), 117.88, 113.21, 47.39.

2,6-Dichloro-9-(2,6-dichlorobenzyl)-9*H*-purine **2h**. White solid, yield 22%, m.p. 183–186 °C. ^{1}H NMR (200 MHz, $CDCl_3$) δ 7.89 (s, 1H), 7.54–7.30 (m, 3H), 5.70 (s, 2H). ^{13}C NMR (50 MHz, $CDCl_3$) δ 153.11, 151.77, 144.82, 136.79, 131.56 (2C), 130.43, 129.37, 129.10 (3C), 43.34.

3.1.2. General Synthetic Procedure to Obtain Substituted Purines **3a–h**

The *N*-benzyl-purines **2a–h** (1.0 mmol), 4-piperidinopiperidine (2.0 mmol), triethylamine (3.0 mmol) and ethanol (5 mL) were added to a microwave reaction flask, and the reaction mixture was irradiated for 15 min at 80 °C. Then, the solvent was evaporated under vacuum, and the crude product was purified by column chromatographic on silica gel using a (8:2) chloroform/methanol mixture.

6-([1,4′-Bipiperidin]-1′-yl)-9-(4-fluorobenzyl)-9*H*-purine **3a**. White solid, yield 49%, m.p. 138–139 °C. ^{1}H NMR (400 MHz, $CDCl_3$) δ 8.57 (s, 1H), 7.90 (s, 1H), 7.47 (t, *J* = 6.4 Hz, 2H), 7.23 (t, *J* = 8.4 Hz, 2H), 5.76 (bs, 2H), 5.53 (s, 2H), 3.25 (t, *J* = 12.3 Hz, 2H), 2.93 (t,

J = 10.9 Hz, 1H), 2.81 (s, 4H), 2.25 (d, *J* = 12.1 Hz, 2H), 1.95–1.77 (m, 6H), 1.67 (bs, 2H). ^{13}C NMR (101 MHz, $CDCl_3$) δ 163.81–161.35 (d, $^1J_{CF}$ = 247.2 Hz), 153.75, 152.71, 150.94, 137.88, 131.73–131.69 (d, $^4J_{CF}$ = 3.2 Hz), 129.55–129.47 (d, $^3J_{CF}$ = 8.3 Hz), 119.79, 116.05–115.83 (d, $^2J_{CF}$ = 21.7 Hz), 63.03, 50.12, 46.33, 44.91, 27.91, 25.83, 24.43. ^{19}F NMR (376 MHz, $CDCl_3$) δ −113.57 (1F). HRMS calcd. for ($C_{22}H_{27}FN_6$ [M + H]$^+$): 395.2354. Found: 395.2350. HPLC purity: 99.97%.

6-([1,4′-Bipiperidin]-1′-yl)-9-(4-chlorobenzyl)-9*H*-purine **3b**. White solid, yield 55%, m.p. 156–157 °C. ^{1}H NMR (400 MHz, $CDCl_3$) δ 8.30 (s, 1H), 7.65 (s, 1H), 7.19 (d, *J* = 29.2 Hz, 4H), 5.48 (s, 2H), 5.26 (s, 2H), 2.98 (b.s, 2H), 2.52 (b.s, 5H), 1.96 (b.s, 2H), 1.73–1.40 (m, 8H). ^{13}C NMR (101 MHz, $CDCl_3$) δ 153.73, 152.72, 150.92, 137.83, 134.39, 129.13 (2C), 128.98 (2C), 119.73, 62.92, 50.12, 46.31, 44.99, 27.99, 25.99, 24.52. HRMS calcd. for ($C_{22}H_{27}ClN_6$ [M + H]$^+$): 411.2058. Found: 411.2057. HPLC purity: 99.39%.

4-((6-([1,4′-Bipiperidin]-1′-yl)-9*H*-purin-9-yl)methyl)benzonitrile **3c**. White solid, yield 41%, m.p. 136–138 °C. ^{1}H NMR (400 MHz, $CDCl_3$) δ 8.29 (s, 1H), 7.71 (s, 1H), 7.58 (d, *J* = 8.3 Hz, 2H), 7.30 (d, *J* = 8.2 Hz, 2H), 5.50 (s, 2H), 5.38 (s, 2H), 3.01 (t, *J* = 11.9 Hz, 2H), 2.63 (ddd, *J* = 11.4, 7.5, 3.4 Hz, 1H), 2.58–2.45 (m, 4H), 1.98 (d, *J* = 12.6 Hz, 2H), 1.64–1.50 (m, 6H), 1.41 (d, *J* = 5.1 Hz, 2H). ^{13}C NMR (101 MHz, $CDCl_3$) δ 153.74, 152.86, 150.88, 141.19, 137.72, 132.74 (2C), 127.99 (2C), 119.69, 118.28, 112.17, 62.82 (2C), 50.14 (2C), 46.43 (2C), 44.96, 28.04, 26.03 (2C), 24.53. HRMS calcd. for ($C_{23}H_{27}N_7$ [M + H]$^+$): 402.2401. Found: 402.2398. HPLC purity: 96.83%.

6-([1,4′-Bipiperidin]-1′-yl)-9-(2,6-dichlorobenzyl)-9*H*-purine **3d**. White solid, yield 59%, m.p. 172–173 °C. ^{1}H NMR (400 MHz, $CDCl_3$) δ 8.23 (s, 1H), 7.30 (s, 1H), 7.23 (s, 1H), 7.17–7.09 (m, 1H), 5.45 (s, 2H), 5.37 (s, 2H), 2.85 (t, *J* = 12.4 Hz, 2H), 2.51 (t, *J* = 11.4 Hz, 1H), 2.40 (s, 4H), 1.83 (d, *J* = 12.3 Hz, 2H), 1.54–1.40 (m, 7H), 1.28 (d, *J* = 4.4 Hz, 2H). ^{13}C NMR (101 MHz, $CDCl_3$) δ 153.71, 152.53, 150.93, 137.05, 136.85, 130.85, 130.82, 128.84 (2C), 119.52, 62.98 (2C), 50.11 (2C), 44.94, 42.47 (2C), 27.97, 26.01 (2C), 24.54. HRMS calcd. for ($C_{22}H_{26}Cl_2N_6$ [M + H]$^+$): 445.1669. Found: 445.1668. HPLC purity: 95.68%.

6-([1,4′-Bipiperidin]-1′-yl)-2-chloro-9-(4-fluorobenzyl)-9*H*-purine **3e**. White solid, yield 58%, m.p. 140–142 °C. ^{1}H NMR (400 MHz, $CDCl_3$) δ 7.82 (s, 1H), 7.47 (dd, *J* = 8.3, 5.5 Hz, 2H), 7.23 (t, *J* = 8.5 Hz, 2H), 5.65 (bs, 2H), 5.47 (s, 2H), 3.24 (s, 2H), 2.90–2.81 (m, 1H), 2.75 (s, 4H), 2.20 (d, *J* = 12.4 Hz, 2H), 1.90–1.71 (m, 6H), 1.65 (d, *J* = 4.6 Hz, 2H). ^{13}C NMR (101 MHz, $CDCl_3$) δ 163.86–161.40 (d, $^1J_{CF}$ = 247.6 Hz), 154.19, 153.82, 152.14, 138.04, 131.35–131.32 (d, $^4J_{CF}$ = 3.3 Hz), 129.78–129.69 (d, $^3J_{CF}$ = 8.3 Hz), 118.54, 116.09–115.88 (d, $^2J_{CF}$ = 21.7 Hz), 62.63, 50.15, 46.39, 44.79, 28.04, 26.12, 24.59. ^{19}F NMR (376 MHz, $CDCl_3$) δ −113.25 (1F). HRMS calcd. for ($C_{22}H_{26}ClFN_6$ [M + H]$^+$): 429.1964. Found: 429.1963. HPLC purity: 98.26%.

6-([1,4′-Bipiperidin]-1′-yl)-2-chloro-9-(4-chlorobenzyl)-9*H*-purine **3f**. White solid, yield 59%, m.p. 139–141 °C. ^{1}H NMR (400 MHz, $CDCl_3$) δ 7.60 (s, 1H), 7.28 (d, *J* = 8.4 Hz, 2H), 7.18 (d, *J* = 8.4 Hz, 2H), 5.42 (s, 2H), 5.25 (s, 2H), 3.01 (s, 2H), 2.63 (ddd, *J* = 11.5, 8.3, 3.5 Hz, 1H), 2.57–2.46 (m, 4H), 1.97 (d, *J* = 12.6 Hz, 2H), 1.67–1.49 (m, 6H), 1.42 (d, *J* = 5.0 Hz, 2H). ^{13}C NMR (101 MHz, $CDCl_3$) δ 154.22, 153.81, 152.14, 138.04, 134.37, 134.00, 129.20 (2C), 129.19 (2C), 118.52, 62.62 (2C), 50.14 (2C), 46.38 (2C), 44.85, 28.03, 26.11 (2C), 24.58. HRMS calcd. for ($C_{22}H_{26}Cl_2N_6$ [M + H]$^+$): 445.1669. Found: 445.1669. HPLC purity: 98.96%.

4-((6-([1,4′-Bipiperidin]-1′-yl)-2-chloro-9*H*-purin-9-yl)methyl)benzonitrile **3g**. White solid, yield 66%, m.p. 187–188 °C. ^{1}H NMR (400 MHz, $CDCl_3$) δ 7.69–7.53 (m, 3H), 7.32 (d, *J* = 7.2 Hz, 2H), 5.62 (bs, 2H), 5.36 (bs, 2H), 3.04 (bs, 2H), 2.66 (bs, 1H), 2.56 (bs, 4H), 2.01 (d, *J* = 11.2 Hz, 2H), 1.62 (bs, 6H), 1.44 (bs, 2H). ^{13}C NMR (101 MHz, $CDCl_3$) δ 154.43, 153.82, 152.16, 140.77, 137.92, 132.81 (2C), 128.17 (2C), 118.50, 118.23, 112.40, 62.62 (2C), 50.17 (2C), 46.46 (2C), 27.99, 26.00 (2C), 24.51. HRMS calcd. for ($C_{23}H_{26}ClN_7$ [M + H]$^+$): 436.2011. Found: 436.2008. HPLC purity: 96.58%.

6-([1,4′-Bipiperidin]-1′-yl)-2-chloro-9-(2,6-dichlorobenzyl)-9*H*-purine **3h**. White solid, yield 52%, m.p. 88–89 °C. ^{1}H NMR (400 MHz, $CDCl_3$) δ 7.22 (d, *J* = 11.4 Hz, 2H), 7.14 (dd, *J* = 8.8, 7.3 Hz, 1H), 5.39 (s, 2H), 5.21 (bs, 2H), 2.85 (s, 2H), 2.53–2.42 (m, 1H), 2.41–2.26 (m, 4H), 1.81 (d, *J* = 12.6 Hz, 2H), 1.52–1.34 (m, 7H), 1.27 (d, *J* = 5.0 Hz, 2H). ^{13}C NMR (101 MHz, $CDCl_3$) δ 154.01, 153.77, 152.15, 137.19, 136.88, 131.01, 130.35, 128.86 (2C), 118.38, 62.67 (2C),

50.12 (2C), 45.06, 42.74 (2C), 27.99, 26.10 (2C), 24.58. HRMS calcd. for ($C_{22}H_{25}Cl_3N_6$ [M + H]$^+$): 479.1279. Found: 479.1280. HPLC purity: 96.93%.

3.1.3. Human Histamine H_3 Radioligand Displacement

Radioligand displacement assays at the human histamine H_3R were performed, as published previously [28]. In summary, the compounds were incubated with membrane preparations of HEK-293 cells stably expressing the human histamine H_3R (20 µg/well) and [^{3}H]N^α-methylhistamine (2 nM, K_D = 3.08 nM) in 200 µL of binding buffer (10 mM $MgCl_2$, 100 mM NaCl and 75 mM Tris/HCl, pH 7.4) for 90 min. At least three independent experiments of each compound in duplicate were conducted with 11 concentrations. Obtained data was analyzed with GraphPad Prism 7 (San Diego, CA, USA) using non-linear least squares fit and the equation "one site competition" (representative Figures given in the SI). K_i values were calculated according to the Cheng–Prusoff equation [29] and are reported as means with a 95% confidence interval. Statistical analyses were performed on the -logK_i values and were converted to mean K_i values and a 95% confidence interval. Differences are considered significant if 95% confidence intervals are not overlapping.

3.1.4. Cell Cultures

Cultures of HEPG2 (ATCC-HB-8065 TM), HEK293 (ATCC CRL-1573 TM) and SHSY-5Y (ATCC CRL-2266 TM) cell lines were used as experimental models. Cells were maintained in a DMEM culture medium supplemented with 10% Foetal Bovine Serum (FBS), in an incubator at 37 °C and a humidified atmosphere with 5% CO_2. Cells were seeded on culture plates, were allowed to grow for 24 h and then were treated with the synthesized compounds for 48 h with 100, 10, 1 and 0.1 µM concentrations. Negative cell death control, corresponding to untreated cells, and positive cell death control, corresponding to cells treated with 10% SDS, were maintained.

3.1.5. Cytotoxicity Assays

In a colorimetric MTT reduction assay [30], sterile 96-well culture plates were used. An amount of 2000–2500 cells per well were seeded. Upon completion of treatment, the culture medium was vacuum aspirated and washed with 1x PBS, and then 100 µL of 0.5 mg/mL MTT solution was added for a period of 4 h at 37 °C for formazan crystal formation. At the end of the 4 h, 100 µL of 10% SDS in HCl was added and kept overnight in an incubator at 37 °C to dissolve the formed crystals. The absorbance of each well was measured on the Synergy HTX microplate reader at 570 nm wavelength.

3.1.6. Docking Studies

The 3D structures of the compounds that were synthesized were built using OECHEM, followed by protonation states, and they were adjusted to a pH of 7.2 using FixpKa from the QUACPAC package (QUACPAC 2.1.3.0: OpenEye Scientific Software, Santa Fe, NM. http://www.eyesopen.com, accessed on 1 November 2021). The conformers were generated using OMEGA software [31]. The H_3R model was downloaded from the GPCR database (https://gpcrdb.org, accessed on 1 May 2022) [32–34]. The preparation of the proteins was performed with Schrodinger Suite 2021–1 [35], and the minimization was performed in the presence of restraints to maintain the protein conformation utilizing force field, OPLS4 [36].

The molecular docking studies were carried out with the induced-fit docking protocol [37,38], considering possible interactions with Asp114 or Glu206. The best poses were refined with the MM-GBSA method [39] in order to obtain the binding free energy by taking into account the solvation energies of the interacting molecules in addition to the molecular mechanics (MM) energies. The contribution of polar solvation energies was computed by the generalized Born (GB) implicit solvent model, whereas the nonpolar contribution of the solvation energy was dependent on solvent-accessible surface area (SA).

The interactions of residues in the active site were identified using a 6 Å radius around the docked position as a reference.

3.1.7. Molecular Dynamics

The molecular dynamic simulation was carried out with Desmond software (Schrödinger Release 2021-1: Desmond Molecular Dynamics System, D. E. Shaw Research, New York, NY, USA, 2021. Maestro-Desmond Interoperability Tools, Schrödinger, New York, NY, USA, 2021). The ligand–receptor complexes were inserted into the POPC membrane, were solvated and were ionized up to a concentration of 0.15 M NaCl using the Membrane Builder module from the System Builder. The protein orientation was defined based on the OPM database [40]. Orthorhombic periodic boundary conditions were set up to specify the shape and size of the repeating unit buffered at 10 Å distances. The simulated systems were first relaxed with 2000 steps of minimization, and then they were gradually heated from 0 to 310 K by repeating 500-step MD simulations every cycle. Except for the lipid tails, which were left to equilibrate for 250 ps, the systems were then fixed. The simulation was then changed to NPT conditions and equilibrated for 2.5 ns while constraining the protein with an initial force constant of 10 kcal/mol^2 that was gradually reduced to 8, 6, 4, 2, 1, 0.5 and 0.05 kcal/mol^2 every 250 ps of the MD simulation. Finally, the systems were run for 50 ns without any limits. The OLPS4 force field described proteins, lipids, and ions. In the production phase, a timestep of 2 fs was used, and PME (Particle Mesh Ewald) was used to tackle long-range electrostatic interactions. Langevin dynamics were used to keep the temperature at 310 K. The Simulation Interaction Diagram module (Schrodinger Suite 2021-1) and the PyMOL program (The PyMOL Molecular Graphics System, Version 2.0 Schrödinger, LLC., New York, NY, USA) were used to analyze the results.

4. Conclusions

In this work, we synthesized eight new purine derivatives in a simple manner and in good yields that include the classical pharmacophore of the H_3R ligands. The results of the affinity assays show that all these derivatives bind to receptors with K_i values on the nanomolar scale (2.91–105 nM), and compound **3d** presented the best affinity with a K_i value of 2.91 nM, which is better than pitolisant. Furthermore, **3d** showed low cytotoxicity for the kidney, liver and neuroblastoma cell lines. By in silico studies, the importance of the N-7 purine scaffold in the stabilization of the ligand–receptor complex through a hydrogen bond interaction with the Tyr374 residue at the binding site could be determined. Finally, the predicted ADME properties indicated that these derivatives fulfill all the requirements for good absorption and penetration into the CNS.

Supplementary Materials: The following supporting information can be downloaded at: https://www.mdpi.com/article/10.3390/ph15050573/s1, Figure S1: Graphical representation of histamine at the H3R binding site; Figure S2: The two best poses were achieved with the induced-fit docking protocol for 3d at the H3R binding site. (A) Piperidine oriented toward Asp114, and (B) piperidine oriented toward Glu206; Figure S3: The RMSD of the two studied complexes (3a in red and 3d in blue) was obtained during 50 ns of MD simulations; Figure S4: The root means square deviation (RMSF) values of each residue averaged over two trajectories for 3a (red line) and 3d (blue line); Figure S5: (A) Histogram plot of the contact H3R-3a system. (B) Timeline plots represent of the interactions and contact with 3a; Figure S6: (A) Histogram plot of the contact H3R-3d system. (B) Timeline plots represent of the interactions and contact with 3d; Figure S7: Graphical representations of 3a and 3d properties in the binding site.

Author Contributions: Conceptualization, C.E.-B., H.S. and C.O.S.; methodology, C.E.-B., L.L., T.A., M.J.S., A.C.-A. and H.S.; investigation, C.E.-B., L.L., T.A., M.J.S., A.d.C., A.C.-A., H.S. and C.O.S.; resources, C.E.-B., A.d.C. and H.S.; writing—original draft preparation, C.E.-B., A.C.-A., H.S. and C.O.S.; writing—review and editing, C.E.-B., A.C.-A., H.S. and C.O.S.; supervision, C.E.-B., A.d.C., H.S. and C.O.S.; project administration, C.E.-B. and C.O.S.; funding acquisition, C.E.-B. and H.S. All authors have read and agreed to the published version of the manuscript.

Funding: C.E.-B. gratefully acknowledges the financial support from FONDECYT Research Grant No. 1180292. The partial support of DFG GRK2158 is greatly acknowledged (by H.S.).

Institutional Review Board Statement: Not applicable.

Informed Consent Statement: Not applicable.

Data Availability Statement: Data is contained within the article and supplementary material.

Acknowledgments: A.C.-A. thanks the OpenEye company and Schrodinger Inc. for academic licences. The authors are grateful to Conrado Camilo Manriquez of the Dirección de Investigaciones Científicas y Tecnológicas de la Pontificia (DICTUC), for the realization and analysis of the mass spectra.

Conflicts of Interest: The authors declare no conflict of interest.

References

1. Panula, P.; Chazot, P.L.; Cowart, M.; Gutzmer, R.; Leurs, R.; Liu, W.L.; Stark, H.; Thurmond, R.L.; Haas, H.L. International Union of Basic and Clinical Pharmacology. XCVIII. Histamine Receptors. *Pharmacol. Rev.* **2015**, *67*, 601–655. [CrossRef] [PubMed]
2. Schlicker, E.; Kathmann, M. Role of the Histamine H_3 Receptor in the Central Nervous System. *Handb. Exp. Pharmacol.* **2017**, *241*, 277–299. [CrossRef] [PubMed]
3. Tiligada, E.; Kyriakidis, K.; Chazot, P.L.; Passani, M.B. Histamine pharmacology and new CNS drug targets. *CNS Neurosci. Ther.* **2011**, *17*, 620–628. [CrossRef] [PubMed]
4. Ghamari, N.; Zarei, O.; Arias-Montano, J.A.; Reiner, D.; Dastmalchi, S.; Stark, H.; Hamzeh-Mivehroud, M. Histamine H_3 receptor antagonists/inverse agonists: Where do they go? *Pharmacol. Ther.* **2019**, *200*, 69–84. [CrossRef] [PubMed]
5. Lamb, Y.N. Pitolisant: A Review in Narcolepsy with or without Cataplexy. *CNS Drugs* **2020**, *34*, 207–218. [CrossRef] [PubMed]
6. Tiligada, E.; Zampeli, E.; Sander, K.; Stark, H. Histamine H_3 and H_4 receptors as novel drug targets. *Expert Opin. Investig. Drugs* **2009**, *18*, 1519–1531. [CrossRef]
7. Labeeuw, O.; Levoin, N.; Poupardin-Olivier, O.; Calmels, T.; Ligneau, X.; Berrebi-Bertrand, I.; Robert, P.; Lecomte, J.M.; Schwartz, J.C.; Capet, M. Novel and highly potent histamine H_3 receptor ligands. Part 3: An alcohol function to improve the pharmacokinetic profile. *Bioorg. Med. Chem. Lett.* **2013**, *23*, 2548–2554. [CrossRef]
8. Wingen, K.; Stark, H. Scaffold variations in amine warhead of histamine H_3 receptor antagonists. *Drug Discov. Today Technol.* **2013**, *10*, e483–e489. [CrossRef]
9. Szczepanska, K.; Kuder, K.; Kiec-Kononowicz, K. Histamine H_3 Receptor Ligands in the Group of (Homo)piperazine Derivatives. *Curr. Med. Chem.* **2018**, *25*, 1609–1626. [CrossRef]
10. Bautista-Aguilera, O.M.; Hagenow, S.; Palomino-Antolin, A.; Farre-Alins, V.; Ismaili, L.; Joffrin, P.L.; Jimeno, M.L.; Soukup, O.; Janockova, J.; Kalinowsky, L.; et al. Multitarget-Directed Ligands Combining Cholinesterase and Monoamine Oxidase Inhibition with Histamine H_3 R Antagonism for Neurodegenerative Diseases. *Angew. Chem. Int. Ed. Engl.* **2017**, *56*, 12765–12769. [CrossRef]
11. Dou, F.; Cao, X.; Jing, P.; Wu, C.; Zhang, Y.; Chen, Y.; Zhang, G. Synthesis and evaluation of histamine H3 receptor ligand based on lactam scaffold as agents for treating neuropathic pain. *Bioorg. Med. Chem. Lett.* **2019**, *29*, 1492–1496. [CrossRef] [PubMed]
12. Espinosa-Bustos, C.; Frank, A.; Arancibia-Opazo, S.; Salas, C.O.; Fierro, A.; Stark, H. New lead elements for histamine H3 receptor ligands in the pyrrolo[2,3-*d*]pyrimidine class. *Bioorg. Med. Chem. Lett.* **2018**, *28*, 2890–2893. [CrossRef] [PubMed]
13. Frank, A.; Meza-Arriagada, F.; Salas, C.O.; Espinosa-Bustos, C.; Stark, H. Nature-inspired pyrrolo[2,3-*d*]pyrimidines targeting the histamine H_3 receptor. *Bioorg. Med. Chem.* **2019**, *27*, 3194–3200. [CrossRef] [PubMed]
14. Zarate, A.M.; Espinosa-Bustos, C.; Guerrero, S.; Fierro, A.; Oyarzun-Ampuero, F.; Quest, A.F.G.; Di Marcotullio, L.; Loricchio, E.; Caimano, M.; Calcaterra, A.; et al. A New Smoothened Antagonist Bearing the Purine Scaffold Shows Antitumour Activity In Vitro and In Vivo. *Int. J. Mol. Sci.* **2021**, *22*, 8372. [CrossRef] [PubMed]
15. Bertrand, J.; Dostalova, H.; Krystof, V.; Jorda, R.; Castro, A.; Mella, J.; Espinosa-Bustos, C.; Maria Zarate, A.; Salas, C.O. New 2,6,9-trisubstituted purine derivatives as Bcr-Abl and Btk inhibitors and as promising agents against leukemia. *Bioorg. Chem.* **2020**, *94*, 103361. [CrossRef] [PubMed]
16. Sharma, S.; Singh, J.; Ojha, R.; Singh, H.; Kaur, M.; Bedi, P.M.S.; Nepali, K. Design strategies, structure activity relationship and mechanistic insights for purines as kinase inhibitors. *Eur. J. Med. Chem.* **2016**, *112*, 298–346. [CrossRef]
17. Legraverend, M.; Grierson, D.S. The purines: Potent and versatile small molecule inhibitors and modulators of key biological targets. *Bioorg. Med. Chem.* **2006**, *14*, 3987–4006. [CrossRef]
18. Giorgi, I.; Scartoni, V. 8-azapurine nucleus: A versatile scaffold for different targets. *Mini Rev. Med. Chem.* **2009**, *9*, 1367–1378. [CrossRef]
19. Shimamura, T.; Shiroishi, M.; Weyand, S.; Tsujimoto, H.; Winter, G.; Katritch, V.; Abagyan, R.; Cherezov, V.; Liu, W.; Han, G.W.; et al. Structure of the human histamine H_1 receptor complex with doxepin. *Nature* **2011**, *475*, 65–70. [CrossRef]
20. Mehta, P.; Miszta, P.; Filipek, S. Molecular Modeling of Histamine Receptors—Recent Advances in Drug Discovery. *Molecules* **2021**, *26*, 1778. [CrossRef]
21. Xin, J.; Hu, M.; Liu, Q.; Zhang, T.T.; Wang, D.M.; Wu, S. Design, synthesis, and biological evaluation of novel iso-flavones derivatives as H_3R antagonists. *J. Enzyme Inhib. Med. Chem.* **2018**, *33*, 1545–1553. [CrossRef] [PubMed]

22. Wágner, G.; Mocking, T.A.M.; Arimont, M.; Provensi, G.; Rani, B.; Silva-Marques, B.; Latacz, G.; Da Costa Pereira, D.; Karatzidou, C.; Vischer, H.F.; et al. 4-(3-Aminoazetidin-1-yl)pyrimidin-2-amines as High-Affinity Non-imidazole Histamine H_3 Receptor Agonists with In Vivo Central Nervous System Activity. *J. Med. Chem.* **2019**, *62*, 10848–10866. [CrossRef] [PubMed]
23. Daina, A.; Michielin, O.; Zoete, V. SwissADME: A free web tool to evaluate pharmacokinetics, drug-likeness and medicinal chemistry friendliness of small molecules. *Sci. Rep.* **2017**, *7*, 42717. [CrossRef] [PubMed]
24. Lipinski, C.A.; Lombardo, F.; Dominy, B.W.; Feeney, P.J. Experimental and computational approaches to estimate solubility and permeability in drug discovery and development settings. *Adv. Drug Deliv. Rev.* **2001**, *46*, 3–26. [CrossRef]
25. Veber, D.F.; Johnson, S.R.; Cheng, H.Y.; Smith, B.R.; Ward, K.W.; Kopple, K.D. Molecular properties that influence the oral bioavailability of drug candidates. *J. Med. Chem.* **2002**, *45*, 2615–2623. [CrossRef] [PubMed]
26. Daina, A.; Zoete, V. A BOILED-Egg To Predict Gastrointestinal Absorption and Brain Penetration of Small Molecules. *ChemMedChem* **2016**, *11*, 1117–1121. [CrossRef]
27. Bakkestuen, A.K.; Gundersen, L.-L.; Utenova, B.T. Synthesis, Biological Activity, and SAR of Antimycobacterial 9-Aryl-, 9-Arylsulfonyl-, and 9-Benzyl-6-(2-furyl)purines. *J. Med. Chem.* **2005**, *48*, 2710–2723. [CrossRef] [PubMed]
28. Sander, K.; Kottke, T.; Weizel, L.; Stark, H. Kojic acid derivatives as histamine H_3 receptor ligands. *Chem. Pharm. Bull. (Tokyo)* **2010**, *58*, 1353–1361. [CrossRef] [PubMed]
29. Cheng, Y.; Prusoff, W.H. Relationship between the inhibition constant (K_1) and the concentration of inhibitor which causes 50 per cent inhibition (I_{50}) of an enzymatic reaction. *Biochem. Pharmacol.* **1973**, *22*, 3099–3108. [CrossRef] [PubMed]
30. Gray, N.S.; Wodicka, L.; Thunnissen, A.M.; Norman, T.C.; Kwon, S.; Espinoza, F.H.; Morgan, D.O.; Barnes, G.; LeClerc, S.; Meijer, L.; et al. Exploiting chemical libraries, structure, and genomics in the search for kinase inhibitors. *Science* **1998**, *281*, 533–538. [CrossRef]
31. Hawkins, P.C.D.; Skillman, A.G.; Warren, G.L.; Ellingson, B.A.; Stahl, M.T. Conformer Generation with OMEGA: Algorithm and Validation Using High Quality Structures from the Protein Databank and Cambridge Structural Database. *J. Chem. Inf. Model.* **2010**, *50*, 572–584. [CrossRef] [PubMed]
32. Kooistra, A.J.; Mordalski, S.; Pándy-Szekeres, G.; Esguerra, M.; Mamyrbekov, A.; Munk, C.; Keserű, G.M.; Gloriam, D.E. GPCRdb in 2021: Integrating GPCR sequence, structure and function. *Nucleic Acids Res.* **2020**, *49*, D335–D343. [CrossRef] [PubMed]
33. Pándy-Szekeres, G.; Munk, C.; Tsonkov, T.M.; Mordalski, S.; Harpsøe, K.; Hauser, A.S.; Bojarski, A.J.; Gloriam, D.E. GPCRdb in 2018: Adding GPCR structure models and ligands. *Nucleic Acids Res.* **2017**, *46*, D440–D446. [CrossRef] [PubMed]
34. Isberg, V.; Mordalski, S.; Munk, C.; Rataj, K.; Harpsøe, K.; Hauser, A.S.; Vroling, B.; Bojarski, A.J.; Vriend, G.; Gloriam, D.E. GPCRdb: An information system for G protein-coupled receptors. *Nucleic Acids Res.* **2016**, *44*, D356–D364. [CrossRef]
35. Sastry, G.M.; Adzhigirey, M.; Day, T.; Annabhimoju, R.; Sherman, W. Protein and ligand preparation: Parameters, protocols, and influence on virtual screening enrichments. *J. Comput-Aided Mol. Des.* **2013**, *27*, 221–234. [CrossRef]
36. Lu, C.; Wu, C.; Ghoreishi, D.; Chen, W.; Wang, L.; Damm, W.; Ross, G.A.; Dahlgren, M.K.; Russell, E.; Von Bargen, C.D.; et al. OPLS4: Improving Force Field Accuracy on Challenging Regimes of Chemical Space. *J. Chem. Theory Comput.* **2021**, *17*, 4291–4300. [CrossRef]
37. Sherman, W.; Day, T.; Jacobson, M.P.; Friesner, R.A.; Farid, R. Novel procedure for modeling ligand/receptor induced fit effects. *J. Med. Chem.* **2006**, *49*, 534–553. [CrossRef]
38. Sherman, W.; Beard, H.S.; Farid, R. Use of an induced fit receptor structure in virtual screening. *Chem. Biol. Drug Des.* **2006**, *67*, 83–84. [CrossRef]
39. Li, J.; Abel, R.; Zhu, K.; Cao, Y.; Zhao, S.; Friesner, R.A. The VSGB 2.0 model: A next generation energy model for high resolution protein structure modeling. *Proteins* **2011**, *79*, 2794–2812. [CrossRef]
40. Lomize, M.A.; Pogozheva, I.D.; Joo, H.; Mosberg, H.I.; Lomize, A.L. OPM database and PPM web server: Resources for positioning of proteins in membranes. *Nucleic Acids Res.* **2012**, *40*, D370–D376. [CrossRef]

Supporting information

Substituted purines as high affinity histamine H_3 receptor ligands

Christian Espinosa-Bustos,[1*] Luisa Leitzbach,[2] Tito Añazco,[1] María J. Silva,[1] Andrea del Campo,[1] Alejandro Castro-Alvarez,[3] Holger Stark,[2] Cristian O. Salas [4*]

[1] Departamento de Farmacia, Facultad de Química y de Farmacia, Pontificia Universidad Católica de Chile, Santiago de Chile 702843, Chile.; ccespino@uc.cl (C.E-B.), taanazco@uc.cl (T.A.); mjsilva15@uc.cl (M.J.S.); andrea.delcampo@uc.cl (A. del C.)

[2] Institute of Pharmaceutical and Medicinal Chemistry, Heinrich Heine University Düsseldorf, Universitaetsstr. 1, 40225 Duesseldorf, Germany.; luisa.leitzbach@hhu.de (L.L.); stark@hhu.de (H.S.)

[3] Laboratorio de Bioproductos Farmacéuticos y Cosméticos, Centro de Excelencia en Medicina Traslacional, Facultad de Medicina, Universidad de La Frontera, Temuco, Chile.; qf.alec.astro@gmail.com (A.C-A.)

[4] Departamento de Química Orgánica, Facultad de Química y de Farmacia, Pontificia Universidad Católica de Chile, 702843 Santiago de Chile, Chile.; cosalas@uc.cl (C.O.S.)

Index

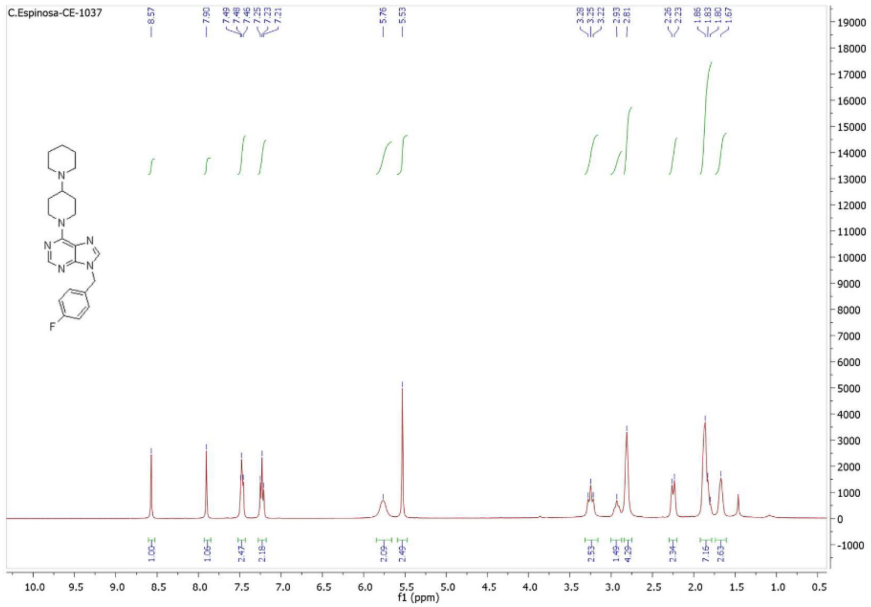
^{1}H and ^{13}C NMR of compounds **3a-h**……pag 02-09

HRMS of compounds **3a-h**……pag 10-13

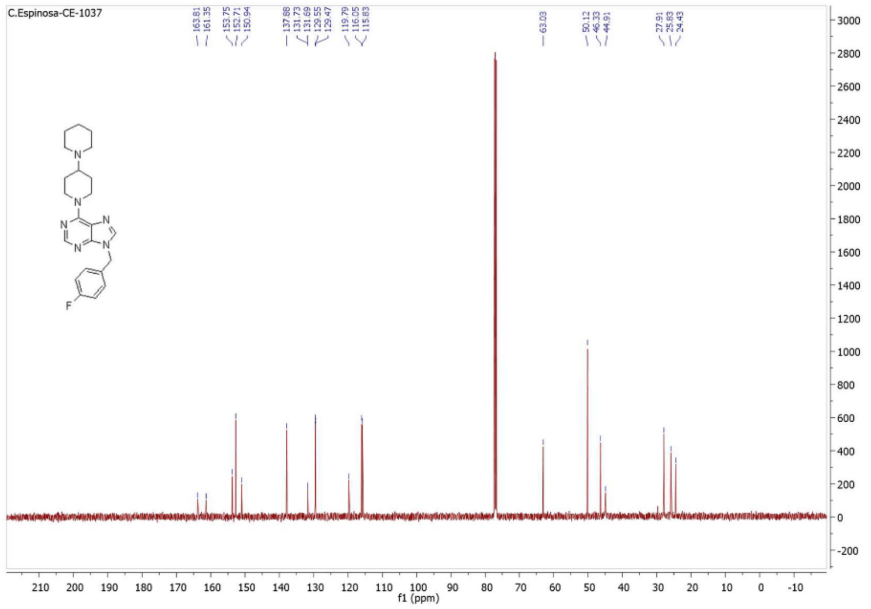
HPLC of compounds **3a-h**……pag 14-17

In silico studies……pag 18-25

^{1}H NMR compound 3a

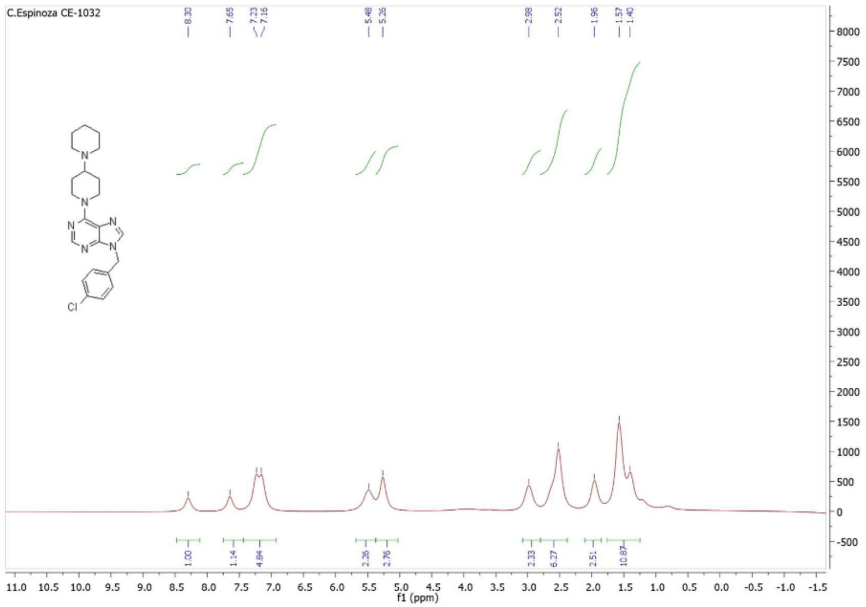


^{13}C NMR compound 3a

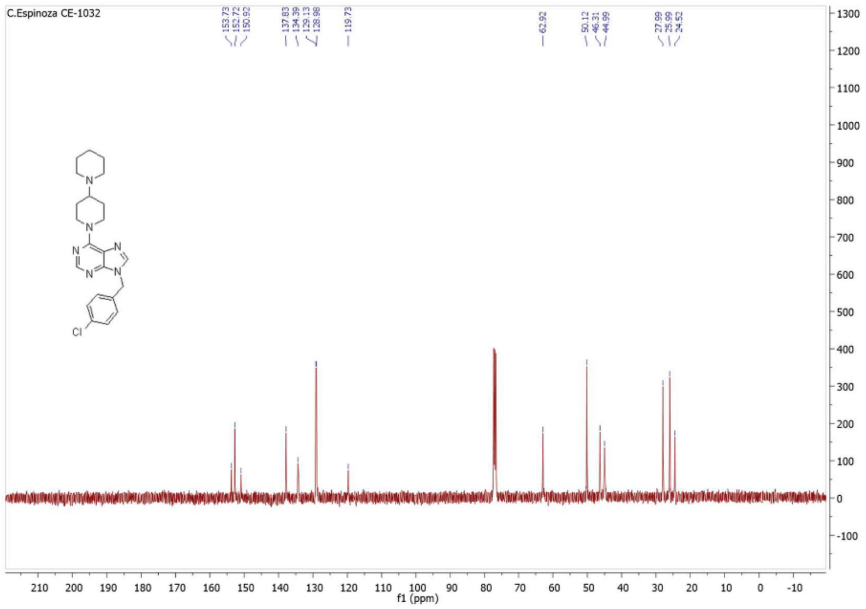


2

^{1}H NMR compound 3b

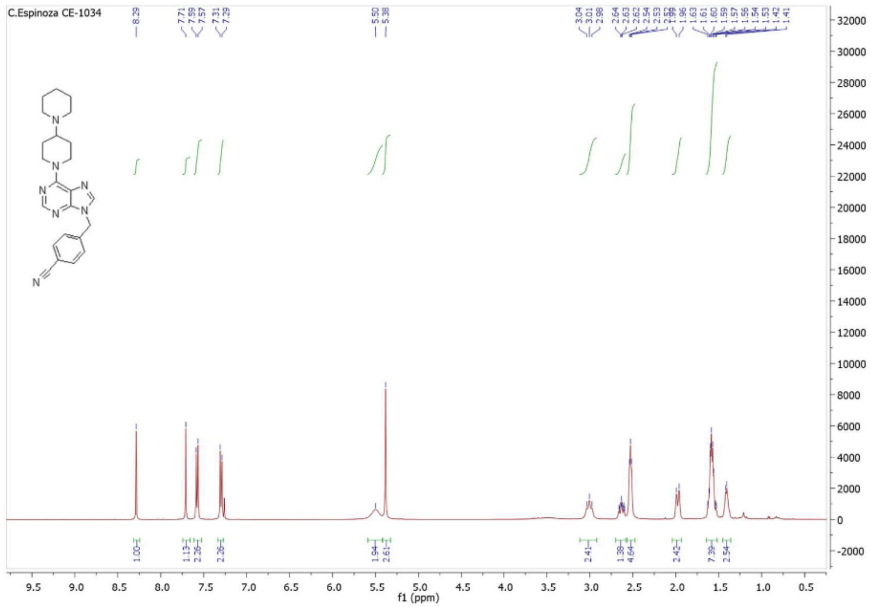


^{13}C NMR compound 3b

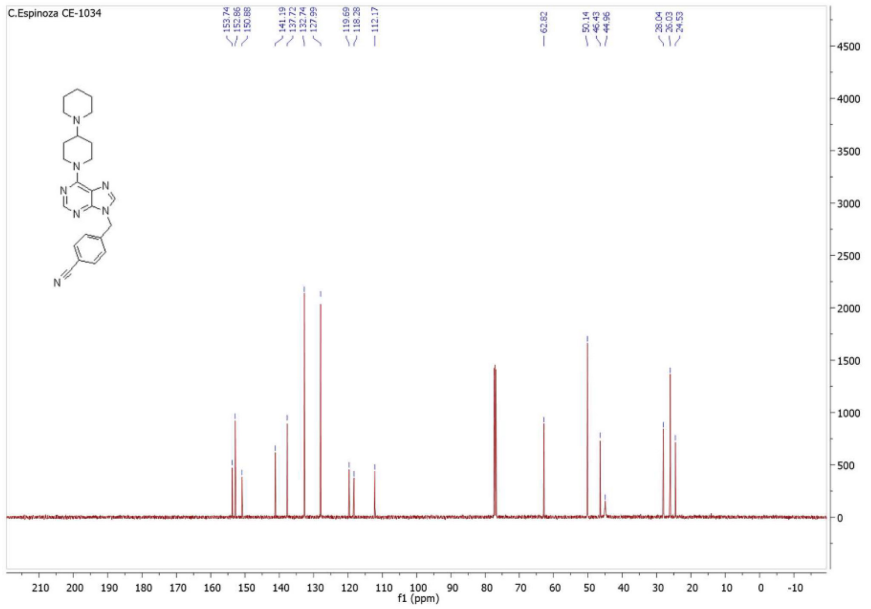


3

^{1}H NMR compound 3c

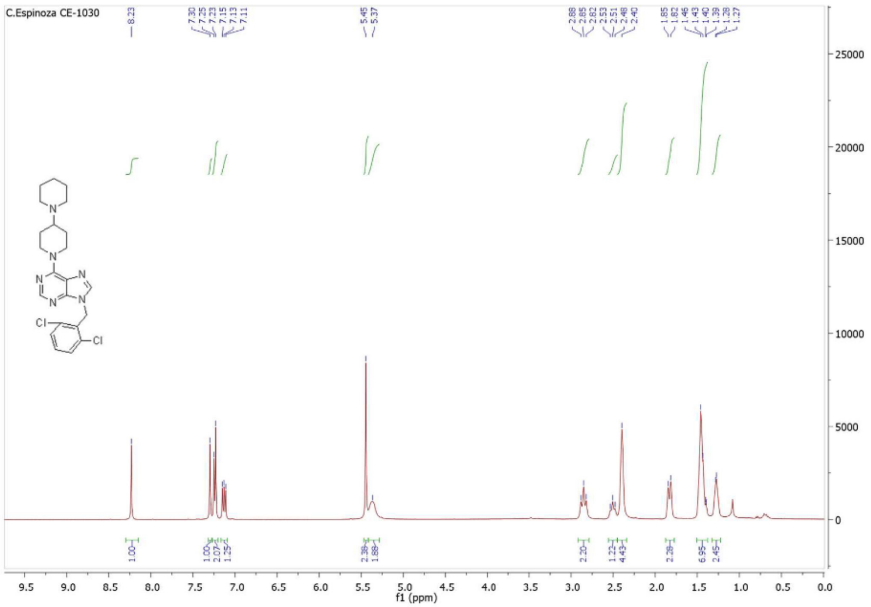


^{13}C NMR compound 3c

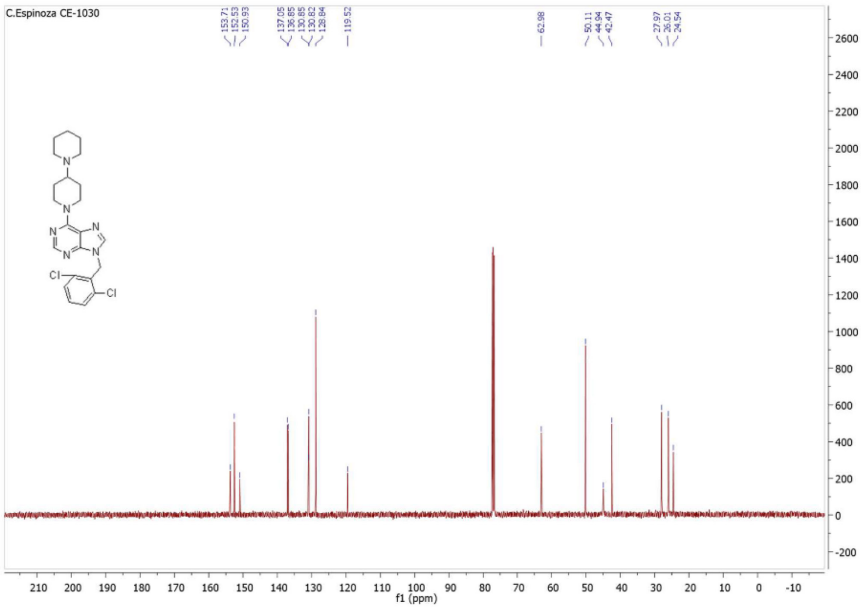


4

^{1}H NMR compound 3d

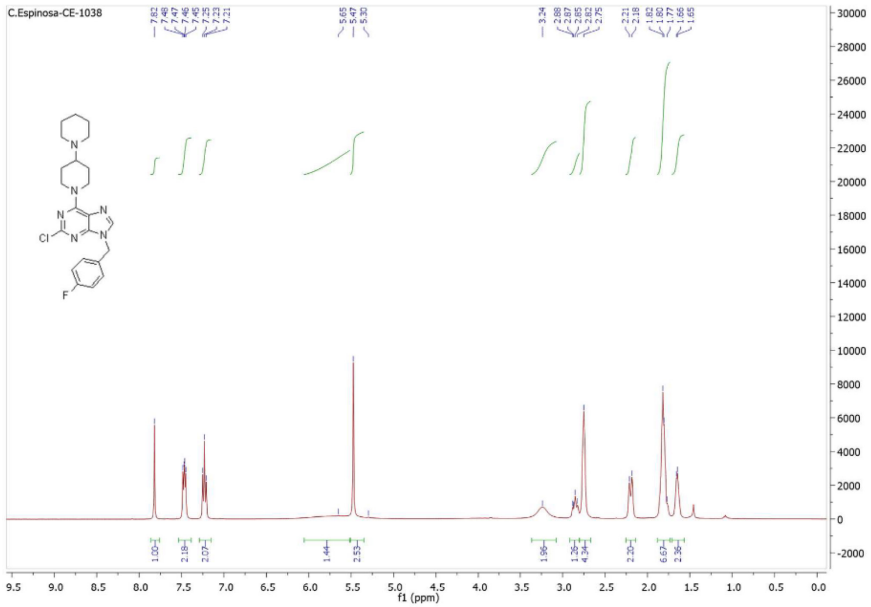


^{13}C NMR compound 3d

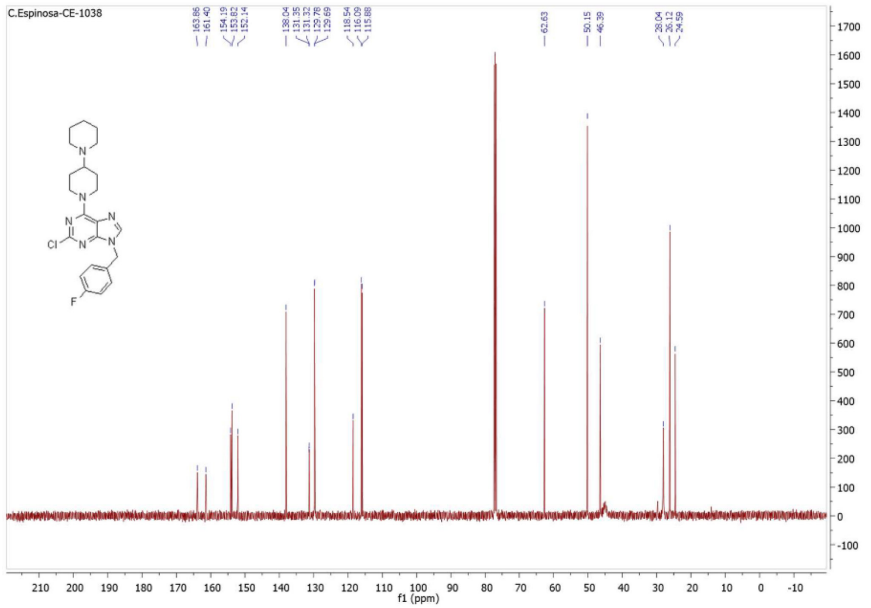


5

^{1}H NMR compound 3e

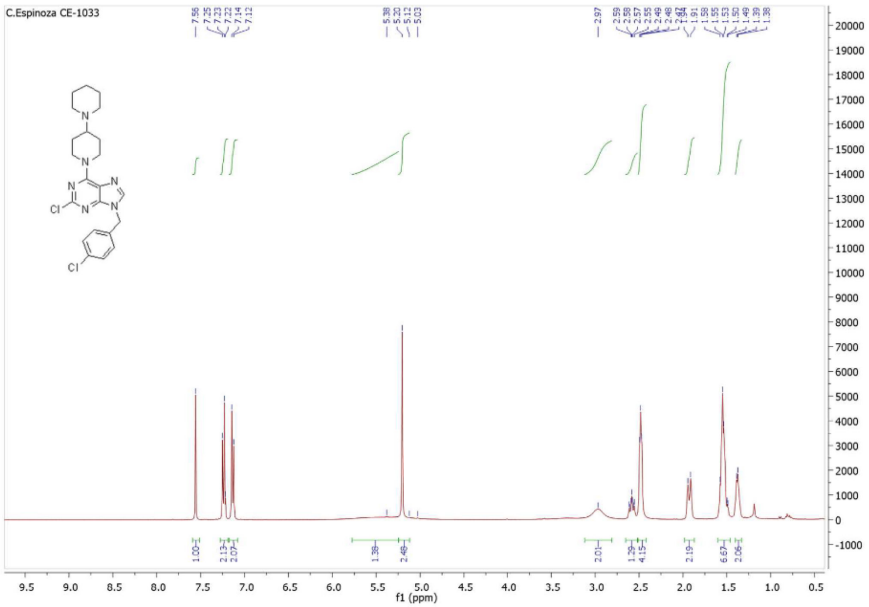


^{13}C NMR compound 3e

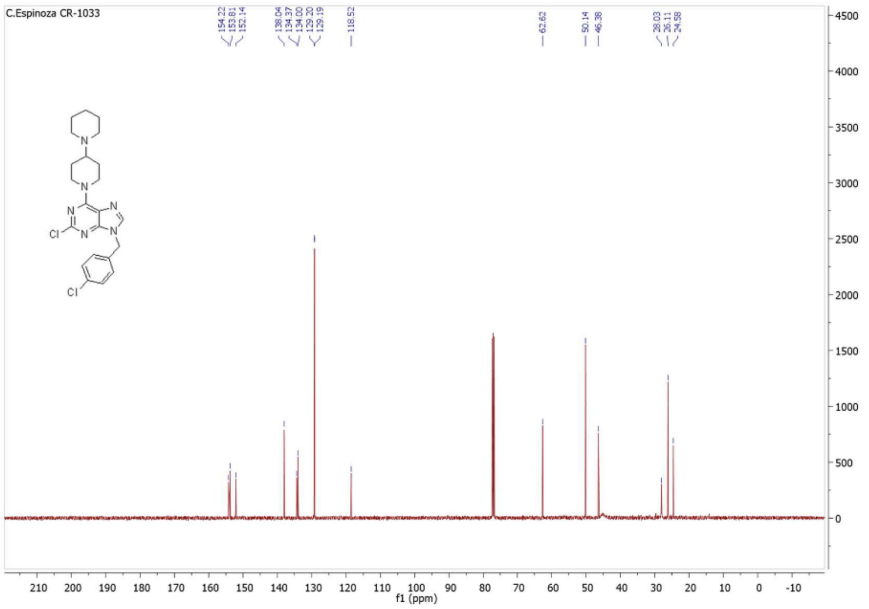


6

^{1}H NMR compound 3f

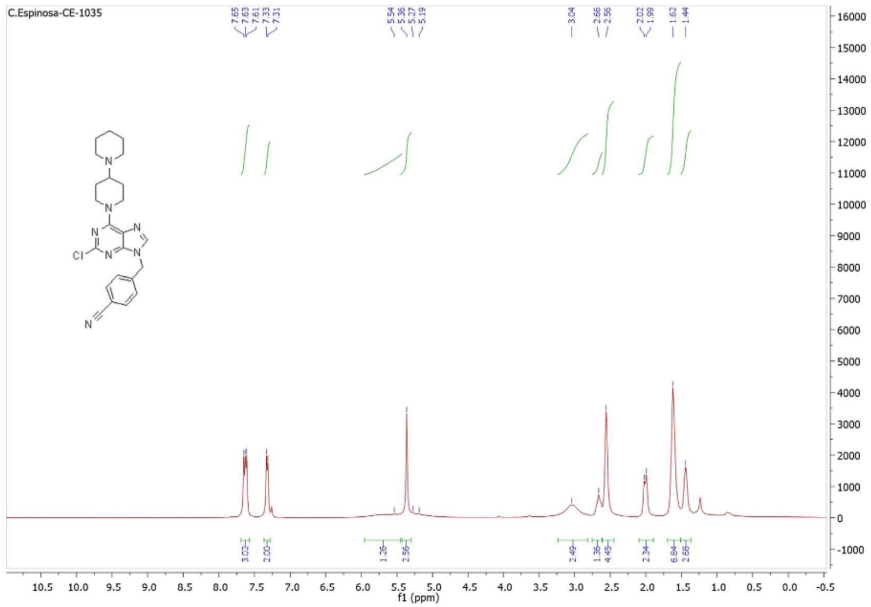


^{13}C NMR compound 3f

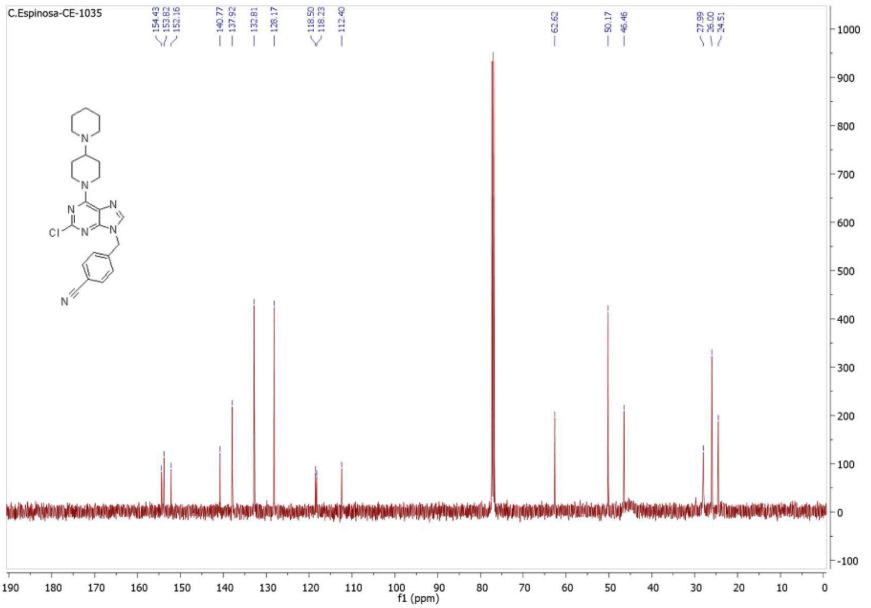


7

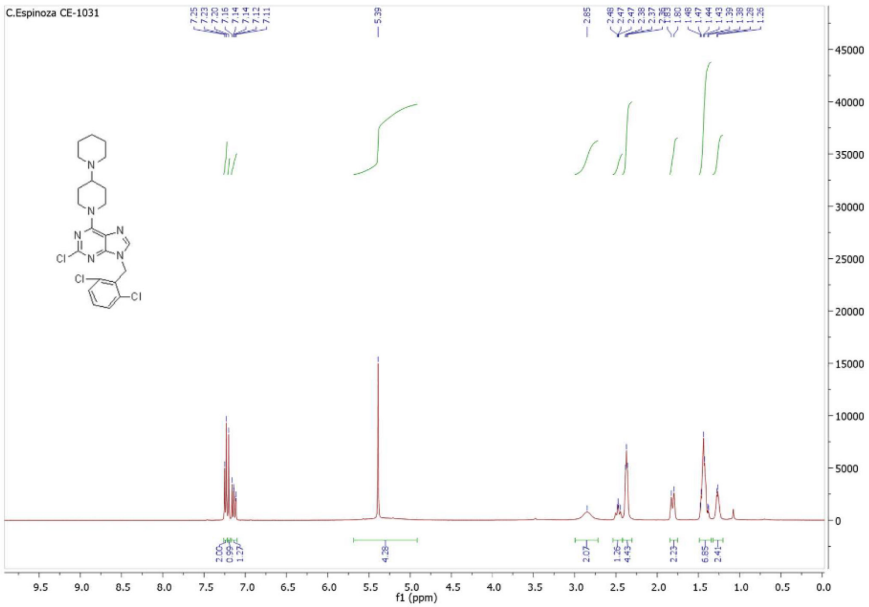
^{1}H NMR compound 3g



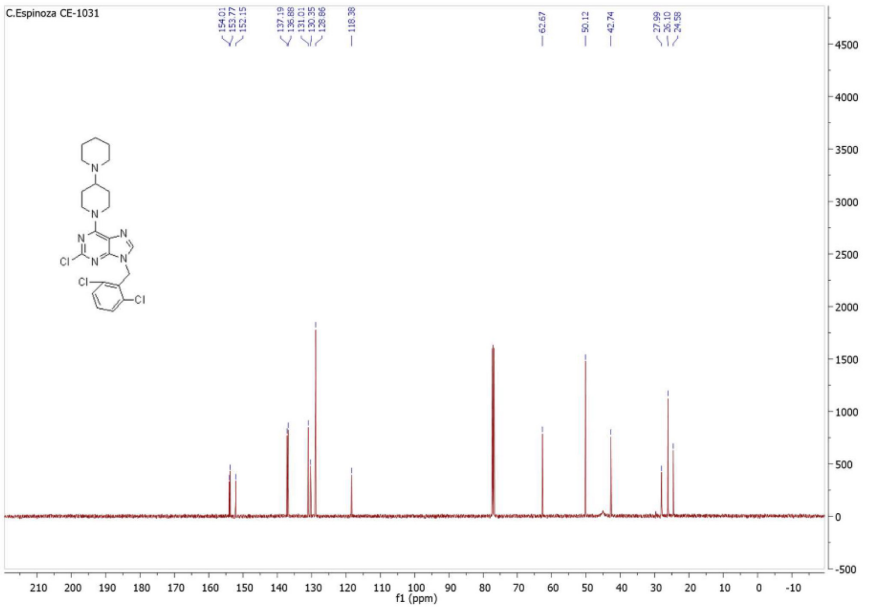
^{13}C NMR compound 3g



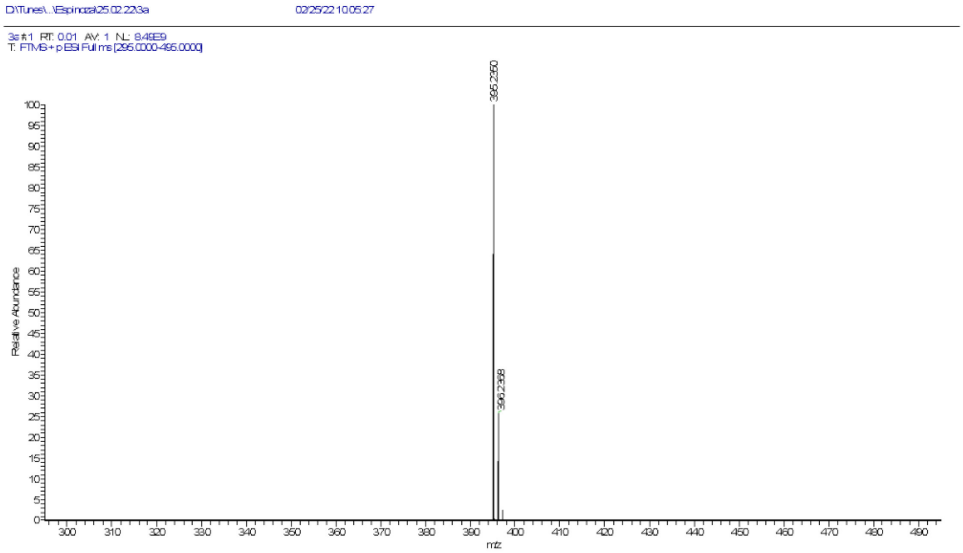
^{1}H NMR compound 3h



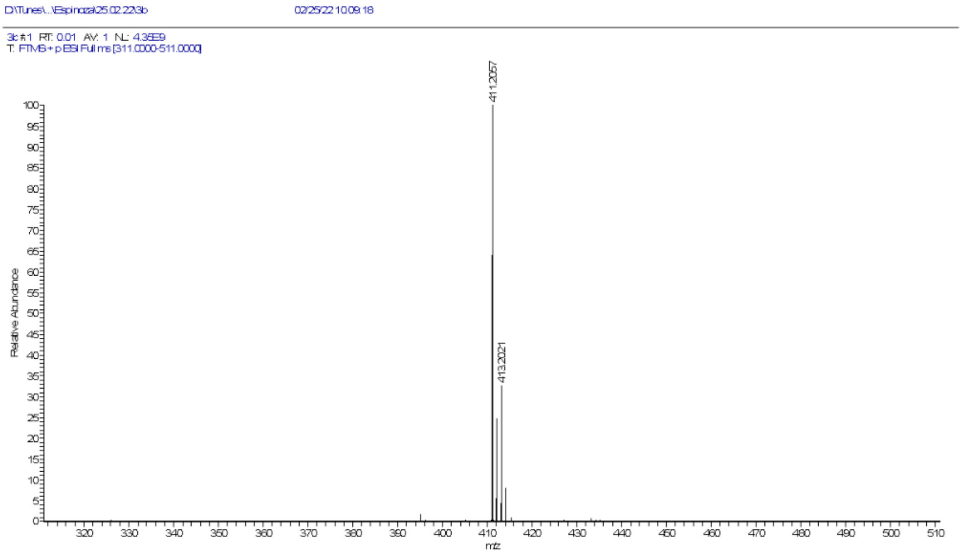
^{13}C NMR compound 3h



Mass spectra compound 3a

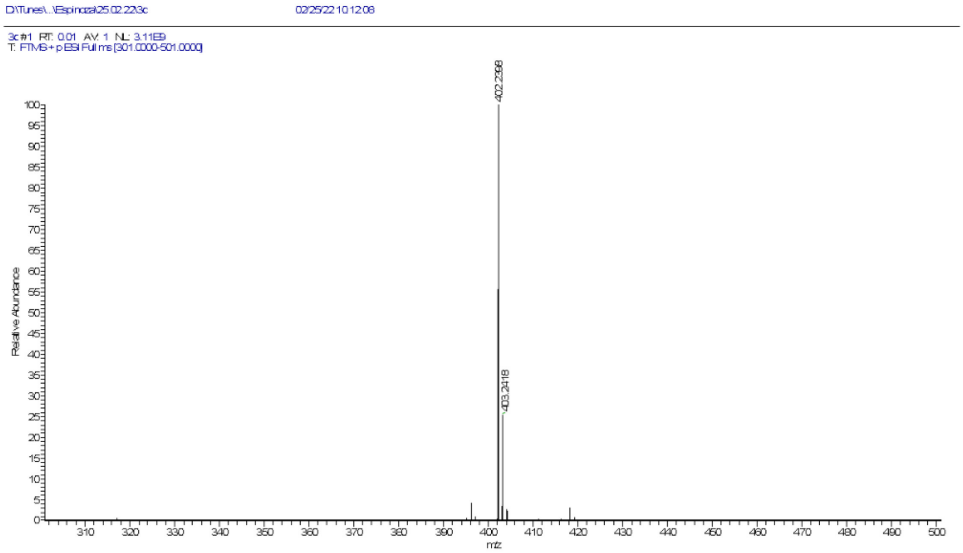


Mass spectra compound 3b

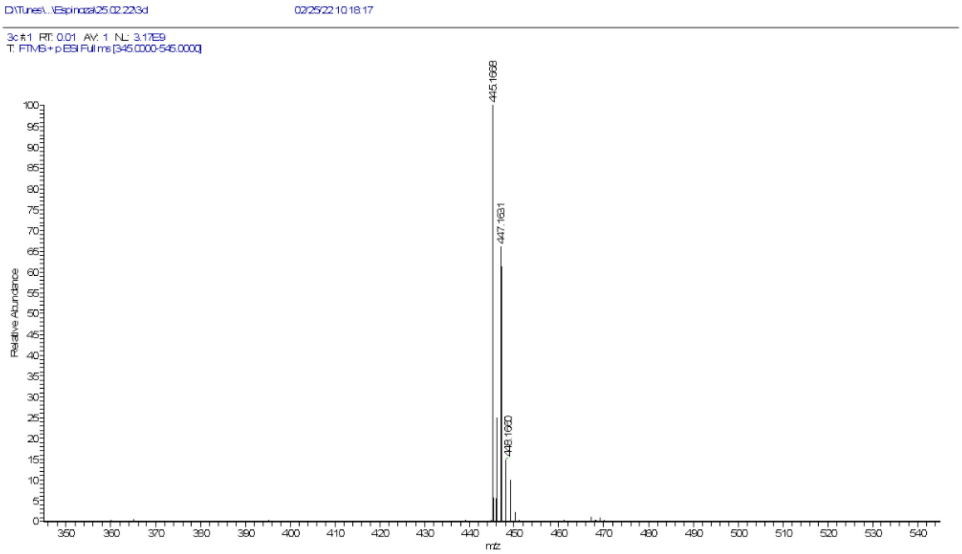


10

Mass spectra compound 3c

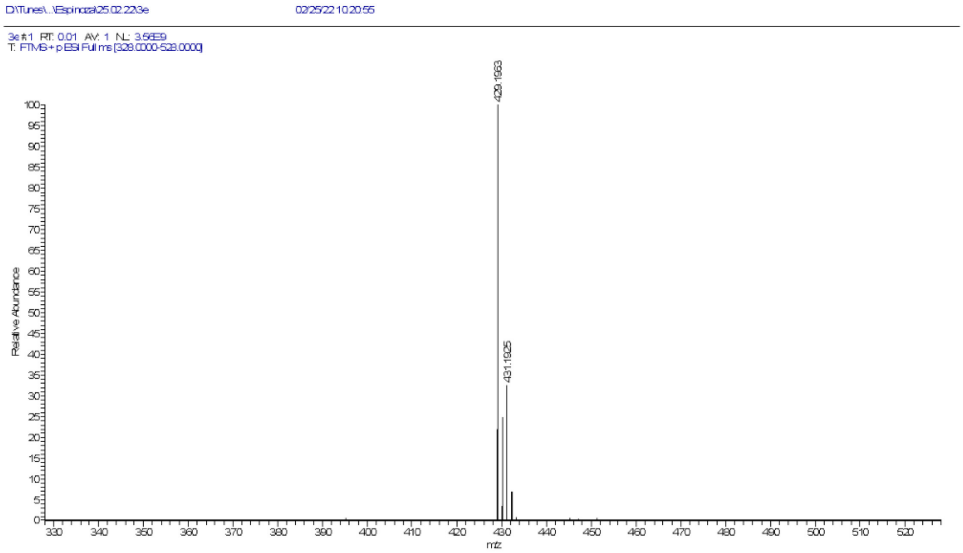


Mass spectra compound 3d

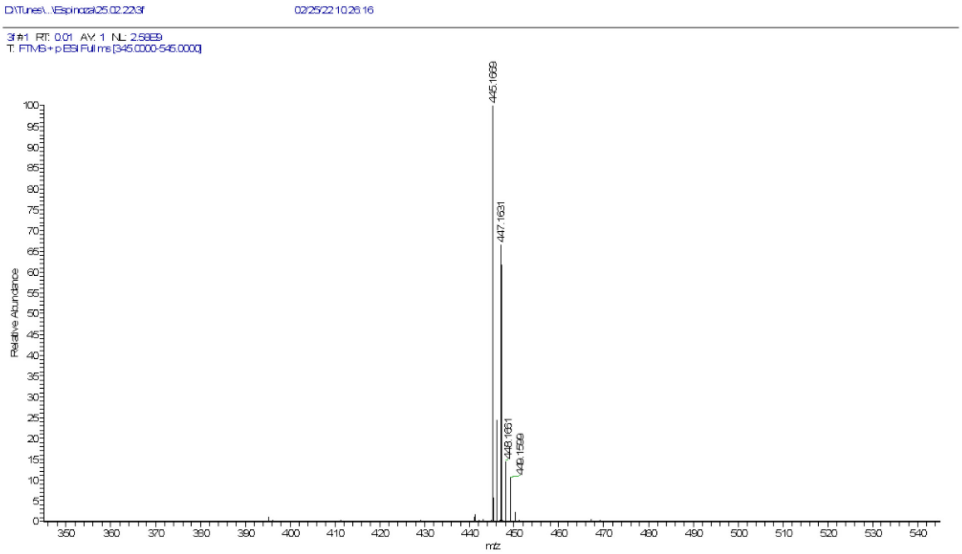


11

Mass spectra compound 3e

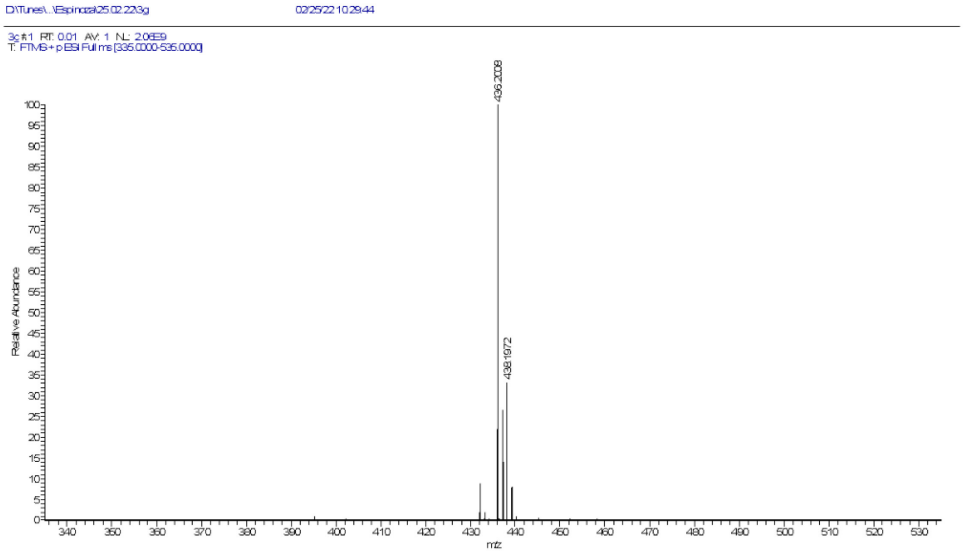


Mass spectra compound 3f

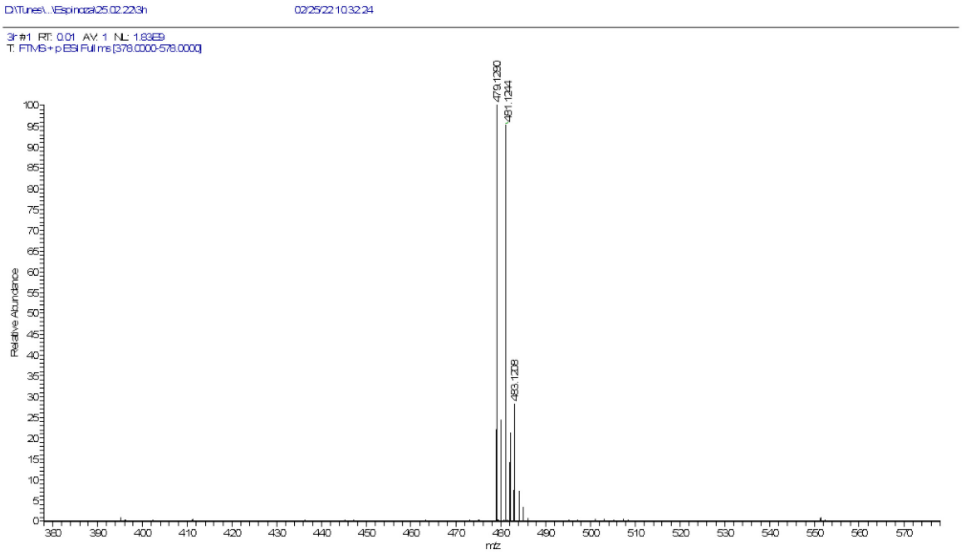


12

Mass spectra compound 3g



Mass spectra compound 3h

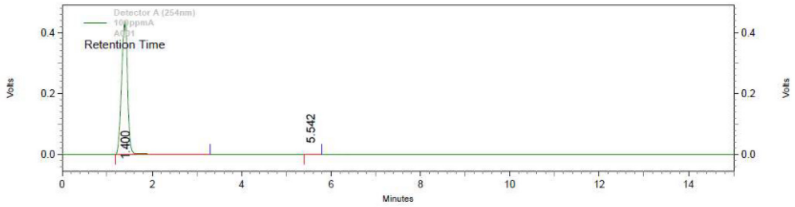


13

HPLC compound 3a

Shimadzu CLASS-VP V6.14 SP2 *Area % Report*
Page 1 of 1

Method Name: C:\CLASS-VP\Methods\Polyphenols_MA_02.met
Data Name: C:\CLASS-VP\Data\Joaquin_Fernandez\Tito\A001
User: Mario
Acquired: 26/04/2022 15:28:18
Printed: 27/04/2022 18:01:27



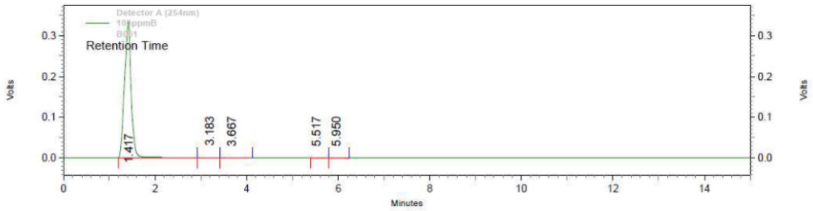
Detector A (254nm)

Pk #	Retention Time	Area	Area %	Height	Height %
1	1.400	3728760	99.979	436126	99.983
2	5.542	766	0.021	74	0.017
Totals		3729526	100.000	436200	100.000

HPLC compound 3b

Shimadzu CLASS-VP V6.14 SP2 *Area % Report*
Page 1 of 1

Method Name: C:\CLASS-VP\Methods\Polyphenols_MA_02.met
Data Name: C:\CLASS-VP\Data\Joaquin_Fernandez\Tito\B001
User: Mario
Acquired: 26/04/2022 15:49:21
Printed: 27/04/2022 18:05:27



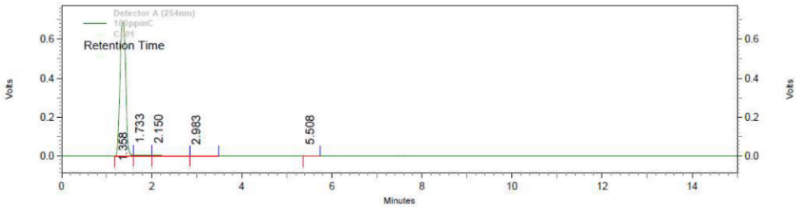
Detector A (254nm)

Pk #	Retention Time	Area	Area %	Height	Height %
1	1.417	3391621	99.397	333696	99.721
2	3.183	7493	0.220	382	0.114
3	3.667	3801	0.111	142	0.042
4	5.517	2954	0.087	116	0.035
5	5.950	6340	0.186	292	0.087
Totals		3412209	100.000	334628	100.000

HPLC compound 3c

Shimadzu CLASS-VP V6.14 SP2 *Area % Report*
Page 1 of 1

Method Name: C:\CLASS-VP\Methods\Polyphenols_MA_02.met
Data Name: C:\CLASS-VP\Data\Joaquin_Fernandez\Tito\C001
User: Mario
Acquired: 26/04/2022 16:11:04
Printed: 27/04/2022 18:06:37



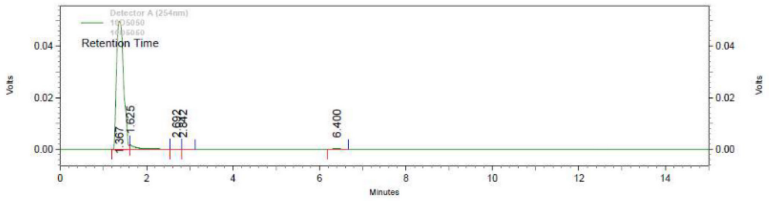
Detector A (254nm)

Pk #	Retention Time	Area	Area %	Height	Height %
1	1.358	6060354	96.830	687561	98.342
2	1.733	107465	1.717	6139	0.878
3	2.150	81529	1.303	4891	0.700
4	2.983	8742	0.140	489	0.070
5	5.508	669	0.011	72	0.010
Totals		6258759	100.000	699152	100.000

HPLC compound 3d

Shimadzu CLASS-VP V6.14 SP2 *Area % Report*
Page 1 of 1

Method Name: C:\CLASS-VP\Methods\Polyphenols_MA_02.met
Data Name: C:\CLASS-VP\Data\Joaquin_Fernandez\Tito\10D5050
User: Mario
Acquired: 27/04/2022 18:30:54
Printed: 27/04/2022 18:46:10



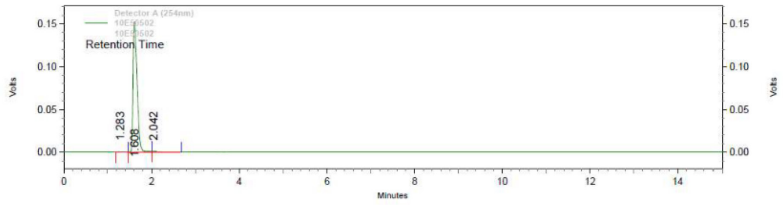
Detector A (254nm)

Pk #	Retention Time	Area	Area %	Height	Height %
1	1.367	566148	95.684	49791	96.241
2	1.625	21737	3.674	1613	3.118
3	2.692	1269	0.214	94	0.182
4	2.842	517	0.087	61	0.118
5	6.400	2016	0.341	177	0.342
Totals		591687	100.000	51736	100.000

HPLC compound 3e

Shimadzu CLASS-VP V6.14 SP2 *Area % Report*
Page 1 of 1

Method Name: C:\CLASS-VP\Methods\Polyphenols_MA_02.met
Data Name: C:\CLASS-VP\Data\Joaquin_Fernandez\Tito\10E50502
User: Mario
Acquired: 27/04/2022 16:46:11
Printed: 27/04/2022 17:25:26



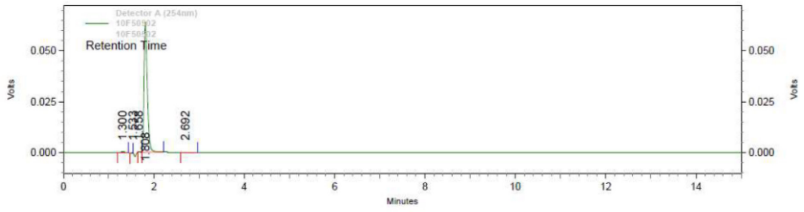
Detector A (254nm)

Pk #	Retention Time	Area	Area %	Height	Height %
1	1.283	5816	0.582	569	0.369
2	1.608	981867	98.261	152566	99.066
3	2.042	11556	1.156	869	0.564
Totals		999239	100.000	154004	100.000

HPLC compound 3f

Shimadzu CLASS-VP V6.14 SP2 *Area % Report*
Page 1 of 1

Method Name: C:\CLASS-VP\Methods\Polyphenols_MA_02.met
Data Name: C:\CLASS-VP\Data\Joaquin_Fernandez\Tito\10F50502
User: Mario
Acquired: 27/04/2022 17:28:14
Printed: 27/04/2022 19:00:00



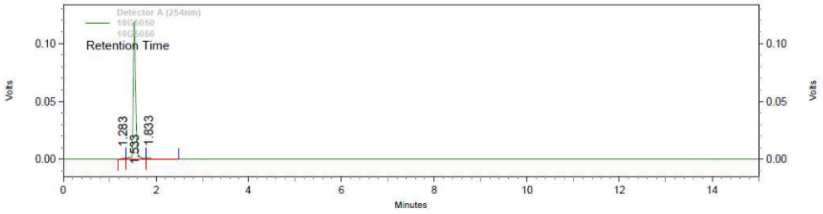
Detector A (254nm)

Pk #	Retention Time	Area	Area %	Height	Height %
1	1.300	1672	0.517	197	0.304
2	1.533	985	0.304	482	0.743
3	1.658	398	0.123	144	0.222
4	1.808	320177	98.962	64044	98.678
5	2.692	302	0.093	35	0.054
Totals		323534	100.000	64902	100.000

HPLC compound 3g

Shimadzu CLASS-VP V6.14 SP2 *Area % Report*
Page 1 of 1

Method Name: C:\CLASS-VP\Methods\Polyphenols_MA_02.met
Data Name: C:\CLASS-VP\Data\Joaquin_Fernandez\Tito\10G5050
User: Mario
Acquired: 27/04/2022 17:48:54
Printed: 27/04/2022 18:14:41



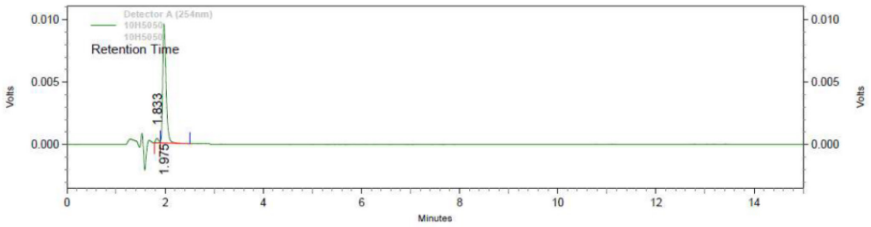
Detector A (254nm)

Pk #	Retention Time	Area	Area %	Height	Height %
1	1.283	4203	0.933	651	0.540
2	1.533	435091	96.588	118814	98.466
3	1.833	11165	2.479	1200	0.994
Totals		450459	100.000	120665	100.000

HPLC compound 3h

Shimadzu CLASS-VP V6.14 SP2 *Area % Report*
Page 1 of 1

Method Name: C:\CLASS-VP\Methods\Polyphenols_MA_02.met
Data Name: C:\CLASS-VP\Data\Joaquin_Fernandez\Tito\10H5050
User: Mario
Acquired: 27/04/2022 18:08:09
Printed: 27/04/2022 19:02:45



Detector A (254nm)

Pk #	Retention Time	Area	Area %	Height	Height %
1	1.833	1436	3.065	350	3.539
2	1.975	45418	96.935	9541	96.461
Totals		46854	100.000	9891	100.000

17

S1. Histamine and H_3R

The simulation of the histamine and H_3R was carried out by superimposing the 3RZE (inactive conformation) and 7DFL (active conformation) crystals. Subsequently, the ligand is removed from the 3RZE crystal and the receptor from the 7DFL crystal. As a result, the new model depicts the arrangement of the amino acids Asp114 and Glu206 in relation to histamine's primary amine and imidazole orientation.

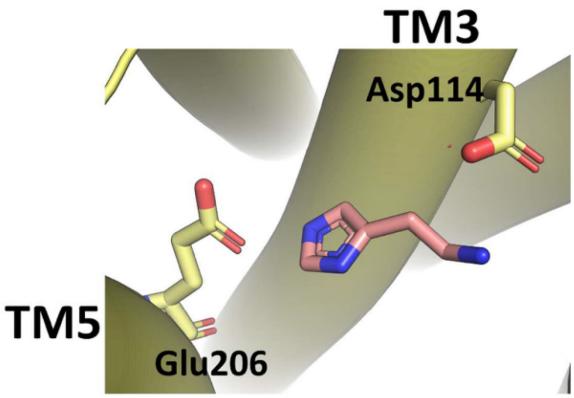


Figure S1. Graphical representation of histamine at the H_3R binding site.

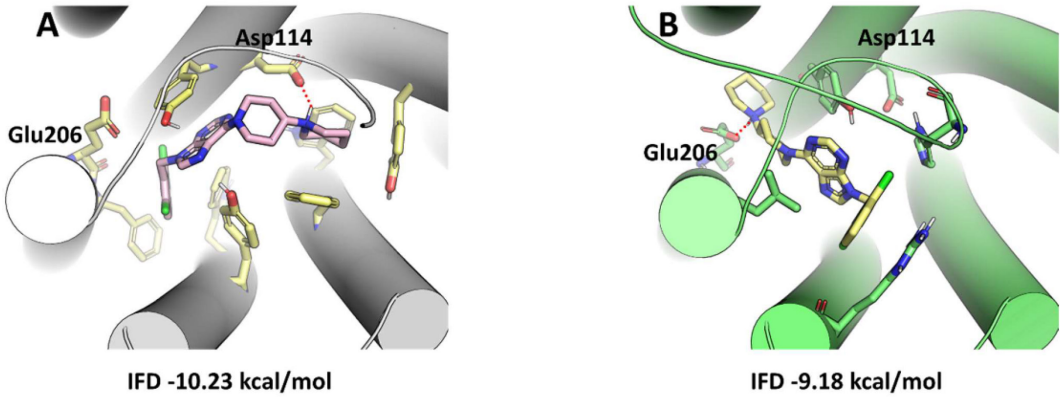


Figure S2. The two best poses were achieved with the induced-fit docking protocol for **3d** at the H3R binding site. (**A**) Piperidine oriented toward Asp114, and (**B**) piperidine oriented toward Glu206.

S2. Molecular dynamics analysis

S2.1. RMSD of systems **3a** and **3d**

The Root Mean Square Deviation (RMSD) is a metric for calculating a group of atoms' average change in displacement concerning a reference frame. It is calculated for each frame of the trajectory. For frame *x*, the RMSD is:

$$RMSD = \sqrt{\frac{1}{N}\sum_{i=1}^{N}\left(r_i'(t_x)\right) - \left(r_i(t_{ref})\right)^2}$$

where N is the number of atoms in the atom selection; t_{ref} is the reference time (typically the first frame is used as the reference, and it is regarded as time $t = 0$); and r' is the position of the selected atoms in frame x after superimposing on the reference frame, where frame x is recorded at time t_x. The procedure is repeated for every frame in the simulation trajectory.

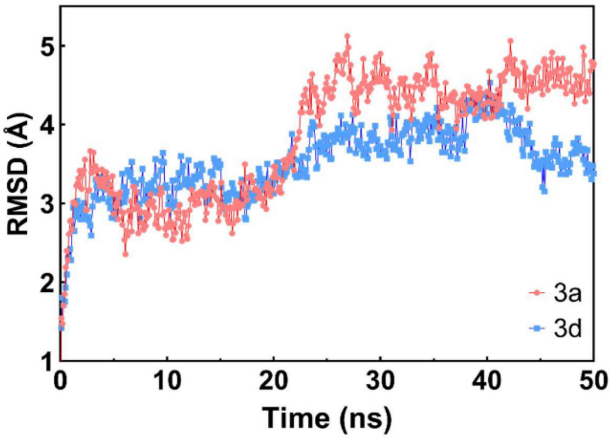


Figure S3. The RMSD of the two studied complexes (**3a** in red and **3d** in blue) was obtained during 50 ns of MD simulations.

The above plot shows the RMSD evolution of a protein (left Y-axis) in angstrom (Å). All protein frames are first aligned on the reference frame Cα of the protein, and then the RMSD is calculated based on the atom selection.

Monitoring the RMSD of the protein can give insights into its structural conformation throughout the simulation. RMSD analysis can indicate if the simulation has equilibrated; its fluctuations towards the end of the simulation are around some thermal average structure. Changes of the order of 1-3 Å are perfectly acceptable for small, globular proteins. However, more extensive changes indicate that the protein undergoes a significant conformational change during the simulation. For example, the H3R-3a system increases its RMSD from 20 ns onwards, the cause of which lies in the displacement of 3a at the binding site due to the low affinity achieved for the halogenated aromatic fragment of the hydrophobic pocket 2 (HP2). In contrast, the H3R-3d system has a better affinity for HP2, achieving a more stable RMSD (~ 3.5 Å).

S2.2. RMSF of systems **3a** and **3d**

The Root Mean Square Fluctuation (RMSF) is useful for characterizing local changes along the protein chain. The RMSF for residue *i* is:

$$RMSF_i = \sqrt{\frac{1}{T}\sum_{t=1}^{T}\langle\left(r_i'(t)\right)^2 - \left(r_i(t_{ref})\right)^2\rangle}$$

where *T* is the trajectory time over which the RMSF is calculated, tref is the reference time, r_i is the position of residue *i*; *r'* is the position of atoms in residue *i* after superposition on the reference, and the angle brackets indicate that the average of the square distance is taken over the selection of atoms in the residue. On this plot, peaks indicate areas of the protein that fluctuate the most during the simulation.

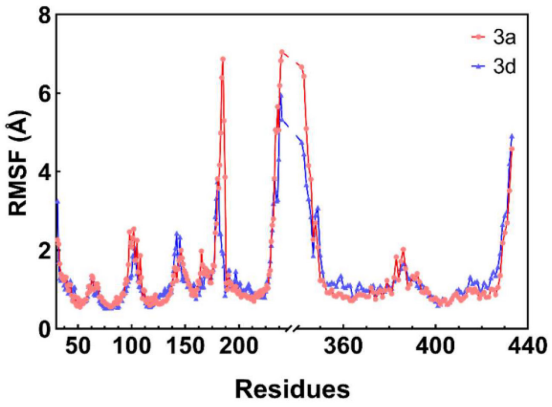


Figure S4. The root means square deviation (RMSF) values of each residue averaged over two trajectories for **3a** (red line) and **3d** (blue line).

S2.3. Ligand-protein contacts

Protein interactions with the ligand can be monitored throughout the simulation. As shown in the plot below, these interactions can be categorized by type and summarized. Protein-ligand interactions (or 'contacts') are categorized into four types: Hydrogen Bonds, Hydrophobic, Ionic, and Water Bridges. The stacked bar charts are normalized throughout the trajectory: for example, a value of 0.7 suggests that the specific interaction is maintained 70% of the simulation time. The threshold was 0.3 (dot line in red of Figure **S5-A** and **S6-A**) residue interactions with the respective ligand.

In Figure **S5-B** and **S6-B**, the top panel shows the total number of specific contacts the protein makes with the ligand for the trajectory (blue graphic). The bottom panel shows which residues interact with the ligand in each trajectory frame. Some residues make more than one specific contact with the ligand, which is represented by a darker shade of orange, according to the scale to the right of the plot.

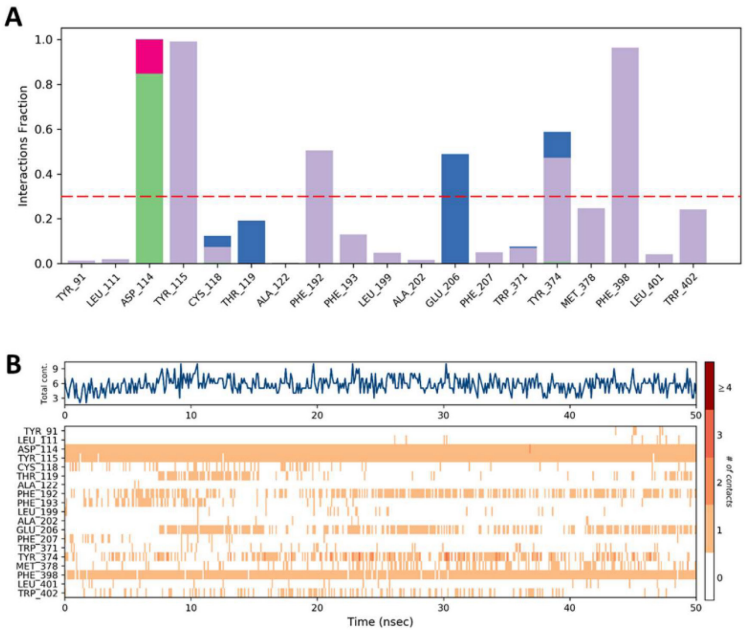


Figure S5. (**A**) Histogram plot of the contact H3R-**3a** system. (**B**) Timeline plots represent of the interactions and contact with **3a**.

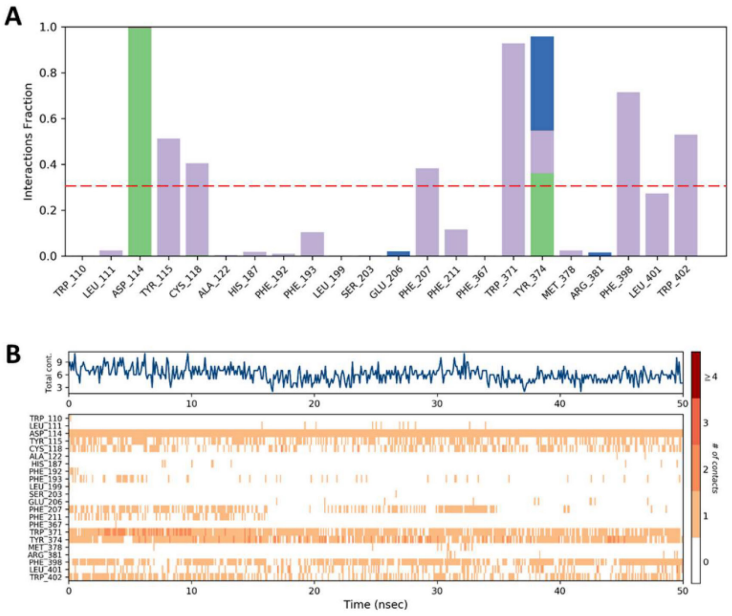


Figure S6. (**A**) Histogram plot of the contact H3R-**3d** system. (**B**) Timeline plots represent of the interactions and contact with **3d**.

According to the H3R-3a system are Asp114, Phe192, Glu206, Tyr374, and Phe398, the 0.3 threshold and only Asp114, Tyr115, and Phe378 exceed 80% during molecular dynamics. In contrast, the H3R-**3d** system has Asp114, Tyr115, Cys118, Trp371, Tyr374, Phe398, Trp402, exceeding the 0.3 thresholds; however, the amino acids Asp114, Trp371, and Tyr374 exceed 80% during molecular dynamics, a pattern of interactions similar to that achieved with pitolisant (10.1111/cbdd.13471)

S2.4. Ligand properties in the binding site

The properties of the ligand give a clear idea about the global interactions affecting the ligand at the binding site, such as the evolution of its RMSD, the radius of gyration, Molecular surface area, Solvent accessible surface area and Polar Surface area, whose properties are defined as:

Ligand RMSD: Root mean square deviation of a ligand with respect to the reference conformation (typically, the first frame is used as the reference, and it is regarded as time t=0).

The radius of Gyration (rGyr): Measures the 'extendedness' of a ligand and is equivalent to its principal moment of inertia.

Molecular Surface Area (MolSA): Molecular surface calculation with 1.4 Å probe radius. This value is

equivalent to a van der Waals surface area.

Solvent Accessible Surface Area (SASA): Surface area of a molecule accessible by a water molecule.

Polar Surface Area (PSA): Solvent accessible surface area in a molecule contributed only by oxygen and nitrogen atoms.

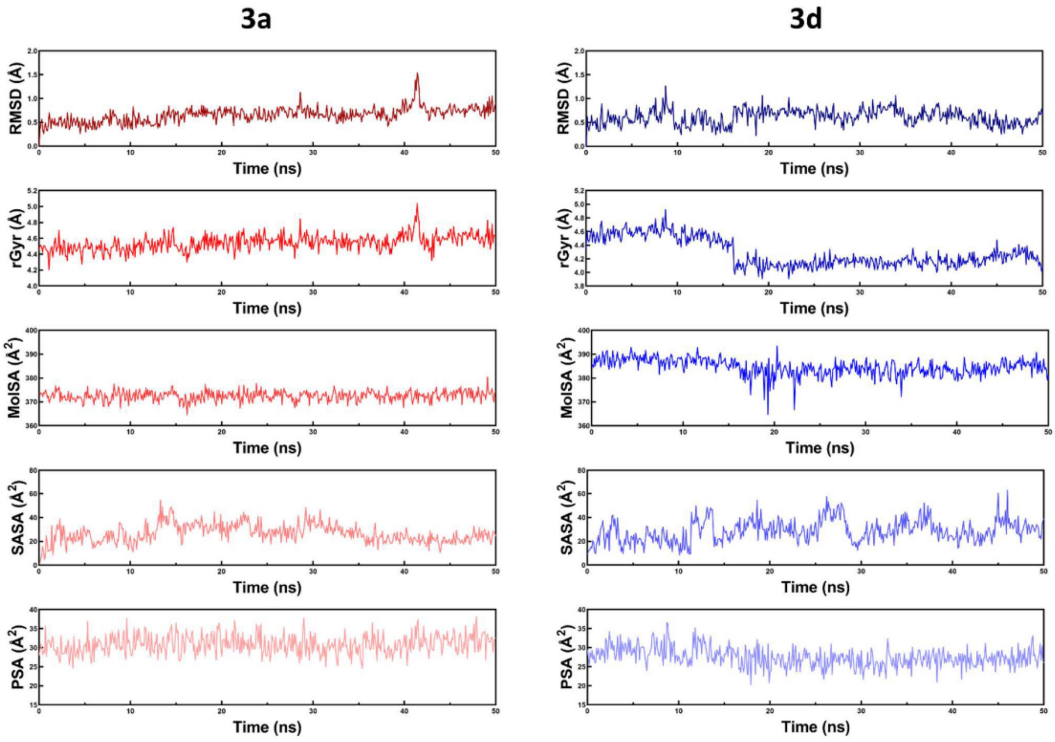


Figure S7. Graphical representations of **3a** and **3d** properties in the binding site.

3.3 Aromatic linker variations in novel dopamine D_2 and D_3 receptor ligands

Cristian di Biase[1], Luisa Leitzbach[1], Annika Frank[1], Aleksandra Zivkovic[1], Holger Stark[1]

[1] Institute of Pharmaceutical and Medicinal Chemistry, Heinrich Heine University Düsseldorf, Duesseldorf Germany

Published in: Archiv der Pharmazie, 2024, e2400071, Vol. 357, http://doi.org/10.1002/ardp.202400071

Impact Factor: 3.6 (2024)

Contribution: L.L. performed most of the in-vitro experiments, interpretation of pharmacological data, partly prepared, reviewed the manuscript and worked on revision of the manuscript.

Check for updates

Received: 26 January 2024 | Revised: 21 April 2024 | Accepted: 22 April 2024

DOI: 10.1002/ardp.202400071

FULL PAPER

ARCH PHARM Archiv der Pharmazie DPhG

Aromatic linker variations in novel dopamine D_2 and D_3 receptor ligands

Cristian Di Biase | Luisa Leitzbach | Annika Frank | Aleksandra Zivkovic | Holger Stark

Institute of Pharmaceutical and Medicinal Chemistry, Heinrich Heine University Düsseldorf, Duesseldorf, Germany

Correspondence
Holger Stark, Heinrich Heine University Düsseldorf, Institute of Pharmaceutical and Medicinal Chemistry, Universitätsstr.1, 40225 Düsseldorf, Germany.
Email: stark@hhu.de

Funding information
None

Abstract

Dopamine D_2-like receptors, especially D_2 and D_3 receptor subtypes, are important targets of antipsychotic agents. Many of these antipsychotics share an aliphatic linker element between a protonable amine group and an acyl-like moiety. Here, we have modified this aliphatic linker into phenylmethyl and phenylethyl linkers substituted in different positions. The design, synthesis, and in vitro evaluation of 18 dopamine D_2 and D_3 receptor ligands were performed in this study. Using a radioligand displacement assay, all ligands were found to have modest nanomolar affinity to D_2R and D_3R. *N*-(4-{2-[4-(2-Methoxyphenyl)piperazin-1-yl]ethyl}phenyl) acetamide (**6c**) demonstrates the highest D_3R and D_2R affinity values (pK_i values of 7.83 [D_2R] and 8.04 [D_3R]), featuring a slight preference to D_3R. This derivative can be taken as a reference structure for the development of a new class of D_2R and D_3R ligands.

KEYWORDS

D_2 receptor, D_3 receptor, ligands, linker, SAR

1 | INTRODUCTION

Motion, emotions, and cognition are regulated by dopamine and multiple human disorders have been related to dysfunctions of the dopaminergic system, especially human brain diseases such as psychiatric disorders, schizophrenia, drug addiction, Parkinson's disease, and Huntington's disease.[1] Functions and dysfunctions of dopaminergic transmission are mediated by the interaction of dopamine with its own receptors which belong to the rhodopsin-like A class of G-protein coupled receptors (GPCRs) sharing the characteristics of seven transmembrane domains. Dopamine receptors are divided into two classes: D_1-like receptors that groups D_1 and D_5 receptors, D_2-like that groups D_2, D_3 and D_4 receptors.[2] Although these two subfamilies have a high level of structural homology, they have different biochemical responses and pharmacological properties.[3,4]

Dopamine D_2-like receptors are considered the main targets for treatment of dopamine-related disorders above mentioned, but the majority of medications cause severe side effects as a result of preferential binding to other monoamine receptors or to off-target receptors.[5] Accordingly, selective ligands of dopamine receptor subtypes are necessary for effective therapy, especially preferring D_2 and D_3 receptor ligands have become a possible solution to the onset of undesired effects,[6,7] thus extensive medicinal chemistry efforts have been made to discover dopamine D_2R/D_3R ligands in the last decades.[8,9]

Substituted *N*-phenylpiperazine based ligands represent a promising option in this matter[10] and the related pharmacophore model

This is an open access article under the terms of the Creative Commons Attribution-NonCommercial License, which permits use, distribution and reproduction in any medium, provided the original work is properly cited and is not used for commercial purposes.
© 2024 The Authors. *Archiv der Pharmazie* published by Wiley-VCH GmbH on behalf of Deutsche Pharmazeutische Gesellschaft.

has been considered for this study. It is characterized by four subunits: an aryl group, an acyl function, a spacer and a basic region, represented by a substituted aryl-piperazine system.[11] Indeed, the structural elements shown in the model are crucial for intrinsic affinity and some preclinical candidates (e.g., BP897)[12] or commercially available drugs like cariprazine[13] feature these or related core moieties. For example, the aryl-piperazine binds the orthosteric binding site (OBS) and the acyl region could bind a secondary binding pocket (SBP) (Figure 1), which have been found among crystal structures of D_2R and D_3R.[14,15] In details, the piperazine is positioning into the OBS which affects eventually the binding at SBP and creates in protonated form a salt-bridge bond with residue Asp110 of the third transmembrane domain (TM-3) located in both of receptors.[16,17] The arylamide moiety or related ones act as H-bond acceptors and donors and might contain a lipophilic residue that allowed diverse modifications including cycloalkyl, aryl, heteroaryl or biphenyl substituents among the structural developments. So, the opposite parts of the pharmacophore model have been objects of numerous variations except the spacer, that was represented mostly by a *n*-butyl chain. Modifications have been applied such as hydroxy or fluor substituents with the purpose of directing the butyl chain to engender an efficient conformation of the ligand inside binding pockets.[18] Generally, a simple alkyl chain of four carbons seems to be the most suitable structure to respect the two most important requirements for optimal D_2R/D_3R binding properties: linearity and extension.[19] Nevertheless, the development of a marketed drug such as cariprazine demonstrated that a variation of the butyl chain is possible and can lead to a further optimization of D_2R and D_3R binding properties.[20–22] The innovation of this drug lies in its structure: the 1,4-disubstituted cyclohexyl unit, used as a linker, is a conformational restriction that reduces the overall number of possible conformations and, as a consequence, favors the molecular recognition by the target receptor,[23] in this case D_2 and D_3 receptors.

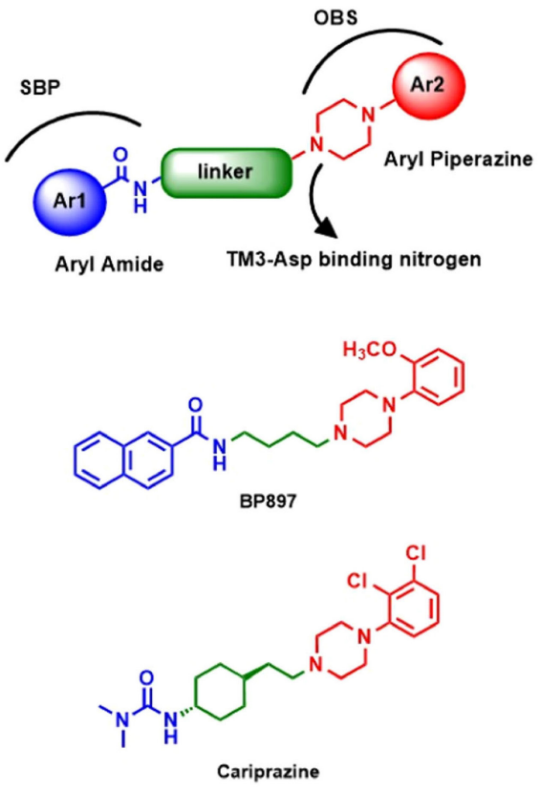


FIGURE 1 Schematic representation of pharmacophore model of selective D_3R ligands with some compounds bearing the core moieties. OBS, orthosteric binding site; SBP, secondary binding pocket; TM-3, third transmembrane domain.

Inspired by this type of lead optimization,[24] we report herein a new set of conformationally restricted 1-(2-methoxyphenyl) piperazine derivatives presenting nanomolar affinity for D_2 and D_3 dopamine receptors. The compounds were designed as aromatic analogs of the drug cariprazine having 1-(2-methoxyphenyl) piperazine moiety for the OBS and a simple methylamide function for SBP which is bioisosterically similar to the urea group supported by cariprazine (Figure 2). We use the piperazine unit presented in BP897 because it is a potent D_2R/D_3R ligand that inhibits cocaine-seeking behaviors without having primary rewarding effects, so it can be used for therapy of drug addiction associated with mental disorders.[25] We propose an aromatic linker with two variations: phenylmethyl and phenylethyl. For each variation, we have evaluated the substitution patterns in *ortho*, *meta* and *para* positions to analyze which conformation is respecting the linearity concept of C4-chain. In addition, we have provided further variations of the amide group of D_2R/D_3R selective pharmacophore model using nitro or cyano as electron-withdrawing group (EWG), aniline, methanamine and acetanilide as electron-donating group (EDG) in different positions thanks to the changeable western end position of our proposed linkers.

2 | RESULTS AND DISCUSSION

2.1 | Chemistry

The synthesis of compounds **1a–c** and **2a–c** was carried out according to our previous study by Hackling et al. with slight modifications.[26] Conditions of alkylation between related benzonitrile halides and 1-(2-methoxyphenyl) piperazine were modified by changing the solvent. Whereas, the reduction of cyano group was performed differently by using the catalyst Raney-Ni leading to the formation of primary amines **2a–c** which were acylated with acetic anhydride and triethylamine in dichloromethane to obtain phenylmethyl linker derivatives **3a–c**. To synthetize the phenylethyl linker derivatives **6a–c**, two different alkylating methods were performed. Compounds **4a**, **4b** were obtained through the alkylation between 1-(2-methoxyphenyl) piperazine and corresponding halides (Method

15214184, 2024, 8, Downloaded from https://onlinelibrary.wiley.com/doi/10.1002/ardp.202400071, Wiley Online Library on [08/10/2025]. See the Terms and Conditions (https://onlinelibrary.wiley.com/terms-and-conditions) on Wiley Online Library for rules of use; OA articles are governed by the applicable Creative Commons License

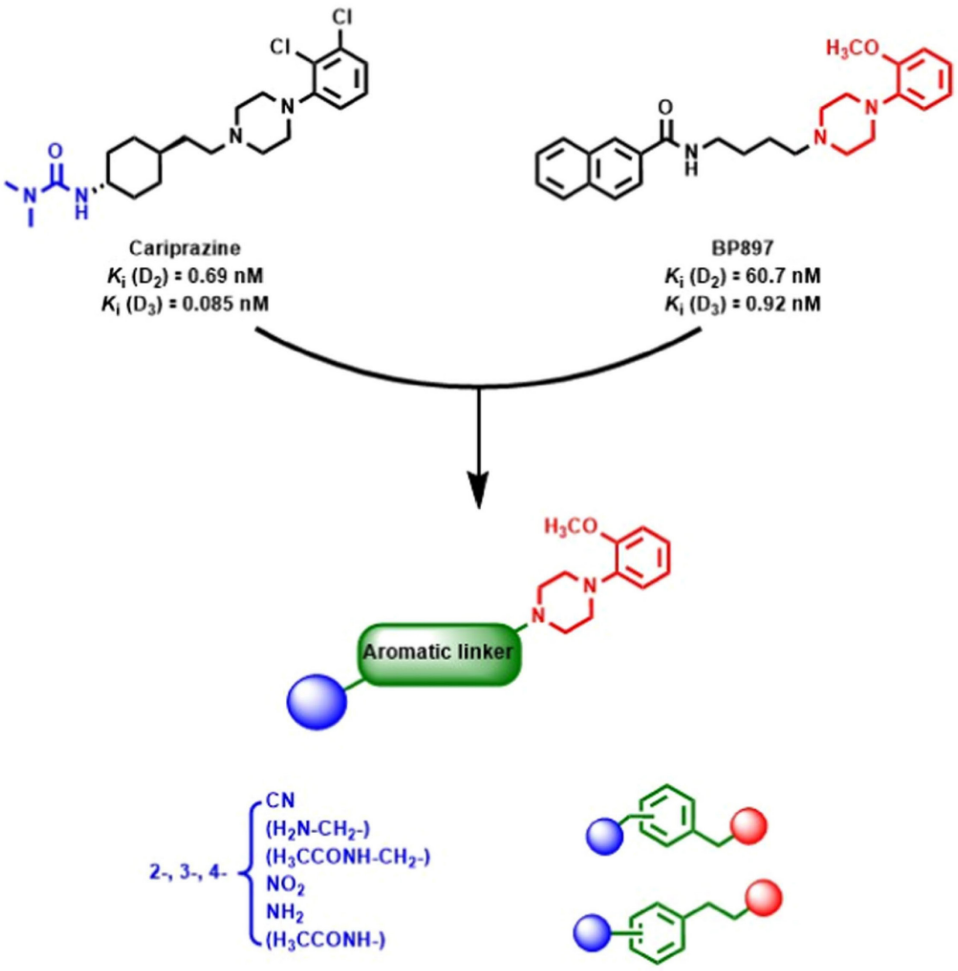


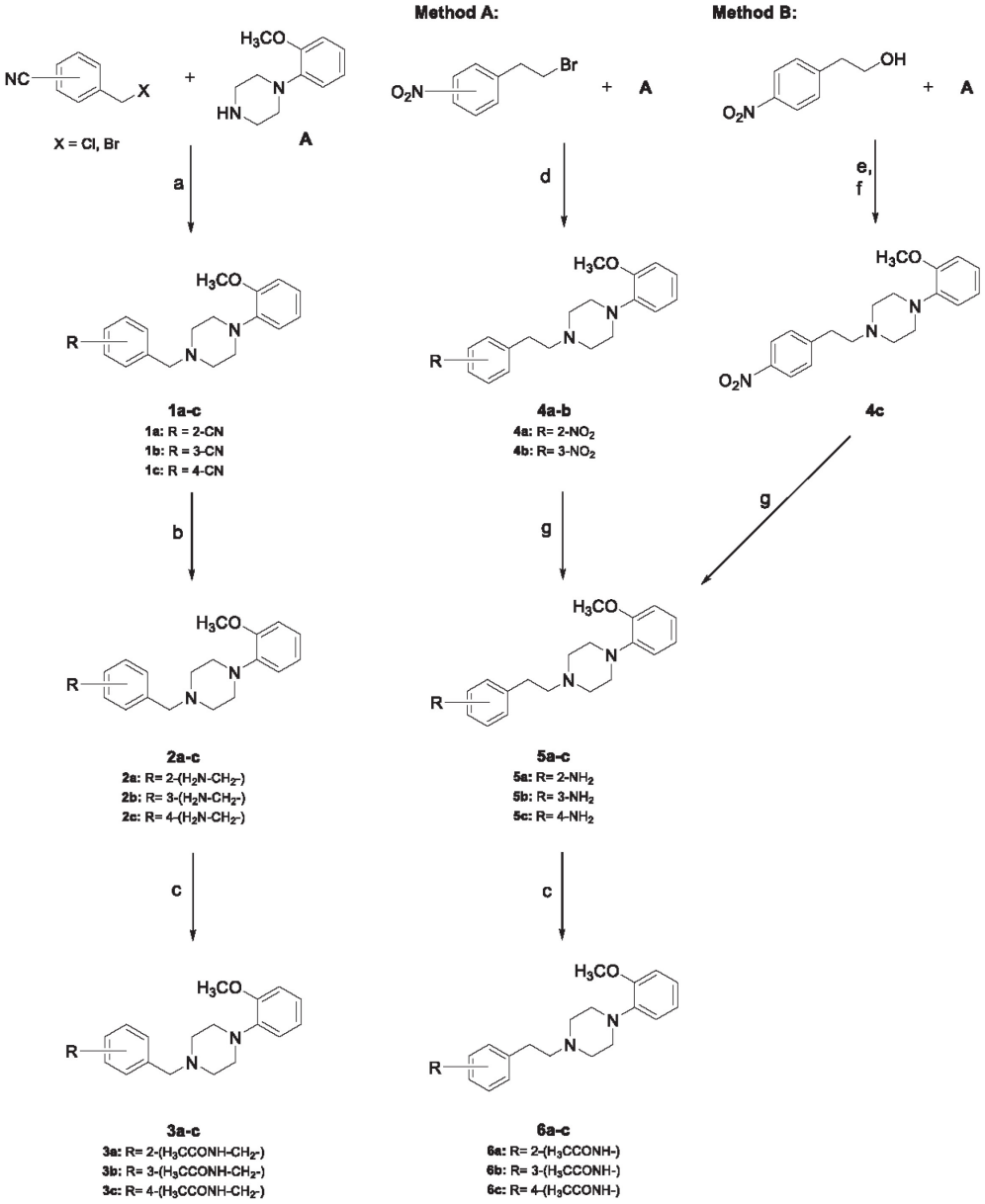
FIGURE 2 Concept of D_2R/D_3R ligands described in this study. The blue moieties are the bioisosteric substitutions of urea. The red moieties represent the aryl-piperazine derived from the second lead compound BP897. The areas marked green show the two new linkers explored in this study.

A), while the precursor **4c** was made activating first the alcohol with methane sulfonyl chloride and then alkylating it with the piperazine **A** (Method B). The nitro precursors **4a–c** were reduced first into anilines (**5a–c**) using the catalyst Pd/C 10% under H_2 atmosphere and subsequently were coupled with acetic anhydride to amides **6a–c** following the procedure, used for derivatives **3a–c**. All synthetic approaches are shown in Scheme 1. All compounds shown in this study were obtained as free base derivatives and crystallized preferentially as hydrochlorides (**1a–b**, **3a**, **3c**, **4a–c**, **6c**). To comply this, a standard procedure was adapted by literature[27] and applied using Et_2O as a solvent to solubilize the free base compounds and adding a solution of HCl in dioxane (2M). Precursor **1c**, amide derivatives **6a**, **6b**, aliphatic primary amines **2a–c** and aromatic primary amines **5a–c** were obtained as free base solids in Et_2O due to their insolubility properties. Compound **3b** featured to have problems with the obtaining of hydrochloride, we believed the reason could be related to its *meta* orientation, therefore oxalic acid was used to form the corresponding crystallized salt according to the previous literature.[28]

2.2 | Pharmacology and SAR

In this study, affinity was tested in radioligand displacement assays for human isoforms of the dopamine D_2 short receptor ($D_{2s}R$) and D_3R according to a general procedure already described.[29–31] Briefly, the membranes expressing the human dopamine $D_{2s}R$ and D_3R were prepared through extraction from CHO-K1 cells. [^{3}H]

15214184, 2024, 8, Downloaded from https://onlinelibrary.wiley.com/doi/10.1002/ardp.202400071, Wiley Online Library on [08/02/2025]. See the Terms and Conditions (https://onlinelibrary.wiley.com/terms-and-conditions) on Wiley Online Library for rules of use; OA articles are governed by the applicable Creative Commons License



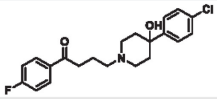
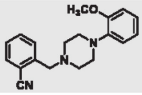
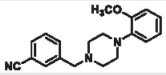
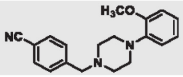
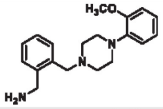
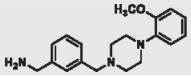
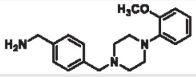
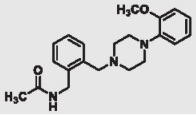
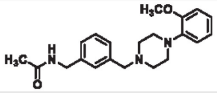
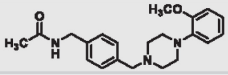
SCHEME 1 Synthesis of compounds **3a–c**, **6a–c**, and the corresponding precursors and intermediates. Reagents and conditions: (a) K_2CO_3, acetonitrile, reflux, 3 h; (b) Raney-Ni, NH_3/MeOH, H_2 5 bar, 40°C, 16 h; (c) Ac_2O, Et_3N, CH_2Cl_2, reflux, 3 h; Method A: (d) K_2CO_3, DMF, 130°C, 4 min, μW; Method B: (e) methane sulfonyl chloride, Et_3N, CH_2Cl_2, 0°C, 15 min; (f) K_2CO_3, acetonitrile, reflux, 16 h; (g) Pd/C 10%, H_2, MeOH, RT, 18 h.

Spiperone has been used as a radioligand and haloperidol to measure unspecific binding and as reference for these assays. The affinity values with the corresponding confidence intervals (CIs) and the ratio indices are listed in Table 1 for the phenylmethyl linker and in Table 2 for the phenylethyl linker derivatives.

Although chemical characterization for **1a–c**, **2a–c**, **3c**, **5c**, and **6c** and different pharmacological evaluations for **1c** and **3c** can be found in previous literature,[26,32–34] a novel scientific viewpoint has been reported in this study focusing on aromatic motif variations to evaluate possibly new SAR with an efficient and simple chemistry.

15214184, 2024, 8, Downloaded from https://onlinelibrary.wiley.com/doi/10.1002/ardp.202400071, Wiley Online Library on [08/02/2025]. See the Terms and Conditions (https://onlinelibrary.wiley.com/terms-and-conditions) on Wiley Online Library for rules of use; OA articles are governed by the applicable Creative Commons License

TABLE 1 Structures, physicochemical properties, and biological data of ligands with substituted phenylmethyl linker.

Name	Structure	mp (°C)	clog*P*[a]	K_i (D_2R) (nM) (95% confidence interval [CI])	K_i (D_3R) (nM) (95% CI)	Ratio (D_2R/D_3R)[b]
Haloperidol		152	3.08	2.61 (2.02, 3.39)	13.5 (10.4, 17.4)	0.2
1a		243–245[c]	3.45	1453 (542, 3898)	9498 (3968, 22,732)	0.2
1b		232[c]	3.45	498 (165, 1499)	2030 (1241, 3322)	0.2
1c		116–118[c]	3.45	580 (143, 2353)	1711 (119, 2459)	0.3
2a		189.5[c]	2.75	7003 (3558, 13782)	35,795 (24,359, 52,600)	0.2
2b		167–170[c]	2.75	1135 (465, 2771)	2402 (1674, 3445)	0.5
2c		97–99[c]	2.75	774 (347, 1725)	627 (321, 1223)	1.2
3a		204[c]	2.58	126 (62.1, 254)	415 (179, 965)	0.3
3b		84[d]	2.58	413 (246, 695)	889 (315, 2511)	0.5
3c		222[e]	2.58	324 (101, 1042)	205 (65.8, 638.6)	1.6

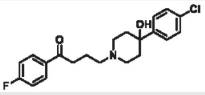
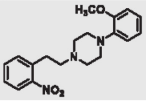
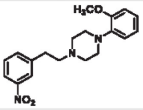
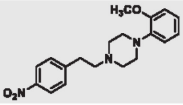
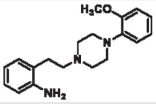
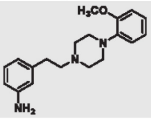
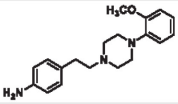
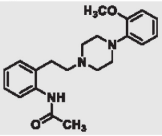
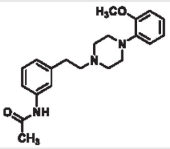
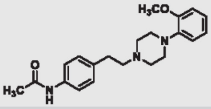
[a]Log *P* values calculated using MarvinSketch by ChemAxon.
[b]Ratio K_i(D_2R)/K_i(D3R).
[c](Re)Crystallized from Et_2O.
[d](Re-)Crystallized from EtOAc.
[e](Re-)Crystallized from EtOH.

Indeed, all compounds show modest to low nanomolar affinity values on both target receptors. Comparing the two linkers proposed in this study, we can affirm that phenylethyl spacer is providing higher binding properties than the phenylmethyl one. The amide derivatives **3a–c** and **6b,c** demonstrate having better binding properties than the corresponding precursors and intermediates. It is not the case for **6a** because **4a** and **5a** showed better affinity values than the corresponding amide analogous. If the positions of the amide group are considered (*ortho*, *meta*, *para*), a progressive increase of the affinity values toward both receptors is observed. Interestingly, only derivative **3a** shows a different tendency with better K_i values than **6a**. The *para* derivatives **3c** and **6c** show a slight preference for D_3R over D_2R, the phenylethyl linker with 4-substituent on the aromatic ring is fully respecting the key points of evaluated pharmacophore model: linearity and extension.[19,26] In contrast, a bent conformation represented by *ortho* and *meta* substitutions for both linkers is giving a slight preference toward dopamine D_2 over D_3 and, as a consequence, the derivatives **3a,b** and **6a,b** have a different pharmacological profile compared to the one of *para* isomers.

Concerning electron density, we can affirm two concepts: (1) The presence of an EWG as nitro or cyano instead of an EDG as amide, aniline or methanamine decreases the affinity to both receptors. (2) The amide unit is working better than the aniline or methanamine function as EDG in terms of binding properties. Of course, the difference of affinity values between the synthetized ligands depends on structural conformation and H-bond/acceptor properties of the

15214184, 2024, 8, Downloaded from https://onlinelibrary.wiley.com/doi/10.1002/ardp.202400071, Wiley Online Library on [08/02/2025]. See the Terms and Conditions (https://onlinelibrary.wiley.com/terms-and-conditions) on Wiley Online Library for rules of use; OA articles are governed by the applicable Creative Commons License

TABLE 2 Structures, physicochemical properties, and biological data of ligands with substituted phenylethyl linker.

Name	Structure	mp (°C)	clogP[a]	K_i (D_2R) (nM) (95% confidence interval [CI])	K_i (D_3R) (nM) (95% CI)	Ratio (D_2R/D_3R)[b]
Haloperidol		152	3.08	2.61 (2.02, 3.39)	13.5 (10.4, 17.4)	0.2
4a		203–205[c]	3.84	221 (23.8, 2044)	294 (142, 609)	0.8
4b		194–196[c]	3.84	365 (66.5, 2000)	239 (82.5, 693)	1.5
4c		222[c]	3.84	206 (55.0, 768)	160 (79.0, 325)	1.3
5a		97.8[c]	3.10	236 (94.7, 588)	434 (106, 1781)	0.5
5b		109.6[c]	3.10	219 (52.6, 913)	195 (65.0, 584)	1.1
5c		87.4[c]	3.10	75.6 (34.3, 167)	106 (51.5, 219)	0.7
6a		115[c]	3.21	498 (330, 750)	1179 (621, 2237)	0.4
6b		124[c]	3.21	193 (87.8, 424)	201 (153, 263)	0.9
6c		296[d]	3.21	14.9 (5.94, 37.4)	9.2 (4.10, 20.7)	1.6

[a]Log *P* values calculated using MarvinSketch by ChemAxon.
[b]Ratio K_i(D2R)/K_i(D3R).
[c](Re)Crystallized from Et_2O.
[d](Re-)Crystallized from iPrOH.

amide group, but manipulation of electron density is a further factor that can play an important role in binding the secondary pocket of D_2R and D_3R. For instance, compound **6c** presents a pharmacological profile 100-fold better than **4c**, this optimization is not found in **5c** even though it has an EDG like **6c**. The latter aspect is also evident for the phenylmethyl linker derivatives (Table 1) whereby intermediates **2a–c** have higher K_i values than corresponding precursors **1a–c** and methylamide ligands (**3a–c**) have the best profiles. Regarding the other phenylethyl ligands, a different situation is observed for **4a**, **5a**, and **6a**, in which the precursor shows better binding properties. We believe

15214184, 2024, 8, Downloaded from https://onlinelibrary.wiley.com/doi/10.1002/ardp.202400071, Wiley Online Library on [08/02/2025]. See the Terms and Conditions (https://onlinelibrary.wiley.com/terms-and-conditions) on Wiley Online Library for rules of use; OA articles are governed by the applicable Creative Commons License

the reason could be the bent conformation and the steric hindrance particularly for **6a**, because the values among **4a** and **5a** are comparable. However, the pharmacological behavior with a positive trend through the change of EWG with EDG is found again for **4b**, **5b**, and **6b** albeit with little intensity.

Compound **6c** is the most promising part of this work with low nanomolar affinity at both receptors (D_2R K_i = 14.9 nM, D_3R K_i = 9.2 nM). The structure of **6c** shows that *para* substitution with phenylethyl linker variation is a suitable orientation for binding the target receptors. The innovation of aromatic spacers proposed in this study is the inclusion of an aromatic ring in the linker itself and not in the carbonyl function, as it is represented by the pharmacophore model. In this sense, the area of the ligand, where the acyl function is supposed to be, becomes a possibility of infinite modifications that allow to investigate deeply the SBP area of D_2R and D_3R. Therefore, derivative **6c** can be conceived as a reference structure for further SAR studies to develop more interesting dopamine D_2 and D_3 receptor ligands.

2.3 | In silico evaluation of compound 6c

The physicochemical properties of **6c**, haloperidol and cariprazine have been evaluated through the pkCSM online tool.[35] Derivative **6c** is fully respecting the Lipinski's rule[36] because it features four H-bond acceptors, one H-bond donor, the molecular weight is lower than 500 and its cLog*P* is lower than 5. Regarding ADMET properties, some key features, that are relevant to the drug-likeness profile of target compound, have been analyzed, therefore values of **6c** have been compared with the ones shown by marketed drugs like haloperidol and cariprazine. The comparison of ADMET in silico prediction is listed in Table 3 whereby *para* acetamide derivative features a profile very similar to reference compounds. Indeed, **6c** shows slightly better solubility in water and intestinal absorption, comparable distribution values confirming that **6c** has an elevated grade of absorption by passive diffusion. As well as the satisfactory value of Blood–Brain Barrier (BBB) permeability indicates that the most promising anilide can be a suitable tool for mental disorder, which requires physico-chemical parameters that are in line with marketed drugs haloperidol and cariprazine. The target derivative is supposed to be a substrate of CYP2D6 and CYP3A4 which are two main isoforms of cytochrome P450 responsible for drug metabolism. Nevertheless, in silico predictions assess that **6c** is likely going to be cytochrome P450 inhibitor (CYP1A2, CYP2D6, and CYP3A4) which is observable also in the considered drugs with the difference that haloperidol is inhibiting CYP2D6 and CYP3A4 while cariprazine only CYP2D6. One main difference is related to toxicity data, showing that **6c** may have mutagenic characteristics due to the positiveness of AMES toxicity test and it could lead to long QT syndrome-fatal ventricular arrhythmia. In conclusion, lead derivative **6c** has promising drug-likeness profile that can be easily compared to ones of marketed drugs like haloperidol and cariprazine, but parameters relative to toxicity hamper possible in vivo screenings. Nevertheless, the structure of **6c** is still open to infinite

TABLE 3 In silico ADMET prediction for compound **6c** and reference compounds.

	Absorption			Distribution		Metabolism						Excretion	Toxicity
						Cyp substrate	Cyp inhibitor						
Compound	Water solubility (log mol/L)[a]	Intestinal absorption in humans (% absorbed)[b]	Caco2 permeability (log Papp in 10^{-6} cm/s)	VDss (human) (log L/Kg)[c]	Blood–Brain Barrier permeability (logBB)[d]	2D6	3A4	1A2	2C19	2C9	2D6	3A4	Total clearance (log mL/min/kg)	AMES toxicity
Haloperidol	−4.1	89.6	0.9	1.4	0.1	Yes	Yes	No	No	No	Yes	Yes	1.1	No
Cariprazine	−4.7	87.2	1.0	0.9	0.2	Yes	Yes	No	No	No	Yes	No	0.6	No
6c	**−3.3**	90.2	0.9	1.1	0.2	Yes	Yes	Yes	No	No	Yes	Yes	0.9	Yes

[a]Water solubility (lo(mol/L)): highly soluble > 0 > very soluble > −2 > soluble > −4 > moderately > −6 > poorly soluble > −10 > insoluble.

[b]Intestinal absorbance value < 30%: poor soluble.

[c]Volume of distribution (VDss): log VDss < −0.15 is low and log VDss > 0.45 is high.

[d]log BB < −1: poorly distributed in the brain. Results were obtained by using the pkCSM online tool available at https://biosig.lab.uq.edu.au/pkcsm/.

15214184, 2024, 8, Downloaded from https://onlinelibrary.wiley.com/doi/10.1002/ardp.202400071, Wiley Online Library on [08/02/2025]. See the Terms and Conditions (https://onlinelibrary.wiley.com/terms-and-conditions) on Wiley Online Library for rules of use; OA articles are governed by the applicable Creative Commons License

variations that might improve toxicity profile and binding properties of phenylethyl linker reported here.

3 | CONCLUSION

All 18 synthesized compounds showed interesting affinity values on both D_2R and D_3R. Most of the compounds revealed a slight preference toward D_2R over D_3R (**1a–c**, **2a,b**, **3a,b**, **4a**, **5a**, **5c**, **6a,b**), whereas **2c**, **3c**, **4b,c**, **5b**, and **6c** showed minor tendency to D_3R over D_2R. Compound **6c** showed the best pharmacological profile with the highest binding properties at both receptors: $pK_i(D_2R) = 7.83$ and $pK_i(D_3R) = 8.04$. SAR evaluation of this work demonstrated that linear and extended conformation of dopamine D_2R and D_3R ligands can also be represented by the linkers proposed here: phenylmethyl and phenylethyl. In particular, the second phenethyl spacer has been shown to be a promising alternative to the widely used chain of four carbon atoms and the cyclohexylethyl linker.[37,38] Furthermore, an EDG in combination with phenethyl linker leads to higher affinity than an electron withdrawing group, especially if EDG is represented by an amide unit.

Considering the results obtained, compound **6c** can be taken as a new starting point for the development of selective dopamine D_2R and D_3R ligands characterized by a new aromatic spacer.

4 | EXPERIMENTAL

4.1 | Chemistry

4.1.1 | General

All starting materials were obtained from Sigma-Aldrich. Analytical thin-layer chromatography was performed on ALUGRAM® silica gel 60-UV_{254} plates and visualized by UV light (Macherey-Nagel) and preparative column chromatography was performed on a silica gel 60M, 0.04-0.063 mm (Macherey-Nagel). ^{1}H-NMR spectra were recorded on a Bruker Advance III spectrometer (Bruker) at 300/600 MHz and ^{13}C-NMR spectra at 75 and 150 MHz The chemical shifts for ^{1}H-NMR and ^{13}C-NMR were referenced to TMS via residual solvent signals (^{1}H, $CDCl_3$ at $\delta = 7.26$ ppm; ^{13}C, $CDCl_3$ at $\delta = 77.36$ ppm; ^{1}H, DMSO-d_6 at $\delta = 2.50$ ppm; ^{13}C, DMSO-d_6 at $\delta = 39.43$ ppm) to identify the signals of protons bonded to aromatic ring Ar = aryl-moiety; Ar-Pip = aryl-piperazine moiety. Chemical shifts are given as parts per million (ppm) and reported as follows: s (singlet), d (doublet), dd (double of doublets), t (triplet), q (quartet), p (pentet), or m (multiplet). The coupling constant (J) is given in Hertz (Hz). Melting points were determined on a M-564 Büchi melting point apparatus (Büchi). Microwave reactions were performed with sealed microwave vials designed for 0.5–2 mL reaction volumes in a Biotage Initiator 2.0 oven (Biotage). Mass values for identity of target compounds were determined on Advion APCI mass spectrometer express CMS in negative and positive mode (Advion) and data are shown as $[M+H^+]^+$. Solvents have been evaporated using a Rotavapor R II (Büchi) with a PC 3001 VARIO Chemie Vacuum pump (Vacuubrand) and CVC 3000 Vacuum controlling system. The compounds have been dried with the high-vacuum pump (Hybrid-Pumpe RC 6; Vacuubrand). Purity determination of the described ligands was performed with LC connected to low-resolution mass spectrometer for **1a–c**, **3a–c**, **4a–c**, **6a–c**, and connected to a high resolution mass spectrometer for **2a–c** and **5a–c**. LC-MS and LC/HR-MS data are shown as $[M+H^+]^+$ with purity grade in brackets (%). The stock solutions for LC-MS measurements (approximately 1 mg/mL) were diluted with methanol hyper grade for LC-MS and concentrations of approximately 0.1–0.2 mg/mL were obtained (injection: 2 µL). Relative purity of the compounds was determined. Ion-trap LC/MS analysis was made with this LC system: Elute SP LC System (Bruker Daltonics) with vacuum degasser, binary pump, autosampler, column oven. Column: Intensity Solo 2 C18 (100 × 2.1 mm); Temperature: 40°C; Mobile phase: A. water hypergrade for LC-MS with 0.1% formic acid (v/v) (Merck); B. Acetonitrile hypergrade for LC-MS (for LC-MS); Flow Rate: 0.2 mL/min; MS-System: amaZon speed ETD ion Trap LC/MS System (Bruker Daltonics); Ionization: electron spray; Polarity: positive; Alternating ion-Polarity:on; Scan Range: *m/z*: 80–1200; Nebulizer: Nitrogen, 15 Psi; Dry Gas: Nitrogen, 8 l/min, 200°C; Mass range Mode: Ultra Scan. Methods of LC-MS measurements: (Method 1 for **1a–c**, **3a–c**, **4a–b**, **6a–c**): Analysis: 0–4 min 98% A, 4–5 min gradient 98%–95% A, 5–9 min 95% A, 9–16 min gradient 95%–5% A, 16–17 min. gradient 5%–0% A, reconditioning: 17–18 min gradient to 0%–98% A, 18–21 min 98% A. (Method 2 for **4c**): Analysis: 0–4 min 95% A, 4–14 min gradient 95%–20% A, 14–16 min gradient 20%–5% A, 16–17 min. gradient 5%–0% A, reconditioning: 17–18 min. gradient to 95% A, 18–21 min 95% A. (Method 3 for **2a–c** and **5a–c**): MS-System: compact (Bruker Daltonics); Ionization: electron spray; Polarity: positive; Scan range: *m/z*: 50–1300; Nebulizer: Nitrogen, 1.8 bar; Dry Gas: Nitrogen, 9 L/min, 220°C; Mass range mode: Ultra Scan. Quantification was done using Extracted Ion Chromatograms (EIC, for Pitolisant 297 ± 1.5, for internal standard 220.5 ± 1.0). Analysis: 0–4 min 98% A, 4–8 min gradient 98% to 95% A, 5–10 min 95% A, 10–20 min gradient 95%–2% A, reconditioning: 20–22 min gradient 2%–98% A. The InChI codes of the investigated compounds, together with affinity values, are provided in Supporting Information.

4.1.2 | General procedure for the synthesis of {[4-(2-methoxyphenyl)piperazin-1-yl]methyl}benzonitrile precursors (**1a–c**)[26]

Following the corresponding reference literature,[26] 1-(2-methoxyphenyl) piperazine (1.1 eq.) and K_2CO_3 (1.1 eq.) were added at room temperature to a solution of the respective halide benzonitrile (1 eq.) in 20 mL acetonitrile and then heated to reflux for 3 h. After cooling to ambient temperature, the inorganic solid was removed by filtration and acetonitrile was removed under reduced pressure. Afterward, the crude reaction was solubilized in ethyl

15214184, 2024, 8, Downloaded from https://onlinelibrary.wiley.com/doi/10.1002/ardp.202400071, Wiley Online Library on [08/02/2025]. See the Terms and Conditions (https://onlinelibrary.wiley.com/terms-and-conditions) on Wiley Online Library for rules of use; OA articles are governed by the applicable Creative Commons License

15214184, 2024, 8, Downloaded from https://onlinelibrary.wiley.com/doi/10.1002/ardp.202400071, Wiley Online Library on [08/02/2025]. See the Terms and Conditions (https://onlinelibrary.wiley.com/terms-and-conditions) on Wiley Online Library for rules of use; OA articles are governed by the applicable Creative Commons License

acetate. The organic phase was washed with an aqueous solution of HCl 1M, which was then neutralized with NaOH 6M and an extraction with dichloromethane was performed three times. The organic layers were combined and dried with Mg_2SO_4. The obtained crude was purified by column chromatography in SiO_2 with dichloromethane/methanol 98:2 to obtain the pure benzonitrile precursors **1a–c**.

2-{[4-(2-Methoxyphenyl)piperazin-1-yl]methyl}benzonitrile hydrochloride (**1a**): Yellow oil. Yield = 95%. The obtained product was solubilized in Et_2O and a solution of HCl in dioxane (2M) was added drop by drop. A white precipitate of HCl salt was obtained which was recrystallized in iPrOH. ^{1}H-NMR (300 MHz, $CDCl_3$) δ = 13.31 (s, 1H), 7.82 (ddd, J = 7.6, 1.4 Hz, 1H Ar), 7.69 (td, J = 7.6, 1.4 Hz, 1H Ar), 7.60 (dt, J = 7.5 Hz, 1H Ar), 7.48 (td, J = 7.5, 1.4 Hz, 1H Ar), 6.97–6.82 (m, 4H Ar-Pip), 3.76 (s, 3H), 3.70 (s, 2H), 2.95 (s, 4H), 2.56 (t, 4H). ^{13}C-NMR (75 MHz, DMSO-d_6) δ = 151.82, 139.26, 139.17, 133.43, 133.12, 132.36, 130.37, 123.49, 120.78, 118.29, 117.22, 113.92, 112.05, 56.59, 55.37, 51.28, 46.66. LC-MS (ESI[+]) m/z [M+H$^+$]$^+$ = 308.12 (98.22%); MS (APCI [+]) m/z [M+H$^+$]$^+$ calculated for $[C_{19}H_{22}N_3O]^+$: 308.1, found 308.2. M = 343.40 g/mol (HCl salt). mp = 243–245°C (Et_2O).

3-{[4-(2-Methoxyphenyl)piperazin-1-yl]methyl}benzonitrile hydrochloride (**1b**): Light-yellow oil. Yield = 76%. The obtained compound was solubilized in Et_2O and a solution of HCl in dioxane (2M) was added drop by drop. A white precipitate of HCl salt was obtained which was recrystallized in iPrOH. ^{1}H-NMR (300 MHz, DMSO-d_6) δ = 11.38 (s, 1H), 8.17 (t, 1H Ar), 7.99 (ddt, J = 7.8 Hz, 2H Ar), 7.70 (t, J = 7.8 Hz, 1H Ar), 7.06–6.86 (m, 4H Ar-Pip), 4.45 (d, 2H), 3.78 (s, 3H), 3.51–3.00 (m, 8H). ^{13}C-NMR (75 MHz, DMSO-d_6) δ = 151.80, 139.20, 136.40, 135.18, 133.00, 131.11, 129.81, 123.44, 120.76, 118.24, 112.01, 111.64, 57.39, 55.32, 50.78, 46.60. LC-MS (ESI [+]) m/z [M+H$^+$]$^+$ = 308.16 (97.53%); MS (APCI [+]) m/z [M+H$^+$]$^+$ calculated for $[C_{19}H_{22}N_3O]^+$: 308.1, found 308.3. M = 343.40 g/mol (HCl salt). mp = 232°C (Et_2O).

4-{[4-(2-Methoxyphenyl)piperazin-1-yl]methyl}benzonitrile (**1c**)[34]: Yellow oil. Yield = 88%. The pure product was obtained as a solid by crystallization in diethyl ether. ^{1}H-NMR (300 MHz, $CDCl_3$) δ = 7.68–7.58 (m, 2H Ar), 7.53–7.45 (m, 2H Ar), 7.04–6.83 (m, 4H Ar-Pip), 3.86 (s, 3H), 3.62 (s, 2H), 3.10 (d, 4H), 2.65 (t, 4H). ^{13}C-NMR = (75 MHz, $CDCl_3$) δ 152.56, 144.45, 141.57, 132.26, 129.73, 123.10, 121.25, 119.07, 118.43, 111.65, 111.16, 62.75, 55.58, 53.66, 50.84. LC-MS (ESI [+]) m/z [M+H$^+$]$^+$ = 308.15 (99.38%); MS (APCI [+]) m/z [M+H$^+$]$^+$ calculated for $[C_{19}H_{22}N_3O]^+$: 308.1, found 307.9. M = 307.40 g/mol (free base). mp = 116–118°C (Et_2O).

4.1.3 | General procedure for the synthesis of {[4-(2-methoxyphenyl)piperazin-1-yl]methyl} phenylmethanamine intermediate derivatives (**2a–c**)[26]

Adapted from Hackling et al.,[26] the catalyst Raney-Ni 50%–50% (1.5 eq.) was added into a solution of NaOH (20 mL) and it was stirred for 1 h at 90°C to activate the catalyst. Then the mixture was washed first with water and then with methanol three times each. Finally, the methanolic solution of activated catalyst was added to the solution of respective benzonitrile precursor (1 eq.) in ammonia/methanol (10 mL). The reaction mixture was stirred at 40°C under H_2 atmosphere into autoclave for 16 h. Afterward, the reaction was filtered off with Celyte through Buchner filter, the solution was concentrated under reduced pressure. The pure intermediates **2a–c** were obtained by column chromatography in SiO_2 with dichloromethane/methanol 95:5.

(2-{[4-(2-Methoxyphenyl)piperazin-1-yl]methyl}phenyl) methanamine (**2a**): White solid. Yield = 96%. The pure product was obtained as a solid by crystallization in diethyl ether. ^{1}H-NMR (300 MHz, $CDCl_3$) δ = 7.36–7.18 (m, 4H Ar), 6.98 (ddt, 1H Ar-Pip), 6.91–6.81 (m, 3H Ar-Pip), 3.91 (s, 2H), 3.85 (s, 3H), 3.60 (s, 2H), 3.35 (s, 2H), 3.04 (s, 4H), 2.68 (t, 4H). ^{13}C-NMR (75 MHz, $CDCl_3$) δ = 152.22, 142.22, 141.14, 136.02, 131.34, 129.58, 128.36, 127.00, 122.98, 120.98, 118.25, 111.16, 61.66, 55.36, 53.17, 50.73, 44.78. LC/HR-MS (ESI [+]) m/z [M+H$^+$]$^+$ = 312.2068 (99.05%); MS (APCI [+]) m/z [M+H$^+$]$^+$ calculated for $[C_{19}H_{26}N_3O]^+$: 312.2, found 312.2. M = 311.43 g/mol (free base). mp = 189.5° C (Et_2O).

(3-{[4-(2-Methoxyphenyl)piperazin-1-yl]methyl}phenyl) methanamine (**2b**): White solid. Yield = 92%. The pure product was obtained as a solid by crystallization in diethyl ether. ^{1}H-NMR (300 MHz, $CDCl_3$) δ = 7.25–7.11 (m, 4H Ar), 6.94–6.81 (m, 3H Ar-Pip), 6.77 (dd, 1H Ar-Pip), 3.79 (s, 2H), 3.77 (s, 3H), 3.50 (s, 2H), 3.01 (t, J = 4.8 Hz, 4H), 2.58 (t, J = 4.8 Hz, 4H), 1.85 (s, 2H). ^{13}C-NMR (75 MHz, $CDCl_3$) δ = 152.28, 143.07, 141.41, 138.38, 128.46, 128.08, 127.93, 125.91, 122.87, 120.98, 118.23, 111.15, 63.19, 55.36, 55.32, 53.39, 50.65, 46.39. LC/HR-MS (ESI [+]) m/z [M+H$^+$]$^+$ = 312.2005 (100%); MS (APCI [+]) m/z [M+H$^+$]$^+$ calculated for $[C_{19}H_{26}N_3O]^+$: 312.2, found 312.3. M = 311,43 g/mol (free base). mp = 167–170°C (Et_2O).

(4-{[4-(2-Methoxyphenyl)piperazin-1-yl]methyl}phenyl) methanamine (**2c**): White sticky oil. Yield = 86%. The pure product was obtained as a solid by crystallization in diethyl ether. ^{1}H-NMR (300 MHz, $CDCl_3$) δ 7.25 (d, 2H Ar), 7.22–7.17 (m, 2H Ar), 6.95–6.76 (m, 4H Ar-pip), 3.78 (s, 2H), 3.77 (s, 3H), 3.50 (s, 2H), 3.01 (t, J = 4.8 Hz, 4H), 2.58 (t, J = 4.8 Hz, 4H), 1.80 (s, 2H). ^{13}C-NMR (75 MHz, $CDCl_3$) δ = 152.28, 141.91, 141.40, 136.61, 129.60, 127.05, 122.86, 120.98, 118.23, 111.15, 62.88, 55.32, 53.31, 50.65, 46.19. LC/HR-MS (ESI [+]) m/z [M+H$^+$]$^+$ = 312.2068 (96.24%); MS (APCI [+]) m/z [M+H$^+$]$^+$ calculated for $[C_{19}H_{26}N_3O]^+$: 312.2, found 312.0. M = 311.43 g/mol (free base). mp = 97–99°C (Et_2O).

4.1.4 | General procedure for the synthesis of 1-(2-methoxyphenyl)-4-(nitrophenethyl)piperazine precursors (**4a**, **4b**): Method A

Into a microwave vial of 0.5–2 mL the corresponding bromide (1 eq.), 1-(2-methoxyphenyl) piperazine (1.25 eq.), and K_2CO_3 (1.25 eq.) were added with dimethylformamide (1 mL). The reaction mixture

was stirred in the microwave oven for 4 min at 130°C. After the removal of inorganic salts by filtration and evaporation of DMF under reduced pressure, the crude was solubilized in EtOAc. The organic phase was washed with HCl 1M three times, the aqueous layers were combined and neutralized with NaOH 6M. The basic aqueous phase was extracted with dichloromethane three times and the organic layers were combined, dried over Mg_2SO_4, and concentrated under reduced pressure. The obtained crude was purified by column chromatography in dichloromethane/methanol 98:2 to have the desired NO_2-derivatives.

1-(2-Methoxyphenyl)−4-(2-nitrophenethyl)piperazine hydrochloride (**4a**): Light yellow oil. Yield = 50%. The product was solubilized in Et_2O and a solution of HCl in dioxane (2M) was added drop by drop. A white precipitate of HCl salt was obtained which was recrystallized in iPrOH. ^{1}H-NMR (300 MHz, $CDCl_3$) δ = 12.98 (s, 1H), 7.91 (dd, 1H Ar), 7.53 (td, 1H Ar), 7.44–7.32 (m, 2H Ar), 7.04–6.83 (m, 4H Ar-Pip), 3.87 (s, 3H), 3.75–3.46 (m, 8H), 3.38 (s, 2H), 3.24 (s, 2H). ^{13}C-NMR (75 MHz, $CDCl_3$) δ = 159.56, 149.63, 134.58, 133.93, 129.04, 126.03, 125.45, 124.75, 121.48, 119.32, 118.21, 111.70, 57.60, 55.70, 52.54, 47.69, 28.59. LC-MS (ESI [+]) *m/z* $[M+H^+]^+$ = 342.17 (100%); MS (APCI [+]) *m/z* $[M+H^+]^+$ calculated for $[C_{19}H_{24}N_3O_3]^+$: 342.1, found 342.2. *M* = 377.41 g/mol (HCl salt) mp = 203–205°C (Et_2O).

1-(2-Methoxyphenyl)−4-(3-nitrophenethyl)piperazine hydrochloride (**4b**): Yellow oil. Yield = 60%. The product was solubilized in Et_2O and a solution of HCl in dioxane (2M) was added drop by drop. A white precipitate of HCl salt was obtained which was recrystallized in iPrOH. ^{1}H-NMR (300 MHz, $CDCl_3$) δ = 12.98 (s, 1H), 8.15–8.04 (m, 2H Ar), 7.57 (dt, 1H Ar), 7.46 (t, 1H Ar), 7.06–6.83 (m, 4H Ar-Pip), 3.87 (s, 3H), 3.18–3.09 (m, 4H), 2.96 (dd, 2H), 2.78–2.70 (m, 6H). ^{13}C-NMR (75 MHz, $CDCl_3$) δ = 155.04, 152.50, 150.97, 135.47, 130.43, 126.64, 123.83, 123.57, 122.85, 121.68, 114.94, 112.20, 55.88, 51.88, 51.83, 48.00, 29.97. LC-MS (ESI [+]) *m/z* $[M+H^+]^+$ = 342.17 (100%); MS (APCI [+]) *m/z* $[M+H^+]^+$ calculated for $[C_{19}H_{24}N_3O_3]^+$: 342.1, found 341.9. *M* = 377.41 g/mol (HCl salt). mp = 194–196°C (Et_2O).

4.1.5 | General procedure for the synthesis of 1-(2-methoxyphenyl)−4-(4-nitrophenethyl) piperazine derivative (**4c**): Method B

2-(4-nitrophenyl) ethan1-ol was solubilized in dichloromethane (20 mL). Into this solution methane sulfonyl chloride (1.1 eq.) and triethylamine (1.5 eq.) were added. The reaction mixture was stirred for 15 min in an ice bath. Then, the crude solution of reaction was washed with iced water, HCl 1M and a saturated aqueous solution of $NaHCO_3$. The organic phase was dried over Mg_2SO_4 and concentrated under reduced pressure. No further purification was needed to perform, the mesylated product was obtained with quantitative yield and used directly for the following step of synthesis. So, 1-(2-methoxyphenyl) piperazine (1eq.) and K_2CO_3 (1 eq.) were added into a solution of 4-nitrophenethyl methane sulfonate in ACN (15 mL) at room temperature. The reaction mixture was left to stir 16 h at reflux. After that, the inorganic salts were filtered off and ACN was removed under reduced pressure. The crude oil was solubilized in EtOAc and washed with HCl 1M. The acidic aqueous solution was neutralized with NaOH 6M and extracted with dichloromethane three times. Organic layers were combined, dried over Mg_2SO_4 and then concentrated under reduced pressure. The crude yellow oil was purified by column chromatography in SiO_2 with dichloromethane/methanol 98:2.

1-(2-Methoxyphenyl)−4-(4-nitrophenethyl)piperazine hydrochloride (**4c**): Yellow oil. Yield = 71%. The free base product was solubilized in Et_2O and a solution of HCl in dioxane (2M) was added drop by drop. A white precipitate of HCl salt was obtained which was recrystallized in iPrOH. ^{1}H-NMR (300 MHz, DMSO-d_6) δ = 10.61 (s, 1H), 8.19–8.12 (m, 2H Ar), 7.59–7.52 (m, 2H Ar), 6.98–6.82 (m, 4H Ar-Pip), 3.77 (s, 3H), 3.66–3.54 (m, 6H), 3.25 (dd, 4H), 3.03 (t, 2H). ^{13}C-NMR (75 MHz, DMSO-d_6) δ = 151.83, 146.51, 145.46, 139.02, 130.13, 123.78, 120.87, 118.41, 112.02, 55.44, 55.28, 51.03, 46.93, 39.25, 29.05. LC-MS (ESI [+]) *m/z* $[M+H^+]^+$ = 342.13 (100%); MS (APCI [+]) *m/z* $[M+H^+]^+$ calculated for $[C_{19}H_{24}N_3O_3]^+$: 342.1, found 342.0. *M* = 377.41 g/mol (HCl salt). mp = 222°C (Et_2O).

4.1.6 | General procedure for the synthesis of aniline intermediate derivatives (**5a–c**)

A round bottom flaks with two necks was charged by the corresponding nitro precursor (1 eq.) and Pd/C 10% (1 eq.) in methanol (15 mL). Subsequently, the flask was purged first with N_2 atmosphere to make dry conditions and then with H_2 atmosphere. The reaction was stirred at room temperature for 18 h. Afterward, the mixture was filtered off with Buchner filter on Celyte, the solution was concentrated under reduced pressure and there was no need for any further purification.

2-{2-[4-(2-Methoxyphenyl)piperazin-1-yl]ethyl}aniline (**5a**): White solid. Yield = 79%. The pure product was obtained as a solid by crystallization in diethyl ether. ^{1}H-NMR (300 MHz, $CDCl_3$) δ = 7.08–6.98 (m, 3H Ar), 6.97–6.91 (m, 2H Ar/Ar-pip), 6.91–6.84 (m, 1H Ar-pip), 6.76–6.64 (m, 2H Ar-pip), 4.03 (s, 2H), 3.87 (s, 3H), 3.13 (s, 4H), 2.87–2.63 (m, 8H). ^{13}C-NMR (75 MHz, $CDCl_3$) δ = 152.28, 145.22, 141.18, 130.27, 127.38, 125.81, 123.03, 121.01, 118.53, 118.20, 115.83, 111.22, 58.82, 55.37, 53.68, 50.71, 29.95. LC/HR-MS (ESI [+]) *m/z* $[M+H^+]^+$ = 312.2088 (100%); MS (APCI [+]) *m/z* $[M+H^+]^+$ calculated for $[C_{19}H_{26}N_3O]^+$: 312.2, found 312.0. *M* = 311.43 (free base). mp = 97.8°C (Et_2O).

3-{2-[4-(2-Methoxyphenyl)piperazin-1-yl]ethyl}aniline (**5b**): Yellow solid. Yield = 92%. The pure product was obtained as a solid by crystallization in diethyl ether. ^{1}H-NMR (300 MHz, $CDCl_3$) δ = 7.12–6.84 (m, 5H Ar/Ar-pip), 6.67–6.50 (m, 3H Ar-pip), 3.87 (s, 3H), 3.76–3.49 (m, 2H), 3.14 (t, 4H), 2.83–2.58 (m, 8H). ^{13}C-NMR (75 MHz, $CDCl_3$) δ = 152.29, 146.48, 141.61, 141.36, 129.34, 122.93, 121.01, 119.06, 118.23, 115.51, 112.95, 111.17, 60.60, 55.39, 53.46, 50.69, 33.64. LC/HR-MS (ESI [+]) *m/z* $[M+H^+]^+$ = 312.2128 (100%); MS (APCI [+]) *m/z* $[M+H^+]^+$ calculated for $[C_{19}H_{26}N_3O]^+$: 311.2, found 312.0. *M* = 311.43 (free base). mp = 109.6°C (Et_2O).

15214184, 2024, 8, Downloaded from https://onlinelibrary.wiley.com/doi/10.1002/ardp.202400071, Wiley Online Library on [08/02/2025]. See the Terms and Conditions (https://onlinelibrary.wiley.com/terms-and-conditions) on Wiley Online Library for rules of use; OA articles are governed by the applicable Creative Commons License

15214184, 2024, 8, Downloaded from https://onlinelibrary.wiley.com/doi/10.1002/ardp.202400071, Wiley Online Library on [08/02/2025]. See the Terms and Conditions (https://onlinelibrary.wiley.com/terms-and-conditions) on Wiley Online Library for rules of use; OA articles are governed by the applicable Creative Commons License

4-{2-[4-(2-Methoxyphenyl)piperazin-1-yl]ethyl}aniline (**5c**)[33]: Light orange solid. Yield = 85%. The pure product was obtained as a solid by crystallization in diethyl ether. ^{1}H-NMR (300 MHz, DMSO-d_6) δ = 7.02–6.83 (m, 6H Ar/Ar-pip), 6.53–6.46 (m, 2H Ar-pip), 4.83 (s, 2H), 3.77 (s, 3H), 2.97 (t, 4H), 2.64–2.52 (m, 6H), 2.50–2.42 (m, 2H). ^{13}C-NMR (75 MHz, DMSO-d_6) δ = 151.93, 146.50, 141.27, 128.94, 127.23, 122.27, 120.80, 117.83, 113.94, 111.86, 60.54, 55.26, 53.00, 50.04, 32.03. LC/HR-MS (ESI [+]) *m/z* $[M+H^+]^+$ = 312.2120 (100%); MS (APCI [+]) *m/z* $[M+H^+]^+$ calculated for $[C_{19}H_{26}N_3O]^+$: 312.2, found 311.9. *M* = 311.43 (free base). mp = 87.4°C (Et_2O).

4.1.7 | General procedure for the synthesis of the amide products (3a–c and 6a–c)

A mixture of respective amine (1 eq.), acetic anhydride (1.1 eq.), and triethylamine (1 eq.) in dichloromethane (30 mL) was stirred at reflux for 3 h. Then, the reaction mixture was washed with water and a saturated solution of $NaHCO_3$, was dried over Mg_2SO_4 and concentrated under reduced pressure. Finally, a purification through column chromatography in SiO_2 with dichloromethane/ammonia in methanol 95:5 was performed to obtain the pure derivatives.

N-(2-{[4-(2-Methoxyphenyl)piperazin-1-yl]methyl}benzyl) acetamide hydrochloride (**3a**): Light brown oil. Yield = 88%. The pure compound was solubilized in Et_2O and a solution of HCl in dioxane (2M) was added drop by drop into it. A white precipitate of HCl salt was obtained which was recrystallized in a solution of iPrOH/EtOH 1:1. ^{1}H-NMR (300 MHz, DMSO-d_6) δ = 10.93 (s, 1H), 9.05 (t, *J* = 5.9 Hz, 1H), 7.67 (dd, 1H Ar), 7.53–7.31 (m, 3H Ar), 7.07–6.85 (m, 4H Ar-Pip), 4.53 (d, 2H), 4.41 (d, *J* = 5.9 Hz, 2H), 3.79 (s, 3H), 3.57–2.99 (m, 8H), 1.89 (s, 3H). ^{13}C-NMR (150 MHz, DMSO-d_6) δ = 170.12, 151.85, 139.80, 139.08, 132.63, 129.98, 129.93, 127.47, 127.37, 123.71, 120.85, 118.38, 112.04, 55.73, 55.43, 51.06, 46.81, 40.06, 22.48. LC-MS (ESI [+]) *m/z* $[M+H^+]^+$ = 354.18 (96.27%); MS (APCI [+]) *m/z* $[M+H^+]^+$ calculated for $[C_{21}H_{28}N_3O_2]^+$: 354.2, found 354.0. *M* = 389.47 g/mol (HCl salt). mp = 204°C (Et_2O).

N-(3-{[4-(2-Methoxyphenyl)piperazin-1-yl]methyl}benzyl) acetamide hydrogenoxalate (**3b**): Brown oil. Yield = 67%. The obtained pure product was solubilized in EtOAc and stirred at room temperature during the dropwise addition of oxalic acid (1.1 eq.) solution in EtOAc. Then the obtained oxalic salt was recrystallized in iPrOH. ^{1}H-NMR (300 MHz, DMSO-d_6) δ = 8.37 (t, *J* = 5.9 Hz, 1H), 7.40–7.23 (m, 4H Ar), 7.02–6.84 (m, 4H Ar-Pip), 4.27 (d, *J* = 5.9 Hz, 2H), 3.97 (s, 2H), 3.77 (s, 3H), 3.08 (s, 4H), 2.93 (s, 4H), 1.88 (s, 3H). ^{13}C-NMR (75 MHz, DMSO-d_6) δ = 168.99, 162.76, 162.39, 157.87, 151.90, 139.83, 128.83, 128.37, 127.03, 126.99, 122.76, 120.76, 118.06, 112.00, 60.56, 55.29, 51.93, 48.56, 41.96, 22.47. LC-MS (ESI [+]) *m/z* $[M+H^+]^+$ = 354.20 (99.91%); MS (APCI [+]) *m/z* $[M+H^+]^+$ calculated for $[C_{21}H_{28}N_3O_2]^+$: 354.2, found 354.2. *M* = 443.50 g/mol (oxalic salt). mp = 84°C (EtOAc).

N-(4-{[4-(2-Methoxyphenyl)piperazin-1-yl]methyl}benzyl) acetamide hydrochloride (**3c**)[32]: Yellowish oil. Yield = 89%. The pure compound was solubilized in EtOH and a solution of HCl in dioxane (2M) was added drop by drop. A white precipitate of HCl salt was obtained which was recrystallized in a solution of i-PrOH/EtOH 1:1. ^{1}H-NMR (300 MHz, DMSO-d_6) δ = 11.12 (s, 1H), 8.43 (t, *J* = 5.9 Hz, 1H), 7.61–7.55 (m, 2H Ar), 7.33 (d, 2H Ar), 7.06–6.83 (m, 4H Ar-Pip), 4.34 (d, 2H), 4.28 (d, *J* = 5.9 Hz, 2H), 3.56 (s, 3H), 3.50–3.29 (m, 4H), 3.22–2.99 (m, 4H), 1.88 (s, 3H). ^{13}C-NMR (150 MHz, DMSO-d_6) δ = 169.25, 151.83, 141.12, 139.12, 131.61, 127.91, 127.46, 123.67, 120.81, 118.35, 111.96, 58.24, 55.38, 50.55, 46.71, 41.78, 22.57. LC-MS (ESI [+]) *m/z* $[M+H^+]^+$ = 354.18 (100%); MS (APCI [+]) *m/z* $[M+H^+]^+$ calculated for $[C_{21}H_{28}N_3O_2]^+$: 354.2, found 354.1. *M* = 389.47 g/mol (HCl salt). mp = 222°C (EtOH).

N-(2-{2-[4-(2-Methoxyphenyl)piperazin-1-yl]ethyl}phenyl) acetamide (**6a**): Pink solid. Yield = 74%. The pure product was obtained as a solid by crystallization in Et_2O. ^{1}H-NMR (300 MHz, DMSO-d_6) δ = 9.53 (s, 1H), 7.42–7.34 (m, 1H Ar), 7.28–7.06 (m, 3H Ar), 6.99–6.83 (m, 4H Ar-Pip), 3.77 (s, 3H), 2.98 (t, *J* = 4.6 Hz, 4H), 2.76 (dd, 4H), 2.59 (t, *J* = 4.6 Hz, 4H), 2.07 (s, 3H). ^{13}C-NMR (75 MHz, DMSO-d_6) δ = 168.25, 151.97, 141.23, 136.22, 134.60, 129.69, 126.06, 125.75, 125.13, 122.26, 120.81, 117.87, 112.04, 58.58, 55.30, 53.00, 49.97, 28.57, 23.36. LC-MS (ESI [+]) *m/z* $[M+H^+]^+$ = 354.19 (99.97%); MS (APCI [+]) *m/z* $[M+H^+]^+$ calculated for $[C_{21}H_{28}N_3O_2]^+$: 354.2, found 354.1. *M* = 353.47 g/mol (free base). mp = 115°C (Et_2O).

N-(3-{2-[4-(2-Methoxyphenyl) piperazin-1-yl]ethyl}phenyl)acetamide (**6b**): White solid. Yield = 74%. The pure product was obtained as a solid by crystallization in Et_2O. ^{1}H-NMR (300 MHz, DMSO-d_6) δ = 9.85 (s, 1H), 7.47–7.36 (m, 2H Ar), 7.19 (t, 1H Ar), 6.96–6.85 (m, 5H Ar/Ar-Pip), 3.77 (s, 3H), 2.95 (d, 4H), 2.72 (dd, 2H), 2.56 (t, 6H), 2.02 (s, 3H). ^{13}C-NMR (75 MHz, DMSO-d_6) δ = 168.08, 151.95, 141.28, 140.85, 139.18, 128.37, 123.31, 122.20, 120.80, 119.18, 117.84, 116.68, 112.03, 59.68, 55.29, 52.91, 49.98, 32.84, 23.88. LC-MS (ESI [+]) *m/z* $[M+H^+]^+$ = 354.18 (99.45%); MS (APCI [+]) *m/z* $[M+H^+]^+$ calculated for $[C_{21}H_{28}N_3O_2]^+$: 354.2, found 354.2. *M* = 353.47 g/mol (free base). mp = 124°C (Et_2O).

N-(4-{2-[4-(2-Methoxyphenyl)piperazin-1-yl]ethyl}phenyl) acetamide hydrochloride (**6c**)[33]: Light yellow oil. Yield = 90%. The free base product was solubilized in iPrOH and a solution of HCl in dioxane (2N) was added drop by drop. A white precipitate of HCl salt was obtained which was recrystallized in iPrOH. ^{1}H-NMR (300 MHz, DMSO-d_6) δ = 10.59 (s, 1H), 9.84 (s, 1H), 7.50–7.44 (m, 2H Ar), 7.18–7.12 (m, 2H Ar), 6.95–6.85 (m, 4H Ar-Pip), 3.77 (s, 3H), 2.96 (t, 5H), 2.70 (dd, 2H), 2.55 (q, 5H), 2.02 (s, 3H). ^{13}C-NMR (75 MHz, DMSO-d_6) δ = 168.25, 151.82, 139.40, 138.12, 131.35, 128.90, 123.48, 120.85, 119.24, 118.26, 111.92, 56.30, 55.37, 51.20, 46.94, 28.76, 23.98. LC-MS (ESI [+]) *m/z* $[M+H^+]^+$ = 354.19 (96.77%); MS (APCI [+]) *m/z* $[M+H^+]^+$ calculated for $[C_{21}H_{28}N_3O_2]^+$: 354.2, found 354.0. *M* = 389.47 g/mol (HCl salt). mp = 296°C (iPrOH).

4.2 | Biological assays

All compounds were tested in D_{2s}R and D_3R binding studies in vitro as described previously.[29–31] In brief, compounds were tested at seven appropriate concentrations in a radioligand displacement

assay. The affinity at human recombinant dopamine receptors was determined by incubation of test compounds, membrane preparations from CHO-K1 cells stably expressing $hD_{2S}R/hD_3R$ and radioligand for 120 min. As radioligand [^{3}H]spiperone was used for $D_{2S}R/D_3R$. Bound radioligand was harvested through GF/B filters (Perkin Elmer) by washing three times with distilled water and measured using liquid scintillation counting. Nonspecific binding was determined using 10 µM Haloperidol. Obtained data from at least three independent experiments in triplicates were analyzed with GraphPad Prism 7 using nonlinear regression (one site competition on logarithmic scale). Cheng–Prusoff equation[39] was used to transform IC_{50} to K_i values. Statistical analysis was performed on pK_i values and transformed into mean K_i values and corresponding 95% CIs.

ACKNOWLEDGMENTS

The authors have nothing to report. Open Access funding enabled and organized by Projekt DEAL.

CONFLICTS OF INTEREST STATEMENT

The authors declare no conflicts of interest.

DATA AVAILABILITY STATEMENT

The data that support the findings of this study are available from the corresponding author upon reasonable request.

ORCID

Cristian Di Biase http://orcid.org/0009-0008-9313-3887
Holger Stark https://orcid.org/0000-0003-3336-1710

REFERENCES

[1] J.-M. Beaulieu, R. R. Gainetdinov, *Pharmacol. Rev.* **2011**, *63*, 182. https://doi.org/10.1124/pr.110.002642.182
[2] D. Vallone, R. Picetti, E. Borrelli, *Neurosci. Biobehav. Rev.* **2000**, *24*, 125. https://doi.org/10.1016/S0149-7634(99)00063-9
[3] D. M. Jackson, A. Westlind-Danielsson, *Pharmacol. Ther.* **1994**, *64*, 291.
[4] C. Missale, S. R. Nash, S. W. Robinson, M. Jaber, M. G. Caron, *Physiol. Rev.* **1998**, *78*, 189.
[5] P. G. Strange, *Pharmacol. Rev.* **2001**, *53*, 119.
[6] F. Boeckler, H. Lanig, P. Gmeiner, *J. Med. Chem.* **2005**, *48*, 694. https://doi.org/10.1021/jm049612a
[7] A. E. Moritz, R. B. Free, D. R. Sibley, *Cell. Signal.* **2018**, *41*, 75. https://doi.org/10.1016/j.cellsig.2017.07.003
[8] G. Campiani, S. Butini, F. Trotta, C. Fattorusso, B. Catalanotti, F. Aiello, S. Gemma, V. Nacci, E. Novellino, J. A. Stark, A. Cagnotto, E. Fumagalli, F. Carnovali, L. Cervo, T. Mennini, *J. Med. Chem.* **2003**, *46*, 3822. https://doi.org/10.1021/jm0211220
[9] F. Boeckler, P. Gmeiner, *Biochim. Biophys. Acta Biomembr.* **2007**, *1768*, 871. https://doi.org/10.1016/j.bbamem.2006.12.001
[10] B. Lee, M. Taylor, S. A. Griffin, T. McInnis, N. Sumien, R. H. Mach, R. R. Luedtke, *Molecules* **2021**, *26*, 3182. https://doi.org/10.3390/molecules26113182
[11] A. E. Hackling, H. Stark, *ChemBioChem* **2002**, *3*, 946. https://doi.org/10.1002/1439-7633(20021004)3:10<946::AID-CBIC946>3.0.CO;2-5
[12] M. Pilla, S. Perachon, F. Sautel, F. Garrido, A. Mann, C. G. Wermuth, J. C. Schwartz, B. J. Everitt, P. Sokoloff, *Nature* **1999**, *400*, 371.
[13] B. Kiss, A. Horváth, Z. Némethy, É. Schmidt, I. Laszlovszky, G. Bugovics, K. Fazekas, K. Hornok, S. Orosz, I. Gyertyán, É. Ágai-Csongor, G. Domány, K. Tihanyi, N. Adham, Z. Szombathelyi, *J. Pharmacol. Exp. Ther.* **2010**, *333*, 328. https://doi.org/10.1124/jpet.109.160432
[14] S. Wang, T. Che, A. Levit, B. K. Shoichet, D. Wacker, B. L. Roth, *Nature* **2018**, *555*, 269. https://doi.org/10.1038/nature25758
[15] E. Y. T. Chien, W. Liu, Q. Zhao, V. Katritch, G. Won Han, M. A. Hanson, L. Shi, A. H. Newman, J. A. Javitch, V. Cherezov, R. C. Stevens, *Science* **2010**, *330*, 1091. https://doi.org/10.1126/science.1197410
[16] S. Maramai, S. Gemma, S. Brogi, G. Campiani, S. Butini, H. Stark, M. Brindisi, *Front. Neurosci.* **2016**, *10*, 1. https://doi.org/10.3389/fnins.2016.00451
[17] A. F. Brito, L. K. S. Moreira, R. Menegatti, E. A. Costa, *Fundam. Clin. Pharmacol.* **2019**, *33*, 13. https://doi.org/10.1111/fcp.12408
[18] A. B. Shaik, V. Kumar, A. Bonifazi, A. M. Guerrero, S. L. Cemaj, A. Gadiano, J. Lam, Z. X. Xi, R. Rais, B. S. Slusher, A. H. Newman, *J. Med. Chem.* **2019**, *62*, 9061. https://doi.org/10.1021/acs.jmedchem.9b00607
[19] S. Butini, K. Nikolic, S. Kassel, H. Brückmann, S. Filipic, D. Agbaba, S. Gemma, S. Brogi, M. Brindisi, G. Campiani, H. Stark, *Prog. Neurobiol.* **2016**, *142*, 68. https://doi.org/10.1016/j.pneurobio.2016.03.011
[20] K. P. Garnock-Jones, *CNS Drugs* **2017**, *31*, 513. https://doi.org/10.1007/s40263-017-0442-z
[21] F. Calabrese, F. I. Tarazi, G. Racagni, M. A. Riva, *CNS Spectr.* **2020**, *25*, 343. https://doi.org/10.1017/S109285291900083X
[22] I. Laszlovszky, Á. Barabássy, G. Németh, *Adv. Ther.* **2021**, *38*, 3652. https://doi.org/10.1007/s12325-021-01797-5
[23] P. de Sena M. Pinheiro, D. A. Rodrigues, R. do Couto Maia, S. Thota, C. A. M. Fraga, *Curr. Top. Med. Chem.* **2019**, *19*, 1712. https://doi.org/10.2174/1568026619666190712205025
[24] T. T. da Silva Cunha, R. R. Silva, D. A. Rodrigues, P. de Sena Murteira Pinheiro, T. Kronenberger, C. M. R. Sant'Anna, F. Noël, C. A. M. Fraga, *Biomolecules* **2022**, *12*, 1112. https://doi.org/10.3390/biom12081112
[25] A. Preti, *Curr. Opin. Invest. Drugs* **2000**, *1*, 110.
[26] A. Hackling, R. Ghosh, S. Perachon, A. Mann, H. D. Höltje, C. G. Wermuth, J. C. Schwartz, W. Sippl, P. Sokoloff, H. Stark, *J. Med. Chem.* **2003**, *46*, 3883. https://doi.org/10.1021/jm030836n
[27] J. M. Kwak, J. S. Moon, J. I. Choi, R. N. Murugan, W. K. Park, J. Y. Gong, H. Y. Lee, H. Y. Koh, *Bull. Korean Chem. Soc.* **2013**, *34*, 3467. https://doi.org/10.5012/bkcs.2013.34.11.3467
[28] M. Bajda, D. Łażewska, J. Godyń, P. Zaręba, K. Kuder, S. Hagenow, K. Łątka, E. Stawarska, H. Stark, K. Kieć-Kononowicz, B. Malawska, *Eur. J. Med. Chem.* **2020**, *185*, 111785. https://doi.org/10.1016/j.ejmech.2019.111785
[29] M. Schübler, B. Sadek, T. Kottke, L. Weizel, H. Stark, *Front. Chem.* **2017**, *5*, 1. https://doi.org/10.3389/fchem.2017.00064
[30] L. Stank, A. Frank, S. Hagenow, H. Stark, *MedChemComm* **2019**, *10*, 1926. https://doi.org/10.1039/c9md00379g
[31] A. Frank, D. J. Kiss, G. M. Keserű, H. Stark, *Sci. Rep.* **2018**, *8*, 12509. https://doi.org/10.1038/s41598-018-30794-y
[32] P. Kowalski, P. Śliwa, G. Satała, R. Kurczab, I. Bartos, K. Zuchowicz, *Arch. Pharm. (Weinheim)* **2017**, *350*, 1. https://doi.org/10.1002/ardp.201700090
[33] J. Mills, US2927924, Eli Lilly, **1960**.
[34] R. Tietze, S. Löber, H. Hübner, P. Gmeiner, T. Kuwert, O. Prante, *Bioorg. Med. Chem. Lett.* **2008**, *18*, 983. https://doi.org/10.1016/j.bmcl.2007.12.026

15214184, 2024, 8, Downloaded from https://onlinelibrary.wiley.com/doi/10.1002/ardp.202400071, Wiley Online Library on [08/02/2025]. See the Terms and Conditions (https://onlinelibrary.wiley.com/terms-and-conditions) on Wiley Online Library for rules of use; OA articles are governed by the applicable Creative Commons License

[35] D. E. V. Pires, T. L. Blundell, D. B. Ascher, *J. Med. Chem.* **2015**, *58*, 4066. https://doi.org/10.1021/acs.jmedchem.5b00104

[36] C. A. Lipinski, F. Lombardo, B. W. Dominy, P. J. Feeney, *Adv. Drug Deliv. Rev.* **1997**, *23*, 3.

[37] G. Németh, R. Csehi, *Front. Psychiatry* **2022**, *13*, 13. https://doi.org/10.3389/fpsyt.2022.1038627

[38] S. Vangveravong, Z. Zhang, M. Taylor, M. Bearden, J. Xu, J. Cui, W. Wang, R. R. Luedtke, R. H. Mach, *Bioorg. Med. Chem.* **2011**, *19*, 3502. https://doi.org/10.1016/j.bmc.2011.04.021

[39] H. C. Cheng, *J. Pharmacol. Toxicol. Methods* **2001**, *46*, 61, https://doi.org/10.1016/S1056-8719(02)00166-1

SUPPORTING INFORMATION

Additional supporting information can be found online in the Supporting Information section at the end of this article.

How to cite this article: C. Di Biase, L. Leitzbach, A. Frank, A. Zivkovic, H. Stark, *Arch. Pharm.* **2024**;*357*:e2400071. https://doi.org/10.1002/ardp.202400071

15214184, 2024, 8, Downloaded from https://onlinelibrary.wiley.com/doi/10.1002/ardp.202400071, Wiley Online Library on [08/02/2025]. See the Terms and Conditions (https://onlinelibrary.wiley.com/terms-and-conditions) on Wiley Online Library for rules of use; OA articles are governed by the applicable Creative Commons License

Supplemental material: ^{1}H-NMR,^{13}C-NMR and HPLC-MS of described compounds

Aromatic linker variations in novel dopamine D_2 and D_3 receptor ligands

Cristian Di Biase[1], Luisa Leitzbach[1], Annika Frank[1], Aleksandra Zivkovic[1], Holger Stark[1]*

1 Institute of Pharmaceutical and Medicinal Chemistry, Heinrich Heine University Düsseldorf, Universitaetsstr.1, Duesseldorf, NRW, Germany

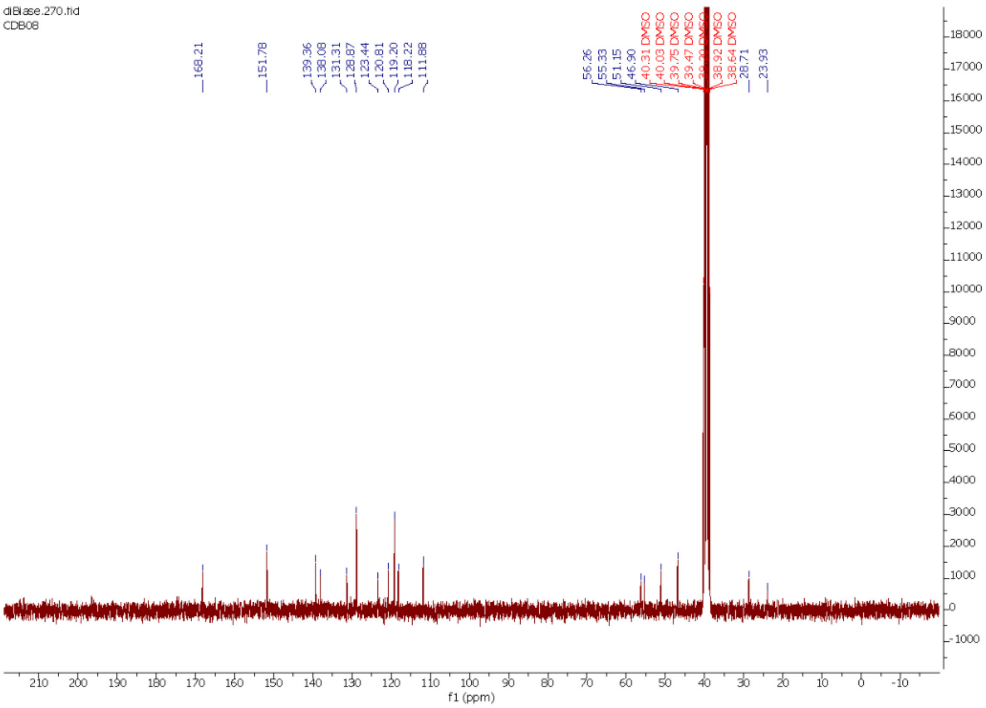
*Correspondence: : Holger Stark, Heinrich Heine University Düsseldorf, Institute of Pharmaceutical and Medicinal Chemistry, Universitätsstr.1, 40225 Düsseldorf, Germany.

Email: stark@hhu.de

Explanatory table for characterization of described compounds

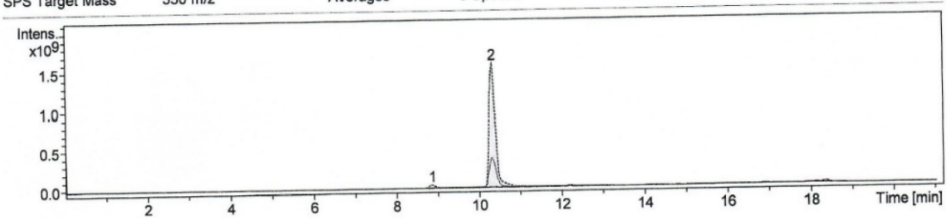
	Identity	*Purity*	
Compound	**APCI-MS**	**HPLC-MS**	**HPLC/HRAM-MS**
1a	X	X	
1b	X	X	
1c	X	X	
2a	X		X
2b	X		X
2c	X		X
3a	X	X	
3b	X	X	
3c	X	X	
4a	X	X	
4b	X	X	
4c	X	X	
5a	X		X
5b	X		X
5c	X		X
6a	X	X	
6b	X	X	
6c	X	X	

^{13}C-NMR



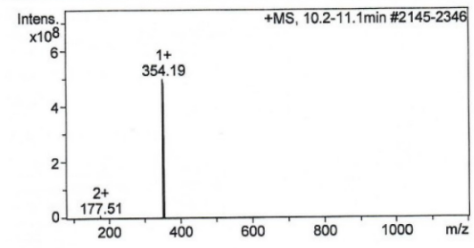
Acquisition Parameter

Ion Source Type	ESI	Ion Polarity	Positive	Alternating Ion Polarity	on
Mass Range Mode	UltraScan	Scan Begin	80 m/z	Scan End	1200 m/z
Accumulation Time	2000 µs	RF Level	59 %	Trap Drive	47.4
SPS Target Mass	350 m/z	Averages	5 Spectra	n/a	n/a



#	RT [min]	Area	S/N	Area Frac. %	Max. m/z
1	8.9	533038400	358.5	3.23	312.16
2	10.3	15976980480	10134.6	96.77	354.19

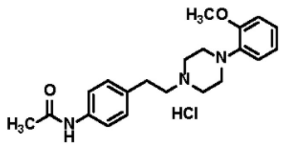
Cmpd 2, 10.3 min



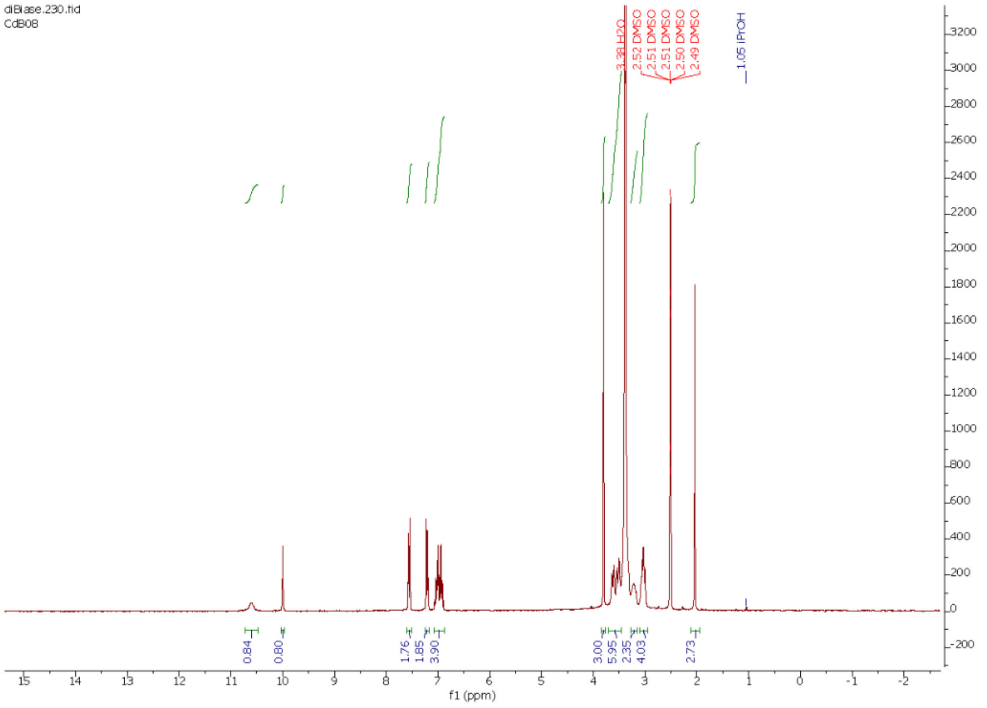
m/z: 354.19 (M+1)

37

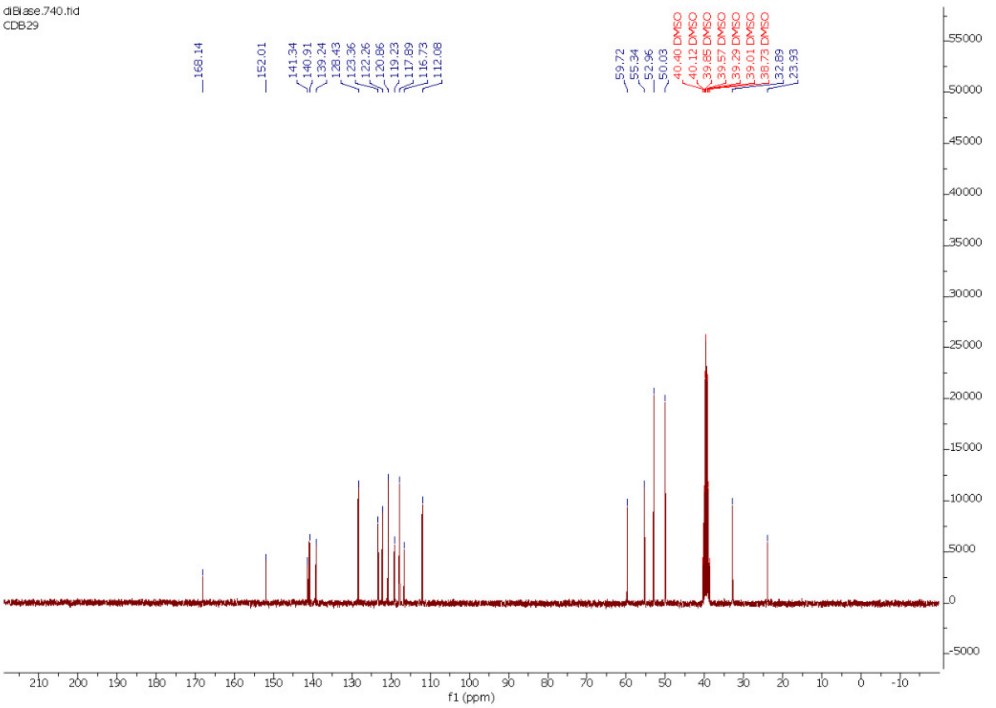
***N*-(4-{2-[4-(2-Methoxyphenyl)piperazin-1-yl]ethyl}phenyl)acetamide hydrochloride (6c)**



^{1}H-NMR

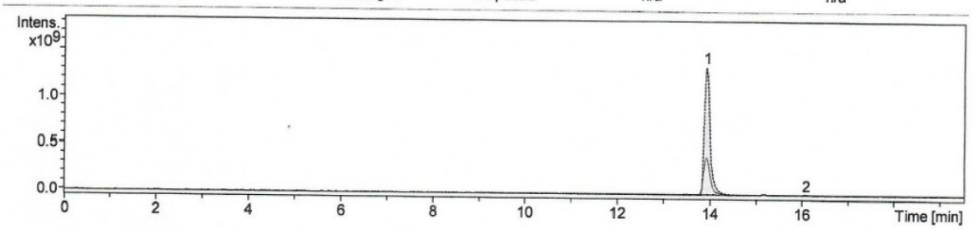


^{13}C-NMR



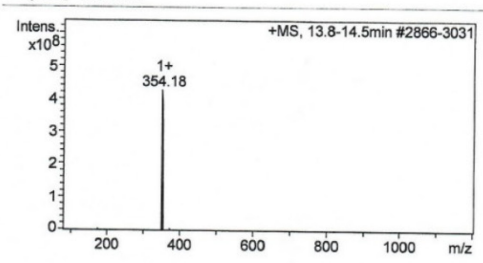
Acquisition Parameter

Ion Source Type	ESI	Ion Polarity	Positive	Alternating Ion Polarity	on
Mass Range Mode	UltraScan	Scan Begin	80 m/z	Scan End	1200 m/z
Accumulation Time	2000 µs	RF Level	59 %	Trap Drive	47.4
SPS Target Mass	350 m/z	Averages	5 Spectra	n/a	n/a



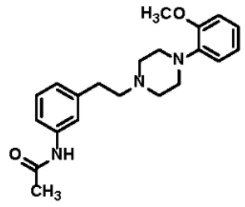
#	RT [min]	Area	S/N	Area Frac. %	Max. m/z
1	13.9	11612632064	7964.0	99.45	354.18
2	16.1	64125736	81.3	0.55	406.19

Cmpd 1, 13.9 min

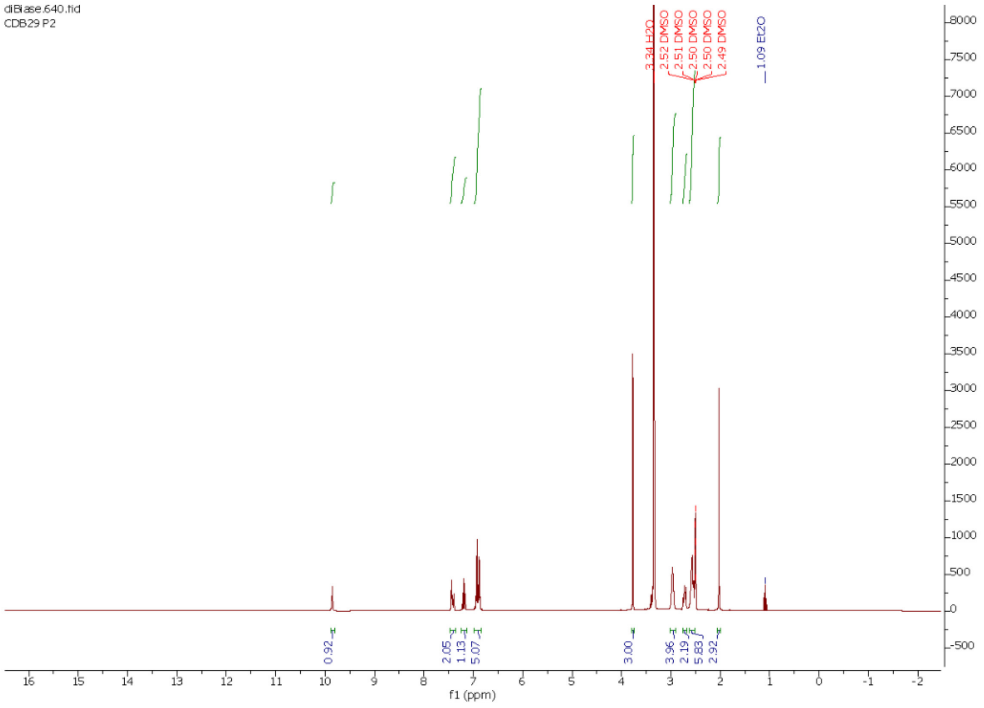


m/z: 354.18 (M+1)

***N*-(3-{2-[4-(2-Methoxyphenyl) piperazin-1-yl]ethyl}phenyl)acetamide (6b)**

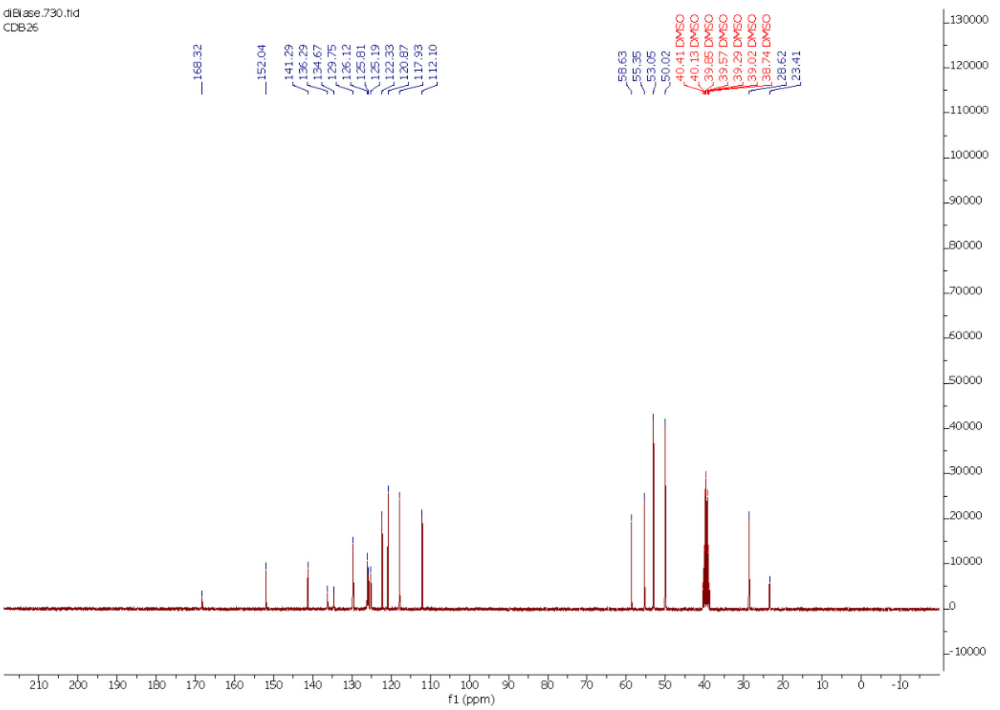


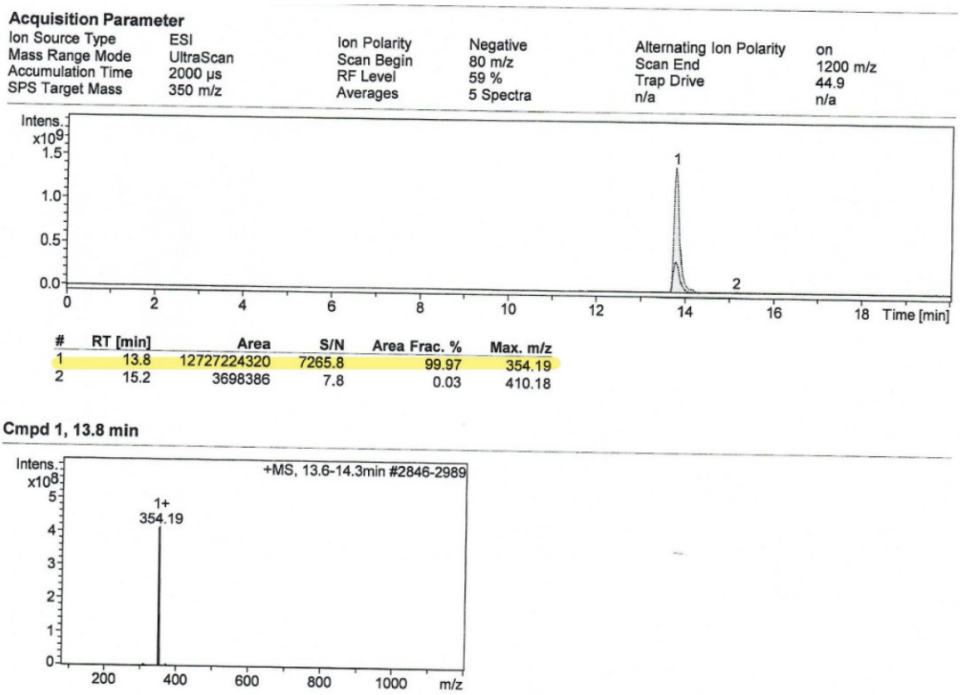
^{1}H-NMR



34

^{13}C-NMR

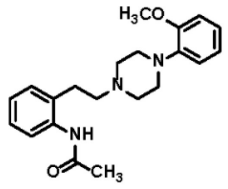




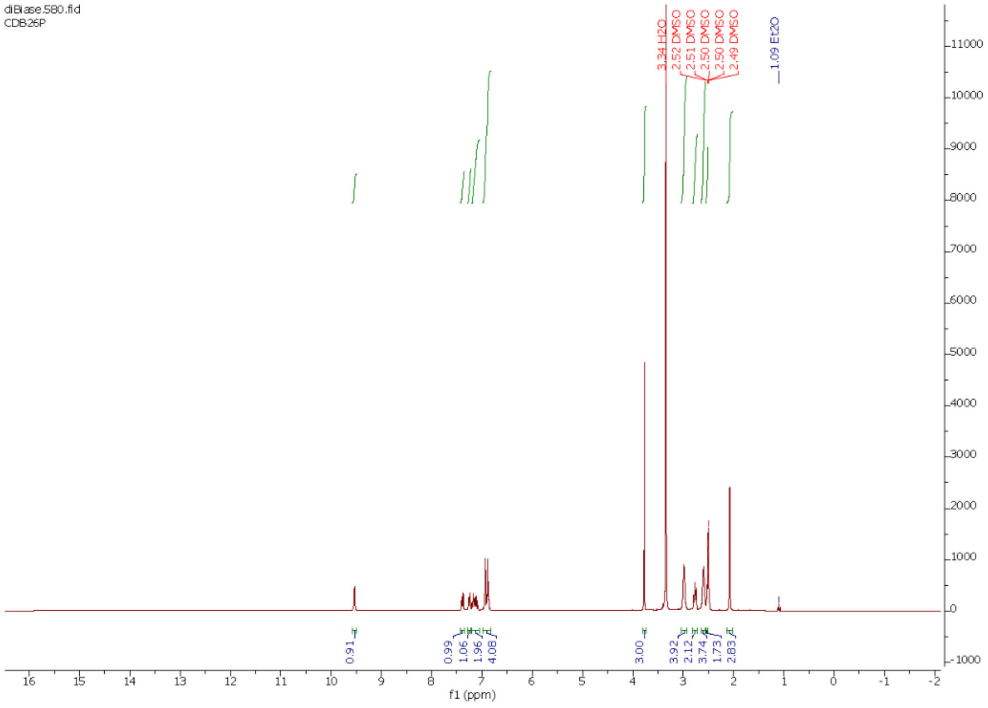
m/z: 354.19 (M+1)

33

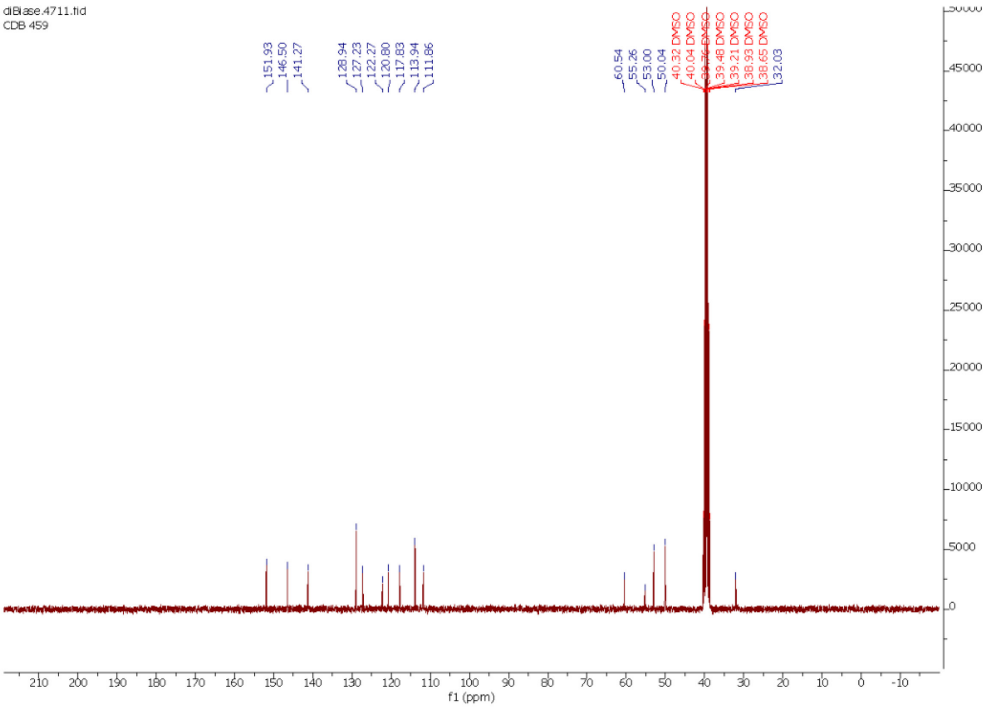
***N*-(2-{2-[4-(2-Methoxyphenyl)piperazin-1-yl]ethyl}phenyl)acetamide (6a)**



^{1}H-NMR

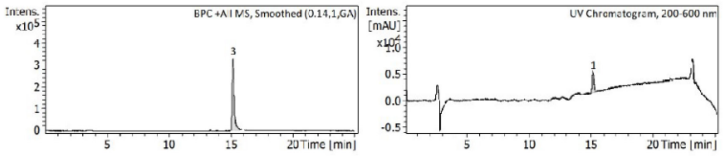


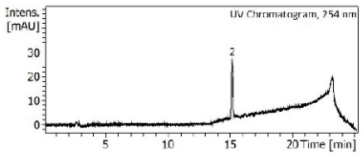
^{13}C-NMR



Acquisition Parameter

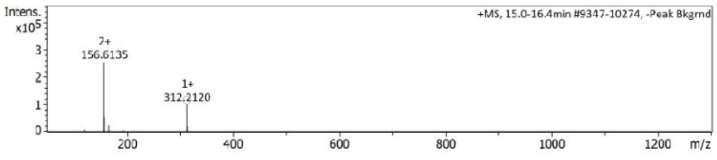
Source Type	ESI	Ion Polarity	Positive	Set Nebulizer	1.8 Bar
Focus	Not active			Set Dry Heater	220 °C
Scan Begin	50 m/z	Set Capillary	4500 V	Set Dry Gas	9.0 l/min
Scan End	1300 m/z	Set End Plate Offset	-500 V	Set Divert Valve	Waste





#	RT [min]	Area	S/N	Max. m/z	FWHM [min]	Area Frac. %
1	15.2	29942.90	45.7		0.1	100.000
2	15.2	200.77	55.0		0.1	100.000
3	15.2	1233117.00	15686.3	156.6135	0.2	100.000

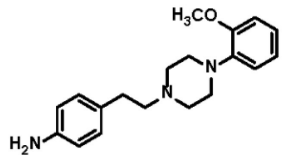
Cmpd 3, 15.2 min



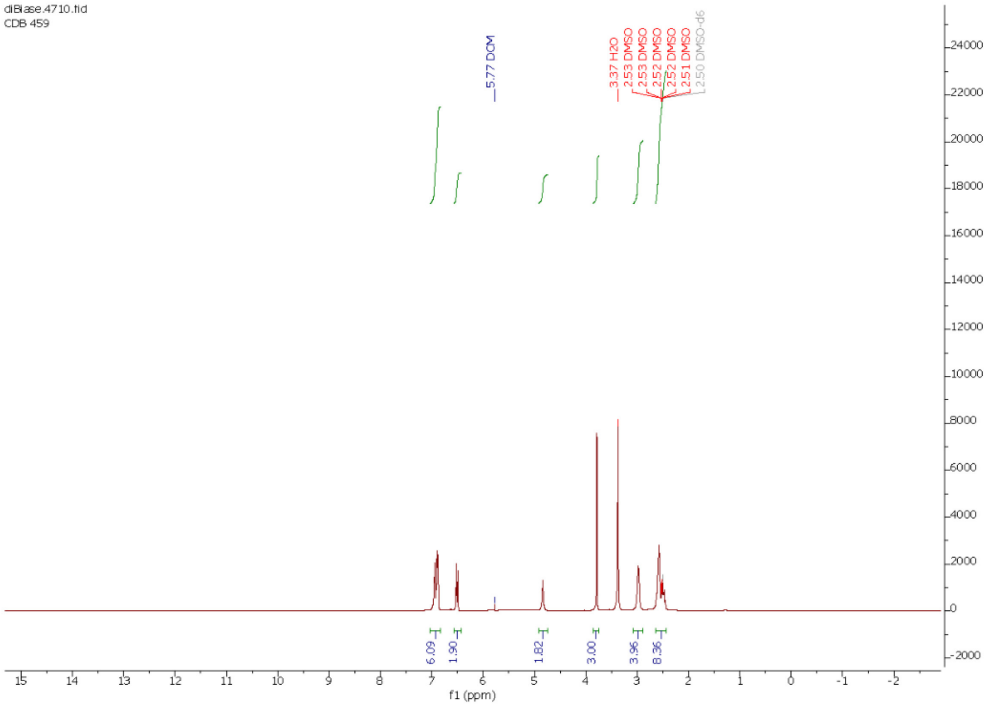
m/z: 312.2120 (M+1)

31

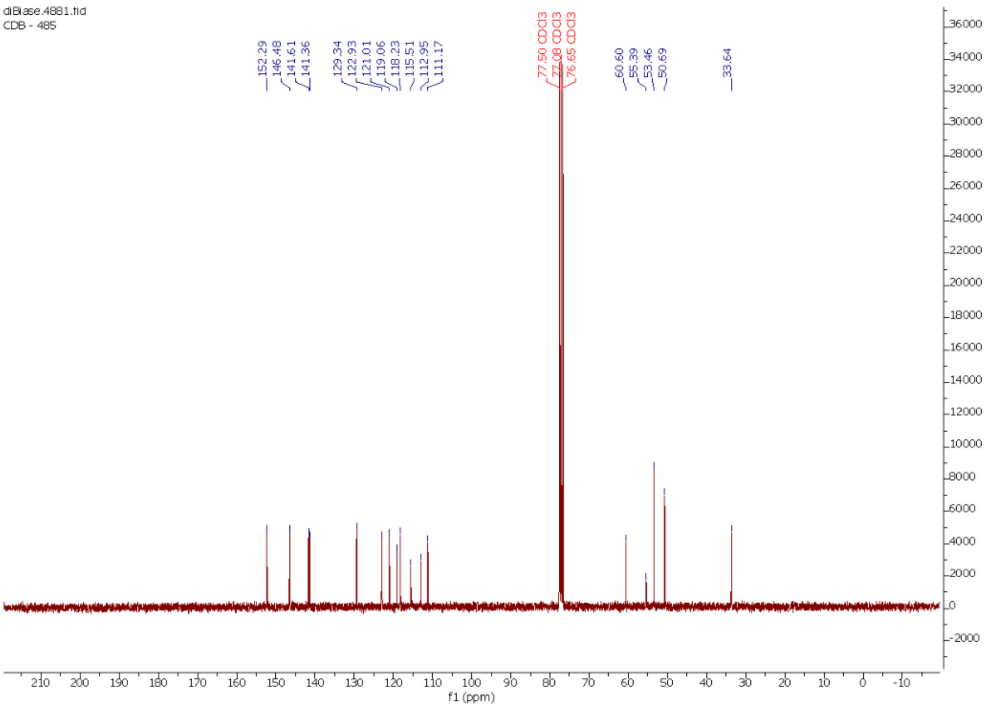
4-{2-[4-(2-Methoxyphenyl) piperazin-1-yl]ethyl}aniline (5c)



^{1}H-NMR

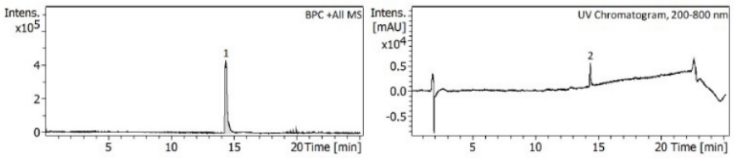


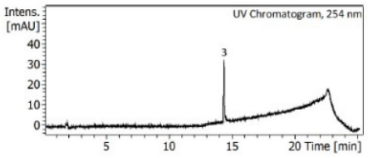
^{13}C-NMR



Acquisition Parameter

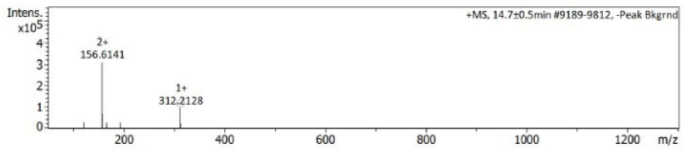
Source Type	ESI	Ion Polarity	Positive	Set Nebulizer	1.8 Bar
Focus	Not active			Set Dry Heater	220 °C
Scan Begin	50 m/z	Set Capillary	4500 V	Set Dry Gas	9.0 l/min
Scan End	1300 m/z	Set End Plate Offset	-500 V	Set Divert Valve	Waste





#	RT [min]	Area	S/N	Max. m/z	FWHM [min]	Area Frac. %
1	14.4	4940661.00	433.2	156.6141	0.2	100.000
2	14.4	24669.65	49.7		0.1	100.000
3	14.4	174.04	60.3		0.1	100.000

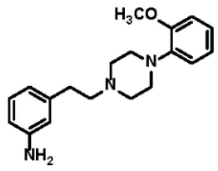
Cmpd 1, 14.4 min



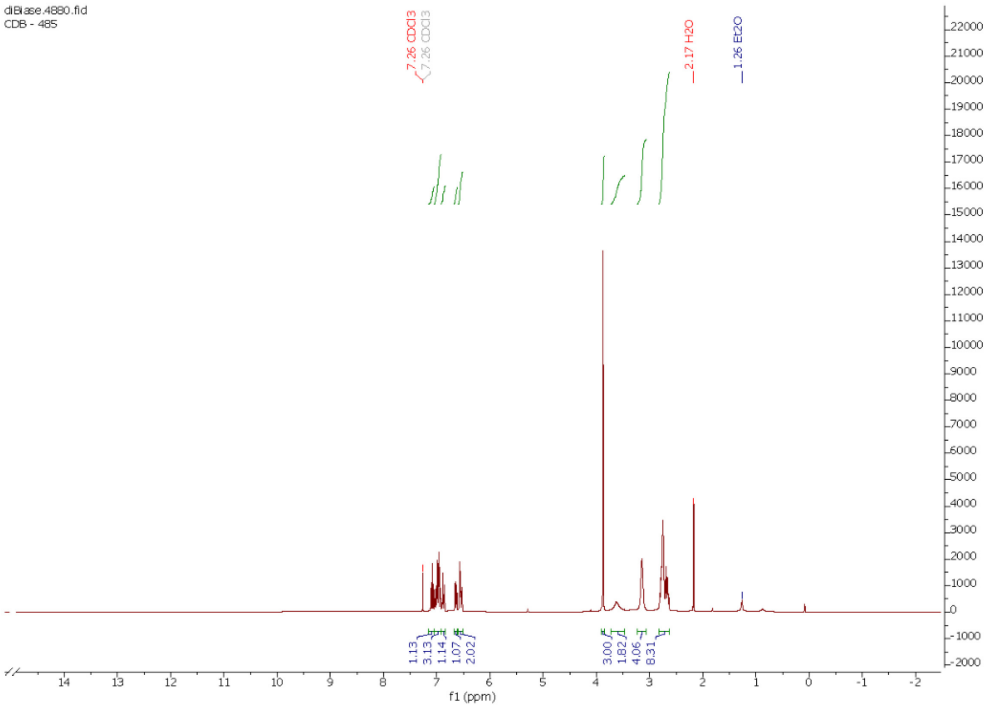
m/z: 312.2128 (M+1)

29

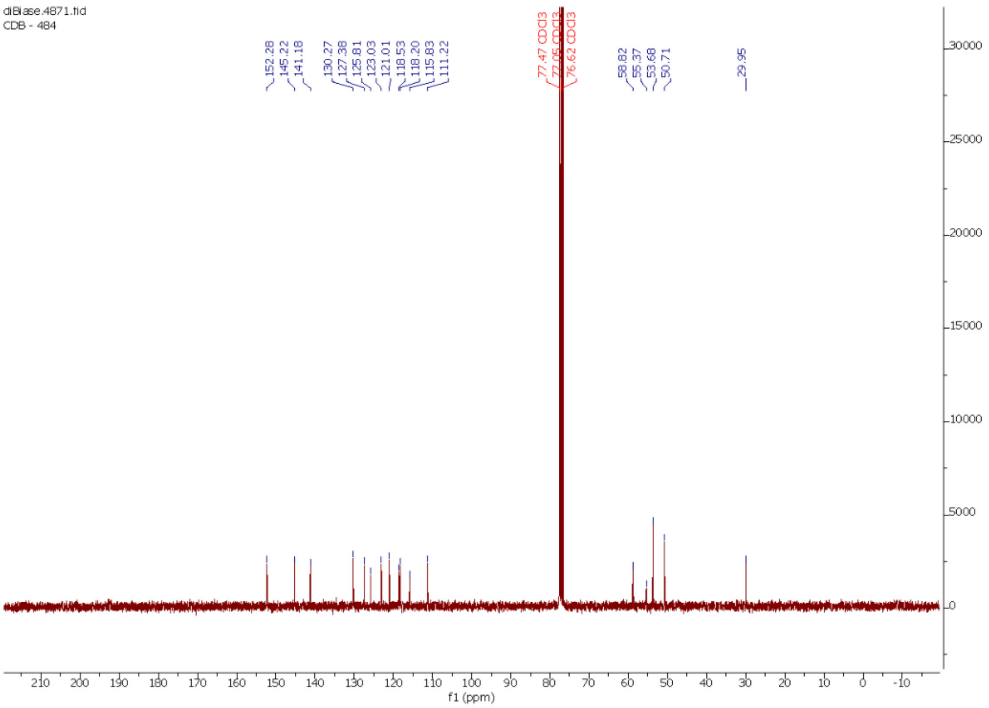
3-{2-[4-(2-Methoxyphenyl)piperazin-1-yl]ethyl}aniline (5b)



^{1}H-NMR

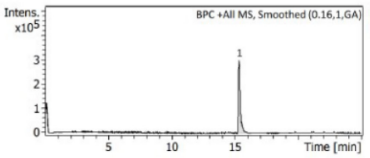


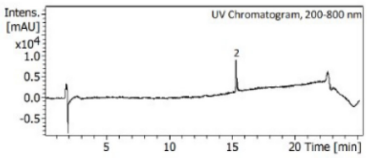
^{13}C-NMR

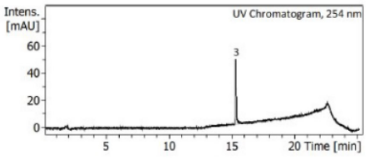


Acquisition Parameter

Source Type	ESI	Ion Polarity	Positive	Set Nebulizer	1.8 Bar
Focus	Not active			Set Dry Heater	220 °C
Scan Begin	50 m/z	Set Capillary	4500 V	Set Dry Gas	9.0 l/min
Scan End	1300 m/z	Set End Plate Offset	-500 V	Set Divert Valve	Waste

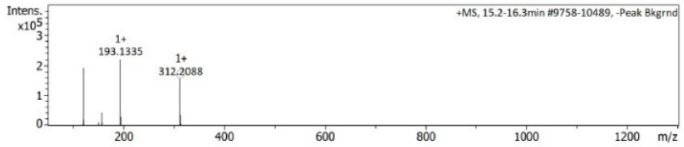






#	RT [min]	Area	S/N	Max. m/z	FWHM [min]	Area Frac. %
1	15.3	3400558.50	686.7	193.1335	0.2	100.00
2	15.3	41581.54	84.0		0.1	100.00
3	15.3	278.06	94.3		0.1	100.00

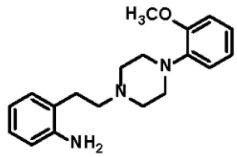
Cmpd 1, 15.3 min



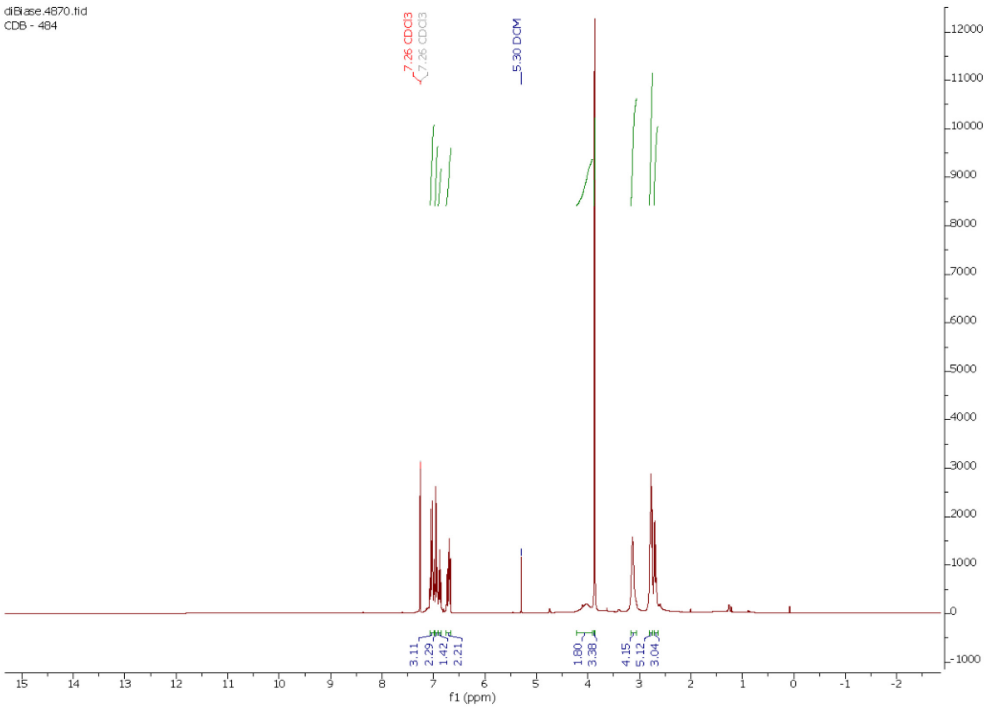
m/z: 312.2088 (M+1)

27

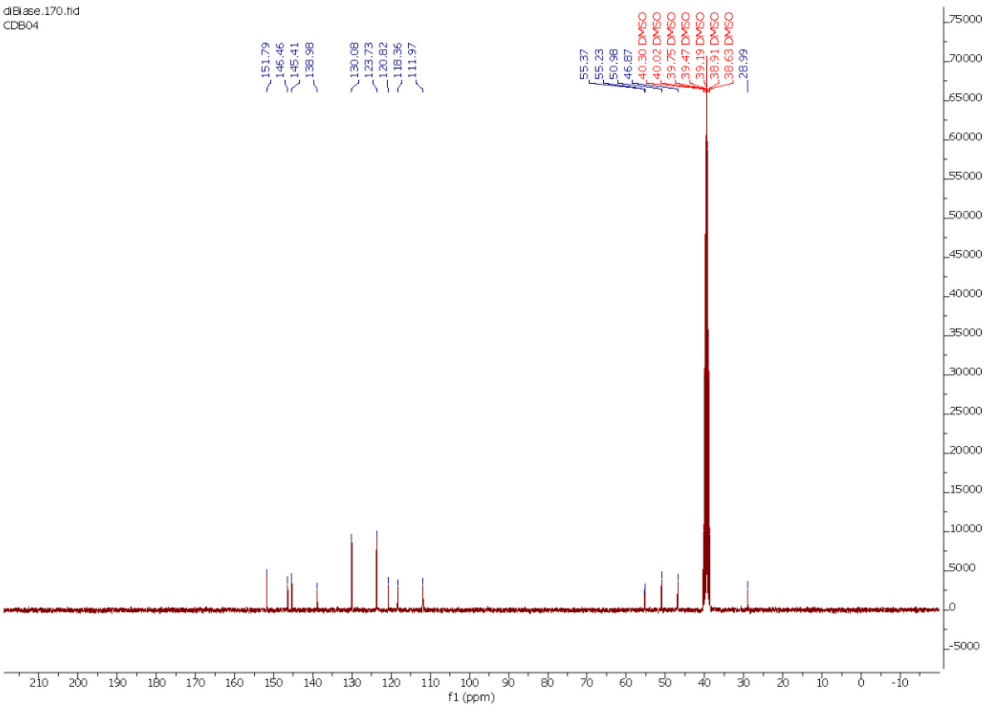
2-{2-[4-(2-Methoxyphenyl)piperazin-1-yl]ethyl}aniline (5a)



1H-NMR

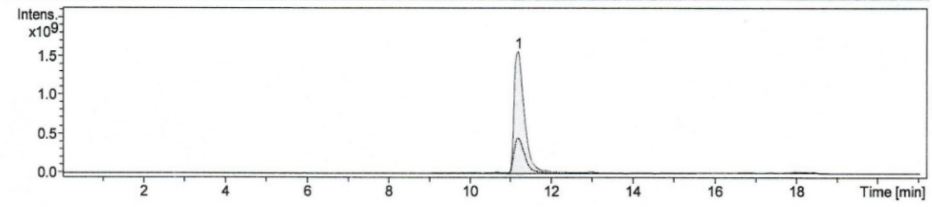


^{13}C-NMR



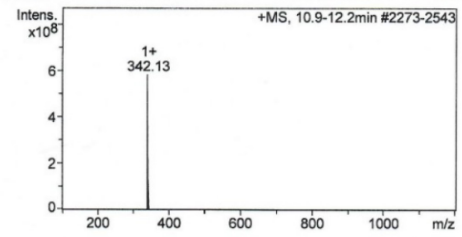
Acquisition Parameter

Ion Source Type	ESI	Ion Polarity	Negative	Alternating Ion Polarity	on
Mass Range Mode	UltraScan	Scan Begin	100 m/z	Scan End	1200 m/z
Accumulation Time	2000 µs	RF Level	59 %	Trap Drive	44.9
SPS Target Mass	350 m/z	Averages	5 Spectra	n/a	n/a



#	RT [min]	Area	S/N	Area Frac. %	Max. m/z
1	11.2	27988297728	21374.6	100.00	342.13

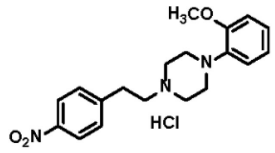
Cmpd 1, 11.2 min



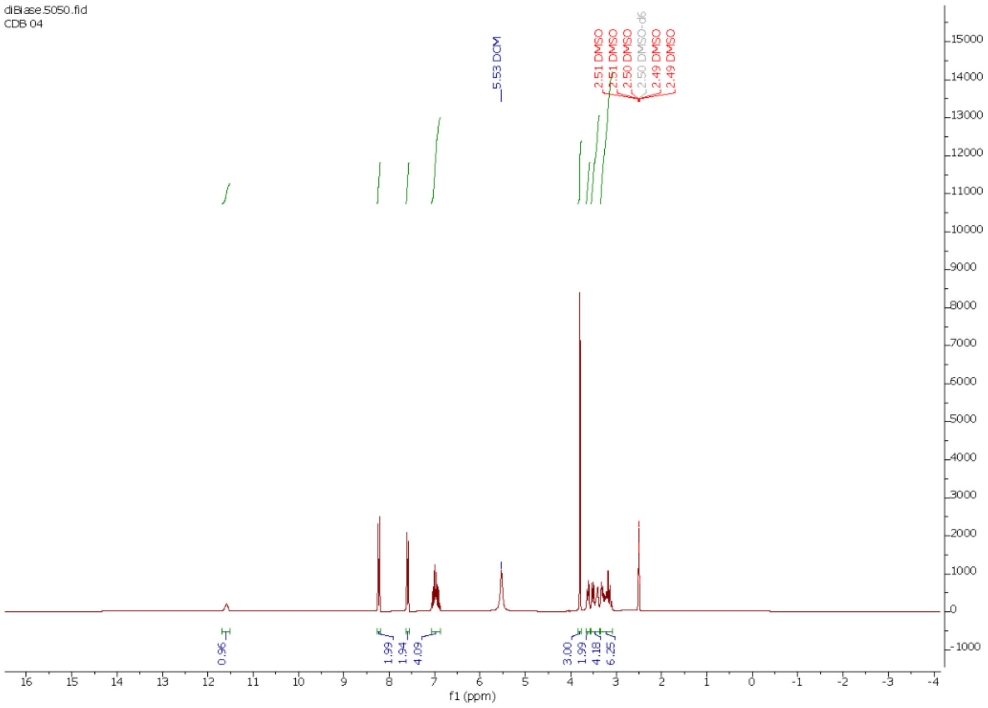
m/z: 342.13 (M+1)

25

1-(2-Methoxyphenyl)-4-(4-nitrophenethyl)piperazine hydrochloride (4c)

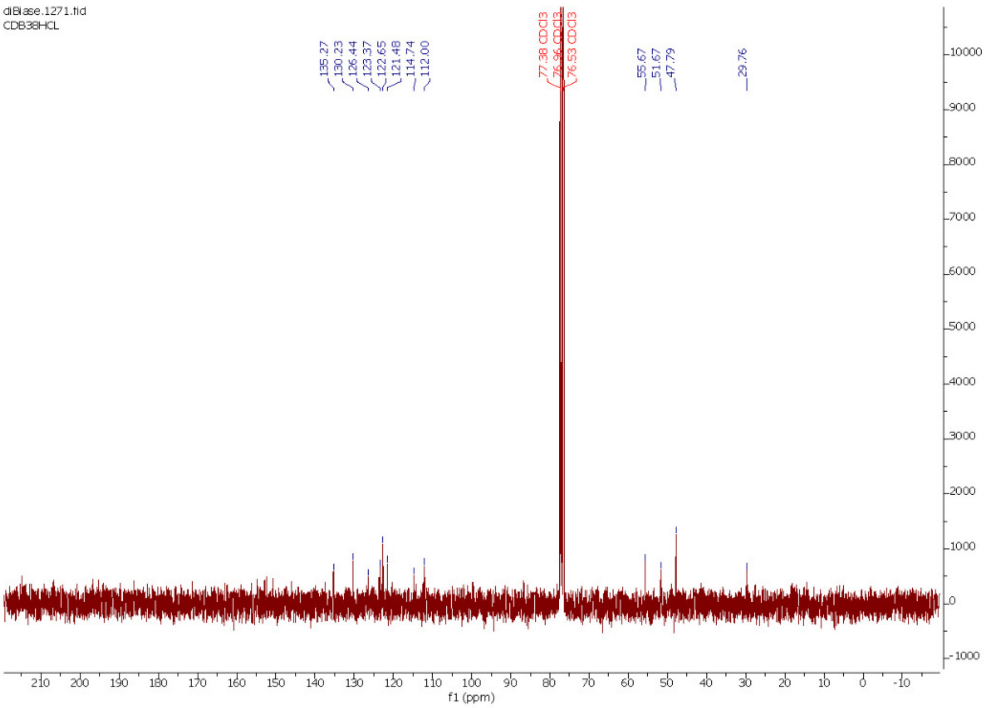


^{1}H-NMR



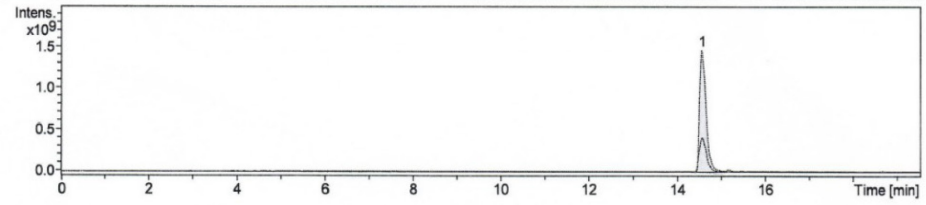
24

^{13}C-NMR



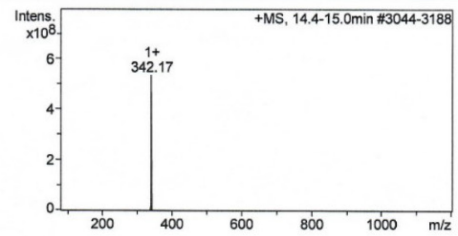
Acquisition Parameter

Ion Source Type	ESI	Ion Polarity	Negative	Alternating Ion Polarity	on
Mass Range Mode	UltraScan	Scan Begin	80 m/z	Scan End	1200 m/z
Accumulation Time	2000 µs	RF Level	59 %	Trap Drive	44.9
SPS Target Mass	350 m/z	Averages	5 Spectra	n/a	n/a



#	RT [min]	Area	S/N	Area Frac. %	Max. m/z
1	14.6	15431892992	7549.5	100.00	342.17

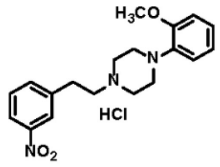
Cmpd 1, 14.6 min



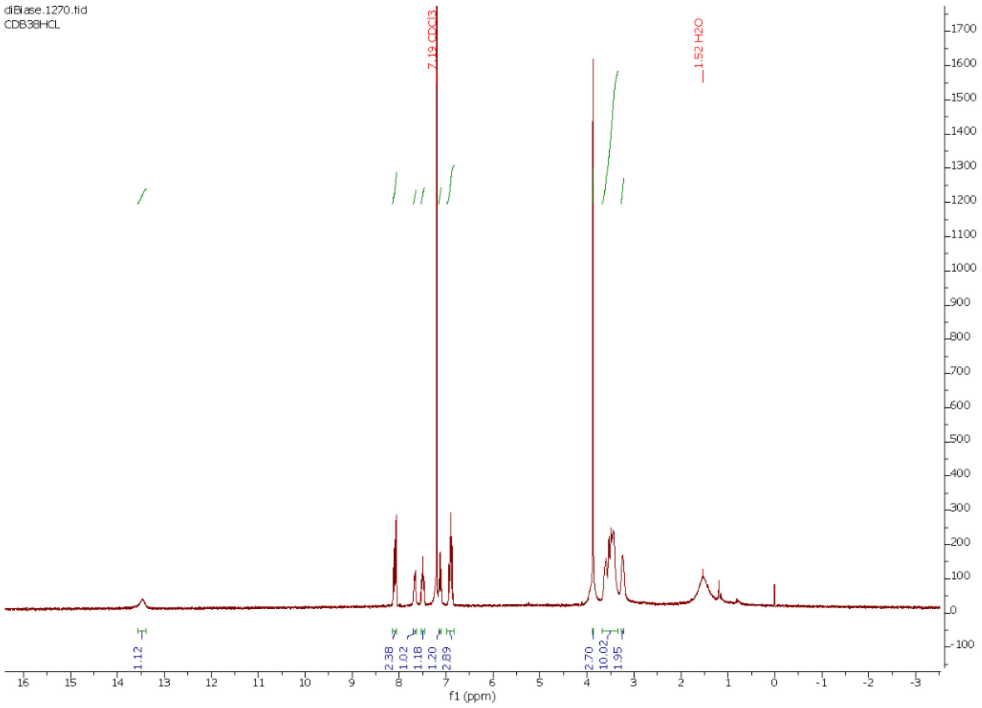
m/z: 342.17 (M+1)

23

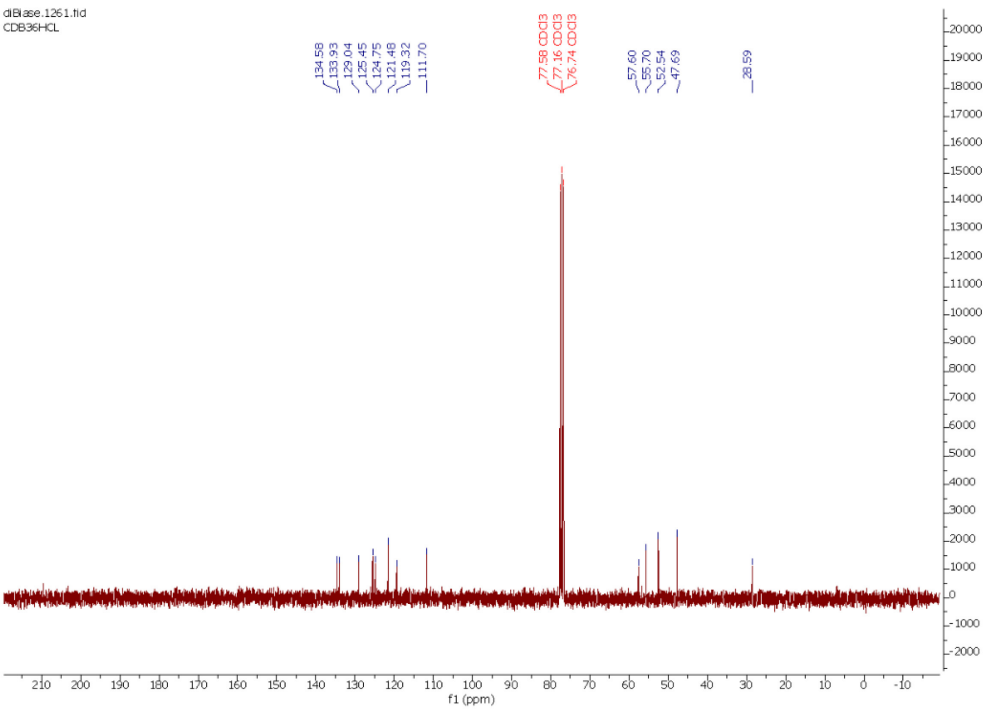
1-(2-Methoxyphenyl)-4-(3-nitrophenethyl)piperazine hydrochloride (4b)



^{1}H-NMR

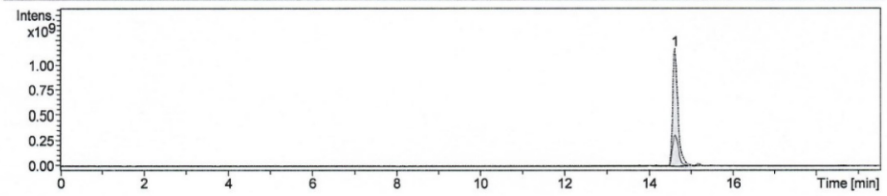


^{13}C-NMR



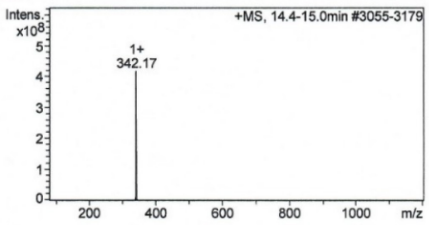
Acquisition Parameter

Ion Source Type	ESI	Ion Polarity	Negative	Alternating Ion Polarity	on
Mass Range Mode	UltraScan	Scan Begin	80 m/z	Scan End	1200 m/z
Accumulation Time	2000 µs	RF Level	59 %	Trap Drive	44.9
SPS Target Mass	350 m/z	Averages	5 Spectra	n/a	n/a



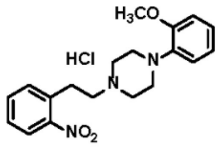
#	RT [min]	Area	S/N	Area Frac. %	Max. m/z
1	14.6	10403288064	5215.2	100.00	342.17

Cmpd 1, 14.6 min

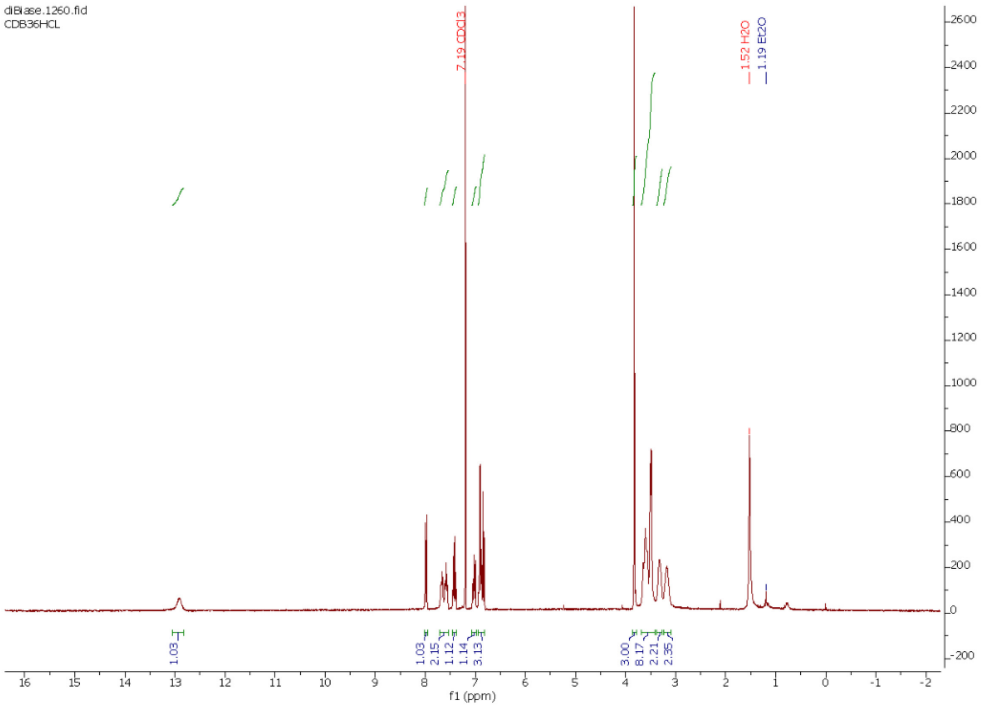


m/z: 342.17 (M+1)

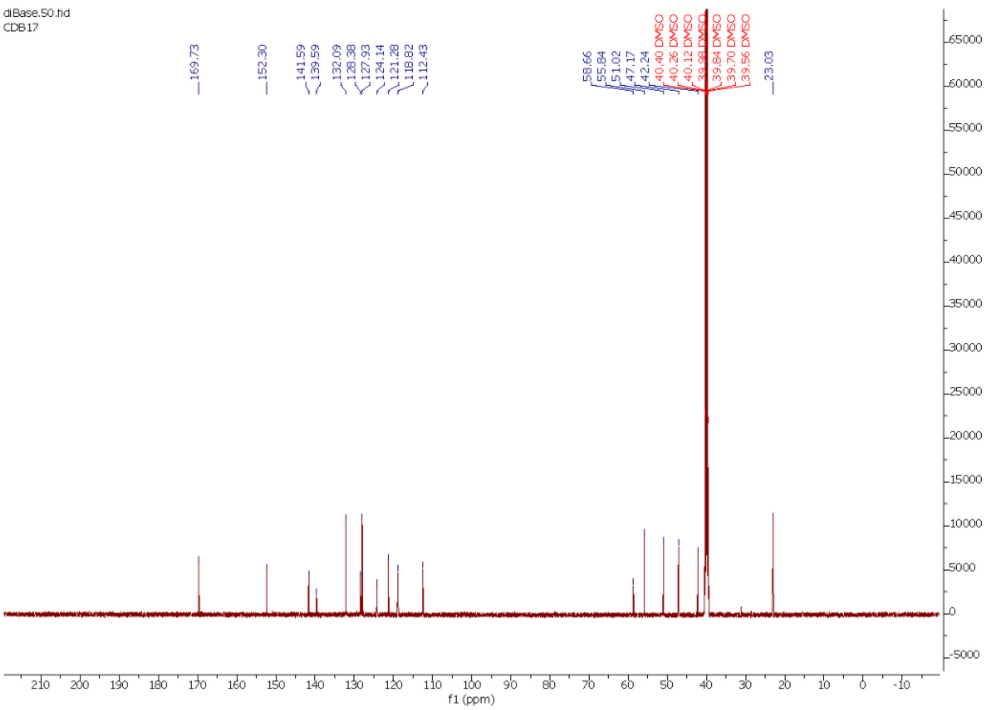
1-(2-Methoxyphenyl)-4-(2-nitrophenethyl)piperazine hydrochloride (4a)

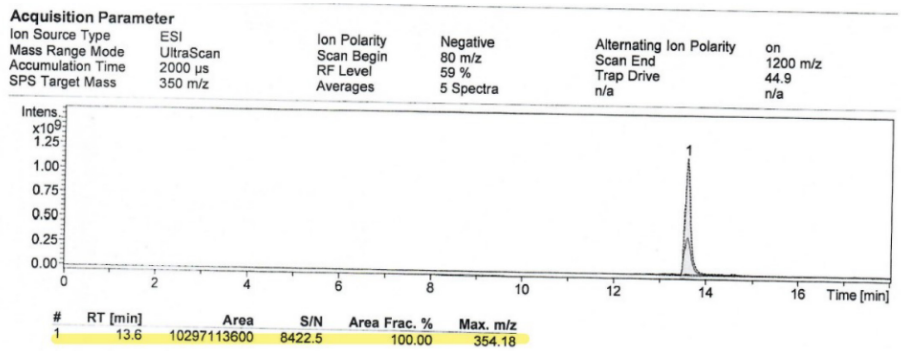


^{1}H-NMR

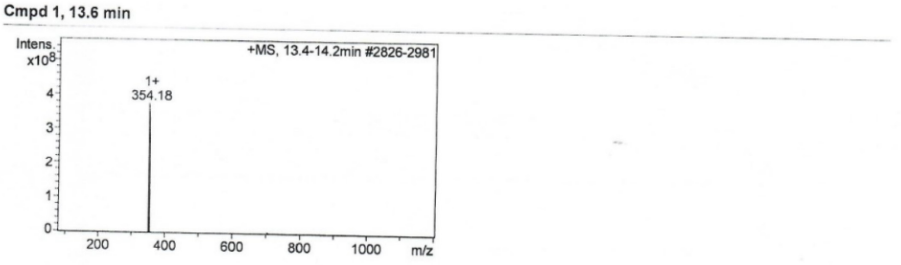


^{13}C-NMR





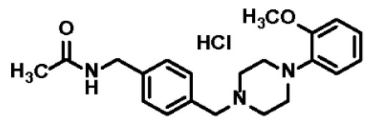
#	RT [min]	Area	S/N	Area Frac. %	Max. m/z
1	13.6	10297113600	8422.5	100.00	354.18



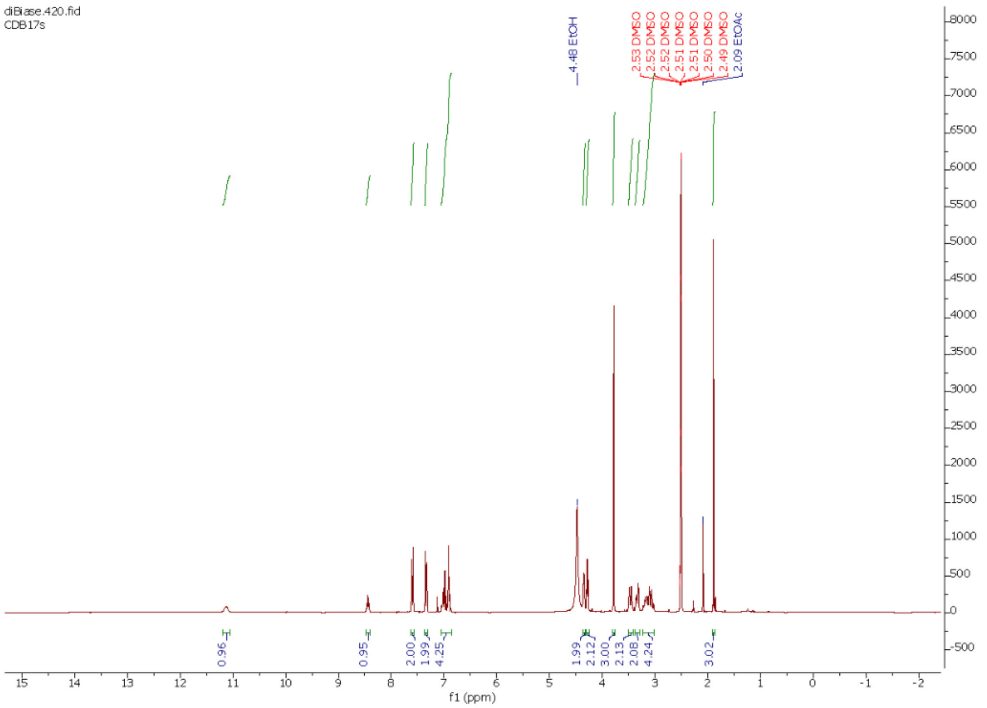
m/z: 354.18 (M+1)

19

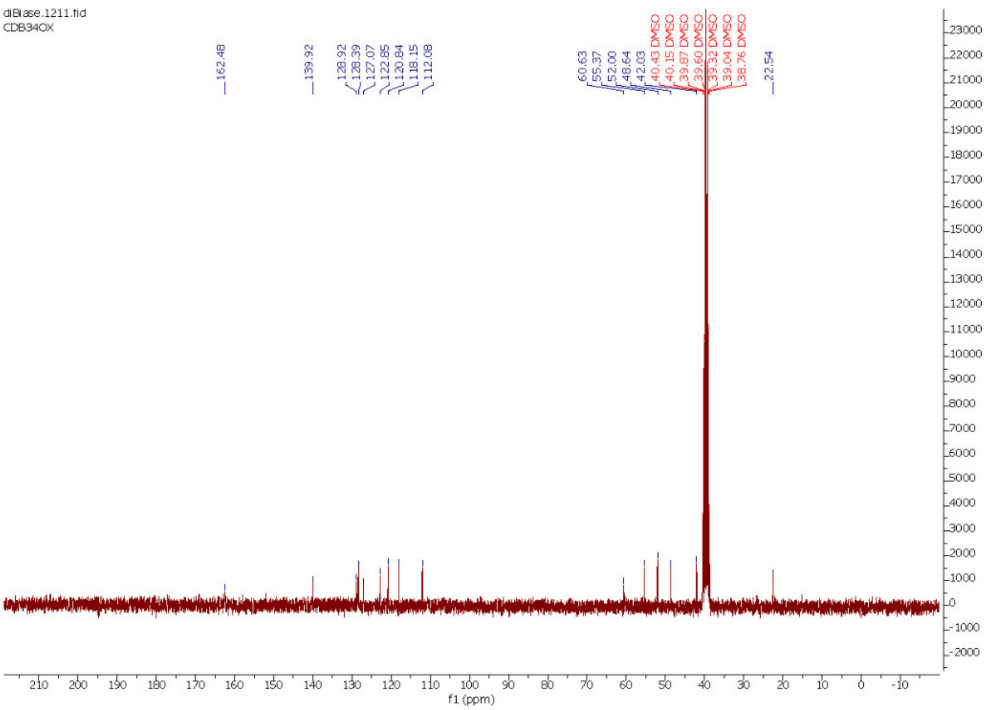
***N*-(4-{[4-(2-Methoxyphenyl)piperazin-1-yl]methyl}benzyl)acetamide hydrochloride (3c)**



^{1}H-NMR

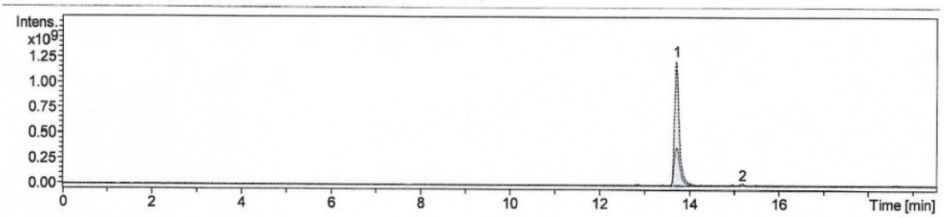


^{13}C-NMR



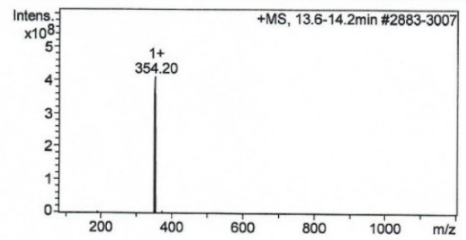
Acquisition Parameter

Ion Source Type	ESI	Ion Polarity	Positive	Alternating Ion Polarity	on
Mass Range Mode	UltraScan	Scan Begin	80 m/z	Scan End	1200 m/z
Accumulation Time	2000 µs	RF Level	59 %	Trap Drive	47.4
SPS Target Mass	350 m/z	Averages	5 Spectra	n/a	n/a



#	RT [min]	Area	S/N	Area Frac. %	Max. m/z
1	13.7	9330502656	4992.1	99.91	354.20
2	15.2	8089282	12.7	0.09	410.18

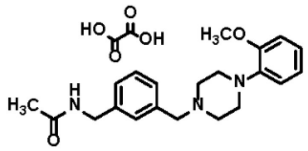
Cmpd 1, 13.7 min



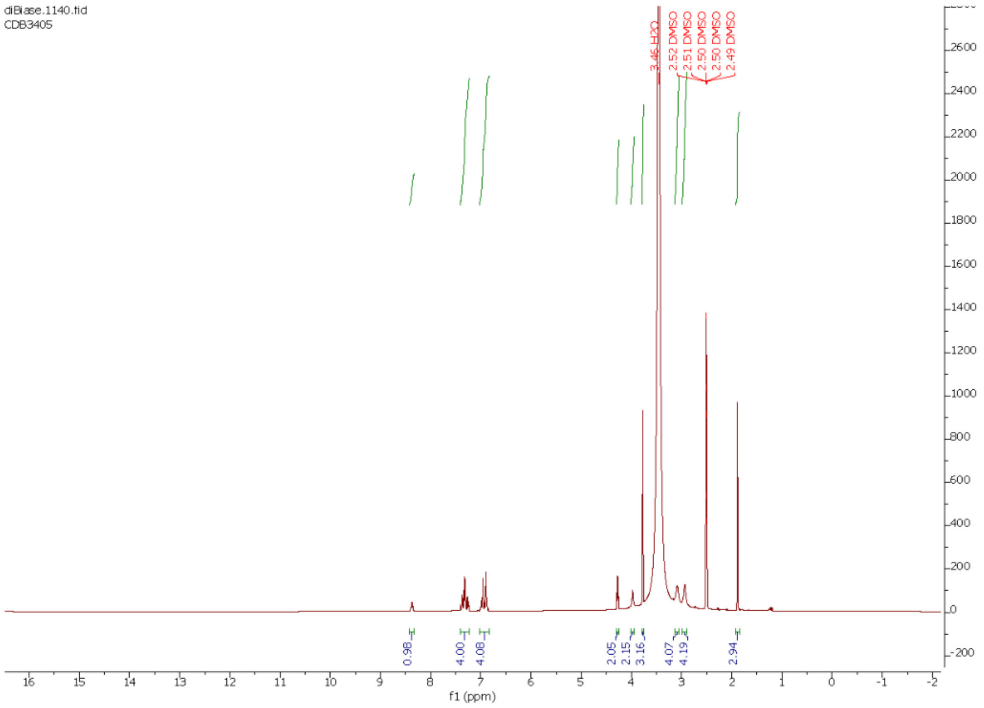
m/z: 354.20 (M+1)

17

***N*-(3-{[4-(2-Methoxyphenyl)piperazin-1-yl]methyl}benzyl)acetamide hydrogenoxalate (3b)**

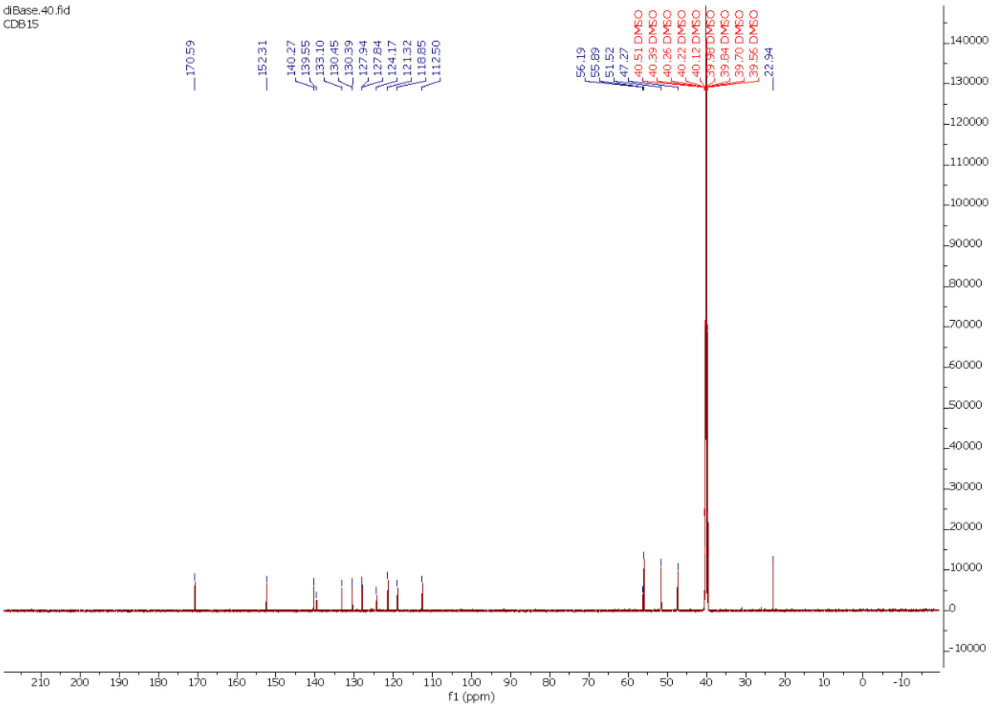


^{1}H-NMR



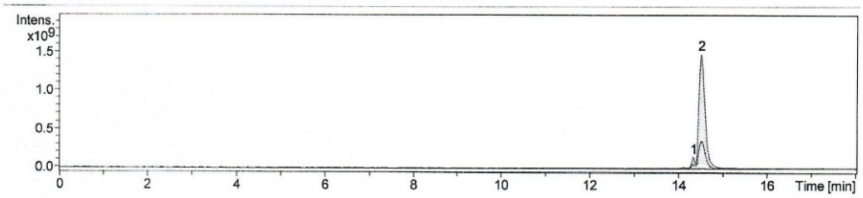
16

^{13}C-NMR



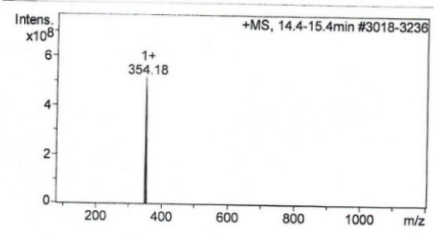
Acquisition Parameter

Ion Source Type	ESI	Ion Polarity	Negative	Alternating Ion Polarity	on
Mass Range Mode	UltraScan	Scan Begin	80 m/z	Scan End	1200 m/z
Accumulation Time	2000 µs	RF Level	59 %	Trap Drive	44.9
SPS Target Mass	350 m/z	Averages	5 Spectra	n/a	n/a



#	RT [min]	Area	S/N	Area Frac. %	Max. m/z
1	14.3	498399712	893.7	3.73	366.19
2	14.5	12853067776	10385.3	96.27	354.18

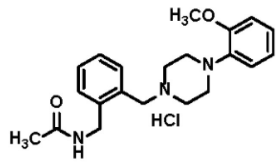
Cmpd 2, 14.5 min



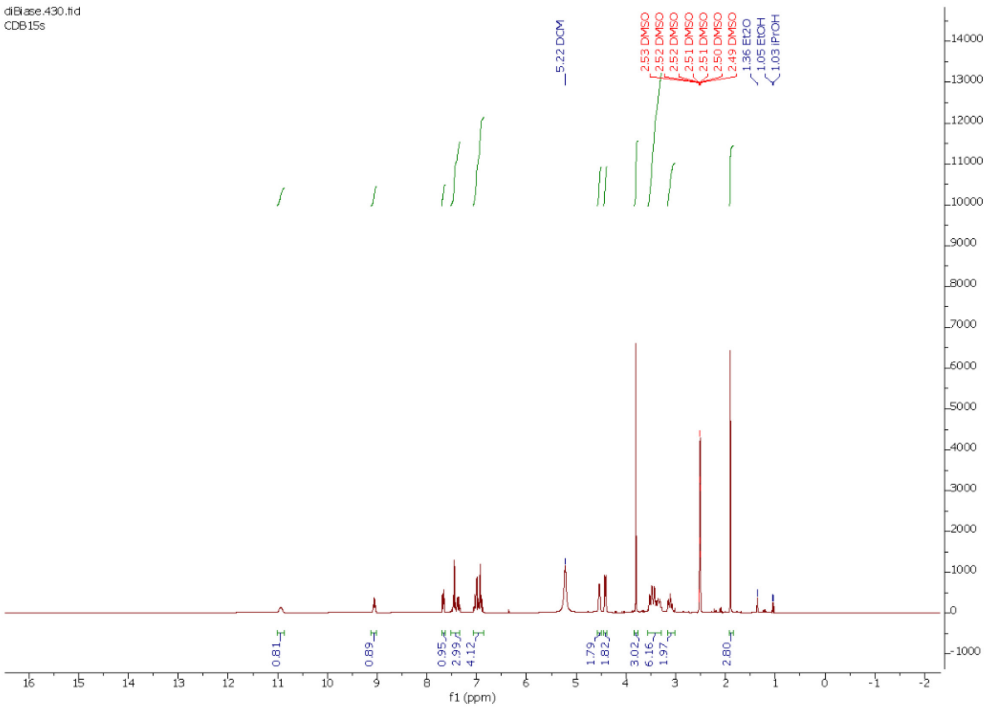
m/z: 354.18 (M+1)

15

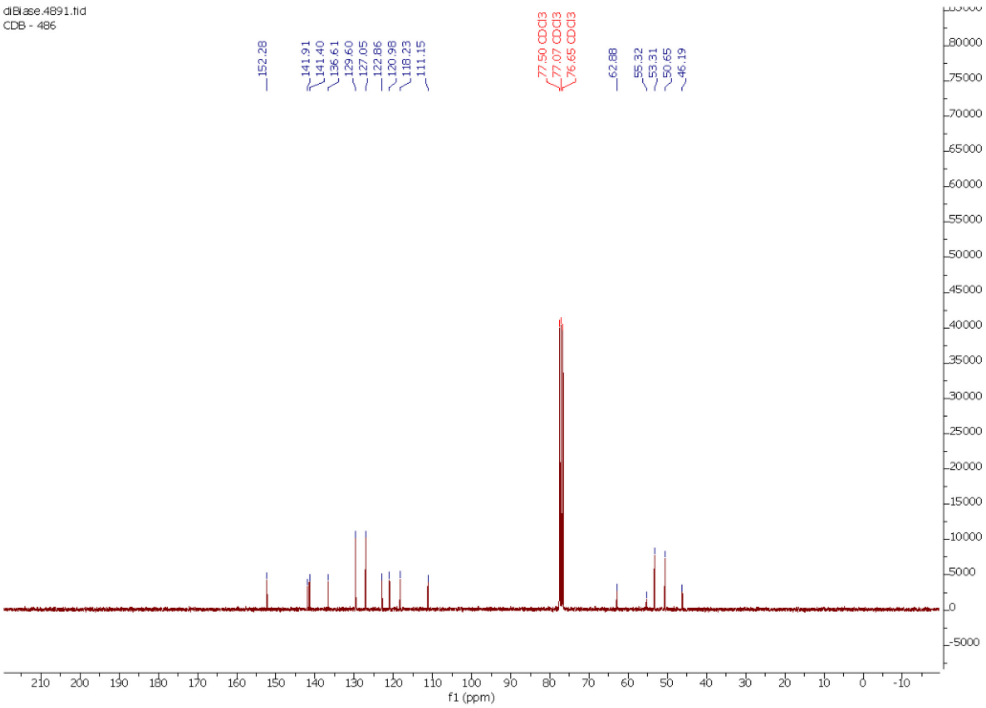
***N*-(2-{[4-(2-Methoxyphenyl)piperazin-1-yl]methyl}benzyl)acetamide hydrochloride (3a)**



^{1}H-NMR

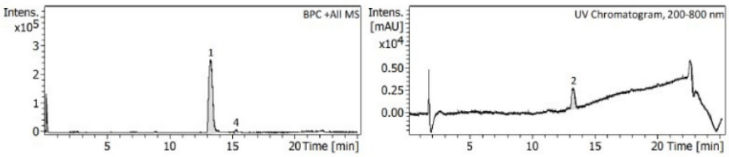


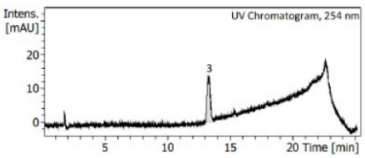
^{13}C-NMR



Acquisition Parameter

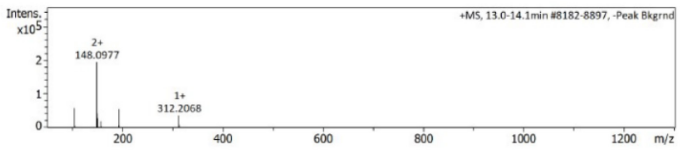
Source Type	ESI	Ion Polarity	Positive	Set Nebulizer	1.8 Bar
Focus	Not active			Set Dry Heater	220 °C
Scan Begin	50 m/z	Set Capillary	4500 V	Set Dry Gas	9.0 l/min
Scan End	1300 m/z	Set End Plate Offset	-500 V	Set Divert Valve	Waste





#	RT [min]	Area	S/N	Max. m/z	FWHM [min]	Area Frac. %
1	13.3	5679828.50	4693.6	148.0977	0.4	96.237
2	13.3	44040.52	24.0		0.3	100.000
3	13.3	250.28	26.5		0.3	100.000
4	15.3	222080.34	253.3	311.1747	0.3	3.763

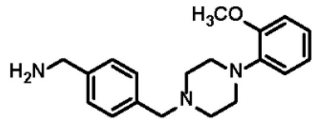
Cmpd 1, 13.3 min



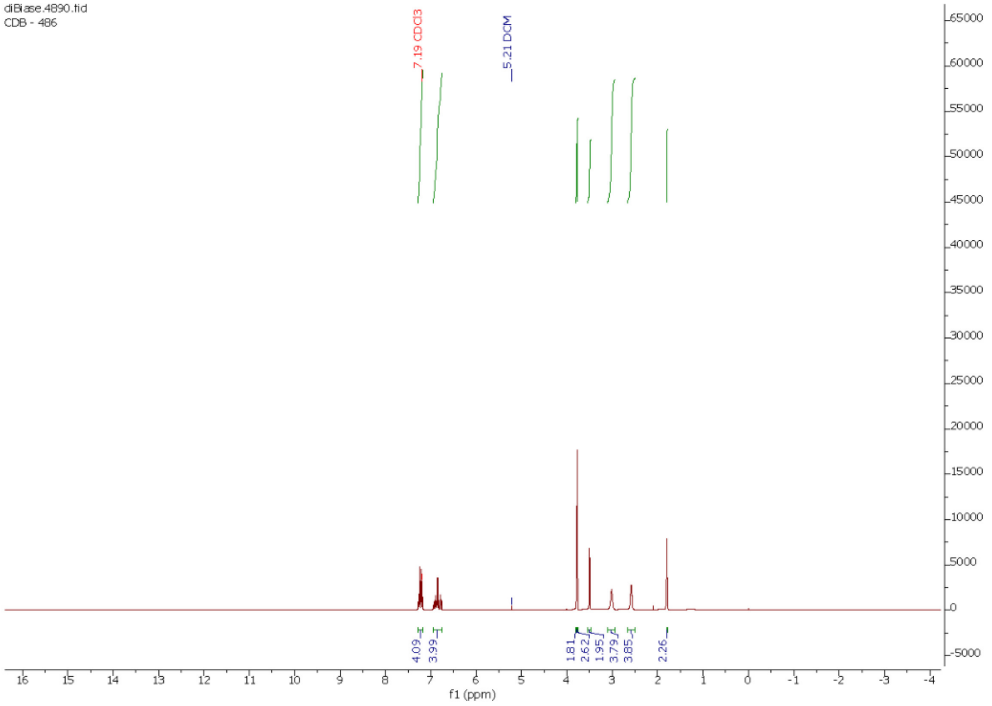
m/z: 312.2068 (M+1)

13

(4-{[4-(2-Methoxyphenyl)piperazin-1-yl]methyl}phenyl)methanamine (2c)

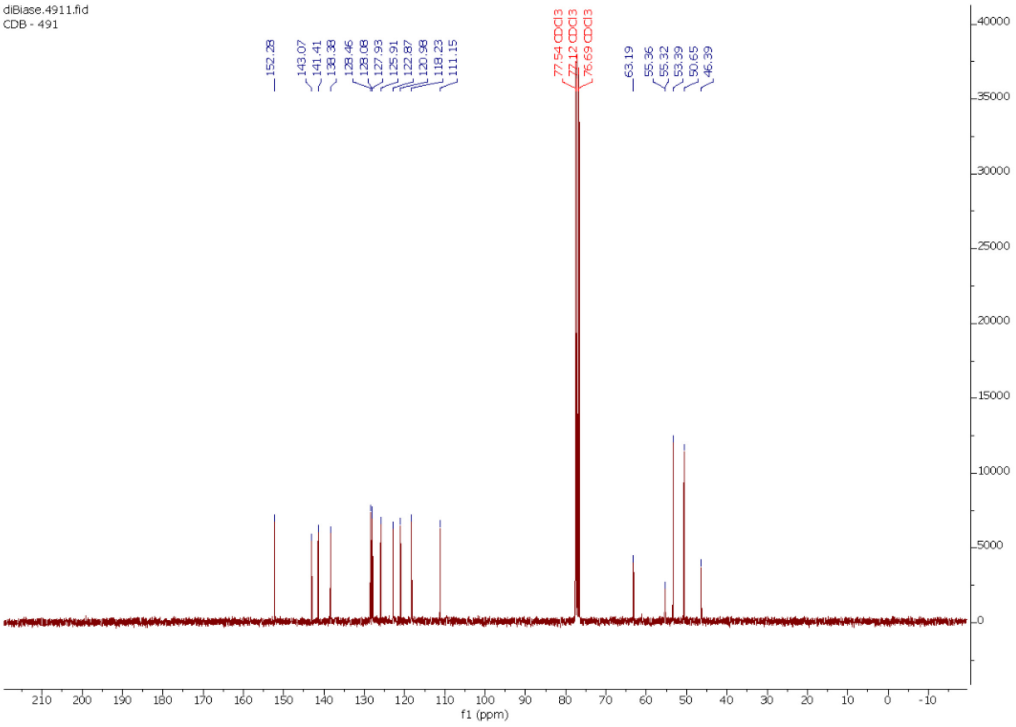


^{1}H-NMR



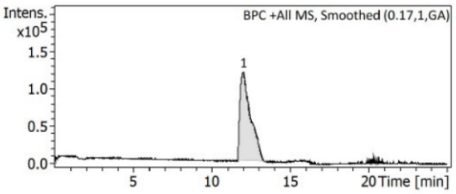
12

^{13}C-NMR



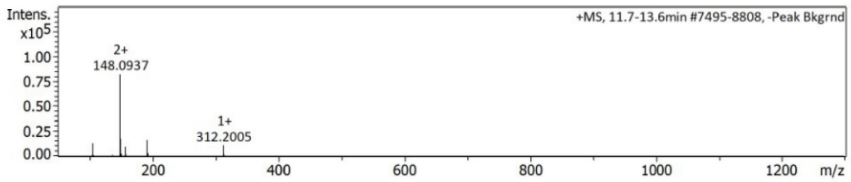
Acquisition Parameter

Source Type	ESI	Ion Polarity	Positive	Set Nebulizer	1.8 Bar
Focus	Not active			Set Dry Heater	220 °C
Scan Begin	50 m/z	Set Capillary	4500 V	Set Dry Gas	9.0 l/min
Scan End	1300 m/z	Set End Plate Offset	-500 V	Set Divert Valve	Waste



#	RT [min]	Area	S/N	Max. m/z	FWHM [min]	Area Frac. %
1	12.0	5530507	276.5	148.0937	0.7	100.00

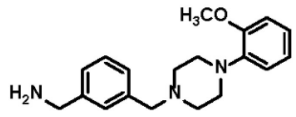
Cmpd 1, 12.0 min



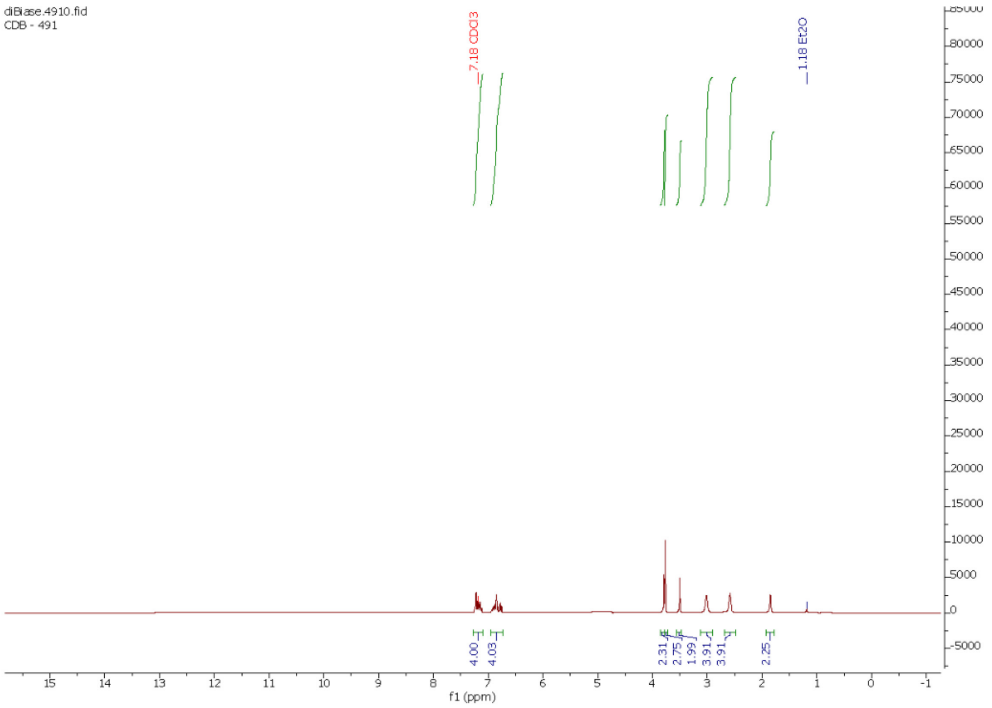
m/z: 312.2005 (M+1)

11

(3-{[4-(2-Methoxyphenyl)piperazin-1-yl]methyl}phenyl)methanamine (2b)

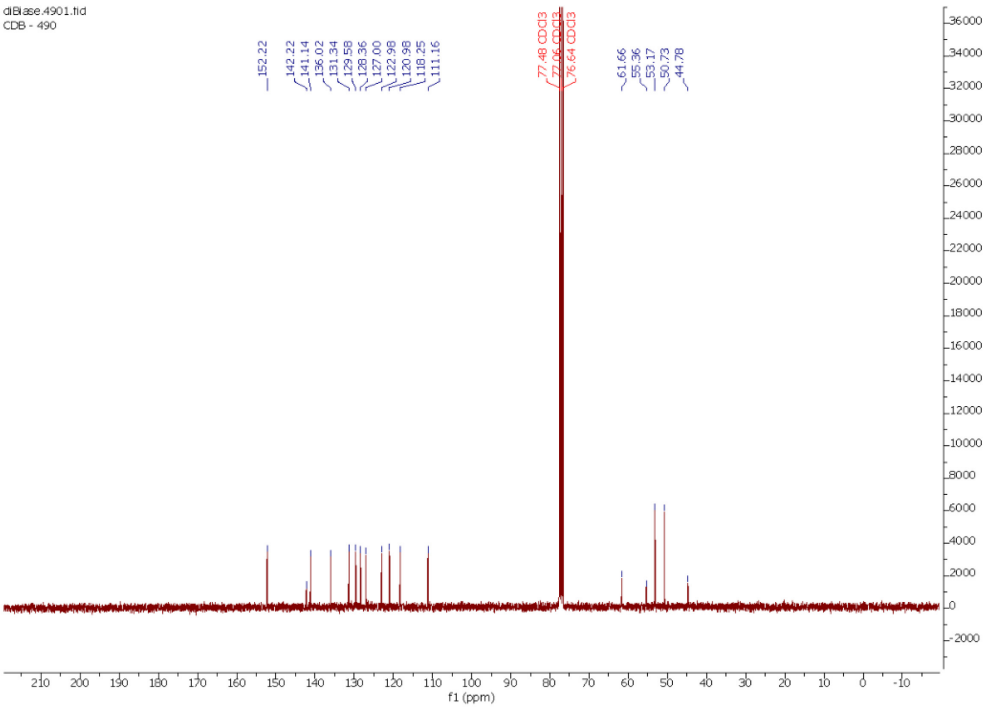


^{1}H-NMR



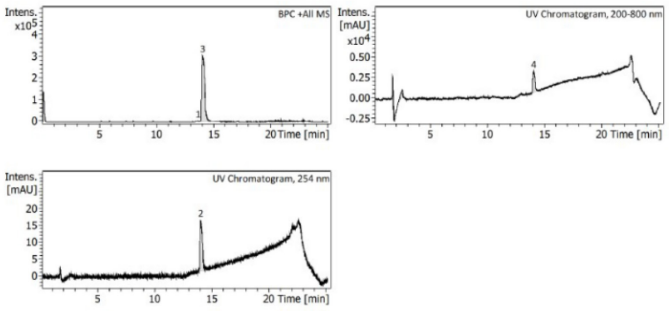
10

^{13}C-NMR



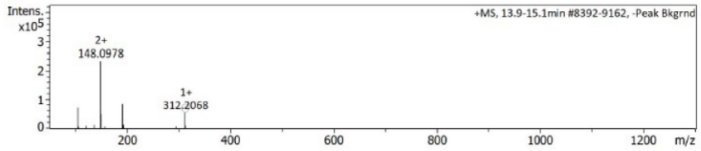
Acquisition Parameter

Source Type	ESI	Ion Polarity	Positive	Set Nebulizer	1.8 Bar
Focus	Not active			Set Dry Heater	220 °C
Scan Begin	50 m/z	Set Capillary	4500 V	Set Dry Gas	9.0 l/min
Scan End	1300 m/z	Set End Plate Offset	-500 V	Set Divert Valve	Waste



#	RT [min]	Area	S/N	Max. m/z	FWHM [min]	Area Frac. %
1	13.7	52756.45	97.3	147.5935	0.3	0.949
2	14.0	204.64	29.5		0.2	100.000
3	14.1	5506976.50	7100.0	148.0978	0.3	99.051
4	14.1	33134.16	27.4		0.2	100.000

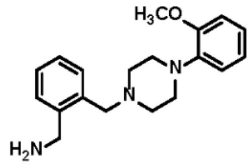
Cmpd 3, 14.1 min



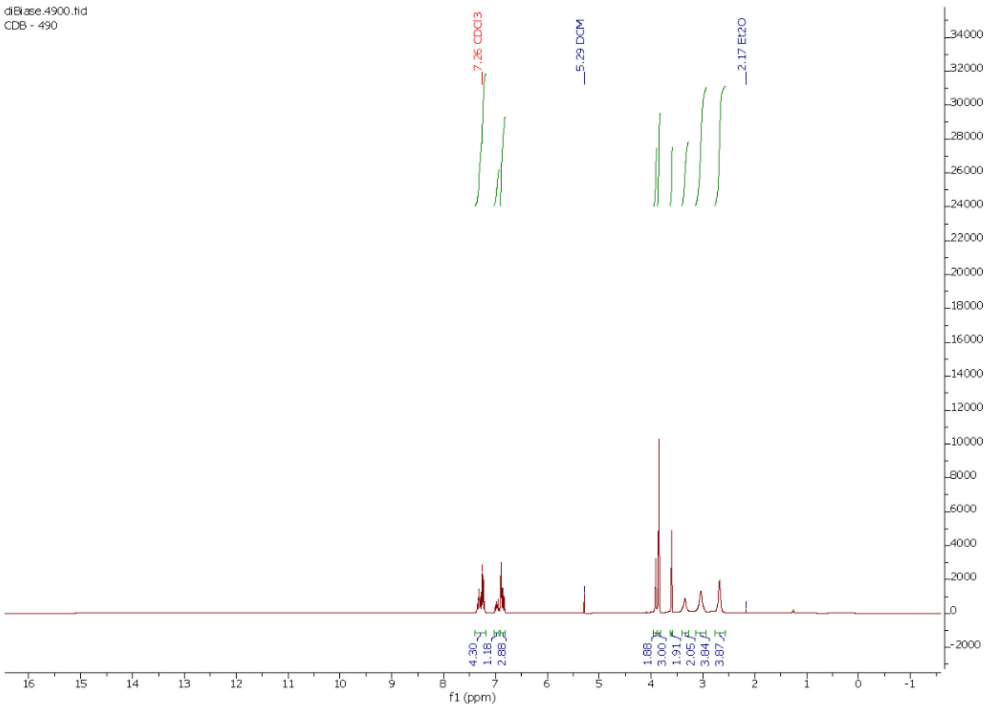
m/z: 312.2068 (M+1)

9

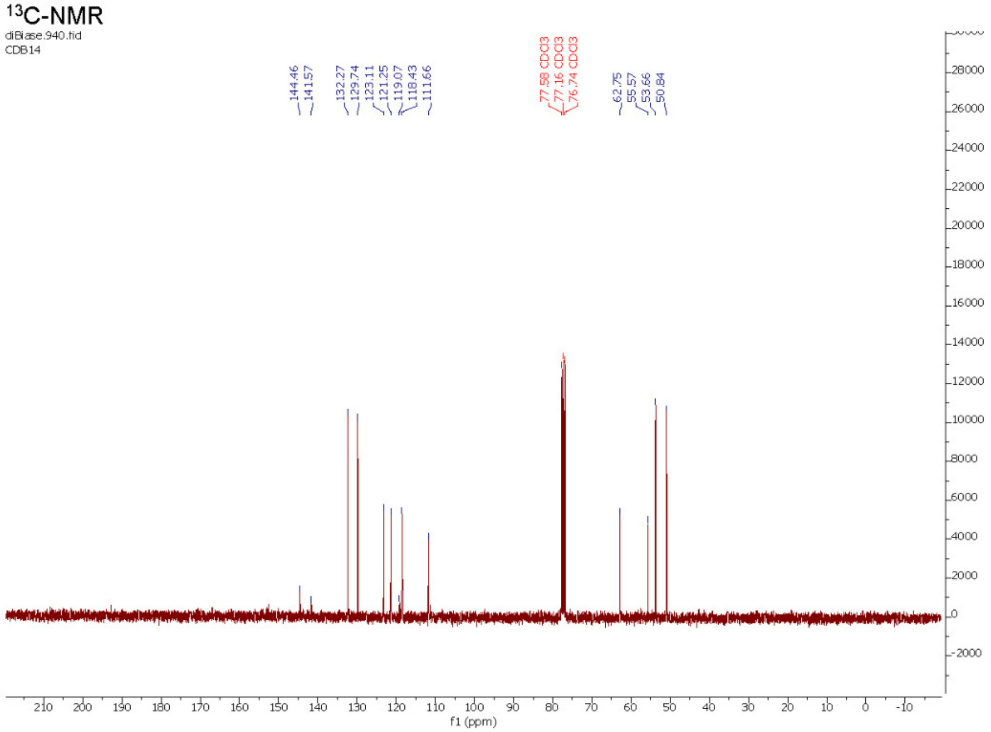
(2-{[4-(2-Methoxyphenyl)piperazin-1-yl]methyl}phenyl)methanamine (2a)

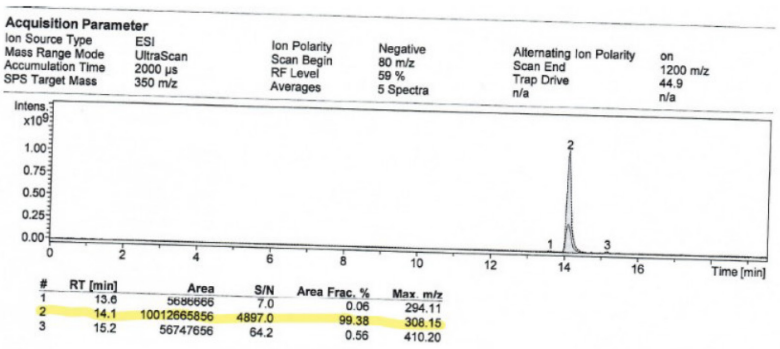


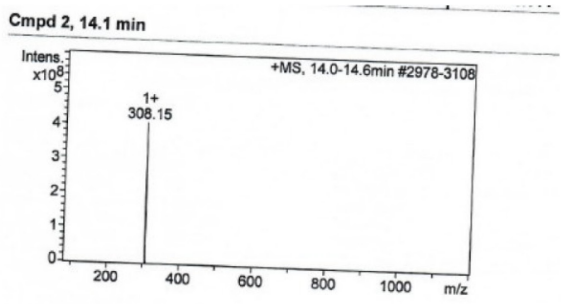
^{1}H-NMR



8


13C-NMR
dBase.940.fid
CDB14
144.46
141.57
132.27
129.74
123.11
121.25
119.07
118.43
111.66
77.58 CDCl3
77.16 CDCl3
76.74 CDCl3
62.75
55.57
53.66
50.84
f1 (ppm)

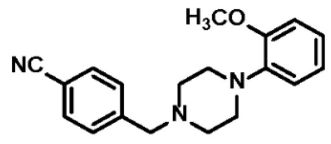

Acquisition Parameter
Ion Source Type ESI
Mass Range Mode UltraScan
Accumulation Time 2000 µs
SPS Target Mass 350 m/z
Ion Polarity Negative
Scan Begin 80 m/z
RF Level 59 %
Averages 5 Spectra
Alternating Ion Polarity on
Scan End 1200 m/z
Trap Drive 44.9
n/a n/a
Intens.
x10^9
Time [min]
RT [min] Area S/N Area Frac. % Max. m/z
1 13.6 5686666 7.0 0.06 294.11
2 14.1 10012665856 4897.0 99.38 308.15
3 15.2 56747656 64.2 0.56 410.20


Cmpd 2, 14.1 min
Intens.
x10^8
+MS, 14.0-14.6min #2978-3108
1+
308.15
m/z

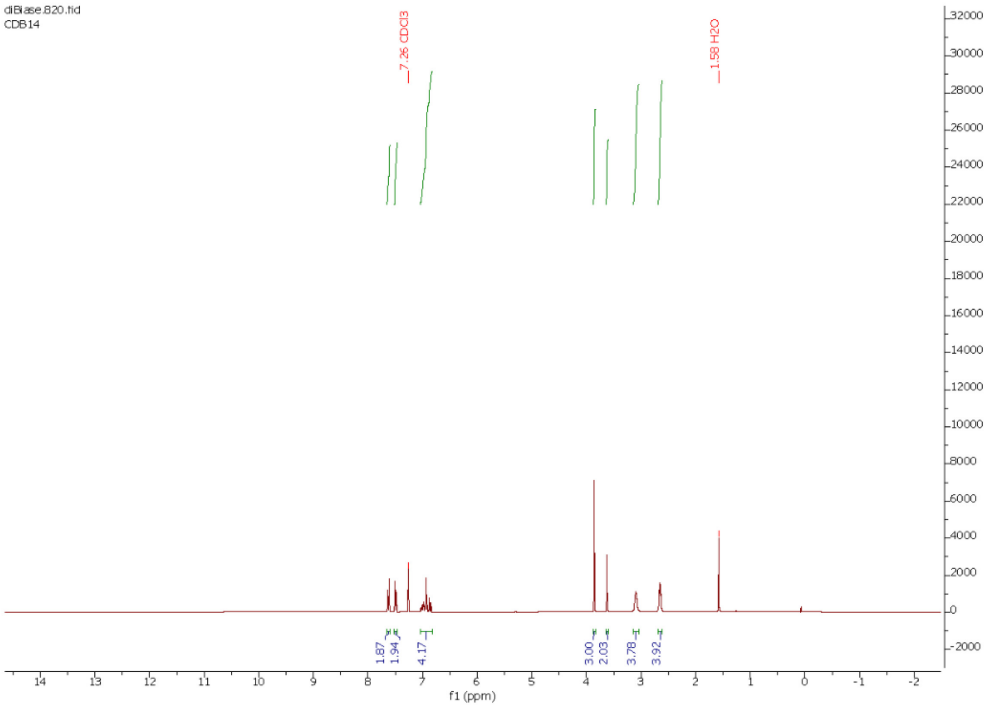
m/z: 308.15 (M+1)

7

4-{[4-(2-Methoxyphenyl)piperazin-1-yl]methyl}benzonitrile (1c)

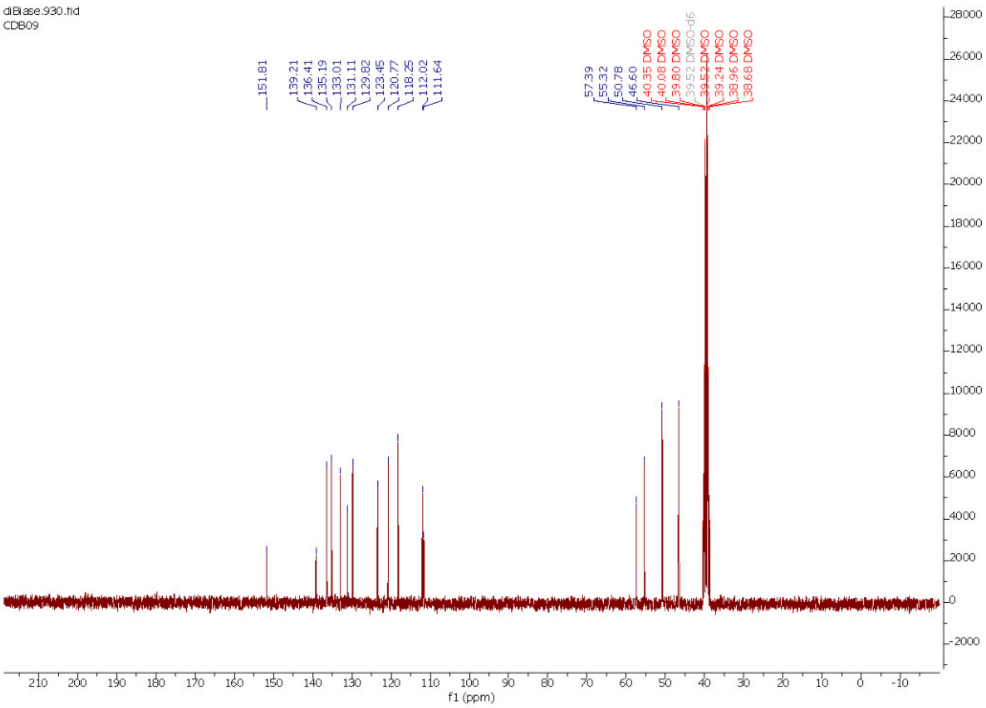


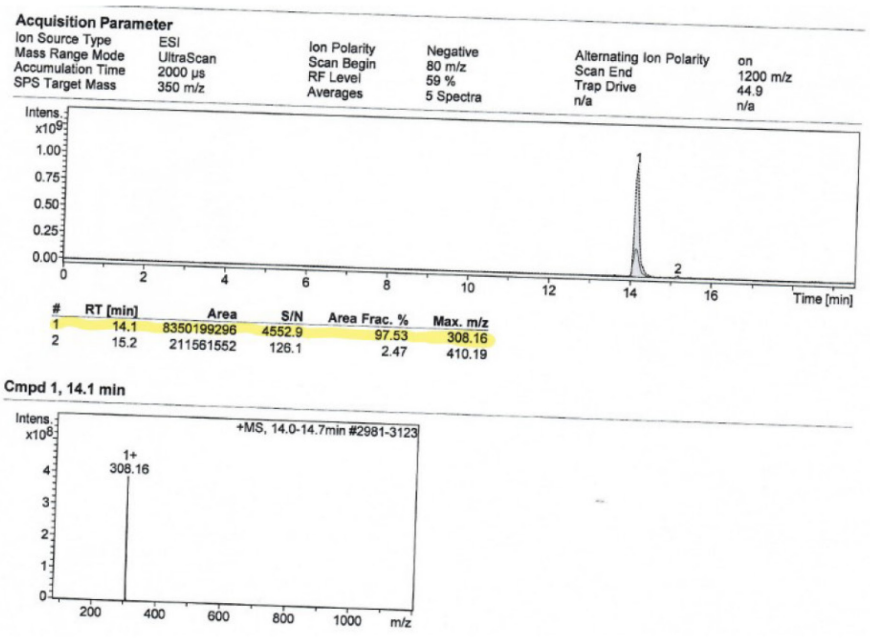
^{1}H-NMR



6

^{13}C-NMR

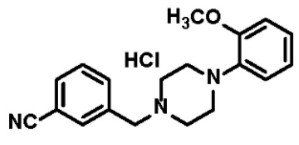




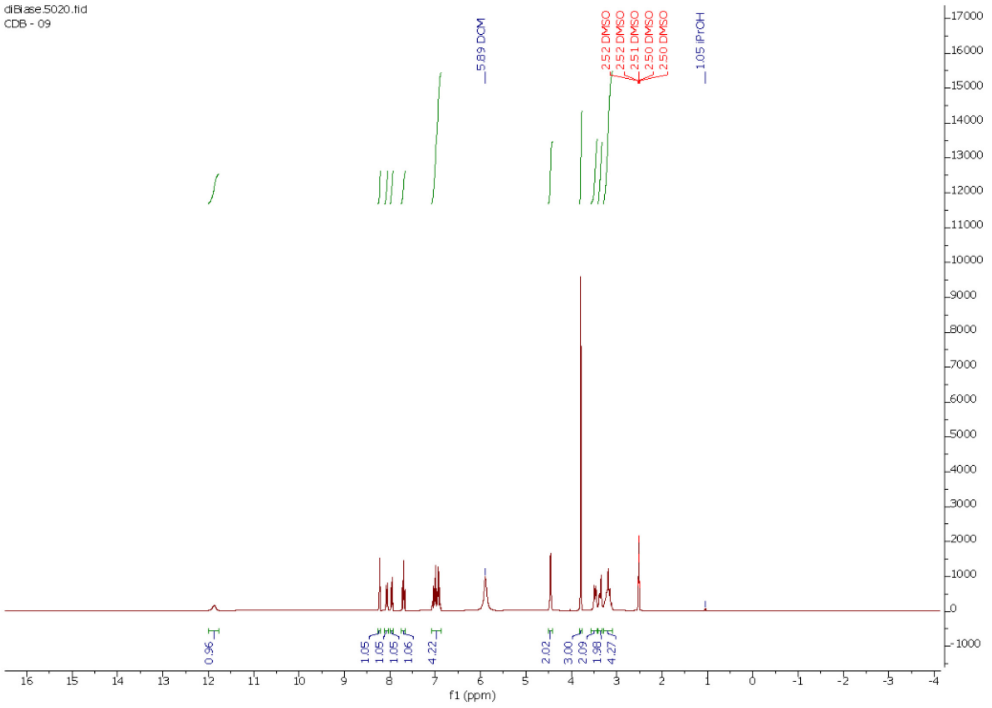
m/z: 308.16 (M+1)

5

3-{[4-(2-Methoxyphenyl)piperazin-1-yl]methyl}benzonitrile hydrochloride (1b)

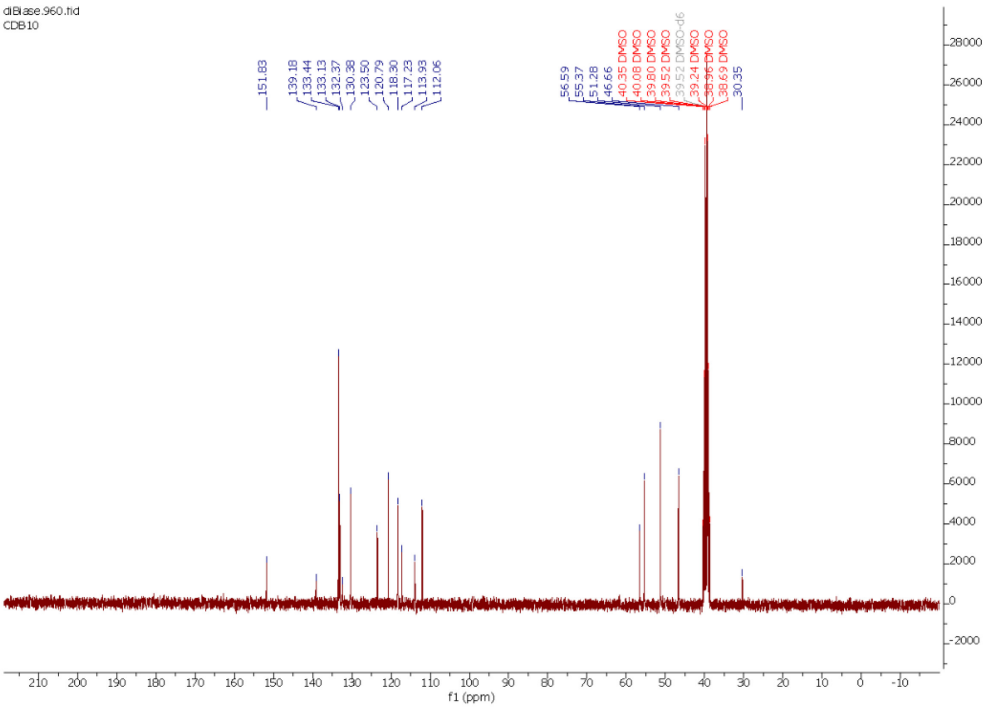


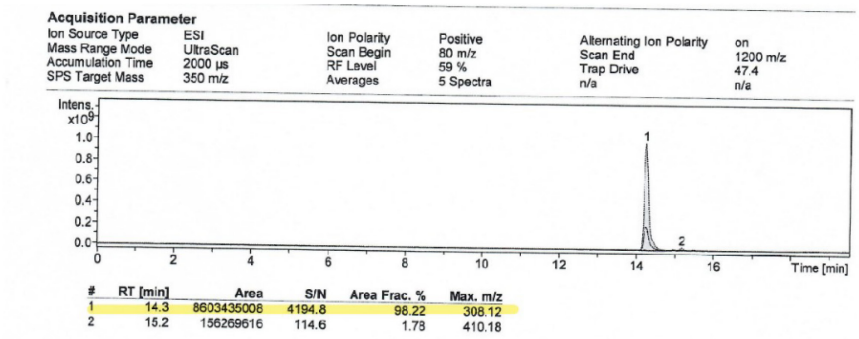
^{1}H-NMR

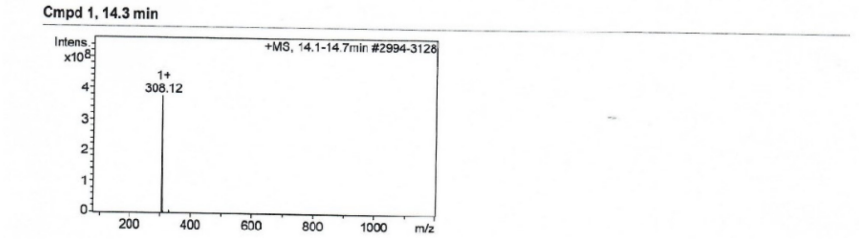


4

^{13}C-NMR



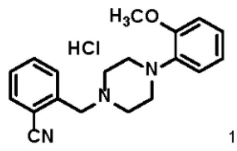




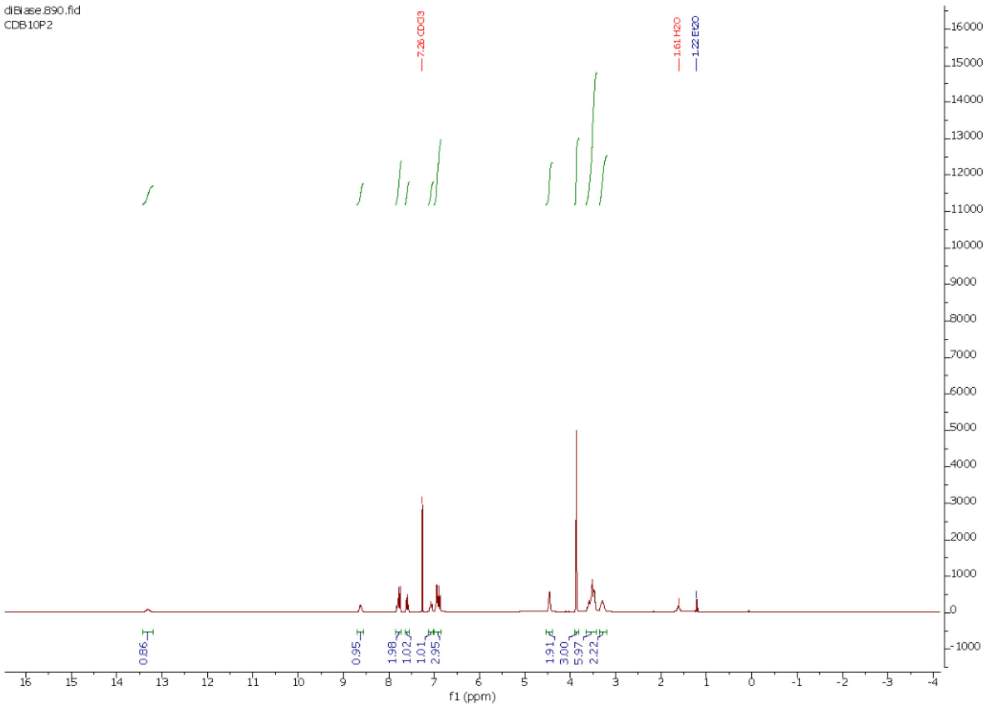
m/z: 308.12 (M+1)

3

2-{[4-(2-Methoxyphenyl)piperazin-1-yl]methyl}benzonitrile hydrochloride (1a)



^{1}H-NMR



2

3.4 Multitargeting approaches to cognitive impairment: Synthesis of aryl-alkylpiperazines and assessment at cholinesterases, histamine H_3 and dopamine D_3 receptors

Cecília M.S.Q. Aranha[1], David Reiner-Link[2], Luisa R. Leitzbach[2], Flavia B. Lopes[1], Holger Stark[2], João Paulo S. Fernandes[1]

[1] Department of Pharmaceutical Sciences, Universidade Federal de Sao Paulo, Diadema, SP, Brazil, [2] Institute for Pharmaceutical and Medicinal Chemistry, Heinrich Heine University Düsseldorf, Duesseldorf, Germany

Published in: Bioorganic & Medicinal Chemistry, 2023, 117132, Vol. 78, https://doi.org/10.1016/j.bmc.2022.117132

Impact Factor: 3.0 (2025)

Contribution: L.L. designed, partially performed and evaluated the histamine H_3R and D_3R binding studies, partially wrote and reviewed the manuscript.

Bioorg. Med. Chem. 78 (2023) 117132

Contents lists available at ScienceDirect

Bioorganic & Medicinal Chemistry

journal homepage: www.elsevier.com/locate/bmc

Multitargeting approaches to cognitive impairment: Synthesis of aryl-alkylpiperazines and assessment at cholinesterases, histamine H_3 and dopamine D_3 receptors

Cecília M.S.Q. Aranha [a], David Reiner-Link [b], Luisa R. Leitzbach [b], Flavia B. Lopes [a], Holger Stark [b,*], João Paulo S. Fernandes [a,*]

[a] Department of Pharmaceutical Sciences, Universidade Federal de São Paulo, Diadema, SP, Brazil
[b] Institute for Pharmaceutical and Medicinal Chemistry, Heinrich Heine University Düsseldorf, Duesseldorf, Germany

ARTICLE INFO

Keywords:
Multitarget ligand
H_3R ligand
D_3R ligand
Cholinesterase inhibitors
Procognitive agents

ABSTRACT

Multitargeting ligands on enzymes and receptors may generate a profile for a potential treatment of cognitive impairment. Considering this, a set of 21 substituted aryl–alkyl-piperazines were designed, prepared and tested for their binding affinities at histamine H_3 and dopamine D_3 receptors (H_3R and D_3R, respectively) as well as acetyl- and butyrylcholinesterases (AChE/BChE) as potentially synergistic profile. Initial screening of the compounds at H_3R and D_3R was done at 1 or 10 μM and 100 μM at AChE and BChE assays. The most promising compounds were then evaluated in full concentration–response curves to estimate the K_i and IC_{50} values. Results showed that several compounds were ligands at H_3R (n = 10), D_3R (n = 6), AChE (n = 3), and BChE (n = 9). Compounds LINS05006 (K_i H_3R 2.8 μM; D_3R 0.7 μM; IC_{50} BChE 26.3 μM) and LINS05015 (K_i H_3R 1.1 μM; D_3R 3.1 μM; IC_{50} AChE 97.8 μM; BChE 43.7 μM) are highlighted since presented affinity in three different. These results suggest that methylpiperazine moiety led to balanced activity at all three classes of targets, and longer linker provided the best affinities. These compounds presented high ligand efficiency values (LE > 0.3) and may have adequate pharmacokinetic profile as suggested by calculated physicochemical properties.

1. Introduction

Designed multiple ligands (DMLs), also referred as multitarget compounds, are molecules designed to interact with more than one target with a single molecule, in a different approach from the classical drugs designed from the "one drug, one target" paradigm,[1] which proposes that by interacting with selected key targets, a positive network effect can be achieved on a given condition, leading to increased therapeutic response. This is especially desirable when designing drugs for CNS disorders that involve cognitive decline that involves a network effect of several distinct brain areas and systems and therefore a complex treatment. However, such complex therapeutic regimen can lead to low adherence, poor efficacy and increased risk for toxicity, especially if considering elderly patients.[2]

The design of DMLs is not a trivial task, since the structural requirements for binding to each target must be considered in a single molecule, and indeed the selection of pharmacological targets should be carried out with some criteria.[1,2] When the targets require similar structural features for ligand binding, merging pharmacophores in a single molecule is a feasible strategy for ligand design.[3] Regarding this, the histamine H_3 receptor (H_3R), dopamine D_3 receptor (D_3R) and cholinesterases (ChEs, acetyl - AChE and butyryl - BChE) were selected as targets for their role in cognitive processes and pharmacophore requirements for ligand binding.

The role of histamine in cognition made the H_3R widely explored as drug target for cognitive disorders.[4,5] H_3R is a presynaptic auto/heteroreceptor in the CNS and thus it may control the production and release of several neurotransmitters including dopamine, acetylcholine and histamine itself.[5] Therefore, by blocking H_3R, an increase in the activity of such neurotransmitters is expected. In addition to histamine, dopamine is also related to cognition, especially by the activation of D_3R.[6] This receptor is mainly expressed in prefrontal cortex, hippocampus and amygdala as an auto-receptor; thus the blockade of this receptor, similarly to the H_3R, may result in increased dopamine levels in these areas, improving the cognition.[6,7] Lastly, the relationship of acetylcholine with cognition is evident, once the main treatment for cognitive decline

* Corresponding authors.
E-mail addresses: stark@hhu.de (H. Stark), joao.fernandes@unifesp.br (J.P.S. Fernandes).

https://doi.org/10.1016/j.bmc.2022.117132
Received 7 October 2022; Received in revised form 5 December 2022; Accepted 12 December 2022
Available online 16 December 2022
0968-0896/© 2022 Elsevier Ltd. All rights reserved.

involves the inhibition of AChE and/or BChE by donepezil, galantamine, rivastigmine and several other drugs.[3,8,9] However, the inhibition of cholinesterases only provides limited therapeutic benefit in short-term due to solely increasing acetylcholine levels but no other neurotransmitters.

The possible interactions and cross-reactivity of dopamine, histamine and acetylcholine neurotransmission is just a cutout of a complex network (Figure 1). By blocking the presynaptic receptors H_3R/D_3R and reducing the hydrolysis rate of acetylcholine by inhibiting the ChEs, a synergistic effect may be achieved to improve the cognitive process at the end. Considering this panorama and these selected targets, in this work we designed a set of compounds as multitarget agents for binding at H_3R, D_3R and cholinesterases. Since the ligands of such targets share similar characteristics, we adopted the merging strategy to design such compounds, which were prepared and assessed for their binding affinity at H_3R, D_3R, AChE and BChE.

2. Results and discussion

The compounds were designed considering the structural requirements for binding at the selected targets (Figure 2). The general structure for histamine H_3R ligands is comprised of a lipophilic region (usually an aromatic system) and a basic moiety attached by a variable linker group with 4–8 atoms.[5,10,11] These characteristics are related to the interactions that H_3R antagonists perform on the target. The lipophilic group performs hydrophobic interactions, while the ionized basic group interacts with a Asp3.32 residue (conserved in several biogenic amine receptors, including dopamine receptors) through a salt brigde.[12] Compounds with variable structure are reported in literature, but compound KSK29 (Figure 2) is a representative compound containing the 4-pyridinyl substituent in the piperazine group, which performs specific interaction leading to increased affinity at H_3R.[13]

Interestingly, the ligands at D_3R and inhibitors of ChEs have also structural similarities with the general structure of H_3R antagonists. Ligands at D_3R usually present an aromatic system (to bind at the secondary binding pocket, SBP) and a basic moiety (to interact with Asp3.32) frequently represented by arylpiperidines or arylpiperazines (to bind at the orthosteric binding pocket, OBP), separated by a linker group.[6,14] BP897 is a representative compound with submicromolar affinity at D_3R containing a phenylpiperazine moiety in as basic unit and an amide group as connecting group. However, H_3R antagonists frequently have oxygen instead of NH in the connecting group, raising important question about the influence of this amide on H_3R affinity.

Finally, inhibitors of ChEs have more variable structures, but donepezil is an example of a potent inhibitor of AChE containing two aromatic groups (to interact with tryptophan residues from the peripherical anionic site, PAS, and the catalytic anionic site, CAS, of the enzyme) and a basic nitrogen in between.[3,15,16] Several ChEs inhibitors roughly fit to this structural framework,[17] including compound DQN7 represented in Figure 2. Considering these pharmacophore elements, we designed a set of compounds namely LINS05 by merging the structural frameworks presented in H_3R, D_3R and ChEs ligands. The compounds are comprised by an aromatic region represented by naphthyl or benzofuranyl groups and a basic moiety represented by *N*-substituted piperazines. These groups are separated by a variable linker group with 2 or 3 methylene units and a connecting functional group (ether, ester or amide) to explore the optimal distance between the aromatic and basic functionalities for each target, as well as the influence of the connecting group on the affinities. Although esters may present considerable metabolic instability *in vivo*, it is important to emphasize that the aim was to explore the role of the hydrogen bond donor or acceptor group in the connecting group.

The compounds were synthesized by conventional organic reactions that resulted in satisfactory over all yields (Schemes 1 and 2). The ethers **01**–**09** were prepared from the corresponding naphthols by reacting with 1,2-ethane or 1,3-propane dibromides, using potassium carbonate as base, leading to yields between 51 and 60 % of the purified ether products **1a-1d**. Afterwards, these products were reacted with the *N*-substituted piperazine (methyl, phenyl or 4-pyridyl) by similar manner to yield 40 to 97 % of the target compounds (Scheme 1). The esters **10**–**20** were prepared by reacting the acyl chlorides and the corresponding chloroalkanols (2-chloroethanol or 3-chloropropanol) in presence of TEA as base, leading to excellent yields. The amide **2f** was obtained when 3-chloropropylamine was employed (Scheme 2). The same synthetic protocol used for the ethers was applied to obtain the target compounds **10**–**21** from the esters **2a-2e** or amide **2f**. Final compounds were converted to their respective salts of maleic acid and used in this form in the assays in order to increase their water solubility.

The compounds were assessed for their affinity at H_3R and D_3R, as well as ChEs (Tables 1 and 2), and summarized SAR information is described in Figure 3. Seven compounds were identified as ligands of two different classes of targets (**07**, **08**, **11**, **16**, **19**, **20** and **21**) while compounds **06** and **15** were ligands of three classes. These compounds showed adequate physicochemical properties to predict high gastrointestinal (GI) absorption after oral administration and ability to cross the blood brain barrier (BBB), as suggested by the calculation at SwissADME

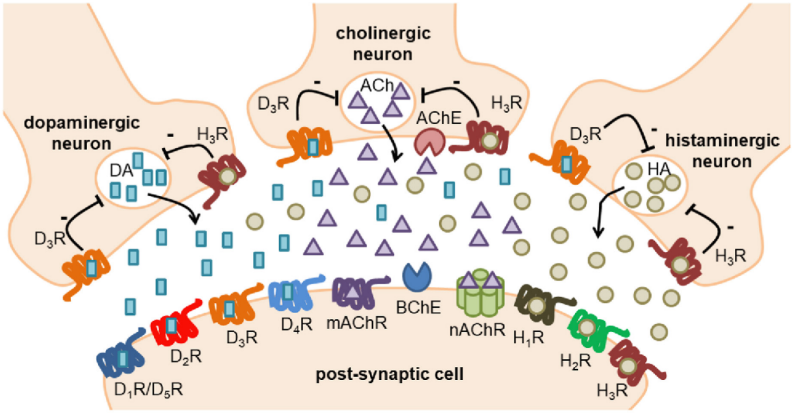


Figure 1. Possible interaction between the dopamine (DA), histamine (HA) and acetylcholine (ACh) neurotransmission. The blockade of D_3R and H_3R may increase the ACh release from cholinergic terminals, while ACh half-life may be increased with the inhibition of ChEs, leading to increased activation of cholinergic muscarinic (mAChR) and/or nicotinic (nAChR) receptors.

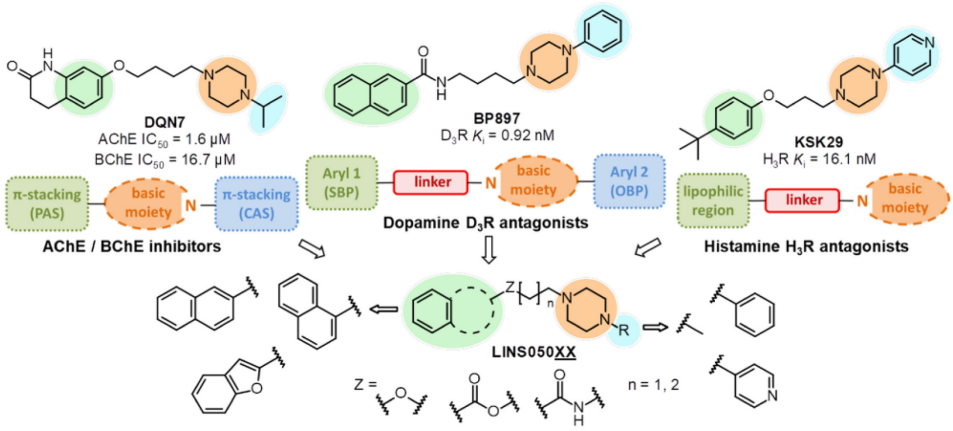
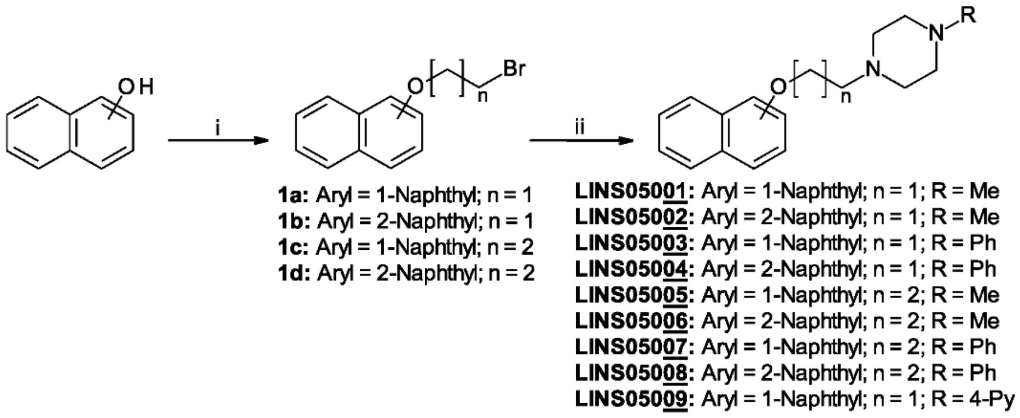


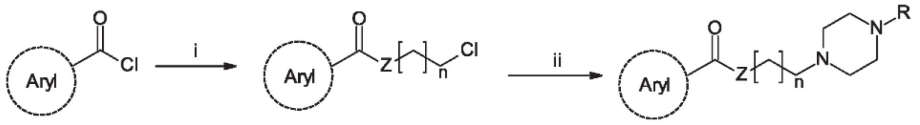
Figure 2. Conception for designing the LINS050XX compounds.



1a: Aryl = 1-Naphthyl; n = 1
1b: Aryl = 2-Naphthyl; n = 1
1c: Aryl = 1-Naphthyl; n = 2
1d: Aryl = 2-Naphthyl; n = 2

LINS05001: Aryl = 1-Naphthyl; n = 1; R = Me
LINS05002: Aryl = 2-Naphthyl; n = 1; R = Me
LINS05003: Aryl = 1-Naphthyl; n = 1; R = Ph
LINS05004: Aryl = 2-Naphthyl; n = 1; R = Ph
LINS05005: Aryl = 1-Naphthyl; n = 2; R = Me
LINS05006: Aryl = 2-Naphthyl; n = 2; R = Me
LINS05007: Aryl = 1-Naphthyl; n = 2; R = Ph
LINS05008: Aryl = 2-Naphthyl; n = 2; R = Ph
LINS05009: Aryl = 1-Naphthyl; n = 1; R = 4-Py

Scheme 1. General preparation of the final ethers. (i) α,ω-dibromoalkan, K_2CO_3, ethanol, reflux, 18–24 h; (ii) R-piperazine, K_2CO_3, KI, ACN, reflux, 24–48 h.

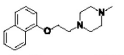
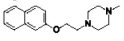
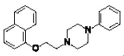
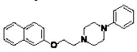
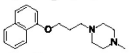
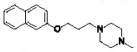
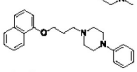
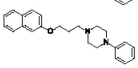
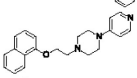
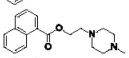
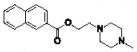
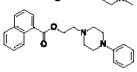
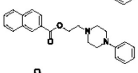
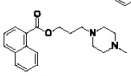
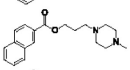
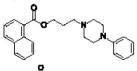
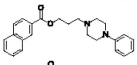
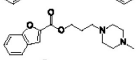
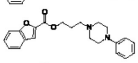
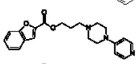
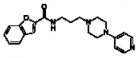


2a: Aryl = 1-Naphthyl; n = 1; Z = O
2b: Aryl = 2-Naphthyl; n = 1; Z = O
2c: Aryl = 1-Naphthyl; n = 2; Z = O
2d: Aryl = 2-Naphthyl; n = 2; Z = O
2e: Aryl = 2-Benzofuranyl; n = 2; Z = O
2f: Aryl = 2-Benzofuranyl; n = 2; Z = NH

LINS05010: Aryl = 1-Naphthyl; n = 1; R = Me; Z = O
LINS05011: Aryl = 2-Naphthyl; n = 1; R = Me; Z = O
LINS05012: Aryl = 1-Naphthyl; n = 1; R = Ph; Z = O
LINS05013: Aryl = 2-Naphthyl; n = 1; R = Ph; Z = O
LINS05014: Aryl = 1-Naphthyl; n = 2; R = Me; Z = O
LINS05015: Aryl = 2-Naphthyl; n = 2; R = Me; Z = O
LINS05016: Aryl = 1-Naphthyl; n = 2; R = Ph; Z = O
LINS05017: Aryl = 2-Naphthyl; n = 2; R = Ph; Z = O
LINS05018: Aryl = 2-Benzofuranyl; n = 2; R = Me; Z = O
LINS05019: Aryl = 2-Benzofuranyl; n = 2; R = Ph; Z = O
LINS05020: Aryl = 2-Benzofuranyl; n = 2; R = 4-Py; Z = O
LINS05021: Aryl = 2-Benzofuranyl; n = 2; R = 4-Py; Z = NH

Scheme 2. General preparation of the final ethers. (i) α,ω-alkoxy or alkylamine chloride, TEA, DCM, 60 °C, 3 h; (ii) R-piperazine, K_2CO_3, KI, ACN, reflux, 24–48 h.

Table 1
Screening of the LINS05 compounds at H_3R, D_3R and ChEs.

Compound LINS050XX		% inhibition (±SD) at 1 or 10 μM		% inhibition (±SD) at 100 μM	
		hH_3R	*h*D_3R	*ee*AChE	*eq*BChE
01[a]		21.3 ± 9.8	33.5 ± 9.5	20.4 ± 7.5	64.9 ± 1.8
02[a]		39.3 ± 16.2	15.2 ± 13.6	8.3 ± 6.0	48.4 ± 8.8
03[a]		39.8 ± 15.6	34.5 ± 11.0	5.3 ± 3.9	26.2 ± 6.3
04[b]		23.3 ± 16.3	45.0 ± 7.2	7.8 ± 8.5	17.5 ± 8.6
05[a]		70.0 ± 7.8	47.8 ± 10.2	45.7 ± 7.7	60.2 ± 9.8
06[a]		80.5 ± 9.0	22.8 ± 21.4	48.8 ± 9.9	70.0 ± 12.1
07[b]		26.3 ± 5.4	59.7 ± 3.1	22.9 ± 10.1	22.7 ± 4.6
08[b]		36.8 ± 12.6	80.5 ± 5.3	11.7 ± 4.0	65.7 ± 11.0
09[b]		54.0 ± 9.7	37.7 ± 11.6	62.2 ± 2.1	65.4 ± 1.6
10[a]		69.0 ± 7.9	49.7 ± 15.5	40.1 ± 4.0	38.3 ± 6.8
11[a]		78.2 ± 6.4	53.7 ± 11.9	43.6 ± 6.8	74.8 ± 0.5
12[a]		71.3 ± 6.8	52.8 ± 10.1	33.0 ± 17.5	24.1 ± 14.1
13[a]		61.5 ± 5.3	32.8 ± 24.4	31.6 ± 10.9	36.5 ± 8.9
14[a]		83.8 ± 6.2	71.5 ± 9.4	39.0 ± 2.6	50.6 ± 5.2
15[a]		96.3 ± 10.1	77.7 ± 10.7	45.7 ± 8.0	85.1 ± 7.4
16[a]		101.2 ± 17.6	86.2 ± 9.0	24.2 ± 3.8	< 10
17[a]		40.8 ± 16.8	65.3 ± 14.1	23.6 ± 8.1	16.6 ± 7.9
18[a]		82.3 ± 8.4	9.0 ± 35.0	44.5 ± 3.6	31.7 ± 2.8
19[a]		80.8 ± 6.1	49.2 ± 16.6	47.0 ± 7.6	46.8 ± 8.2
20[b]		88.8 ± 1.5	18.0 ± 8.6	63.6 ± 2.8	49.9 ± 5.6
21[b]		80.5 ± 6.5	23.5 ± 8.9	49.1 ± 4.0	54.5 ± 8.2
Pitolisant		99.8 ± 5.9			
Haloperidol			100.2 ± 2.0		
Donepezil				>95	
Neostigmine					>95

[a] 10 μM at *h*H_3R and *h*D_3R; [b] 1 μM at *h*H_3R and *h*D_3R.

platform (Table 4).[18] Most compounds should not be P-glycoprotein substrates, suggesting high bioavailability and penetration into the CNS.

Regarding the binding affinity at H_3R, the results showed that the carbonyl-containing compounds (ester and amides) are better ligands than the ether analogues, since only the ethers **06** and **07** presented considerable affinity to this receptor, suggesting the involvement of the carbonyl in a specific interaction with H_3R. It is possible to note that only compounds containing the propylene linker showed important affinity to H_3R, and none of the ethylene-containing compounds were reasonably active on such receptor. The carbonylated compounds are one-atom longer than the ether counterparts, also suggesting that longer linkers play a role in the affinity to H_3R. Moreover, it is possible that compounds containing a basic nitrogen farther from the aromatic region present higher affinity at H_3R, as corroborated by other reports from literature.[5,19,20] The phenylpiperazine derivatives showed lower affinity to H_3R than the methylpiperazines. None of these compounds showed relevant affinity to H_4R (cf. Supporting Information), despite the high sequence similarity of this receptor with the H_3R.

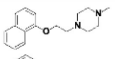
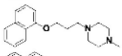
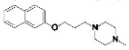
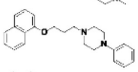
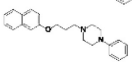
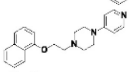
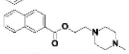
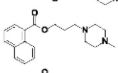
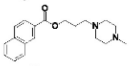
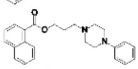
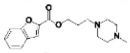
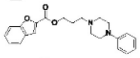
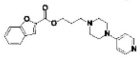
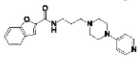
Previous works from literature reported that the 4-pyridylpiperazine moiety may increase the affinity at H_3R by performing specific interactions at H_3R by hydrogen-bond formation and π-π interactions.[11,13] Taking advantage of this structural motif, compounds **09**, **20** and **21** were prepared and assessed. Compounds **20** and **21** were the best of the series as H_3R ligands, showing nanomolar affinity (0.27 and 0.91 μM, respectively), while compound with shorter linker (**09**) presented low affinity at H_3R (Table 2). Since compound **20** has higher affinity at H_3R than the amide analogue **21**, it is suggested that presence of a hydrogen bond acceptor (–O–) from ester group has positive role on the affinity, while the donor (–NH–) from amide decreases the binding affinity at H_3R.

Compounds with high affinity at dopamine D_2-like receptors frequently present an arylpiperazine moiety,[6,7] and thus insertion of the phenylpiperazine motif was considered on the design of the multitarget compounds. Compounds bearing this motif (**07**, **08**, **16** and **19**) showed submicromolar affinities at D_3R, although it usually does not provide selectivity over D_2R (Tables 1 and S1).[21,22] For instance, compounds **07** and **08** presented similar affinity at both D_2R (0.48 and 0.28 μM, respectively) and D_3R. The 4-pyridylpiperazine motif was also considered to obtain affinity at both D_3R and H_3R, but unfortunately compounds **09**, **20** and **21** did not show important affinity to D_3R, suggesting that 4-pyridinyl group affects the affinity at D_3R. Compounds containing 2-methoxyphenyl or 2,3-dichlorophenyl piperazine were reported with high affinity and certain selectivity towards D_3R,[22] however arylpiperazine analogues generally present low affinities at H_3R, except for the 4-pyridylpiperazine containing analogues.[13]

Regarding the inhibitory activity on ChEs, the compounds showed general preference to inhibit BChE over AChE. Although we expected that compounds with longer linkers could have better inhibitory activity, no important differences were noted when comparing ethylene and propylene compounds, suggesting that variations in the linker region poorly affected the activity. Literature suggests that compounds with long linker region usually present higher inhibitory activity at ChEs,[3] however Queda et al.[23] and Bautista-Aguilera et al.[16] reported compounds containing short linkers with considerable inhibition at AChE.

On the other hand, variations in the basic group influenced the inhibitory activity. The methylpiperazine compounds **01**, **05**, **06**, **11** and **15** showed considerable activity on BChE, suggesting that this motif leads to higher affinity for this enzyme. Compounds **09** and **20** that bear the 4-pyridylpiperazine moiety showed affinity at both AChE and BChE, suggesting this fragment is important for the activity on AChE. The compounds that contain phenylpiperazine as basic motif showed poor inhibitory activity at ChEs. Considering that ChEs may hydrolyze esters, a kinetic study with compound **20** was performed to investigate if this compound could serve as substrate. The result revealed that this compound is a competitive inhibitor of AChE and is not hydrolyzed by this enzyme (see Supplementary Information). It is also important to

Table 2
Affinity data to the selected compounds at H_3R, D_3R and ChEs.

Compound LINS050XX		K_i [μM] (CI 95 %)		IC_{50} [μM] (CI 95 %)	
		hH_3R	*h*D_3R	*ee*AChE	*eq*BChE
01		n.d.	n.d.	n.d.	58.9 (25.1–134.1)
05		n.d.	n.d.	n.d.	78.5 (27.0–207.0)
06		2.8 (1.6–5.1)	0.70 (0.06–7.40)	n.d.	26.3 (14.4–51.8)
07		4.0 (2.5–6.2)	0.92 (0.41–2.07)	n.d.	n.d.
08		> 10	0.34 (0.25–0.47)	n.d.	53.7 (34.7–83.7)
09		n.d.	n.d.	53.7 (33.7–85.8)	40.7 (32.8–53.5)
11		2.2 (1.2–4.0)	> 10	n.d.	57.5 (13.8–242.8)
14		3.7 (0.9–15.4)	> 10	n.d.	n.d.
15		1.1 (0.6–2.3)	3.1 (0.7–13.2)	97.8 (74.1–129.1)	43.7 (7.5–253.7)
16		1.9 (0.9–3.7)	0.86 (0.40–1.70)	n.d.	n.d.
18		3.3 (1.9–5.9)	>10	n.d.	n.d.
19		1.7 (0.5–6.0)	1.4 (0.2–8.5)	n.d.	n.d.
20		0.27 (0.1–0.77)	>10	57.2 (38.1–85.8)	97.7 (71.5–138.6)
21		0.91 (0.7–1.19)	>10	n.d.	85.1 (49.1–144.9)
Pitolisant		13.4 nM (9.0–19.9)			
Haloperidol			53.7 nM (4.0–71.4)		
Donepezil				7.3 nM (3.2–17.2)	
Neostigmine					0.16 (0.12–0.22)

n.d.: not determined.

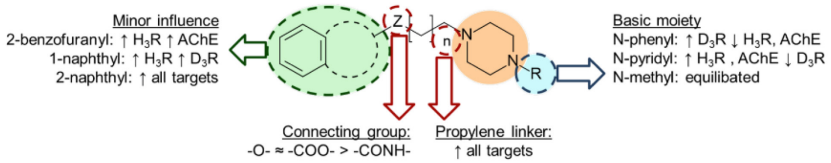


Figure 3. Summarized SAR information obtained from the results of this work.

mention that these esters were stable under assay conditions.

Considering compounds with dual activity, three compounds containing the phenylpiperazine moiety (**07**, **08** and **16**) showed nanomolar affinity at D_3R (K_i 0.92, 0.34 and 0.86 μM, respectively) along with considerable affinity to H_3R (compounds **07** and **16**, K_i 4.0 and 1.9 μM, respectively) or BChE (compound **08**, IC_{50} 53.7 μM). These data reinforces the importance of the phenylpiperazine fragment to the affinity at dopamine receptors, although the methylpiperazine compound **06** showed the higher LE value at D_3R. On the other side, the compounds containing the 4-pyridylpiperazine motif and longer linker **20** and **21** had moderate nanomolar affinities at H_3R along with considerable inhibition of ChEs. Compound **20** must be highlighted due its high potency at H_3R and inhibitory activity against both AChE (IC_{50} 57.2 μM) and BChE (IC_{50} 97.7 μM).

From the results, it is possible to note that compounds containing a propylene methylpiperazine moiety (**06** and **15**) presented triplex affinity at H_3R, D_3R and ChEs. They represent suitable candidates for multitarget purposes, since they presented equilibrated activity in each.

This is important in the multitarget perspective, especially when considering the synergistic effect that H_3R/D_3R antagonism and ChE inhibition may cause in the ACh levels on synaptic cleft (Figure 1). Compound **15** showed ligand activity in all tested targets, presenting much equilibrated activity in each (K_i H_3R 1.1, D_3R 3.1 μM; IC_{50} AChE 97.8, BChE 43.7 μM). On the other hand, compound **06** must be highlighted due its higher LE values at H_3R, D_3R and BChE (0.38, 0.42 and 0.31, respectively), better stability and offers opportunities for future modifications.[24] It is known that during development process, the molecular weight (MW) frequently increases, leading to negative influence on LE values, and therefore compounds like **06** (with lower MW than that of **15**) are considered more interesting prototypes for additional modification. Moreover, both compounds had high predicted GI absorption and BBB permeability, suggesting that they may be orally bioavailable and properly reach the CNS (Table 3), although future modification should be considered on ester moiety of compound **15** as potential motif for hydrolysis to increase its metabolic stability *in vivo*.

In summary, compounds with multitarget activity at H_3R, D_3R and ChEs were identified with adequate physicochemical profile. These compounds are noteworthy prototypes for further modifications in order to increase the potency and optimize the pharmacological potential. It is important to stress that this is one of the first reports reporting compounds with triplex activity at H_3R, D_3R and ChEs, and thus these compounds should be considered useful additional examples of such profile.

3. Material and methods

3.1. Reagents and equipment

Chemicals were obtained in adequate purity from Sigma-Aldrich Co. (Saint Louis, MO, USA) and LabSynt Co. (Diadema, Brazil) and used without any further purification. ^1H and ^{13}C NMR spectra were recorded on a Bruker Ultrashield 300 spectrometer, operating at 300 and 75 MHz, respectively, using $CDCl_3$ or DMSO-d_6 as solvents and tetramethylsilane (TMS) as internal standard. Chemical shifts (δ) were determined from TMS and are reported in parts per million (ppm). Coupling constants (*J*) are reported in units of Hertz (Hz), if applicable. All NMR data was obtained using the compounds as free bases. Elemental analysis was performed for the hydrogenmaleate salts in a Perkin Elmer 2400 CHNS elemental analyzer. Data is reported as the percentage of each element.

The *Electrophorus electricus* AChE (*ee*AChE) and BChE from equine serum (*eq*BChE) were obtained from Sigma-Aldrich Co. Stock solutions of the enzymes were prepared as indicated by the supplier. For cholinesterase assays, test compounds (as hydrogenmaleate salts), donepezil hydrochloride and neostigmine mesylate were prepared as stock solutions from 1 mM to 100 μM. The assay was performed in a microplate spectrophotometer (PowerWave HT, BioTek).

3.2. Synthesis of the compounds

*General procedure for the preparation of ether intermediates (**1a-1d**).* In a flask, 3 mmol of the adequate naphthol, 9 mmol of the alkyl dibromide (1,2-dibromoethane or 1,3-dibromopropane) and 3 mmol of K_2CO_3 were added with 20 mL of ethanol. The reaction mixture was stirred under reflux for 18–24 h until completion (TLC monitoring). The solvent was evaporated, and the residue was taken up in 20 mL of ethyl acetate, washed with 2 × 20 mL of water and the organic layer was dried over anhydrous Na_2SO_4 and evaporated. The crude oil was purified through column chromatography using hexane:AcOEt (9:1) as eluent (Scheme 1).

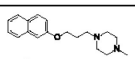
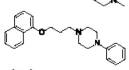
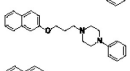
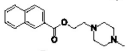
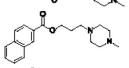
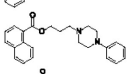
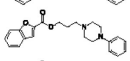
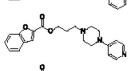
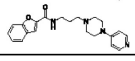
*1-(2-Bromoethoxy)naphthalene (**1a**).* Yellowish oil. Yield 51 %. ^1H NMR (300 MHz, $CDCl_3$) δ 8.27 (dd, *J* = 6.2, 3.3 Hz, 1H), 7.73 (dd, *J* = 6.2, 3.3 Hz, 1H), 7.43 (m, 2H), 7.40 (dd, *J* = 8.1 Hz, 1H), 7.27 (t, *J* = 8.1 Hz, 1H), 6.64 (dd, *J* = 7.3, 1.6 Hz, 1H), 4.28 (t, *J* = 6.2 Hz, 2H), 3.62 (t, *J* = 6.2 Hz, 2H). Spectral data in accordance to Pomilio et al.[25]

*2-(2-Bromoethoxy)naphthalene (**1b**).* Colorless oil. Yield 57 %. ^1H NMR (300 MHz, $CDCl_3$) δ 7.81–7.68 (m, 3H), 7.50–7.41 (m, 1H), 7.36 (dd, *J* = 11.0, 4.0 Hz, 1H), 7.22–7.10 (m, 2H), 4.42 (t, *J* = 6.3 Hz, 2H), 3.71 (t, *J* = 6.3 Hz, 2H). Spectral data in accordance to Guo et al.[26]

*1-(3-Bromopropoxy)naphthalene (**1c**).* Colorless oil. Yield 58 %. ^1H NMR (300 MHz, $CDCl_3$) δ 8.23 (dd, *J* = 6.3, 3.3 Hz, 1H), 7.78–7.81 (m, 1H), 7.50–7.32 (m, 4H), 6.82 (d, *J* = 7.3 Hz, 1H), 4.28 (t, *J* = 6.0 Hz, 2H), 3.70 (t, *J* = 6.0 Hz, 2H), 2.33 (quint, *J* = 6.0 Hz, 2H). Spectral data in accordance to Tada et al.[27]

*2-(3-Bromopropoxy)naphthalene (**1d**).* Colorless oil. Yield 60 %. ^1H NMR (300 MHz, $CDCl_3$) δ 7.74–7.80 (m, 3H), 7.48 (t, *J* = 6.9 Hz, 1H), 7.44 (t, *J* = 6.0 Hz, 1H), 7.15–7.19 (m, 2H), 4.26 (t, *J* = 6.0 Hz, 2H), 3.68

Table 3
LE analysis and pharmacokinetic prediction for the multitarget compounds, carried out with the Swiss ADME prediction tools.[18]

Compound LINS050XX		LE				GI absorption	BBB permeant	P-gp substrate
		H_3R	D_3R	AChE	BChE			
06		0.38	0.42	-	0.31	High	+	No
07		0.28	0.32	–	–	High	+	Yes
08		–	0.34	–	0.22	High	+	Yes
11		0.35	–	–	0.26	High	+	No
15		0.35	0.33	0.24	0.26	High	+	No
16		0.28	0.30	–	–	High	+	No
19		0.29	0.30	–	–	High	+	No
20		0.33	–	0.22	0.20	High	+	No
21		0.31	–	–	0.21	High	+	Yes

(t, J = 6.4, 2H), 2.39–2.45 (quint, J = 6.0, 2H). Spectral data in accordance to Sword et al.[28]

*General procedure for the preparation of ester intermediates (**2a-2f**).* In a flask, the adequate acyl chloride (naphthalene or 2-benzofurancarbonyl chloride, 2 mmol), the alkoxyl chloride (2-chloroethanol or 3-chloropropanol, 6 mmol) and triethylamine (TEA, 2 mmol) were added to 15 mL of dichloromethane (DCM). The mixture was stirred at 60 °C for 1–4 h (TLC monitoring). The resulting solution was washed with 2x 20 mL of saturated aqueous $NaHCO_3$ solution and 20 mL of water. The organic layer was dried over anhydrous Na_2SO_4 and evaporated, giving analytically pure products (Scheme 2).

*2-Chloroethyl naphthalene-1-carboxylate (**2a**).* Yellowish oil. Yield 79 %. ^{1}H NMR (300 MHz, $CDCl_3$) δ 8.93 (d, J = 8.6 Hz, 1H), 8.23 (d, J = 7.3 Hz, 1H), 7.99 (d, J = 8.2 Hz, 1H), 7.84 (d, J = 7.8 Hz, 1H), 7.63–7.57 (m, 1H), 7.54–7.43 (m, 2H), 4.62 (t, J = 5.6 Hz, 2H), 3.83 (t, J = 5.6 Hz, 2H).

*2-Chloroethyl naphthalene-2-carboxylate (**2b**).* Yellowish oil. Yield 70 %. ^{1}H NMR (300 MHz, $CDCl_3$) δ 8.61 (s, 1H), 8.05 (dd, J = 8.6, 1.5 Hz, 1H), 7.92 (d, J = 7.8 Hz, 1H), 7.84 (d, J = 8.9 Hz, 2H), 7.59–7.46 (m, 2H), 4.60 (t, J = 5.7 Hz, 2H), 3.83 (t, J = 5.7 Hz, 2H). Spectral data in accordance to Sattenapally et al.[29]

*3-Chloropropyl naphthalene-1-carboxylate (**2c**).* Yellowish oil. Yield 95 %. ^{1}H NMR (300 MHz, $CDCl_3$) δ 8.90 (d, J = 8.6 Hz, 1H), 8.17 (dd, J = 7.3, 1.0 Hz, 1H), 8.03 (d, J = 8.2 Hz, 1H), 7.89 (d, J = 8.0 Hz, 1H), 7.66–7.45 (m, 3H), 4.57 (t, J = 6.2 Hz, 2H), 3.74 (t, J = 6.2 Hz, 2H), 2.29 (quint, J = 6.2 Hz, 2H).

*3-Chloropropyl naphthalene-2-carboxylate (**2d**).* Yellowish oil. Yield 85 %. ^{1}H NMR (300 MHz, $CDCl_3$) δ 8.59 (s, 1H), 8.04 (dd, J = 8.6, 1.2 Hz, 1H), 7.94 (d, J = 7.8 Hz, 1H), 7.86 (d, J = 8.6 Hz, 2H), 7.62–7.49 (m, 2H), 4.53 (t, J = 6.2 Hz, 2H), 3.67 (t, J = 6.2 Hz, 2H), 2.27 (quint, J = 6.2 Hz, 2H).

*3-Chloropropyl benzofuran-2-carboxylate (**2e**).* Yellowish oil. Yield 59 %. ^{1}H NMR (300 MHz, $CDCl_3$) δ 7.68 (d, J = 7.8 Hz, 1H), 7.59 (d, J = 8.4 Hz, 1H), 7.54 (s, 1H), 7.49–7.41 (m, 1H), 7.30 (m, 1H), 4.54 (t, J = 6.1 Hz, 2H), 3.71 (t, J = 6.1 Hz, 2H), 2.26 (quint, J = 6.1 Hz, 2H).

*Synthesis of N-(3-chloropropyl)benzofuran-2-carboxamide (**2f**).* The procedure was performed following the same protocol for ester preparation, but using the 3-chloro-1-propylamine as reactant. After the reaction was completed, the solution was washed with 2x 15 mL aqueous HCl 0.1 M, 2x 15 mL of aqueous NaOH 0.1 M and 15 mL of water. The organic layer was dried over anhydrous Na_2SO_4 and evaporated, giving analytically pure product as colorless oil (Scheme 2). Yield 95 %. ^{1}H NMR (300 MHz, $CDCl_3$) δ 7.67 (d, J = 7.8 Hz, 1H), 7.55–7.36 (m, 3H), 7.35–7.22 (m, 1H), 6.82 (br.s, 1H), 3.7 (tt, J = 6.5, 3.4 Hz, 4H), 2.15 (quint, J = 6.5 Hz, 2H).

*General procedure for the preparation of final compounds (**LINS05001-LINS05021**).* In a flask, the adequate intermediate **1a-1d** (0.5 mmol), the substituted piperazine (1 mmol for 1-phenylpiperazine and 1-(4-pyridyl)piperazine, and 2 mmol for 1-methylpiperazine), K_2CO_3 (2 mmol) and KI (2 mmol) were added with 15 mL of acetonitrile. The reaction was stirred under reflux up to 48 h (TLC monitoring), and afterwards the solvent was evaporated. The residue was taken up with 15 mL of dichloromethane and washed with 2 × 15 mL of water. The organic layer was dried over anhydrous Na_2SO_4 and evaporated. The crude material was purified through column chromatography using DCM:MeOH (9:1) as eluent (Schemes 1 and 2). The NMR data was obtained for the final compounds as free bases. These were converted into salts of maleic acid to increase buffer solubility in the assays by neutralization with excess of maleic acid and precipitation of the obtained salts in diethyl ether.

1-Methyl-4-[2-(1-naphthyloxy)ethyl]piperazine (**LINS05001**). Yellow ish oil. Yield 97 % ^{1}H NMR (300 MHz, $CDCl_3$) δ 8.30–8.20 (m, 1H), 7.80–7.77 (m, 1H), 7.53–7.30 (m, 4H), 6.80 (d, J = 7.4 Hz, 1H), 4.29 (t, J = 5.7 Hz, 2H), 2.98 (t, J = 5.7 Hz, 2H), 2.71 (br.s, 4H), 2.49 (br.s, 4H), 2.30 (s, 3H). ^{13}C NMR (75 MHz, $CDCl_3$) δ 154.5, 134.5, 127.5, 126.4, 125.9, 125.7, 125.2, 122.1, 120.4, 104.8, 66.6, 57.2, 55.1, 53.6, 46.0. Elemental anal. calcd. for $C_{17}H_{22}N_2O.2C_4H_4O_4$: C 59.75, H 6.0, N 5.75 %. Found: C 59.7, H 6.0, N 5.6 %.

1-Methyl-4-[2-(2-naphthyloxy)ethyl]piperazine (**LINS05002**). Yellow ish oil. Yield 88 %. ^{1}H NMR (300 MHz, $CDCl_3$) δ 7.81–7.66 (m, 3H), 7.47–7.38 (m, 1H), 7.33 (dd, J = 10.9, 4.0 Hz, 1H), 7.20–7.09 (m, 2H), 4.23 (t, J = 5.8 Hz, 2H), 2.89 (t, J = 5.8 Hz, 2H), 2.67 (br.s, 4H), 2.51 (br. s, 4H), 2.31 (s, 3H). ^{13}C NMR (75 MHz, DMSO) δ 155.6, 133.0, 128.7, 127.9, 126.9, 126.1, 125.8, 123.0, 118.1, 106.2, 64.6, 54.9, 52.0, 49.3, 41.7. Elemental anal. calcd. for $C_{17}H_{22}N_2O.2C_4H_4O_4$: C 59.75, H 6.0, N 5.75 %. Found: C 59.8, H 6.05, N 5.6 %.

1-[2-(1-Naphthyloxy)ethyl]-4-phenyl-piperazine (**LINS05003**). White solid. Yield 63 %. ^{1}H NMR (300 MHz, $CDCl_3$) δ 8.33–8.22 (m, 1H), 7.80–7.77 (m, 1H), 7.53–7.31 (m, 4H), 7.29–7.19 (m, 2H), 6.91 (d, J = 8.1 Hz, 2H), 6.83 (dd, J = 15.1, 7.5 Hz, 2H), 4.31 (t, J = 5.6 Hz, 2H), 3.23–3.15 (m, 4H), 3.00 (t, J = 5.6 Hz, 2H), 2.83–2.77 (m, 4H). ^{13}C NMR (75 MHz, $CDCl_3$) δ 154.6, 151.4, 134.6, 129.2, 127.6, 126.5, 125.9, 125.8, 125.3, 122.1, 120.5, 119.8, 116.1, 104.9, 66.7, 57.4, 53.8, 49.3. Elemental anal. calcd. for $C_{22}H_{24}N_2O.C_4H_4O_4$: C 69.6, H 6.3, N 6.25 %. Found: C 69.6, H 6.3, N 6.2 %.

1-[2-(2-Naphthyloxy)ethyl]-4-phenyl-piperazine (**LINS05004**). Yellow ish solid. Yield 56 %. ^{1}H NMR (300 MHz, $CDCl_3$) δ 7.82–7.68 (m, 3H), 7.43 (dd, J = 11.1, 4.0 Hz, 1H), 7.31–7.22 (m, 3H), 7.21–7.12 (m, 2H), 6.94 (d, J = 8.0 Hz, 2H), 6.86 (t, J = 7.3 Hz, 1H), 4.28 (t, J = 5.8 Hz, 2H), 3.28–3.23 (m, 4H), 2.95 (t, J = 5.8 Hz, 2H), 2.82–2.76 (m, 4H). ^{13}C NMR (75 MHz, $CDCl_3$) δ 156.1, 150.3, 135.6, 129.9, 129.6, 129.2, 128.8, 128.1, 127.2, 127.1, 124.4, 120.3, 119.0, 116.3, 107.8, 55.5, 52.3, 46.6. Elemental anal. calcd. for $C_{22}H_{24}N_2O.C_4H_4O_4$: C 69.6, H 6.3, N 6.25 %. Found: C 69.6, H 6.3, N 6.15 %.

1-Methyl-4-[3-(1-naphthyloxy)propyl]piperazine (**LINS05005**). Yellow solid. Yield 60 %. ^{1}H NMR (300 MHz, $CDCl_3$) δ 8.30–8.22 (m, 1H), 7.79–7.76 (m, 1H), 7.51–7.29 (m, 4H), 6.79 (d, J = 7.2 Hz, 1H), 4.16 (t, J = 6.2 Hz, 2H), 2.86–2.32 (m, 10*H*), 2.28 (s, 3H), 2.15–2.04 (m, 2H). ^{13}C RMN (75 MHz, DMSO) δ 154.4, 134.5, 128.0, 127.0, 126.7, 125.8, 125.4, 121.9, 120.4, 105.6, 66.1, 54.0, 52.9, 50.3, 43.1, 26.0. Elemental anal. calcd. for $C_{18}H_{24}N_2O.C_4H_4O_4$: C 60.4, H 6.2, N 5.4 %. Found: C 60.6, H 6.1, N 5.1 %.

1-Methyl-4-[3-(2-naphthyloxy)propyl]piperazine (**LINS05006**). Yellow oil. Yield 38 %. ^{1}H NMR (300 MHz, $CDCl_3$) δ 7.77–7.67 (m, 3H), 7.42 (dd, J = 11.0, 4.0 Hz, 1H), 7.32 (dd, J = 11.0, 3.9 Hz, 1H), 7.16–7.10 (m, 2H), 4.11 (t, J = 6.3 Hz, 2H), 2.33–2.78 (m, 10*H*), 2.30 (s, 3H), 2.09–1.96 (m, 2H). ^{13}C NMR (75 MHz, DMSO) δ 156.9, 134.7, 129.8, 128.9, 128.0, 127.1, 126.9, 124.1, 119.1, 107.1, 65.9, 53.9, 52.9, 50.3, 43.1, 25.9. Elemental anal. calcd. for $C_{18}H_{24}N_2O.C_4H_4O_4$: C 60.4, H 6.2, N 5.4 %. Found: C 60.0, H 5.9, N 5.5 %.

1-[2-(1-Naphthyloxy)propyl]-4-phenyl-piperazine (**LINS05007**). Yell owish solid. Yield 72 %. ^{1}H NMR (300 MHz, $CDCl_3$) δ 8.33–8.23 (m, 1H), 7.84–7.74 (m, 1H), 7.54–7.32 (m, 4H), 7.24–7.27 (m, 2H), 6.94 (d, J = 7.9 Hz, 2H), 6.85 (dd, J = 12.8, 6.7 Hz, 2H), 4.23 (t, J = 6.2 Hz, 2H), 3.24 (t, J = 7.0 Hz, 4H), 2.67–2.73 (m, 6H), 2.25–2.09 (m, 2H). ^{13}C NMR (75 MHz, $CDCl_3$) δ 156.9, 151.3, 134.6, 129.4, 129.1, 129.0, 127.6, 126.7, 126.4, 123.6, 119.8, 118.9, 116.1, 106.7, 66.2, 55.3, 53.3, 49.1, 26.7. Elemental anal. calcd. for $C_{22}H_{24}N_2O.C_4H_4O_4$: C 69.6, H 6.3, N 6.25 %. Found: C 69.8, H 6.1, N 5.9 %.

1-[2-(2-Naphthyloxy)propyl]-4-phenyl-piperazine (**LINS05008**). Yell owish solid. Yield 57 %. ^{1}H NMR (300 MHz, $CDCl_3$) δ 7.80–7.68 (m, 3H), 7.43 (t, J = 7.5 Hz, 1H), 7.37–7.20 (m, 3H), 7.13–7.17 (m, 2H), 6.94 (d, J = 8.0 Hz, 2H), 6.86 (t, J = 7.3 Hz, 1H), 4.17 (t, J = 6.3 Hz, 2H), 3.29–3.17 (m, 4H), 2.63–2.70 (m, 6H), 2.09 (quint, J = 6.9 Hz, 2H). ^{13}C NMR (75 MHz, $CDCl_3$) δ 156.9, 151.3, 134.6, 129.4, 129.1, 129.0, 127.6, 126.7, 126.4, 123.6, 119.8, 118.9, 116.1, 106.7, 66.2, 55.3, 53.3, 49.1, 26.7. Elemental anal. calcd. for $C_{22}H_{24}N_2O.C_4H_4O_4$: C 69.6, H 6.3, N 6.25 %. Found: C 69.75, H 6.35, N 6.0 %.

1-[2-(1-Naphthyloxy)ethyl]-4-(4-pyridyl)-piperazine (**LINS05009**). White solid. Yield 45 %. ^{1}H NMR (300 MHz, $CDCl_3$) δ 8.32–8.18 (m, 3H), 7.85–7.73 (m, 1H), 7.54–7.30 (m, 4H), 6.84–6.76 (m, 1H), 6.61 (d, J = 5.6 Hz, 2H), 4.29 (t, J = 5.4 Hz, 2H), 3.32 (t, J = 6.0 Hz, 4H), 2.98 (t, J = 5.3 Hz, 2H), 2.74 (t, J = 6.0 Hz, 4H). ^{13}C NMR (75 MHz, $CDCl_3$) δ 155.0,

154.4, 149.7, 134.6, 127.6, 126.5, 125.9, 125.7, 125.3, 122.0, 120.5, 108.3, 104.9, 66.6, 57.2, 53.1, 46.0. Elemental anal. calcd. for $C_{21}H_{23}N_3O.2C_4H_4O_4$: C 61.6, H 5.5, N 7.4 %. Found: C 61.45, H 5.9, N 7.05 %.

2-(4-Methylpiperazin-1-yl)ethyl naphthalene-1-carboxylate (**LINS05010**). Yellow oil. Yield 21 %. ^{1}H NMR (300 MHz, $CDCl_3$) δ 8.92 (d, $J = 8.5$ Hz, 1H), 8.16 (d, $J = 7.2$ Hz, 1H), 8.02 (d, $J = 8.2$ Hz, 1H), 7.89 (d, $J = 7.9$ Hz, 1H), 7.65–7.45 (m, 3H), 4.55 (t, $J = 5.8$ Hz, 2H), 2.86 (t, $J = 5.8$ Hz, 2H), 2.69 (br.s, 4H), 2.56 (br.s, 4H), 2.34 (s, 3H). ^{13}C NMR (75 MHz, $CDCl_3$) δ 167.6, 133.8, 133.3, 131.3, 130.1, 128.5, 127.7, 127.4, 126.2, 125.9, 124.5, 62.4, 56.6, 55.1, 53.0, 45.8. Elemental anal. calcd. for $C_{18}H_{22}N_2O_2.2C_4H_4O_4$: C 58.8, H 5.7, N 5.2 %. Found: C 58.4, H 5.2, N 5.5 %.

2-(4-Methylpiperazin-1-yl)ethyl naphthalene-2-carboxylate (**LINS05011**). Yellow oil. Yield 17 %. ^{1}H NMR (300 MHz, $CDCl_3$) δ 8.60 (s, 1H), 8.05 (dd, $J = 8.6$, 1.5 Hz, 1H), 7.96 (d, $J = 7.8$ Hz, 1H), 7,88 (d, $J = 8.5$ Hz, 2H), 7.63–7.50 (m, 2H), 4.52 (t, $J = 6.0$ Hz, 2H), 2.85 (t, $J = 6.0$ Hz, 2H), 2.67 (br.s, 4H), 2.50 (br.s, 4H), 2.30 (s, 3H). ^{13}C NMR (75 MHz, $CDCl_3$) δ 166.7, 135.6, 132.5, 131.1, 129.4, 128.3, 128.2, 127.8, 127.5, 126.7, 125.3, 62.8, 56.7, 55.1, 53.4, 46.0. Elemental anal. calcd. for $C_{18}H_{22}N_2O_2.2C_4H_4O_4$: C 58.8, H 5.7, N 5.3 %. Found: C 58.4, H 5.4, N 5.0 %.

2-(4-Phenylpiperazin-1-yl)ethyl naphthalene-1-carboxylate (**LINS05012**). Yellow oil. Yield 78 %. ^{1}H NMR (300 MHz, $CDCl_3$) δ 8.93 (d, $J = 8.7$ Hz, 1H), 8.17 (dd, $J = 7.3$, 1.1 Hz, 1H), 8.02 (d, $J = 8.2$ Hz, 1H), 7.88 (d, $J = 7.7$ Hz, 1H), 7.65–7.43 (m, 3H), 7.31–7.20 (m, 2H), 6.93 (d, $J = 7.9$ Hz, 2H), 6.85 (t, $J = 7.3$ Hz, 1H), 4.58 (t, $J = 5.8$ Hz, 2H), 3.23 (t, $J = 5.0$ Hz, 4H), 2.90 (t, $J = 5.8$ Hz, 2H), 2.77 (t, $J = 5.0$ Hz, 4H). ^{13}C NMR (75 MHz, $CDCl_3$) δ 167.6, 151.3, 133.9, 133.3, 131.3, 130.1, 129.1, 128.6, 127.8, 127.5, 126.3, 125.9, 124.5, 119.8, 116.1, 62.4, 56.8, 53.5, 49.2. Elemental anal. calcd. for $C_{23}H_{24}N_2O_2.C_4H_4O_4$: C 68.05, H 5.9, N 5.9 %. Found: C 67.9, H 5.5, N 5.8 %.

2-(4-Phenylpiperazin-1-yl)ethyl naphthalene-2-carboxylate (**LINS05013**). Yellow solid. Yield 45 %. ^{1}H NMR (300 MHz, $CDCl_3$) δ 8.62 (s, 1H), 8.07 (d, $J = 8.5$ Hz, 1H), 7.97 (d, $J = 7.4$ Hz, 1H), 7.89 (d, $J = 8.6$ Hz, 2H), 7.65–7.50 (m, 2H), 7.30–7.21 (m, 2H), 6.94 (d, $J = 8.0$ Hz, 2H), 6.86 (t, $J = 7.3$ Hz, 1H), 4.57 (t, $J = 5.9$ Hz, 2H), 3.24 (t, $J = 4.5$ Hz, 4H), 2.91 (t, $J = 6.0$ Hz, 2H), 2.79 (t, $J = 4.5$ Hz, 4H). ^{13}C NMR (75 MHz, $CDCl_3$) δ 166.7, 151.3, 135.6, 132.5, 131.2, 129.4, 129.1, 128.3, 128.2, 127.8, 127.5, 126.7, 125.3, 119.8, 116.1, 62.7, 56.8, 53.5, 49.2. Elemental anal. calcd. for $C_{23}H_{24}N_2O_2.C_4H_4O_4$: C 68.05, H 5.9, N 5.9 %. Found: C 67.8, H 5.5, N 5.7 %.

3-(4-Methylpiperazin-1-yl)propyl naphthalene-1-carboxylate (**LINS05014**). Yellow oil. Yield 18 %. ^{1}H NMR (300 MHz, $CDCl_3$) δ 8.90 (d, $J = 8.5$ Hz, 1H), 8.17 (d, $J = 6.6$ Hz, 1H), 8.03 (d, $J = 8.3$ Hz, 1H), 7.89 (d, $J = 7.8$ Hz, 1H), 7.65–7.46 (m, 3H), 4.47 (t, $J = 6.2$ Hz, 2H), 2.73–2.39 (m, 10*H*), 2.35 (s, 3H), 2,03 (quint, $J = 6$,2 Hz, 2H). ^{13}C NMR (75 MHz, $CDCl_3$) δ 167.6, 133.9, 133.3, 131.4, 130.1, 128.5, 127.7, 127.4, 126.2, 125.8, 124.5, 63.6, 55.2, 55.1, 53.2, 46.0, 26.3. Elemental anal. calcd. for $C_{19}H_{24}N_2O_2.2C_4H_4O_4$: C 59.55, H 5.9, N 5.1 %. Found C 59.65, H 5.7, N 5.2 %.

3-(4-Methylpiperazin-1-yl)propyl naphthalene-2-carboxylate (**LINS05015**). Yellow oil. Yield 20 %. ^{1}H NMR (300 MHz, $CDCl_3$) δ 8.60 (s, 1H), 8.08–8.02 (m, 1H), 7.96 (d, $J = 7.7$ Hz, 1H), 7.88 (d, $J = 8.5$ Hz, 2H), 7.62–7.51 (m, 2H), 4.44 (t, $J = 6.5$ Hz, 2H), 2.81–2.38 (m, 10*H*), 2.35 (s, 3H), 2.08–1.95 (m, 2H). ^{13}C NMR (75 MHz, $CDCl_3$) δ 166.8, 135.5, 132.5, 131.0, 129.4, 128.3, 128.2, 127.8, 127.6, 126.7, 125.2, 63.5, 55.0, 54.9, 52.7, 45.7, 26.3. Elemental anal. calcd. for $C_{19}H_{24}N_2O_2.2C_4H_4O_4$: C 59.55, H 5.9, N 5.1 %. Found: C 59.2, H 5.7, N 5.1 %.

3-(4-Phenylpiperazin-1-yl)propyl naphthalene-1-carboxylate (**LINS05016**). Yellow oil. Yield 81 %. ^{1}H NMR (300 MHz, $CDCl_3$) δ 8.91 (d, $J = 8.6$ Hz, 1H), 8.18 (dd, $J = 7.2$, 0.9 Hz, 1H), 8.02 (d, $J = 8.2$ Hz, 1H), 7.88 (d, $J = 7.9$ Hz, 1H), 7.66–7.45 (m, 3H), 7.26 (dd, $J = 12.8$, 3.6 Hz, 2H), 6.93 (d, $J = 8.1$ Hz, 2H), 6.85 (t, $J = 7.3$ Hz, 1H), 4.50 (t, $J = 6.5$ Hz, 2H), 3.27–3.16 (m, 4H), 2.71–2.54 (m, 6H), 2.06 (quint, $J = 6.9$ Hz, 2H). ^{13}C NMR (75 MHz, DMSO) δ 167.7, 150.1, 135.9, 134.0, 133.9, 130.9, 130.6, 129.6, 129.3, 128.4, 127.0, 125.5, 125.4, 120.5, 116.4, 62.8, 53.6, 51.7, 46.4, 23.9. Elemental anal. calcd. for $C_{24}H_{26}N_2O_2.C_4H_4O_4$: C 68.5, H 6.1, N 5.7 %. Found: C 68.1, H 5.7, N 5.5 %.

3-(4-Phenylpiperazin-1-yl)propyl naphthalene-2-carboxylate (**LINS05017**). Yellow solid. Yield 87 %. ^{1}H NMR (300 MHz, $CDCl_3$) δ 8.61 (s, 1H), 8.07 (d, $J = 8.6$ Hz, 1H), 7.96 (d, $J = 7.8$ Hz, 1H), 7.88 (d, $J = 8.5$ Hz, 2H), 7.63–7.49 (m, 2H), 7.30–7.22 (m, 2H), 6.93 (d, $J = 8.1$ Hz, 2H), 6.86 (t, $J = 7.3$ Hz, 1H), 4.47 (t, $J = 6.4$ Hz, 2H), 3.23 (t, $J = 6.0$ Hz, 4H), 2.73–2.58 (m, 6H), 2.08 (quint, $J = 6.0$ Hz, 2H). ^{13}C NMR (75 MHz, $CDCl_3$) δ 166.8, 151.3, 135.6, 132.5, 131.0, 129.4, 129.1, 128.3, 128.2, 127.8, 127.6, 126.7, 125.3, 119.8, 116.1, 63.6, 55.2, 53.3, 49.1, 26.3. Elemental anal. calcd. for $C_{24}H_{26}N_2O_2.C_4H_4O_4$: C 68.5, H 6.1, N 5.7 %. Found: C 68.2, H 5.8, N 5.8 %.

3-(4-Methylpiperazin-1-yl)propyl benzofuran-2-carboxylate (**LINS05018**). Yellow oil. Yield 38 %. ^{1}H NMR (300 MHz, $CDCl_3$) δ 7.69 (d, $J = 7.8$ Hz, 1H), 7.60 (d, $J = 8.4$ Hz, 1H), 7.52 (s, 1H), 7.49–7.41 (m, 1H), 7.34–7.28 (m, 1H), 4.44 (t, $J = 6.5$ Hz, 2H), 2.71–2.36 (m, 10*H*), 2.32 (s, 3H), 1.99 (quint, $J = 6.4$ Hz, 2H). ^{13}C NMR (75 MHz, $CDCl_3$) δ 159.6, 155.7, 145.6, 127.6, 127.0, 123.8, 122.8, 113.8, 112.4, 64.0, 55.1, 54.9, 53.2, 49.0, 26.2. Elemental anal. calcd. for $C_{17}H_{22}N_2O_3.2C_4H_4O_4$: C 56.2, H 5.7, N 5.2 %. Found: C 56.1, H 5.9, N 5.3 %.

3-(4-Phenylpiperazin-1-yl)propyl benzofuran-2-carboxylate (**LINS05019**). Yellow solid. Yield 21 %. ^{1}H NMR (300 MHz, $CDCl_3$) δ 7.68 (d, $J = 7.8$ Hz, 1H), 7.60 (d, $J = 8.4$ Hz, 1H), 7.53 (s, 1H), 7.45 (dt, $J = 8.3$, 1.2 Hz, 1H), 7.33–7.23 (m, 3H), 6.92 (d, $J = 8.0$ Hz, 2H), 6.85 (t, $J = 7.3$ Hz, 1H), 4.47 (t, $J = 6.6$ Hz, 2H), 3.21 (t, $J = 4.5$ Hz, 4H), 2.69–2.61 (m, 4H), 2.57 (t, $J = 7.3$ Hz, 2H), 2.03 (quint, $J = 6.0$ Hz, 2H). ^{13}C NMR (75 MHz, $CDCl_3$) δ 159.7, 155.8, 151.3, 145.6, 129.1, 127.7, 127.0, 123.8, 122.8, 119.7, 116.1, 113.9, 112.4, 63.9, 55.0, 53.3, 49.1, 26.2. Elemental anal. calcd. for $C_{22}H_{24}N_2O_3.C_4H_4O_4$: C 64.9, H 5.9, N 5.8 %. Found: C 64.6, H 5.9, N 5.7 %.

3-[4-(4-Pyridyl)piperazin-1-yl]propyl benzofuran-1-carboxylate (**LINS05020**). Yellowish solid. Yield 49 %. ^{1}H NMR (300 MHz, $CDCl_3$) δ 8.26 (d, $J = 4.2$ Hz, 2H), 7.68 (d, $J = 7.8$ Hz, 1H), 7.59 (d, $J = 8.4$ Hz, 1H), 7.53 (s, 1H), 7.45 (dt, $J = 8.3$, 1.2 Hz, 1H), 7.31 (t, $J = 7.6$ Hz, 1H), 6.65 (d, $J = 4.2$ Hz, 2H), 4.48 (t, $J = 6.5$ Hz, 2H), 3.37–3.27 (m, 4H), 2.63–2.51 (m, 6H), 2.02 (quint, $J = 6.9$ Hz, 2H). ^{13}C NMR (75 MHz, $CDCl_3$) δ 159.6, 155.7, 155.0, 149.7, 145.5, 127.7, 126.9, 123.9, 122.8, 113.9, 112.4, 108.3, 63.8, 54.8, 52.6, 45.9, 26.1. Elemental anal. calcd. for $C_{21}H_{23}N_3O_3.2C_4H_4O_4$: C 58.3, H 5.2, N 7.0 %. Found C 58.4, H 5.45, N 7.15 %.

3-[4-(4-Pyridyl)piperazin-1-yl]propyl benzofuran-1-carboxylate (**LINS05021**). White solid. Yield 49 %. ^{1}H NMR (300 MHz, $CDCl_3$) δ 8.68 (br. s, 1H), 8.32 (d, $J = 6.4$ Hz, 2H), 7.65–7.61 (m, 1H), 7.44 (d, $J = 0.8$ Hz, 1H), 7.24–7.15 (m, 2H), 7.10–7.00 (m, 1H), 6.72 (d, $J = 6.4$ Hz, 2H), 3.64 (q, $J = 5.6$ Hz, 2H), 3.56–3.45 (m, 4H), 2.75–2.61 (m, 6H), 1.85 (quint, $J = 5.9$ Hz, 2H). ^{13}C NMR (75 MHz, $CDCl_3$) δ 158.7, 154.5, 150.3, 150.3, 149.3, 127.7, 126.7, 123.7, 122.7, 111.2, 110.1, 108.5, 58.3, 52.8, 46.0, 40.1, 24.6. Elemental anal. calcd. for $C_{21}H_{24}N_4O_2.2C_4H_4O_4$: C 58.4, H 5.4, N 9.4 %. Found C 58.2, H 5.3, N 9.5 %.

3.3. Binding assays at human H_3R and D_3R

The hydogenmaleate salts of the compounds were assessed using radioligand displacement assays at the human H_3R and D_3R as reported previously.[21,30,31] The assessment at the human H_3R and D_3R were performed using radioligand displacement assays following the previously reported method. The compounds were initially screened at single concentration of 1 or 10 μM (Table 1). For the most interesting, full concentration response curves were performed. The binding affinity constants (K_i) were calculated through non-linear regression (results are depicted in Table 2). Selected compounds were also tested at the human H_4R and D_2R for selectivity assessment (Table S1), following similar conditions.[21,30]

3.4. Inhibition of cholinesterases

The compounds (as hydrogenmaleate salts) were evaluated for their inhibitory activity on *ee*AChE and *eq*BChE in a 96-well microplate following the Ellman's method as described by our group.[32] The assay is based on the generation of thiocholine from the enzyme-catalyzed hydrolysis of acetylthiocholine (ATCI), which reacts with 5,5′-dithiobis-2-nitrobenzoic acid (DTNB) to form the yellowish products detected in the spectrophotometer.[33] In each well, 100 μL of DTNB, 20 μL of the enzyme (*ee*AChE or *eq*BChE), 40 μL of phosphate buffer (pH 7.0 or 8.0, respectively) and 20 μL of each compound were added. Donepezil hydrochloride and neostigmine mesylate were used as pharmacological standards. The plates were incubated at 37 °C for 15 min and then 20 μL of ATCI solution was added, and then monitored every 3 min over 30 min at 415 nm wavelength. The obtained data (average ± standard error mean, SEM) is presented as percentage of enzymatic activity in Table 1. This data was used to estimate the concentration to reduce the activity by 50 % (IC_{50}) through non-linear regression, and expressed as -logIC_{50} (pIC_{50} ± SEM). These data are presented in Table 2.

3.5. Prediction of physicochemical and pharmacokinetic properties

Selected compounds had their physicochemical properties calculated by the SwissADME on-line platform (https://www.swissadme.ch).[18] The tool uses these physicochemical descriptors to predict pharmacokinetic parameters such as gastrointestinal (GI) absorption, ability to cross the blood–brain barrier (BBB) and probability to be a substrate and/or inhibitor of P-glycoprotein (P-gp), CYP enzymes and other functionalities. The results are presented in Table 3.

3.6. Ligand efficiency analysis

The selected compounds had their ligand efficiency (LE) values calculated following the classical formulae: LE = pK_i or $pIC_{50} \times 1.37/HA$ where HA is the number of non-hydrogen atoms in the compound.[24] The obtained values are described for each target in Table 3.

Declaration of Competing Interest

The authors declare that they have no known competing financial interests or personal relationships that could have appeared to influence the work reported in this paper.

Data availability

Data will be made available on request.

Acknowledgements

The authors are grateful to São Paulo Research Foundation – FAPESP (grant n° 2019/24028-8) to the financial support and scholarship to FBL (grant n° 2021/03387-0). JPSF is also grateful to National Council for Scientific and Technological Development – CNPq (grant n° 307829/2021-9) for the scientific fellowship awarded. Authors are also grateful to Coordination of Higher Education Personnel Improvement – CAPES (financial code 001).

Appendix A. Supplementary material

Supplementary data to this article can be found online at https://doi.org/10.1016/j.bmc.2022.117132.

References

1 Morphy R, Rankovic Z. Designing multiple ligands – medicinal chemistry strategies and challenges. *Curr Pharm Des*. 2009;15:587–600. https://doi.org/10.2174/138161209787315594.
2 Cavalli A, Bolognesi ML, Minarini A, et al. Multi-target-directed ligands to combat neurodegenerative diseases. J Med Chem. 2008;51(7):2326–2326. doi:10.1021/jm800210c.
3 Lopes FB, Aranha CMSQ, Fernandes JPS. Histamine H 3 receptor and cholinesterases as synergistic targets for cognitive decline: strategies to the rational design of multitarget ligands. *Chem Biol Drug Des*. 2021;98:212–225. https://doi.org/10.1111/cbdd.13866.
4 Provensi G, Fabbri R, Munari L, et al. Histaminergic neurotransmission as a gateway for the cognitive effect of oleoylethanolamide in contextual fear conditioning. *Int J Neuropsychopharmacol*. 2017;20:392–399. https://doi.org/10.1093/ijnp/pyw110.
5 Sadek B, Saad A, Sadeq A, Jalal F, Stark H. Histamine H3 receptor as a potential target for cognitive symptoms in neuropsychiatric diseases. *Behav Brain Res*. 2016;312:415–430. https://doi.org/10.1016/j.bbr.2016.06.051.
6 Maramai S, Gemma S, Brogi S, et al. Dopamine D3 receptor antagonists as potential therapeutics for the treatment of neurological diseases. *Front Neurosci*. 2016;10:451. https://doi.org/10.3389/fnins.2016.00451.
7 Micheli F, Heidbreder C. Selective dopamine D3 receptor antagonists: a review 2001–2005. *Recent Pat CNS Drug Discov*. 2006;1:271–288. https://doi.org/10.2174/157488906778773634.
8 Provensi G, Costa A, Passani MB, Blandina P. Donepezil, an acetylcholine esterase inhibitor, and ABT-239, a histamine H3 receptor antagonist/inverse agonist, require the integrity of brain histamine system to exert biochemical and procognitive effects in the mouse. *Neuropharmacology*. 2016;109:139–147. https://doi.org/10.1016/j.neuropharm.2016.06.010.
9 Rizzo S, Bartolini M, Ceccarini L, et al. Targeting Alzheimer's disease: Novel indanone hybrids bearing a pharmacophoric fragment of AP2238. *Bioorganic Med Chem*. 2010;18:1749–1760. https://doi.org/10.1016/j.bmc.2010.01.071.
10 Ghamari N, Zarei O, Arias-Montaño JA, et al. Histamine H3 receptor antagonists/inverse agonists: where do they go? *Pharmacol Ther*. 2019;200:69–84. https://doi.org/10.1016/j.pharmthera.2019.04.007.
11 Szczepańska K, Karcz T, Mogilski S, et al. Synthesis and biological activity of novel tert-butyl and tert-pentylphenoxyalkyl piperazine derivatives as histamine H3R ligands. *Eur J Med Chem*. 2018;152:223–234. https://doi.org/10.1016/j.ejmech.2018.04.043.
12 Mehta P, Miszta P, Filipek S. Molecular modeling of histamine receptors—recent advances in drug discovery. *Molecules*. 2021;26:1778. https://doi.org/10.3390/molecules26061778.
13 Szczepańska K, Karcz T, Siwek A, et al. Structural modifications and in vitro pharmacological evaluation of 4-pyridyl-piperazine derivatives as an active and selective histamine H3 receptor ligands. *Bioorg Chem*. 2019;91, 103071. https://doi.org/10.1016/j.bioorg.2019.103071.
14 Garcia-Ladona FJ, Cox BF. BP 897, a selective dopamine D3 receptor ligand with therapeutic potential for the treatment of cocaine-addiction. *CNS Drug Rev*. 2006;9:141–158. https://doi.org/10.1111/j.1527-3458.2003.tb00246.x.
15 Sugimoto H, Yamanish Y, Iimura Y, Kawakami Y. Donepezil hydrochloride (E2020) and other acetylcholinesterase inhibitors. *Curr Med Chem*. 2000;7:303–339. https://doi.org/10.2174/0929867003375191.
16 Bautista-Aguilera ÓM, Ismaili L, Chioua M, et al. Acetylcholinesterase inhibition of diversely functionalized quinolinones for Alzheimer's disease therapy. *Int J Mol Sci*. 2020;21:3913. https://doi.org/10.3390/ijms21113913.
17 Rodrigues Simoes M, Dias Viegas F, Moreira M, et al. Donepezil: an important prototype to the design of new drug candidates for Alzheimer's disease. *Mini-Rev Med Chem*. 2014;14:2–19. https://doi.org/10.2174/1389557513666131119201353.
18 Daina A, Michielin O, Zoete V. SwissADME: a free web tool to evaluate pharmacokinetics, drug-likeness and medicinal chemistry friendliness of small molecules. *Sci Rep*. 2017;7:42717. https://doi.org/10.1038/srep42717.
19 Łazewska D, Kieć-Kononowicz K. New developments around histamine H3 receptor antagonists/inverse agonists: a patent review (2010-present). *Expert Opin Ther Pat*. 2014;24:89–111. https://doi.org/10.1517/13543776.2014.848197.
20 Correa MF, Fernandes JPS. QSAR modeling of histamine H3R antagonists/inverse agonists as future drugs for neurodegenerative diseases. *Curr Neuropharmacol*. 2018;16:749–757. https://doi.org/10.2174/1570159X15666170818100644.
21 Corrêa MF, Reiner D, Fernandes GAB, et al. Profiling of LINS01 compounds at human dopamine D2 and D3 receptors. *J Chem Sci*. 2020;132:5. https://doi.org/10.1007/s12039-019-1694-6.
22 Newman AH, Beuming T, Banala AK, et al. Molecular determinants of selectivity and efficacy at the dopamine D3 receptor. *J Med Chem*. 2012;55:6689–6699. https://doi.org/10.1021/jm300482h.
23 Queda F, Calò S, Gwizdala K, et al. Novel donepezil-arylsulfonamide hybrids as multitarget-directed ligands for potential treatment of Alzheimer's disease. *Molecules*. 2021;26:1658. https://doi.org/10.3390/molecules26061658.
24 Hopkins AL, Keseru GM, Leeson PD, Rees DC, Reynolds CH. The role of ligand efficiency metrics in drug discovery. *Nat Rev Drug Discov*. 2014;13:105–121. https://doi.org/10.1038/nrd4163.
25 Pomilio AB, Tettamanzi MC, Romanelli GP, Autino JC, Vitale AA. NMR study of substituted 1-bromo-2-aryloxyethanes and monosubstituted xanthones. *Magn Reson Chem*. 1996;34:165–171. https://doi.org/10.1002/(SICI)1097-458X(199602)34:2<165::AID-OMR837>3.0.CO;2-C.
26 Guo X, Ma X, Yang Q, et al. Discovery of 1-aryloxyethyl piperazine derivatives as Kv1.5 potassium channel inhibitors (part I). *Eur J Med Chem*. 2014;81:89–94. https://doi.org/10.1016/j.ejmech.2014.03.075.

27 Tada M, Hiratsuka M, Goto H. Photolyses of (3-naphthoxypropyl)-, (4-naphthylbutyl)-, and (4-naphthyl-4-oxobutyl)cobaloxime. *J Org Chem.* 1990;55:4364–4370. https://doi.org/10.1021/jo00301a030.

28 Sword R, Baldwin LA, Murphy JA. Fragmentations observed in the reactions of α-methoxy-γ-alkoxyalkyl iodide substrates with super-electron-donors derived from 4-DMAP and N-methylbenzimidazole. *Org Biomol Chem.* 2011;9:3560. https://doi.org/10.1039/c0ob01282c.

29 Sattenapally N, Sharma J, Hou Y. Selective conversion of primary amides to esters promoted by KHSO4. *ARKIVOC.* 2018;2018:174–183. https://doi.org/10.24820/ark.5550190.p010.392.

30 Frank A, Kiss DJ, Keserü GM, Stark H. Binding kinetics of cariprazine and aripiprazole at the dopamine D3 receptor. *Sci Rep.* 2018;8:12509. https://doi.org/10.1038/s41598-018-30794-y.

31 Kottke T, Sander K, Weizel L, Schneider EH, Seifert R, Stark H. Receptor-specific functional efficacies of alkyl imidazoles as dual histamine H3/H4 receptor ligands. *Eur J Pharmacol.* 2011;654:200–208. https://doi.org/10.1016/j.ejphar.2010.12.033.

32 Lopes FB, Aranha CMSQ, Corrêa MF, et al. Evaluation of the histamine H_3 receptor antagonists from LINS01 series as cholinesterases inhibitors: enzymatic and modeling studies. *Chem Biol Drug Des.* 2022;100:722–729. https://doi.org/10.1111/cbdd.14139.

33 Ellman GL, Courtney KD, Andres V, Featherstone RM. A new and rapid colorimetric determination of acetylcholinesterase activity. *Biochem Pharmacol.* 1961;7:88–95. https://doi.org/10.1016/0006-2952(61)90145-9.

Multitargeting Approaches to Cognitive Impairment: Synthesis of Aryl-alkylpiperazines and Assessment at Cholinesterases, Histamine H_3 and Dopamine D_3 Receptors

Cecília M.S.Q. Aranha,[1] David Reiner-Link,[2] Luisa R. Leitzbach,[2] Flavia B. Lopes,[1] Holger Stark[2,*] and João Paulo S. Fernandes[1,*]

[1]*Department of Pharmaceutical Sciences, Universidade Federal de São Paulo, Diadema-SP, Brazil*

[2]*Institute for Pharmaceutical and Medicinal Chemistry, Heinrich Heine University Düsseldorf, Duesseldorf, Germany*

*Corresponding authors. E-Mail: stark@hhu.de; joao.fernandes@unifesp.br

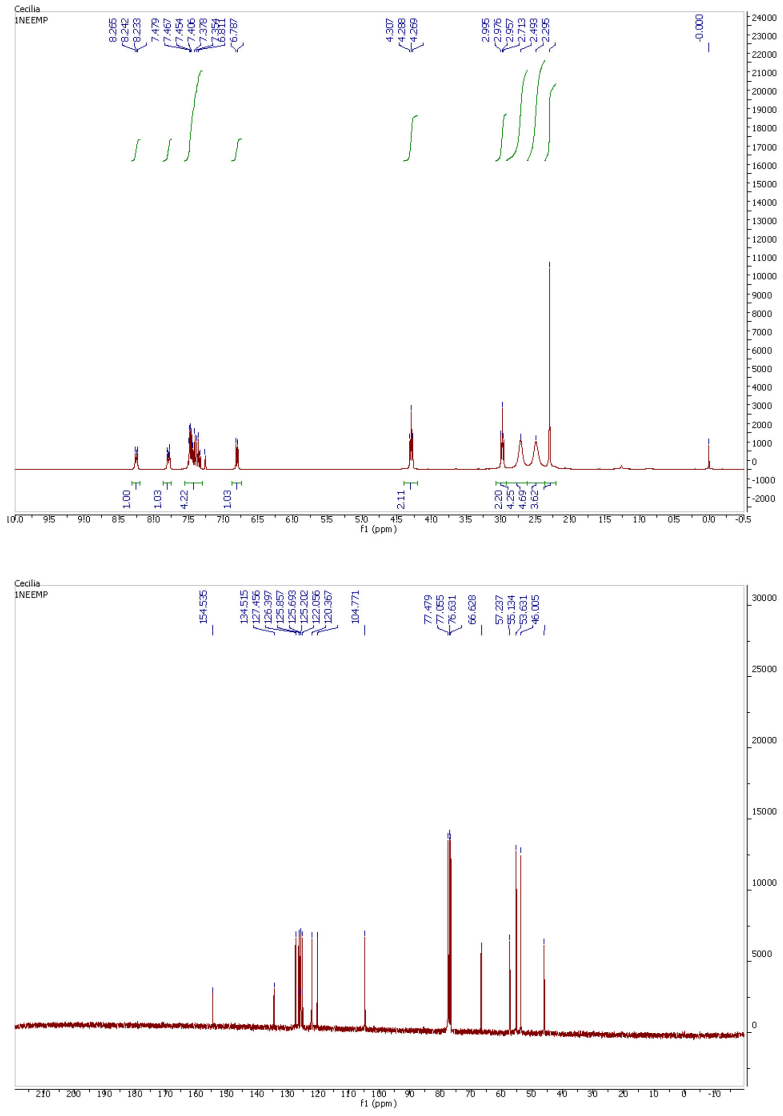
SUPPLEMENTARY MATERIAL

Copies of the NMR spectra for final compounds ……S2-S22

Screening results at H_4R and D_2R……...S23-S24

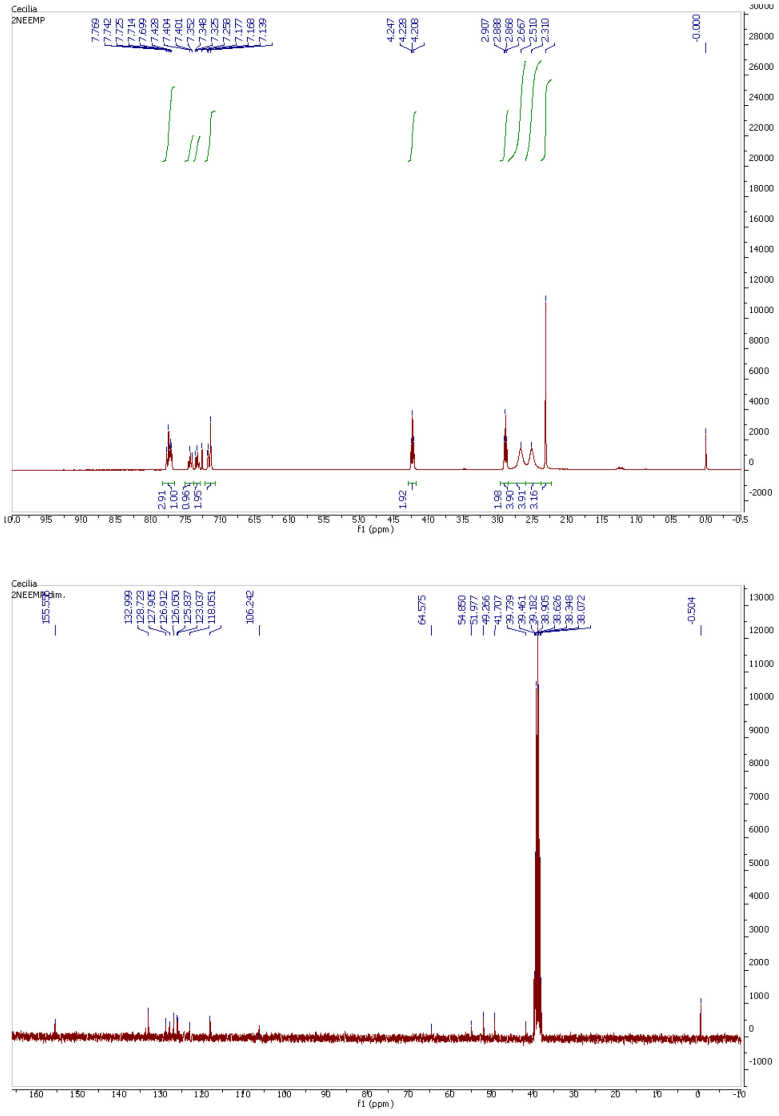
Kinetic studies on compound **20**……..S24-S25

S2

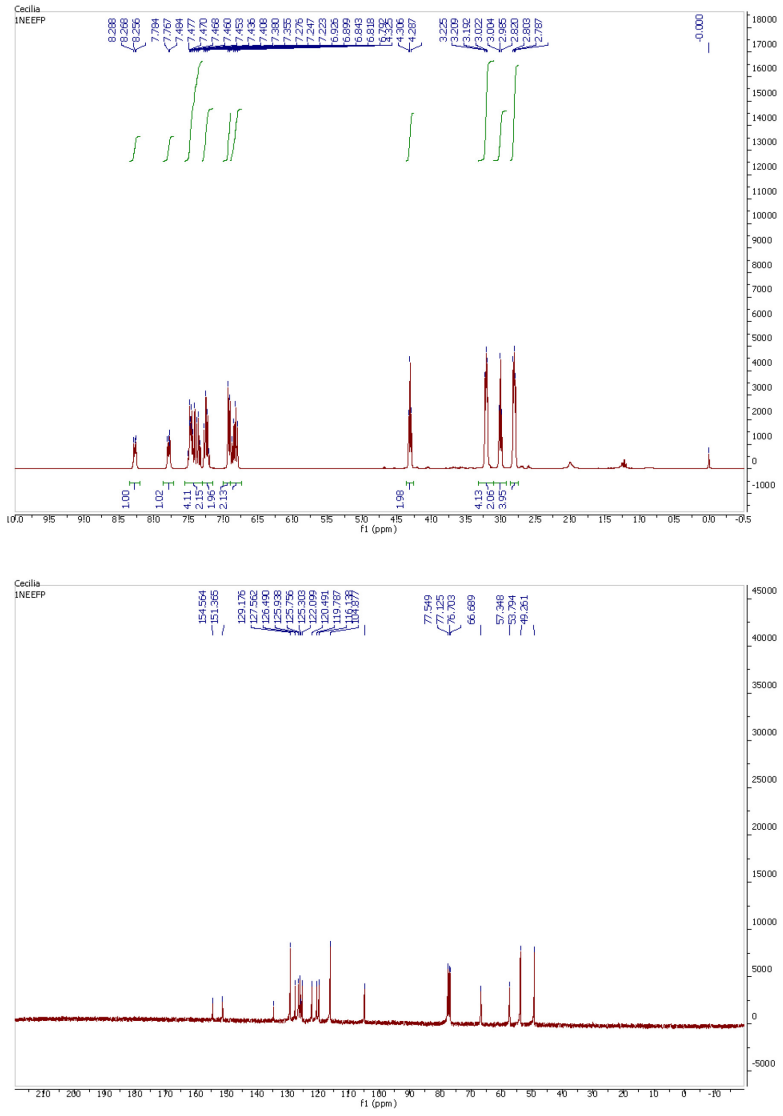


1-Methyl-4-[2-(1-naphthyloxy)ethyl]piperazine (**LINS05001**). ^{1}H NMR (300 MHz, $CDCl_3$) δ 8.30–8.20 (m, 1H), 7.80–7.77 (m, 1H), 7.53–7.30 (m, 4H), 6.80 (d, *J* = 7.4 Hz, 1H), 4.29 (t, *J* = 5.7 Hz, 2H), 2.98 (t, *J* = 5.7 Hz, 2H), 2.71 (br.s, 4H), 2.49 (br.s, 4H), 2.30 (s, 3H). ^{13}C NMR (75 MHz, $CDCl_3$) δ 154.5, 134.5, 127.5, 126.4, 125.9, 125.7, 125.2, 122.1, 120.4, 104.8, 66.6, 57.2, 55.1, 53.6, 46.0.

S3

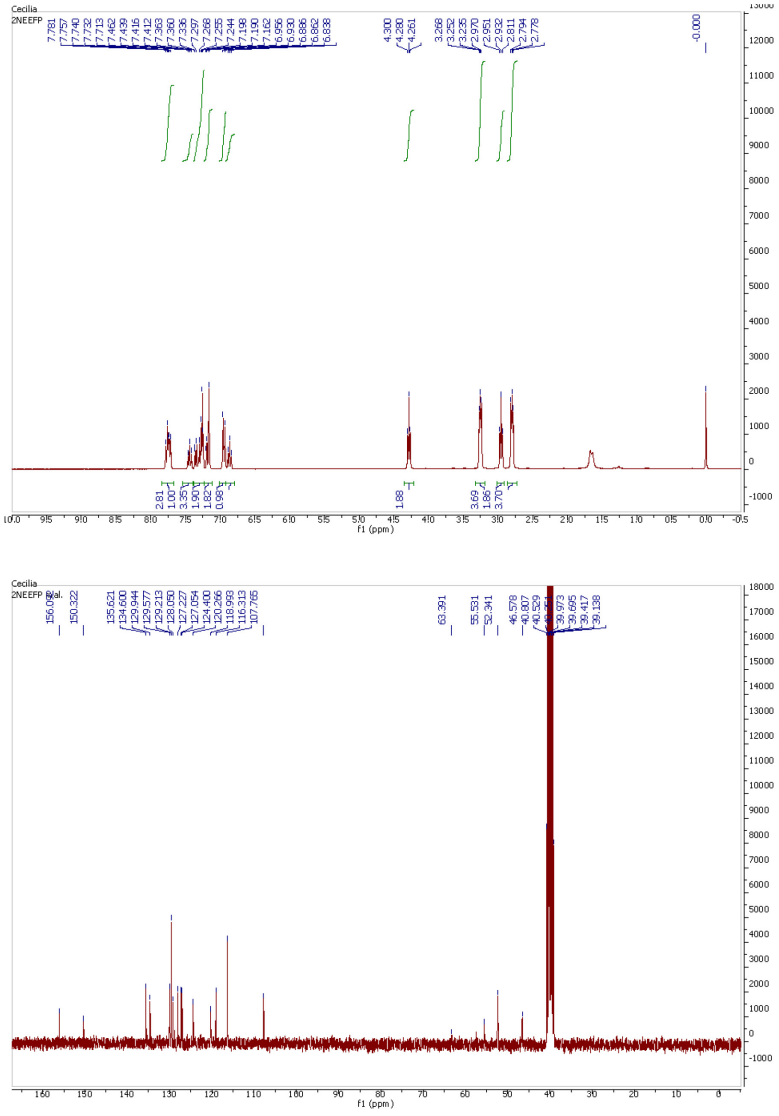


1-Methyl-4-[2-(2-naphthyloxy)ethyl]piperazine (**LINS05002**). ^{1}H NMR (300 MHz, $CDCl_3$) δ 7.81–7.66 (m, 3H), 7.47–7.38 (m, 1H), 7.33 (dd, *J* = 10.9, 4.0 Hz, 1H), 7.20–7.09 (m, 2H), 4.23 (t, *J* = 5.8 Hz, 2H), 2.89 (t, *J* = 5.8 Hz, 2H), 2.67 (br.s, 4H), 2.51 (br.s, 4H), 2.31 (s, 3H). ^{13}C NMR (75 MHz, DMSO) δ 155.6, 133.0, 128.7, 127.9, 126.9, 126.1, 125.8, 123.0, 118.1, 106.2, 64.6, 54.9, 52.0, 49.3, 41.7.



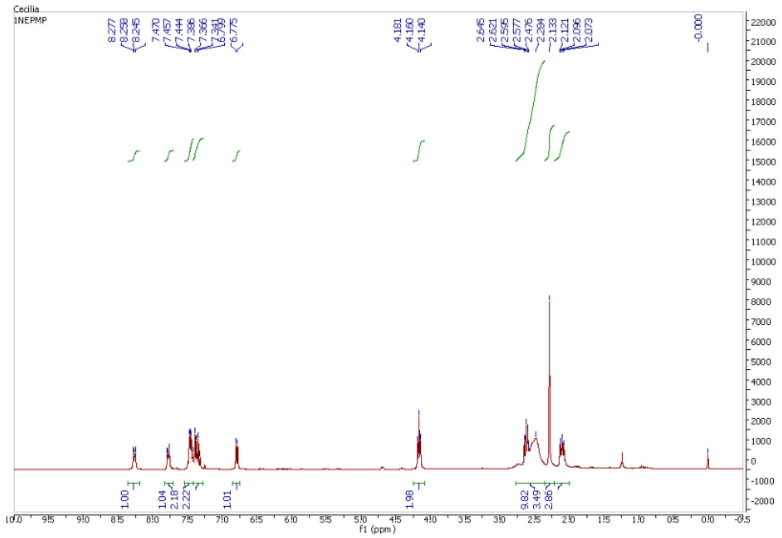
1-[2-(1-Naphthyloxy)ethyl]-4-phenyl-piperazine (**LINS05003**). ^{1}H NMR (300 MHz, $CDCl_3$) δ 8.33–8.22 (m, 1H), 7.80–7.77 (m, 1H), 7.53–7.31 (m, 4H), 7.29–7.19 (m, 2H), 6.91 (d, *J* = 8.1 Hz, 2H), 6.83 (dd, *J* = 15.1, 7.5 Hz, 2H), 4.31 (t, *J* = 5.6 Hz, 2H), 3.23–3.15 (m, 4H), 3.00 (t, *J* = 5.6 Hz, 2H), 2.83–2.77 (m, 4H). ^{13}C NMR (75 MHz, $CDCl_3$) δ 154.6, 151.4, 134.6, 129.2, 127.6, 126.5, 125.9, 125.8, 125.3, 122.1, 120.5, 119.8, 116.1, 104.9, 66.7, 57.4, 53.8, 49.3.

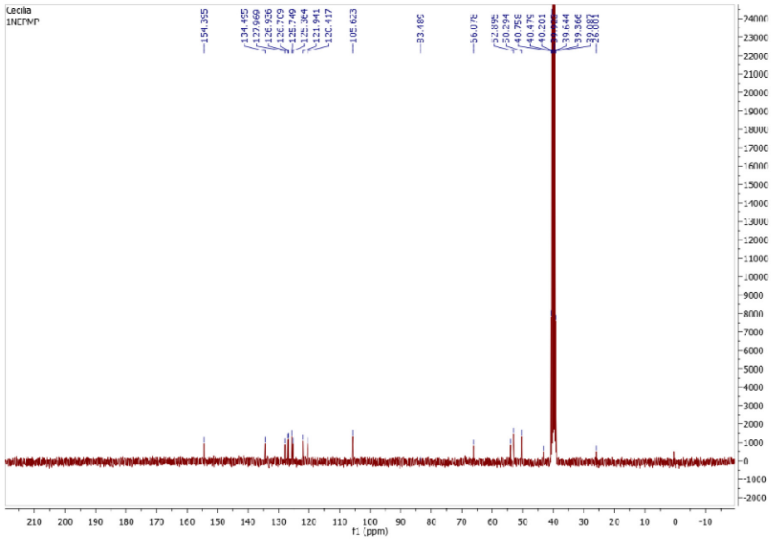
S5



1-[2-(2-Naphthyloxy)ethyl]-4-phenyl-piperazine (**LINS05004**). ^{1}H NMR (300 MHz, $CDCl_3$) δ 7.82–7.68 (m, 3H), 7.43 (dd, *J* = 11.1, 4.0 Hz, 1H), 7.31–7.22 (m, 3H), 7.21–7.12 (m, 2H), 6.94 (d, *J* = 8.0 Hz, 2H), 6.86 (t, *J* = 7.3 Hz, 1H), 4.28 (t, *J* = 5.8 Hz, 2H), 3.28–3.23 (m, 4H), 2.95 (t, *J* = 5.8 Hz, 2H), 2.82–2.76 (m, 4H). ^{13}C NMR (75 MHz, DMSO) δ 156.1, 150.3, 135.6, 129.9, 129.6, 129.2, 128.8, 128.1, 127.2, 127.1, 124.4, 120.3, 119.0, 116.3, 107.8, 55.5, 52.3, 46.6.

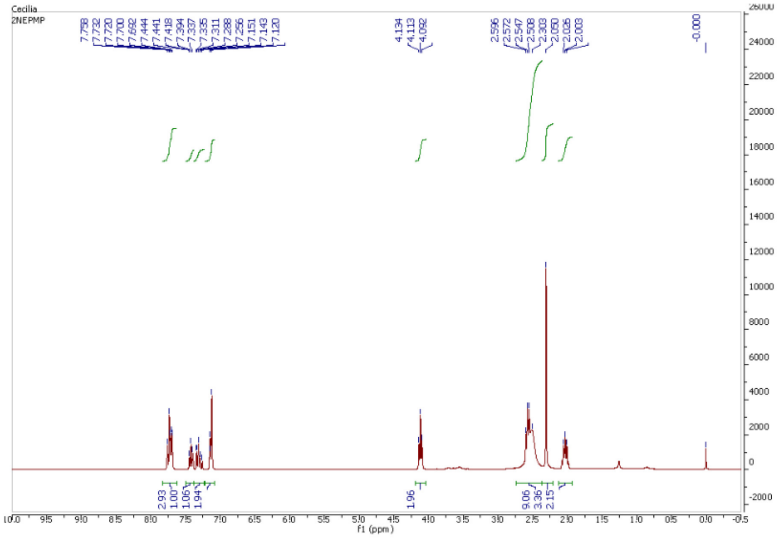
S6

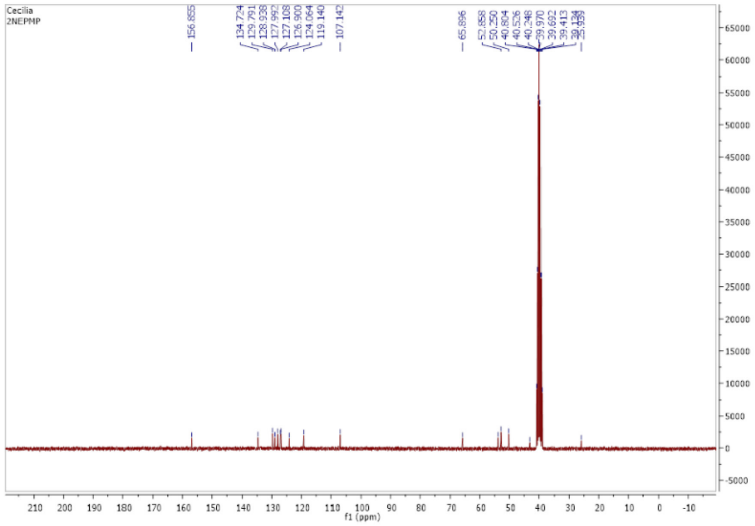




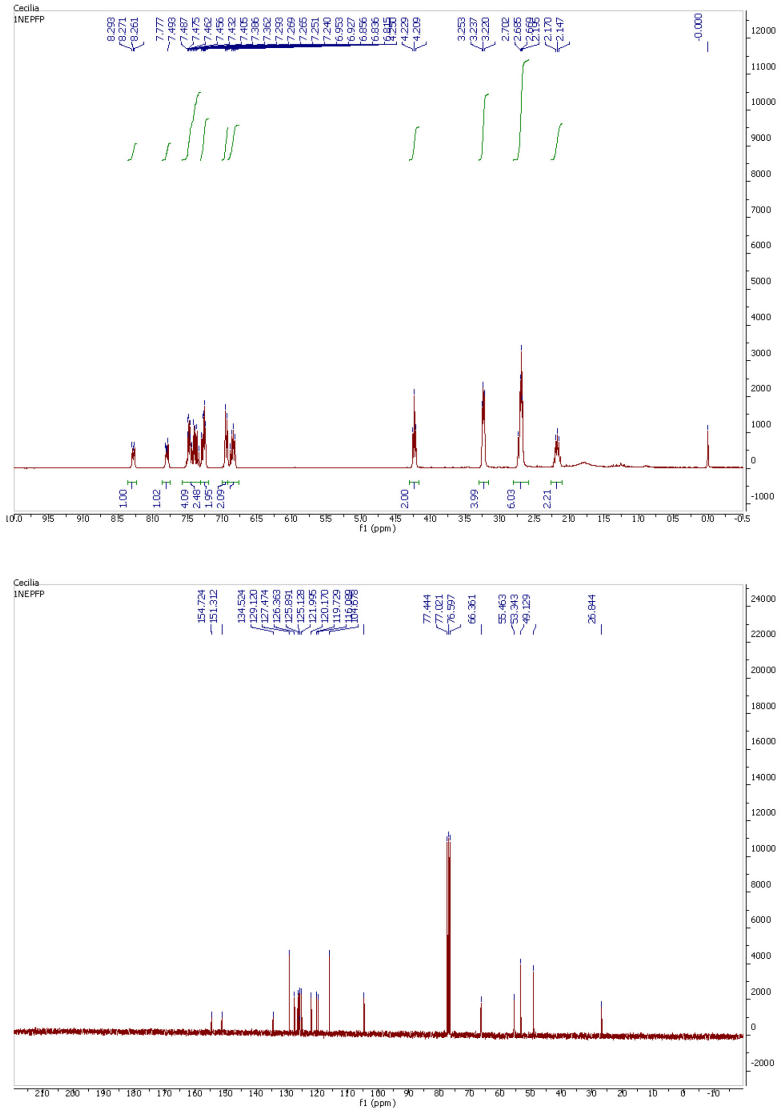
1-Methyl-4-[3-(1-naphthyloxy)propyl]piperazine (**LINS05005**). ^{1}H NMR (300 MHz, $CDCl_3$) δ 8.30–8.22 (m, 1H), 7.79–7.76 (m, 1H), 7.51–7.29 (m, 4H), 6.79 (d, *J* = 7.2 Hz, 1H), 4.16 (t, *J* = 6.2 Hz, 2H), 2.86–2.32 (m, 10H), 2.28 (s, 3H), 2.15–2.04 (m, 2H). ^{13}C RMN (75 MHz, DMSO) δ 154.4, 134.5, 128.0, 127.0, 126.7, 125.8, 125.4, 121.9, 120.4, 105.6, 66.1, 54.0, 52.9, 50.3, 43.1, 26.0.

S7



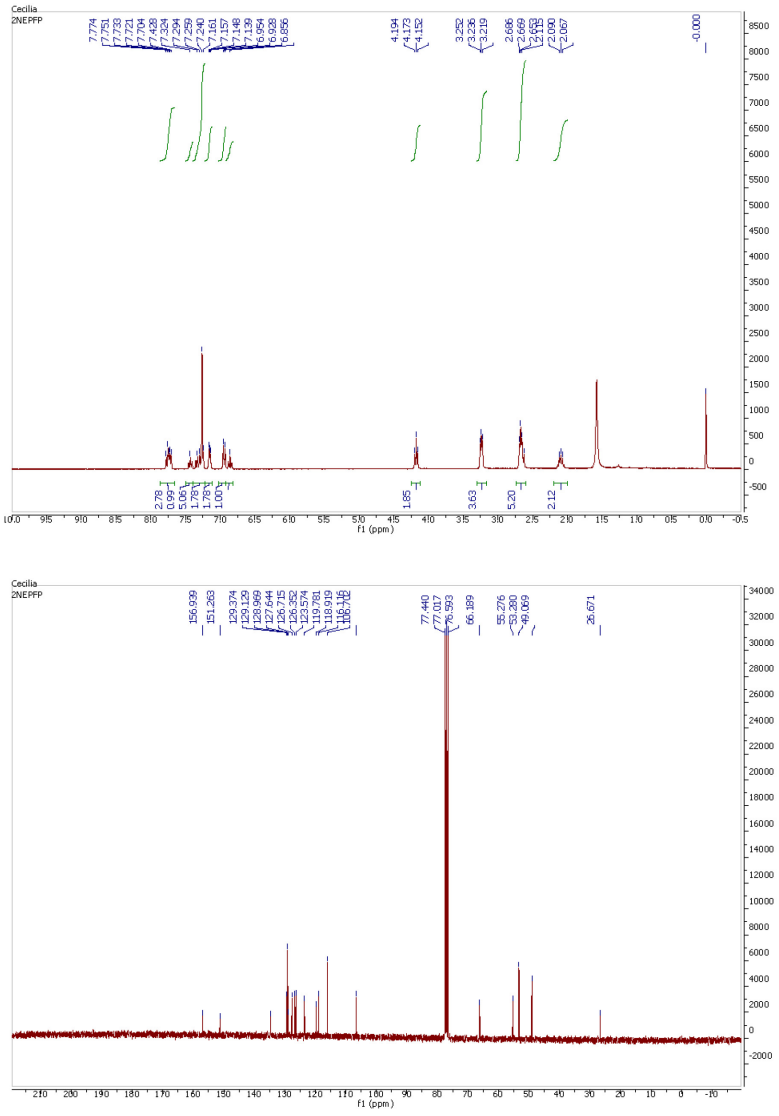


1-Methyl-4-[3-(2-naphthyloxy)propyl]piperazine (**LINS05006**). ^{1}H NMR (300 MHz, $CDCl_3$) δ 7.77–7.67 (m, 3H), 7.42 (dd, *J* = 11.0, 4.0 Hz, 1H), 7.32 (dd, *J* = 11.0, 3.9 Hz, 1H), 7.16–7.10 (m, 2H), 4.11 (t, *J* = 6.3 Hz, 2H), 2.33–2.78 (m, 10H), 2.30 (s, 3H), 2.09–1.96 (m, 2H). ^{13}C NMR (75 MHz, DMSO) δ 156.9, 134.7, 129.8, 128.9, 128.0, 127.1, 126.9, 124.1, 119.1, 107.1, 65.9, 53.9, 52.9, 50.3, 43.1, 25.9.

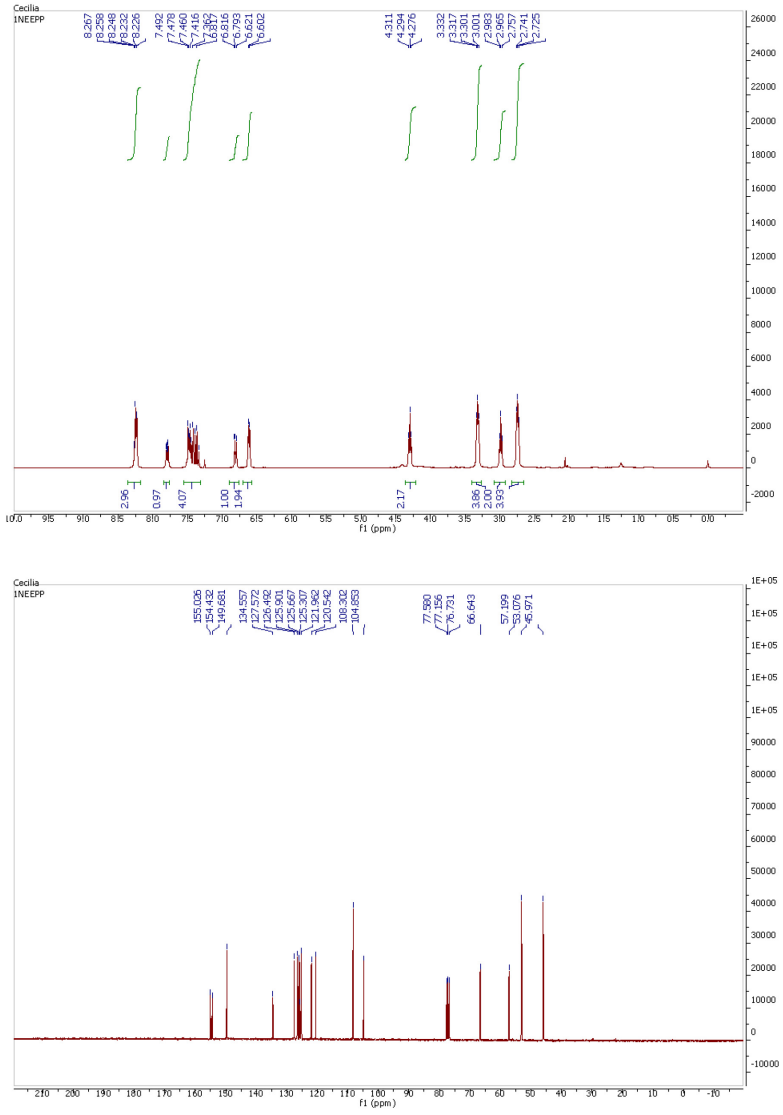


1-[2-(1-Naphthyloxy)propyl]-4-phenyl-piperazine (**LINS05007**). ^{1}H NMR (300 MHz, $CDCl_3$) δ 8.33–8.23 (m, 1H), 7.84–7.74 (m, 1H), 7.54–7.32 (m, 4H), 7.24–7.27 (m, 2H), 6.94 (d, *J* = 7.9 Hz, 2H), 6.85 (dd, *J* = 12.8, 6.7 Hz, 2H), 4.23 (t, *J* = 6.2 Hz, 2H), 3.24 (t, *J* = 7.0 Hz, 4H), 2.67–2.73 (m, 6H), 2.25–2.09 (m, 2H). ^{13}C NMR (75 MHz, $CDCl_3$) δ 156.9, 151.3, 134.6, 129.4, 129.1, 129.0, 127.6, 126.7, 126.4, 123.6, 119.8, 118.9, 116.1, 106.7, 66.2, 55.3, 53.3, 49.1, 26.7.

S9

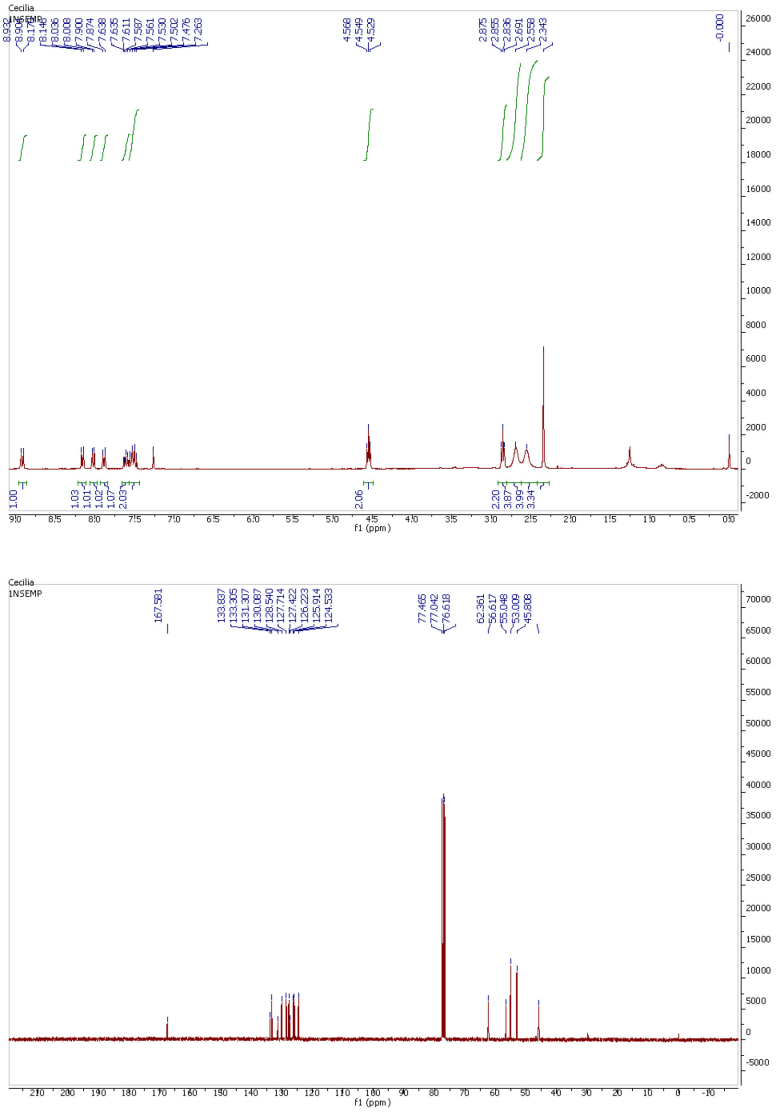


1-[2-(2-Naphthyloxy)propyl]-4-phenyl-piperazine (**LINS05008**). ^{1}H NMR (300 MHz, $CDCl_3$) δ 7.80–7.68 (m, 3H), 7.43 (t, *J* = 7.5 Hz, 1H), 7.37–7.20 (m, 3H), 7.13–7.17 (m, 2H), 6.94 (d, *J* = 8.0 Hz, 2H), 6.86 (t, *J* = 7.3 Hz, 1H), 4.17 (t, *J* = 6.3 Hz, 2H), 3.29–3.17 (m, 4H), 2.63–2.70 (m, 6H), 2.09 (quint, *J* = 6.9 Hz, 2H). ^{13}C NMR (75 MHz, $CDCl_3$) δ 156.9, 151.3, 134.6, 129.4, 129.1, 129.0, 127.6, 126.7, 126.4, 123.6, 119.8, 118.9, 116.1, 106.7, 66.2, 55.3, 53.3, 49.1, 26.7.

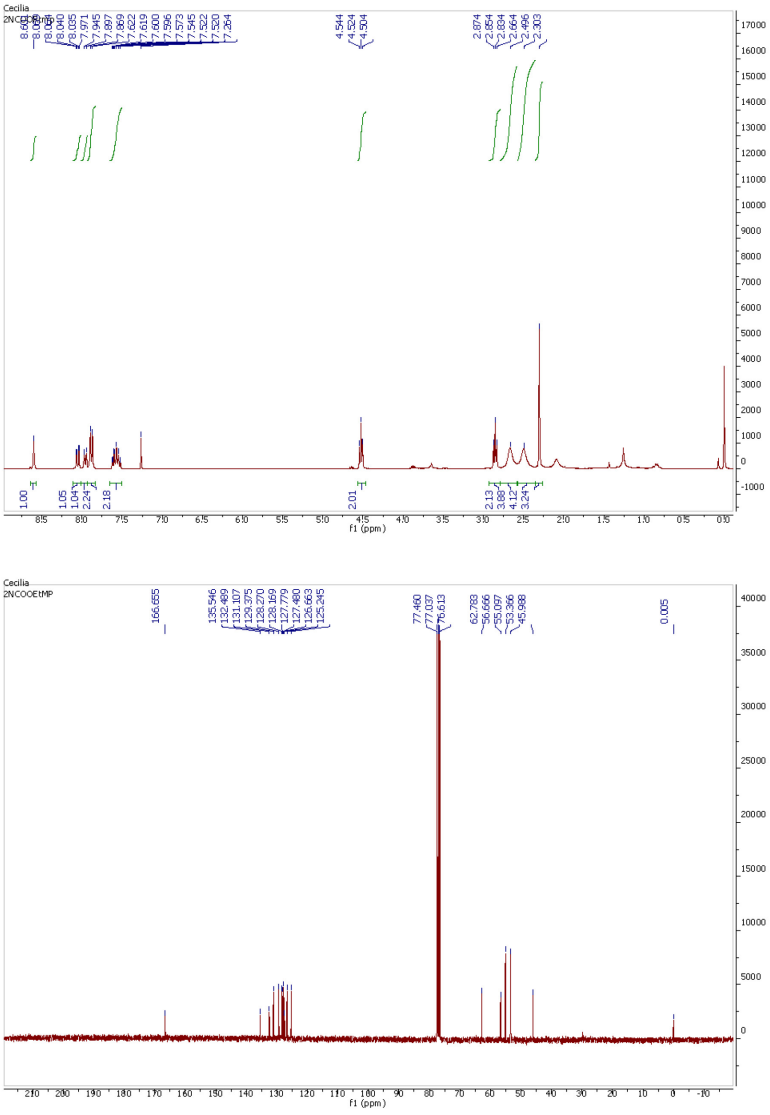


1-[2-(1-Naphthyloxy)ethyl]-4-(4-pyridyl)-piperazine (**LINS05009**). ^{1}H NMR (300 MHz, $CDCl_3$) δ 8.32–8.18 (m, 3H), 7.85–7.73 (m, 1H), 7.54–7.30 (m, 4H), 6.84–6.76 (m, 1H), 6.61 (d, *J* = 5.6 Hz, 2H), 4.29 (t, *J* = 5.4 Hz, 2H), 3.32 (t, *J* = 6.0 Hz, 4H), 2.98 (t, *J* = 5.3 Hz, 2H), 2.74 (t, *J* = 6.0 Hz, 4H). ^{13}C NMR (75 MHz, $CDCl_3$) δ 155.0, 154.4, 149.7, 134.6, 127.6, 126.5, 125.9, 125.7, 125.3, 122.0, 120.5, 108.3, 104.9, 66.6, 57.2, 53.1, 46.0.

S11

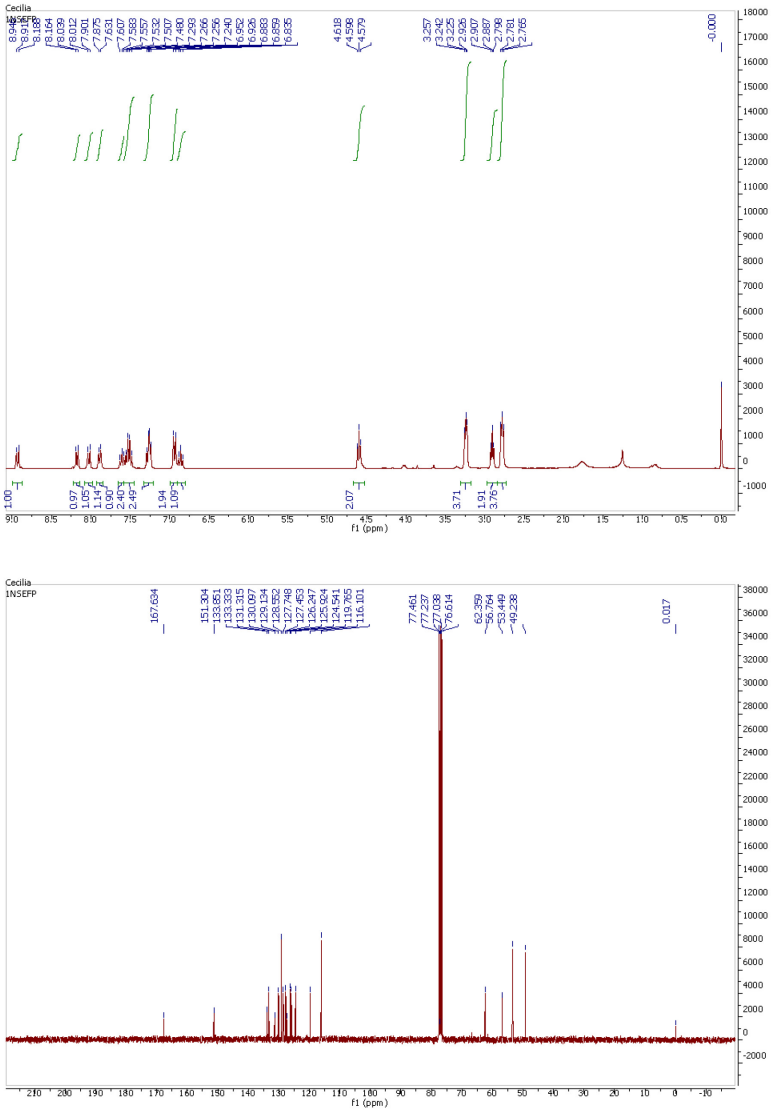


2-(4-Methylpiperazin-1-yl)ethyl naphthalene-1-carboxylate (**LINS05010**). ^{1}H NMR (300 MHz, $CDCl_3$) δ 8.92 (d, *J* = 8.5 Hz, 1H), 8.16 (d, *J* = 7.2 Hz, 1H), 8.02 (d, *J* = 8.2 Hz, 1H), 7.89 (d, *J* = 7.9 Hz, 1H), 7.65–7.45 (m, 3H), 4.55 (t, *J* = 5.8 Hz, 2H), 2.86 (t, *J* = 5.8 Hz, 2H), 2.69 (br.s, 4H), 2.56 (br.s, 4H), 2.34 (s, 3H). ^{13}C NMR (75 MHz, $CDCl_3$) δ 167.6, 133.8, 133.3, 131.3, 130.1, 128.5, 127.7, 127.4, 126.2, 125.9, 124.5, 62.4, 56.6, 55.1, 53.0, 45.8.

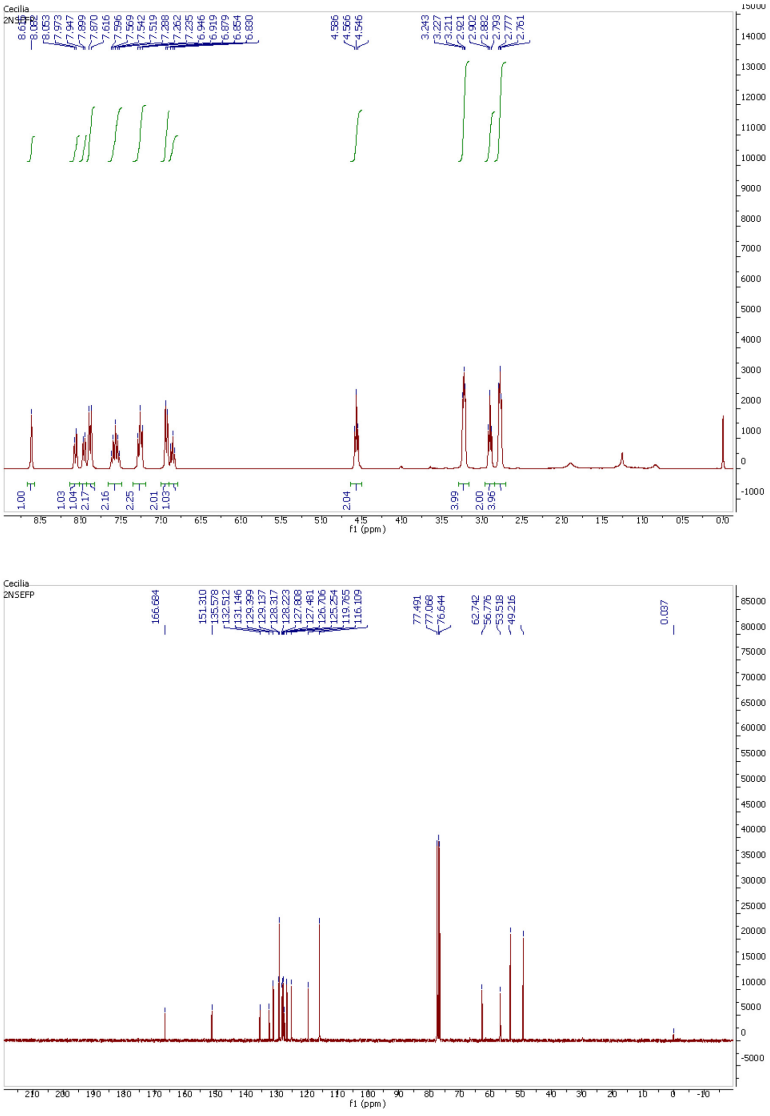


2-(4-Methylpiperazin-1-yl)ethyl naphthalene-2-carboxylate (**LINS05011**). ^{1}H NMR (300 MHz, $CDCl_3$) δ 8.60 (s, 1H), 8.05 (dd, *J* = 8.6, 1.5 Hz, 1H), 7.96 (d, *J* = 7.8 Hz, 1H), 7,88 (d, *J* = 8.5 Hz, 2H), 7.63–7.50 (m, 2H), 4.52 (t, *J* = 6.0 Hz, 2H), 2.85 (t, *J* = 6.0 Hz, 2H), 2.67 (br.s, 4H), 2.50 (br.s, 4H), 2.30 (s, 3H). ^{13}C NMR (75 MHz, $CDCl_3$) δ 166.7, 135.6, 132.5, 131.1, 129.4, 128.3, 128.2, 127.8, 127.5, 126.7, 125.3, 62.8, 56.7, 55.1, 53.4, 46.0.

S13

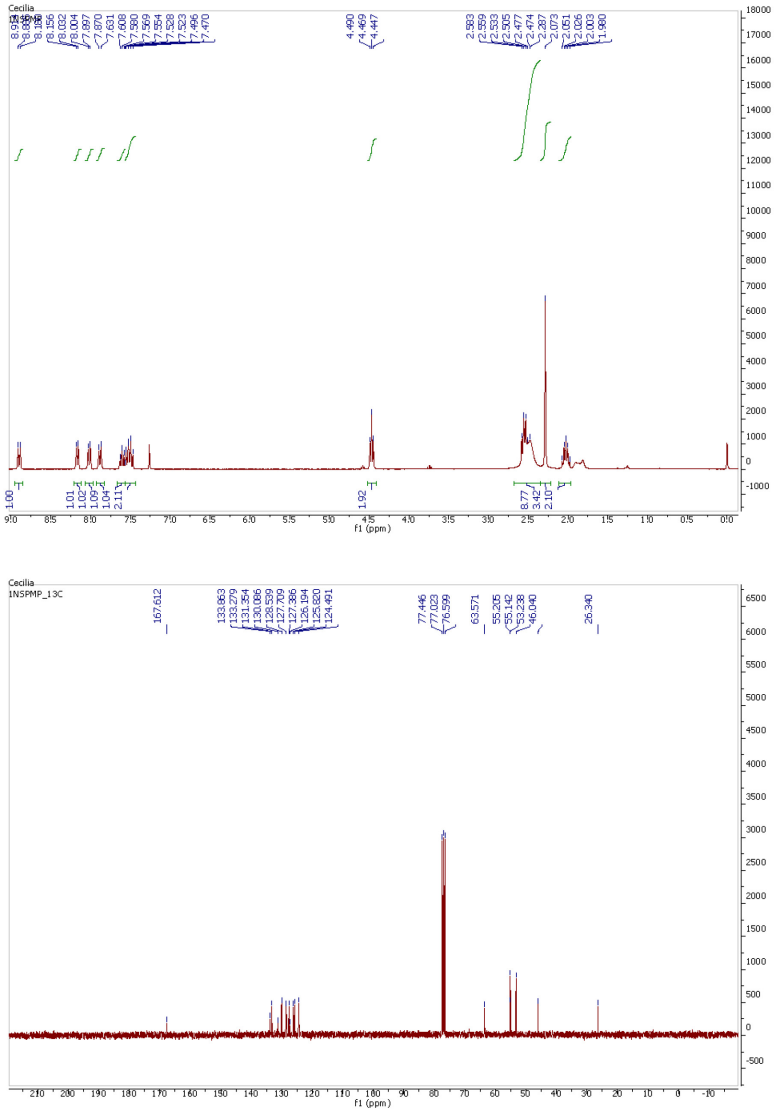


2-(4-Phenylpiperazin-1-yl)ethyl naphthalene-1-carboxylate (**LINS05012**). ^{1}H NMR (300 MHz, $CDCl_3$) δ 8.93 (d, *J* = 8.7 Hz, 1H), 8.17 (dd, *J* = 7.3, 1.1 Hz, 1H), 8.02 (d, *J* = 8.2 Hz, 1H), 7.88 (d, *J* = 7.7 Hz, 1H), 7.65–7.43 (m, 3H), 7.31–7.20 (m, 2H), 6.93 (d, *J* = 7.9 Hz, 2H), 6.85 (t, *J* = 7.3 Hz, 1H), 4.58 (t, *J* = 5.8 Hz, 2H), 3.23 (t, *J* = 5.0 Hz, 4H), 2.90 (t, *J* = 5.8 Hz, 2H), 2.77 (t, *J* = 5.0 Hz, 4H). ^{13}C NMR (75 MHz, $CDCl_3$) δ 167.6, 151.3, 133.9, 133.3, 131.3, 130.1, 129.1, 128.6, 127.8, 127.5, 126.3, 125.9, 124.5, 119.8, 116.1, 62.4, 56.8, 53.5, 49.2.

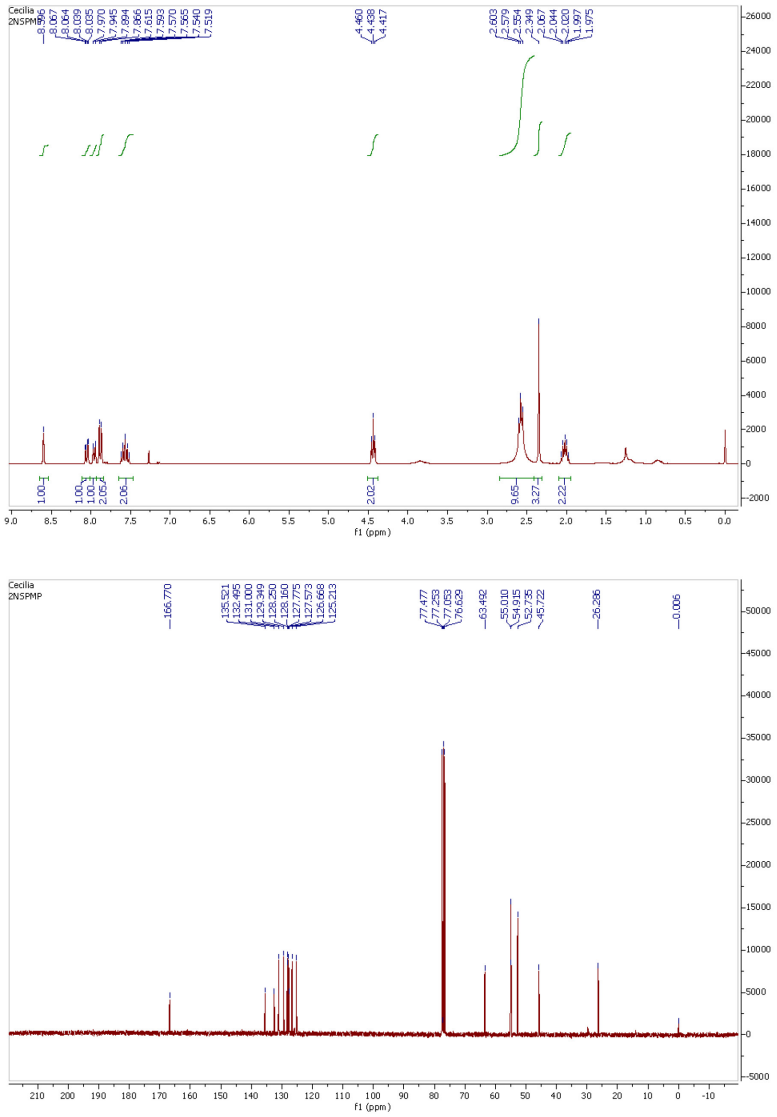


2-(4-Phenylpiperazin-1-yl)ethyl naphthalene-2-carboxylate (**LINS05013**). ^{1}H NMR (300 MHz, $CDCl_3$) δ 8.62 (s, 1H), 8.07 (d, *J* = 8.5 Hz, 1H), 7.97 (d, *J* = 7.4 Hz, 1H), 7.89 (d, *J* = 8.6 Hz, 2H), 7.65–7.50 (m, 2H), 7.30–7.21 (m, 2H), 6.94 (d, *J* = 8.0 Hz, 2H), 6.86 (t, *J* = 7.3 Hz, 1H), 4.57 (t, *J* = 5.9 Hz, 2H), 3.24 (t, *J* = 4.5 Hz, 4H), 2.91 (t, *J* = 6.0 Hz, 2H), 2.79 (t, *J* = 4.5 Hz, 4H). ^{13}C NMR (75 MHz, $CDCl_3$) δ 166.7, 151.3, 135.6, 132.5, 131.2, 129.4, 129.1, 128.3, 128.2, 127.8, 127.5, 126.7, 125.3, 119.8, 116.1, 62.7, 56.8, 53.5, 49.2.

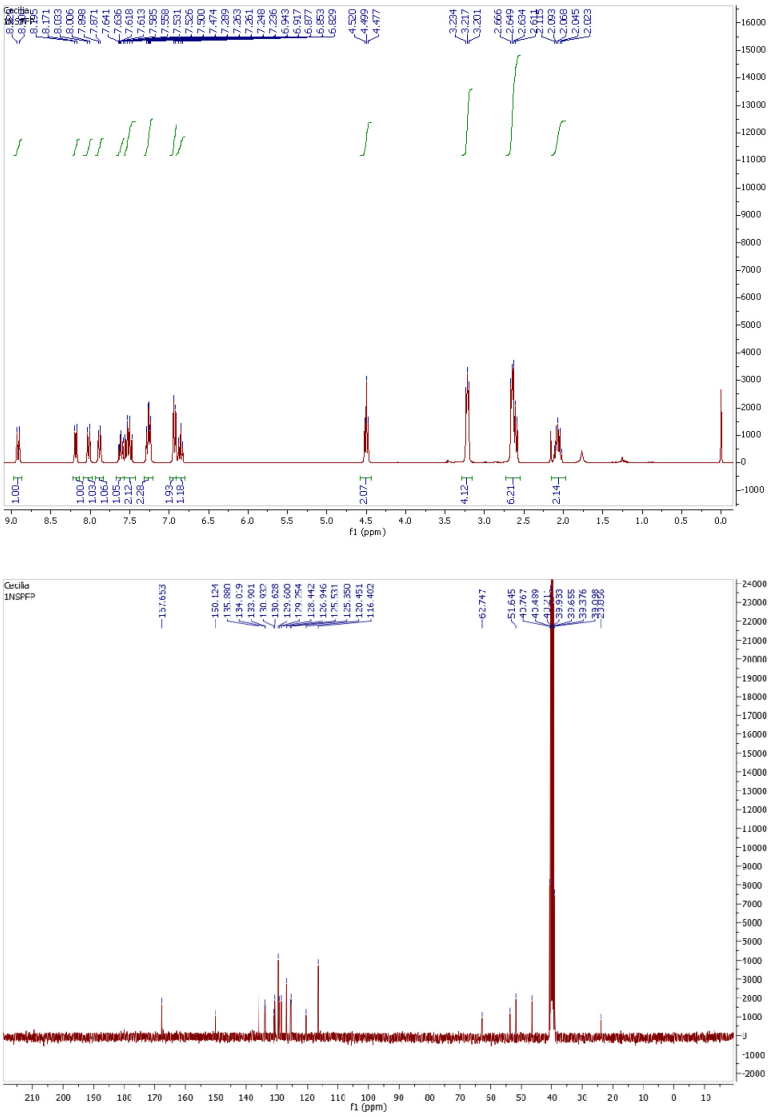
S15



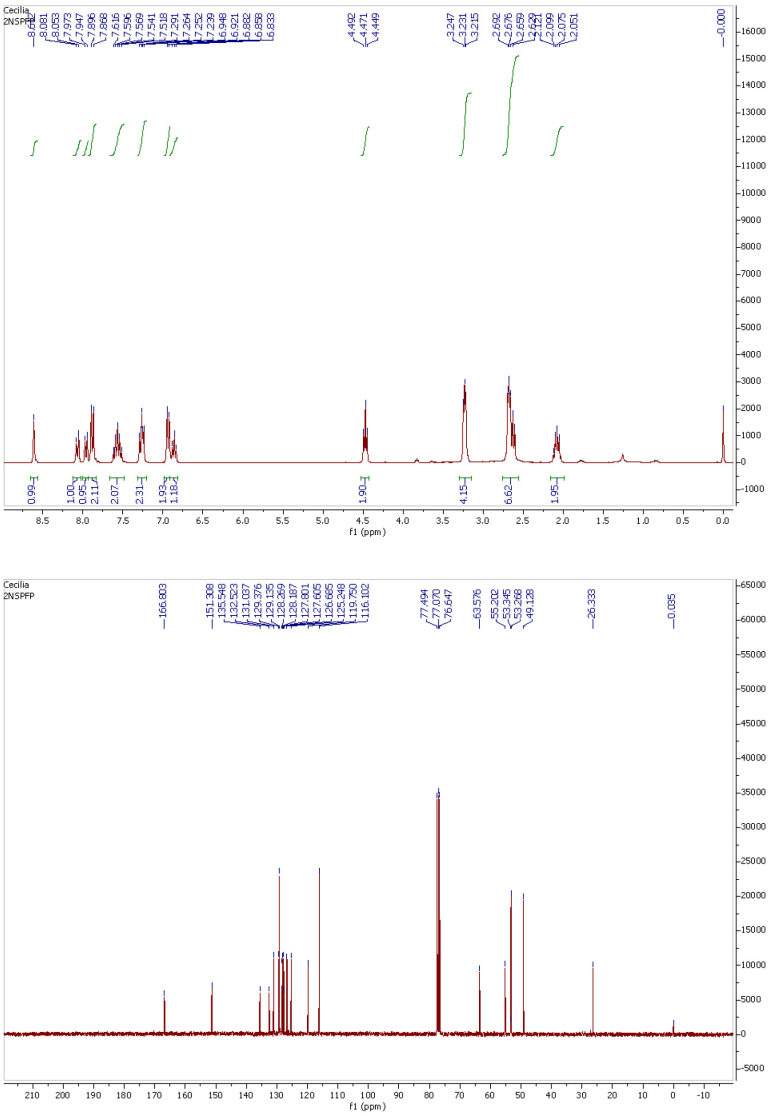
3-(4-Methylpiperazin-1-yl)propyl naphthalene-1-carboxylate (**LINS05014**). ^{1}H NMR (300 MHz, $CDCl_3$) δ 8.90 (d, *J* = 8.5 Hz, 1H), 8.17 (d, *J* = 6.6 Hz, 1H), 8.03 (d, *J* = 8.3 Hz, 1H), 7.89 (d, *J* = 7.8 Hz, 1H), 7.65–7.46 (m, 3H), 4.47 (t, *J* = 6.2 Hz, 2H), 2.73–2.39 (m, 10H), 2.35 (s, 3H), 2,03 (quint, *J* = 6,2 Hz, 2H). ^{13}C NMR (75 MHz, $CDCl_3$) δ 167.6, 133.9, 133.3, 131.4, 130.1, 128.5, 127.7, 127.4, 126.2, 125.8, 124.5, 63.6, 55.2, 55.1, 53.2, 46.0, 26.3.



3-(4-Methylpiperazin-1-yl)propyl naphthalene-2-carboxylate (**LINS05015**). ^{1}H NMR (300 MHz, $CDCl_3$) δ 8.60 (s, 1H), 8.08–8.02 (m, 1H), 7.96 (d, *J* = 7.7 Hz, 1H), 7.88 (d, *J* = 8.5 Hz, 2H), 7.62–7.51 (m, 2H), 4.44 (t, *J* = 6.5 Hz, 2H), 2.81–2.38 (m, 10H), 2.35 (s, 3H), 2.08–1.95 (m, 2H). ^{13}C NMR (75 MHz, $CDCl_3$) δ 166.8, 135.5, 132.5, 131.0, 129.4, 128.3, 128.2, 127.8, 127.6, 126.7, 125.2, 63.5, 55.0, 54.9, 52.7, 45.7, 26.3.

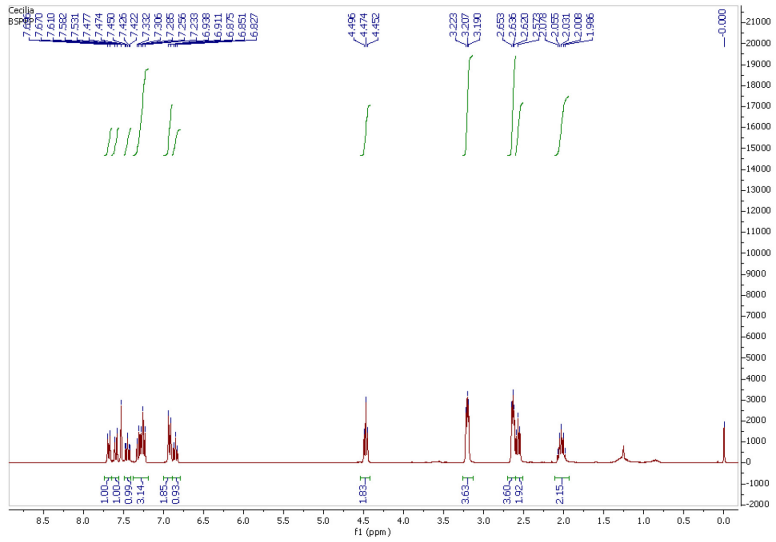


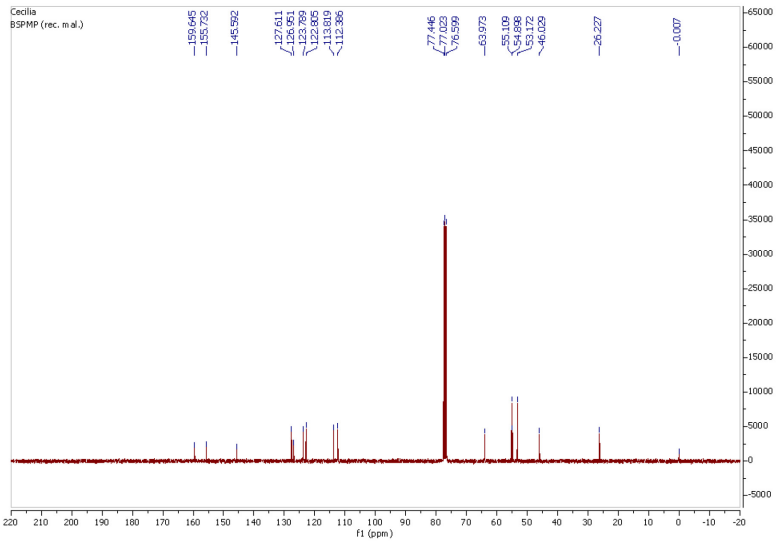
3-(4-Phenylpiperazin-1-yl)propyl naphthalene-1-carboxylate (**LINS05016**). ^{1}H NMR (300 MHz, $CDCl_3$) δ 8.91 (d, *J* = 8.6 Hz, 1H), 8.18 (dd, *J* = 7.2, 0.9 Hz, 1H), 8.02 (d, *J* = 8.2 Hz, 1H), 7.88 (d, *J* = 7.9 Hz, 1H), 7.66–7.45 (m, 3H), 7.26 (dd, *J* = 12.8, 3.6 Hz, 2H), 6.93 (d, *J* = 8.1 Hz, 2H), 6.85 (t, *J* = 7.3 Hz, 1H), 4.50 (t, *J* = 6.5 Hz, 2H), 3.27–3.16 (m, 4H), 2.71–2.54 (m, 6H), 2.06 (quint, *J* = 6.9 Hz, 2H). ^{13}C NMR (75 MHz, DMSO) δ 167.7, 150.1, 135.9, 134.0, 133.9, 130.9, 130.6, 129.6, 129.3, 128.4, 127.0, 125.5, 125.4, 120.5, 116.4, 62.8, 53.6, 51.7, 46.4, 23.9.



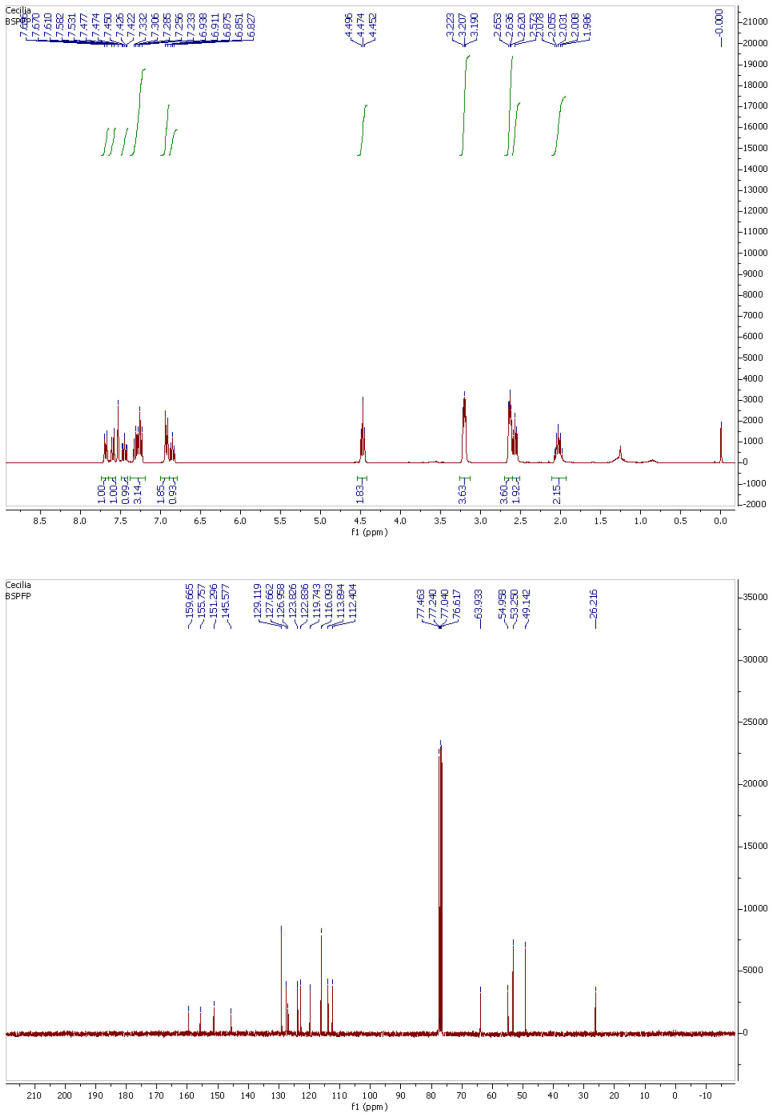
3-(4-Phenylpiperazin-1-yl)propyl naphthalene-2-carboxylate (**LINS05017**). ^{1}H NMR (300 MHz, $CDCl_3$) δ 8.61 (s, 1H), 8.07 (d, *J* = 8.6 Hz, 1H), 7.96 (d, *J* = 7.8 Hz, 1H), 7.88 (d, *J* = 8.5 Hz, 2H), 7.63–7.49 (m, 2H), 7.30–7.22 (m, 2H), 6.93 (d, *J* = 8.1 Hz, 2H), 6.86 (t, *J* = 7.3 Hz, 1H), 4.47 (t, *J* = 6.4 Hz, 2H), 3.23 (t, *J* = 6.0 Hz, 4H), 2.73–2.58 (m, 6H), 2.08 (quint, *J* = 6.0 Hz, 2H). ^{13}C NMR (75 MHz, $CDCl_3$) δ 166.8, 151.3, 135.6, 132.5, 131.0, 129.4, 129.1, 128.3, 128.2, 127.8, 127.6, 126.7, 125.3, 119.8, 116.1, 63.6, 55.2, 53.3, 49.1, 26.3.

S19



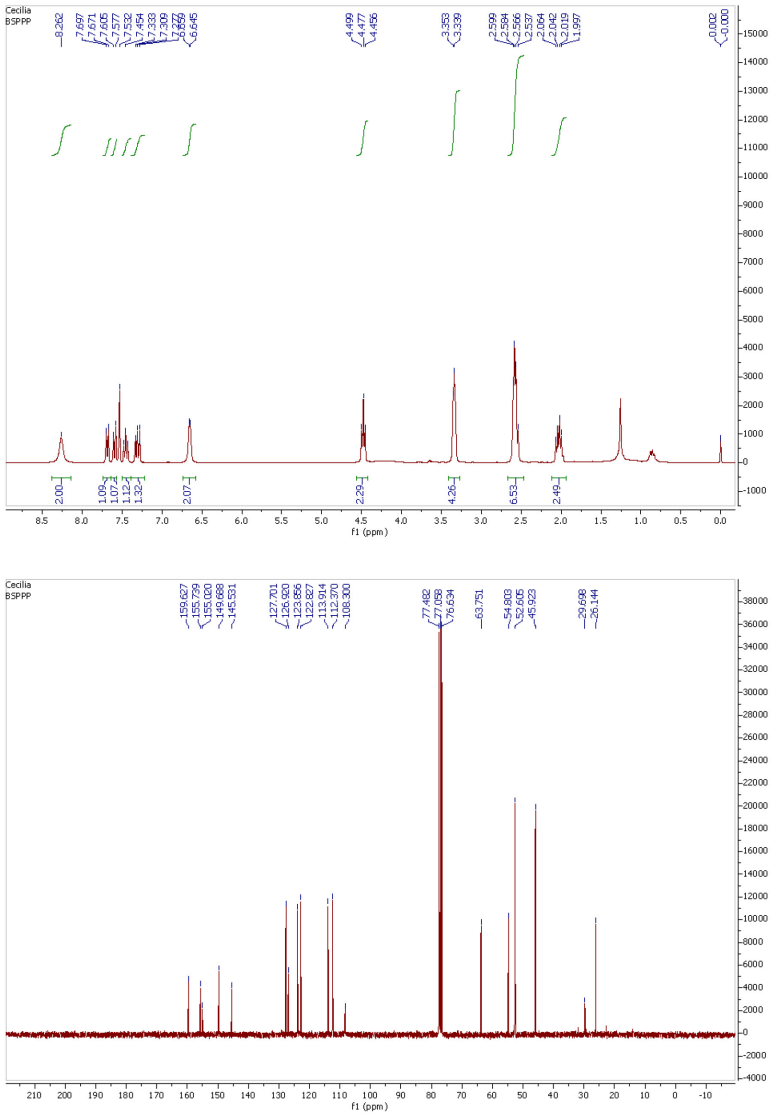


3-(4-Methylpiperazin-1-yl)propyl benzofuran-2-carboxylate (**LINS05018**). ^{1}H NMR (300 MHz, $CDCl_3$) δ 7.69 (d, *J* = 7.8 Hz, 1H), 7.60 (d, *J* = 8.4 Hz, 1H), 7.52 (s, 1H), 7.49–7.41 (m, 1H), 7.34–7.28 (m, 1H), 4.44 (t, *J* = 6.5 Hz, 2H), 2.71–2.36 (m, 10H), 2.32 (s, 3H), 1.99 (quint, *J* = 6.4 Hz, 2H). ^{13}C NMR (75 MHz, $CDCl_3$) δ 159.6, 155.7, 145.6, 127.6, 127.0, 123.8, 122.8, 113.8, 112.4, 64.0, 55.1, 54.9, 53.2, 49.0, 26.2.



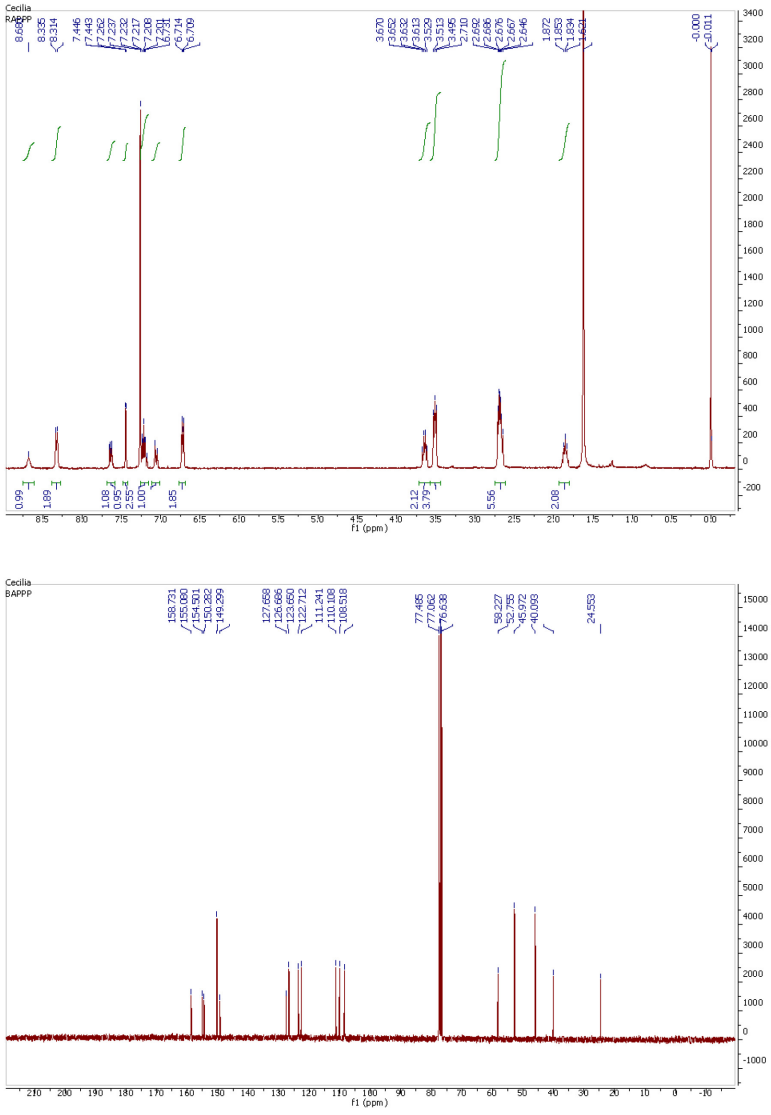
3-(4-Phenylpiperazin-1-yl)propyl benzofuran-2-carboxylate (**LINS05019**). ^{1}H NMR (300 MHz, $CDCl_3$) δ 7.68 (d, *J* = 7.8 Hz, 1H), 7.60 (d, *J* = 8.4 Hz, 1H), 7.53 (s, 1H), 7.45 (dt, *J* = 8.3, 1.2 Hz, 1H), 7.33–7.23 (m, 3H), 6.92 (d, *J* = 8.0 Hz, 2H), 6.85 (t, *J* = 7.3 Hz, 1H), 4.47 (t, *J* = 6.6 Hz, 2H), 3.21 (t, *J* = 4.5 Hz, 4H), 2.69–2.61 (m, 4H), 2.57 (t, *J* = 7.3 Hz, 2H), 2.03 (quint, *J* = 6.0 Hz, 2H).^{13}C NMR (75 MHz, $CDCl_3$) δ 159.7, 155.8, 151.3, 145.6, 129.1, 127.7, 127.0, 123.8, 122.8, 119.7, 116.1, 113.9, 112.4, 63.9, 55.0, 53.3, 49.1, 26.2.

S21



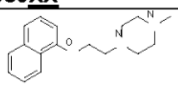
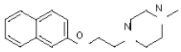
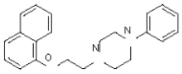
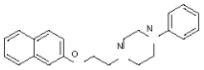
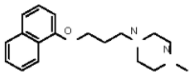
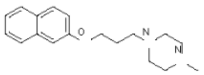
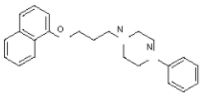
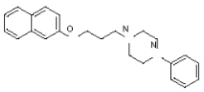
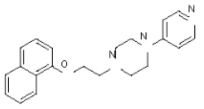
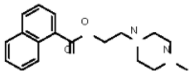
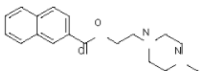
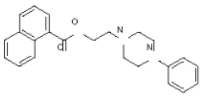
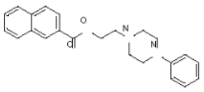
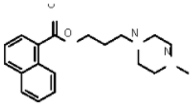
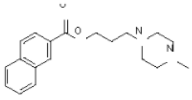
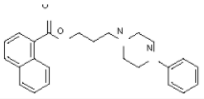
3-[4-(4-Pyridyl)piperazin-1-yl]propyl benzofuran-1-carboxylate (**LINS05020**). ^{1}H NMR (300 MHz, $CDCl_3$) δ 8.26 (d, *J* = 4.2 Hz, 2H), 7.68 (d, *J* = 7.8 Hz, 1H), 7.59 (d, *J* = 8.4 Hz, 1H), 7.53 (s, 1H), 7.45 (dt, *J* = 8.3, 1.2 Hz, 1H), 7.31 (t, *J* = 7.6 Hz, 1H), 6.65 (d, *J* = 4.2 Hz, 2H), 4.48 (t, *J* = 6.5 Hz, 2H), 3.37–3.27 (m, 4H), 2.63–2.51 (m, 6H), 2.02 (quint, *J* = 6.9 Hz, 2H). ^{13}C NMR (75 MHz, $CDCl_3$) δ 159.6, 155.7, 155.0, 149.7, 145.5, 127.7, 126.9, 123.9, 122.8, 113.9, 112.4, 108.3, 63.8, 54.8, 52.6, 45.9, 26.1.

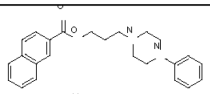
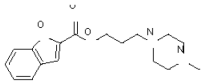
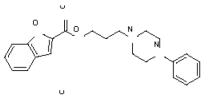
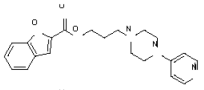
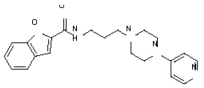
S22



3-[4-(4-Pyridyl)piperazin-1-yl]propyl benzofuran-1-carboxylate (**LINS05021**). ^{1}H NMR (300 MHz, $CDCl_3$) δ 8.68 (br.s, 1H), 8.32 (d, *J* = 6.4 Hz, 2H), 7.65–7.61 (m, 1H), 7.44 (d, *J* = 0.8 Hz, 1H), 7.24–7.15 (m, 2H), 7.10–7.00 (m, 1H), 6.72 (d, *J* = 6.4 Hz, 2H), 3.64 (q, *J* = 5.6 Hz, 2H), 3.56–3.45 (m, 4H), 2.75–2.61 (m, 6H), 1.85 (quint, *J* = 5.9 Hz, 2H). ^{13}C NMR (75 MHz, $CDCl_3$) δ 158.7, 154.5, 150.3, 150.3, 149.3, 127.7, 126.7, 123.7, 122.7, 111.2, 110.1, 108.5, 58.3, 52.8, 46.0, 40.1, 24.6.

Table S1. Screening of the LINS05 compounds at H_4R and D_2R.

Compound LINS050XX		%inhibition (±SD) at 1 or 10 µM	
		hH_4R	*h*D_2R
01[a]		n.t.	23.7 ±5.9
02[a]		n.t.	-1.5 ±6.9
03[a]		n.t.	18.3 ±7.6
04[b]		n.t.	9.3 ±4.5
05[a]		20.2 ±11.3	-20.8 ±14.0
06[a]		40.5 ±20.4	-50.5 ±17.3
07[b]		n.t.	21.0 ±3.7
08[b]		n.t.	67.3 ±16.9
09[b]		n.t.	37.8 ±23.2
10[a]		26.7 ±13.9	-35.0 ±13.3
11[a]		40.8 ±15.8	-30.7 ±19.1
12[a]		45.3 ±14.5	26.5 ±17.9
13[a]		49.5 ±11.1	-5.8 ±8.8
14[a]		53.2 ±17.7	-23.5 ±26.6
15[a]		58.2 ±15.7	-19.5 ±18.1
16[a]		83.7 ±10.6	71.5 ±7.4

17[a]		-10.0 ±14.9	33.3 ±10.6
18[a]		38.5 ±17.1	-34.7 ±17.9
19[a]		43.8 ±20.4	31.2 ±4.5
20[b]		n.t.	2.8 ±5.0
21[b]		n.t.	0.7 ±5.0
Pitolisant		85.7 ±7.1	
Haloperidol			94.8 ±3.5

[a]10 µM at *h*H$_3$R and *h*D$_3$R; [b]1 µM at *h*H$_3$R and *h*D$_3$R. n.t.: not tested

Kinetic studies

The protocol was performed with the same substrate from inhibition assays (ATCI) with concentrations varying from 0.25 to 4 mM, and same concentrations to DTNB and enzymes. The study was performed for compound **20** as inhibitor, in concentrations varying from 10 to 75 µM. The experiments were performed in triplicate. The V_{maxapp} and K_{Mapp} values of the Michaelis-Menten kinetics were estimated through non-linear regression from substrate/velocity curves. Obtained data was used to build the Linewearver-Burk plot by using linear regression. The results from kinetic studies (Figure S1) suggest that the mechanism for inhibition of the *ee*AChE by compound **20** occurs through competitive inhibition. Increasing concentrations of the inhibitor affected only the K_{Mapp} value but not the V_{maxapp} value, leading to an intercept of the linear regression lines on the velocity axis of the Lineweaver-Burk plot.

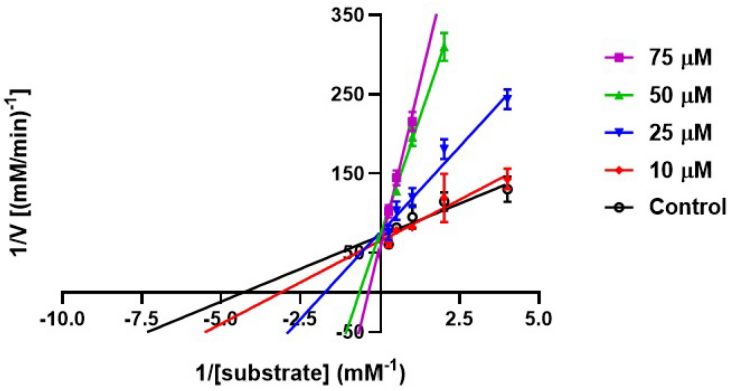


Figure S1. Lineweaver-Burk plot showing competitive inhibition of *ee*AChE activity by compound **20**.

3.5 Design, synthesis and biological in vitro properties of dual acting ligands as histamine H_3 receptor and L-type Ca^{2+} channel inhibitors

Luisa Leitzbach[1], Sicheng Zhong[1], Aleksandra Zivkovic[1], Ferenc Török[2], Lucia Zanetti[2, 3], Nadine J. Ortner[2], Mustafa Sindi[4], Philipp Albrecht[4, 5,] Jörg Striessnig[2], Holger Stark[1*]

[1] Heinrich Heine University Düsseldorf, Institute of Pharmaceutical and Medicinal Chemistry, Universitaetsstr. 1, 40225 Duesseldorf, Germany, [2] University of Innsbruck, Department of Pharmacology and Toxicology, Center for Molecular Biosciences, Innrain 80-82, 6020 Innsbruck, Austria, [3] Scuola Internazionale Superiore degli Studi Avanzati, Department of Neuroscience, Via Bonomea 256, 34136 Trieste, Italy, [4] Department of Neurology, Medical Faculty and University Hospital, Heinrich Heine University Düsseldorf, Universitaetsstr. 1, 40225 Düsseldorf, Germany, [5] Department of Neurology, Maria Hilf Clinics, Viersener Str. 450, 41063 Mönchengladbach, Germany.

Published in: In preparation

Contribution: L.L. designed and performed most of the in-vitro experiments, interpretation of pharmacological data, wrote the manuscript.

.

Design, synthesis and biological in vitro properties of dual acting ligands as histamine H3 receptor and L-type Ca^{2+} channel inhibitors

Luisa Leitzbach[1], Sicheng Zhong[1], Aleksandra Zivkovic[1], Ferenc Török[2], Lucia Zanetti[2, 3], Nadine J. Ortner[2], Mustafa Sindi[4], Philipp Albrecht[4, 5], Jörg Striessnig[2], Holger Stark[1*]

[1] Heinrich Heine University Düsseldorf, Institute of Pharmaceutical and Medicinal Chemistry, Universitaetsstr. 1, 40225 Duesseldorf, Germany

[2] University of Innsbruck, Department of Pharmacology and Toxicology, Center for Molecular Biosciences, Innrain 80-82, 6020 Innsbruck, Austria

[3] Scuola Internazionale Superiore degli Studi Avanzati, Department of Neuroscience, Via Bonomea 256, 34136 Trieste, Italy

[4] Department of Neurology, Medical Faculty and University Hospital, Heinrich Heine University Düsseldorf, Universitaetsstr. 1, 40225 Düsseldorf, Germany

[5] Department of Neurology, Maria Hilf Clinics, Viersener Str. 450, 41063 Mönchengladbach, Germany.

*Correspondence: HS, stark@hhu.de

Preprint not peer reviewed

This preprint research paper has not been peer reviewed. Electronic copy available at: https://ssrn.com/abstract=5133249

Abstract

The challenging development of drugs for neurological diseases caused by multifactorial characteristics and imbalances of several neurotransmitters and ions in the CNS demonstrates the importance for new therapeutic options. Multitarget-directed ligands might be advantageous for these indications since they act simultaneously on multiple involved targets and synergistic effects are conceivable. Herein, we report the design, synthesis and biological evaluation of dual target directed ligands by combining a histamine H_3R antagonist structural motif to various pharmacophores for Ca^{2+} channel inhibition including dihydropyridines and dihydropyrimidines. Besides the H_3R affinities, we were particularly interested in the activity at two specific L-type Ca^{2+} channels ($Ca_V1.2$ and $Ca_V1.3$) due to their potential pathophysiological role for several neurological disorders, including Parkinson´s disease. Compounds **3f (**1-(2,6-dimethyl-4-phenyl-5-(4-(3-(piperidin-1-yl)propoxy)benzoyl)-1,4-dihydropyridin-3-yl)ethan-1-one) and **5b** (1-cyclohexyl-3-(3-(4-(3-(piperidin-1-yl)propoxy)phenyl)propyl)urea) were identified as lead compounds with nanomolar affinity to the H_3R (K_i values of 1.56 nM and 8.41 nM, respectively) and micromolar Ca^{2+} channel inhibition ($Ca_V1.2$ IC_{50} = 25.5 and 103.9 µM, $Ca_V1.3$ IC_{50} = 40.9 and 43.5 µM) and were further evaluated for their use-dependency. Interestingly, the keto-substituted dihydropyridine **3f** with H_3R pharmacophore linked directly to the dihydropyridine showed the best H_3R affinity. The urea derivatives with cyclohexyl side chain (**5a**, **5b** and **5e**) showed a preference for $Ca_V1.3$. The results of this study provide new insights in the structure activity relationship of these dual-actingligands and are essential for lead structure optimization to accomplish balanced dual inhibitory effects.

Keywords: Multitarget-directed ligand, histamine H_3 receptor, calcium channel, Parkinson's disease, neurological disease

Preprint not peer reviewed

This preprint research paper has not been peer reviewed. Electronic copy available at: https://ssrn.com/abstract=5133249

Introduction

Histamine is a biogenic amine and neurotransmitter, which stimulates four subtypes of G-protein coupled receptors (H_1-H_4R). In the central nervous system (CNS), histamine plays a role in cognition, memory, and the sleep-wake cycle. The histamine H_3R is mainly located in the CNS [1] acting pre- and postsynaptically as control for the synthesis and release of histamine and other neurotransmitters such as dopamine or noradrenaline [2]. Several histamine H_3 receptors (H_3R) antagonists/inverse agonists showed potential in modulating memory and cognition, mood and sleep-wake cycle and therefore suggesting its potential role in neurodegenerative and neurocognitive diseases [3]. Much effort has been made to develop drug candidates targeting the H_3R for the treatment of Parkinson's disease (PD), Alzheimer disease (AD), schizophrenia, depression, and other cognitive disorders [4, 5]. Nevertheless, pitolisant presents so far the only approved drug as H_3 receptor antagonist/inverse agonist for the treatment of narcolepsy with or without cataplexy [6-8]. The indications of pitolisant were extended with the authorization of Ozawade® by EMA for excessive daytime sleepiness in obstructive sleep apnea in 2021[9]. In addition, preclinical and clinical failure rates in CNS diseases are higher than for non-CNS medicinal products. Low efficacy, safety concerns, the multifactorial characteristics and the lack of understanding the entire underlying mechanism(s) of neurological diseases challenge the development of new drugs [10].

In recent years, multitarget directed ligands (MTDL) became increasingly important in the development of drugs for multifactorial diseases to overcome these drawbacks. Rational design of target combinations can lead to innovative drug candidates with several advantages over the single target approach[11]. Synergistic effects with increased therapeutic efficacy, higher compliance, and simplified therapeutic regimen are just a few to mention here [12]. Despite this, balanced activity on the carefully selected targets and avoidance of off-targets effects is important for the successful development of MTDL [13].

Malek et al. [14, 15] described the design and evaluation of multitarget directed ligands combining H_3R antagonism, Ca^{2+} channel inhibition and acetyl- (AChE) and butyrylcholinesterase (BuChE) inhibition as potential lead compounds for AD. Their lead compounds 3p (or Han 25) [14] and 3e [15] (shown in

Preprint not peer reviewed

This preprint research paper has not been peer reviewed. Electronic copy available at: https://ssrn.com/abstract=5133249

Figure 1) showed promising effects in-vivo in an AD mouse model despite their low potencies for Ca^{2+} channels (IC_{50} 21 µM and 72.8 µM, respectively).

The importance of proper Ca^{2+} signaling is evident from a number of human diseases associated with Ca^{2+} dysregulation [19-21]. Cav1.2 and Cav1.3 L-type Ca^{2+} channels (LTCCs) are expressed in most excitable cells and are implicated in multiple pathologies including neurological disorders and neuropsychiatric symptoms [21]. Genetic variants enhancing LTCC activity cause the multisystem disorder Timothy syndrome (Cav1.2, [22]) or a rare neurodevelopmental disorder (Cav1.3, [23]). Furthermore, Cav1.3 is linked to mitochondrial oxidative stress in substantia nigra (SN) pars compacta neurons since they contribute to Ca^{2+} oscillations during autonomous pacemaking and to bursting in these neurons [24]. This possibly underlies the high vulnerability and subsequent loss of SN pars compacta neurons in PD, rendering Cav1.3 inhibition a potential disease-modifying strategy in early PD [25].

The aim of this study is the development of dual target-directed ligands by combination of a histamine H_3R antagonist pharmacophore to that of Ca^{2+} channel inhibitors as potential ligands for neurological disorders. The investigation of the mutual influence of the combined pharmacophores on the binding properties is in the focus of this study. In particular, $Ca_V1.3$ selective inhibitors are of special interest, which would spare peripheral vasodilatatory and blood pressure lowering effects, but suitable candidates have so far not been reported [25, 26].

N-(3-Phenoxypropyl)piperidine as in the H_3R antagonist JNJ-5207852 [27, 28] fits in the general pharmacophore model of H_3R antagonists and was selected as H_3R structural element. In the first series of compounds, it was combined with widely used dihydropyridine (DHP) LTCC inhibitors [29] and derivatized. Secondly, two barbituric acid derivatives and urea precursors were designed to include the pyrimidine-2,4,6,-trione, which were identified as low potency modulators of $Ca_V1.3$ [30-32]. In the last series, dihydropyrimidines (DHPM) as in the Ca^{2+} channel modulator SQ 32926 [18] were combined with the H_3R pharmacophore to avoid the metabolic instability of DHPs [a] [33]. The chemical structures of known Ca^{2+} channel modulators are displayed in **Figure 1**. Based on the results of H_3R and Ca^{2+}

[a] Parts of this work are based on the dissertation of S. Zhong.

This preprint research paper has not been peer reviewed. Electronic copy available at: https://ssrn.com/abstract=5133249

Preprint not peer reviewed

channel screening, eight compounds were tested for their selectivity to the H_3R. Additionally, we decided to further evaluate **3f** and **5b** in patch-clamp experiments for their use-dependency on $Ca_V1.3$.

Results and discussion

Chemistry

The synthesis of the symmetric 1,4-DHP (**3a-e**) has been carried out by Hantzsch DHP synthesis (**Scheme 1**) with substituted benzaldehyde (**1a-c**) and the corresponding β-diketones (**2a, 2b**) or iminobutanenitrile (**2c**). The substituted β-diketone was prepared by a crossed Claisen condensation from acetophenone derivative **2d** and EtOAc in the presence of NaH and 18-crown-6-ether in THF. The Claisen product reacted further with NH_4OAc in MeOH to obtain the corresponding iminophenylbutanone derivative **2e**. The Knoevenagel condensation product **1d** was prepared from benzaldehyde and acetylacetone with $AlCl_3$ as catalyst. Compound **3f** was obtained from several convergent synthetic steps (

Scheme 2). Compounds **2e** and **1d** were radiated in the microwave to obtain the desired asymmetric, racemized dihydropyridine **3f** (yield 22%). The low yield may be caused by the low reactivity of **1d** as Michael acceptor.

The benzylamine and phenyl propylamine derivatives (**4a**, **4b**) were prepared as described previously [34]. The urea derivatives **5a-d** have been synthesized by amines **4a** and **4b** and cyclohexyl isocyanate or phenyl isocyanate in THF at ambient temperature (**Scheme 3**). The derivatives with ethyl linker (**5e**, **5f**) were prepared from tyramine hydrochloride in several subsequent steps. The obtained yields range from 29 to 70%. The barbituric acid derivatives **6a** and **6b** were synthesized by acylating *N,N*-substituted urea's with malonic acid in acetic acid anhydride [35].

The DHPM derivatives have been synthesized by using 4-hydroxybenzaldehyde, urea and either acetylacetone or ethyl acetoacetate. The reaction was catalyzed by HCl or $ZrCl_4$ as shown in **Scheme 4** [36, 37]. The obtained phenols **7a** and **7b** reacted with 1-(3-chloropropyl)piperidine resulted to ligands **8a** and **8b** by Williamson ether syntheses under Finkelstein catalysis. The acylated derivatives **8c** and

Preprint not peer reviewed

This preprint research paper has not been peer reviewed. Electronic copy available at: https://ssrn.com/abstract=5133249

8d were obtained by acylating the **8a** and **8b** with acetic anhydride in the presence of 4-dimethyl aminopyridine (DMAP) and triethylamine in a microwave reaction [38]. The dihydropyrimidines were obtained in yields from 78 to 94%.

Pharmacology

The affinity at the human H_3R was determined by radioligand displacement assay as presented in **Table 1**. All DHP derivatives (**3a-f**) showed binding affinities to the H_3R in the nanomolar range. The asymmetric derivative **3f** with H_3R pharmacophore linked directly to the DHP ring showed the lowest K_i value of 1.56 nM in this series. The binding affinities increased for derivatives **3c** and **3d** with electron withdrawing nitro group (70.9 nM and 222 nM, respectively). The lowest K_i value of the urea compounds is displayed by the cyclohexyl derivative **5b** (8.41 nM). A longer linker length of the cyclohexyl derivatives (**5a**, **5b** and **5e**) tends to increase affinity but this is not statistically significant. The same trend is observed for the phenyl derivatives (**5c**, **5d** and **5f**) and the barbituric acid derivatives (**6a** and **6b**). Derivative **8b** of the DHPM derivatives (**8a-d**) showed the lowest K_i value of 45.2 nM for. Varying the ethyl ester and methylketone substitution on the DHPM ring does not influence the binding properties to the H_3R significantly. Overall, the 18 tested compounds demonstrated high affinities at the H_3R in nanomolar concentration range between 1 and 130 nM with clear structure-activity relationships. Three derivatives (**3a, 3f** and **5b**) are in the low nanomolar range, even surpassing the affinity of reference compound pitolisant.

Selectivity for H_3R over other GPCRs (hH_1R and hH_4R) of the most promising derivatives was tested. The H_3R affinity of the investigated compounds is at least 40 times lower than to the other histamine receptors tested. None of the derivates showed affinity at the H_4R up to 100 µM.

All synthesized compounds were investigated in a fluorescence-based assay to assess the inhibition of Ca^{2+} channel subtypes $Ca_V1.2$ and $Ca_V1.3$. The compounds were screened for their IC_{50} values if inhibition at a concentration of 100 µM was higher than 50%. The results are provided in **Table 1**. Three DHP derivatives namely **3b** [14], **3d**, and **3f** inhibited both Ca^{2+} channel subtypes to the same extent. In comparison to **3b** [14] with IC_{50} values of 40.9 µM ($Ca_V1.2$) and 36.8 µM ($Ca_V1.3$), the nitro substitution (**3d**) increased the potency for both LTCC isoforms (IC_{50} 14.0 µM and 11.1 µM, respectively). The

This preprint research paper has not been peer reviewed. Electronic copy available at: https://ssrn.com/abstract=5133249

electron-withdrawing substitution on the phenyl ring is similar as in nimodipine, a blood-brain barrier penetrant drug used for ischemic neurological deficits due to cerebral vasospasms following aneurysmal subarachnoid hemorrhage [39]. Interestingly, the keto-substituted DHP derivative **3f** showed similar IC_{50} values as derivate **3b**. It is the only asymmetric derivative without *para*-substituted phenyl ring, indicating that the *para*-substitution reduces the potency at the Ca^{2+} channels. None of the derivatives showed preference for either of the tested LTCCs. This is consistent with the study of Chang et al., in which DHPs only showed modest preference for $Ca_V1.3$ [40]. The keto substitution at the DHP (**3a** and **3c**) decreased inhibition of the Ca^{2+} channels compared to the ester substitution (**3b** and **3d**). Of the urea derivatives, **5b** and **5d** with propyl linker showed the highest inhibition values with 103.9 or 56.4 µM ($Ca_V1.2$) and 43.5 or 43.3 µM ($Ca_V1.3$). In comparison to the phenyl derivatives, the cyclohexyl group led to a tendency towards the $Ca_V1.3$ isoform (**5b**, **5d** and **5e**). The barbituric acid (**6a** and **6b**) and DHPM (**8a**-**8d**) compounds showed only minor inhibition of the Ca^{2+} channels. The barbituric acid-derived calcium channel inhibitors showed weaker inhibition than that reported for the pyrimidine-2,4,6-trione compound cp-PYT with IC_{50}= 24.3 µM ($Ca_V1.3$) with 100-fold selectivity over $Ca_V1.2$ [16]. However, the results obtained for cp-PYT are contradictory across different laboratories and show a high variation due to the determination methods. Huang et al determined $Ca_V1.3$inhibition of 43% at 50 µM [32] and comparable Cav1.2 inhibition, and Ortner et al. suggest cp-PYT even as activator due to altered current kinetics [31]. For the DHPM ester derivative **8d** with *N3*-substitution the inhibition values are slightly higher with 30.4% ($Ca_V1.2$) and 36.0% ($Ca_V1.3$) compared to the other three derivatives. This indicates that *N3*-substitution and ester functionality are crucial for LTCC inhibition as in SQ 32926 [18].

In summary, five derivatives with IC_{50} values in the micromolar range were identified including the already described derivative **3b** [14]. Despite this, none of the compounds showed LTCC inhibition in the nanomolar range as shown for the control compound isradipine. The decline of LTCC activity of the DHPs compared to the reference isradipine is probably caused by the keto-substitution and the position of the linked H_3R pharmacophore. Furthermore, we were unable to verify Ca^{2+} channel inhibition of DHPM derivatives as shown by Malek et al [15]. This discrepancy may be attributed to the used cell line in the Ca^{2+} assay namely SH-SY5Y human neuroblastoma cells. Their lead compound 3e with in-

Preprint not peer reviewed

This preprint research paper has not been peer reviewed. Electronic copy available at: https://ssrn.com/abstract=5133249

vivo properties in restoring cognitive function in scopolamine treated AD mice is structurally similar to compound **8d** but differs in the linker length of the H_3R pharmacophore and the additional AChE pharmacophore. This raises the questions on which other Ca^{2+} channel subtype(s) the DHPM of Malek et al. bind to and to what extent the structural differences influence the binding properties.

The influence of the Ca^{2+} channel inhibitor pharmacophores on the H_3R affinity is much weaker. Notably the electron-withdrawing group in the DHPs leads to decreased H_3R affinity and therefore to an unfavorable interplay of these dual target ligands. High H_3R affinity values below 100 nM were achieved for all tested Ca^{2+} channel pharmacophore combinations with only two exceptions (**3d**, **5c**). These results could guide further lead structure optimization if dual inhibitory effect on histamine H_3R and LTCCs is required.

Due to the low nanomolar H_3R affinity and simultaneous LTCC inhibition, compounds **3f** and **5b** were further investigated at a concentration of 30 µM in whole-cell patch-clamp experiments with two different frequencies (0.1 and 1 Hz) to analyze the frequency-dependency at $Ca_V1.3$ (**Table 2**, Figure 2B). Compound **5b** inhibited about 20% of $Ca_V1.3$ current with low potency and its potency was not increased at a higher frequency suggesting that it does not act in a frequency-dependent manner. Compound **3f** was slightly more potent with an IC_{50} close to 30 µM at 0.1 Hz stimulation frequency. A minor, but significant increase in potency was observed at 1 Hz frequency, indicating a weak use-dependent mechanism of action (unpaired student's t-test, $p<0.01$)Despite this, both compounds are much less potent than the DHP isradipine (IC_{50} around 100 nM at 0.1 Hz stimulation frequency and negative holding potential (-89 mV)) [41].

To gain insights into the influence of these compounds on cell viability and to test for their cytotoxic effects, we screened the compounds for their cytotoxicity in a cell-based assay using neuronal SH-SY5Y cells. Compared to the toxin MPP^+, which led to a cytotoxicity of ~90 %, none of these compounds showed cytotoxic effect at a concentration of 10 µM as shown in **Table 1**.

Conclusion

We designed dual targeting ligands comprising H_3R antagonist pharmacophore merged to various Ca^{2+} channel inhibitors and identified two derivatives (**3f** and **5b**) with low nanomolar affinity at the human

This preprint research paper has not been peer reviewed. Electronic copy available at: https://ssrn.com/abstract=5133249

H_3R (K_i = 1.56 – 8.41), micromolar LTCC inhibition ($Ca_V1.2$ IC_{50} =25.5 and 103.9 µM, $Ca_V1.3$ IC_{50} = 40.9 and 43.5 µM) and non-existent cytotoxic effects on SH-SY5Y cells. Our results provide new insights into the binding properties of the dual-acting ligands. Furthermore, we observed a tendency of cyclohexyl-3-urea derivatives to $Ca_V1.3$ compared to $Ca_V1.2$. The study certainly adds to our understanding of the mutual influence of the linked pharmacophores.

The herein designed compounds are suitable as a starting point for further structural optimization to obtain desired and balanced binding properties on both investigated targets. Future studies will elucidate whether such novel multi target directed ligands will prove useful for the treatment of complex neurological and neurodegenerative diseases such as PD and AD.

Preprint not peer reviewed

This preprint research paper has not been peer reviewed. Electronic copy available at: https://ssrn.com/abstract=5133249

Materials & methods

Human H_1, H_3 and H_4 Receptor Radioligand Displacement Assays

Radioligand displacement assays at the human histamine H_1R, H_3R and H_4R were performed, as published previously [42, 43]. In summary, the compounds were incubated with membrane preparations of CHO- or HEK-293 cells stably expressing the human histamine H_1R (40 µg/well), H_3R (20 µg/well) and H_4R (30 µg) and the corresponding radioligand [^{3}H]-Pyrilamine (1 nM, K_D = [^{3}H]*N*$^\alpha$-methylhistamine (2 nM, K_D = 3.08 nM) and [3H]-histamine (10 nM, K_D = 10.6 nM) in 200 µL (H_1 and H_3) or 100 µL (H_4) binding buffer (10 mM $MgCl_2$, 100 mM NaCl and 75 mM Tris/HCl, pH 7.4) for 90 or 120 min. At least three independent experiments of each compound in duplicate were conducted with seven to 11 concentrations. Obtained data was analysed with GraphPad Prism 10 (San Diego, CA, USA) using non-linear least squares fit and the equation "one site competition". K_i values were calculated according to the Cheng–Prusoff equation [44] and are reported as means with a 95% confidence interval. Statistical analyses were performed on the -logK_i values and were converted to mean K_i values and a 95% confidence interval. Differences are considered significant if 95% confidence intervals do not overlap.

Ca^{2+} Channel Assays

HEK293 cells stably expressing full-length Cav1.2 or C-terminally short Cav1.3 α1 subunits together with β3 and α2δ1 (tsA-$Ca_V1.2_{77WT}$ and tsA-$Ca_V1.3_s$, respectively [45]) were cultured in DMEM (Sigma-Aldrich), supplemented with 10% FBS (Gibco), 1% L-Glutamine and Penicillin/streptomycin. Selection media was applied for one week after thawing with supplementation of Blasticidin S HCl (Gibco), Hygromycin B and G418.

Cells were seeded onto black, clear bottom 384-well plates (Product number 3764, Corning Life Sciences) and incubated at 37 °C, 5% CO_2 for 48h to achieve 100% confluence. Doxycycline (1 µg/ml) was added to induce expression of α_1-subunit. After 7 to 8 hours, cells were washed twice with Krebs-Hepes buffer (pH 7.4), and Fluo-4 AM dye (4 µM) was added and incubated (37 °C, 5% CO_2) for 45 minutes. Cells were washed twice with Krebs-Hepes buffer and once with HBSS buffer (5 mM Hepes

Preprint not peer reviewed

This preprint research paper has not been peer reviewed. Electronic copy available at: https://ssrn.com/abstract=5133249

added, pH 7.4) to remove excess of dye. Compound dilutions were prepared by subsequent dilution of DMSO stocks (10 mM) to the required concentrations in HBSS buffer. DMSO (1%) was used as control and isradipine as reference. Final volume of each well was 50 µL. Measurement was conducted by Infinite M1000 Pro (Tecan) reader with the following settings: λ_{Ex} = 485 nm, λ_{Em} = 520 nm bandwidth 10 nm, Gain 90. Each well was measured for 60 s with an interval of one second, after measuring the baseline for 10 s KCl (final concentration 90 mM) was injected to initiate Ca^{2+} influx. For one-point measurements at 100 µM, quadruplicate of at least three independent experiments were determined and analysed as global fit. For compounds with inhibition values > 50%, IC_{50} values were determined. Fluorescence increase after injection was calculated ($\Delta F = F_{max} - F_{baseline}$) and normalized to the mean of control (1% DMSO). Data were analysed with GraphPad Prism 9 (San Diego, CA, USA). Nonlinear regression was calculated with log(inhibitor) vs. normalized response – variable slope.

Patch-clamp experiments

Patch clamp recordings were determined on HEK-293T cells stably expressing human $Ca_V1.3$s. External bath solution contains 170 mM choline chloride, 10 mM HEPES, 1 mM $MgCl_2$, 2 mM $CaCl_2$, pH of 7.3 adjusted with CsOH solution. Internal pipette solution contains: 135 mM CsCl, 10 mM Cs-EGTA, 1 mM $MgCl_2$, 10 mM HEPES, 4 mM ATP (pH 7.3). Current–voltage (I–V) relationships were obtained by 25-ms square pulse depolarizations from the holding potential (HP) of -89 mV (corrected for liquid junction potential of -9 mV) to different test potentials in 5 mV increments to determine the voltage of maximal conductance (V_{max}). For the pharmacological experiments cells were depolarized from the same HP to the V_{max} of the individual cell with a frequency of 0.1 or 1 Hz. Cells were perfused with external bath solution (2 mM Ca^{2+}, flow rate 0.35-0.5 ml/min) with or without test compounds. Control recordings were performed daily with bath solution and the application of compounds was started after three constant control sweeps. Stock solution (10 mM in DMSO) of compounds were diluted to test concentration of 30 µM in external bath solution. Effects of compounds were corrected assuming linear current decay in absence of compound. As positive control 3 µM isradipine were applied at the end of the experiment to fully inhibit L-type current. Data were analyzed using MatLab 9.12.0 (The Mathworks, Inc.) and Clampfit 10.7 (Axon Instruments). Statistical evaluation (unpaired student's t-

This preprint research paper has not been peer reviewed. Electronic copy available at: https://ssrn.com/abstract=5133249

test) was done with GraphPad Prism 8.0.1 software (GraphPad Software, La Jolla, CA). Data are presented as mean ± SEM.

Cytotoxicity Assay

SH-SY5Y cells were cultured in MEME (Sigma-Aldrich) containing 10% FBS, 1% L-Glutamine and non-essential amino acids. Cells were seeded onto 96 well cell culture plates (Product number 83.3924.300, Sarstedt) with a cell density of 8000 cells/well in a volume of 90 µL and incubated for 24h (37 °C, 5% CO_2). Compound dilutions (10x concentrated) were added to the wells in triplicate at the concentration of 10 µM and incubated again for 24h (37 °C, 5% CO_2). 1-Methyl-4-phenylpyridinium iodide (MPP^+) in a concentration of 1 mM was used as positive control and 1% DMSO as negative control. The media was removed after the incubation time and resazurin (stock concentration 440 µM) diluted in RPMI buffer (Sigma) was added and incubated for 2h. Fluorescence was measured with a Tecan Infinite M1000 Pro multimode reader with the following settings: λ_{Ex} = 535 nm, λ_{Em} = 590 nm, bandwidth 5 nm, gain 70. Cell viability was calculated by normalizing data to negative control. Cytotoxicity was calculated by subtracting cell viability from 100%.

Chemistry

General

All starting materials were obtained from Sigma Aldrich (Merck) and VWR and used without further purification. Analytical thin-layer chromatography was done on precoated TLC sheets ALUGRAM® Xtra SIL G/UC254 (Macherey-Nagel) with visualization under UV light. Mass spectra have been determined with Advion Mass Express (Advion, Ithaca, USA) and atmospheric-pressure chemical ionization (APCI+/-) or Bruker UHR-QTOF maXis 4G (Bruker Daltonics, Billerica, USA) and electrospray ionization (ESI+/-). Melting points were determined with Büchi M-565 (Büchi Flawil, Switzerland) with an open capillary tube. ^1H and ^{13}C NMR spectra were measured at Bruker Avance-III 300 and Bruker Avance-III 600. Deuterated dimethyl sulfoxide (DMSO-d^6) was used as solvent for NMR and tetramethylsilane as standard. Chemical shifts are given as parts per million (ppm) and reported as follows: s (singlet), d (doublet), dd (double of doublets), t (triplet), q (quartet), p (pentet), or

Preprint not peer reviewed

This preprint research paper has not been peer reviewed. Electronic copy available at: https://ssrn.com/abstract=5133249

m (multiplet). The coupling constant (J) is given in Hertz (Hz). Purification of the compounds was carried out using flash chromatography Biotage Isolera Spektra Systems with ACI™ and Assist (Biotage) with SNAP KP-Sil and SNAP KP Sil ULTRA (Biotage) as stationary phase and dichlormethane and methanol as mobile phase. Solvents have been evaporated with a Rotavapor R II (Büchi) with a PC 3001 VARIO vacuum pump (Vacuubrand) and CVC 3000 Vacuum controlling system. The compounds have been dried with a high-vacuum pump (Hybrid-Pumpe RC 6; Vaccubrand). Elemental analysis was performed on Vario MICRO cube Elemental Analyzer (Hanau, Germany). Liquid chromatography-mass spectrometry (LC-MS) was measured on an Elute SP (HPG 700) Bruker Daltronics and amaZon speed ion trap LC/MSn system (ESI-MS). Method: Alternating ion polarity on; scan range: m/z 80-1200; nebulizer: nitrogen 15 Psi; dry gas: nitrogen, 8 l/min, 200 °C; mass range mode: UltraScan, column: Intensity Solo 2 C18 (100 x 2.1 mm); temperature: 50 °C; mobile phase: A (water hypergrade for LC-MS with 0.1 % formic acid (v/v); B (acetonitrile hypergrade for LC-MS); method 1 analysis: 0-4 min 98% A, 4-5 min gradient to 95% A, 5-9 min 95% A, 9-16 min gradient to 5% A, 16-17 min gradient to 0% A, reconditioning: 17-18 min gradient to 98% A, 18-21 min 98% A.

Method 2: 0-2 min 40% A, 2-24 min gradient to 2% A, 24-25 min gradient to 0% A, reconditioning: 25-26 min gradient to 40% A. Method 3: 0-4 min 40% A, 4-5 min gradient to 35% A, 5-16 min gradient to 5% A, 16-25 min gradient to 0%, reconditioning: 25-28 min gradient to 40% A. Method 4: 0-4 min 95% A, 4-16 min gradient to 5% A, 16-17 min gradient to 0% A, reconditioning: 17-18 min gradient to 95%, 18-21 min 95%.

General procedure for the synthesis of dihydropyridine derivatives

Compounds **3a-d** were prepared via a modified method reported previously [46] . The aldehyde **1a** (for **3a, b**), **1b** (for **3c, d**) (**3a**: 2.04 mmol, **3b**: 2 mmol, **3c**: 1,85 mmol, **3d**: 1 mmol) was dissolved in 1 mL EtOH. This solution was added to acetylacetone (0.4 mL, 4 mmol) for compound **3a, 3c** or ethyl acetoacetate (4 mmol or rather 2 mmol) for compound **3b, 3d** and $(NH_4)_2CO_3$ (0.31 g, 2 mmol or 1 mmol) in 5 mL H_2O. The mixture was heated to 60 °C for 4 h (**3a**) or 55°C for 18h (**3b**), respectively 55°C for 4 h (**3d**). After the completion of the reaction monitored via TLC, the mixture was diluted with 10 mL H_2O and extracted with three portions of 20 mL DCM. The combined organic layer was dried

This preprint research paper has not been peer reviewed. Electronic copy available at: https://ssrn.com/abstract=5133249

with anhydrous $MgSO_4$ and concentrated in a rotary evaporator. The residue was purified[45] with column chromatography using the solvent gradients consisting of DCM and MeOH in ratio from 95:5 to 85:15 as eluents. Compound **3d** the product was converted to the corresponding HCl salt by treating with HCl in 2-propanol.

Compound **3e** was synthesized via an adapted method previously reported (Sanad et al, 2016). Aldehyde **1a** (1 mmol) and 3-aminocrotononitrile (2 mmol) were dissolved in 1 mL AcOH. This solution was radiated in the MW at 120 °C for 10 min and poured into crushed ice after completion. To adjust the p*H* of the solution to 9-10 6 M NaOH solution (aq.) was added. The aqueous solution was extracted three times with 30 mL DCM, the combined organic layer was dried over anhydrous $MgSO_4$ and concentrated in a rotary evaporator. Purification was carried out by column chromatography using a solvent mixture of DCM and MeOH in a ratio of 95:5 as eluent.

For the synthesis of **3f**, benzaldehyde and acetyl acetone with DCM catalyzed by $AlCl_3$ resulted in the Knoevenagel condensation product **1c** after 3 h. **2e** was prepared by a crossed Claisen condensation from derivative **2d** with EtOAc, NaH and 18-crown-6-ether in THF. NH_4OAc in MeOH was added to the Claisen product of the reaction and boiled under reflux for 2 h to result in derivative **2e**. **1c** (1.5 mmol) and **2e** (1.5 mmol) dissolved in 2 mL EtOH have been heated in a microwave at 160 °C for 15 min. The solvent was removed in rotary evaporator and the residue purified by column chromatography with a solvent mixture of DCM and MeOH (85:15).

Melting point, NMR, MS, LC-MS and elemental analysis data for final compounds **3a** – **3f** (**^{1}H and ^{13}C NMRs see Figure S1-S12)**

3a: 3,5-Diacetyl-2,6-dimethyl-4-{4-[3-(piperidin-1-yl)propoxy]phenyl}-1,4-dihydropyridine (**3a**). Light yellow solid, yield 11%, m.p. 151.5 °C. ^{1}H NMR (300 MHz, $CDCl_3$) δ 7.12 (d, *J* = 8.3 Hz, 2H), 6.74 (d, *J* = 8.2 Hz, 2H), 6.06 (s, 1H), 5.02 (s, 1H), 3.93 (t, *J* = 6.4 Hz, 2H), 2.50-2.33 (m, 6H overlap), 2.30 (s, 6H), 2.25 (s, 6H), 1.92 (p, *J* = 6.5 Hz, 2H), 1.57 (p, *J* = 5.5 Hz, 4H), 1.48-1.36 (m, 2H). ^{13}C NMR (75 MHz, $CDCl_3$) δ 198.24, 157.83, 142.91, 138.42, 128.58, 114.53, 114.09, 66.53, 56.13, 54.75, 39.40, 30.22, 26.97, 26.10, 24.56, 20.54. APCI-MS (+): m/z 411.4 $[M+H]^+$,anal. calcd. for $C_{25}H_{34}N_2O_3$: C, 73.14%, H, 8.35%, N, 6.82%. Found: C, 72.99%, H, 8.52%, N, 6.52%.

This preprint research paper has not been peer reviewed. Electronic copy available at: https://ssrn.com/abstract=5133249

3b: Diethyl-2,6-dimethyl-4-{4-[3-(piperidin-1-yl)-propoxy]phenyl}-1,4-dihydropyridine-3,5-dicarboxylate (**3b**). Yellowish viscous liquid, yield 33%. ^{1}H NMR (300 MHz, DMSO-d^6) δ 8.74 (s, 1H), 7.03 (d, *J* = 8.7 Hz, 2H), 6.73 (d, *J* = 8.7 Hz, 2H), 4.78 (s, 1H), 4.04-3.93 (m, 4H), 3.89 (t, *J* = 6.3 Hz, 2H), 2.37-2.26 (m, 6H, overlap), 2.24 (s, 6H), 1.79 (p, *J* = 6.6 Hz, 2H), 1.47 (p, *J* = 5.4 Hz), 1.40-131 (m, 2H), 1.13 (t, *J* = 7.1 Hz, 6H). ^{13}C NMR (75 MHz, DMSO-d^6) δ 167.04, 156.89, 144.97, 140.44, 128.33, 113.74, 102.16, 65.74, 58.95, 55.23, 54.13, 37.97, 26.39, 25.61, 24.17, 18.22, 14.21. APCI-MS (+): m/z 471.2 $[M+H]^+$,anal. calcd. for $C_{27}H_{38}N_2O_5$: C, 68.91%, H, 8.14%, N, 5.95%. Found: C, 68.82%, H, 8.42%, N, 5.75%.

3c: 3,5-Diacetyl-2,6-dimethyl-4-{3-nitro-4-[3-(piperidin-1-yl)propoxy]phenyl}-1,4-dihydropyridine (**3c**). Yellow solid, yield 14%, m.p. 139.6 °C. ^{1}H NMR (300 MHz, DMSO-d^6) δ 9.01 (s, 1H), 7.52 (d, ^4J = 2.3 Hz, 1H), 7.37 (dd, $^{3,4}J$ = 8.7, 2.4 Hz, 1H), 7.19 (d, *J* = 8.8 Hz, 1H), 5.04 (s, 1H), 4.09 (t, *J* = 6.1 Hz, 2H), 2.37-2.23 (m, 12H, overlap), 2.20 (s, 6H), 1.80 (p, *J* = 6.5 Hz, 2H), 1.45 (p, *J* = 5.3 Hz, 4H), 1.39-1.31 (m, 2H). ^{13}C NMR (75 MHz, DMSO-d^6) δ 195.96, 149.83, 145.34, 139.43, 139.04, 133.11, 123.13, 115.01, 112.29, 67.53, 54.79, 54.10, 37.23, 30.44, 26.02, 25.60, 24.14, 19.21. APCI-MS (+): m/z 456.4 $[M+H]^+$,anal. calcd. for $C_{25}H_{33}N_3O_5$: C, 65.91%, H, 7.30%, N, 9.22%. Found: C, 65.93%, H, 7.55%, N, 8.84%.

3d: Diethyl-2,6-dimethyl-4-{3-nitro-4-[3-(piperidin-1-yl)propoxy]phenyl}-1,4-dihydropyridine-3,5-dicarboxylate hydrochloride (**3d**). Hygroscopic yellow solid, yield 41%, m.p. 111.8 °C. ^{1}H NMR (300 MHz, $CDCl_3$) δ 7.74 (d, 4J = 2.2 Hz, 1H), 7.46 (dd, $^{3,4}J$ = 8.6, 2.3 Hz, 1H), 6.87 (d, *J* = 8.6 Hz, 1H), 6.50 (s, 1H), 4.96 (s, 1H), 4.15 (t, *J* = 5.4 Hz, 2H), 4.12-4.01 (m, 4H), 3.22-2.93 (m, 6H, overlap), 2.51-2.38 (m, 2H), 2.35 (s, 6H), 2.02 (br, 4H), 1.65 (br, 2H), 1.21 (t, *J* = 7.1 Hz, 6H). ^{13}C NMR (75 MHz, $CDCl_3$) δ 167.38, 150.21, 145.16, 141.77, 139.00, 134.45, 125.31, 114.16, 103.14, 66.72, 60.00, 55.20, 53.81, 39.06, 24.18, 22.81, 22.31, 19.56, 14.40. LC-MS (ESI)for $C_{27}H_{37}N_3O_7$ m/z calculated 516.27, found 516.32 $[M+H]^+$ purity 98.5%.

3e: 3,5-Dicyano-2,6-dimethyl-4-{4-[3-(piperidin-1-yl)propoxy]phenyl}-1,4-dihydropyridine (**3e**). White solid, yield 19%, m.p. 131.6 °C. ^{1}H NMR (300 MHz, $CDCl_3$) δ 7.15 (d, *J* = 8.6 Hz, 2H), 6.87 (d, *J* = 8.6 Hz, 2H), 6.71 (br, 1H), 4.26 (s, 1H), 3.99 (t, *J* = 6.3 Hz, 2H), 2.57-2.35 (m, 6H, overlap=, 2.06

This preprint research paper has not been peer reviewed. Electronic copy available at: https://ssrn.com/abstract=5133249

(s, 6H), 2.03-1.93 (m, 2H), 1.62 (p, *J* = 5.6 Hz, 4H), 1.52-1.40 (m, 2H). ^{13}C NMR (75 MHz, $CDCl_3$) δ 158.92, 145.16, 135.11, 128.90, 118.99, 115.05, 85.39, 66.52, 56.03, 54.67, 41.42, 26.70, 25.81, 24.35, 18.56. LC-MS (ESI) for $C_{23}H_{28}N_4O$ m/z calculated 377.23, found 377.15 $[M+H]^+$ purity 96.16%.

3f: 3-Acetyl-2,6-dimethyl-4-phenyl-5-{4-[3-(piperidin-1-yl)propoxy]benzoyl}-1,4-dihydropyridine (**3f**). Yellow solid, yield 22%, m. p. 74.0 °C. ^{1}H NMR (300 MHz, $CDCl_3$) δ 7.52 (d, *J* = 8.8 Hz, 2H), 7.22-7.13 (m, 2H), 7.13-7.03 (m, 3H, overlap), 6.82 (d, *J* = 8.8 Hz, 2H), 6.13 (s, 1H), 5.08 (s, 1H), 4.02 (t, *J* = 6.3 Hz, 2H), 2.56-2.49 (m, 2H), 2.49-2.44 (m, 4H), 2.42 (s, 3H), 2.07 (s, 2H), 2.05-1.92 (m, 2H), 1.73 (s, 3H), 1.62 (p, *J* = 5.6 Hz, 4H), 1.51-1.39 (m, 2H). ^{13}C NMR (75 MHz, $CDCl_3$) δ 198.86, 197.56, 162.40, 145.78, 145.64, 136.32, 132.47, 131.02, 128.72, 127.12, 126.68, 115.25, 114.29, 109.78, 66.62, 55.87, 54.62, 43.41, 29.60, 26.46, 25.67, 24.24, 20.70, 18.39. LC-MS (ESI) for $C_{30}H_{36}N_2O_3$ m/z calculated 473.28, found 473.23 $[M+H]^+$ purity 97.39%.

General procedure of the synthesis of urea derivatives

Compound **5b** was synthesized by adding 4 mL $LiAlH_4$ (1 M) in THF dropwise to a solution of carboxamide derivative **4b** (1.37 mmol) in 20 mL THF at r.t. The reaction was heated at reflux for 2 h and quenched with H_2O dropwise at 0 °C until no more gas developed. The mixture was filtered, the filtrate collected and dried in a rotary evaporator. It was dissolved in EtOAc and washed with 20 mL H_2O, 20 mL 1 M NaOH and 20 mL brine. The organic layer was dried with $MgSO_4$ and concentrated in a rotary evaporator. The obtained product phenylpropylamine derivative was directly used in the next steps.

Compounds **5a-d** were synthesized by dissolving benzylamine derivative **4a** (10.2 or 1 mmol; compound **5a**, 5c) or phenylpropylamine derivative **4b** (0.5 mmol; compound **5b**, **5d**) and cyclohexyl isocyanate (**5a**:11.9 mmol, **5b**: 0.5 mmol) respectively phenyl isocyanate (0.9 mmol; **5c**, **5d**) in 80 (**5a**) or 10 mL (**5b-d**) THF at r.t. For compound **5c** TEA (2.5 mmol) was added to reveal the primary amine. The reaction was stirred for 18 h and concentrated in a rotary evaporator.

Compounds **5e** and **5f** were synthesized from Tyramine hydrochloride (1.5 mmol) and TEA (1.95 mmol) stirred in 25 mL MeCN for 1 h. Subsequently, c-Hexyl or phenyl isocyanate (1.5 mmol) was added to

This preprint research paper has not been peer reviewed. Electronic copy available at: https://ssrn.com/abstract=5133249

the solution and stirred at r.t. for 18 h. 1-(3-Chloropropyl)piperidine (**5e**: 5 mmol, **5f**: 1 mmol), K_2CO_3 (**5e**: 20 mmol, **5f**: 2.90 mmol) and KI (**5e**: 0.5 mmol, **5f**: catalytic amount) were added to the reaction mixture. For compound **5e** 30 mL acetone were added and boiled under reflux for 18 (**5e**) or 24 h (**5f**). After cooling down to r.t., the suspension was filtered and rinsed with 20 mL acetone. The filtrate was combined, concentrated in a rotary evaporator.

The residues were purified with column chromatography using DCM and MeOH as eluents (gradient ratio 95:5 to 90:10). To obtain compound **5a**, the purified product was treated with HCl in dioxane to obtain the corresponding salt.

Melting point, NMR, MS, LC-MS and elemental analysis data for final compounds **5a** – **5f** (**^{1}H and ^{13}C NMRs see Figure S13-S24)**

5a: 1-Cyclohexyl-3-{4-[3-(piperidin-1-yl)propoxy]benzyl}urea hydrochloride (**5a**). White solid, yield quantitative, m.p. 189.3 °C. ^{1}H NMR (300 MHz, DMSO-d^6) δ 11.13 (s, 1H), 7.57 (d, *J* = 8.6 Hz, 2H), 7.29 (d, *J* = 8.6 Hz, 2H), 4.53 (s, 2H), 4.43 (t, *J* = 6.1 Hz, 2H), 3.92-3.70 (m, 3H, overlap), 3.55 (dt, *J* = 10.5, 5.1 Hz, 2H), 3.28 (dt, *J* = 12.0, 8.3 Hz, 2H), 2.60 (dq, *J* = 11.7, 6.1 Hz, 2H), 2.36-1.36 (m, 16H, overlap), ^{13}C NMR (75 MHz, DMSO-d^6) δ 157.47, 157.03, 133.25, 128.31, 114.26, 65.07, 53.40, 51.94, 47.79, 42.22, 33.29, 25.34, 24.46, 23.28, 21.43. LC-MS (ESI) for $C_{22}H_{35}N_3O_2$ m/z calculated 374.28, found m/z 374.23 $[M+H]^+$ purity 100%.

5b: 1-Cyclohexyl-3-(3-{4-[3-(piperidin-1yl)propoxy]phenyl}propyl)urea hydrochloride (**5b**). White solid, yield 55%, m.p. 134.9 °C. ^{1}H NMR (300 MHz, DMSO-d^6) δ 10.61 (s, 1H), 7.10 (d, *J* = 8.5 Hz, 2H), 6.84 (d, *J* = 8.6 Hz, 2H), 4.00 (t, *J* = 6.0 Hz, 2H), 3.50-3.36 (m, 2H), 3.37-3.27 (m, 1H), 3.13 (dt, *J* = 8.3, 5.1 Hz, 2H), 2.94 (t, *J* = 6.9 Hz, 2H), 2.89-2.76 (m, 2H), 2.54-2.43 (m, 2H), 2.18 (dq, *J* = 11.7, 6.0 Hz, 2H), 1-93-0.89 (m, 18H, overlap). ^{13}C NMR (75 MHz, DMSO-d^6) δ 157.43, 156.29, 133.98, 129.08, 114.30, 64.98, 53.32, 51.88, 47.60, 38.57, 33.16, 31.88, 31.47, 25.23, 24-31, 23.24, 22.18, 21.29. LC-MS (ESI) for $C_{24}H_{39}N_3O_2$ m/z calculated 402.31, found 402.27 $[M+H]^+$ purity 95.63%.

5c: 1-Phenyl-3-{4-[3-(piperidin-1-yl)propoxy]benzyl}urea (**5c**). White solid, yield 44%, m.p. 145.2 °C. ^{1}H NMR (300 MHz, DMSO-d^6) δ 8.47 (s, 1H), 7.39 (dd, *J* = 8.7, 1.1 Hz, 2H), 7.27-7.15 (m, 4H, overlap),

This preprint research paper has not been peer reviewed. Electronic copy available at: https://ssrn.com/abstract=5133249

6.94-6.82 (m, 3H, overlap), 6.49 (t, *J* = 5.9 Hz, 1H), 4.21 (d, *J* = 5.8 Hz, 2H), 3.95 (t, *J* = 6.4 Hz, 2H), 2.41-2.26 (m, 6H, overlap), 1.83 (p, *J* = 6.5 Hz, 2H), 1.48 (p, *J* = 5.5 Hz, 4H), 1.42-1.29 (m, 2H). ^{13}C NMR (75 MHz, DMSO-d^6) δ 157.59, 155.16, 140.48, 132.13, 128.64, 128.48, 121.04, 117.64, 114.29, 65.93, 55.18, 54.13, 42.20, 26.32, 25.62, 24.16. LC-MS (ESI) for $C_{22}H_{29}N_3O_2$ m/z calculated 368.23, found 368.15 $[M+H]^+$ purity 97.90%.

5d: 1-Phenyl-3-(3-{4-[3-(piperidin-1-yl)propoxy]phenyl}propyl)urea hydrochloride (**5d**). White solid, yield 58%, m.p. 173.2 °C. ^{1}H NMR (300 MHz, DMSO-d^6) δ 10.30 (br, 1H), 8.84 (s, 1H), 7.39 (d, *J* = 8.0 Hz, 2H), 7.19 (t, *J* = 7.8 Hz, 2H), 7.14 (d, *J* = 8.1 Hz, 2H), 6.85 (d, *J* = 8.1 Hz, 3H), 6.52 (t, *J* = 5.6 Hz, 1H), 4.01 (t, *J* = 6.0 Hz, 2H), 3.45-3.40 (m, 2H), 3.14 (t, *J* = 7.9 Hz, 2H), 3.05 (q, *J* = 6.5 Hz, 2H), 2.90-2.81 (m, 2H), 2.55 (t, *J* = 7.6 Hz, 2H), 2.16 (dq, *J* = 11.9, 6.1 Hz, 2H), 1.82-1.74 (m, 4H, overlap), 1.71-1.64 (m, 3H, overlap), 1-42-1.34 (m, 1H). ^{13}C NMR (75 MHz, DMSO-d^6) δ 156.38, 155.38, 140.74, 133.91, 129.28, 128.57, 120.73, 117.38, 114.33, 64.91, 53.45, 52.00, 38.40, 31.78, 31.51, 23.35, 22.38, 21.38. LC-MS (ESI) for $C_{24}H_{33}N_3O_2$ m/z calculated 396.27, found 396.20 $[M+H]^+$ purity 95.05%.

5e: 1-Cyclohexyl-3-{4-[3-[piperidin-1-yl)propoxy]phenethyl}urea hydrochloride (**5e**). White to light beige solid, yield 70%, m.p. 160.2 °C. ^{1}H NMR (300 MHz, DMSO-d^6) δ 10.74 (s, 1H), 7.10 (d, *J* = 8.6 Hz, 2H), 6.85 (d, *J* = 8.6 Hz,2H), 4.00 (t, *J* = 6.1 Hz, 2H), 3.46-3.36 (m, 2H), 3.32 (dt, *J* = 10.0, 3.8 Hz, 1H), 3.21-3.06 (m, 4H, overlap), 2.86 (tdd, *J* = 12.2, 9.1, 3.7 Hz, 2H), 2.58 (t, *J* = 7.3 Hz, 2H), 2.18 (dq, *J* = 11.6, 6.1 Hz, 2H), 2.58 (t, *J* = 7.3 Hz, 2H), 2.18 (dq, *J* = 11.6, 6.1 Hz, 2H), 1.94-0.95 (m, 16H, overlap). ^{13}C NMR (75 MHz, DMSO-d^6) δ 157.40, 156.63, 131.96, 129.62, 114.36, 65.02, 53.41, 51.94, 47.70, 41.14, 35.30, 33.28, 25.33, 24.46, 23.30, 22.31, 21.43. LC-MS (ESI) for $C_{23}H_{27}N_3O_2$ m/z calculated 388.30, found 388.27 $[M+H]^+$ purity 98.71%.

5f: 1-Phenyl-3-{4-[3-(piperidin-1-yl)propoxy]phenethyl}urea (**5f**). White to light beige solid, yield 29%, m.p. 133.0 °C. ^{1}H NMR (300 MHz, $CDCl_3$) δ. 7.34-7.22 (m, 4H), 7.14-6.98 (m, 3H, overlap), 6.88 (s, 1H), 6.82 (d, *J* = 8.6 Hz, 2H), 5.13 (t, *J* = 5.7 Hz, 1H), 3.99 (t, *J* = 6.3 Hz, 2H), 3.44 (q, *J* = 6.7 Hz, 2H), 2.75 (t, *J* = 6.8 Hz, 2H), 2.60-2.44 (m, 6H, overlap), 2.10-1.93 (m, 2H), 1.66 (p, *J* = 5.5 Hz, 4H), 1.55-1.43 (m, 2H). ^{13}C NMR (75 MHz, $CDCl_3$) δ 157.68, 156.26, 139.22, 131.31, 129.83, 129.18,

This preprint research paper has not been peer reviewed. Electronic copy available at: https://ssrn.com/abstract=5133249

Preprint not peer reviewed

123.29, 120.56, 114.90, 66.48, 55.98, 54.69, 41.72, 35.51, 26.68, 25.77, 24.33. LC-MS (ESI) for $C_{23}H_{31}N_3O_2$ m/z calculated 382.25, found 382.18 $[M+H]^+$ purity 100%.

General procedure for the synthesis of *N,N'*-disubstituted barbituric acid derivatives

Compounds **6a** and **6b** were synthesized as reported previously [34].The urea derivatives **5a** or rather **5e** (2 mmol) and malonic acid (2 mmol) were dissolved in 8 mL of $(Ac)_2O$. and the obtained mixture was radiated in the microwave at 60 °C for 10 min. The reaction was quenched by adding 3 mL of H_2O dropwise at 0 °C and the solution was concentrated in the rotary evaporator. The residue was purified with column chromatography by using solvent mixtures of DCM and MeOH (gradient ratio from 90:10 to 85:15) as eluents. The corresponding salts were obtained by treating with HCl in EtOAc.

Melting point, NMR, MS, LC-MS and elemental analysis data for final compounds **6a**,**6b** (**^{1}H** and ^{13}C NMRs see **Figure S25-S28)**

6a: 1-Cyclohexyl-3-{4-[3-(piperidin-1-yl)propoxy]benzyl}-1,3-diazinane-2,4,6-trione hydrochloride (**6a**). White solid, yield 78%, m.p. 229.2 °C. ^{1}H NMR (300 MHz, $CDCl_3$) δ 12.15 (s, 1H), 7.34 (d, *J* = 8.7 Hz, 2H), 6.77 (d, *J* = 8.7 Hz, 2H), 4.92 (s, 2H), 4.56 (tt, $^{3,4}J$ = 12.3, 3.7 Hz, 1H), 4.03 (t, *J* = 5.5. Hz, 2H), 3.60 (s, 2H), 3.59-3.49 (m, 2H), 3.12 (dt, *J* = 10.5, 5.2 Hz, 2H), 2.74-2.56 (m, 4H), 1.68-1.51 (m, 2H), 1.50-1.07 (m, 6H). ^{13}C NMR (75 MHz, $CDCl_3$) δ 184.85, 164.80, 158.03, 151.42, 130.88, 129.22, 114.38, 65.05, 55.57, 55.40, 53.55, 44.39, 40.47, 29.11, 26.35, 25.16, 23.91, 22.63, 22.21. LC-MS (ESI) for $C_{25}H_{35}N_3O_4$ m/z calculated 442.27, found 442.23 $[M+H]^+$ purity 99.35%.

6b: 1-Cyclohexyl-3-{4-[3-(piperidin-1-yl)propoxy]phenethyl}-1,3-diazinane-2,4,6-trione hydrochloride (6b). White to light beige solid, yield 33%, m.p. 185.4 °C. ^{1}H NMR (300 MHz, $CDCl_3$) δ 12.17 (s, 1H), 7.12 (d, *J* = 8.5 Hz, 2H), 6.76 (d, *J* = 8.6 Hz, 2H), 4.56 (tt, $^{3,4}J$ = 12.2, 3.7 Hz, 1H), 4.06-3.95 (m, 4H, overlap), 3.61-3.51 (m, 4H, overlap), 3.20-3.07 (m, 2H), 2.35-2.13 (m, 4H), 1.97-1.74 (m, 6H), 1.70-1.51 (m, 2H), 1.50-1.09 (m, 4H). ^{13}C NMR (75 MHz, $CDCl_3$) δ 164.91, 164.62, 157.14, 151.21, 130.69, 130.14, 114.49, 65.03, 55.50, 55.41, 53.58, 43.14, 40.34, 33.15, 29.15, 26.38, 25.19, 23.97, 22.64, 22.24. LC-MS (ESI) for $C_{26}H_{37}N_3O_4$ m/z calculated 456.29, found 456.24 $[M+H]^+$ purity 98.62%.

Preprint not peer reviewed

This preprint research paper has not been peer reviewed. Electronic copy available at: https://ssrn.com/abstract=5133249

General procedure for the synthesis of dihydropyrimidine derivatives

Compound **8a**, **b** were synthesized as follows, the Biginelli product **7a** (1.91 mmol, for **8a**) or **7b** (3.33 mmol, for **8b**), alkyl chloride 2 (2 or 3.34 mmol), KI (1 mmol or catalytic amoiunt), and K_2CO_3 (6 or 8 mmol) were dissolved in 15 mL DMF respectively 30 mL acetone. The reaction was heated to 70 °C for 40 h. The purification was performed via column chromatography using DCM and MeOH as eluent (gradient 95:5 to 85:15). The purified product of compound **8a** was treated with HCl in EtOAc to obtain the corresponding salt.

Compounds **8c** and **8d** were synthesized via a modified method reported previously [37]. Compound **8a** or **8b** (1.4 or 0.5 mmol), Ac_2O (3.5 or 1.2 mmol), TEA (3.5 or 1.2 mmol), and DMAP (0.28 or 0.1 mmol) were dissolved in 3 or 1 mL MeCN. The solution was heated in the microwave to 130 °C for 10 min. The obtained solution was concentrated in a rotary evaporator and purified with column chromatography with DCM and MeOH as eluents (ratio from 95:5 to 90:10).

Melting point, NMR, MS, LC-MS and elemental analysis data for final compounds **8a** – **8d** (**^{1}H and ^{13}C NMRs see Figure S29-S36)**

8a: 5-Acetyl-6-methyl-4-{4-[3-(piperidin-1-yl)propoxy]phenyl}-3,4-dihydropyrimidine-2(1*H*)-one hydrochloride (**8a**). Light yellowish solid, yield 78%, m.p. 228.7 °C. ^{1}H NMR (300 MHz, DMSO-d^6) δ 10.66 (s, 1H), 9.15 (d, ^4J = 2.0 Hz, 1H), 7.77 (dd, $^{3,4}J$ = 3.6, 2.0 Hz, 1H), 7.16 (d, J = 8.7 Hz, 2H), 6.89 (d, J = 8.7 Hz, 2H), 5.20 (d, J = 3.4 Hz, 1H), 4.02 (t, J = 6.0 Hz, 2H), 3.41 (d, J = 12.3 Hz, 2H), 3.19-3.05 (m, 2H), 2.94-2.76 (m, 2H), 2.28 (s, 3H), 2.25-2.10 (m, 2H), 2.07 (s, 3H), 1.89-1.64 (m, 5H, overlap), 1.45-1.31 (m, 1H). ^{13}C NMR (75 MHz, DMSO-d^6) δ 194.34, 157.52, 152.07, 147.89, 136.65, 127.67, 114.43, 109.57, 65.07, 53.37, 53.24, 51.93, 30.19, 23.23, 22.30, 21.41, 18.85. LC-MS (ESI) for $C_{21}H_{29}N_3O_3$ m/z calculated 372.23 found 372.29 $[M+H]^+$ purity 100%

8b: Ethyl-6-methyl-2-oxo-4-{4-[3-(piperidin-1-yl)-propoxy]phenyl}-1,2,3,4-tetrahydropyrimidine-5-carboxylate (**8b**). White solid, yield 84%, m.p. 147.4 °C. ^{1}H NMR (300 MHz, DMSO-d^6) δ 9.14 (d, ^4J = 2.0 Hz, 1H), 7.65 (dd, $^{3,4}J$ 2.1 Hz, 1H), 7.13 (d, J = 8.7 Hz, 2H), 6.86 (d, J = 8.7 Hz, 1H), 5.08 (d, J = 3.3 Hz, 1H), 4.07-3.90 (m, 4H, overlap), 2.51-2.31 (m, 6H, overlap), 2.23 (s, 3H), 1.93-1.79 (m, 2H),

Preprint not peer reviewed

This preprint research paper has not been peer reviewed. Electronic copy available at: https://ssrn.com/abstract=5133249

1.59-1.45 (m, 4H), 1.44-1,34 (m, 2H), 1.10 (t, *J* = 7.1 Hz, 3H). ^{13}C NMR (75 MHz, DMSO-d^6) δ 165.38, 157.79, 152.15, 148.00, 137.02, 127.40, 114.24, 99.56, 65.77, 59.15, 54.94, 53.85, 53.34, 25.92, 25.20, 23.78, 17.77, 14.11. LC-MS (ESI) for $C_{22}H_{31}N_3O_4$ m/z calculated 402.24, found 402.28 $[M+H]^+$ purity 100%.

8c: 3,5-Diacetyl-6-methyl-4-{4-[3-(piperidin-1-yl)propoxy]phenyl}-3,4-dihydropyrimidine-2(1*H*)-one (**8c**). Beige solid, yield 78%, m.p. 163.7 °C. ^{1}H NMR (300 MHz, $CDCl_3$) δ 8.23 (s, 1H), 7.23 (d, *J* = 8.7 Hz, 2H), 6.80 (d, *J* = 8.8 Hz, 2H), 6.64 (s, 1H), 3,95 (t, *J* = 6.3 Hz, 2H), 2.54 (s, 3H), 2.50-2.34 (m, 9H, overlap), 2.18 (s, 3H), 2.02-1.87 (m, 2H), 1.58 (p, *J* = 5.5 Hz, 4H, 1.49-1.36 (m, 2H). ^{13}C NMR (75 MHz, $CDCl_3$) δ 195.68, 171.63, 159.20, 151.91, 144.92, 130.55, 128.74, 114.86, 113.46, 66.55, 56.01, 54.71, 53.16, 29.74, 26.76, 26.54, 25.95, 24.46, 18.61. LC-MS (ESI) for $C_{23}H_{31}N_3O_4$ m/z calculated 414.24, found 414.26 $[M+H]^+$ purity 100%.

8d: Ethyl 3-acetyl-6-methyl-2-oxo-4-{4-[3-piperidin-1-yl)propoxy]phenyl}-1,2,3,4-tetrahydro-pyrimidine-5-carboxylate (**8d**). Light yellowish solid, yield 94%, m.p. 159.2 °C. ^{1}H NMR (300 MHz, $CDCl_3$) δ 8.04 (s, 1H), 7.23 (d, *J* = 8.7 Hz, 2H), 6.78 (d, *J* = 8.8 Hz, 2H), 6.56 (s, 1H), 4.15 (q, *J* = 7.1 Hz, 2H), 3.95 (t, *J* = 6.3 Hz, 2H), 2.54 (s, 3H), 2.52-2.41 (m, 6H, overlap), 2.40 (s, 3H), 2.02-1.90 (m, 2H), 1.60 (p, *J* = 5.5 Hz, 4H), 1.49-1.39 (m, 2H), 1.23 (t, *J* = 7.1 Hz, 3H). ^{13}C NMR (75 MHz, $CDCl_3$) δ 171.61, 165.15, 158.82, 152.31, 145.10, 132.03, 128.34, 114.53, 105.90, 66.48, 60.61, 56.04, 54.68, 53.18, 26.76, 26.72, 25.87, 24.41, 17.91, 14.35. LC-MS (ESI) for $C_{24}H_{33}N_3O_5$ m/z calculated 444.25, found 444.29 $[M+H]^+$ purity 100%.

Preprint not peer reviewed

This preprint research paper has not been peer reviewed. Electronic copy available at: https://ssrn.com/abstract=5133249

Declaration of Competing Interest

Philipp Albrecht has participated in meetings sponsored by, received speaker honoraria or travel funding from Abbvie, Biogen, Celgene/Bristol Meyers Squibb, Ipsen, Janssen, Lilly, Merck, Merz, Novartis, Roche, Sanofi-Genzyme and Teva, and received honoraria for consulting Abbvie, Novartis, Roche. He has received unrestricted research grants from German Research Association (DFG), EFRE-NRW, Celgene/Bristol Meyers Squibb, Merz, Novartis, and Roche. The other authors declare no competing interests.

Acknowledgments

This work was supported by the European Community Marie Skłodowska-Curie COFUND (847681, ARDRE) and in part by the Austrian Science Fund (FWF, DOI 10.55776/P35722, DOI 10.55776/P35087, DOI 10.55776/DOC30, 10.55776/DOC178).

Preprint not peer reviewed

This preprint research paper has not been peer reviewed. Electronic copy available at: https://ssrn.com/abstract=5133249

References

[1] Lovenberg, T.W., et al., Cloning and Functional Expression of the Human Histamine H 3 Receptor. Mol. Pharmacol., 55 (1999) 1101-1107. DOI: 10.1124/mol.55.6.1101.
[2] Jutel, M., M. Akdis, and C.A. Akdis, Histamine, histamine receptors and their role in immune pathology. Clin. Exp. Allergy, 39 (2009) 1786-800. DOI: 10.1111/j.1365-2222.2009.03374.x.
[3] Alhusaini, M., et al., Revisiting Preclinical Observations of Several Histamine H3 Receptor Antagonists/Inverse Agonists in Cognitive Impairment, Anxiety, Depression, and Sleep-Wake Cycle Disorder. Front. Pharmacol., 13 (2022) 861094. DOI: 10.3389/fphar.2022.861094.
[4] Panula, P. and S. Nuutinen, The histaminergic network in the brain: basic organization and role in disease. Nat. Rev. Neurosci., 14 (2013) 472-487. DOI: 10.1038/nrn3526.
[5] Shan, L., A.-M. Bao, and D.F. Swaab, The human histaminergic system in neuropsychiatric disorders. Trends Neurosci., 38 (2015) 167-177. DOI: 10.1016/j.tins.2014.12.008.
[6] Schwartz, J.-C., The histamine H3 receptor: from discovery to clinical trials with pitolisant. Br. J. Pharmacol., 163 (2011) 713-721. DOI: 10.1111/j.1476-5381.2011.01286.x.
[7] European Medicines Agency. Wakix -EPAR: summary public. EMA/63272. 2016. [accessed on: Feb. 02, 2025]. Available from: https://www.ema.europa.eu/en/medicines/human/EPAR/wakix.
[8] Food Drug Administration. Wakix (pitolisant) NDA Approval. NDA 211150. 2019. [accessed on: Feb. 02, 2025]. Available from: https://www.accessdata.fda.gov/scripts/cder/daf/index.cfm?event=BasicSearch.process.
[9] European Medicines Agency. Ozawade - EPAR: medicines overview. EMA/371398. 2021. [accessed on: Feb. 02, 2025]. Available from: https://www.ema.europa.eu/en/medicines/human/EPAR/ozawade.
[10] Gribkoff, V.K. and L.K. Kaczmarek, The need for new approaches in CNS drug discovery: Why drugs have failed, and what can be done to improve outcomes. Neuropharmacol., 120 (2017) 11-19. DOI: 10.1016/j.neuropharm.2016.03.021.
[11] Proschak, E., H. Stark, and D. Merk, Polypharmacology by Design: A Medicinal Chemist's Perspective on Multitargeting Compounds. J. Med. Chem., 62 (2019) 420-444. DOI: 10.1021/acs.jmedchem.8b00760.
[12] Anighoro, A., J. Bajorath, and G. Rastelli, Polypharmacology: challenges and opportunities in drug discovery. J. Med. Chem., 57 (2014) 7874-7887. DOI: 10.1021/jm5006463.
[13] Khanfar, M.A., et al., Multiple Targeting Approaches on Histamine H3 Receptor Antagonists. Front. Neurosci., 10 (2016) 201. DOI: 10.3389/fnins.2016.00201.
[14] Malek, R., et al., New Dual Small Molecules for Alzheimer's Disease Therapy Combining Histamine H3 Receptor (H3R) Antagonism and Calcium Channels Blockade with Additional Cholinesterase Inhibition. J. Med. Chem., 62 (2019) 11416-11422. DOI: 10.1021/acs.jmedchem.9b00937.
[15] Malek, R., et al., Discovery of New Highly Potent Histamine H3 Receptor Antagonists, Calcium Channel Blockers, and Acetylcholinesterase Inhibitors. ACS Chem. Neurosci., 15 (2024) 3363-3383. DOI: 10.1021/acschemneuro.4c00341.
[16] Kang, S., et al., CaV1.3-selective L-type calcium channel antagonists as potential new therapeutics for Parkinson's disease. Nat. Commun., 3 (2012) 1146. DOI: 10.1038/ncomms2149.
[17] Scriabine, A. and W. van den Kerckhoff, Pharmacology of nimodipine. A review. Ann. N. Y. Acad. Sci., 522 (1988) 698-706. DOI: 10.1111/j.1749-6632.1988.tb33415.x.
[18] Grover, G.J., et al., Pharmacologic Profile of the Dihydropyrimidine Calcium Channel Blockers SQ 32,547 and SQ 32,946. J. Cardiovasc. Pharmacol., 26 (1995) 289. DOI: 10.1097/00005344-199508000-00015.
[19] Cain, S.M. and T.P. Snutch, Voltage-gated calcium channels and disease. BioFactors, 37 (2011) 197-205. DOI: 10.1002/biof.158.
[20] Striessnig, J., Voltage-Gated Ca(2+)-Channel alpha1-Subunit de novo Missense Mutations: Gain or Loss of Function - Implications for Potential Therapies. Front. Synaptic Neurosci., 13 (2021) 634760. DOI: 10.3389/fnsyn.2021.634760.
[21] Kabir, Z.D., A. Martinez-Rivera, and A.M. Rajadhyaksha, From Gene to Behavior: L-Type Calcium Channel Mechanisms Underlying Neuropsychiatric Symptoms. Neurotherapeutics, 14 (2017) 588-613. DOI: 10.1007/s13311-017-0532-0.

This preprint research paper has not been peer reviewed. Electronic copy available at: https://ssrn.com/abstract=5133249

[22] Splawski, I., et al., Ca(V)1.2 calcium channel dysfunction causes a multisystem disorder including arrhythmia and autism. Cell, 119 (2004) 19-31. DOI: 10.1016/j.cell.2004.09.011.
[23] Ortner, N.J., et al., De novo CACNA1D Ca(2+) channelopathies: clinical phenotypes and molecular mechanism. Pflügers Arch., 472 (2020) 755-773. DOI: 10.1007/s00424-020-02418-w.
[24] Guzman, J.N., et al., Oxidant stress evoked by pacemaking in dopaminergic neurons is attenuated by DJ-1. Nature, 468 (2010) 696-700. DOI: 10.1038/nature09536.
[25] Filippini, L., et al., Cav 1.3-selective inhibitors of voltage-gated L-type Ca2+ channels: Fact or (still) fiction? Br. J. Pharmacol., 180 (2023) 1289-1303. DOI: 10.1111/bph.16060.
[26] Pasternak, B., et al., Use of calcium channel blockers and Parkinson's disease. Am. J. Epidemiol., 175 (2012) 627-635. DOI: 10.1093/aje/kwr362.
[27] Barbier, A.J., et al., Acute wake-promoting actions of JNJ-5207852, a novel, diamine-based H3 antagonist. Br. J. Pharmacol., 143 (2004) 649-661. DOI: 10.1038/sj.bjp.0705964.
[28] Wingen, K. and H. Stark, Scaffold variations in amine warhead of histamine H_3 receptor antagonists. Drug Discov. Today Technol., 10 (2013) e483-9. DOI: 10.1016/j.ddtec.2013.07.001.
[29] Striessnig, J., et al., The Molecular Basis of Ca2+ Antagonist Drug Action-Recent Developments, in Voltage-Gated Calcium Channels, G.W. Zamponi, Editor. 2005, Eurekah.com and Kluwer Academic / Plenum Publishers: Boston, MA. p. 262-280.
[30] Cooper, G., et al., A Single Amino Acid Determines the Selectivity and Efficacy of Selective Negative Allosteric Modulators of CaV1.3 L-Type Calcium Channels. ACS Chem. Biol., 15 (2020) 2539-2550. DOI: 10.1021/acschembio.0c00577.
[31] Ortner, N.J., et al., Pyrimidine-2,4,6-triones are a new class of voltage-gated L-type Ca2+ channel activators. Nat. Commun., 5 (2014) 3897. DOI: 10.1038/ncomms4897.
[32] Huang, H., et al., Modest CaV1.342-selective inhibition by compound 8 is beta-subunit dependent. Nat. Commun., 5 (2014) 4481. DOI: 10.1038/ncomms5481.
[33] Zhong, S., Syntheses and evaluation of novel histamine H3 receptor ligands and multi-target-directed ligands as neuroprotective agents. 2021, Heinrich-Heine Universität: Düsseldorf.
[34] Sander, K., et al., Kojic acid derivatives as histamine H(3) receptor ligands. Chem. Pharm. Bull. (Tokyo), 58 (2010) 1353-1361. DOI: 10.1248/cpb.58.1353.
[35] Milite, C., et al., A novel cell-permeable, selective, and noncompetitive inhibitor of KAT3 histone acetyltransferases from a combined molecular pruning/classical isosterism approach. J. Med. Chem., 58 (2015) 2779-2798. DOI: 10.1021/jm5019687.
[36] Yang, X.-B., et al., Zirconium(IV) 4-sulphophenylethyliminobismethylphosphonate as an efficient and reusable catalyst for one-pot synthesis of 3,4-dihydropyrimidones under solvent-free conditions. Chem. Pap., 65 (2011) 829-834. DOI: 10.2478/s11696-011-0091-5.
[37] Kiyani, H. and M. Ghiasi, Solvent-free efficient one-pot synthesis of Biginelli and Hantzsch compounds catalyzed by potassium phthalimide as a green and reusable organocatalyst. Res. Chem. Intermed., 41 (2015) 5177-5203. DOI: 10.1007/s11164-014-1621-x.
[38] Dallinger, D., N.Y. Gorobets, and C.O. Kappe, High-throughput synthesis of N3-acylated dihydropyrimidines combining microwave-assisted synthesis and scavenging techniques. Org. Lett., 5 (2003) 1205-1208. DOI: 10.1021/ol034085v.
[39] Yasuda, S.U. and K.J. Tietze, Nimodipine in the treatment of subarachnoid hemorrhage. DICP, 23 (1989) 451-455. DOI: 10.1177/106002808902300602.
[40] Chang, C.-C., et al., Antagonism of 4-substituted 1,4-dihydropyridine-3,5-dicarboxylates toward voltage-dependent L-type Ca2+ channels Ca V 1.3 and Ca V 1.2. Biorg. Med. Chem., 18 (2010) 3147-3158. DOI: 10.1016/j.bmc.2010.03.038.
[41] Török, F., et al., Inactivation induced by pathogenic Ca(v)1.3 L-type Ca(2+)-channel variants enhances sensitivity for dihydropyridine Ca(2+) channel blockers. Br. J. Pharmacol., 182 (2025) 181-197. DOI: 10.1111/bph.17357.
[42] Kottke, T., et al., Receptor-specific functional efficacies of alkyl imidazoles as dual histamine H3/H4 receptor ligands. Eur. J. Pharmacol., 654 (2011) 200-208. DOI: 10.1016/j.ejphar.2010.12.033.
[43] Sander, K., et al., First metal-containing histamine H3 receptor ligands. Org. Lett., 12 (2010) 2578-2581. DOI: 10.1021/ol100419y.
[44] Cheng, Y.-C. and W.H. Prusoff, Relationship between the inhibition constant (KI) and the concentration of inhibitor which causes 50 per cent inhibition (I50) of an enzymatic reaction. Biochem. Pharmacol., 23 (1973) 3099-3108. DOI: 10.1016/0006-2952(73)90196-2.

This preprint research paper has not been peer reviewed. Electronic copy available at: https://ssrn.com/abstract=5133249

[45] Ortner, N.J., et al., Lower Affinity of Isradipine for L-Type Ca2+ Channels during Substantia Nigra Dopamine Neuron-Like Activity: Implications for Neuroprotection in Parkinson's Disease. J. Neurosci., 37 (2017) 6761-6777. DOI: 10.1523/JNEUROSCI.2946-16.2017.
[46] Tamaddon, F., Z. Razmi, and A.A. Jafari, Synthesis of 3,4-dihydropyrimidin-2(1H)-ones and 1,4-dihydropyridines using ammonium carbonate in water. Tetrahedron Lett., 51 (2010) 1187-1189. DOI: 10.1016/j.tetlet.2009.12.098.

Preprint not peer reviewed

This preprint research paper has not been peer reviewed. Electronic copy available at: https://ssrn.com/abstract=5133249

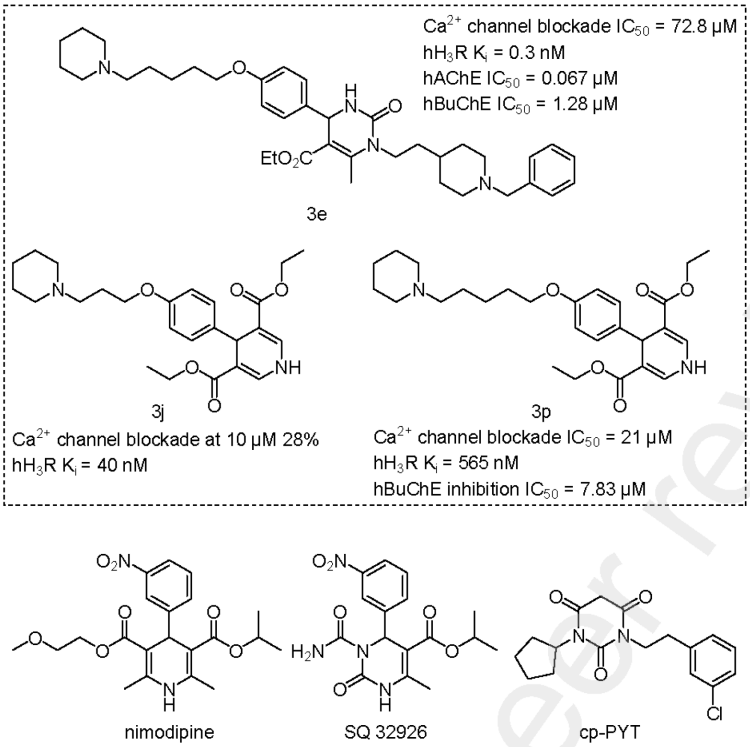
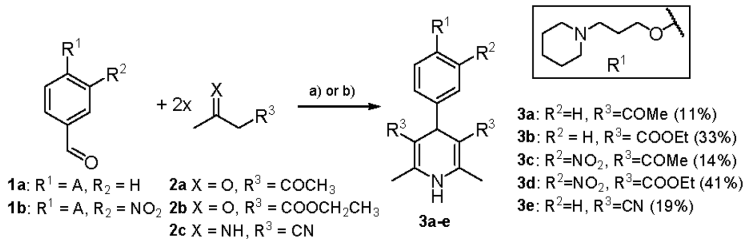


Figure 1: Chemical structures and their biological activities of multi target-directed ligands combining H_3R and Ca^{2+} channel inhibition and chemical structures of known Ca^{2+} channel blockers taken as lead motifs [16.18]. Data for compound 3e [15], for compounds 3j and 3p [14].

Preprint not peer reviewed

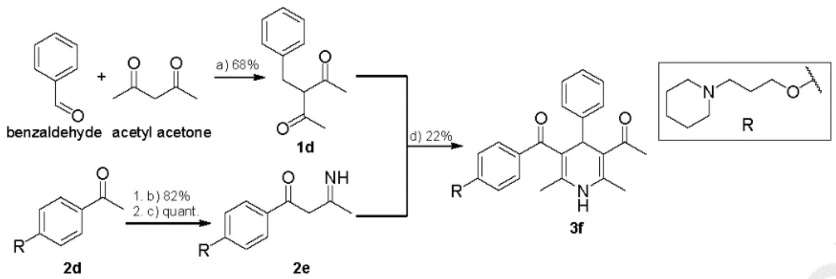
This preprint research paper has not been peer reviewed. Electronic copy available at: https://ssrn.com/abstract=5133249



Scheme 1: Preparation of symmetric dihydropyridines. Chemicals and conditions: a) $(NH_4)_2CO_3$, corresponding α, β-diketone, H_2O, EtOH, 55-60 °C, 4 h; b) AcOH, 120 °C, MW, 10 min.

Preprint not peer reviewed

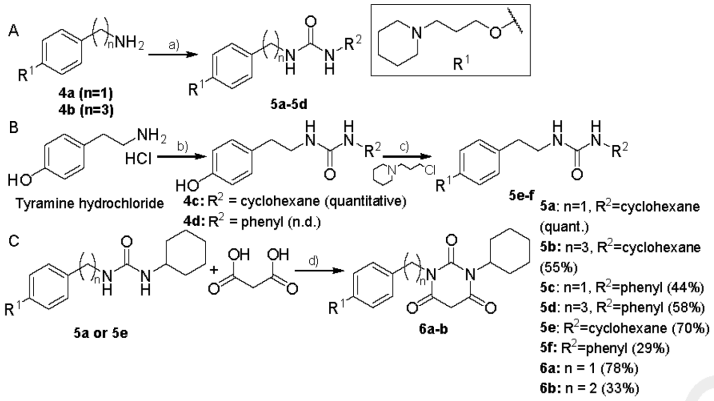
This preprint research paper has not been peer reviewed. Electronic copy available at: https://ssrn.com/abstract=5133249



Scheme 2: Preparation of the asymmetric dihydropyridine. Chemicals and conditions: a) $AlCl_3$, DCM, r.t., 3 h; d) EtOH, MW, 160 °C, 15 min; b) NaH, EtOAc, 18-crown-6-ether, THF, reflux, 3 h c) NH_4OAc, MeOH, reflux, 2 h.

Preprint not peer reviewed

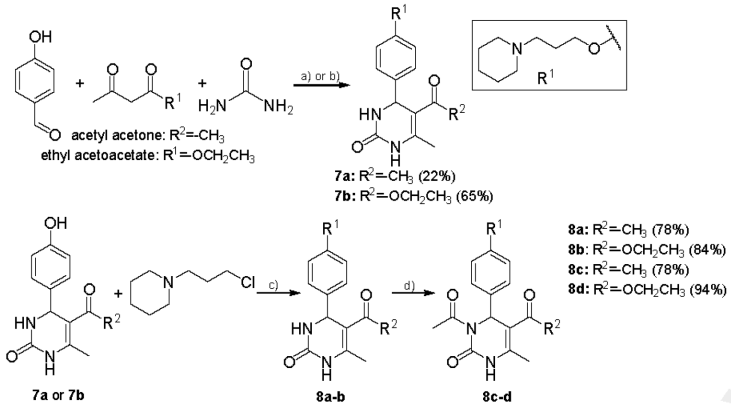
This preprint research paper has not been peer reviewed. Electronic copy available at: https://ssrn.com/abstract=5133249



Scheme 3: Syntheses of urea (A, B) and corresponding barbituric acid derivatives (C). Chemicals and conditions: a) c-hexyl or phenyl isocyanates, THF, r.t. 2 h; b) c-hexyl or phenyl isocyanates, TEA, THF (4c) or MeCN (4d), r.t.; c) K_2CO_3, KI, acetone (4c) or MeCN (4d), reflux, 18 h; d) Ac_2O, MW, 60 °C, 10 min.

Preprint not peer reviewed

This preprint research paper has not been peer reviewed. Electronic copy available at: https://ssrn.com/abstract=5133249



Scheme 4: Biginelli syntheses of dihydropyrimidine derivatives. Chemicals and conditions: a) EtOH, HCl (37%, aq., catalytic amount), reflux, 18 h; b) EtOH, ZrCl4 (catalytic amount), reflux, 15 h; c) acetone, K_2CO_3, KI, reflux, 18 h; d) Ac_2O, TEA, DMAP, MeCN, 130 °C, MW, 10 min.

Preprint not peer reviewed

This preprint research paper has not been peer reviewed. Electronic copy available at: https://ssrn.com/abstract=5133249

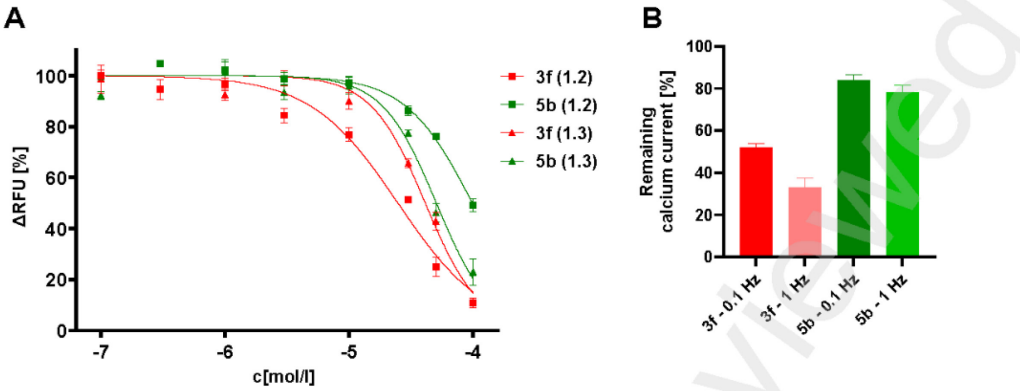


Figure 2: Activity of derivative 3f and 5b over $Ca_V1.2$ and $Ca_V1.3$ Ca^{2+} channels determined by fluorescence assay. (A) Concentration response curves for inhibition of $Ca_V1.2$ and $Ca_V1.3$ under application of various concentrations. Data are presented as mean ± SEM of at least three independent experiments. Inhibition curves of $Ca_V1.2$ and $Ca_V1.3$ channels from derivatives 3f and 5b**. (B)** Remaining Ca^{2+} currents ($Ca_V1.3$) in patch clamp experiments at 0.1 and 1 Hz stimulation frequency.

Preprint not peer reviewed

This preprint research paper has not been peer reviewed. Electronic copy available at: https://ssrn.com/abstract=5133249

Table 1: Results of radioligand displacement assays of hH_3R, hH_1R and hH_4R, and fluorescence Ca^{2+} channel and cytotoxicity assay.

Compound	hH_3 K_i [b] [nM]	hH_1 K_i [b] [nM]	hH_4 K_i [b] [nM]	$Ca_v1.2$ % inhibition[c,d]	$Ca_V1.2$ IC_{50}[c] [µM]	$Ca_V1.3$ % inhibition[c,d]	$Ca_V1.3$ IC_{50}[c] [µM]	Cytotoxicity[c,e] [%]
Pitolisant	12.1 [7.5-19.4]							
Chlorpheniramine		20.2 [12.7-32.0]						
JNJ7777120			9.6 [5.6-16.3]					
Isradipine				103 (± 6.5)	0.0015 (± 0.0009)	102 (±4.5)	0.0089 (±0.001)	
MPP^+								89.3 (±1.9)
3a	3.09 [0.77-12.5]	3942 [674-23071]	>100000	23.8 (± 8.5)		18.7 (± 9.0)		-9.2 (±3.3)
3b[f]	11.4 [5.21-24.8]	1869 [515-6780]	>100000	69.8 (± 12.2)	40.9 (± 2.5)	92.9 (± 3.8)	37.6 (± 1.9)	-1.5 (±5.0)
3c	70.9 [29.0-174]			27.6 (± 4.0)		34.0 (± 7.1)		12.1 (±5.9)
3d	222 [89-554]	9724 [5419-17449]	>100000	96.2 (± 3.7)	14.0 (± 1.1)	95.0 (± 4.9)	11.1 (± 0.8)	11.0 (±3.8)
3e	29.1 [3.14-270]			29.1 (± 15.1)		33.0 (± 9.2)		0.9 (±5.2)
3f	1.56 [0.68-3.60]	2260 [1019-5013]	>100000	76.7 (± 2.6)	25.5 (± 0.7)	88.1 (± 3.9)	40.9 (± 2.0)	-1.9 (±4.3)
5a	18.6 [7.13-48.5]	4214 [1040-17071]	>100000	18.6 (± 5.9)		23.1 (± 10.4)		-6.7 (±2.6)
5b	8.41 [5.96-11.9]	1708 [721-4044]	>100000	26.9 (± 10.7)	103.9 (± 9.4)	82.3 (± 8.0)	43.5 (± 9.8)	-5.0 (±1.8)
5c	125 [82.5-191]			29.3 (± 7.1)		32.5 (± 8.7)		-9.0 (±2.4)
5d	15.4 [2.30-103]	1145 [906-1448]	>100000	63.2 (± 6.1)	56.4 (± 3.6)	82.1 (± 11.7)	43.3 (± 3.6)	-7.1 (±2.7)
5e	29.2 [7.6-112]			13.1 (± 9.3)		48.4 (± 17.7)		-4.2 (±4.9)
5f	21.0 [1.92-229]	3650 [1511-8818]	>100000	31.5 (± 7.9)		32.7 (± 14.7)		-9.9 (±1.9)
6a	98.8 [29.0-337]			12.5 (± 11.5)		22.5 (± 7.6)		-8.1 (±1.7)
6b	34.5 [11.5-104]			16.9 (± 10.9)		23.8 (± 14.2)		-1.3 (±4.1)
8a	61.5 [19.8-191]			6.4 (± 6.1)		2.0 (± 8.5)		-4.2 (±2.1)
8b	45.2 [13.6-151]			12.9 (± 8.8)		18.7 (± 13.8)		0.1 (±1.7)
8c	83.9 [38.5-183]			10.4 (± 5.9)		4.5 (± 7.6)		-4.8 (±4.3)
8d	77.3 [57.1-105]			30.4 (± 7.9)		36.0 (± 8.2)		-2.4 (±5.0)

[b] K_i values are presented as mean with confidence interval (95%) of at least three independent experiments.
[c] Data are presented as mean ± SEM of at least three independent experiments.
[d] One point inhibition values were measured at a concentration of 100 µM.
[e] Cytotoxicity was calculated by subtracting normalized response (cell viability) from 100%.
[f] Compound published as 3f from Malek et al with Ca^{2+} channel blockade 28%, hH_3R K_i value of 40 nM [14].

This preprint research paper has not been peer reviewed. Electronic copy available at: https://ssrn.com/abstract=5133249

Preprint not peer reviewed

Table 2: Inhibition of $Ca_V1.3$ channels by 30 µM of compounds 3f and 5b determined in patch clamp experiments. The remaining Ca^{2+} currents [%] at 0.1 and 1 Hz stimulation frequency is given as mean ± SEM (n-number). Statistics: unpaired student's t-test $^{**}P < 0.01$; no significant difference was observed between 0.1 and 1 Hz for 5b.

compound	Remaining Ca^{2+} current [%] (n)	
	0.1 Hz	1 Hz
3f	52.1 ± 1.81** (4)	33.0 ± 4.51** (4)
5b	83.8 ± 2.56 (3)	78.1 ± 3.63 (3)
Isradipine	IC_{50} = 98.1 nM [41]	-

Preprint not peer reviewed

This preprint research paper has not been peer reviewed. Electronic copy available at: https://ssrn.com/abstract=5133249

3.6 Dual piperidine-based histamine H_3 and sigma-1 receptor ligands in the treatment of nociceptive and neuropathic pain

Katarzyna Szczepańska[1,2], Tadeusz Karcz[1], Maria Dichiara[3], Szczepan Mogilski[4], Justyna Kalinowska-Tłusć ik[3], Bogusław Pilarski[5], Arkadiusz Leniak[7], Wojciech Pietrus[2,7], Sabina Podlewska[2], Katarzyna Popiołek-Barczyk[8], Laura J. Humphrys[9], M. Carmen Ruiz-Cantero[10], David Reiner-Link[11], Luisa Leitzbach[11], Dorota Łażewska[1], Steffen Pockes[9], Michał Górka[7], Adam Zmysłowski[7], Thierry Calmels[12], Enrique J. Cobos[10], Agostino Marrazzo[3], Holger Stark[11], Andrzej J. Bojarski[2], Emanuele Amata[3], and Katarzyna Kieć-Kononowicz[1]

[1]Department of Technology and Biotechnology of Drugs, Faculty of Pharmacy, Jagiellonian University Medical College, Medyczna 9, 30-688 Krakow, Poland, [2]Department of Medicinal Chemistry, Maj Institute of Pharmacology, Polish Academy of Sciences, Smetna 12, 31-343 Krakow, Poland, [3]Department of Drug and Health Sciences, University of Catania, V.le A. Doria, 95125 Catania, Italy, [4]Department of Pharmacodynamics, Faculty of Pharmacy, Jagiellonian University Medical College, Medyczna 9, 30-688 Krakow, Poland, [5]Department of Crystal Chemistry and Crystal Physics, Faculty of Chemistry, Jagiellonian University, Gronostajowa 2, 30-387 Krakow, Poland, [6]Cerko Sp. z o.o. Sp.k, Al. Zwyciestwa 96/98, 81-451 Gdynia, Poland, [7]Celon Pharma S.A., R&D Centre, Marymoncka 15, 05-152 Kazun Nowy, Poland, [8]Department of Medicinal Chemistry, Maj Institute of Pharmacology, Polish Academy of Sciences, Smetna 12, 31-343 Krakow, Poland, [9]Institute of Pharmacy, Faculty of Chemistry and Pharmacy, University [10]Department of Pharmacology and Neurosciences Institute (Biomedical Research Center), University of Granada, and Biosanitary Research Institute ibs. Granada, Avenida de la Investigacion 11, 18016 Granada, Spain, [11]Institute of Pharmaceutical and Medicinal Chemistry, Heinrich Heine University Düsseldorf, Universitaetsstr. 1, 40225 Düsseldorf, Germany, [12]Bioprojet-Biotech, 4rue du Chesnay Beauregard, 35762 Saint-Gregoire Cedex, France

Published in: Journal of Medicinal Chemistry, 2023, 9658-9683, Vol. 66, https://doi.org/10.1021/acs.jmedchem.3c00430

Impact Factor: 6.8 (2024)

Contribution: L.L. designed, partially performed the histamine H_3 receptor binding studies and evaluated the receptor binding data and reviewed the manuscript.

Journal of Medicinal Chemistry

pubs.acs.org/jmc Article

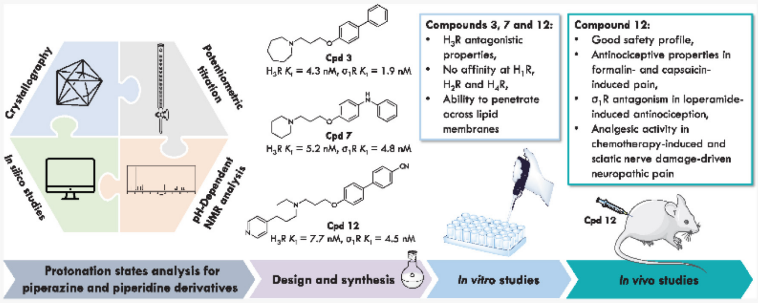
Dual Piperidine-Based Histamine H_3 and Sigma-1 Receptor Ligands in the Treatment of Nociceptive and Neuropathic Pain

Katarzyna Szczepańska,[◊] Tadeusz Karcz,*[,◊] Maria Dichiara, Szczepan Mogilski, Justyna Kalinowska-Tłuścik, Bogusław Pilarski, Arkadiusz Leniak, Wojciech Pietruś, Sabina Podlewska, Katarzyna Popiołek-Barczyk, Laura J. Humphrys, M. Carmen Ruiz-Cantero, David Reiner-Link, Luisa Leitzbach, Dorota Łażewska, Steffen Pockes, Michał Górka, Adam Zmysłowski, Thierry Calmels, Enrique J. Cobos, Agostino Marrazzo, Holger Stark, Andrzej J. Bojarski, Emanuele Amata,* and Katarzyna Kieć-Kononowicz*

Cite This: *J. Med. Chem.* 2023, 66, 9658−9683 Read Online

ACCESS | Metrics & More | Article Recommendations | Supporting Information

Downloaded via 93.195.59.121 on November 26, 2024 at 15:52:48 (UTC).
See https://pubs.acs.org/sharingguidelines for options on how to legitimately share published articles.



ABSTRACT: In search of new dual-acting histamine H_3/sigma-1 receptor ligands, we designed a series of compounds structurally based on highly active *in vivo* ligands previously studied and described by our team. However, we kept in mind that within the previous series, a pair of closely related compounds, **KSK67** and **KSK68**, differing only in the piperazine/piperidine moiety in the structural core showed a significantly different affinity at sigma-1 receptors (σ_1Rs). Therefore, we first focused on an in-depth analysis of the protonation states of piperazine and piperidine derivatives in the studied compounds. In a series of 16 new ligands, mainly based on the piperidine core, we selected three lead structures (**3**, **7**, and **12**) for further biological evaluation. Compound **12** showed a broad spectrum of analgesic activity in both nociceptive and neuropathic pain models based on the novel molecular mechanism.

1. INTRODUCTION

The treatment of complex, multifactorial diseases by single target-oriented therapies rarely results in good efficacy. For this reason, the approach based on the simultaneous modulation of multiple targets' activity captured the interest of the pharmaceutical industry and academia. The increasing number of evidence indicates improvement in both the therapeutic safety and efficacy of multitarget-directed ligands (MTDLs) compared with single-target drugs.[1,2]

The histamine H_3 receptor (H_3R) is a G protein-coupled receptor (GPCR) highly expressed in the central nervous system (CNS), where it acts as an auto- and heteroreceptor to regulate neurotransmission.[3] Thus, it has been considered a relevant target in the treatment of varied disorders, such as Alzheimer's disease, schizophrenia, and attention deficit hyperactivity disorder.[4] Furthermore, being localized in several CNS regions responsible for nociception, H_3Rs are also associated with pain[5] through the involvement in the central sensitization of pain.

A range of competitive antagonists/inverse agonists have been discovered and progressed into clinical trials, among which pitolisant was approved in 2016 for the treatment of narcolepsy (Figure 1).[6,7] As a consequence, the interest in the clinical application of novel H_3R antagonists, especially those with multifunctional profiles, has clearly increased.[8−12]

Received: March 10, 2023
Published: July 7, 2023



ACS Publications © 2023 The Authors. Published by American Chemical Society

https://doi.org/10.1021/acs.jmedchem.3c00430
J. Med. Chem. 2023, 66, 9658−9683

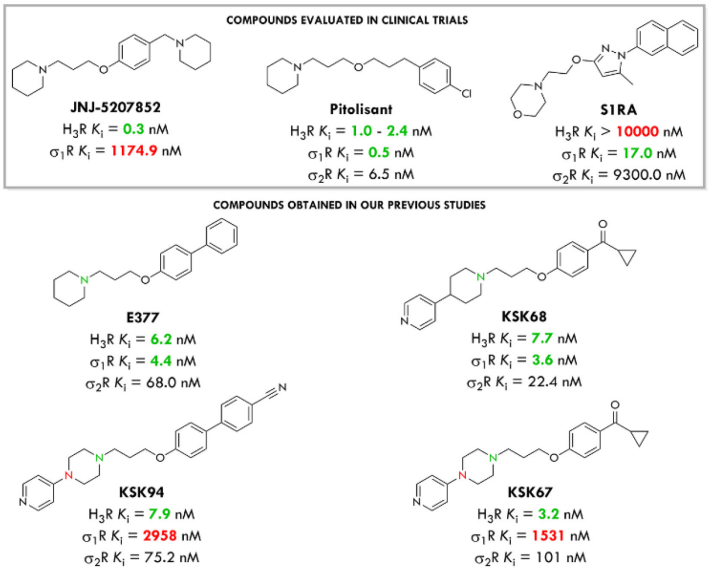


Figure 1. Structures of selective and dual-targeting compounds evaluated in clinical trials and obtained in our previous work.[23]

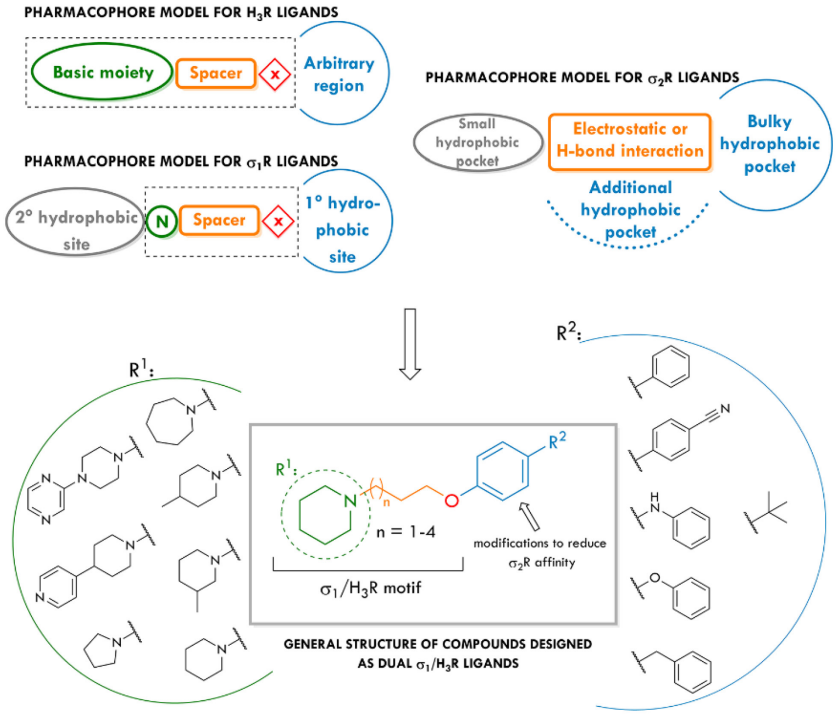
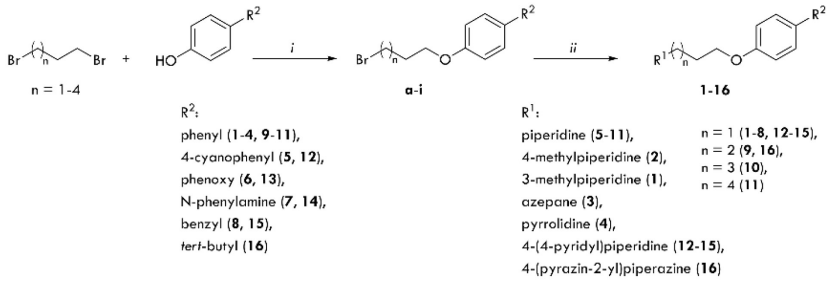


Figure 2. Pharmacophore models for H_3R, σ_1R, and σ_2R ligands. General structures of compounds described in this work.

Importantly, recent studies have shown that some clinically evaluated H_3R antagonists possess additional affinity at sigma-1 receptors, which may play an important role in their pharmacology and underlie the differences in the reported preclinical and clinical efficacy.[13,14] For example, JNJ-5207852 was highly selective for H_3R compared to the sigma-1 receptor, and the approved agent pitolisant displayed similar affinity toward both receptors (Figure 1).[13] Therefore, sigma-1 affinity

https://doi.org/10.1021/acs.jmedchem.3c00430
J. Med. Chem. 2023, 66, 9658−9683

Scheme 1. General Synthetic Pathway for Starting Ethers a−i and Compounds 1−16[a]



[a]Reagents and conditions: (i) proper α,ω-dibromoalkane, $CH_3CH_2CH_2ONa$, 60 °C: 3 h, reflux: 3 h; (ii) proper cycloalkylamine, K_2CO_3, KI, $EtOH/H_2O$ (5:1), reflux: 8−12 h.

should be always considered when interpreting the *in vivo* efficacy of novel H_3R ligands.

Sigma (σ) receptors, initially described as a subtype of opioid receptors, are now considered a separate class. Pharmacological studies have distinguished two types of σ receptors, namely, σ_1 and σ_2.[15] The sigma-1 receptor (σ_1R) is a ligand-regulated chaperone protein that modulates the signaling of proteins (receptors, enzymes) with which it interacts.[16] It is a unique and poorly understood biological target engaged in physiological mechanisms of learning and memory, depression, anxiety, and schizophrenia.[17] Sigma-1 antagonists are reported to be effective agents in neuropathic pain,[18] and although the mechanism of action is not well understood, several studies suggest the involvement of σ_1Rs in the regulation of ion channel function (including NMDA/GluN receptors and K^+/Ca^{2+} channels), which are involved in the pathogenesis of pain.[17] Many ion channels are located at the nociceptor peripheral terminal, affecting neuron excitability after injury and as a result affecting pain sensation.[17] In this context, the highly selective σ_1 antagonist **S1RA** (Figure 1) is in phase II clinical trials for pain treatment, with an intended indication for enhancing opioid analgesia and amelioration of neuropathic pain.[18]

Considering the clear relation between H_3R and σ_1R, along with the fact that dual-targeting compounds can lead to several improvements when compared to selective drugs, great efforts should be made to develop such ligands for the treatment of various pain conditions. Answering this challenge, in our recent studies, we investigated 20 previously reported H_3R ligands for their affinity toward σRs to check whether their high preclinical *in vivo* efficacy is related to a synergistic effect of the dual H_3R and σ_1R modulation.[19−22] According to the obtained results, compounds **E377** and **KSK68** (Figure 1) turned out to be high-affinity histamine H_3 and σ_1 receptor antagonists with negligible affinity at the other histamine receptor subtypes and promising antinociceptive *in vivo* activity.[23] Moreover, the piperidine moiety in the basic part of those compounds has been established as a critical structural feature for dual H_3/σ_1 receptor activity as can be seen by comparing the data for compounds **KSK67** and **KSK68** (Figure 1). The piperidine derivatives in protonated form are involved in the essential salt bridge interaction with Glu172 in the σ_1R binding pocket, being responsible for the high biological activity of the studied ligands. As discussed in our previous work, this phenomenon can be attributed to a change in the protonation state or states at physiological pH.[23] Therefore, in the initial step of designing the next series of ligands, we focused on an in-depth analysis of the protonation states of piperazine vs piperidine derivatives using crystallography, potentiometric titration, and NMR spectroscopy measurements in a pH-controlled environment. Next, we designed a series of 16 new compounds, mainly based on the piperidine core, with the general structure presented in Figure 2 and performed their pharmacological characterization using *in vitro* methods. Finally, lead compounds were tested in animal models of nociceptive and neuropathic pain.

2. RESULTS AND DISCUSSION

2.1. Chemistry. The synthesis of the desired final compounds **1−16** was achieved through the synthetic route presented in Scheme 1. According to the previously described procedure,[19,21,22,24,25] the phenoxy alkyl bromides **a−i** were obtained mainly by one-step alkylation of commercially available phenols with 1,3-dibromopropane (**a**−**e**), 1,4-dibromobutane (**f**, i), 1,5-dibromopentane (**g**), or 1,6-dibromohexane (**h**) in propan-1-ol under reflux conditions. Obtained precursor bromides were then coupled with 3-methylpiperidine (**1**), 4-methylpiperidine (**2**), azepane (**3**), pyrrolidine (**4**), piperidine (**5−11**), 4-(piperidin-4-yl)pyridine (**12−15**), or 2-(piperazin-1-yl)pyrazine (**16**) in a mixture of ethanol/water with powdered potassium carbonate and a catalytic amount of potassium iodide. The final products were obtained as free bases and isolated as oxalate or hydrogen oxalate salts.

2.2. Protonation Investigation Based on Crystal Structure Analysis. To determine the potential differences in the protonation of piperidine and piperazine derivatives, we selected two pairs of compounds for crystallographic studies, differing only in the basic part. The first contains the cyclopropylmethanone derivatives **KSK67** and **KSK68** obtained in our previous work[22,23] (Figure 1), whereas the second contains two nitrile derivatives: **KSK94** (also published earlier,[22,23] Figure 1) and compound **12** (structure in Pharmacology, Table 2). In the **KSK67** and **KSK68** oxalate crystals, the total charge of the main organic compound is +2, with protonation centers at N1 (pyridine) and N10 (piperazine/piperidine) nitrogen atoms. The resulting positive charge is compensated by oxalate anions that form charge-assisted hydrogen bonds with the mentioned protonated amine (Figures S1 and S2). An interesting geometry is observed for N1-H-O3A interaction in structure **KSK68** (distances: N1···O3A 2.581 Å, N1-H 1.305 Å, O3A-H 1.278 Å; angle: N1-H-O3A 175.66°), suggesting possible proton transfer between

https://doi.org/10.1021/acs.jmedchem.3c00430
J. Med. Chem. 2023, 66, 9658−9683

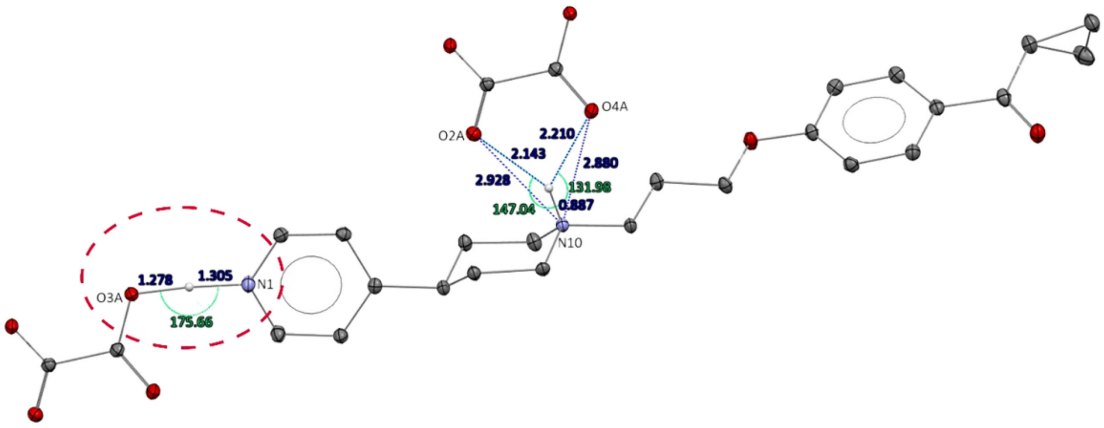
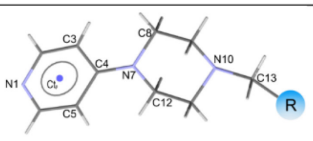
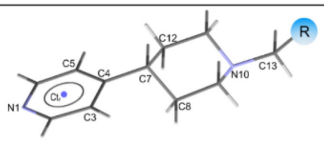


Figure 3. The geometrical parameters of the strongest interactions observed in the crystal structure of **KSK68** (charge-assisted hydrogen bonds N^+-H···O^- type; distances in dark blue, angles in light green). The weaker basicity of the N1 atom in the pyridine ring is manifested by the hydrogen shift toward oxalate anion (discussed fragment is depicted with a dashed-line ellipsoid). Displacement ellipsoids of nonhydrogen atoms are drawn at the 30% probability level. H atoms not involved in the described interactions were removed for figure clarity.

Table 1. Selected Geometrical Parameters Defined for the Determined Crystal Structures[a]



4-pyridylpiperazine fragment



4-pyridylpiperidine fragment

Geometrical parameter	Structure								
	KSK67	KSK68	KSK68_OH	KSK67_fb	KSK68_fb		KSK94_fb		12_fb
(mol. total charge)	(+2)	(+2)	(+1)	(+1)	mol. 1 (0)	mol. 2 (0)	mol. 1 (+1)	mol. 2 (0)	(0)
C4-N7/C7	**1.350 Å**	1.508 Å	1.511 Å	**1.340 Å**	1.514 Å	1.518 Å	**1.351 Å**	**1.360 Å**	1.507 Å
N10-C13	1.543 Å	1.492 Å	1.543 Å	1.477 Å	1.467 Å	1.469 Å	1.460 Å	1.481 Å	1.464 Å
C4-N7/C7-C8	**124.00°**	109.82°	110.75°	**123.43°**	109.76°	115.00°	**120.22°**	**119.42°**	111.97°
C4-N7/C7-C12	**125.95°**	112.11°	114.68°	**124.24°**	115.59°	110.96°	**119.95°**	**118.96°**	113.78°
C8-N7/C7-C12	110.05°	109.92°	108.22°	110.89°	107.92°	108.25°	115.15°	115.86°	108.93°
C3-C4-N7/C7-C8	**–0.92°**	–65.58°	–92.40°	**5.92°**	15.12°	–74.31°	**169.53°**	**–14.11°**	129.33°
C5-C4-N7/C7-C12	**–1.47°**	–124.30°	–35.46°	**–10.16°**	70.06°	–19.69°	**–166.79°**	**14.98°**	72.41°
N1···N10	6.881 Å	7.031 Å	7.131 Å	6.982 Å	7.079 Å	7.105 Å	7.037 Å	7.033 Å	7.107 Å
N10···Ct_p	5.545 Å	5.684 Å	5.753 Å	5.629 Å	5.705 Å	5.727 Å	5.658 Å	5.633 Å	5.719 Å
N10··· N7/C7··· Ct_p	155.78°	150.40°	155.94°	168.00°	151. 68°	153. 78°	174.79°	171.98°	155.57°

[a]Ct_p: geometrical center of the pyridine ring.

pyridine nitrogen N1 and O3A of the carboxylic group (Figure 3). That may imply weaker basic properties of N1 compared to the piperidine N10 protonation center for **KSK68**. This can be deduced also based on the obtained **KSK68_OH** crystal structure, where increased pH led to +1 cation, with sole protonation at N10 (Figure S3).

The crystal structures obtained for the free bases **KSK67_fb**, **KSK68_fb**, **KSK94_fb**, and **12_fb** from water/organic solvents revealed peculiar properties of molecules with 4-pyridylpiperazine moiety. Surprisingly, molecules containing the mentioned fragment (**KSK67_fb** and **KSK94_fb**) did not crystalize in the neutral form. The pyridine nitrogen of those compounds is a very strong base and easily protonates in the solution (Figures S4 and S6). Thus, in the crystal, an iodide salt is observed. The counter ion I^- was introduced during the synthesis, where the catalytic amount of potassium iodide was applied (see Chemistry Section 2.1.). An analogous basic property of N1 is not observed for **KSK68_fb** and **12_fb** with 4-pyridylpiperidine moiety. For these samples, crystals with the neutral form of the compound were obtained (Figures S5 and S7).

The observed strong basic character of N1 in structures **KSK67_fb** and **KSK94_fb** is a consequence of the increased availability of lone pair electrons correlated with the electron source at the para position (lone pair of N7 nitrogen atom of the piperazine ring). The N7-lone pair shift manifests in N7-C4 bond shortening to ∼1.35 Å (Table 1), which implies a partial double bond character and decreasing pyramidality of N7 atom. The last observation is confirmed by angles C4-N7-C8 and C4-N7-C12 being ∼120° (Table 1) and defining nearly flat geometry around N7. The observed change of N7 hybridization from sp^3 to sp^2 leads to the quasi-planar mutual orientation of pyridine and piperazine (torsion angles C3-C4-N7-C8 and C5-C4-N7-C12 closer to 0/180°; Table 1). Such effect and geometry are often observed for arylpiperazine fragments. However, it may strongly depend on substituents or

https://doi.org/10.1021/acs.jmedchem.3c00430
J. Med. Chem. 2023, 66, 9658−9683

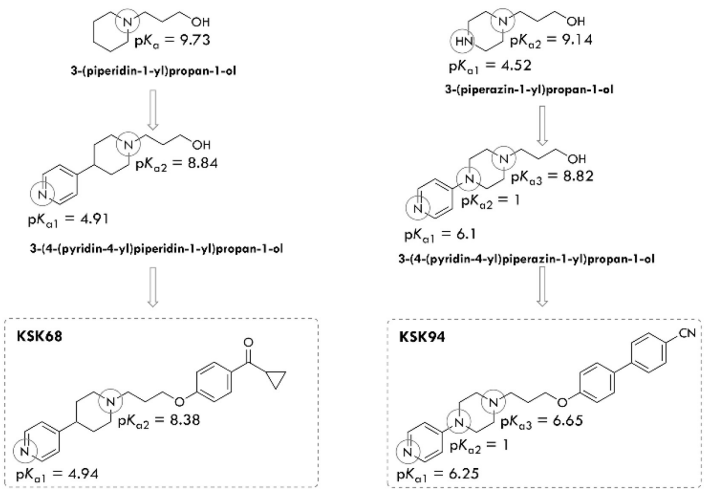


Figure 4. Structure and experimental pK_a values of KSK compounds and corresponding amino alcohols.

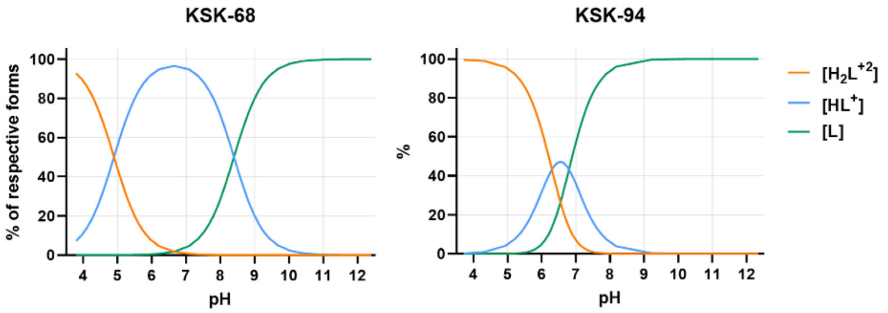


Figure 5. The protonation states of **KSK68** and **KSK94** as a function of pH. The species distribution was generated from the CerkoLab software based on titration curves of investigated compounds (see Figure S8). The equilibria between the species are as follows: **KSK68**: $H_2L^{+2} = H^+ + HL^+$, pK_1 = 4.94 and $HL^+ = H^+ + L^0$, pK_2 = 8.38; **KSK94**: $H_2L^{+2} = H^+ + HL^+$, pK_2 = 6.25 and $HL^+ = H^+ + L^0$, pK_2 = 6.65.

heteroatoms in the aromatic fragment.[26] Nevertheless, the observed phenomenon is responsible for the rigidity of the 4-pyridylpiperazine fragment that determines the highly basic character of N1 as well as the orientation of π-electrons of the aromatic fragment. This last characteristic may be a strong geometrical feature responsible for effective ligand−protein recognition and may explain the observed selectivity of the investigated compounds containing the 4-pyridylpiperazine fragment for H_3R.

2.3. Determination of the Basicity of Selected Piperidine and Piperazine Derivatives by Potentiometric Titration. Several key physicochemical properties that influence absorption and distribution processes, such as lipophilicity and solubility, depend on pK_a. The ionization state is a key parameter not only in ADME profiling but also during ligand−receptor mutual recognition and interaction, as it usually occurs in an aqueous environment at physiological pH.

Thus, we evaluated two representative compounds, **KSK68** and **KSK94**, containing a piperidine or piperazine substituted with a 4-pyridyl moiety in pK_a studies. In addition, we tested the amino alcohol fragments of these compounds to carefully monitor the influence of individual protonated nitrogen atoms on the obtained pK_a values (Figure 4). Considering the structural differences between **KSK68** and **KSK94**, it seems obvious that their different binding potency toward σ_1R should be attributed to the change in protonation state at physiological pH. Based on a previously modified potentiometric procedure,[27,28] a series of titrations were performed, and the pK_a values were determined using the Kostrowicki and Liwo algorithm.[29,30] Experimental pK_a data show that **KSK68** exists exclusively in the monoprotonated form in an aqueous solution at physiological pH (approximately 90% of $[HL^+]$ form, Figure 5). That explains the surprising result of free base crystallization attempts where iodide salt was obtained instead of the neutral form. On the other hand, in the same environment, **KSK94** exists in two forms: the monoprotonated form $[HL^+]$ (20.56%) and the free ligand [L] (77.72%, Figure 5). Experimental data show how replacing the piperidine system with a piperazine ring drastically affects the acid−base properties of the molecule. **KSK68** can be characterized as a basic ligand with pK_{a1} = 4.9 (pyridine N) and pK_{a2} = 8.4 (piperidine N). The pK_a values are consistent with those determined by the same procedure for the corresponding amino alcohol 3-(4-(pyridin-4-yl)piperidin-1-yl)propan-1-ol (Figure 4). In contrast to **KSK68**, the **KSK94** compound

https://doi.org/10.1021/acs.jmedchem.3c00430
J. Med. Chem. 2023, 66, 9658−9683

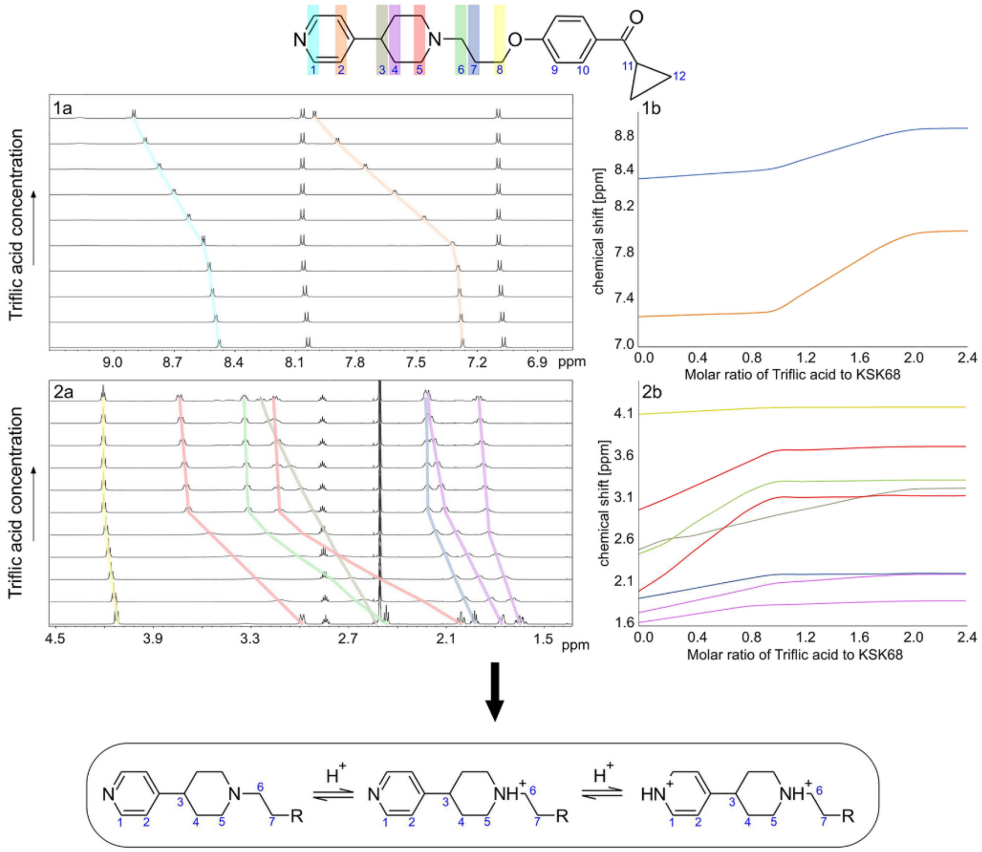


Figure 6. NMR titration experiment for **KSK68** presents stacked ^{1}H NMR spectra of (1a) the aromatic region of chemical shifts and (2a) the aliphatic one. The concentration of acid is rising in an upward direction by 0.2 molar equivalents. (1b, 2b) Graphs that represent the change in the chemical shift of the individual signals on the ^{1}H NMR spectra as the concentration of triflic acid in the solution increases. Panel 1b corresponds to the aromatic region of chemical shits and 2b to the aliphatic one. The colors on the top structure of **KSK68** refer to the signals marked on the spectra with exact color lines and to the colors of the lines on the graphs. The largest changes in the difference in chemical shifts $\Delta\Delta\delta$ are observed for signals of protons that are adjacent to the nitrogen atoms, which undergo protonation. Tracking these changes in $\Delta\Delta\delta$ while increasing the concentration of triflic acid in the solution allows one to assess the order of protonation of individual nitrogen atoms in the molecule (when nitrogen functions possess significant difference in pK_a) and determine the integer number of nitrogen atoms that undergo protonation. For a detailed analysis, see the Supporting Information.

belongs to the group of ligands with an acidic center located at the N7 nitrogen of the piperazine ring with a pK_{a2} value of approximately 1 (Figure 4). A similarly low pK_{a2} value for the N7 piperazine nitrogen atom was also determined for the corresponding amino alcohol 3-(4-(pyridin-4-yl)piperazin-1-yl)propan-1-ol (Figure 4), which is in agreement with the value obtained for 1-phenyl-4-methyl piperazine reported in the literature.[31] Moreover, the literature pK_a values of 1-aryl-4-propylpiperazines range from 7.59 to 8.39 for the N-CH_2-CH_2 moiety. The lowest value was determined for 4-nitrophenyl, and the highest was for 2-methylphenyl derivatives.[32]

2.4. Protonation Investigation Based on NMR Spectroscopy Measurements in the pH-Controlled Environment. Another attempt to determine the order of protonation of nitrogen atoms in studied molecules was carried out using NMR spectroscopy.

All signals in the ^{1}H and ^{13}C spectra were assigned based on 2D correlation spectra for compounds **KSK68** and **KSK94** (piperidine and piperazine derivatives, respectively) to follow the course of changes in their chemical shifts during titration with trifluoromethanesulfonic acid (triflic acid or TfOH), one of the strongest organic acids (pK_a ~(−15)). A detailed description of the chemical shifts upon the addition of triflic acid is described in the Supporting Information.

In the case of **KSK68**, the nitrogen atom in the piperidine ring is protonated first (Figure 6). Protonation of the nitrogen atom in the pyridine ring begins after full saturation to a molar ratio of 1.0:1.0. This is clearly visible in the shifts of protons in the vicinity of individual nitrogen atoms. The sole signal on the spectrum that shifts toward higher frequencies during the titration process comes from the H3 proton, which is located near both nitrogen atoms and links the two rings. The observed effect is characteristic for systems in which the pK_a

https://doi.org/10.1021/acs.jmedchem.3c00430
J. Med. Chem. 2023, 66, 9658−9683

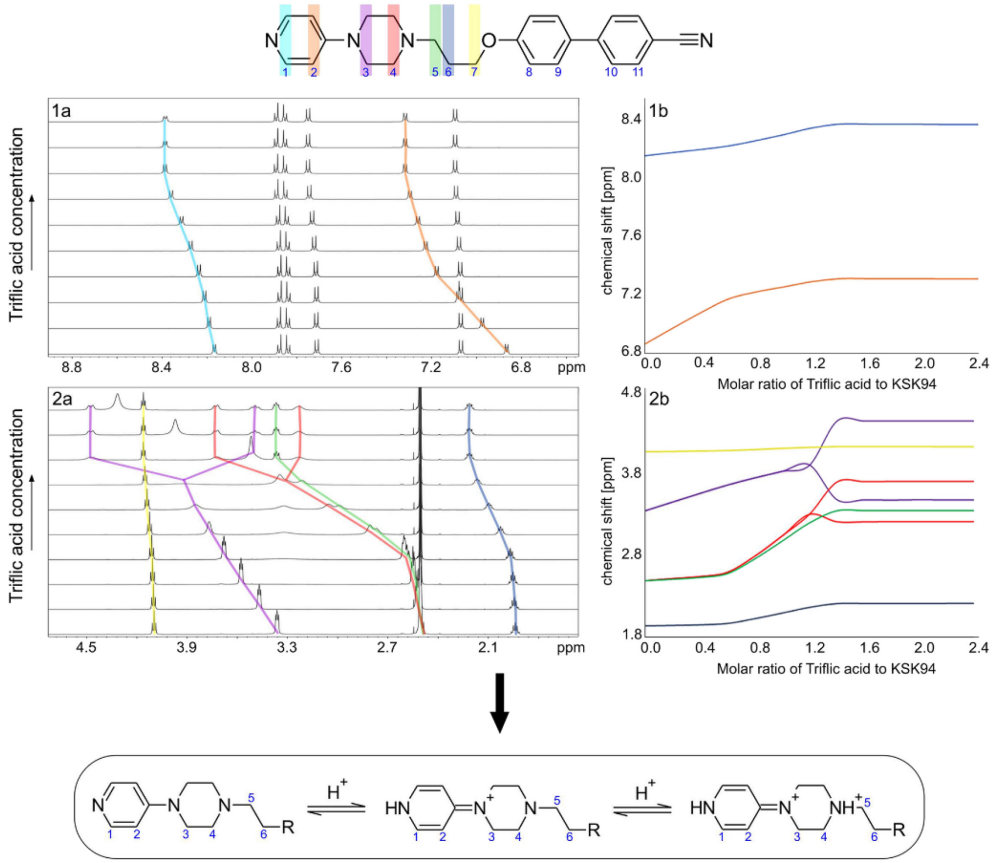


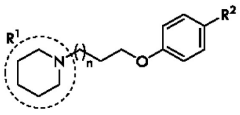
Figure 7. NMR titration experiment for **KSK94** presents stacked ^{1}H NMR spectra of (1a) the aromatic region of chemical shifts and (2a) the aliphatic one. The concentration of acid is rising in an upward direction by 0.2 molar equivalents. (1b, 2b) Graphs that represent the change in the chemical shift of the individual signals on the ^{1}H NMR spectra as the concentration of triflic acid in the solution increases. Panel 1b corresponds to the aromatic region of chemical shits and 2b to the aliphatic one. The colors on the top structure of **KSK94** refer to the signals marked on the spectra with exact color lines and to the colors of the lines on the graphs. The largest changes in the difference in chemical shifts $\Delta\Delta\delta$ are observed for signals of protons that are adjacent to the nitrogen atoms, which undergo protonation. Tracking these changes in $\Delta\Delta\delta$ while increasing the concentration of triflic acid in the solution allows one to assess the order of protonation of individual nitrogen atoms in the molecule (when nitrogen functions possess significant difference in pK_a) and determine the integer number of nitrogen atoms that undergo protonation. For a detailed analysis, see the Supporting Information.

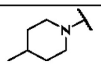
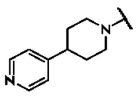
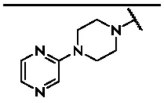
values for the two basic centers differ significantly. Here, the pK_a for piperidine nitrogen is higher in value than that for pyridine nitrogen, which is in line with the theoretical data.

For **KSK94**, the model is more complicated than for **KSK68** (Figure 7). H1, H2, and H3 protons are affected by a change in the chemical environment at first, with H2 protons being the least affected. Thus, the proton environment is mostly changed in the proximity of the pyridine nitrogen atom and near the piperazine nitrogen closer to the pyridine. Taking further into account the difference of 94 ppm in ^{15}N chemical shift for pyridine nitrogen, it can be concluded that the nature of the pyridine nitrogen atom changes dramatically from purely aromatic to an intermediate form between heterocyclic and amine. As a consequence, the pyridine nitrogen atom is protonated first, but the positive charge is transferred to the piperazine nitrogen atom by appropriate resonance structures. The second piperazine nitrogen atom is initially unprotonated, as indicated by no change in the chemical shift of proton signals from its immediate vicinity. From an acid molar ratio of 0.6:1.0, protonation of the second nitrogen atom in the piperazine ring can be observed. The proton signals in the vicinity of this nitrogen atom broaden by losing multiplicity and start to move toward higher frequencies. This is analogous to the first protonation step of **KSK68**. At this point, both nitrogen functions protonate at the same time, as both the aromatic and aliphatic proton signals shift toward higher frequencies, indicating similar pK_a values, with the value of the first stage being higher. Because of the loss of one symmetry element and likely conformational stiffening of the piperazine ring, the signals from the H3 and H4 protons, which were integrated as four protons, split into axial and equatorial components, and now each is integrated as two. At a ratio of 1.4:1.0, saturation occurs, and no further changes were observed despite reaching the molar ratio of 3:0:1.0.

https://doi.org/10.1021/acs.jmedchem.3c00430
J. Med. Chem. 2023, 66, 9658−9683

Table 2. Structures of Compounds 1−16 and Their *in Vitro* Binding Affinities at the Human Histamine H_3 Receptor (hH_3R) and Rat Sigma-1 (σ_1R) and Sigma-2 (σ_2R) Receptors[f]



Compound	n	R1	R2	x̄ [CI 95%] hH_3R K_i [nM]	σ_1R K_i [nM]	σ_2R K_i [nM]	σ_2/σ_1 ratio
1	1		phenyl	31 [11, 90]	1.5 [0.5, 4.1]	17 [9, 32]	11.3
2	1		phenyl	10.3 [1.7, 62.4]	2.4 [0.7, 8.2]	16 [12, 22]	6.7
3	1		phenyl	4.3 [1.4, 13.0]	1.9 [0.6, 5.8]	25 [7.6, 83]	13.2
4	1		phenyl	19.5 [4.7, 81.2]	24 [8.4, 66]	65 [34, 128]	2.7
5	1		4-cyanophenyl	6.2 [1.5, 26][a]	28 [5.7, 136]	47 [21, 105]	1.7
6	1		phenoxy	2.7 [1.1, 5.8]	18 [8.2, 39]	103 [48, 223]	5.7
7	1		N-phenylamine	5.2 [2.1, 12.6]	4.8 [2.8, 8.4]	116 [70, 191]	24.2
8	1		benzyl	27.5.0 [9.1, 83.4]	5.5 [1.1, 27]	47 [22, 102]	8.5
9	2		phenyl	22 [7, 73]	95 [36, 252]	33 [14, 74]	0.3
10	3		phenyl	21.7 [3.9, 110][b]	140 [78, 251]	19 [8.8, 41]	0.1
11	4		phenyl	88.9 [42, 187][b]	118 [31, 449]	46 [18, 114]	0.4
12	1		4-cyanophenyl	7.7 [1.1, 52.5]	4.5 [1.3, 15]	10 [5.6, 20]	2.2
13	1		phenoxy	24.2 [3.1, 187.6]	5.6 [2.8, 11]	4 [0.8, 19]	0.7
14	1		N-phenylamine	69 [18.8, 253.4]	3.3 [1.6, 7.1]	29 [14, 59]	8.8
15	1		benzyl	76.1 [18.4, 315.7]	2.8 [1.3, 6]	9.9 [3.6, 27]	3.5
16	2		*tert*-butyl	5477 [1034, 29027][e]	7.6 [4, 14]	27 [11, 67]	3.6
Pitolisant				11.2 [6.7, 18.4]	0.5[d]	6.5[d]	13
(+)-Pentazocine					4.3[e]	1465[e]	340.7
DTG					124[e]	18[e]	0.1

[a]Data published in ref 25. [b]Recalculated from data published in ref 24. [c]Data published in ref 19. [d]Data published in ref 7. [e]Data published in ref 61. [f]Given data represent mean values within the 95% confidence interval (CI).

2.5. *In Vitro* Pharmacology. *2.5.1. Affinity at H_3R and σRs.* *In vitro* affinity data for the newly synthesized ligands are assembled in Table 2. Interestingly, almost all compounds (except **16**) showed high affinity at histamine H_3 receptors with K_i values below 100 nM. Moreover, all the described ligands showed more or less significant activity to both sigma receptors but with different binding affinities. In the case of compound **16**, the only piperazine derivative in this series, the lack of activity toward H_3R is related to the pyrazine-2-yl group in the basic part of the molecule, as discussed in our previous work.[19,20] Nevertheless, **16** was still very active on both sigma receptors (σ_1R K_i = 7.6 nM, σ_2R K_i = 27 nM). The

https://doi.org/10.1021/acs.jmedchem.3c00430
J. Med. Chem. 2023, 66, 9658−9683

unsubstituted piperidine ring in the basic part of the compounds seems to be the most influential on affinity at human H_3R (hH_3R), as can be seen by comparing compounds **5**–**7** with their 4-pyridyl analogues **12**–**14** (hH_3R K_i = 6.2, 2.7, and 5.2 nM vs 7.7, 24.2, and 69 nM, respectively). Moreover, this structural relationship is also observed in the case of ligands **1** and **2**, which are methyl analogues of the lead compound **E377** (Figure 1) published in our previous paper[23] (hH_3R K_i = 31 and 10.3 nM vs 6.2 nM, respectively). However, for both sigma receptors, 4-pyridylpiperidine derivatives **12**–**14** were more potent than unsubstituted piperidines (**5**–**7**), especially when comparing affinity values toward sigma-1 receptors (σ_1R K_i = 4.5, 5.6, and 3.3 nM vs 28, 18, and 4.8 nM, respectively; σ_2R K_i = 10, 4, and 29 nM vs 47, 103, and 116 nM, respectively). For all the described piperidine derivatives, the effect of the alkyl chain can only be observed at the H_3R, where the extension of the linker length decreased the affinity of biphenyl analogues **9**, **10**, and **11** (hH_3R K_i = 22, 21.7, and 88.9 nM, respectively). In our previous work, we found a critical structural feature that distinguishes the dual H_3/σ_1Rs ligands and selective H_3R-targeting compounds.[23] One of the lead structures, **KSK68** with the 4-pyridylpiperidine moiety as the fundamental part of the molecule, showed high affinity at both histamine H_3 and σ_1 receptors, whereas its piperazine analogue **KSK67** was highly selective for H_3R (Figure 1). Interestingly, this time, we also confirmed this structural phenomenon, as can be seen by comparing the nitrile derivative **12** with its piperazine analogue **KSK94** described in our previous work (Figure 1, hH_3R K_i = 7.7 nM and σ_1R K_i = 4.5 nM vs hH_3R K_i = 7.9 nM and σ_1R K_i = 2958 nM, respectively). Again, the piperidine derivative **12** showed dual H_3/σ_1Rs activity, whereas the piperazine-based compound **KSK94** was highly selective for H_3R. Taking into account the selectivity toward sigma-2 receptors in the group of biphenyl derivatives with three-carbon chains, the highest values were observed for compounds **1** and **3** (σ_2/σ_1 ratio 11.3 and 13.2, respectively). Furthermore, extending the carbon chain from four to six methylene groups significantly reduced this parameter (ligands **9**–**11**). Aniline derivative **7** showed the highest σ_2/σ_1 ratio among all described derivatives (24.2).

As lead structures for further evaluation, we selected two piperidine derivatives, **3** and **7**, with high affinity at both H_3R and σ_1R as well as the highest σ_2/σ_1 selectivity factor. In this choice, we were guided by the fact that the highly selective σ_1R antagonist **S1RA**, so far the only one tested in clinical trials for pain treatment, showed no affinity at σ_2R.[18] On the other hand, bearing in mind recently reported studies with novel σ_2R-selective ligands, which suggest that they may also modulate nociception,[33] we included nitrile derivative **12** exhibiting activity toward σ_2R at a comparable level as toward H_3R and σ_1R. Moreover, its piperazine analogue, compound **KSK94**, was extensively tested in the obesity model in our previous studies and showed a good safety profile.[22]

2.5.2. Affinity at Other Histamine Receptors. To check the selectivity profile of our lead structures, radioligand binding studies at other histamine receptor subtypes were carried out. Compounds **3**, **7**, and **12** in their oxalate forms were tested at human recombinant histamine H_1, H_2, and H_4 receptor subtypes stably expressed in HEK293T cells. Obtained results clearly indicate the high selectivity of the tested derivatives toward human H_3R (Table 3).

2.5.3. Intrinsic Activity toward H_3R. To identify the lead compounds' functional profile, their intrinsic activity was tested in a 3′,5′-cyclic adenosine monophosphate (cAMP) accumulation assay in HEK cells expressing human recombinant H_3R.[34] All tested compounds reversed the *R*-α-methylhistamine inhibition of cAMP production in forskolin-stimulated cells and were therefore classified as H_3R antagonists/inverse agonists. The IC_{50} values obtained in the H_3R functional assay are assembled in Table 3.

Table 3. Radioligand Binding Assay at Human Histamine H_1 (hH_1R), H_2 (hH_2R), and H_4 (hH_4R) Receptors and Functional Study at the Human Histamine H_3 Receptor (hH_3R)[a]

compound	hH_1R (K_i [nM] x̄ [CI 95%])	hH_2R (K_i [nM] x̄ [CI 95%])	hH_4R (K_i [nM] x̄ [CI 95%])	hH_3R (IC_{50} [nM] ± SD)
3	7615 [4024; 14,407]	>10,000	>10,000	83.4 ± 15.9
7	>10,000	>10,000	>10,000	83.7 ± 2.1
12	653 [259; 1647]	>10,000	>10,000	215 ± 108
thioperamide				375 ± 30
pitolisant				1.96 ± 0.80

[a]Given data represent the mean K_i (nM) values within the 95% confidence interval (CI) (n = 3, triplicate) or the mean IC_{50} values of tested compounds in the cAMP assay ± standard deviation (n = 2, triplicate).

2.6. *In Silico* Studies. Molecular Modeling: Docking Studies and Molecular Dynamics Simulations. In addition to experimental studies, the protonation states of compounds were also evaluated *in silico* using two software packages: InstantJChem and Epik (Figure 8). Although there are slight differences in the numerical values of predicted pK_a, the overall tendencies observed for the performed experiments are preserved: nitrogen atoms belonging to the piperidine moieties are characterized by higher pK_a values than those of piperazine, and therefore, they are less likely to protonate at physiological pH.

To further investigate the influence of structural differences between the 4-pyridylpiperazine and 4-pyridylpiperidine moieties on their molecular mechanism of action, the binding with sigma-1 and histamine H_3 receptors was evaluated using molecular modeling methods. Analysis of the binding mode of **KSK94** and **12** to σ_1R shows coherent binding modes of 4-pyridylpiperidine/piperazine fragment in comparison to our previous studies[22,23] (Figure 9A). However, because of the use of induced-fit docking, which allows relaxing the binding pocket and fitting of adjacent amino acids to the molecular core of compounds, we observed that the 4-cyanophenyl fragment occupies a hydrophobic pocket with the stabilizing hydrogen bond (HB) between the nitrile group and the main chain of Ser99. Then, on the basis of both NMR analysis and crystallographic results, we decided to dock all protonation and tautomeric states of **KSK94** and **12** using *ab initio* docking (quantum polarized ligand docking, QPLD) and energy calculations applying the Molecular Mechanics Generalized Born Surface Area (MM-GBSA) method (Table S5, SI). First, we estimated the energy loss of piperazine derivatives to piperidine ones for σ_1R. The result showed that the tautomeric monoprotonated pyrimidine structure (the most populated protonation state) of **KSK94** has a higher ΔG value vs **12** (Table 4), indicating a loss of ligand–receptor interaction energy, which is also reflected in the *in vitro* results (Table 2). In the case of the monoprotonated tautomeric form, a loss of

https://doi.org/10.1021/acs.jmedchem.3c00430
J. Med. Chem. 2023, 66, 9658–9683

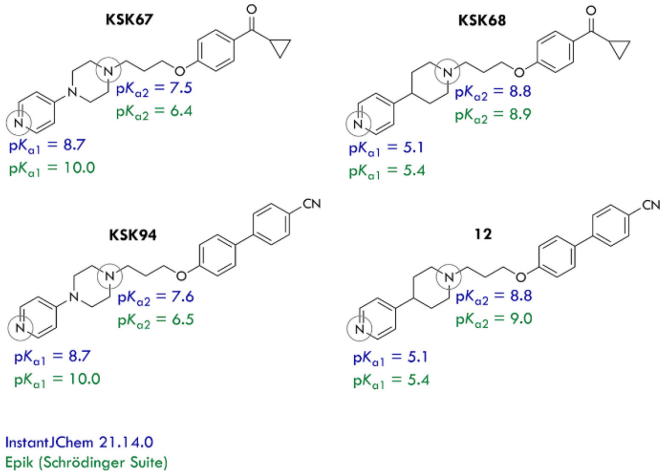


Figure 8. Results of *in silico* protonation studies of compounds **KSK67**, **KSK68**, **KSK94**, and **12**.

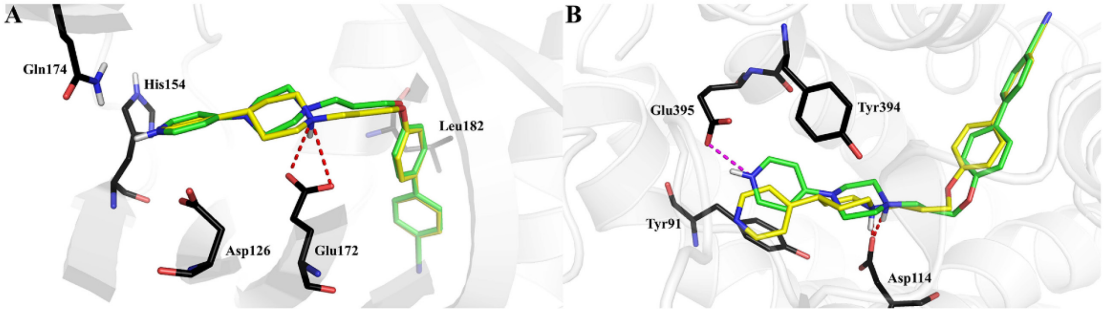
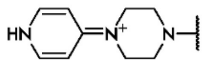
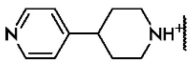


Figure 9. Comparison of the binding mode of **KSK94** (green) in tautomeric monoprotonated state and **12** (yellow) in the σ_1R (PDB ID: 6DJZ) (A). Comparison of the binding mode of **KSK67** (green) in the tautomeric monoprotonated state and **KSK68** (yellow) in the H_3R binding site (homology model) (B). The corresponding salt bridges are marked in red and magenta.

Table 4. Comparison of Free Binding Energies and Docking Scores of the Most Populated Protonation States with the *In Vitro* Activity of KSK67, KSK68, KSK94, and 12 with σ_1 and H_3 Receptors

Form	Compound	σ_1R			H_3R		
		K_i [nM]	Docking score	ΔG [kcal/mol]	K_i [nM]	Docking score	ΔG [kcal/mol]
	**KSK67**	1531	−8.04	−61.24	3.2	−9.67	−98.11
	KSK94	2958	−10.45	−81.44	7.9	−10.22	−95.71
	**KSK68**	3.6	−9.56	−99.29	7.7	−10.79	−98.69
	12	4.5	−11.51	−99.47	7.7	−10.47	−97.64

the essential salt bridge interaction with Glu172 (Figure 9A) can explain the decrease in biological activity. A similar correlation between *in vitro* results and ΔG value can be noticed for **KSK67** and **KSK68** compounds (Table 4). When analyzing the interactions of lead compounds, it is worth noting that ligands **3** and **7** occupy exactly the same place as **12** despite the lack of a heteroaromatic ring connected to the saturated basic fragment (Figure S25). Notably, enriched by the assembled experimental evidence and observations, in this study, more complex and sophisticated molecular modeling methods were applied compared to the previous studies,[23] resulting in different binding modes observed. Analysis of the previously described **KSK68** binding mode showed significant changes compared to the results presented here, where a salt bridge with Asp114 (D3.32) was formed. However, the two compound poses are flipped with respect to each other. In our earlier studies, the conformation of **KSK68** was almost linear (Figure S24), whereas in the current study, the conformation resembles the one observed for the sigma-1 receptor (Figure 9A,B). In fact, four distinct binding modes of H_3R ligands have

https://doi.org/10.1021/acs.jmedchem.3c00430
J. Med. Chem. 2023, 66, 9658−9683

been reported so far in the literature;[35−44] however, we decided to focus on the one that does not involve Glu206. This orientation was also similar to the alternative binding modes of ciproxifan in the H_3R binding pocket.[37,45] Because of the expansion of the tertiary amine fragment compared to ciproxifan (replacement of imidazole with 4-pyridylpiperazine), compound **12** additionally forms contacts with Tyr91 (TM3), Tyr394 (TM7), as well as Glu395 (TM7). To explain the slight difference in the biological activity of **KSK94** and **12** toward H_3R (Table 2), *ab initio* molecular docking of all protonation and tautomeric forms was performed (Table S5, SI). The results showed that for the monoprotonated tautomeric form of **KSK94**, the loss of the ligand−receptor interaction energy (ΔG) is insignificant (Table 4), which is related to formation of an additional stabilizing salt bridge with Glu395, which also correlates with the biological activity observed. Moreover, the compounds occupy the same region of the binding pocket, and because of the nature of the homology modeling procedure applied to generate the H_3R model, alternative binding mechanisms cannot be excluded. For the monoprotonated tautomeric form of **KSK67**, compared to **KSK68**, the ΔG values are close, which correlate well with the experimental results (Table 4). The observed salt bridge with D3.32 (the strongest interaction in ligand−receptor interactions)[46] fixes the position occupied by the ligands, which can be seen by comparing lead compounds **3** and **7** (Figure S26). The *N*-phenylamine (**7**) or phenyl (**3**) fragment penetrates deep into the binding pocket because of its hydrophobic environment and, as with compound **12**, interacts through hydrophobic effects or $\pi-\pi$ stacking interactions (Figure S26).

To confirm the validity of the docking poses discussed above, the molecular dynamics (MD) simulations were carried out. The obtained data were analyzed both in terms of the variation in the ligand-protein contacts as well as *via* the examination of ligands' RMSDs. Both approaches confirmed the stability of the obtained docking poses: the compounds occupied the same region of the binding pocket during the whole simulation process, and the patterns of ligand−protein interactions in general remain the same (Figures S27 and S28).

We are aware of the H_3R crystal structure, which was released in late October 2022 in the PDB repository (PDB ID: 7F61).[47] The crystalized complex contains an antagonist in the binding pocket, PF03654746, as well as the unexpected cholesterol binding at the allosteric site. According to the authors, the H_3R orthosteric binding pocket is shallow, and PF03654746 occupies an extended part of it (EBD). To evaluate the quality of our homology model, we docked PF03654746 to the model, and we obtained a similar pose to that observed in the crystal structure (Figure S29). The RMSD (root-mean-square deviation) of ligands was 1.48 Å, and it is less than the crystal resolution (2.6 Å), which indicated that our model was coherent with the crystal structure. It is worth to stress that the proposed binding mode of KSK ligands engaged the same protein helices (especially TM7) and crucial amino acids.[47] For this reason, we decided not to perform *in silico* calculations once again using an experimental H_3R structure.

2.7. Determination of Selected ADMET Parameters. *2.7.1. Permeability Profile.* During the research and development of new drugs directed to the central nervous system, there is a considerable attrition rate caused by their hampered access to the brain by the blood−brain barrier. Throughout the years, several *in vitro* models have been developed in an attempt to mimic critical functionalities of the blood−brain barrier and reliably predict the permeability of drug candidates. Therefore, the ability of selected compounds (**3**, **7**, **12**, and **S1RA**) to penetrate across lipid membranes was estimated by a parallel artificial membrane permeability assay (PAMPA). In medicinal chemistry, PAMPA is a method that determines the permeability of substances from a donor compartment through a lipid-infused artificial membrane into an acceptor compartment; passive diffusion is the predominant absorption mechanism of most commercial drugs.[48] By using UPLC−MS with an internal standard, the exact quantity of molecules that penetrated from donor to acceptor wells through the phospholipid membrane was measured. The results were expressed as permeability coefficient P_e calculated according to the formulas described in the literature.[49] Taking into account the collected data and comparing them with two standards: well-permeable caffeine ($P_e = 10.49 \times 10^{-6}$ cm/s) and low-permeable sulpiride ($P_e = 0.05 \times 10^{-6}$ cm/s), it seems justified to consider the tested molecules as substances with highly passive transport through biological membranes (Table 5). In general, compounds with a P_e value above 4×10^{-6} cm/s are considered permeable, whereas those with a lower value are considered impermeable. All tested ligands showed P_e values greater than the threshold value.

Table 5. PAMPA Results (Permeability Coefficient P_e) for Tested Compounds

compound	P_e (10^{-6} cm/s)
S1RA	5.26
3	6.57
7	10.63
12	12.00
caffeine	10.49
sulpiride	0.05

Moreover, taking into account an intracellular localization of sigma receptors, the high ability of tested compounds to penetrate lipid membranes and, at the same time, the possibility of interacting with σ_1R seem to be an important feature of dual histamine H_3/σ_1R ligands.

2.7.2. Serum Metabolic Stability. A successful drug-lead candidate must possess favorable characteristics, including, among others, good serum stability; therefore, we decided to test this parameter for compound **12**. Using LC−MS with imipramine as an internal standard, the exact amount of molecule remaining in the serum was measured at six time points (0, 1, 2, 4, 6, and 24 h) for three initial concentrations (0.1, 0.5, and 1 μM). The response ratio was calculated by dividing the test peak area by the internal standard peak area and converted to % of test compound remaining in the serum. The % of test compound remaining was then plotted vs time (Figure 10). Upon the curve fitting using a one phase decay model, the half-life parameter was calculated to characterize the serum stability of compound **12** ($t_{1/2} = 7.7 \pm 1.4$ h). As a reference drug, we used highly stable atenolol at an initial concentration of 1 μM. The % of atenolol remaining in the serum after 24 h of incubation was significantly higher than compound **12** (82.3 vs 17.5%); thus, **12** can be considered a moderately stable ligand.

2.8. *In Vivo* Pharmacological Activity. *2.8.1. Safety Pharmacology: Influence of Lead Compounds on Sponta-*

https://doi.org/10.1021/acs.jmedchem.3c00430
J. Med. Chem. 2023, 66, 9658−9683

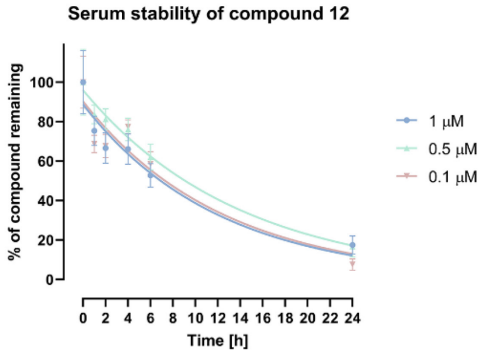


Figure 10. Serum stability of compound **12**. The % of test compound remaining in the serum is plotted vs time, and the curve is fitted using a one phase decay model.

neous Locomotor Activity and Motor Coordination in the Rotarod Test. The high sedative activity of analgesics is considered an undesirable property, which may lead to an incorrect or ambiguous interpretation of the *in vivo* results. Moreover, it may limit the potential clinical application of new drug candidates. Therefore, we tested the influence of compounds **3**, **7**, and **12** on spontaneous locomotor activity to investigate their sedative properties. The data presented in Figure S30 indicate that compounds **3** and **7** at the dose of 15 mg/kg showed high and significant sedative effects ($F_{(2,21)}$ = 28.36; $p < 0.0001$). In contrast, **12** at the same dose decreased spontaneous locomotor activity, but the effect was not statistically significant, which proved the less pronounced sedative property of this compound. It significantly decreased locomotor activity at the dose of 30 mg/kg ($F_{(3,32)} = 4.97$; $p < 0.01$). The estimated ED_{50} value for the ligand in this test was 21.97 mg/kg (Figure S31).

The neurotoxicity of the new compounds can result in impaired motor functions of the experimental animals, which may subsequently cause false interpretation of the results of *in vivo* tests. Understandably, neurotoxicity is also the frequent reason for eliminating the tested compound from further studies. To minimize that risk, we investigated the influence of our lead structures on motor coordination in the rotarod test, which is the classical test used for assessing motor coordination and balance in rodents. It provides a quick and simple estimation of neuromuscular coordination. During our test, the vehicle-treated mice did not demonstrate any signs of impaired motor coordination. The time spent on the rotarod apparatus was 60 s for each control mouse. Compound **7** at the dose of 15 mg/kg significantly decreased the time spent on the rod at 18 and 24 rpm ($F_{(3,20)}$ = 31.32; $p < 0.0001$). Although the effect of **3** was less pronounced, the compound also significantly impaired the motor coordination of mice at the administrated dose (15 mg/kg) and two tested speeds (18 and 24 rpm) ($F_{(3,20)} = 3.33$; $p < 0.05$). Compound **12** at the same conditions slightly affected motor coordination, but the effect was not statistically significant ($F_{(3,20)}$ = 2.31; p = 0.107) (Figure S32). The results showed that **12** is characterized by a better safety profile than the other two tested compounds.

2.8.2. Antinociceptive Activity in the Formalin Test. The formalin test is one of the most useful screening models for testing potentially clinically relevant antinociceptive molecules because of its ease of administration, standardization, and validation with reference drugs.[50] The subcutaneous injection of formalin results in a focal injury that stimulates and then damages sensory endings. Two distinct phases of nociceptive response are associated with the immediate activation of nociceptors and sensitization of spinal reflex circuits during phase I and II responses, respectively.[51] Moreover, it has been recently suggested that formalin injection results in pathological changes that resemble those observed in nerve injury.[52] The intraperitoneal (i.p.) administration of compound **7** prior to the subcutaneous injection of formalin significantly affected the duration of the nociceptive response in the acute phase of the formalin test ($F_{(4,40)} = 21.36$; $p < 0.0001$). This ligand also significantly attenuated the late phase of the test ($F_{(4,40)}$ = 16.50; $p < 0.0001$). The calculated ED_{50} value in phase I was found to be 11.9 mg/kg, whereas the ED_{50} value in phase II was found to be 11.7 mg/kg (Figure 11b). The treatment with **3** resulted in a significant decrease in nociceptive response in both the acute phase ($F_{(3,34)} = 43.20$; $p < 0.0001$) and the late phase ($F_{(3,32)}$ = 17.63; $p < 0.0001$). The potency of the compound expressed as the ED_{50} value was slightly lower than that obtained for the previous compound and was 14.21 and 13.31 mg/kg for the acute and late phases, respectively (Figure 11A). Ligand **12** showed high analgesic activity in the acute phase ($F_{(4,40)}$ = 13.73; $p < 0.0001$) and late phase ($F_{(4,40)}$ = 9.51; $p < 0.0001$) of the test (Figure 11C). Interestingly, the obtained ED_{50} values (6.17 and 12.32 mg/kg for the acute and late phase, respectively) reveal the particularly high potency of this compound in the acute, neurogenic phase, which suggests that it may affect the mechanisms of neurotransmitter release from neuronal cells.

Taking all data from preliminary studies, we decided to select compound **12** for further analysis of its analgesic activity. Although all three compounds showed significant activity in the formalin test, the safety profile of **12** was better than the other ligands. The chosen compound did not affect motor coordination significantly, and its ED_{50} value in the formalin test was almost two times lower than that obtained in the evaluation of the sedative activity. We used other models of pain to assess the range of analgesic activity of the compound with particular emphasis on neuropathic pain of different origins.

2.8.3. Effects of 12 on Capsaicin-Induced Nociception. Because compound **12** had a strong effect on the acute phase of the formalin test, we decided to evaluate its activity in capsaicin-induced pain, which is another model of neurogenic pain. Formalin-induced pain is mainly dependent on the chemical stimulation of the TRPA1 receptor on somatosensory nerve endings, whereas capsaicin is an agonist of TRPV1 receptors.[53]

As shown in Figure 12, the selected compound significantly decreased the paw licking or biting behavior in that test at all administrated doses (10, 15, and 30 mg/kg) ($F_{(3,34)} = 28.48$, $p < 0.0001$). The ED_{50} value calculated for **12** in the capsaicin test was 10.32 mg/kg.

The high potency of **12** in both formalin- and capsaicin-induced pain shows that this compound has the potential to attenuate neurogenic pain independent of the mechanism of its induction. This suggests a broad spectrum of activity of this ligand.

2.8.4. Effects of 12 on Loperamide-Induced Antinociception. As it is well known that σ_1R antagonism enhances opioid analgesia, we tested the effects of compound **12** on antinociception induced by the opioid agonist loperamide.

https://doi.org/10.1021/acs.jmedchem.3c00430
J. Med. Chem. 2023, 66, 9658−9683

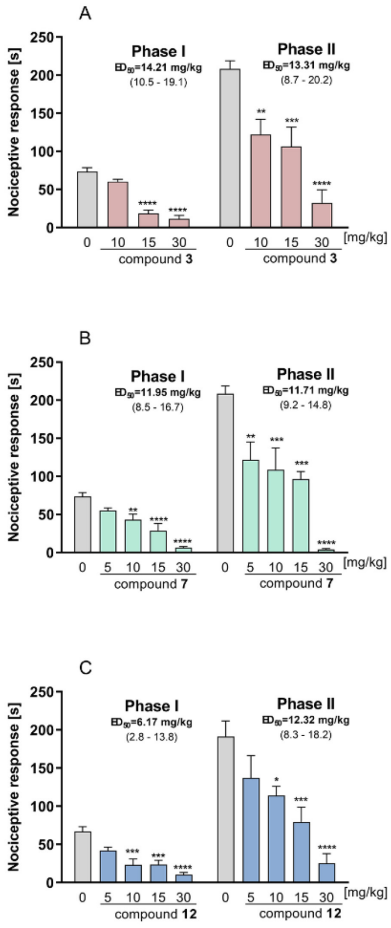


Figure 11. Antinociceptive activity of **3** (A), **7** (B), and **12** (C) in the formalin test. Results are shown as time of licking in phase I (0−5 min after intraplantar injection of formalin) and in phase II (15−30 min after formalin injection). Each value represents the mean ± S.E.M. for 8−10 animals. 0: vehicle (1% Tween 80). Statistical analysis: one-way ANOVA followed by *post hoc* Dunnett's test. Statistical significance compared to vehicle-treated animals: $*p < 0.05$, $**p < 0.01$, $***p < 0.001$, and $****p < 0.0001$.

S1RA was used as a σ_1R reference antagonist and administered intraplantarly (i.pl.) at two doses of 50 and 100 μg. Compound **12** was tested at 12.5 and 25 μg. The antinociceptive effect of the treatments was tested in mice by monitoring the latency to struggle in response to a nociceptive mechanical stimulus applied to the paw. The subcutaneous (s.c.) administration of loperamide (4 mg/kg) induced a minimal (nonsignificant) increase in the struggle response latency in comparison to the values from mice treated with its solvent (Figure 13). The administration of **S1RA** alone (100 μg) did not change the response to the mechanical stimulus but significantly and dose-dependently (50−100 μg) increased the antinociceptive effect induced by loperamide and only in the paw injected with the σ_1R antagonist (Figure 13). The administration of compound **12** (25 μg) did not have any effect *per se* but dose-dependently

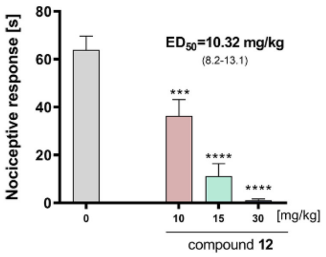


Figure 12. Antinociceptive activity of compound **12** in the capsaicin test. Results are shown as time of nociceptive response in 5 min period after intraplantar injection of capsaicin. Each value represents the mean ± S.E.M. for 8−10 animals. Statistical analysis: one-way ANOVA followed by *post hoc* Dunnett's test. Statistical significance compared to vehicle-treated animals (Tween): $****p < 0.0001$. 0: vehicle treated mice (1% Tween 80).

(12.5−25 μg) increased the antinociceptive effect of loperamide at the injected paw, mirroring the effects induced by **S1RA** (Figure 13). Hence, the potency of compound **12** to enhance loperamide-induced antinociception was much higher than **S1RA**. Notably, the coadministration of the σ_1R agonist PRE-084 (75 μg) with **S1RA**, and also with **12**, was able to markedly reverse the effect of these compounds on loperamide-induced antinociception (Figure 13). These data strongly support that not only **S1RA** but also compound **12** is a σ_1 receptor antagonists. Moreover, the effect of **S1RA** and **12** was also reversed by naloxone-methiodide that is a peripheral opioid antagonist. This means that the observed pharmacological effect is due to the peripheral potentiation of opioid antinociception by sigma-1 receptor antagonism.

In further studies, we used two different models of neuropathic pain to test the influence of **12** on pain associated with neuronal tissue damage: the oxaliplatin-induced model and the chronic constriction injury (CCI) model. The mechanism of neuron impairment is different in both, which may relate to the different efficacy of potential treatments. In the oxaliplatin-induced model, neurons are directly affected by this chemotherapeutic agent. That leads to mechanical allodynia resulting from the impaired regulation of ion channels and destruction of mitochondrial DNA, among others.[54] In CCI, neuropathy impairs peripheral nerve function, and neuronal damage results from a persistent mechanical stimulus and its complications such as vascular and metabolic dysfunctions.

2.8.5. Oxaliplatin (OXPT)-Induced Neuropathy. The neuropathy manifests as a decrease in the pain threshold and can be observed in hours or in days after oxaliplatin administration, which is called the early or late phase of neuropathic pain, respectively. We tested the influence of compound **12** on tactile allodynia using the von Frey method 3 h and 7 days after the induction of neuropathy.[12]

In the group treated with **12** at the dose of 5 mg/kg (Figure 14), the initial value of 5.53 ± 0.34 (baseline) was decreased to the value of 3.51 ± 0.17 (63.5% of the baseline) and 4.30 ± 0.08 (77.7% of the baseline) in the early and late phase, respectively. The single administration of **12** partially reversed the effect of OXPT in the early phase (88.6% of the baseline; $F_{(2.136,\ 19.22)} = 7.66$, $p < 0.01$) but not in the late phase. In the group treated with **12** at the dose of 10 mg/kg, the initial value of 5.83 ± 0.41 was decreased to the value of 2.94 ± 0.36

https://doi.org/10.1021/acs.jmedchem.3c00430
J. Med. Chem. 2023, 66, 9658−9683

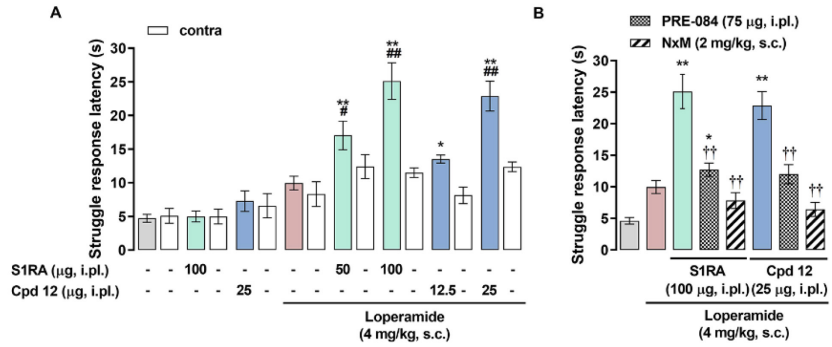


Figure 13. Effects of **S1RA** and **12** on loperamide-induced antinociception. The results represent the struggle response latency during stimulation with 450 g pressure in mice intraplantarly (i.pl.) administered **S1RA** (50−100 μg), **12** (12.5−25 μg), or saline and treated subcutaneously (s.c.) with loperamide (4 mg/kg) or its solvent (1% DMSO in ultrapure water). (A) Effect of treatments on the response latency to mechanical stimulation in the paw i.pl. injected with the σ_1R ligands (ipsi) and in the contralateral paw (contra). (B) Effect of the i.pl. administration of PRE-084 (75 μg) and the s.c. administration of naloxone-methiodide (NxM, 2 mg/kg) on the potentiation of loperamide-induced antinociception by **S1RA** and **12**. Each bar and vertical line represent the mean ± SEM of values obtained in six to eight animals. Two-way analysis of variance followed by the Bonferroni test was used to determine statistically significant differences (A and B) between the values obtained in the group treated with the solvent of the drugs and the rest of the groups (*$p < 0.05$, **$p < 0.01$), (A) between the ipsi and the contra paws (##$p < 0.01$), and (B) between the values of the ipsi paw from loperamide-treated mice injected with **S1RA** or **12** alone and coadministered with PRE-084 or with the association with NxM (†÷$p < 0.01$).

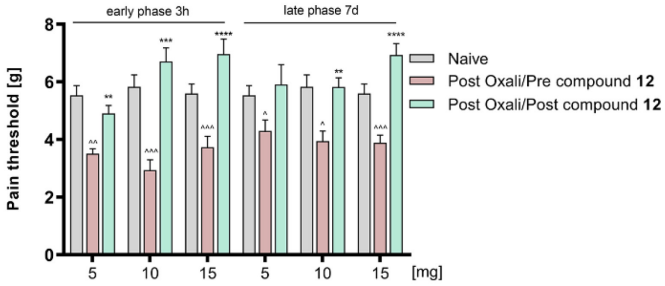


Figure 14. Antiallodynic effects of compound **12** in the tactile allodynia evaluated in the von Frey test in oxaliplatin-induced peripheral neuropathy. Each experimental group consisted of 8−10 animals. **$p < 0.01$, ***$p < 0.001$, and ****$p < 0.0001$ (repeated measures analysis of variance (ANOVA) followed by Dunnett's *post hoc* test) when the groups were compared to oxaliplatin treatment; ^$p < 0.05$, ^^$p < 0.01$, and ^^^$p < 0.001$ (repeated measures analysis of variance ANOVA followed by *post hoc* Dunnett's test) when the groups were compared to naive animals.

(50.4% of the baseline) and 3.94 ± 0.36 (67.6% of the baseline) in the early and the late phase, respectively. The single administration of **12** reversed the effect of OXPT in both the early phase (115.0% of the baseline) and the late phase (99.8% of the baseline) ($F_{(2.574, 20.59)} = 17.84$, $p < 0.0001$). In the group treated with **12** at the dose of 15 mg/kg, the initial value of 5.60 ± 0.33 was decreased to the value of 3.73 ± 0.38 (66.6% of the baseline) and 3.88 ± 0.27 (69.3% of the baseline) in the early and late phase, respectively. The single administration of **12** completely reversed the effect of OXPT and even elevated the pain threshold above the baseline in both the early phase (124.3% of the baseline) and the late phase (123.7% of the baseline) ($F_{(2.317, 41.71)} = 21.67$, $p < 0.0001$).

These results indicate that compound **12** exhibits potency for relieving chemotherapy-induced neuropathic pain (all the tested doses were significantly active), which confirms its wide range of analgesic activity and encourages further research.

2.8.6. Effects of 12 on Neuropathic Pain Symptoms in CCI-Exposed Mice. Behavioral assessment of **12** was performed 14 days after the sciatic nerve injury. Mice were randomly assigned to four treatment groups: vehicle-treated (i.p.) and **12**-treated (5, 10, and 15 mg/kg, i.p.). Baseline measurements (basal) for all tests were performed before compound injections, and the results are presented as percentages of the maximal possible effect (% MPE). We observed a significant effect of the tested compound in the von Frey test at all tested time points (30 min: $F_{(3, 26)} = 12.38$, $p < 0,0001$; 90 min: $F_{(3, 26)} = 12.65$, $p < 0.0001$; 180 min: $F_{(3, 26)} = 6.464$, $p = 0.0020$). In CCI-exposed mice, **12** exhibited significant analgesic effects 30 min after injection of 5 ($p < 0.0001$) and 10 mg/kg ($p = 0.0201$) in the von Frey test compared with vehicle-treated animals (Figure 15A). However, a single injection of compound **12** only at a dose of 10 mg/kg increased the withdrawal thresholds in the von Frey test at 90 ($p < 0.0001$) and 180 ($p = 0.0014$) min after administration (Figure 15A). We also observed a significant effect of treatment on the contralateral paw 90 min after injection ($F_{(3, 26)} = 5.741$, $p = 0.0037$). Further analysis showed no effects of compound **12** (for doses 5 and 10 mg/kg) on tactile allodynia in the von Frey test at all time points after treatment. However, **12** at dose 15 mg/kg reduced the withdrawal

https://doi.org/10.1021/acs.jmedchem.3c00430
J. Med. Chem. 2023, 66, 9658−9683

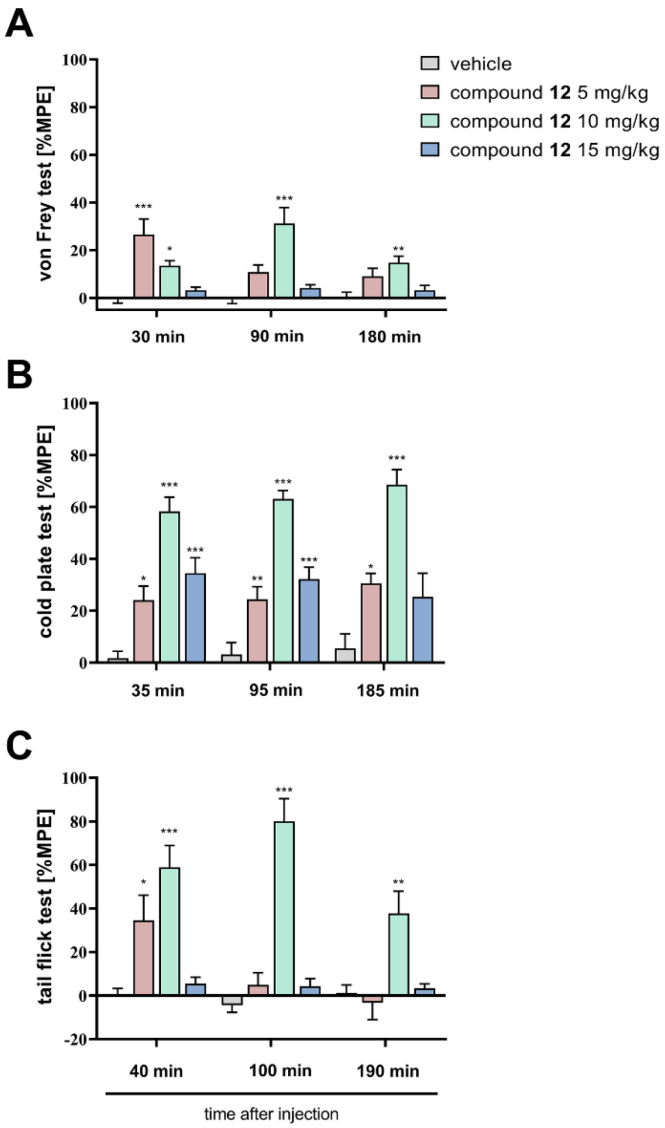


Figure 15. The effects of single i.p. administration of **12** (5, 10 and 15 mg/kg) on mechanical (A, von Frey test) and thermal (B, cold plate test; C, tail flick test) stimulus on day 14 following CCI to the sciatic nerve were evaluated (n = 7–8 animals per group). The results are presented as percentages of the maximal possible effect (% MPE; means ± SEM). Intergroup differences were analyzed by one-way ANOVA with Bonferroni's multiple comparison *post hoc* test. *p < 0.05, **p < 0.01, and ***p < 0.001 vs vehicle-treated group.

threshold 30 and 180 min after injection, although this effect was not statistically significant at those time points. But 90 min after injection, we observed a significant effect (p = 0.0056) (Figure S33). We have also observed a significant effect of treatment on thermal stimuli as measured in a cold plate test at all tested time points (35 min: $F_{(3, 26)}$ = 20.77, p < 0.0001; 95 min: $F_{(3, 26)}$ = 32.42, p < 0.0001; 185 min: $F_{(3, 26)}$ = 16.11, p < 0.0001). Here, analgesic effects of **12** single injection were observed at 35 min for all tested doses as compared with control animals (5 mg/kg: p = 0.019; 10 mg/kg: p < 0.0001; 15 mg/kg: p = 0.0004) (Figure 15B). This antihyperalgesic effect was also observed 95 min after injection (5 mg/kg: p = 0.0072; 10 mg/kg: p < 0.0001; 15 mg/kg: p = 0.0002) (Figure 15B). However, 185 min after treatment, the analgesic effect was significant only for doses 5 (p = 0.0482) and 10 mg/kg (p < 0.0001). The measurements of spinal responses assessed by the tail flick test also revealed a significant effect of treatments (40 min: $F_{(3, 25)}$ = 11.74, p < 0.0001; 100 min: $F_{(3, 25)}$ = 35.93, p < 0.0001; 190 min: $F_{(3, 25)}$ = 7.479, p = 0.001). The analysis of the tail flick test results (Figure 15C) showed significant analgesic action of **12** at 40 min (for doses 5 (p = 0.021) and 10 mg/kg (p < 0.0001)) after injection as compared with

https://doi.org/10.1021/acs.jmedchem.3c00430
J. Med. Chem. 2023, 66, 9658−9683

vehicle-treated mice. At the further time points (100 and 190 min), only the 10 mg/kg dose had significant analgesic effects ($p < 0.0001$ and $p = 0.0033$, respectively) (Figure 15C).

3. CONCLUSIONS

Comprehensive and rational drug discovery requires a multidisciplinary approach involving many techniques and methods. A deeper understanding of the molecule's physicochemical properties and its conformational preferences may be very helpful, especially in the case of selective or dual (multi)-target therapeutic agent design.

In our study, we decided to combine chemical, biological, and computational methods to reveal molecular properties responsible for histamine H_3R and σ_1R selective or dual-target binding of the studied compounds. Considering the different abilities of piperidine and piperazine derivatives substituted with a 4-pyridyl moiety to form a salt bridge with Glu172 in the σ_1R binding pocket, which is a crucial interaction for ligand−protein complex stability and thus the high biological activity, we performed an in-depth analysis of their protonation states with three different methods. In the case of piperidine derivatives, the crystal structure confirmed the presence of two protonation centers with higher basic properties of the piperidine vs pyridine nitrogen atom. In contrast, for the piperazine derivatives, we observed a strong basic character of the pyridine nitrogen atom as a consequence of the increased availability of the lone pair electrons. The former is correlated with the source of electrons located at the para position, originated in the piperazine ring's nitrogen atom with its lone pair of electrons being involved in the π-electron resonance. The observed rigidity of the 4-pyridylpiperazine fragment not only determines the highly basic character of pyridine nitrogen atom but also strongly defines the spatial orientation of π-electrons of the aromatic fragment. This geometrical feature is most likely responsible for the effective ligand−protein recognition and may explain the observed selectivity of the investigated compounds containing 4-pyridylpiperazine fragment for H_3R. Moreover, the order of protonation of individual nitrogen atoms based on NMR spectroscopy measurements in a pH-controlled environment stays in agreement with the crystallographic data for both piperidines and piperazines. Interestingly, for the piperazine derivative **KSK94**, we observed a transfer of the positive charge from the pyridine nitrogen atom, which was protonated first, to the piperazine nitrogen through appropriate resonance structures. This observation is fully consistent with the crystallographic data and explains the inability of 4-pyridylpiperazine derivatives to form a salt bridge with Glu172 in the σ_1R binding pocket. This is caused by the low basicity of the second piperazine nitrogen atom, which was initially unprotonated. A series of titrations allowed determining pK_a values of individual nitrogen atoms and recognizing piperidine derivative **KSK68** as a basic ligand with $pK_{a1} = 4.9$ (pyridine N) and $pK_{a2} = 8.4$ (piperidine N). In turn, the **KSK94** compound belongs to ligands with an acidic center located on the piperazine nitrogen atom to which the pyridine ring is directly attached ($pK_{a2} = 1$). The protonation states of the compounds were also assessed *in silico*, and the obtained results were consistent with the experimental data.

In the next step, we designed and synthesized a series of 16 novel compounds, mainly piperidine derivatives, and determined their affinity at H_3R, σ_1R, and σ_2R. We confirmed the previously described phenomenon and identified a second pair of similar compounds, differing only in the 4-pyridylpiperazine/piperidine core with dual H_3/σ_1R activity of the piperidine derivative **12** and no affinity toward σ_1R of its piperazine analogue **KSK94**. To further investigate the impact of structural differences between these moieties on their molecular mode of action, the binding to σ_1R and H_3R was evaluated using molecular modeling techniques and molecular dynamics simulations. Both the free binding energies and the docking scores of the most abundant protonation states correlated with the *in vitro* activity of the tested ligands.

As the lead structures for further evaluation, we selected compounds **3** and **7** with the highest σ_2/σ_1 selectivity factor (13.2 and 24.2, respectively) and ligand **12** with the same high σ_2R activity as for major biological targets. It is well known that sigma receptors modulate nociception, offering a potential therapeutic target for pain management, but relatively little is known about the role of σ_2R in the pathomechanism of this condition. Interestingly, recent studies with the highly σ_2R-selective compound CM-398 showed that it ameliorates inflammatory and chronic neuropathic pain in established mouse models, suggesting possible mediation of nociception by σ2R.[33] Therefore, it seems reasonable to test triple-targeting $H_3/\sigma_1/\sigma_2R$ ligand **12** alongside the dual-acting compounds **3** and **7**.

All lead structures had no affinity at other histamine receptor subtypes and were characterized as potent H_3R antagonists in the cAMP accumulation assay. Moreover, we checked their ability to penetrate lipid membranes by parallel artificial membrane permeability assay. All tested molecules can be considered substances with high passive transport through biological membranes. Taking into account an intracellular localization of σ_1R, the satisfactory level of lipid membranes penetration and thus the ability of studied compounds to reach this biological target seem to be an important feature of dual H_3/σ_1R ligands. Furthermore, we also tested the serum stability of compound **12**, and the obtained data clearly indicate that it can be considered as a moderately stable ligand, which is relatively rapidly degraded by serum enzymes. This is associated with the presence of a hydrolysis-susceptible nitrile group within its structure. On the other hand, this moiety was one of the key structural element responsible for the pharmacological activity of **12**. Thus, the identification of other groups in this region, less sensitive to serum enzymes activity, will be the subject of our further studies. Knowledge of the permeability profile and stability in plasma of tested ligand is a very preliminary step in predicting its exposure required for *in vivo* efficacy.

Finally, we tested the efficacy of compounds **3**, **7**, and **12** in animal models of pain. We started by testing the safety pharmacology and checked their influence on spontaneous locomotor activity and motor coordination in the rotarod test. Compounds **3** and **7** showed high and significant sedative effects and significantly impaired motor coordination in mice at the administrated doses. In contrast, the obtained results showed that **12** is characterized by a better safety profile than the other two tested compounds; hence, we chose this ligand for further analysis of its analgesic activity. The high potency of **12** in both formalin- and capsaicin-induced pain shows that this compound has the potential to attenuate neurogenic pain regardless of the mechanism of its induction. We then tested the effect of **12** on antinociception induced by the opioid agonist loperamide. Administration of compound **12** enhanced the effect of loperamide, which was markedly reversed by co-

https://doi.org/10.1021/acs.jmedchem.3c00430
J. Med. Chem. 2023, 66, 9658−9683

administration of the σ_1R agonist PRE-084. These data strongly support that **12** is a potent σ_1R antagonist. Finally, we used two different models of neuropathic pain to test the influence of **12** on pain associated with neuronal tissue damage. The obtained results indicate that compound **12** has the potential to alleviate both chemotherapy-induced neuropathic pain and pain resulting from sciatic nerve damage. This confirms its broad spectrum of analgesic activity, which may be related to the dual H_3/σ_1R modulation as well as the additional interaction with σ_2R. Determining the exact mechanism of action of compound **12** will be the subject of our further studies.

4. EXPERIMENTAL PROTOCOLS

4.1. Chemistry. All reagents were purchased from commercial suppliers and were used without further purification. Melting points (m.p.) were determined on a MEL-TEMP melting point apparatus II (LD Inc., USA) and are uncorrected. HPLC analysis were performed on an Agilent 1290 UHPLC system coupled with an Agilent QTOF 6545 mass spectrometer (a Phenomenex Kinetex 1.7 μm EVO C18 (100 Å, 50 × 2.1 mm) reversed-phase column was used). Mass spectra (LC/MS) were carried out on a system consisting of a Waters Acquity UPLC coupled to a Waters TQD mass spectrometer. Retention times (t_R) are given in minutes. High-resolution mass spectrometry (HRMS) was performed on Thermo Scientific Orbitrap Exploris 240 mass spectrometer. ^{1}H NMR spectra were recorded on a Varian Mercury 300 MHz PFG spectrometer in DMSO-d_6. Chemical shifts were expressed in parts per million (ppm) using the solvent signal as an internal standard. Data are reported in the following order: multiplicity (s, singlet; d, doublet; dd, double of doublets; t, triplet; tt, triplet of triplets; quin, quintet; qd, quartet of doublets; m, multiplet; br, broad), approximate coupling constants J expressed in hertz (Hz), and number of protons. ^{13}C NMR spectra were recorded on a Varian-Mercury-VX 300 MHz PFG or Bruker 400 MHz spectrometer at 75 MHz in DMSO-d_6. Elemental analyses (C, H, N) were performed on a Vario El III elemental analyzer (Hanau, Germany). For CC purification (column chromatography using silica gel 60 (0.063−0.20 mm); Merck), the following solvent systems were used: I: petroleum ether/EtOAc (9:1); II: CH_2Cl_2/MeOH (9:1). Chemical compounds' names were generated using Chem Draw Professional 18.0.0.231 (4029).

All final compounds are >95% pure by HPLC analysis.

*4.1.1. General Synthetic Procedure for Compounds **a**−**i**.* All compounds were obtained using methods described previously.[19,21,22,24,25] To a solution of freshly prepared sodium 1-propanolate (0.1 mol, 100 mL), proper substituted phenols (0.1 mol) were added and stirred in room temperature for 5 min. α,ω-Dibromoalkanes (0.2 mol) were then added dropwise in the time of 1 h. The reaction mixture was stirred in 60 °C for 3 h and then refluxed for another 3 h. After cooling down to RT, the mixture was filtrated and evaporated. To a rough product, 100 mL of 10% NaOH was added and left overnight in the cold. To a resulting white oil, CH_2Cl_2 was added and mixed, and layers were then separated. The organic layer was dried over sodium sulfate, filtered, and evaporated. The rough product was used for further reactions after purification.

*4.1.1.1. 4-(3-Bromopropoxy)-1,1′-biphenyl (**a**).* Compound previously described in the literature.[21] Obtained 22.13 g of raw product, purified by CC (I), yield 76%. CAS113795-28-1.

*4.1.1.2. 4′-(3-Bromopropoxy)-[1,1′-biphenyl]-4-carbonitrile (**b**).* Compound previously described in the literature.[22] Obtained 17.71 g of raw product, purified by CC (I), yield 56%. CAS134880-32-3.

*4.1.1.3. 1-(3-Bromopropoxy)-4-phenoxybenzene (**c**).* Compound previously described in the literature.[22] Obtained 16.59 g of raw product, purified by CC (I). yield 54%. CAS63457-51-2.

*4.1.1.4. 4-(3-Bromopropoxy)-N-phenylaniline (**d**).* Compound previously described in the literature.[22] Obtained 15.92 g of raw product, purified by CC (I), yield 52%.

*4.1.1.5. 1-Benzyl-4-(3-bromopropoxy)benzene (**e**).* Compound previously described in the literature.[22] Obtained 17.40 g of raw product, purified by CC (I), yield 57%. CAS60859-24-7.

*4.1.1.6. 4-(4-Bromobutoxy)-1,1′-biphenyl (**f**).* Compound previously described in the literature.[55] Obtained 12.51 g of raw product, purified by CC (I), yield 41%. CAS53669-78-6.

*4.1.1.7. 4-((5-Bromopentyl)oxy)-1,1′-biphenyl (**g**).* Compound previously described in the literature.[24] Obtained 7.66 g of raw product, purified by CC (I), yield 24%. CAS52273-19-5.

*4.1.1.8. 4-((6-Bromohexyl)oxy)-1,1′-biphenyl (**h**).* Compound previously described in the literature.[24] Obtained 8.33 g of raw product, purified by CC (I), yield 25%. CAS158136-46-0.

*4.1.1.9. 1-(4-Bromobutoxy)-4-(tert-butyl)benzene (**i**).* Compound previously described in the literature.[19] Obtained 19.68 g of raw product, purified by CC (I), yield 69%. CAS53669-73-1.

*4.1.2. General Synthetic Procedure for Compounds **1**−**16**.* All compounds were obtained using methods described previously.[19,21,22,24,25] To a suspension of potassium carbonate (8.5 mmol) and a catalytic amount of potassium iodide in water (10 mL), a mixture of proper amine (5 mmol) and compound **a**−**i** (5 mmol) in ethanol (50 mL) was added as previously described.[19,21,22,24,25] The mixture was then refluxed for 8−12 h (TLC controlled). After cooling down to room temperature, reaction mixture was filtrated, evaporated, and purified. To the resulting oil, 100 mL of CH_2Cl_2 was added and washed with 0.5% HCl solution, 0.5% NaOH solution, and water. After drying over anhydrous Na_2SO_4 and evaporation of the organic layer, the product was further purified using CC (II). Compounds **5**, **10**, **11**, and **16** were obtained as in previous studies and used in the biological assays with high purity estimated using LC/MS; details of their synthesis and analyses are described elsewhere.[19,24,25]

*4.1.2.1. 1-(3-([1,1′-Biphenyl]-4-yloxy)propyl)-3-methylpiperidine Oxalate (**1**).* White solid, yield 30%, m.p. 169−172 °C, $C_{21}H_{27}NO\cdot C_2H_2O_4$ (MW = 399.49). RP-HPLC: 99.67% (t_R = 2.890, k' = 14.21). ^{1}H NMR (500 MHz, DMSO-d_6) δ ppm: 7.57 (dd, J = 2.00, 8.31 Hz, 4H), 7.39 (t, J = 7.73 Hz, 2H), 7.24−7.31 (m, 1H), 6.99 (d, J = 8.59 Hz, 2H), 4.04 (t, J = 6.01 Hz, 2H), 3.28−3.42 (m, 2H), 3.10 (t, J = 7.59 Hz, 2H), 2.71 (t, J = 10.74 Hz, 1H), 2.43 (br. s., 1H), 2.11 (quin, J = 6.80 Hz, 2H), 1.79−1.90 (m, 1H), 1.62−1.78 (m, 3H), 0.95−1.09 (m, 1H), 0.86 (d, J = 6.59 Hz, 3H). ^{13}C NMR (126 MHz, DMSO-d_6) δ ppm: 165.2, 158.4, 140.3, 133.3, 129.4, 128.3, 127.3, 126.7, 115.5, 65.7, 58.1, 54.0, 54.0, 52.2, 30.6, 29.1, 24.1, 22.8, 22.8, 19.1. LC−MS: purity 100.00%, t_R = 5.53, (ESI) m/z $[M + H]^+$ 310.22. Anal. calcd. for $C_{23}H_{29}NO_5$: C, 69.15; H, 7.32; N, 3.51%. Found: C, 68.94; H, 7.08; N, 3.46%.

*4.1.2.2. 1-(3-([1,1′-Biphenyl]-4-yloxy)propyl)-4-methylpiperidine Oxalate (**2**).* White solid, yield 38%, m.p. 222−224 °C, $C_{21}H_{27}NO\cdot C_2H_2O_4$ (MW = 399.49). RP-HPLC: 97.96% (t_R = 2.888, k' = 14.20). ^{1}H NMR (500 MHz, DMSO-d_6) δ ppm: 7.57 (d, J = 8.59 Hz, 4H), 7.39 (t, J = 7.73 Hz, 2H), 7.24−7.30 (m, 1H), 6.99 (d, J = 8.59 Hz, 2H), 4.05 (t, J = 6.01 Hz, 2H), 3.37 (d, J = 10.60 Hz, 2H), 3.06−3.15 (m, 2H), 2.83 (br. s., 2H), 2.02−2.15 (m, 2H), 1.74 (d, J = 13.46 Hz, 2H), 1.57 (br. s., 1H), 1.27−1.40 (m, 2H), 0.89 (d, J = 6.30 Hz, 3H). ^{13}C NMR (126 MHz, DMSO-d_6) δ ppm: 140.28, 133.34, 129.42, 128.32, 126.71, 115.48, 100.00, 65.60, 24.28. LC−MS: purity 97.76%, t_R = 5.47, (ESI) m/z $[M + H]^+$ 310.22. Anal. calcd. for $C_{23}H_{29}NO_5$: C, 69.15; H, 7.32; N, 3.51%. Found: C, 68.82; H, 7.53; N, 3.38%.

*4.1.2.3. 1-(3-([1,1′-Biphenyl]-4-yloxy)propyl)azepane Oxalate (**3**).* White solid, yield 38%, m.p. 187−190 °C, $C_{21}H_{27}NO\cdot C_2H_2O_4$ (MW = 399.49). RP-HPLC: 96.06% (t_R = 2.875, k' = 14.13). ^{1}H NMR (500 MHz, DMSO-d_6) δ ppm: 7.57 (d, J = 7.73 Hz, 4H), 7.39 (t, J = 7.30 Hz, 2H), 7.27 (t, J = 7.16 Hz, 1H), 7.00 (d, J = 8.31 Hz, 2H), 4.05 (t, J = 5.58 Hz, 2H), 2.93−3.40 (m, 6H), 2.10 (br. s., 2H), 1.76 (br. s., 4H), 1.40−1.63 (m, 4H). ^{13}C NMR (126 MHz, DMSO-d_6) δ ppm: 165.1, 158.4, 140.3, 133.3, 129.4, 128.3, 127.3, 126.7, 115.5, 65.6, 54.3, 54.2, 26.5, 24.5, 23.7. LC−MS: purity 96.08%, t_R = 5.51, (ESI) m/z $[M + H]^+$ 310.22. Anal. calcd. for $C_{23}H_{29}NO_5$: C, 69.15; H, 7.32; N, 3.51%. Found: C, 68.71; H, 7.08; N, 3.38%.

*4.1.2.4. 1-(3-([1,1′-Biphenyl]-4-yloxy)propyl)pyrrolidine Oxalate (**4**).* White solid, yield 42%, m.p. 204−206 °C, $C_{19}H_{23}NO\cdot C_2H_2O_4$

https://doi.org/10.1021/acs.jmedchem.3c00430
J. Med. Chem. 2023, 66, 9658−9683

(MW = 371.43). RP-HPLC: 96.58% (t_R = 2.768, k' = 13.57). ^{1}H NMR (500 MHz, DMSO-d_6) δ ppm: 7.57 (d, J = 8.31 Hz, 4H), 7.39 (t, J = 7.59 Hz, 2H), 7.23−7.31 (m, 1H), 6.99 (d, J = 8.59 Hz, 2H), 4.05 (t, J = 5.87 Hz, 2H), 3.01−3.42 (m, 6H), 2.03−2.13 (m, 2H), 1.89 (br. s., 4H). ^{13}C NMR (126 MHz, DMSO-d_6) δ ppm: 165.0, 158.4, 140.3, 133.3, 129.4, 128.3, 127.3, 126.7, 115.6, 115.5, 65.4, 53.7, 51.9, 25.9, 23.2. LC−MS: purity 100.00%, t_R = 5.10 (ESI) m/z [M + H]$^+$ 282.137. HRMS (MALDI): m/z [M + H]$^+$ 282.1856.

4.1.2.5. 4′-(3-(Piperidin-1-yl)propoxy)-[1,1′-biphenyl]-4-carbonitrile Oxalate (5). Compound previously described in the literature.[25] White solid, yield 37%. RP-HPLC: 95.63% (t_R = 2.731, k' = 13.37). LC−MS: purity 93.82%, t_R = 4.64, (ESI) m/z [M + H]$^+$ 321.26. HRMS (MALDI): m/z [M + H]$^+$ 321.1966.

4.1.2.6. 1-(3-(4-Phenoxyphenoxy)propyl)piperidine Oxalate (6). White solid, yield 46%, m.p. 137−140 °C, $C_{20}H_{25}NO_2 \cdot C_2H_2O_4$ (MW = 401.46). RP-HPLC: 100.00% (t_R = 2.808, k' = 13.78). ^{1}H NMR (500 MHz, DMSO-d_6) δ ppm: 7.26−7.36 (m, 2H), 7.03 (t, J = 7.30 Hz, 1H), 6.90−6.98 (m, 4H), 6.87 (d, J = 7.73 Hz, 2H), 3.98 (t, J = 6.01 Hz, 2H), 2.79−3.36 (m, 6H), 2.00−2.16 (m, 2H), 1.60−1.77 (m, 4H), 1.49 (br. s., 2H). ^{13}C NMR (126 MHz, DMSO-d_6) δ ppm: 165.3, 158.5, 155.2, 150.1, 130.4, 123.2, 121.2, 117.9, 116.3, 66.0, 54.0, 52.6, 24.1, 23.1, 22.0. LC−MS: purity 97.09%, t_R = 5.19, (ESI) m/z [M + H]$^+$ 312.41. Anal. calcd. for $C_{22}H_{27}NO_6$: C, 65.82; H, 6.78; N, 3.49%. Found: C, 65.59; H, 6.61; N, 3.39%.

4.1.2.7. N-Phenyl-4-(3-(piperidin-1-yl)propoxy)aniline Oxalate (7). White solid, yield 34%, m.p. 130−133 °C, $C_{20}H_{26}N_2O \cdot C_2H_2O_4$ (MW = 400.48). RP-HPLC: 99.41% (t_R = 2.726, k' = 13.35). ^{1}H NMR (400 MHz, DMSO-d_6) δ ppm: 7.87 (br. s., 1H), 7.12−7.22 (m, 2H), 7.04 (d, J = 9.00 Hz, 2H), 6.83−6.96 (m, 4H), 6.72 (t, J = 7.24 Hz, 1H), 3.98 (t, J = 5.87 Hz, 2H), 2.91−3.32 (m, 6H), 2.04−2.20 (m, 2H), 1.63−1.84 (m, 4H), 1.53 (br. s., 2H). ^{13}C NMR (101 MHz, DMSO-d_6) δ ppm: 165.1, 153.1, 145.4, 136.9, 129.6, 120.6, 118.8, 115.8, 115.4, 65.8, 54.1, 52.6, 24.1, 23.2, 22.0. LC−MS: purity 100%, t_R = 4.88, (ESI) m/z [M + H]$^+$ 311.41. Anal. calcd. for $C_{22}H_{28}N_2O_5$: C, 65.98; H, 7.05; N, 7.00%. Found: C, 66.25; H, 6.89; N, 7.00%.

4.1.2.8. 1-(3-(4-Benzylphenoxy)propyl)piperidine Oxalate (8). White solid, yield 39%, m.p. 152−155 °C, $C_{21}H_{27}NO \cdot C_2H_2O_4$ (MW = 399.49). RP-HPLC: 98.02% (t_R = 2.866, k' = 14.08). ^{1}H NMR (500 MHz, DMSO-d_6) δ ppm: 7.19−7.29 (m, 2H), 7.03−7.18 (m, 5H), 6.81 (d, J = 8.59 Hz, 2H), 3.94 (t, J = 6.01 Hz, 2H), 3.82 (s, 2H), 2.76−3.43 (m, 6H), 1.98−2.11 (m, 2H), 1.62−1.75 (m, 4H), 1.47 (br. s., 2H). ^{13}C NMR (126 MHz, DMSO-d_6) δ ppm: 165.3, 157.1, 142.3, 134.1, 130.2, 129.1, 128.9, 126.4, 115.0, 65.5, 54.0, 52.6, 24.0, 23.1, 22.0. LC−MS: purity 100.00%, t_R = 5.35, (ESI) m/z [M + H]$^+$ 310.47. Anal. calcd. for $C_{23}H_{29}NO_5$: C, 69.15; H, 7.32; N, 3.51%. Found: C, 68.46; H, 7.53; N, 3.36%.

4.1.2.9. 1-(4-([1,1′-Biphenyl]-4-yloxy)butyl)piperidine Oxalate (9). White solid, yield 24%, m.p. 182−185 °C, $C_{21}H_{27}NO \cdot C_2H_2O_4$ (MW = 399.49). RP-HPLC: 97.54% (t_R = 2.863, k' = 14.07). ^{1}H NMR (500 MHz, DMSO-d_6) δ ppm: 7.56 (dd, J = 5.58, 7.59 Hz, 4H), 7.39 (t, J = 7.73 Hz, 2H), 7.18−7.31 (m, 1H), 6.88−7.06 (m, 2H), 4.00 (t, J = 5.87 Hz, 2H), 2.72−3.49 (m, 6H), 1.58−1.86 (m, 8H), 1.29−1.58 (m, 2H). ^{13}C NMR (126 MHz, DMSO-d_6) δ ppm: 165.1, 165.1, 165.0, 158.7, 140.3, 133.1, 129.4, 128.3, 127.3, 126.7, 115.5, 67.4, 56.1, 52.5, 26.5, 23.1, 22.0, 20.8. LC−MS: purity 96.17%, t_R = 5.46, (ESI) m/z [M + H]$^+$ 310.22. Anal. calcd. for $C_{23}H_{29}NO_5$: C, 69.15; H, 7.32; N, 3.51%. Found: C, 68.78; H, 7.47; N, 3.31%.

4.1.2.10. 1-(5-([1,1′-Biphenyl]-4-yloxy)pentyl)piperidine Oxalate (10). Compound previously described in the literature.[24] White solid, yield 66%. RP-HPLC: 98.88% (t_R = 2.934, k' = 14.44). LC−MS: purity 99.60%, t_R = 5.81, (ESI) m/z [M + H]$^+$ 324.44.

4.1.2.11. 1-(6-([1,1′-Biphenyl]-4-yloxy)hexyl)piperidine Oxalate (11). Compound previously described in the literature.[24] White solid, yield 60%. RP-HPLC: 100.00% (t_R = 3.013, k' = 14.86). LC−MS: purity 100.00%, t_R = 6.18, (ESI) m/z [M + H]$^+$ 338.47.

4.1.2.12. 4′-(3-(4-(Pyridin-4-yl)piperidin-1-yl)propoxy)-[1,1′-biphenyl]-4-carbonitrile Oxalate (12). White solid, yield 32%, m.p. 157−160 °C, $C_{26}H_{27}N_3O \cdot C_2H_2O_4$ (MW = 487.56). RP-HPLC: 100.00% (t_R = 2.431, k' = 11.79). ^{1}H NMR (500 MHz, DMSO-d_6) δ ppm: 8.40−8.43 (m, 2H), 7.79−7.86 (m, 4H), 7.65−7.69 (m, 2H), 7.22−7.24 (m, 2H), 7.01−7.04 (m, 2H), 4.04 (t, J = 6.44 Hz, 2H), 2.95 (d, J = 11.46 Hz, 2H), 2.48−2.52 (m, 1H), 2.43 (t, J = 7.16 Hz, 2H), 1.93−2.01 (m, 2H), 1.88 (quin, J = 6.73 Hz, 2H), 1.69−1.76 (m, 2H), 1.55−1.65 (m, 2H). ^{13}C NMR (126 MHz, DMSO-d_6) δ ppm: 159.9, 155.3, 150.1, 144.8, 133.3, 128.9, 127.4, 122.9, 115.7, 109.6, 66.6, 55.2, 54.1, 32.6, 26.9. LC−MS: purity 100.00%, t_R = 3.54, (ESI) m/z [M + H]$^+$ 398.12. HRMS (MALDI): m/z [M + H]$^+$ 398.2230.

4.1.2.13. 4-(1-(3-(4-Phenoxyphenoxy)propyl)piperidin-4-yl)-pyridine Oxalate (13). White solid, yield 34%, m.p. 143−146 °C, $C_{25}H_{28}N_2O_2 \cdot C_2H_2O_4$ (MW = 478.55). RP-HPLC: 100.00% (t_R = 2.492, k' = 12.12). ^{1}H NMR (500 MHz, DMSO-d_6) δ ppm: 8.41−8.43 (m, 2H), 7.28−7.32 (m, 2H), 7.22−7.25 (m, 2H), 7.02 (tt, J = 7.41, 1.04 Hz, 1H), 6.90−6.96 (m, 4H), 6.86−6.89 (m, 2H), 3.96 (t, J = 6.30 Hz, 2H), 2.95 (d, J = 11.46 Hz, 2H), 2.48−2.52 (m, 1H), 2.42 (t, J = 7.30 Hz, 2H), 1.93−2.00 (m, 2H), 1.82−1.89 (m, 2H), 1.72 (d, J = 12.60 Hz, 2H), 1.60 (qd, J = 12.36, 3.58 Hz, 2H). ^{13}C NMR (126 MHz, DMSO-d_6) δ ppm: 158.6, 155.6, 149.8, 130.4, 122.9, 117.8, 116.2, 66.8, 55.2, 54.1, 32.6, 27.0. LC−MS: purity 100.00%, t_R = 3.94, (ESI) m/z [M + H]$^+$ 389.23. HRMS (MALDI): m/z [M + H]$^+$ 389.2227.

4.1.2.14. N-Phenyl-4-(3-(4-(pyridin-4-yl)piperidin-1-yl)propoxy)-aniline Oxalate (14). White solid, yield 38%, m.p. 182−185 °C, $C_{25}H_{29}N_3O \cdot C_2H_2O_4$ (MW = 477.56). RP-HPLC: 100.00% (t_R = 2.400, k' = 11.63). ^{1}H NMR (500 MHz, DMSO-d_6) δ ppm: 8.41−8.43 (m, 2H), 7.80 (s, 1H), 7.22−7.24 (m, 2H), 7.09−7.13 (m, 2H), 6.97−7.01 (m, 2H), 6.86−6.89 (m, 2H), 6.80−6.84 (m, 2H), 6.66 (tt, J = 7.30, 1.15 Hz, 1H), 3.92 (t, J = 6.30 Hz, 2H), 2.97 (d, J = 10.02 Hz, 2H), 2.48−2.54 (m, 2H), 2.00 (br. s., 2H), 1.84 (quin, J = 6.73 Hz, 2H), 1.73 (d, J = 12.03 Hz, 2H), 1.61 (qd, J = 12.32, 3.44 Hz, 2H). ^{13}C NMR (126 MHz, DMSO-d_6) δ ppm: 155.3, 153.6, 150.1, 145.6, 136.6, 129.6, 122.9, 120.8, 118.8, 115.7, 115.3, 66.6, 55.3, 54.0, 32.5, 26.9. LC−MS: purity 100.00%, t_R = 3.62, (ESI) m/z [M + H]$^+$ 388. HRMS (MALDI): m/z [M + H]$^+$ 388.2387.

4.1.2.15. 4-(1-(3-(4-Benzylphenoxy)propyl)piperidin-4-yl)pyridine Oxalate (15). White solid, yield 41%, m.p. 135−138 °C, $C_{26}H_{30}N_2O \cdot C_2H_2O_4$ (MW = 476.57). RP-HPLC: 98.95% (t_R = 2.538, k' = 12.36). ^{1}H NMR (500 MHz, DMSO-d_6) δ ppm: 8.40−8.43 (m, 2H), 7.21−7.25 (m, 4H), 7.06−7.17 (m, 5H), 6.78−6.82 (m, 2H), 3.92 (t, J = 6.44 Hz, 2H), 3.82 (s, 2H), 3.29 (br. s., 1H), 2.94 (d, J = 10.88 Hz, 2H), 2.37−2.44 (m, 2H), 1.90−2.04 (m, 2H), 1.83 (quin, J = 6.80 Hz, 2H), 1.71 (d, J = 12.03 Hz, 2H), 1.59 (qd, J = 12.32, 3.72 Hz, 2H). ^{13}C NMR (126 MHz, DMSO-d_6) δ ppm: 157.5, 155.3, 150.1, 142.3, 133.7, 130.2, 128.9, 122.9, 114.9, 66.3, 55.5, 55.2, 54.0, 32.6, 26.9. LC−MS: purity 100.00%, t_R = 4.17, (ESI) m/z [M + H]$^+$ 387.22. HRMS (MALDI): m/z [M + H]$^+$ 387.2434.

4.1.2.16. 2-(4-(4-(4-(tert-Butyl)phenoxy)butyl)piperazin-1-yl)-pyrazine Oxalate (16). Compound previously described in the literature.[19] White solid, yield 61%. RP-HPLC: 100.00% (t_R = 2.874, k' = 14.13). LC−MS: purity 98.64%, t_R = 5.38, (ESI) m/z [M + H]$^+$ 370.51.

4.2. pH-Dependent Crystallization and Crystal Structure Determination. Single crystals were obtained by crystallization in two sets of samples, oxalate salts of compounds **KSK67** and **KSK68**, followed by free base samples of **KSK67_fb**, **KSK68_fb**, **KSK94_fb**, and **12_fb**. The **KSK67** and **KSK68** oxalate salts were initially crystallized by slow evaporation of the solvent at ambient conditions from propan-2-ol solution with few drops of water. This procedure resulted in obtaining crystals suitable for the X-ray experiment. In the next step, the attempts to crystallize the mentioned samples in three batches were conducted: (1) from the water solution (solution pH: 4.5−5) and (2) with the addition of 1 M HCl (the solution pH: 3.5) and (3) 1 M NaOH (solution pH: 7−7.5). **KSK68** is more soluble in H_2O than **KSK67**. The solubility of both samples increases in acidic conditions, whereas the addition of alkali leads to rapid precipitation. The controlled, dropwise addition of NaOH allowed obtaining a clear solution at equilibrium. The described crystallization procedures of the oxalate salts resulted in good quality crystals only for **KSK68** with addition of NaOH (named as **KSK68_OH**). The free base samples of **KSK67_fb**, **KSK68_fb**, **KSK94_fb**, and **12_fb** are not highly soluble

https://doi.org/10.1021/acs.jmedchem.3c00430
J. Med. Chem. 2023, 66, 9658−9683

in water. To solve all samples, an addition of organic solvents mixture was required: propan-2-ol and acetone (2:1, v:v; for **KSK67_fb** and **KSK68_fb**) or propan-2-ol, acetone, and THF (2:5:1, v:v:v; for **KSK94_fb** and **12_fb**). The final pH of solutions was in the range 6.5−7. All samples showed very good solubility in acidic conditions (pH 3.5) and were insoluble after adding the NaOH solution. The above described crystallization procedures of free bases resulted in good quality crystals only for the water/organic solutions. X-ray single-crystal diffraction data sets were collected using an XtaLAB Synergy-S four-circle diffractometer with a mirror monochromator and a microfocus Cu Kα radiation source (λ = 1.5418 Å). The CryoStream cryostat system was used to allow low-temperature experiments performed at 100(2) K. The obtained data sets were processed with the CrysAlisPro software (Rigaku-Oxford Diffraction; CrysAlisPro Oxford Diffraction Ltd., Abingdon, England, V 1. 171. 36. 2 (release 27-06-2012 CN) 2006). The phase problem was solved with direct methods using SHELXT.[56] Parameters of the obtained model were refined by full-matrix least-squares on F^2 using SHELXL-2014/6.[57] Calculations were performed using the WinGX integrated system (ver. 2014.1).[58] Figures were prepared with the Mercury 4.0 software.[59] All nonhydrogen atoms were refined anisotropically. All hydrogen atoms attached to carbon atoms were positioned with the idealized geometry and refined using the riding model with the isotropic displacement parameter U_{iso}[H] = 1.2 U_{eq}[C]. The hydrogen atoms attached to nitrogens (N1 and/or N10) as a result of protonation of the basic center were located on the Fourier difference map. Hydrogen atoms of water molecules present in the crystal lattice were, in most cases, defined based on the Fourier difference map and were refined using the riding model with the isotropic displacement parameter U_{iso}[H] = 1.5 U_{eq}[O]. In many cases, restraints on distances and angles (DFIX and DANG commands, respectively) were required to maintain relatively good water molecule geometry. Only for structure **KSK67**, where interpretation of the Fourier difference map did not allow water molecules' hydrogen atoms location, was the CALC-OH predictive algorithm[60] available in the WinGX suite[58] applied. In structures **KSK67**, **KSK68_fb**, and **KSK94_fb**, a positional disorder within the molecule was observed. This disorder was modeled based on the Fourier difference map inspection, and the site occupancies were determined during the refinement procedure. Crystal data and refinement results are shown in Tables S1 (for oxalate salts) and S2 (for free bases) in the Supporting Information file. The asymmetric units of all obtained crystal structures, presenting atom labeling as well as the positional disordered observed for tested compounds, are shown in Figures S1−S7 in the SI file. Crystallographic data have been deposited with the Cambridge Crystallographic Data Centre (CCDC) as supplementary publication nos. CCDC2245077 (**KSK67**), CCDC2245079 (**KSK68**), CCDC2245081 (**KSK68_OH**), CCDC2245080 (**KSK67_fb**), CCDC2245078 (**KSK68_fb**), CCDC2245082 (**KSK94_fb**), and CCDC2245083 (**12_fb**). Copies of the data can be obtained, free of charge, on application to CCDC (e-mail: deposit@ccdc.cam.ac.uk).

4.3. Potentiometric Titration. The potentiometric microtitration was performed in a thermostated 20 mL cell using a CerkoLab microtitration unit fitted with a pH electrode (Hydromet ERH-13-6). The electrode was calibrated with the use of buffer solutions: pH = 4.00, 7.00, and 10.00. Titrant T (0.1 M KOH) was standardized according to the general analytical procedure and protected from carbon dioxide. Double distilled water with a conductivity of about 0.18 mS/cm was used to prepare all aqueous solutions. DMSO (HPLC grade, 99.5%) was supplied by Sigma Aldrich. The concentration of the titrant solution (D) was 0.0025−0.005 M. The solubilization procedure was follows: The appropriate amount of KSK compound was dissolved in 1 mL 0.1 M HCl and 1 mL DMSO to prepare a 25 mL stock solution. The developed solubilization system can be recommended for poorly soluble derivatives. The analytical procedure was a follows: volume V_0 = 4.5 mL of titrant D was titrated with 0.1 M titrant T using the CerkoLab System equipped with a 5 mL syringe pump. Titrant T was added to titrant D in 0.005 mL increments with 10 s intervals. pK_a values were calculated from the experimental data points $\{(V_j, pH_j)/j = 1, ..., N\}$ according to the Kostrowicki and Liwo algorithm.[29,30]

4.4. NMR Spectroscopy Measurements in the pH-Controlled Environment. NMR spectra were measured on a JEOL JNM-ECZR 600 MHz spectrometer equipped with a Royal HFX probe. All measurements were carried out at stable 303 K. DMSO-d_6 of purity 99.8% was purchased from Eurisotop and stored over A3 molecular sieves for a few days. Proton spectra were collected from 16 scans and 32,768 points with an acquisition time of 2.42 s and relaxation delay of 5 s. A standard sequence with one 45° pulse on the proton channel before acquisition was used. Titrations were conducted using trifluoromethylsulfonic (triflic) acid purchased from Sigma-Aldrich with a purity of over 99%. A solution of 0.5 M concentration in DMSO-d_6 was made and further used. Analysis of the results was carried out using the JEOL JASON software. Titrations were performed by adding successive portions of the TfOH acid solution to the test compound solution in portions of 0.2 molar equivalents. All spectra and chemical shift tables from the titration experiments are available in the Supporting Information.

4.5. *In Vitro* Pharmacology. *4.5.1. Affinity at σ_1 and σ_2 Receptors.* Brain and liver homogenates for σ_1R and σ_2R binding assays were prepared from male Dunkin-Hartley guinea pigs and Sprague-Dawley rats, respectively (ENVIGO RMS S.R.L., Udine, Italy), as previously reported.[23,61,62] *In vitro* σ_1R ligand binding assays were carried out in a Tris buffer (50 mM, pH 7.4) for 150 min at 37 °C. The thawed membrane preparation of the guinea pig brain cortex was incubated with increasing concentrations of test compounds and [^{3}H](+)-pentazocine (2 nM) in a final volume of 0.5 mL. Unlabeled (+)-pentazocine (10 μM) was used to measure nonspecific binding. Bound and free radioligands were separated by fast filtration under reduced pressure using a Millipore filter apparatus through Whatman GF 6 glass fiber filters, which were presoaked in a 0.5% poly(ethyleneimine) water solution. Each filter paper was rinsed three times with ice-cold Tris buffer (50 mM, pH 7.4), dried at rt, and incubated overnight with scintillation fluid into pony vials. The bound radioactivity was determined using a liquid scintillation counter (Beckman LS 6500).[61,63] *In vitro* σ_2R ligand binding assays were carried out in Tris buffer (50 mM, pH 8.0) for 120 min at rt. The thawed membrane preparation of rat liver was incubated with increasing concentrations of test compounds and [^{3}H]DTG (2 nM) in the presence of (+)-pentazocine (5 μM) as σ_1 masking agent in a final volume of 0.5 mL. Nonspecific binding was evaluated with unlabeled DTG (10 μM). Bound and free radioligands were separated by fast filtration under reduced pressure using a Millipore filter apparatus through Whatman GF 6 glass fiber filters, which were presoaked in a 0.5% poly(ethyleneimine) water solution. Each filter paper was rinsed three times with ice-cold Tris buffer (10 mM, pH 8), dried at rt, and incubated overnight with scintillation fluid into pony vials. The bound radioactivity was determined using a liquid scintillation counter (Beckman LS 6500).[64] The K_i values were calculated with the program GraphPad Prism 7.0 (GraphPad Software, San Diego, CA, USA). The K_i values are given as mean value ± CI from at least two independent experiments performed in duplicate.

4.5.2. Affinity at Histamine Receptors. Compounds (as oxalate salts) were tested in H_3R *in vitro* binding studies using the methods described previously.[21−23] Ligands were tested at 5 to 11 appropriate concentrations in a [^{3}H]N^α-methylhistamine (K_D = 3.08 nM) radioligand depletion assay to determine the affinity at human recombinant histamine H_3R stably expressed in HEK-293 cells. Radioligand binding experiments at the H_1R, H_2R, and H_4R were performed as previously described in Rosier et al.[65] and Bartole et al.[66] The following radioligands and concentrations were used: [^{3}H]mepyramine (hH_1R, K_d = 5.1 nM, c = 5 nM) (Novandi Chemistry AB, Södertälje, Sweden), [^{3}H]UR-DE257 (hH_2R, K_d = 66.9 nM, c = 50 nM),[67] and [^{3}H]UR-PI294 (hH_4R, K_d = 3.6 nM, c = 4 nM)[68] at HEK293T-SP-FLAG-hH_xR (x = 1, 2, or 4) expressing the respective hHR. Data represent mean values ± CI from three independent experiments, each performed in triplicate. The normalized competition binding curves were then fitted with a four-

https://doi.org/10.1021/acs.jmedchem.3c00430
J. Med. Chem. 2023, 66, 9658−9683

parameter logistic fit yielding IC_{50} values using the Prism 8.4.3 software (GraphPad, San Diego, CA). The K_i values were estimated from the Cheng–Prusoff equation.[69]

4.5.3. Cyclic Adenosine Monophosphate (cAMP) Accumulation Assay. The LANCE Ultra cAMP assay (Perkin Elmer), a homogeneous time-resolved fluorescence resonance energy transfer (TR-FRET) immunoassay, is designed to measure cAMP produced upon modulation of adenylyl cyclase activity by GPCRs. The assay is based on the competition between the europium (Eu) chelate-labeled cAMP tracer and sample cAMP for binding sites on cAMP-specific monoclonal antibodies labeled with the ULight dye. For measurement, HEK293 cells expressing hH_3R[34] were resuspended in HBSS buffer containing 0.1% BSA, HEPES (5 mM), and phosphodiesterase inhibitor RO-201724 (100 μM) as previously described.[22] An antagonist dose–response experiment was performed in 384-well white opaque plates using 3000 cells/well stimulated with 3 μM forskolin and 30 nM (*R*)-(−)-α-methylhistamine as reference H_3R agonist. Cell treatments were performed for 30 min at room temperature, and the cAMP production was assayed by the addition of Eu-cAMP tracer and ULight-anti-cAMP solution in detection buffer according to the manufacturer's instructions. The TR-FRET signal was measured 60 min later using the EnVision microplate reader (Perkin Elmer), and the amount of released cAMP was calculated based on the cAMP standard curve. Experiments were conducted twice in triplicates, and IC_{50} values were determined using the Prism 8.4.3 software.

4.6. *In Silico* Studies. Molecular Modeling: Docking Studies and Molecular Dynamics Simulations. *4.6.1. Structures of the Receptors.* The histamine H_3 receptor homology model was built using the AlphaFold server,[70,71] and we chose the model with the highest values of the predicted local-distance difference test (pLDDT). The structures of σ_1R were retrieved from the Protein Data Bank[72,73] (PDB ID: 5HK1,[74] 5HK2,[74] 6DJZ,[75] 6DK0,[75] 6DK1[75]); however, on the basis of the similarity of crystalized ligand and preliminary research, we choose the crystal structure of σ_1R in complex with the antagonist haloperidol[17] (PDB ID: 6DJZ).

4.6.2. Induced Fit Docking (IFD). The three-dimensional structures of the ligands were prepared using LigPrep v3.6,[76] and the appropriate ionization states at pH = 7.0 ± 0.5 were assigned using Epik v3.4.[77] The Protein Preparation Wizard[78] was used to assign the bond orders and appropriate amino acid ionization states and to check for steric clashes for the sigma-1 crystals. The receptor grid was generated (OPLS3 force field)[79] by centering the grid box of the sigma-1 receptor with a size of 8 Å on crystalized ligands and the grid box of histamine H_3R with a size of 10 Å on D3.32. Automated flexible docking was performed using Glide v6.9[80,81] at the SP level.

4.6.3. The QM/MM Optimization. The L-R complexes selected in IFD procedure were next optimized using the QM/MM approach using QSite.[82] The QM area containing the ligand and the amino acid side chains interacting with ligands was described by a combination of DFT hybrid functional B3LYP and LACVP* basis sets, whereas the rest of the system was optimized using the OPLS3 force field.

4.6.4. Quantum Polarized Ligand Docking (QPLD). The optimized complexes of **KSK68** and **12** were used as a grid for the next steps. The receptor grids were generated (OPLS3 force field) by centering the grid box with a size of 8 Å on **KSK68** and **12**. Docking was performed by the quantum-polarized ligand docking (QPLD) procedure[83] that involves the QM-derived ligand atomic charges in the protein environment at the 3-21G/BLYP level. For each ligand, the five poses were obtained.

4.6.5. Binding Free Energy Calculations. GBSA (generalized-born/surface area) was used to calculate the binding free energy based on the ligand–receptor complexes generated by the QPLD procedure. The ligand poses were minimized using the local optimization feature in Prime, the flexible residue distance was set to 6 Å from a ligand pose, and the ligand charges obtained in the QPLD stage were used. The energies of complexes were calculated with the OPLS3e force field and generalized-born/surface area continuum solvent model. To assess the influence of an appropriate tautomeric and protonation state, the $\Delta\Delta G$ was calculated as a difference between binding free energy (ΔG) of the piperidine monoprotonated derivative and piperazine analogues.

4.6.6. Molecular Dynamics Simulations. Selected ligand–receptor complexes underwent MD simulations to confirm the stability of docking poses obtained in previous stages. They were carried out in Desmond,[16] with the application of the TIP3P solvent model[17] and POPC membrane model in the case of the H_3R. The remaining conditions were as follows: OPLS3e force-field, pressure of 1.01325 bar, temperature of 300 K, orthorhombic box shape with a size of +10 Å × +10 Å × +10 Å, application of the neutralization of the system by addition of the appropriate number of Cl− ions and relaxation before simulation, simulation length: 1000 ns. Ligand–protein contacts occurring during MD simulations were analyzed with the use of the Simulation Interaction Diagram (Schrödinger Suite).

4.6.7. Protonation Studies. The protonation studies were carried out in two software packages: InstantJChem and Epik.[77] In the latter case, water was selected as a solvent.

4.7. Determination of Selected ADMET Parameters. *4.7.1. Permeability across Lipid Membranes.* The precoated PAMPA Plate System Gentest was obtained from Corning (Tewksbury, MA, USA). It consists of a 96-well receiver filter plate that has been precoated with structured layers of phospholipids and a matched donor microplate. The stock solutions of tested compounds and reference drugs were diluted in the PBS buffer (pH 7.4) to the final concentration of 100 μM according to the method described previously.[21] The compounds were applied into the donor wells (300 μL), and PBS buffer was placed in acceptor wells (200 μL). Plates were incubated in RT for 5 h. By using the UPLC–MS spectrometry (Waters ACQUITY TQD system with the TQ Detector, Waters, Milford, USA) with an internal standard, the exact quantity of molecules that penetrated from donor to acceptor wells through phospholipid membrane was estimated. The permeability coefficients (P_e, cm/s) were calculated using the formula provided by the PAMPA Plate System manufacturer.[49]

4.7.2. Serum Metabolic Stability. Acetonitrile (LC–MS grade), formic acid (LC–MS grade), and DMSO (HPLC grade) were obtained from Sigma Aldrich. Imipramine was also acquired from Sigma Aldrich. Water MilliQ was used for chromatography with 18 MΩ·cm.

The plasma was warmed to 37 °C for 10 min, mixed, and centrifuged to pellet any aggregated protein. Calcium chloride (500 mM, 0.5 mL added to 25 mL of plasma) was then added to the plasma to allow clot formation. The plasma was centrifuged at 4 °C for 30 min at 14,000 rpm to remove the clot. The clear supernatant (serum) was then transferred to an assay plate (249 μL) using the Bravo Automated Liquid Handling Platform (Agilent Technologies). The serum was equilibrated to 37 °C, and biotransformation was initiated by adding 1 μL of the compound solution in DMSO to achieve final concentrations of 0.1, 0.5, and 1 mM with 250 μL final incubation volume. Samples (25 μL) were taken at 0, 1, 2, 4, 6, and 24 h and added to 100 μL acetonitrile with 100 nM imipramine as internal standard for plasma deproteinization. The samples were vortexed for 1 min and then centrifuged at 4 °C for 30 min at 14,000 rpm. The clear supernatants were analyzed by LC–MS. An Exion HPLC system consisting of a degasser (DGU-20A) and an autosampler (SIL-HTA) was used. LC was performed on an analytical column (Waters BEH C18; 1.7 μm, 50 × 2.1 mm). The mobile phase consisted of acetonitrile–water with 0.1% formic acid. The flow rate was 0.5 mL/min with a column compartment temperature of 50 °C and injection volume of 1 μL.

4.8. *In Vivo* Pharmacology. *4.8.1. Influence on Spontaneous Locomotor Activity.* This test was carried out according to the procedure described elsewhere.[84] The animals were injected (i.p.) with **12** at doses of 5, 15, and 30 mg/kg and placed in the activity cages individually (30 min before the experiment). The number of light-beam crossings was counted in each group during the next 30 min in 10 min intervals.

4.8.2. Influence on Motor Coordination in the Rotarod Test. The test was carried out on the semiautomatic rotarod apparatus (Rotarod apparatus Panlab/Harvard Apparatus, LE 8200, Spain) according to

https://doi.org/10.1021/acs.jmedchem.3c00430
J. Med. Chem. 2023, 66, 9658−9683

the method previously described in the literature.[85] The mice were trained for 3 days on the rod rotating at a constant speed of 18 rotations per minute (rpm). During each training session, the animals were placed on the rod for 3 min with an unlimited number of trials. On the test day (24 h after the final training trial), 30 min before the rotarod test, the mice were pretreated (i.p.) with the test compound (15 mg/kg). Then, the animals were tested on the rotarod revolving at 6, 18, and then 24 rpm. Motor impairments, defined as the inability to remain on the rotating rod for 1 min, were measured at each speed.

4.8.3. Formalin Test. The procedure used was essentially the same as that described previously.[86,87] Briefly, 20 μL of 1.5% formalin solution was injected intraplantarly (i.pl.) into the mice right hind paw using a 26-gauge needle. Immediately after formalin injection, the animals were placed individually in an observation chamber made of glass and were observed for the next 30 min. The total time (in seconds) spent on licking the injected paw during periods of 0−5 min (early phase, neurogenic) and 15−30 min (late phase, inflammatory) was measured and was considered as an indicator of nociceptive behavior. Before formalin injection, different groups of mice were treated i.p. with the vehicle (10 mL/kg, negative control) and the varying doses of **12** (5, 10, 15, and 30 mg/kg).

4.8.4. Capsaicin-Induced Nociception. The procedure used was similar to that described previously.[88,89] The pain reaction was induced by the injection of 20 μL of capsaicin solution (1.6 μg/paw made in PBS) under the skin of the dorsal surface of the mice right hindpaw. The animals were observed individually in an observation chamber for 5 min following capsaicin injection. The amount of time spent licking the injected paw was recorded by means of the stopwatch and was considered as indicative of pain. The animals were pretreated with the vehicle (10 mL/kg, negative control) and investigated compound (10, 15, and 30 mg/kg).

4.8.5. Loperamide-Induced Antinociception. Female CD1 mice (Charles River, Barcelona, Spain) were used in all experiments. The experiments were performed during the light phase (from 9:00 a.m. to 3:00 p.m.). Animal care was provided in accordance with institutional (Research Ethics Committee of the University of Granada, Granada, Spain), regional (Junta de Andalucía, Spain), and international standards (European Communities Council directive 2010/63).

We aimed to test whether compound **12** behaved *in vivo* as σ_1 antagonists or agonists. As reference σ_1 compounds, we used **S1RA** (4-[2-[[5-methyl-1-(2-naphthalenyl)1*H*-pyraol-3-yl]oxy]ethyl]-morpholine hydrochloride), a known selective σ_1 receptor antagonist (DC Chemicals, Shanghai, China), and PRE-084 (2-[4-morpholinethyl]1-phenylcyclohexanecarboxylate hydrochloride) (Tocris Cookson Ltd., Bristol, United Kingdom), a selective σ_1 receptor agonist.[18] **S1RA** and PRE-084 were dissolved in sterile physiologic saline (0.9% NaCl). Compound **12** was dissolved in 2% Tween 80 (Sigma-Aldrich, Madrid, Spain) in ultrapure water and heated until dissolved before injection. We previously tested that this solvent did not alter the animals' behavioral response to the mechanical stimulation (data not shown). All these compounds (or their solvents) were administered intraplantarly (i.pl.) into the right hind paw in a volume of 20 μL using a 1710 TLL Hamilton microsyringe (Teknokroma, Barcelona, Spain) with a $30^{1/2}$-gauge needle. The i.pl. injection was made 5 min before nociceptive testing to minimize systemic absorption of the compounds. When PRE-084 was associated with **S1RA** or **12**, drugs were dissolved in the same solution and injected together to avoid paw lesions from multiple injections.

As it is known that σ_1 antagonism can enhance opioid antinociception and that σ_1 agonism reverses this effect,[90] we tested whether our compound modulated the antinociceptive effect induced by the opioid agonist loperamide hydrochloride (Sigma-Aldrich). This drug was dissolved in 1% dimethylsulfoxide (DMSO) (Merck KGaA, Darmstadt, Germany) in ultrapure water and injected subcutaneously into the interscapular area in a volume of 5 mL/kg 30 min before behavioral testing. Naloxone methiodide (Sigma-Aldrich) was used as a peripheral opioid antagonist[91] and was dissolved in physiological saline and s.c. administered 5 min before loperamide injection.

Nociceptive stimulation of the hind paw of the animals was made with an Analgesimeter (Model 37215, Ugo-Basile, Varese, Italy) as previously described.[23,90] After drug administration, mice were gently pincer grasped between the thumb and index fingers by the skin above the interscapular area. Then, a blunt cone-shaped paw-presser was applied at a constant intensity of 450 g to the dorsal surface of the hind paw until the animal showed a struggle response. The struggle latency was measured with a chronometer. Evaluations were done twice alternately to each hind paw at intervals of 1 min between stimulations.

Statistical analysis was carried out with the two-way analysis of variance (ANOVA) followed by a Bonferroni *post hoc* test. ANOVA was performed with the SigmaPlot 12.0 program. The differences between values were considered significant when the p value was below 0.05.

4.8.6. Oxaliplatin-Induced Neuropathy. Neuropathy was induced by the administration of a single dose (10 mg/kg) of oxaliplatin (OXPT) dissolved in a 5% glucose solution (Polfa Kutno, Poland). To assess the sensitivity to mechanical stimuli, the von Frey test was carried out using the electronic von Frey unit (Bioseb, France). The apparatus was supplied with a single flexible filament, which was used to apply increasing force (from 0 to 10 g) against the plantar surface of the hind paw of the mouse. The crossing of pain threshold resulted in the paw withdrawal and subsequent recording of the mechanical pressure that evoked the nocifensive response. The measurement was done before the OXPT administration and 3 h and 7 days afterward. The compounds were administrated to the animals with tactile allodynia observed as a statistically significant decrease in pain threshold. On the day of the experiment, each mouse was placed in an observation chamber with a wire mesh bottom and was allowed to habituate for 1 h. After the habituation period, the mouse pain threshold was tested three times alternately with at least 30 s gap between each measurement. The mean of these three consecutive measurements was taken as the baseline value. The mice with tactile allodynia were i.p. pretreated with the tested compound, and 30 min later, the animals were tested again according to the same procedure.[92]

4.8.7. Chronic Constriction Injury of the Sciatic Nerve. All animal procedures were performed following the recommendations of the International Association for the Study of Pain[93] and the NIH Guide for the Care and Use of Laboratory Animals. Experiments were approved by the II Local Ethics Committee Branch of the National Ethics Committee for Experiments on Animals based at the Maj Institute of Pharmacology, Polish Academy of Sciences, Krakow, Poland (approval number: 24/2022). Care was taken to minimize animal suffering and minimize the number of animals used (3R policy). Adult male albino Swiss CD-1 mice (initially weighing 18−20 g) were purchased from Charles River Laboratories (Hamburg, Germany). The animals were housed in groups of seven under controlled conditions (temp. 21 ± 2 °C; 12 h light/dark cycle, lights on at 6:00 a.m.) with *ad libitum* food and water.

The model of chronic constriction injury (CCI) to the sciatic nerve was established according to Bennett and Xie.[94] The surgical method was performed under isoflurate anesthesia (2% isoflurane in 100% oxygen with a flow of 1.5 L/min).[95] Below the right hipbone, a small incision was performed, and three ligatures (4/0 silk) around the sciatic nerve were made (with 1 mm spacing) until a brief twitch in the respective hind limb was observed. All mice that underwent the CCI procedure developed hypersensitivity to mechanical and thermal stimuli. Behavioral tests were performed at day 14 after injury. Compound **12** was dissolved in 10% DMSO/10% (2-hydroxypropyl)-β-cyclodextrin/water and administered i.p. at doses 5, 10, and 15 mg/kg (injection volume 10 mL/kg of body weight). The control group received the vehicle (10% DMSO/10% (2-hydroxypropyl)-β-cyclodextrin/water).

4.8.7.1. Behavioral Tests. Behavioral experiments were performed between 8:00 a.m. and 2:00 p.m. Across the experiments, we compared vehicle-treated mice with **12**-treated animals. Experiments were performed 30, 90, and 180 min (von Frey test); 35, 95, and 185

https://doi.org/10.1021/acs.jmedchem.3c00430
J. Med. Chem. 2023, 66, 9658−9683

min (cold plate test); and 40, 100, and 190 min (tail flick test) after the vehicle or **12** administration.

The von Frey test was used to measure mechanical hypersensitivity as described in a previous publication.[95] The animals were placed in cages with a wire net floor. The reaction (paw withdrawal, shaking, or licking) of the ipsilateral (Figure 15) and contralateral (Figure S33) paw of CCI-exposed mice to the mechanical stimulator (calibrated nylon monofilaments (0.6−6 g; Stoelting)) in serial increments was observed.

Sensitivity to noxious thermal stimuli was assessed with the cold plate test (Cold/Hot Plate Analgesia Meter, Columbus Instruments) as previously described.[95] The temperature of the plate was kept at 2 °C, and the cutoff latency was 30 s. The mice were placed on the cold plate, and the time until lifting of the injured paw was recorded.

The responsiveness to thermally induced pain was determined by a tail flick analgesic meter (Tail-Flick Unit; Ugo Basile) as previously described.[95] Tail flick latency was measured on the dorsal part of the tail at two-thirds of its length by applying a focused beam of light (thermal stimulus). The time interval between onset of the thermal stimulus and withdrawal of the tail from the beam was recorded; the cutoff latency was 9 s to prevent tissue damage.

4.8.7.2. Data and Statistical Analysis. The behavioral data in Figure 14 are presented as a percentage of the maximal possible effect [% MPE = 100% × (measured response − basal)(cutoff value − basal)] of drug action. In the Supporting Information, the results from the von Frey test are expressed as pressure (g) applied with the filament. The behavioral data are presented as mean ± SEM. The one-way ANOVA was performed, and the differences between the groups were further analyzed with Bonferroni's *post hoc* test. Significant differences between group are indicated when $*p < 0.05$, $**p < 0.01$, and $***p < 0.001$. The analysis and charts were prepared using GraphPad Prism v.9.1.2 (GraphPad Software, La Jolla, CA, USA).

■ ASSOCIATED CONTENT

Supporting Information

The Supporting Information is available free of charge at https://pubs.acs.org/doi/10.1021/acs.jmedchem.3c00430.

Protonation investigation based on crystal structure analysis; determination of the basicity of selected piperidine and piperazine derivatives by potentiometric titration; protonation investigation based on NMR spectroscopy measurements in pH-controlled environment; *in vivo* pharmacological activity; *in silico* studies; molecular modeling: docking studies and molecular dynamics simulations; and ^{1}H and ^{13}C NMR spectra HRMS analysis and HPLC traces (PDF)

Molecular formula strings (CSV)

3_in_H3 (PDB)

3_in_sigma1 (PDB)

7_in_H3 (PDB)

7_in_sigma1 (PDB)

H3_compound_3 (PDB)

H3_compound_7 (PDB)

KSK67_in_H3_pose1 (PDB)

KSK67_in_H3_pose2 (PDB)

KSK68_in_H3 (PDB)

KSK94_in_sigma1_pose1 (PDB)

KSK94_in_sigma1_pose2 (PDB)

KSK100_in_sigma1 (PDB)

sigma_compound_3 (PDB)

sigma_compound_7 (PDB)

■ AUTHOR INFORMATION

Corresponding Authors

Tadeusz Karcz − *Department of Technology and Biotechnology of Drugs, Faculty of Pharmacy, Jagiellonian University Medical College, 30-688 Kraków, Poland*; Email: t.karcz@uj.edu.pl

Emanuele Amata − *Department of Drug and Health Sciences, University of Catania, 95125 Catania, Italy*; orcid.org/0000-0002-4750-3479; Email: eamata@unict.it

Katarzyna Kieć-Kononowicz − *Department of Technology and Biotechnology of Drugs, Faculty of Pharmacy, Jagiellonian University Medical College, 30-688 Kraków, Poland*; Email: mfkonono@cyf-kr.edu.pl

Authors

Katarzyna Szczepańska − *Department of Technology and Biotechnology of Drugs, Faculty of Pharmacy, Jagiellonian University Medical College, 30-688 Kraków, Poland; Department of Medicinal Chemistry, Maj Institute of Pharmacology, Polish Academy of Sciences, 31-343 Kraków, Poland*; orcid.org/0000-0002-6110-9400

Maria Dichiara − *Department of Drug and Health Sciences, University of Catania, 95125 Catania, Italy*; orcid.org/0000-0001-6380-7176

Szczepan Mogilski − *Department of Pharmacodynamics, Faculty of Pharmacy, Jagiellonian University Medical College, 30-688 Kraków, Poland*

Justyna Kalinowska-Tłuścik − *Department of Crystal Chemistry and Crystal Physics, Faculty of Chemistry, Jagiellonian University, 30-387 Kraków, Poland*

Bogusław Pilarski − *Cerko Sp. z o.o. Sp.k, 81-451 Gdynia, Poland*

Arkadiusz Leniak − *Celon Pharma S.A., R&D Centre, 05-152 Kazuń Nowy, Poland*

Wojciech Pietruś − *Department of Medicinal Chemistry, Maj Institute of Pharmacology, Polish Academy of Sciences, 31-343 Kraków, Poland; Celon Pharma S.A., R&D Centre, 05-152 Kazuń Nowy, Poland*; orcid.org/0000-0002-8563-7929

Sabina Podlewska − *Department of Medicinal Chemistry, Maj Institute of Pharmacology, Polish Academy of Sciences, 31-343 Kraków, Poland*; orcid.org/0000-0002-2891-5603

Katarzyna Popiołek-Barczyk − *Department of Neurochemistry, Maj Institute of Pharmacology, Polish Academy of Sciences, 31-343 Kraków, Poland*

Laura J. Humphrys − *Institute of Pharmacy, Faculty of Chemistry and Pharmacy, University of Regensburg, D-93053 Regensburg, Germany*; orcid.org/0000-0003-4019-5538

M. Carmen Ruiz-Cantero − *Department of Pharmacology and Neurosciences Institute (Biomedical Research Center), University of Granada, and Biosanitary Research Institute ibs. Granada, 18016 Granada, Spain*; orcid.org/0000-0001-6968-0946

David Reiner-Link − *Institute of Pharmaceutical and Medicinal Chemistry, Heinrich Heine University Düsseldorf, 40225 Düsseldorf, Germany*

Luisa Leitzbach − *Institute of Pharmaceutical and Medicinal Chemistry, Heinrich Heine University Düsseldorf, 40225 Düsseldorf, Germany*

Dorota Łażewska − *Department of Technology and Biotechnology of Drugs, Faculty of Pharmacy, Jagiellonian University Medical College, 30-688 Kraków, Poland*; orcid.org/0000-0001-8454-4440

Steffen Pockes – *Institute of Pharmacy, Faculty of Chemistry and Pharmacy, University of Regensburg, D-93053 Regensburg, Germany;* orcid.org/0000-0002-2211-9868
Michał Górka – *Celon Pharma S.A., R&D Centre, 05-152 Kazuń Nowy, Poland*
Adam Zmysłowski – *Celon Pharma S.A., R&D Centre, 05-152 Kazuń Nowy, Poland*
Thierry Calmels – *Bioprojet-Biotech, 4rue du Chesnay Beauregard, 35762 Saint-Gregoire, France*
Enrique J. Cobos – *Department of Pharmacology and Neurosciences Institute (Biomedical Research Center), University of Granada, and Biosanitary Research Institute ibs. Granada, 18016 Granada, Spain*
Agostino Marrazzo – *Department of Drug and Health Sciences, University of Catania, 95125 Catania, Italy;* orcid.org/0000-0002-8728-8857
Holger Stark – *Institute of Pharmaceutical and Medicinal Chemistry, Heinrich Heine University Düsseldorf, 40225 Düsseldorf, Germany;* orcid.org/0000-0003-3336-1710
Andrzej J. Bojarski – *Department of Medicinal Chemistry, Maj Institute of Pharmacology, Polish Academy of Sciences, 31-343 Kraków, Poland;* orcid.org/0000-0003-1417-6333

Complete contact information is available at: https://pubs.acs.org/10.1021/acs.jmedchem.3c00430

Author Contributions

♢K.S. and T.K. contributed equally. K.K.-K., K.S., T.K., H.S., E.A., S.Poc., A.M., and A.J.B. participated in research design. K.S. and D.Ł. synthesized, purified, and characterized all compounds. J.K.-T. conducted crystallographic experiments. B.P. conducted potentiometric titrations. A.L. conducted NMR analysis in a pH-controlled environment. M.D., L.H., D.R.-L., L.L., T.C., M.G., A.Z., and T.K. conducted *in vitro* experiments. S.M., K.P.-B., M.C.R.C., and E.J.C. conducted *in vivo* pharmacology experiments. S.Pod. and W.P. conducted *in silico* experiments. K.S., M.D., and M.C.R.C. contributed reagents, materials, and analysis tools. K.S. and T.K. performed data analysis. K.S. wrote the original draft. T.K. and J.K.-T. wrote and contributed to the writing of the manuscript. All authors have given approval to the final version of the manuscript.

Funding

We are pleased to acknowledge the generous support of the National Science Center, Poland, granted based on decisions 2020/36/C/NZ7/00284, 2019/35/D/NZ7/01042, and 2020/04/X/NZ7/01338. This study was partly supported by statutory funds from the Faculty of Pharmacy Jagiellonian University Medical College, Krakow, Poland (N42/DBS/000242). Support by ERNEST COST Action 18133 is also acknowledged. We also acknowledge funding from the University of Catania, PIA.CE.RI. 2020–2022 Linea di intervento 3 Starting Grant project CARETO (grant 57722172136 to E. Amata). S.Poc. was supported by the Fonds der Chemischen Industrie (grant 661688). L.J.H. was funded by the Deutsche Forschungsgemeinschaft (DFG, Research Training Group GRK 1910). The crystal structure analysis was performed on the equipment purchased thanks to the financial support of the Ministry of Science and Higher Education, Warsaw, Poland (grant 6903/IA/SP/2018).

Notes

The authors declare no competing financial interest.

■ ACKNOWLEDGMENTS

We would like to thank Maria Kaleta and Annika Frank for technical assistance.

■ ABBREVIATIONS

ADME, absorption, distribution, metabolism, excretion; br, broad; cAMP, 3′,5′-cyclic adenosine monophosphate; CC, column chromatography; CCDC, Cambridge Crystallographic Data Centre; CCI, chronic constriction injury; CI, confidence interval; CNS, central nervous system; d, doublet; dd, doublet of doublets; DMSO, dimethyl sulfoxide; GPCR, G protein-coupled receptor; H_1R, histamine H_1 receptor; H_2R, histamine H_2 receptor; H_3R, histamine H_3 receptor; HB, hydrogen bond; HEK, human embryonic kidney cells; HPLC, high-performance liquid chromatography; HRMS, high-resolution mass spectra; i.p., intraperitoneal; IFD, induced fit docking; m.p., melting point; m, multiplet; MD, molecular dynamics; MM-GBSA, molecular mechanics generalized born surface area; MPE, maximum possible effect; MTDLs, multitarget-directed ligands; NMDA, *N*-methyl-D-aspartate receptor; NMR, nuclear magnetic resonance spectroscopy; OXPT, oxaliplatin; PAMPA, parallel artificial membrane permeability assay; PDB, Protein Data Bank; P_e, permeability coefficient; ppm, parts per million; qd, quartet of doublets; QPLD, quantum polarized ligand docking; quin, quintet; RMSD, root-mean-square deviation; RT, room temperature; s.c., subcutaneous; s, singlet; SD, standard deviation; SEM, standard error of the mean; t, triplet; TfOH, trifluoromethanesulfonic acid (triflic acid); TLC, thin-layer chromatography; t_R, retention time; TR-FRET, time-resolved fluorescence resonance energy transfer; TRPV1, transient receptor potential vanilloid type 1; tt, triplet of triplets; UPLC–MS, ultra-performance liquid chromatography–mass spectrometry; σ_1R, sigma-1 receptor; σ_2R, sigma-2 receptor

■ REFERENCES

(1) Zimmermann, G. R.; Lehár, J.; Keith, C. T. Multi-target therapeutics: when the whole is greater than the sum of the parts. *Drug Discovery Today* **2007**, *12*, 34–42.
(2) Proschak, E.; Stark, H.; Merk, D. Polypharmacology by Design: A Medicinal Chemist's Perspective on Multitargeting Compounds. *J. Med. Chem.* **2019**, *62*, 420–444.
(3) Walter, M.; Stark, H. Histamine receptor subtypes: a century of rational drug design. *Front Biosci* **2012**, *S4*, 461–488.
(4) Łażewska, D.; Kieć-Kononowicz, K. New developments around histamine H(3) receptor antagonists/inverse agonists: a patent review (2010 - present). *Expert Opin. Ther. Pat.* **2014**, *24*, 89–111.
(5) Hsieh, G. C.; Honore, P.; Pai, M.; Wensink, E. J.; Chandran, P.; Salyers, A. K.; Wetter, J. M.; Zhao, C.; Liu, H.; Decker, M. W.; Esbenshade, T. A.; Cowart, M. D.; Brioni, J. D. Antinociceptive effects of histamine H_3 receptor antagonist in the preclinical models of pain in rats and the involvement of central noradrenergic systems. *Brain Res.* **2010**, *1354*, 74–84.
(6) Ghamari, N.; Zarei, O.; Arias-Montaño, J. A.; Reiner, D.; Dastmalchi, S.; Stark, H.; Hamzeh-Mivehroud, M. Histamine H_3 receptor antagonists/inverse agonists: Where do they go? *Pharmacol. Ther.* **2019**, *200*, 69–84.
(7) European Medicines Agency *Wakix (pitolisant) - Assessment report*; 2015;*44* (November), 1–91.
(8) Imeri, F.; Stepanovska Tanturovska, B.; Zivkovic, A.; Enzmann, G.; Schwalm, S.; Pfeilschifter, J.; Homann, T.; Kleuser, B.; Engelhardt, B.; Stark, H.; Huwiler, A. Novel compounds with dual S1P receptor agonist and histamine H_3 receptor antagonist activities act protective in a mouse model of multiple sclerosis. *Neuropharmacology* **2021**, *186*, No. 108464.

(9) Szczepańska, K.; Kincses, A.; Vincze, K.; Szymańska, E.; Latacz, G.; Kuder, K. J.; Stark, H.; Spengler, G.; Handzlik, J.; Kieć-Kononowicz, K. N-Substituted piperazine derivatives as potential multitarget agents acting on histamine H_3 receptor and cancer resistance proteins. *Bioorg. Med. Chem. Lett.* **2020**, *30*, No. 127522.
(10) Reiner, D.; Seifert, L.; Deck, C.; Schüle, R.; Jung, M.; Stark, H. Epigenetics meets GPCR: inhibition of histone H3 methyltransferase (G9a) and histamine H_3 receptor for Prader-Willi Syndrome. *Sci. Rep.* **2020**, *10*, 13558.
(11) Bautista-Aguilera, Ó. M.; Hagenow, S.; Palomino-Antolin, A.; Farré-Alins, V.; Ismaili, L.; Joffrin, P.-L.; Jimeno, M. L.; Soukup, O.; Janočková, J.; Kalinowsky, L.; Proschak, E.; Iriepa, I.; Moraleda, I.; Schwed, J. S.; Romero Martínez, A.; López-Muñoz, F.; Chioua, M.; Egea, J.; Ramsay, R. R.; Marco-Contelles, J.; Stark, H. Multitarget-Directed Ligands Combining Cholinesterase and Monoamine Oxidase Inhibition with Histamine H_3 R Antagonism for Neurodegenerative Diseases. *Angew. Chem., Int. Ed. Engl.* **2017**, *56*, 12765−12769.
(12) Łażewska, D.; Bajda, M.; Kaleta, M.; Zaręba, P.; Doroz-Płonka, A.; Siwek, A.; Alachkar, A.; Mogilski, S.; Saad, A.; Kuder, K.; Olejarz-Maciej, A.; Godyń, J.; Stary, D.; Sudoł, S.; Więcek, M.; Latacz, G.; Walczak, M.; Handzlik, J.; Sadek, B.; Malawska, B.; Kieć-Kononowicz, K. Rational design of new multitarget histamine H_3 receptor ligands as potential candidates for treatment of Alzheimer's disease. *Eur. J. Med. Chem.* **2020**, *207*, No. 112743.
(13) Riddy, D. M.; Cook, A. E.; Shackleford, D. M.; Pierce, T. L.; Mocaer, E.; la Cour, C. M.; Sors, A.; Charman, W. N.; Summers, R. J.; Sexton, P. M.; Christopoulos, A.; Langmead, C. J. Drug-receptor kinetics and sigma-1 receptor affinity differentiate clinically evaluated histamine H_3 receptor antagonists. *Neuropharmacology* **2019**, *144*, 244−255.
(14) Leurs, R.; Tulp, M. T. M.; Menge, W. M. B. P.; Adolfs, M. J. P.; Zuiderveld, O. P.; Timmerman, H. Evaluation of the receptor selectivity of the H_3 receptor antagonists, iodophenpropit and thioperamide: an interaction with the 5-HT_3 receptor revealed. *Br. J. Pharmacol.* **1995**, *116*, 2315−2321.
(15) Turnaturi, R.; Montenegro, L.; Marrazzo, A.; Parenti, R.; Pasquinucci, L.; Parenti, C. Benzomorphan skeleton, a versatile scaffold for different targets: A comprehensive review. *Eur. J. Med. Chem.* **2018**, *155*, 492−502.
(16) Arena, E.; Dichiara, M.; Floresta, G.; Parenti, C.; Marrazzo, A.; Pittalà, V.; Amata, E.; Prezzavento, O. Novel Sigma-1 receptor antagonists: from opioids to small molecules: what is new? *Future Med. Chem.* **2018**, *10*, 231−256.
(17) Cobos, E. J.; Entrena, J. M.; Nieto, F. R.; Cendán, C. M.; Del Pozo, E. Pharmacology and therapeutic potential of sigma(1) receptor ligands. *Curr. Neuropharmacol.* **2008**, *6*, 344−366.
(18) Ruiz-Cantero, M. C.; González-Cano, R.; Tejada, M. Á.; Santos-Caballero, M.; Perazzoli, G.; Nieto, F. R.; Cobos, E. J. Sigma-1 receptor: A drug target for the modulation of neuroimmune and neuroglial interactions during chronic pain. *Pharmacol. Res.* **2021**, *163*, No. 105339.
(19) Szczepańska, K.; Karcz, T.; Mogilski, S.; Siwek, A.; Kuder, K. J.; Latacz, G.; Kubacka, M.; Hagenow, S.; Lubelska, A.; Olejarz, A.; Kotańska, M.; Sadek, B.; Stark, H.; Kieć-Kononowicz, K. Synthesis and biological activity of novel *tert*-butyl and *tert*-pentylphenoxyalkyl piperazine derivatives as histamine H_3R ligands. *Eur. J. Med. Chem.* **2018**, *152*, 223−234.
(20) Szczepańska, K.; Karcz, T.; Kotańska, M.; Siwek, A.; Kuder, K. J.; Latacz, G.; Mogilski, S.; Hagenow, S.; Lubelska, A.; Sobolewski, M.; Stark, H.; Kieć-Kononowicz, K. Optimization and preclinical evaluation of novel histamine H_3receptor ligands: Acetyl and propionyl phenoxyalkyl piperazine derivatives. *Bioorg. Med. Chem.* **2018**, *26*, 6056−6066.
(21) Szczepańska, K.; Karcz, T.; Siwek, A.; Kuder, K. J.; Latacz, G.; Bednarski, M.; Szafarz, M.; Hagenow, S.; Lubelska, A.; Olejarz-Maciej, A.; Sobolewski, M.; Mika, K.; Kotańska, M.; Stark, H.; Kieć-Kononowicz, K. Structural modifications and *in vitro* pharmacological evaluation of 4-pyridyl-piperazine derivatives as an active and selective histamine H_3 receptor ligands. *Bioorg. Chem.* **2019**, *91*, No. 103071.
(22) Szczepańska, K.; Pockes, S.; Podlewska, S.; Höring, C.; Mika, K.; Latacz, G.; Bednarski, M.; Siwek, A.; Karcz, T.; Nagl, M.; Bresinsky, M.; Mönnich, D.; Seibel, U.; Kuder, K. J.; Kotańska, M.; Stark, H.; Elz, S.; Kieć-Kononowicz, K. Structural modifications in the distal, regulatory region of histamine H_3 receptor antagonists leading to the identification of a potent anti-obesity agent. *Eur. J. Med. Chem.* **2021**, *213*, No. 113041.
(23) Szczepańska, K.; Podlewska, S.; Dichiara, M.; Gentile, D.; Patamia, V.; Rosier, N.; Mönnich, D.; Ruiz Cantero, M. C.; Karcz, T.; Łażewska, D.; Siwek, A.; Pockes, S.; Cobos, E. J.; Marrazzo, A.; Stark, H.; Rescifina, A.; Bojarski, A. J.; Amata, E.; Kieć-Kononowicz, K. Structural and Molecular Insight into Piperazine and Piperidine Derivatives as Histamine H_3 and Sigma-1 Receptor Antagonists with Promising Antinociceptive Properties. *ACS Chem. Neurosci.* **2022**, *13*, 1−15.
(24) Łażewska, D.; Kaleta, M.; Schwed, J. S.; Karcz, T.; Mogilski, S.; Latacz, G.; Olejarz, A.; Siwek, A.; Kubacka, M.; Lubelska, A.; Honkisz, E.; Handzlik, J.; Filipek, B.; Stark, H.; Kieć-Kononowicz, K. Biphenyloxy-alkyl-piperidine and azepane derivatives as histamine H_3 receptor ligands. *Bioorg. Med. Chem.* **2017**, *25*, 5341−5354.
(25) Godyń, J.; Zaręba, P.; Łażewska, D.; Stary, D.; Reiner-Link, D.; Frank, A.; Latacz, G.; Mogilski, S.; Kaleta, M.; Doroz-Płonka, A.; Lubelska, A.; Honkisz-Orzechowska, E.; Olejarz-Maciej, A.; Handzlik, J.; Stark, H.; Kieć-Kononowicz, K.; Malawska, B.; Bajda, M. Cyanobiphenyls: Novel H_3 receptor ligands with cholinesterase and MAO B inhibitory activity as multitarget compounds for potential treatment of Alzheimer's disease. *Bioorg. Chem.* **2021**, *114*, No. 105129.
(26) Rzęsikowska, K.; Jabłoński, M.; Kalinowska-Tłuścik, J. Flat or angular? The impact of the nitrogen atom hybridization on the docking results for arylpiperazine derivatives as an example. *Struct. Chem.* **2020**, *31*, 823−829.
(27) Pilarski, B.; Kaliszan, R.; Wyrzykowski, D.; Młodzianowski, J.; Balińska, A. General analytical procedure for determination of acidity parameters of weak acids and bases. *J. Anal. Methods Chem.* **2015**, *2015*, No. 530731.
(28) Hogendorf, A. S.; Hogendorf, A.; Popiołek-Barczyk, K.; Ciechanowska, A.; Mika, J.; Satała, G.; Walczak, M.; Latacz, G.; Handzlik, J.; Kieć-Kononowicz, K.; Ponimaskin, E.; Schade, S.; Zeug, A.; Bijata, M.; Kubicki, M.; Kurczab, R.; Lenda, T.; Staroń, J.; Bugno, R.; Duszyńska, B.; Pilarski, B.; Bojarski, A. J. Fluorinated indole-imidazole conjugates: Selective orally bioavailable 5-HT_7 receptor low-basicity agonists, potential neuropathic painkillers. *Eur. J. Med. Chem.* **2019**, *170*, 261−275.
(29) Kostrowicki, J.; Liwo, A. A general method for the determination of the stoichiometry of unknown species in multicomponent systems from physicochemical measurements. *Comput. Chem.* **1987**, *11*, 195−210.
(30) Kostrowicki, J.; Liwo, A. Determination of equilibrium parameters by minimization of an extended sum of squares. *Talanta* **1990**, *37*, 645−650.
(31) Khalili, F.; Henni, A.; East, A. L. L. pK_a Values of Some Piperazines at (298, 303, 313, and 323) K. *J. Chem. Eng. Data* **2009**, *54*, 2914−2917.
(32) Lacivita, E.; Leopoldo, M.; De Giorgio, P.; Berardi, F.; Perrone, R. Determination of 1-aryl-4-propylpiperazine pKa values: The substituent on aryl modulates basicity. *Bioorg. Med. Chem.* **2009**, *17*, 1339−1344.
(33) Wilson, L. L.; Alleyne, A. R.; Eans, S. O.; Cirino, T. J.; Stacy, H. M.; Mottinelli, M.; Intagliata, S.; McCurdy, C. R.; McLaughlin, J. P. Characterization of CM-398, a Novel Selective Sigma-2 Receptor Ligand, as a Potential Therapeutic for Neuropathic Pain. *Molecules* **2022**, *27*, 3617.
(34) Ligneau, X.; Perrin, D.; Landais, L.; Camelin, J. C.; Calmels, T. P.; Berrebi-Bertrand, I.; Lecomte, J. M.; Parmentier, R.; Anaclet, C.; Lin, J. S.; Bertaina-Anglade, V.; la Rochelle, C. D.; d'Aniello, F.; Rouleau, A.; Gbahou, F.; Arrang, J.-M.; Ganellin, C. R.; Stark, H.;

https://doi.org/10.1021/acs.jmedchem.3c00430
J. Med. Chem. 2023, 66, 9658−9683

Schunack, W.; Schwartz, J.-C. BF2.649 [1-{3-[3-(4-Chlorophenyl)-propoxy]propyl}piperidine, hydrochloride], a nonimidazole inverse agonist/antagonist at the human histamine H3 receptor: Preclinical pharmacology. *J. Pharmacol. Exp. Ther.* **2007**, *320*, 365−375.
(35) Dastmalchi, S.; Hamzeh-Mivehroud, M.; Ghafourian, T.; Hamzeiy, H. Molecular modeling of histamine H_3 receptor and QSAR studies on arylbenzofuran derived H_3 antagonists. *J. Mol. Graphics Modell.* **2008**, *26*, 834−844.
(36) Lorenzi, S.; Mor, M.; Bordi, F.; Rivara, S.; Rivara, M.; Morini, G.; Bertoni, S.; Ballabeni, V.; Barocelli, E.; Plazzi, P. V. Validation of a histamine H_3 receptor model through structure-activity relationships for classical H_3 antagonists. *Bioorg. Med. Chem.* **2005**, *13*, 5647−5657.
(37) Rai, B. K.; Tawa, G. J.; Katz, A. H.; Humblet, C. Modeling G protein-coupled receptors for structure-based drug discovery using low-frequency normal modes for refinement of homology models: Application to H_3 antagonists. *Proteins: Struct., Funct., Bioinf.* **2010**, *78*, 457−473.
(38) Axe, F. U.; Bembenek, S. D.; Szalma, S. Three-dimensional models of histamine H_3 receptor antagonist complexes and their pharmacophore. *J. Mol. Graphics Modell.* **2006**, *24*, 456−464.
(39) Morini, G.; Comini, M.; Rivara, M.; Rivara, S.; Lorenzi, S.; Bordi, F.; Mor, M.; Flammini, L.; Bertoni, S.; Ballabeni, V.; Barocelli, E.; Plazzi, P. V. Dibasic non-imidazole histamine H_3 receptor antagonists with a rigid biphenyl scaffold. *Bioorg. Med. Chem. Lett.* **2006**, *16*, 4063−4067.
(40) Stark, H.; Sippl, W.; Ligneau, X.; Arrang, J. M.; Ganellin, C. R.; Schwartz, J. C.; Schunack, W. Different antagonist binding properties of human and rat histamine H3 receptors. *Bioorg. Med. Chem. Lett.* **2001**, *11*, 951−954.
(41) Uveges, A. J.; Kowal, D.; Zhang, Y.; Spangler, T. B.; Dunlop, J.; Semus, S.; Jones, P. G. The role of transmembrane helix 5 in agonist binding to the human H_3 receptor. *J. Pharmacol. Exp. Ther.* **2002**, *301*, 451−458.
(42) Yao, B. B.; Witte, D. G.; Miller, T. R.; Carr, T. L.; Kang, C. H.; Cassar, S.; Faghih, R.; Bennani, Y. L.; Surber, B. W.; Hancock, A. A.; Esbenshade, T. A. Use of an inverse agonist radioligand [^{3}H]A-317920 reveals distinct pharmacological profiles of the rat histamine H_3 receptor. *Neuropharmacology* **2006**, *50*, 468−478.
(43) Schlegel, B.; Laggner, C.; Meier, R.; Langer, T.; Schnell, D.; Seifert, R.; Stark, H.; Höltje, H. D.; Sippl, W. Generation of a homology model of the human histamine H(3) receptor for ligand docking and pharmacophore-based screening. *J. Comput.-Aided Mol. Des.* **2007**, *21*, 437−453.
(44) Levoin, N.; Calmels, T.; Poupardin-Olivier, O.; Labeeuw, O.; Danvy, D.; Robert, P.; Berrebi-Bertrand, I.; Ganellin, C. R.; Schunack, W.; Stark, H.; Capet, M. Refined docking as a valuable tool for lead optimization: application to histamine H_3 receptor antagonists. *Arch. Pharm.* **2008**, *341*, 610−623.
(45) Kim, S. K.; Fristrup, P.; Abrol, R.; Goddard, W. A., III Structure-based prediction of subtype selectivity of histamine H_3 receptor selective antagonists in clinical trials. *J. Chem. Inf. Model.* **2011**, *51*, 3262−3274.
(46) Kurczab, R.; Śliwa, P.; Rataj, K.; Kafel, R.; Bojarski, A. J. Salt Bridge in Ligand-Protein Complexes - Systematic Theoretical and Statistical Investigations. *J. Chem. Inf. Model.* **2018**, *58*, 2224−2238.
(47) Peng, X.; Yang, L.; Liu, Z.; Lou, S.; Mei, S.; Li, M.; Chen, Z.; Zhang, H. Structural basis for recognition of antihistamine drug by human histamine receptor. *Nat. Commun.* **2022**, *13*, 6105.
(48) Bicker, J.; Alves, G.; Fortuna, A.; Falcão, A. Blood-brain barrier models and their relevance for a successful development of CNS drug delivery systems: A review. *Eur. J. Pharm. Biopharm.* **2014**, *87*, 409−432.
(49) Chen, X.; Murawski, A.; Patel, K.; Crespi, C. L.; Balimane, P. V. A novel design of artificial membrane for improving the PAMPA model. *Pharm. Res.* **2008**, *25*, 1511−1520.
(50) Tjølsen, A.; Berge, O. G.; Hunskaar, S.; Rosland, J. H.; Hole, K. The formalin test: an evaluation of the method. *Pain* **1992**, *51*, 5−17.
(51) Vierck, C. J.; Yezierski, R. P.; Light, A. R. Long-lasting hyperalgesia and sympathetic dysregulation after formalin injection into the rat hind paw. *Neuroscience* **2008**, *153*, 501−506.
(52) Salinas-Abarca, A. B.; Avila-Rojas, S. H.; Barragán-Iglesias, P.; Pineda-Farias, J. B.; Granados-Soto, V. Formalin injection produces long-lasting hypersensitivity with characteristics of neuropathic pain. *Eur. J. Pharmacol.* **2017**, *797*, 83−93.
(53) Frias, B.; Merighi, A. Capsaicin, Nociception and Pain. *Molecules* **2016**, *21*, 797.
(54) Joseph, E. K.; Levine, J. D. Comparison of Oxaliplatin- and Cisplatin-Induced Painful Peripheral Neuropathy in the Rat. *J Pain* **2009**, *10*, 534−541.
(55) Chambers, J. E.; Chambers, H. W.; Funck, K. E.; Meek, E. C.; Pringle, R. B.; Ross, M. K. Efficacy of novel phenoxyalkyl pyridinium oximes as brain-penetrating reactivators of cholinesterase inhibited by surrogates of sarin and VX. *Chem.-Biol. Interact.* **2016**, *259*, 154−159.
(56) Sheldrick, G. M. SHELXT - Integrated space-group and crystal-structure determination. *Acta Crystallogr., Sect. A: Found. Crystallogr.* **2015**, *71*, 3−8.
(57) Sheldrick, G. M. A short history of SHELX. *Acta Crystallogr., Sect. A: Found. Crystallogr.* **2008**, *64*, 112−122.
(58) Farrugia, L. J. WinGX suite for small-molecule single-crystal crystallography. *J. Appl. Crystallogr.* **1999**, *32*, 837−838.
(59) Macrae, C. F.; Sovago, I.; Cottrell, S. J.; Galek, P. T. A.; McCabe, P.; Pidcock, E.; Platings, M.; Shields, G. P.; Stevens, J. S.; Towler, M.; Wood, P. A. *Mercury 4.0*: from visualization to analysis, design and prediction. *J. Appl. Crystallogr.* **2020**, *53*, 226−235.
(60) Nardelli, M. Modeling hydroxyl and water H atoms. *J. Appl. Crystallogr.* **1999**, *32*, 563−571.
(61) Amata, E.; Dichiara, M.; Gentile, D.; Marrazzo, A.; Turnaturi, R.; Arena, E.; La Mantia, A.; Tomasello, B. R.; Acquaviva, R.; Di Giacomo, C.; Rescifina, A.; Prezzavento, O. Sigma Receptor Ligands Carrying a Nitric Oxide Donor Nitrate Moiety: Synthesis, *In Silico*, and Biological Evaluation. *ACS Med. Chem. Lett.* **2020**, *11*, 889−894.
(62) Dichiara, M.; Artacho-Cordón, A.; Turnaturi, R.; Santos-Caballero, M.; González-Cano, R.; Pasquinucci, L.; Barbaraci, C.; Rodríguez-Gómez, I.; Gómez-Guzmán, M.; Marrazzo, A.; Cobos, E. J.; Amata, E. Dual Sigma-1 receptor antagonists and hydrogen sulfide-releasing compounds for pain treatment: Design, synthesis, and pharmacological evaluation. *Eur. J. Med. Chem.* **2022**, *230*, No. 114091.
(63) Amata, E.; Rescifina, A.; Prezzavento, O.; Arena, E.; Dichiara, M.; Pittalà, V.; Montilla-García, Á.; Punzo, F.; Merino, P.; Cobos, E. J.; Marrazzo, A. (+)-Methyl (1R,2S)-2-{[4-(4-Chlorophenyl)-4-hydroxypiperidin-1-yl]methyl}-1-phenylcyclopropanecarboxylate [(+)-MR200] Derivatives as Potent and Selective Sigma Receptor Ligands: Stereochemistry and Pharmacological Properties. *J. Med. Chem.* **2018**, *61*, 372−384.
(64) Amata, E.; Dichiara, M.; Arena, E.; Pittalà, V.; Pistarà, V.; Cardile, V.; Graziano, A. C. E.; Fraix, A.; Marrazzo, A.; Sortino, S.; Prezzavento, O. Novel Sigma Receptor Ligand-Nitric Oxide Photo-donors: Molecular Hybrids for Double-Targeted Antiproliferative Effect. *J. Med. Chem.* **2017**, *60*, 9531−9544.
(65) Rosier, N.; Grätz, L.; Schihada, H.; Möller, J.; Işbilir, A.; Humphrys, L. J.; Nagl, M.; Seibel, U.; Lohse, M. J.; Pockes, S. A Versatile Sub-Nanomolar Fluorescent Ligand Enables NanoBRET Binding Studies and Single-Molecule Microscopy at the Histamine H_3 Receptor. *J. Med. Chem.* **2021**, *64*, 11695−11708.
(66) Bartole, E.; Grätz, L.; Littmann, T.; Wifling, D.; Seibel, U.; Buschauer, A.; Bernhardt, G. UR-DEBa242: A Py-5-Labeled Fluorescent Multipurpose Probe for Investigations on the Histamine H_3 and H_4 Receptors. *J. Med. Chem.* **2020**, *63*, 5297−5311.
(67) Baumeister, P.; Erdmann, D.; Biselli, S.; Kagermeier, N.; Elz, S.; Bernhardt, G.; Buschauer, A. [^{3}H]UR-DE257: development of a tritium-labeled squaramide-type selective histamine H_2 receptor antagonist. *ChemMedChem* **2015**, *10*, 83−93.
(68) Igel, P.; Schnell, D.; Bernhardt, G.; Seifert, R.; Buschauer, A. Tritium-labeled N^1-[3-(1H-imidazol-4-yl)propyl]-N^2-propionylguani-

https://doi.org/10.1021/acs.jmedchem.3c00430
J. Med. Chem. 2023, 66, 9658−9683

dine ([^{3}H]UR-PI294), a high-affinity histamine H_3 and H_4 receptor radioligand. *ChemMedChem* **2009**, *4*, 225−231.
(69) Cheng, Y.; Prusoff, W. H. Relationship between the inhibition constant (K_I) and the concentration of inhibitor which causes 50 per cent inhibition (I_{50}) of an enzymatic reaction. *Biochem. Pharmacol.* **1973**, *22*, 3099−3108.
(70) Varadi, M.; Anyango, S.; Deshpande, M.; Nair, S.; Natassia, C.; Yordanova, G.; Yuan, D.; Stroe, O.; Wood, G.; Laydon, A.; Žídek, A.; Green, T.; Tunyasuvunakool, K.; Petersen, S.; Jumper, J.; Clancy, E.; Green, R.; Vora, A.; Lutfi, M.; Figurnov, M.; Cowie, A.; Hobbs, N.; Kohli, P.; Kleywegt, G.; Birney, E.; Hassabis, D.; Velankar, S. AlphaFold Protein Structure Database: massively expanding the structural coverage of protein-sequence space with high-accuracy models. *Nucleic Acids Res.* **2022**, *50*, D439−D444.
(71) Jumper, J.; Evans, R.; Pritzel, A.; Green, T.; Figurnov, M.; Ronneberger, O.; Tunyasuvunakool, K.; Bates, R.; Žídek, A.; Potapenko, A.; Bridgland, A.; Meyer, C.; Kohl, S. A. A.; Ballard, A. J.; Cowie, A.; Romera-Paredes, B.; Nikolov, S.; Jain, R.; Adler, J.; Back, T.; Petersen, S.; Reiman, D.; Clancy, E.; Zielinski, M.; Steinegger, M.; Pacholska, M.; Berghammer, T.; Bodenstein, S.; Silver, D.; Vinyals, O.; Senior, A. W.; Kavukcuoglu, K.; Kohli, P.; Hassabis, D. Highly accurate protein structure prediction with AlphaFold. *Nature* **2021**, *596*, 583−589.
(72) Berman, H. M. The Protein Data Bank. *Nucleic Acids Res.* **2000**, *28*, 235−242.
(73) Burley, S. K.; Bhikadiya, C.; Bi, C.; Bittrich, S.; Chen, L.; Crichlow, G. V.; Christie, C. H.; Dalenberg, K.; Di Costanzo, L.; Duarte, J. M.; Dutta, S.; Feng, Z.; Ganesan, S.; Goodsell, D. S.; Ghosh, S.; Green, R. K.; Guranović, V.; Guzenko, D.; Hudson, B. P.; Lawson, C. L.; Liang, Y.; Lowe, R.; Namkoong, H.; Peisach, E.; Persikova, I.; Randle, C.; Rose, A.; Rose, Y.; Sali, A.; Segura, J.; Sekharan, M.; Shao, C.; Tao, Y. P.; Voigt, M.; Westbrook, J. D.; Young, J. Y.; Zardecki, C.; Zhuravleva, M. RCSB Protein Data Bank: powerful new tools for exploring 3D structures of biological macromolecules for basic and applied research and education in fundamental biology, biomedicine, biotechnology, bioengineering and energy sciences. *Nucleic Acids Res.* **2021**, *49*, D437−D451.
(74) Schmidt, H. R.; Zheng, S.; Gurpinar, E.; Koehl, A.; Manglik, A.; Kruse, A. C. Crystal structure of the human σ_1 receptor. *Nature* **2016**, *532*, 527−530.
(75) Schmidt, H. R.; Betz, R. M.; Dror, R. O.; Kruse, A. C. Structural basis for σ_1 receptor ligand recognition. *Nat. Struct. Mol. Biol.* **2018**, *25*, 981−987.
(76) *Schrodinger Release 2017−3*; LigPrep. 2017.
(77) Shelley, J. C.; Cholleti, A.; Frye, L. L.; Greenwood, J. R.; Timlin, M. R.; Uchimaya, M. Epik: A software program for pK_a prediction and protonation state generation for drug-like molecules. *J. Comput.-Aided Mol. Des.* **2007**, *21*, 681−691.
(78) Madhavi Sastry, G.; Adzhigirey, M.; Day, T.; Annabhimoju, R.; Sherman, W. Protein and ligand preparation: Parameters, protocols, and influence on virtual screening enrichments. *J. Comput.-Aided Mol. Des.* **2013**, *27*, 221−234.
(79) Harder, E.; Damm, W.; Maple, J.; Wu, C.; Reboul, M.; Xiang, J. Y.; Wang, L.; Lupyan, D.; Dahlgren, M. K.; Knight, J. L.; Kaus, J. W.; Cerutti, D. S.; Krilov, G.; Jorgensen, W. L.; Abel, R.; Friesner, R. A. OPLS3: A Force Field Providing Broad Coverage of Drug-like Small Molecules and Proteins. *J. Chem. Theory Comput.* **2016**, *12*, 281−296.
(80) Friesner, R. A.; Murphy, R. B.; Repasky, M. P.; Frye, L. L.; Greenwood, J. R.; Halgren, T. A.; Sanschagrin, P. C.; Mainz, D. T. Extra precision glide: docking and scoring incorporating a model of hydrophobic enclosure for protein-ligand complexes. *J. Med. Chem.* **2006 Oct 19**, *49*, 6177−6196.
(81) Halgren, T. A.; Murphy, R. B.; Friesner, R. A.; Beard, H. S.; Frye, L. L.; Pollard, W. T.; Banks, J. L. Glide: a new approach for rapid, accurate docking and scoring. 2. Enrichment factors in database screening. *J. Med. Chem.* **2004**, *47*, 1750−1759.
(82) Murphy, R. B.; Philipp, D. M.; Friesner, R. A. A Mixed Quantum Mechanics/Molecular Mechanics (QM/MM) Method for Large-Scale Modeling of Chemistry in Protein Environments. *J. Comput. Chem.* **2000**, *21*, 1442−1457.
(83) Cho, A. E.; Guallar, V.; Berne, B. J.; Friesner, R. Importance of accurate charges in molecular docking: Quantum Mechanical/Molecular Mechanical (QM/MM) approach. *J. Comput. Chem.* **2005**, *26*, 915−931.
(84) Mogilski, S.; Kubacka, M.; Łażewska, D.; Więcek, M.; Głuch-Lutwin, M.; Tyszka-Czochara, M.; Bukowska-Strakova, K.; Filipek, B.; Kieć-Kononowicz, K. Aryl-1,3,5-triazine ligands of histamine H_4 receptor attenuate inflammatory and nociceptive response to carrageen, zymosan and lipopolysaccharide. *Inflammation Res.* **2017**, *66*, 79−95.
(85) Sałat, K.; Cios, A.; Wyska, E.; Sałat, R.; Mogilski, S.; Filipek, B.; Więckowski, K.; Malawska, B. Antiallodynic and antihyperalgesic activity of 3-[4-(3-trifluoromethyl-phenyl)-piperazin-1-yl]-dihydrofuran-2-one compared to pregabalin in chemotherapy-induced neuropathic pain in mice. *Pharmacol., Biochem. Behav.* **2014 Jul**, *122*, 173−181.
(86) Milano, J.; Oliveira, S. M.; Rossato, M. F.; Sauzem, P. D.; Machado, P.; Beck, P.; Zanatta, N.; Martins, M. A. P.; Mello, C. F.; Rubin, M. A.; Ferreira, J.; Bonacorso, H. G. Antinociceptive effect of novel trihalomethyl-substituted pyrazoline methyl esters in formalin and hot-plate tests in mice. *Eur. J. Pharmacol.* **2008**, *581*, 86−96.
(87) Pavao-de-Souza, G. F.; Zarpelon, A. C.; Tedeschi, G. C.; Mizokami, S. S.; Sanson, J. S.; Cunha, T. M.; Ferreira, S. H.; Cunha, F. Q.; Casagrande, R.; Verri, W. A., Jr. Acetic acid- and phenyl-p-benzoquinone-induced overt pain-like behavior depends on spinal activation of MAP kinases, PI_3K and microglia in mice. *Pharmacol., Biochem. Behav.* **2012 May**, *101*, 320−328.
(88) Lopes, S. C.; da Silva, A. V. L.; Arruda, B. R.; Morais, T. C.; Rios, J. B.; Trevisan, M. T. S.; Rao, V. S.; Santos, F. A. Peripheral antinociceptive action of mangiferin in mouse models of experimental pain: role of endogenous opioids, K(ATP)-channels and adenosine. *Pharmacol., Biochem. Behav.* **2013**, *110*, 19−26.
(89) Mogilski, S.; Kubacka, M.; Redzicka, A.; Kazek, G.; Dudek, M.; Malinka, W.; Filipek, B. Antinociceptive, anti-inflammatory and smooth muscle relaxant activities of the pyrrolo[3,4-d]pyridazinone derivatives: Possible mechanisms of action. *Pharmacol., Biochem. Behav.* **2015 Jun**, *133*, 99−110.
(90) Sánchez-Fernández, C.; Montilla-García, Á.; González-Cano, R.; Nieto, F. R.; Romero, L.; Artacho-Cordón, A.; Montes, R.; Fernández-Pastor, B.; Merlos, M.; Baeyens, J. M.; Entrena, J. M.; Cobos, E. J. Modulation of peripheral μ-opioid analgesia by σ_1 receptors. *J. Pharmacol. Exp. Ther.* **2014**, *348*, 32−45.
(91) Ruiz-Cantero, M. C.; Cortés-Montero, E.; Jain, A.; Montilla-García, Á.; Bravo-Caparrós, I.; Shim, J.; Sánchez-Blázquez, P.; Woolf, C. J.; Baeyens, J. M.; Cobos, E. J. The sigma-1 receptor curtails endogenous opioid analgesia during sensitization of TRPV1 nociceptors. *Br. J. Pharmacol.* **2023**, *180*, 1148−1167.
(92) Sałat, K.; Kołaczkowski, M.; Furgała, A.; Rojek, A.; Śniecikowska, J.; Varney, M. A.; Newman-Tancredi, A. Antinociceptive, antiallodynic and antihyperalgesic effects of the 5-HT_{1A} receptor selective agonist, NLX-112 in mouse models of pain. *Neuropharmacology* **2017 Oct**, *125*, 181−188.
(93) Zimmermann, M. Ethical guidelines for investigations of experimental pain in conscious animals. *Pain* **1983 Jun**, *16*, 109−110.
(94) Bennett, G. J.; Xie, Y. K. A peripheral mononeuropathy in rat that produces disorders of pain sensation like those seen in man. *Pain* **1988 Apr**, 33, 87−107.
(95) Popiolek-Barczyk, K.; Łażewska, D.; Latacz, G.; Olejarz, A.; Makuch, W.; Stark, H.; Kieć-Kononowicz, K.; Mika, J. Antinociceptive effects of novel histamine H_3 and H_4 receptor antagonists and their influence on morphine analgesia of neuropathic pain in the mouse. *Br. J. Pharmacol.* **2018**, *175*, 2897−2910.

https://doi.org/10.1021/acs.jmedchem.3c00430
J. Med. Chem. 2023, 66, 9658−9683

Supplementary Information

Dual piperidine-based histamine H_3 and sigma-1 receptor ligands in the treatment of nociceptive and neuropathic pain

Katarzyna Szczepańska[+ a,b], Tadeusz Karcz[+ a,*], Maria Dichiara [c], Szczepan Mogilski [d], Justyna Kalinowska-Tłuścik [e], Bogusław Pilarski [f], Arkadiusz Leniak [g], Wojciech Pietruś [b,g], Sabina Podlewska [b], Katarzyna Popiołek-Barczyk [h], Laura J. Humphrys [i], M. Carmen Ruiz-Cantero [j], David Reiner-Link [k], Luisa Leitzbach [k], Dorota Łażewska [a], Steffen Pockes [i], Michał Górka [g], Adam Zmysłowski [g], Thierry Calmels [l], Enrique J. Cobos [j], Agostino Marrazzo [c], Holger Stark [k], Andrzej J. Bojarski [b], Emanuele Amata [c,*], Katarzyna Kieć-Kononowicz [a,*]

[a] *Department of Technology and Biotechnology of Drugs, Faculty of Pharmacy, Jagiellonian University Medical College, Medyczna 9, Kraków 30-688, Poland*
[b] *Maj Institute of Pharmacology, Polish Academy of Sciences, Department of Medicinal Chemistry, Smętna 12, Kraków 31-343, Poland*
[c] *Department of Drug and Health Sciences, University of Catania, V.le A. Doria, 95125 Catania, Italy*
[d] *Department of Pharmacodynamics, Faculty of Pharmacy, Jagiellonian University Medical College, Medyczna 9, Kraków 30-688, Poland*
[e] *Department of Crystal Chemistry and Crystal Physics, Faculty of Chemistry Jagiellonian University, Gronostajowa 2, 30-387 Kraków, Poland*
[f] *Cerko Sp. z o.o. Sp.k, Al. Zwycięstwa 96/98, 81-451 Gdynia, Poland*
[g] *Celon Pharma S.A., R&D Centre, Marymoncka 15, 05-152, Kazuń Nowy, Poland*
[h] *Maj Institute of Pharmacology, Polish Academy of Sciences, Department of Neurochemistry, Smętna 12, Kraków 31-343, Poland*
[i] *Institute of Pharmacy, Faculty of Chemistry and Pharmacy, University of Regensburg, Universitätsstraße 31, D-93053 Regensburg, Germany*
[j] *Department of Pharmacology and Neurosciences Institute (Biomedical Research Center), University of Granada, and Biosanitary Research Institute ibs.Granada, Avenida de la Investigación 11, 18016 Granada, Spain*
[k] *Institute of Pharmaceutical and Medicinal Chemistry, Heinrich Heine University Düsseldorf, Universitaetsstr. 1, 40225 Duesseldorf, Germany*
[l] *Bioprojet-Biotech, 4rue du Chesnay Beauregard, 35762 Saint-Gregoire Cedex, France*

* Corresponding authors. E-mail addresses: t.karcz@uj.edu.pl (Tadeusz Karcz), eamata@unict.it (Emanuele Amata), mfkonono@cyf-kr.edu.pl (Katarzyna Kieć-Kononowicz).
[+] These authors contributed equally to this work.

Contents

1. Protonation investigation based on crystal structure analysis 2
2. Determination of the basicity of selected piperidine and piperazine derivatives by potentiometric titration 11
3. Protonation investigation based on NMR spectroscopy measurements in pH-controlled environment..... 12
4. *In silico* studies. Molecular modeling: docking studies and molecular dynamics simulations..... 27
5. *In vivo* pharmacological activity 32
6. ^{1}H-, ^{13}C-NMR spectra, HRMS analysis and HPLC traces 34

1. Protonation investigation based on crystal structure analysis

Table S1. Crystal data and final refinement results for structures of oxalate salts.

	KSK67	**KSK68**	**KSK68_OH**
Empirical moiety formula	$C_{22}H_{29}N_3O_{12}$, 2 C_2HO_4, 2 H_2O	$C_{25}H_{30}N_2O_6$, 0.5 $C_2H_2O_4$	$C_{23}H_{29}N_2O_2$, 0.5 C_2O_4, 4 H_2O
Formula weight [g/mol]	581.57	499.53	481.55
Crystal system	Monoclinic	Monoclinic	Triclinic
Space group	C2	C2/*c*	$P\bar{1}$
Unite cell dimensions	a = 15.0969(8) Å b = 5.7291(3) Å c = 30.7622(8) Å α=90° β=94.626(3)° γ=90°	a = 21.5545(6) Å b = 8.4549(2) Å c = 28.2827(8) Å α=90° β=111.415(3)° γ=90°	a = 8.5168(5) Å b = 9.6493(4) Å c = 16.1458(9) Å α=89.241(4)° β=89.175(5)° γ=72.737(5)°
Volume [$Å^3$]	2652.0(2)	4798.4(2)	1266.92(12)
Z	4	8	2
D_{calc} [Mg/m^3]	1.457	1.383	1.262
μ [mm^{-1}]	0.985	0.856	0.783
F(000)	1232	2120	518
Crystal size [mm^3]	0.2 x 0.15 x 0.02	0.3 x 0.2 x 0.02	0.3 x 0.2 x 0.1
Θ range	2.882° to 75.520°	3.357° to 75.541°	2.737° to 77.567°
Index ranges	-18 ≤ h ≤ 17, -7 ≤ k ≤ 5, -36 ≤ l ≤ 38	-26 ≤ h ≤ 26, -10 ≤ k ≤ 8, -35 ≤ l ≤ 34	-10 ≤ h ≤ 10, -12 ≤ k ≤ 9, -20 ≤ l ≤ 20
Refl. collected	12977	23308	12391
Independent reflections	4718 [R(int) = 0.0785]	4842 [R(int) = 0.0684]	4996 [R(int) = 0.0553]
Completeness [%] to Θ	99.9 (Θ 67.684°)	97.2 (Θ 75.541°)	92.6 (Θ 77.567°)
Absorption correction	Multi-scan	Multi-scan	Multi-scan
Tmin. and Tmax.	0.688 and 1.000	0.778 and 1.000	0.787 and 1.000
Data/ restraints/parameters	4718 / 16 / 504	4847 / 1 / 338	4996 / 4 / 316
GooF on F2	1.101	1.125	1.078
Final R indices [I>2sigma(I)]	R1= 0.0947, wR2= 0.2510	R1= 0.0694, wR2= 0.2063	R1= 0.0727, wR2= 0.2021
R indices (all data)	R1= 0.0947, wR2= 0.2517	R1= 0.0733, wR2= 0.2104	R1= 0.0809, wR2= 0.2131
$\Delta\rho_{max}$, $\Delta\rho_{min}$ [$e \cdot Å^{-3}$]	0.632 and -0.585	0.469 and -0.434	0.765 and -0.533
Absolute structure parameter	0.07(14)	-	-

Table S2. Crystal data and final refinement results for free bases.

	KSK67_fb	**KSK68_fb**	**KSK94_fb**	**KSK100_fb**
Empirical moiety formula	$C_{22}H_{27}N_3O_2$, HI, 2 H_2O	$C_{23}H_{28}N_2O_2$	2 $C_{25}H_{26}N_4O$, HI, 2 H_2O	$C_{26}H_{27}N_3O$
Formula weight [g/mol]	529.40	364.47	960.93	397.50
Crystal system	Monoclinic	Monoclinic	Monoclinic	Triclinic
Space group	$P2_1/n$	$P2_1$	$P2_1/c$	$P\bar{1}$
Unite cell dimensions	a = 10.9621(1) Å b = 8.9179(1) Å c = 23.5157(1) Å α=90° β=94.814(1)° γ=90°	a = 10.3351(1) Å b = 11.6636(1) Å c = 16.9247(1) Å α=90° β=105.438(1)° γ=90°	a = 10.4940(1) Å b = 17.3517(2) Å c = 25.4093(3) Å α=90° β=91.703(1)° γ=90°	a = 7.5156(1) Å b = 10.7481(1) Å c = 13.7353(1) Å α=104.711(1)° β=96.758(1)° γ=96.212(1)°
Volume [Å^3]	2290.76(3)	1966.57(3)	4624.7(9)	1054.62(2)
Z	4	4	4	2
D_{calc} [Mg/m^3]	1.535	1.231	1.380	1.252
μ [mm^{-1}]	11.251	0.618	5.867	0.603
F(000)	1080	784	1992	424
Crystal size [mm^3]	0.3 x 0.15 x 0.07	0.3 x 0.15 x 0.1	0.1 x 0.05 x 0.02	0.3 x 0.2 x 0.01
Θ range	3.773° to 80.481°	2.709° to 80.458°	3.084° to 80.621°	3.365° to 80.401°
Index ranges	-14 ≤ h ≤ 13, -10 ≤ k ≤ 11, -29 ≤ l ≤ 30	-13 ≤ h ≤ 13, -14 ≤ k ≤ 13, -21 ≤ l ≤ 21	-13 ≤ h ≤ 13, -20 ≤ k ≤ 22, -32 ≤ l ≤ 31	-9 ≤ h ≤ 9, -13 ≤ k ≤ 13, -17 ≤ l ≤ 17
Refl. collected	65243	68587	64583	33862
Independent reflections	4983 [R(int) = 0.0614]	8403 [R(int) = 0.0423]	10037 [R(int) = 0.0761]	4538 [R(int) = 0.0506]
Completeness [%] to Θ	99.4 (Θ 80.481°)	98.0 (Θ 80.458°)	98.9 (Θ 80.621°)	98.1 (Θ 80.401°)
Absorption correction	Multi-scan	Multi-scan	Multi-scan	Multi-scan
Tmin. and Tmax.	0.633 and 1.000	0.830 and 1.000	0.722 and 1.000	0.548 and 1.000
Data/ restraints/parameters	4983 / 2 / 291	8403 / 1 / 553	10037 / 4 / 612	4538 / 0 / 271
GooF on F2	1.085	1.051	1.0896	1.071
Final R indices [I>2sigma(I)]	R1= 0.0219, wR2= 0.0583	R1= 0.0454, wR2= 0.1235	R1= 0.0578, wR2= 0.1420	R1= 0.0397, wR2= 0.1070
R indices (all data)	R1= 0.0222, wR2= 0.0586	R1= 0.0464, wR2= 0.1248	R1= 0.0634, wR2= 0.1454	R1= 0.0422, wR2= 0.1096
$\Delta\rho_{max}$, $\Delta\rho_{min}$ [e·Å^{-3}]	0.533 and -0.832	0.391 and -0.213	1.211 and -1.014	0.196 and -0.255
Absolute structure parameter	-	0.2(2)	-	-

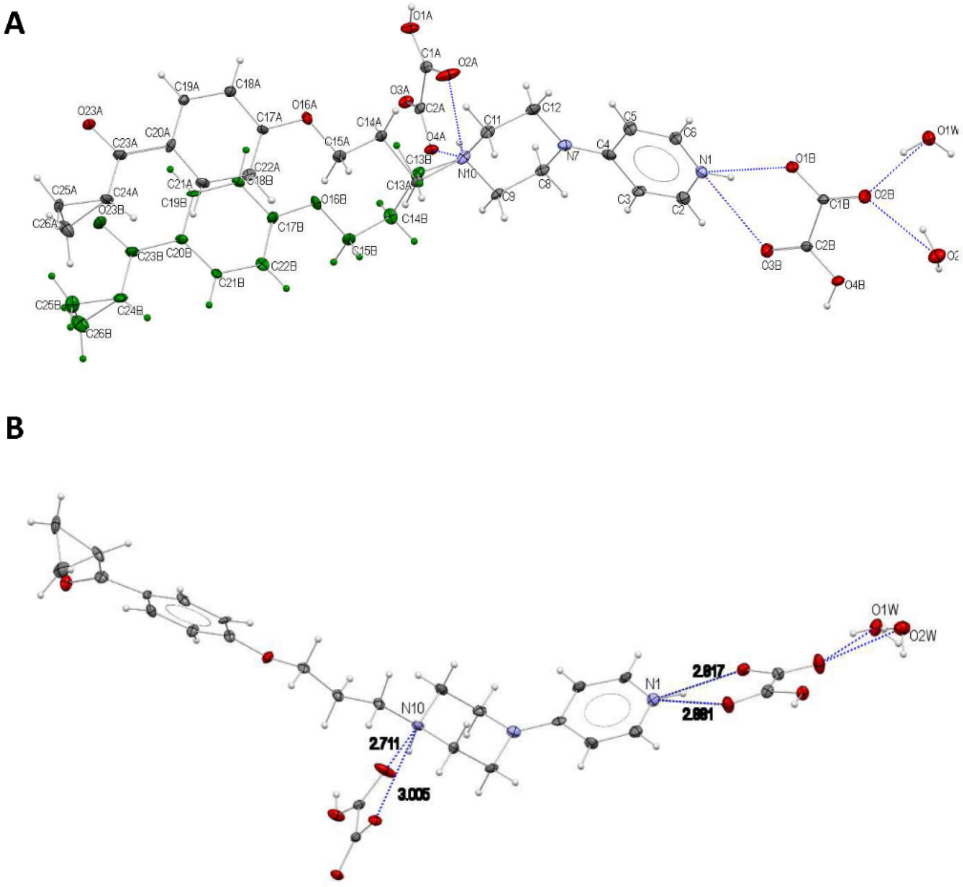


Figure S1. **A**: The asymmetric unit of **KSK67** crystal structure with the atom labeling scheme. A positional disorder is observed – the molecule adopts two alternative conformations in the crystal lattice with site occupancies of 60% and 40% (the less abundant conformation is marked with C and H-atoms in green and labels with B letters at the end of a symbol). **B**: The strongest interactions stabilizing crystal lattice (charge-assisted hydrogen bonds between protonated nitrogen atoms of the main organic compound and oxalate anion & hydrogen bonds involving water molecules incorporated in the crystal structure). Displacement ellipsoids of non-hydrogen atoms are drawn at the 30% probability level. H atoms are presented as small spheres with an arbitrary radius .

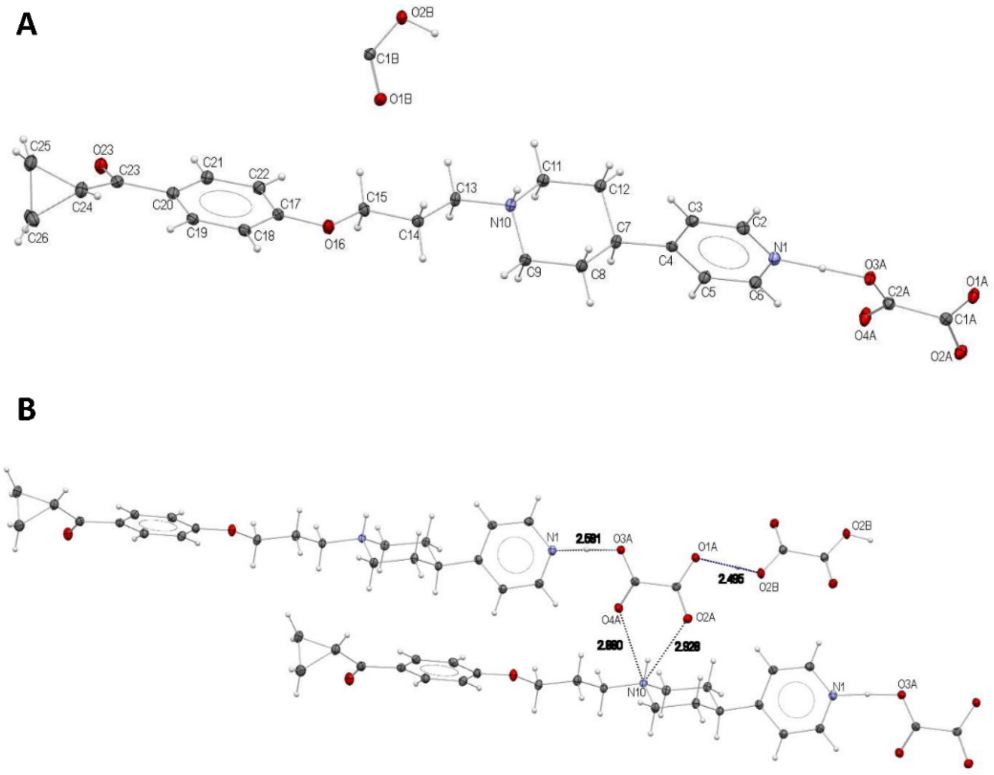


Figure S2. **A**: The asymmetric unit of **KSK68** crystal structure showing the atom labeling scheme. **B**: The strongest interactions stabilizing crystal lattice (charge-assisted hydrogen bonds between protonated nitrogen atoms of the main organic compound and oxalate anion & hydrogen bonds involving neutral oxalic acid molecules as an H-bond donor. Displacement ellipsoids of non-hydrogen atoms are drawn at the 30% probability level. H atoms are presented as small spheres with an arbitrary radius.

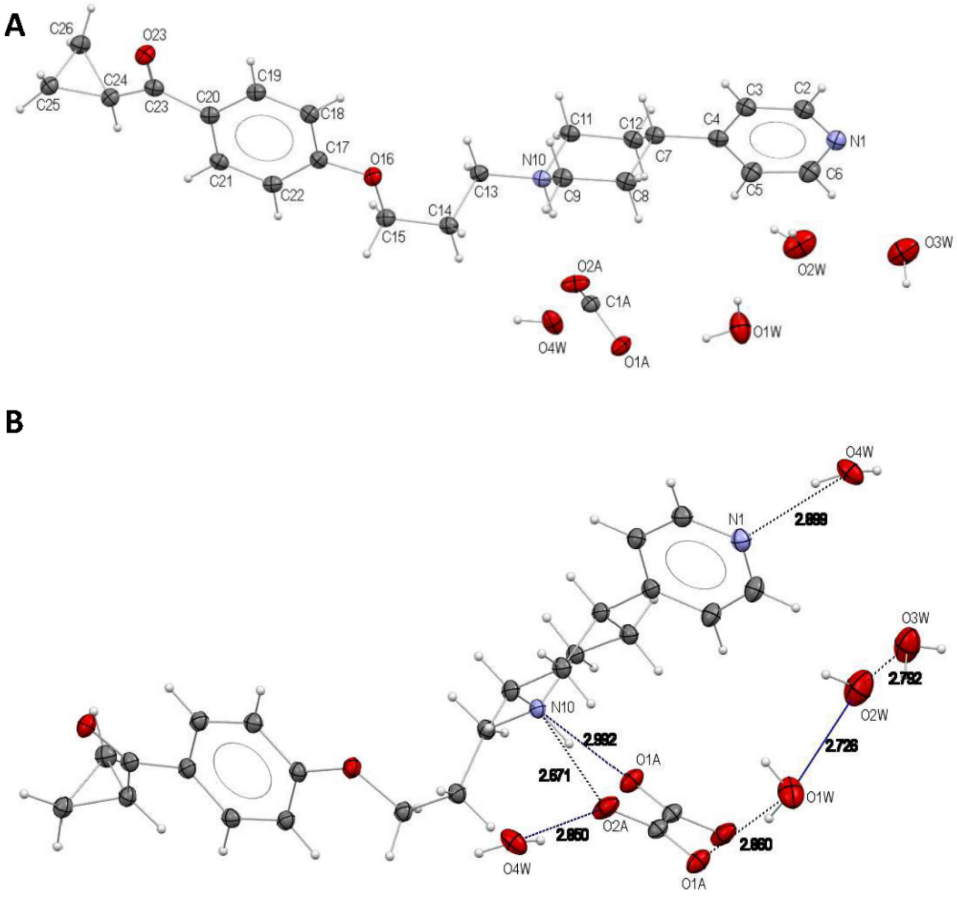


Figure S3. **A**: The asymmetric unit of **KSK68_OH** crystal structure presenting the atom labeling scheme. **B**: The strongest interactions stabilizing crystal lattice (charge-assisted hydrogen bonds between the protonated nitrogen atom of the piperidine moiety and oxalate anion & hydrogen bonds involving water molecules incorporated in the crystal structure, forming expanded H-bonds motifs propagating along [100] axis. Displacement ellipsoids of non-hydrogen atoms are drawn at the 30% probability level. H atoms are presented as small spheres with an arbitrary radius.

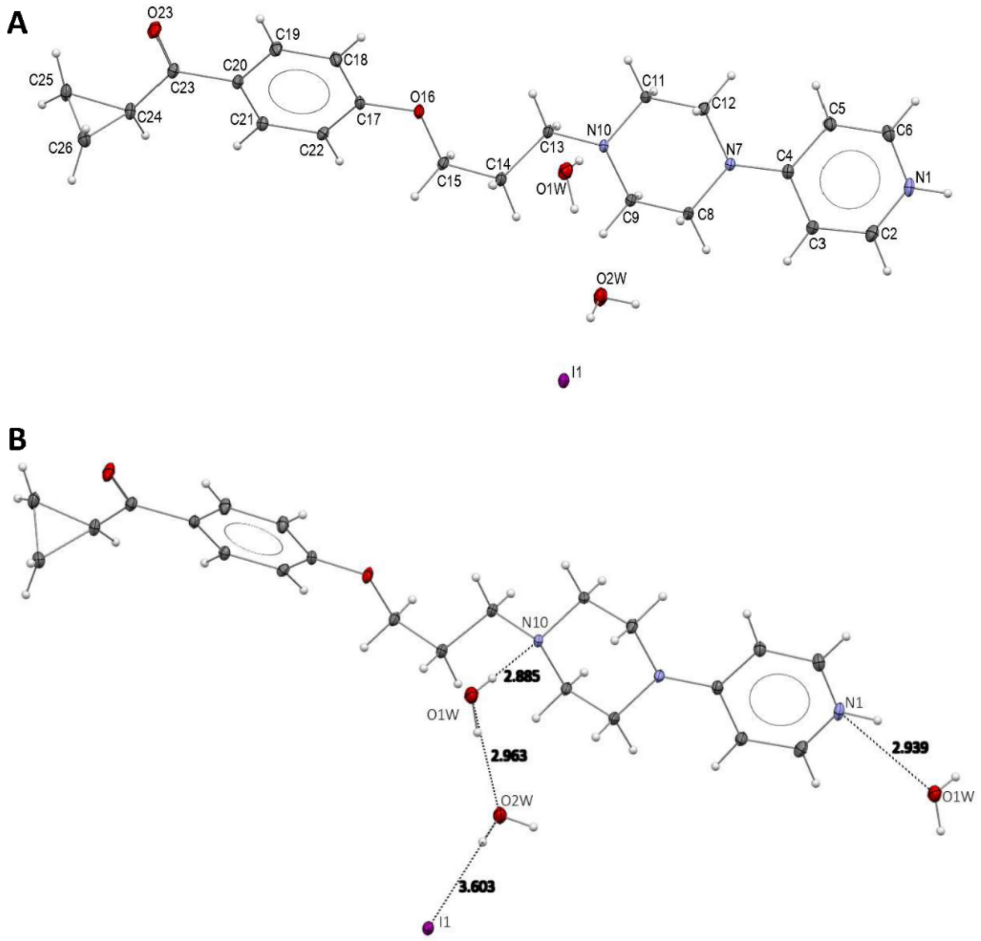


Figure S4. **A**: The asymmetric unit of **KSK67_fb** crystal structure with the atom labeling scheme. The postulated free base was not observed in the neutral form. Instead, an iodide salt was present, with the protonation center at N1 (pyridine) nitrogen atom, suggesting a strongly basic character of this molecular fragment. **B**: The strongest interactions stabilizing crystal lattice. Interestingly, the charge-assisted interaction between counter-ions was not observed. Both cation and anion are involved in hydrogen bonds with water molecules incorporated in the crystal structure. Displacement ellipsoids of non-hydrogen atoms are drawn at the 30% probability level. H atoms are presented as small spheres with an arbitrary radius.

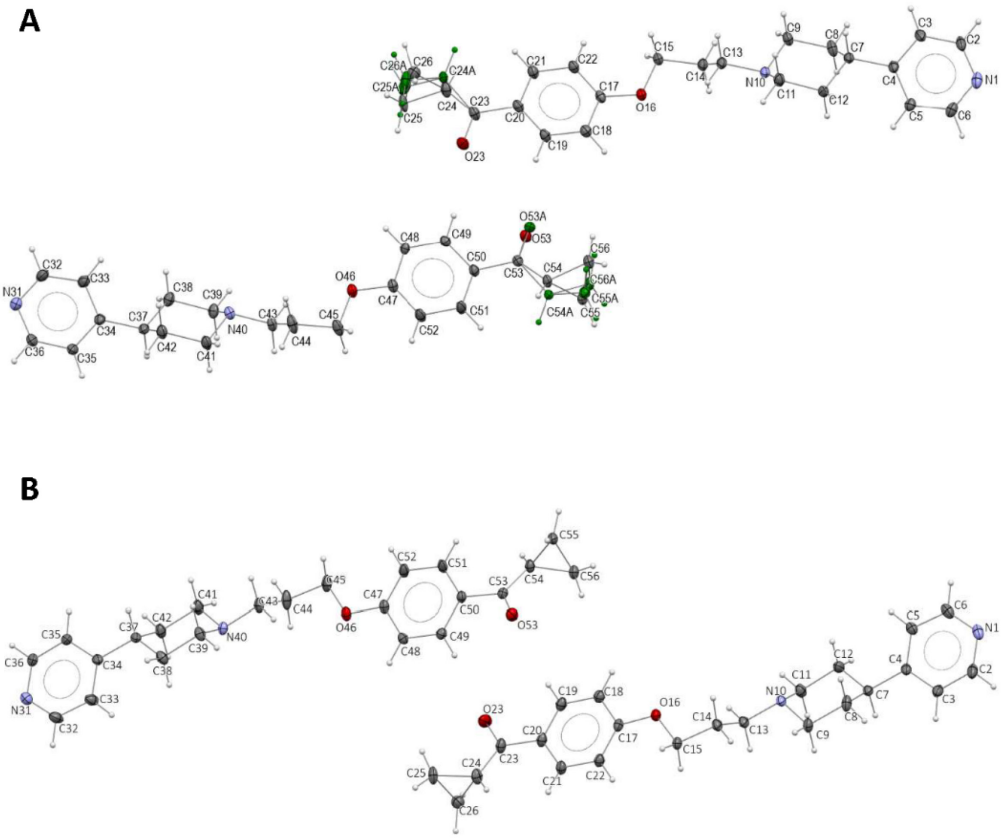


Figure S5. **A**: The asymmetric unit of **KSK68_fb** crystal structure presenting the atom labeling scheme. The asymmetric unit consists of two independent molecules adopting alternative conformations in the crystal lattice. Additionally, a positional disorder is observed for both molecules within the cyclopropyl fragment with site occupancies of 53% and 47% for molecules 1 (with label numbers 1-26), and 51% and 49% for molecule 2 (with label numbers 31-56) - the less abundant conformation for each molecule is marked with C and H-atoms in green and labels with an additional A letter at the end of a symbol. **B**: The asymmetric unit presenting only the most abundant conformations. Displacement ellipsoids of non-hydrogen atoms are drawn at the 30% probability level. H atoms are presented as small spheres with an arbitrary radius.

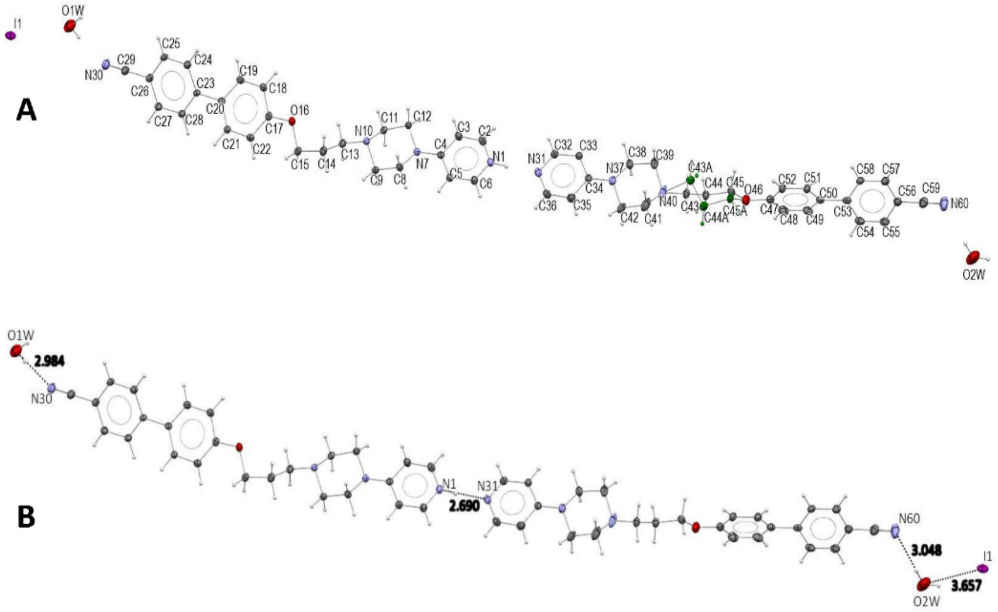


Figure S6. A: The asymmetric unit of **KSK94_fb** crystal structure with the atom labeling scheme. The asymmetric unit consists of two independent molecules adopting alternative conformations in the crystal lattice. For one of them (molecule 2 with label numbers 31-60) a positional disorder is observed for the propyl chain, existing in two alternative conformations (site occupancies 63% and 37%; the less abundant conformation is marked with C and H-atoms in green and labels with A letters at the end of a symbol). **B**: The strongest interactions stabilizing crystal lattice. Similarly to **KSK67_fb**, also here a free base form was expected. However, the strongest base (N1 of the pyridine ring in molecule 1) is protonated and forms an interaction with the corresponding basic center N31 in molecule 2. No charge-assisted interaction between counter-ions was observed. The iodide anion is involved in hydrogen bonds with water molecules incorporated in the crystal structure. Water molecules form additional hydrogen bonds with a nitrile nitrogen atom as an acceptor. Displacement ellipsoids of non-hydrogen atoms are drawn at the 30% probability level. H atoms are presented as small spheres with an arbitrary radius.

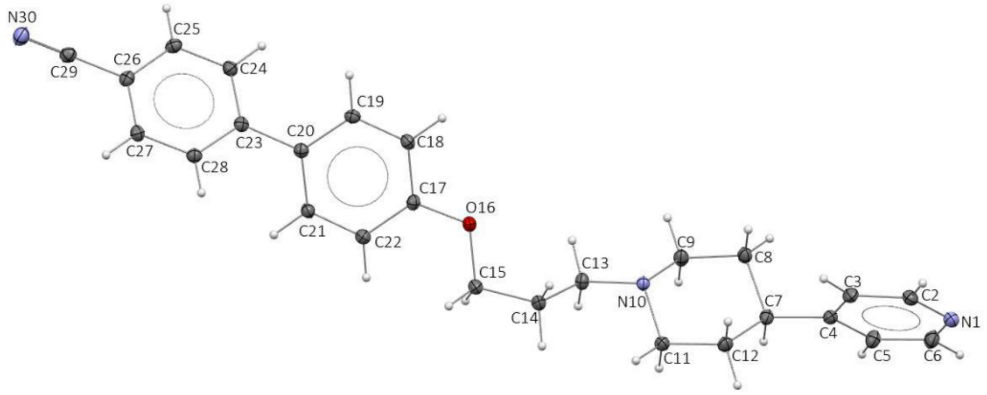


Figure S7. The asymmetric unit of **12_fb** crystal structure showing the atom labeling scheme. The crystal is stabilized only by weak interactions with the predominant number of weak hydrogen bonds with C-H donor. Displacement ellipsoids of non-hydrogen atoms are drawn at the 30% probability level. H atoms are presented as small spheres with an arbitrary radius.

2. Determination of the basicity of selected piperidine and piperazine derivatives by potentiometric titration

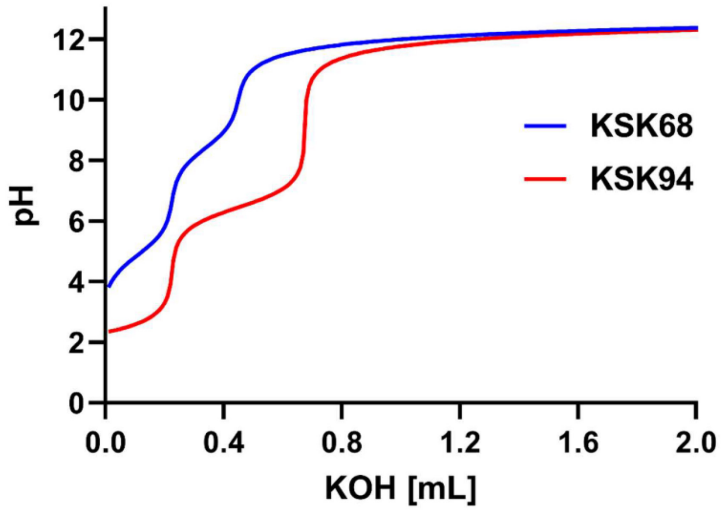


Figure S8. Titration curves of compounds **KSK68** and **KSK94** used to generate their protonation states.

3. Protonation investigation based on NMR spectroscopy measurements in pH-controlled environment

All signals in the ^{1}H and ^{13}C spectra were assigned based on 2D correlation spectra for compounds **KSK68** and **KSK94** to follow the course of changes in their chemical shifts during titration with trifluoromethanesulfonic acid (TfOH).

The spectrum of **KSK68** consists two main groups of signals: aromatic and alkyl. The signals of the methylene groups of the piperidine ring differentiate into equatorial and axial positions on the spectrum due to the different chemical environment in the ring's chair conformation. The H3 proton signal is covered by the DMSO-d_6 signal. All other signals are separable and have a distinct multiplet structure.

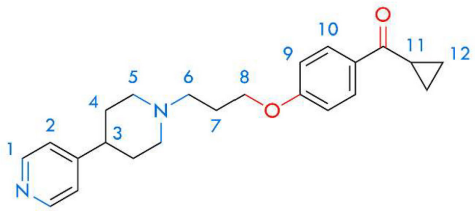


Figure S9. Structure of **KSK68** with numbered hydrogen atoms.

The addition of the first portion of TfOH in the amount of 0.2 molar equivalents does not cause any fundamental changes in the chemical shifts and multiplet structures of the signals in the aromatic part of the spectrum and for signals from H8 to H12. In contrast, the proton signals of the piperidine ring and the adjacent proton signals of H6, H7 shift toward higher frequencies. This signals undergo significant broadening and loss of multiplet structure. That behaviour can be explained to the occurrence of the dynamics of the transition of the piperidine ring from the protonated form to the free form of the nitrogen function, which entails conformational changes that are too slow on the NMR time scale. The signals of protons closer to the piperidine nitrogen undergo stronger chemical shift changes. As the titration continues, the protons H1, H1' also shift slightly towards higher frequencies. This trend is observed until a molar ratio of 1.0 : 1.0 is reached. With this acid concentration the piperidine ring proton signals and adjacent signals of H6, H7 protons recover the multiplet structure. It is associated with a shift in exchange dynamics toward the protonated form only. Further addition of acid does not cause any change in the structure and chemical shift of the aliphatic signals except for the proton H3 signal, which is the nodal proton between the pyridine and piperidine ring.

From a ratio of 1.2 : 1.0, the aromatic pyridine signals begin to shift toward higher frequencies, with shift change values for protons H1, H1' being larger than for H2, H2'. The change in the chemical shifts of the signals for the pyridine protons and H3 continues up to an acid content of 2.0 : 1.0. Above this value, there is no longer any change in the signal structure

of compound **KSK68** in the NMR spectrum. Only increasing concentrations of free triflic acid can be observed.

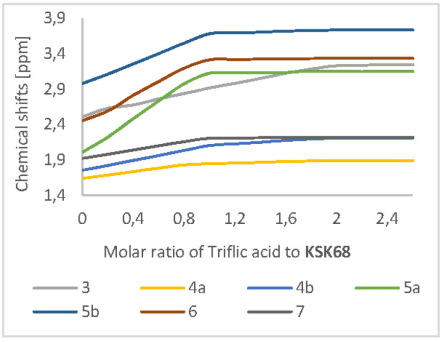


Figure S10. Proton chemical shifts in increasing molar ratio of triflic acid to **KSK68** for the significant aliphatic signals.

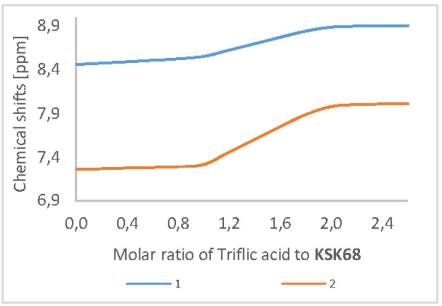


Figure S11. Proton chemical shifts in increasing molar ratio of triflic acid to **KSK68** for the significant aromatic signals.

Similar to **KSK68**, the spectrum of **KSK94** contains two major groups of signals. The aromatic part, which is enriched with two signals of an additional ring, and the aliphatic part with a simplified structure in comparison to the above case of **KSK68**. In contrast to the piperidine ring, the signals of protons of H3, H3' and H4, H4' in piperazine ring do not differentiate into equatorial and axial positions - they appear as single signals with integration referred as equal to 4. The signals of protons H4, H4' and H5 are covered by DMSO-d_6 signal.

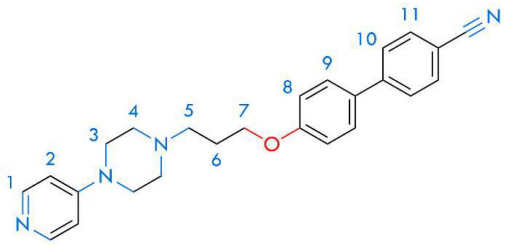


Figure S12. Structure of **KSK94** with numbered hydrogen atoms.

Titration with triflic acid to a molar ratio of 0.6 : 1.0 results in a strong shift of the aromatic signals H1, H1' towards higher frequencies. Identical behaviour is observed for H3, H3' aliphatic protons of the piperazine ring. The aromatic protons H2, H2' also shift in the same direction but with lower step difference values. The remaining aliphatic proton signals show no change in structure or chemical shift. Further titration with acid cause a decrease in the dynamics of changes in chemical shifts of aromatic protons, which still occurs but is much more subtle. On the other hand, significant changes could be observed in the aliphatic range of the spectrum. The signals of H3, H4, H5 and H6 protons have broadened and lost their multiplet structure. The situation is analogous to the case of compound **KSK68**. At a molar ratio of 1.2 : 1.0, the signals of protons H3, H3' and H4, H4' start to split into signals originating from protons in axial and equatorial positions in the piperazine ring. At this acid concentration all aliphatic signals have recovered

their multiplet structure. Above a ratio of 1:4 : 1.0, there are no more changes in the NMR spectral image except for increasing TfOH acid content.

As the titration progresses, a very broad signal associated with protonated nitrogen functions begins to grow out of the baseline in the range of 12 ppm to 14 ppm. At a molar ratio of 0.6 : 0.1 its chemical shift is about 13 ppm. Up to a ratio of 1.0 : 1.0 it shifts toward lower frequencies resulting in a very broad signal. At 1.2 : 1.0 signal splits into two independent signals at 9.86 ppm and 13.60 ppm, each one corresponds to different protonated nitrogen atom.

For compound **KSK94**, $^{1}H\{^{15}N\}$ HMBC nitrogen spectra were collected for the free base form and after the titration was completed. The chemical shift for pyridinic nitrogen before the addition of acid is -115 ppm relative to nitromethane (0 ppm). The same pyridinic nitrogen after the titration showed a chemical shift value of -209 ppm. The difference in shifts is 94 ppm.

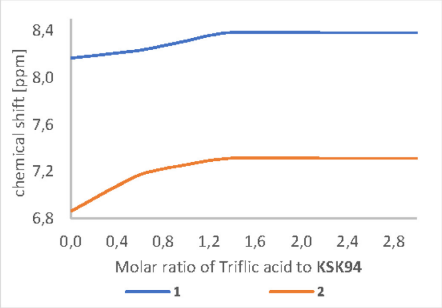


Figure S13. Proton chemical shifts in increasing molar ratio of triflic acid to **KSK94** for the significant aromatic signals.

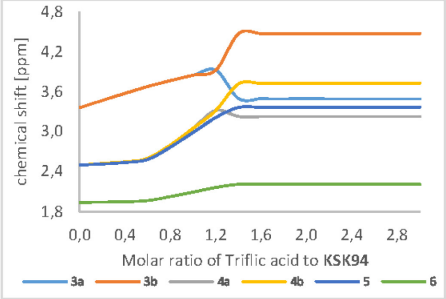


Figure S14. Proton chemical shifts in increasing molar ratio of triflic acid to **KSK94** for the significant aliphatic signals.

All spectra were measured on a JEOL JNM_ECZR 600 MHz spectrometer equipped with a Royal HFX probe. Full structural analysis with assignment of ^{1}H and ^{13}C signals performed using JASON software.

KSK68

Spectra and structural analysis

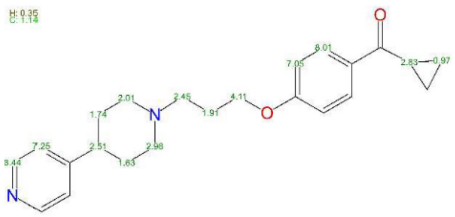


Figure S15. Structure of **KSK68** with ^{1}H chemical shifts applied on.

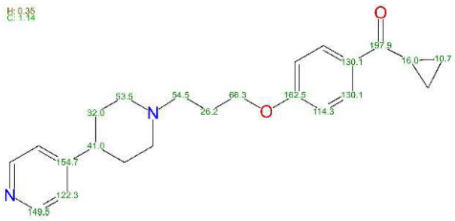
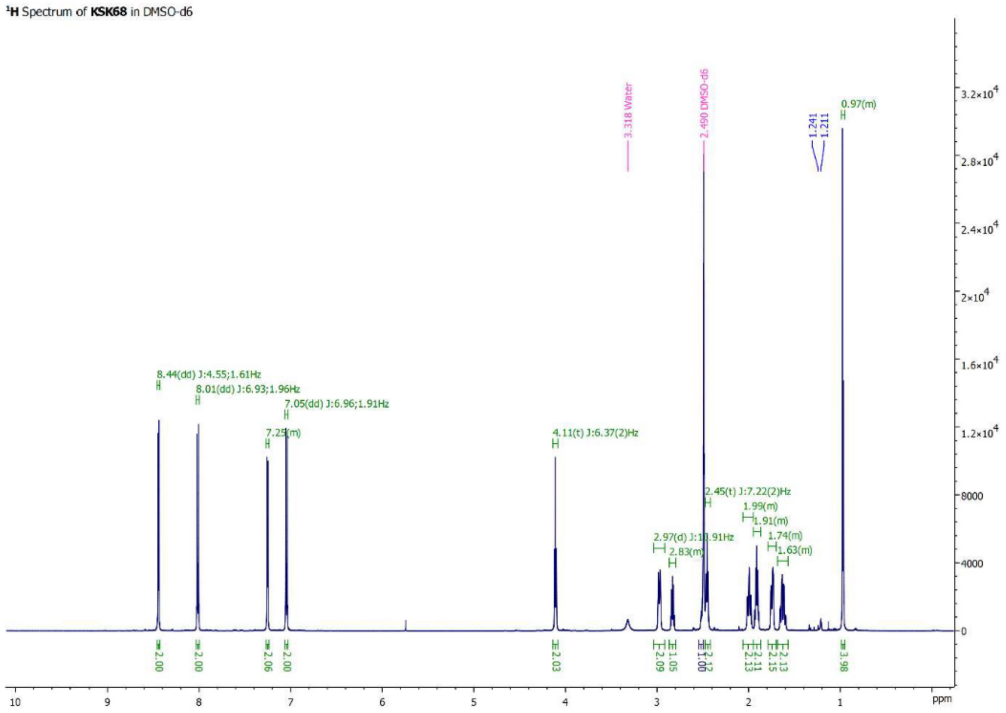
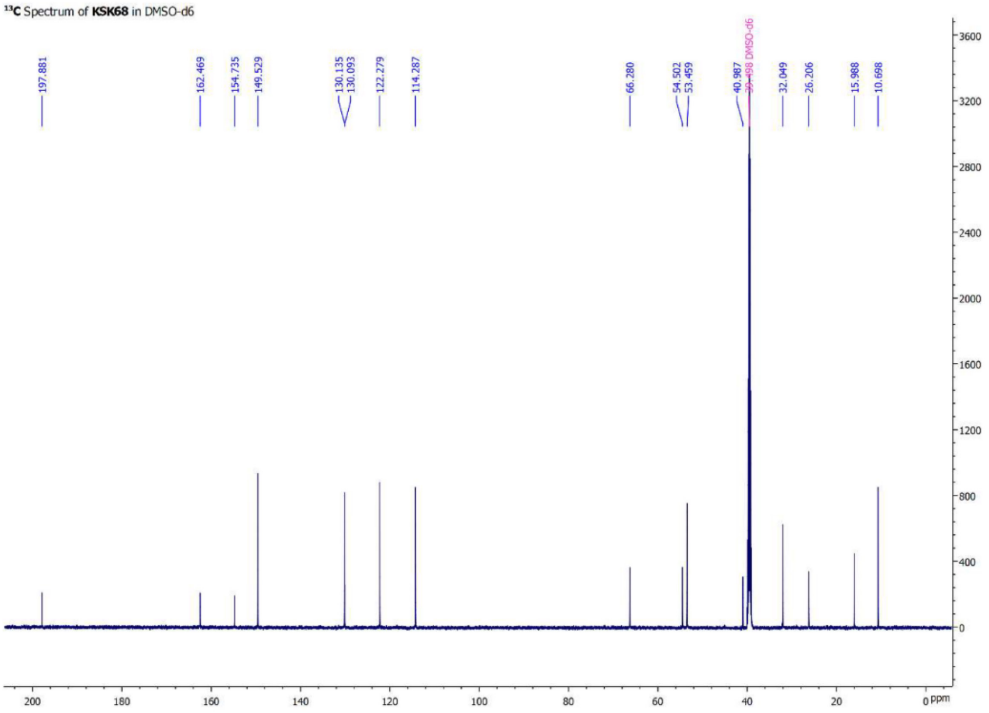
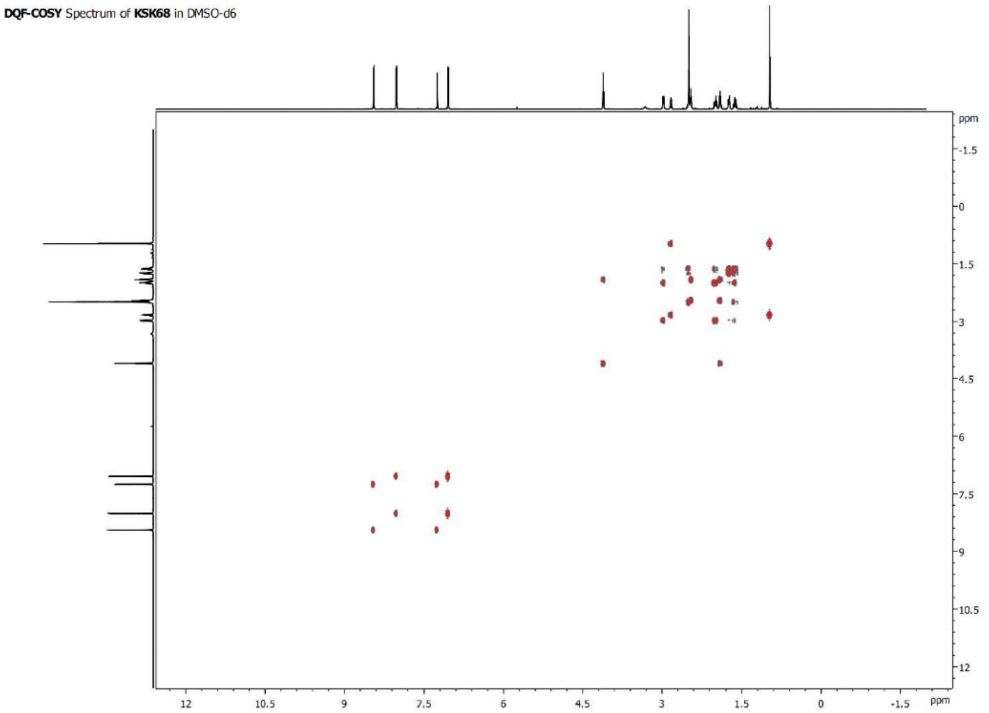


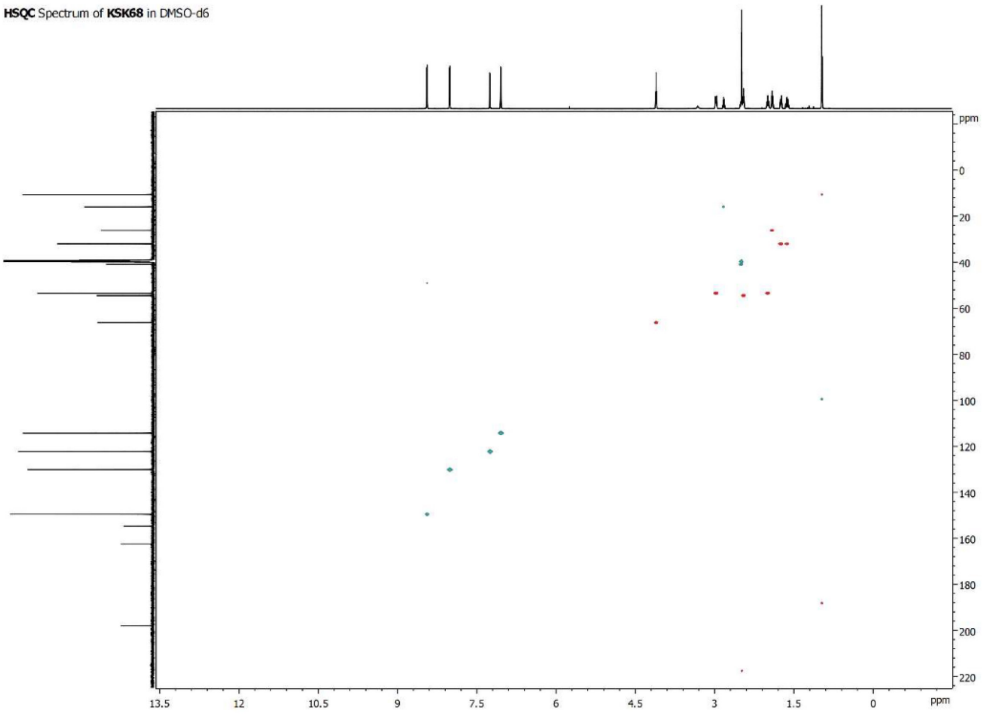
Figure S16. Structure of **KSK68** with ^{13}C chemical shifts applied on.

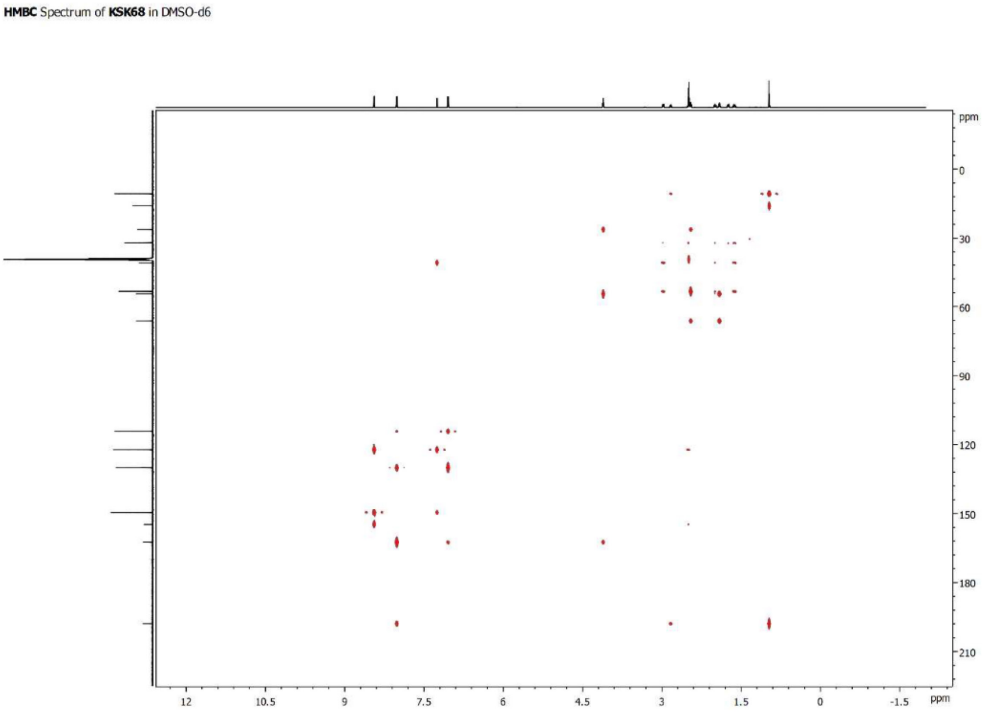



^{13}C Spectrum of KSK68 in DMSO-d6
197.881
162.469
154.735
149.529
130.135
130.093
122.279
114.287
66.280
54.502
53.459
40.987
39.498 DMSO-d6
32.049
26.206
15.988
10.698
ppm


DQF-COSY Spectrum of KSK68 in DMSO-d6
ppm

S16


HSQC Spectrum of KSK68 in DMSO-d6
ppm
0
20
40
60
80
100
120
140
160
180
200
220
13.5
12
10.5
9
7.5
6
4.5
3
1.5
0
ppm


HMBC Spectrum of KSK68 in DMSO-d6
ppm
0
30
60
90
120
150
180
210
12
10.5
9
7.5
6
4.5
3
1.5
0
-1.5
ppm

S17

KSK68

Titration experiment

Table S3. Proton chemical shifts of signals of compound **KSK68** with increasing TfOH concentration during titration.

	Chemical shifts [ppm] in reference to TMS in DMSO-d_6													
Atom label	1	2	3	4a	4b	5a	5b	6	7	8	9	10	11	12
Molarity of acid														
0.0	8.462	7.264	2.513	1.642	1.760	2.011	2.985	2.460	1.927	4.127	7.061	8.030	2.841	0.994
0.2	8.478	7.272	2.634	1.690	1.827	2.226	3.117	2.595	1.985	4.143	7.068	8.038	2.845	0.997
0.4	8.495	7.280	2.680	1.739	1.898	2.487	3.261	2.817	2.045	4.160	7.075	8.045	2.849	1.001
0.6	8.512	7.288	2.766	1.789	1.967	2.737	3.407	3.012	2.106	4.176	7.082	8.053	2.854	1.003
0.8	8.528	7.295	2.841	1.835	2.039	2.979	3.554	3.200	2.164	4.192	7.089	8.061	2.858	1.005
1.0	8.556	7.321	2.920	1.852	2.108	3.128	3.686	3.318	2.213	4.204	7.094	8.066	2.861	1.007
1.2	8.629	7.463	2.987	1.860	2.132	3.133	3.698	3.323	2.215	4.205	7.094	8.066	2.861	1.007
1.4	8.702	7.608	3.055	1.871	2.155	3.139	3.709	3.328	2.218	4.206	7.094	8.066	2.861	1.006
1.6	8.775	7.754	3.127	1.882	2.180	3.141	3.723	3.333	2.219	4.207	7.095	8.066	2.861	1.006
1.8	8.845	7.892	3.188	1.891	2.199	3.159	3.734	3.338	2.219	4.208	7.095	8.065	2.861	1.006
2.0	8.890	7.983	3.234	1.897	2.213	3.155	3.739	3.341	2.227	4.209	7.095	8.065	2.861	1.006
2.2	8.901	8.006	3.242	1.900	2.215	3.153	3.741	3.341	2.227	4.208	7.095	8.065	2.861	1.006
2.4	8.903	8.011	3.245	1.900	2.216	3.155	3.741	3.342	2.226	4.208	7.095	8.065	2.861	1.005
2.6	8.904	8.014	3.247	1.900	2.216	3.155	3.741	3.341	2.225	4.208	7.095	8.064	2.861	1.005

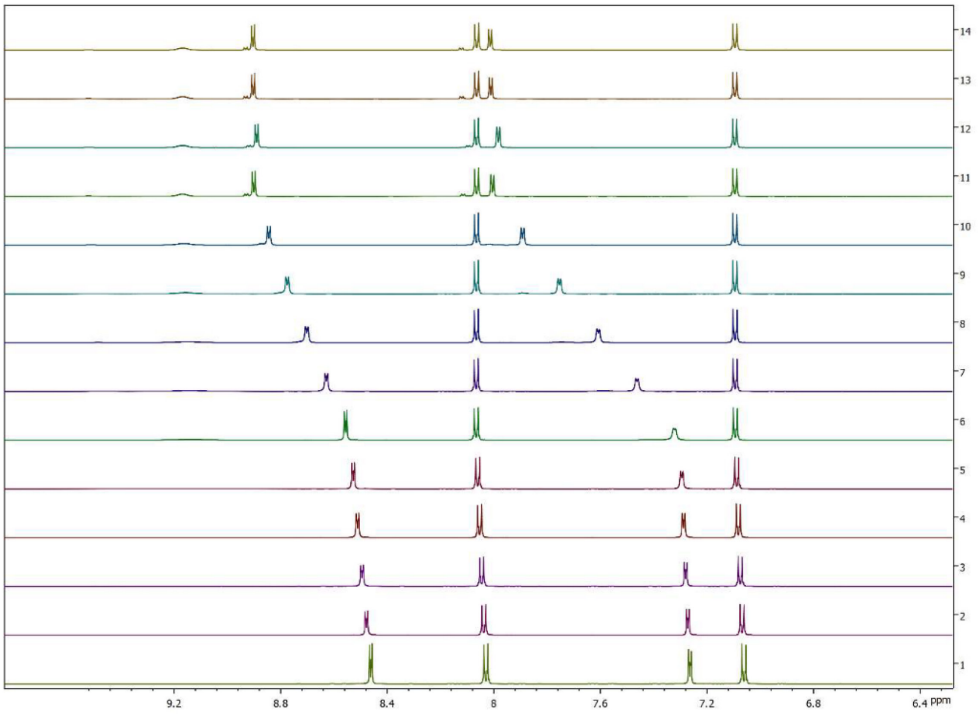


Figure S17. Stacked ^{1}H spectra of **KSK68** with increasing TfOH concentration. Aromatic region of spectrum. Acid concentration is increasing from the bottom spectrum (no acid) in steps of molar equivalents equal to 0.2.

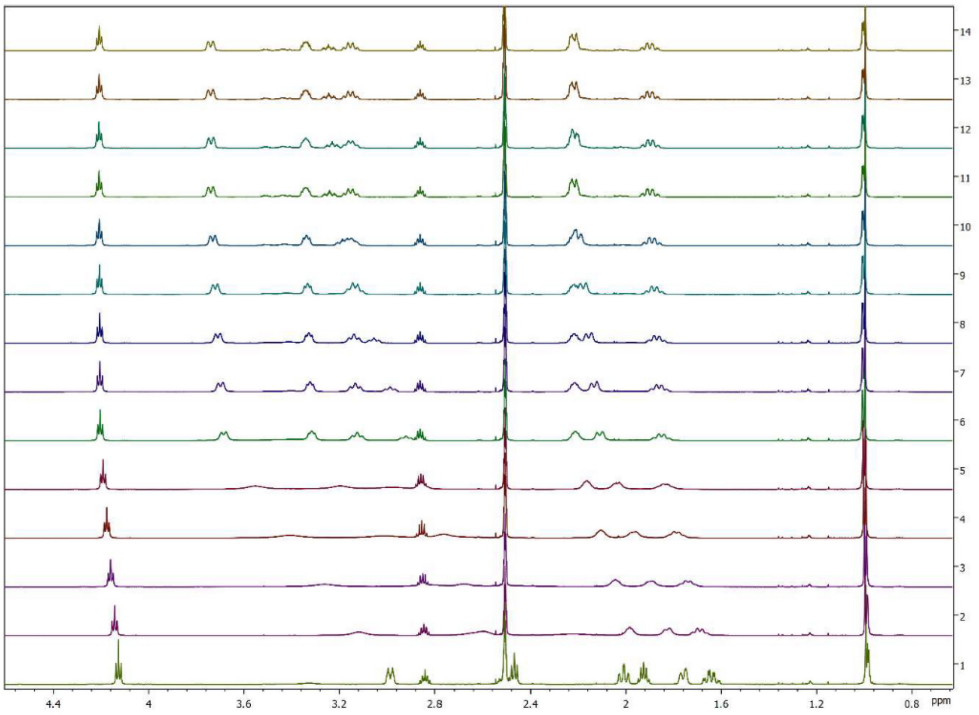


Figure S18. Stacked ^{1}H spectra of **KSK68** with increasing TfOH concentration. Aliphatic region of spectrum. Acid concentration is increasing from the bottom spectrum (no acid) in steps of molar equivalents equal to 0.2.

KSK94

Spectra and structural analysis

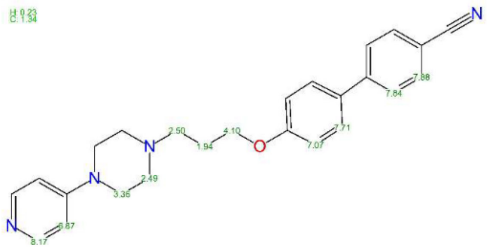


Figure S19. Structure of **KSK94** with ^{1}H chemical shifts applied on.

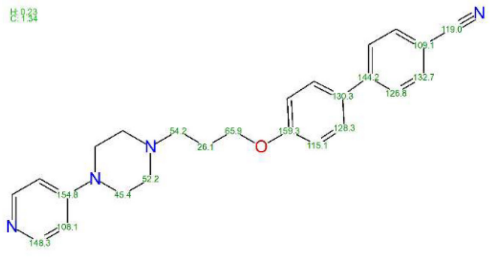
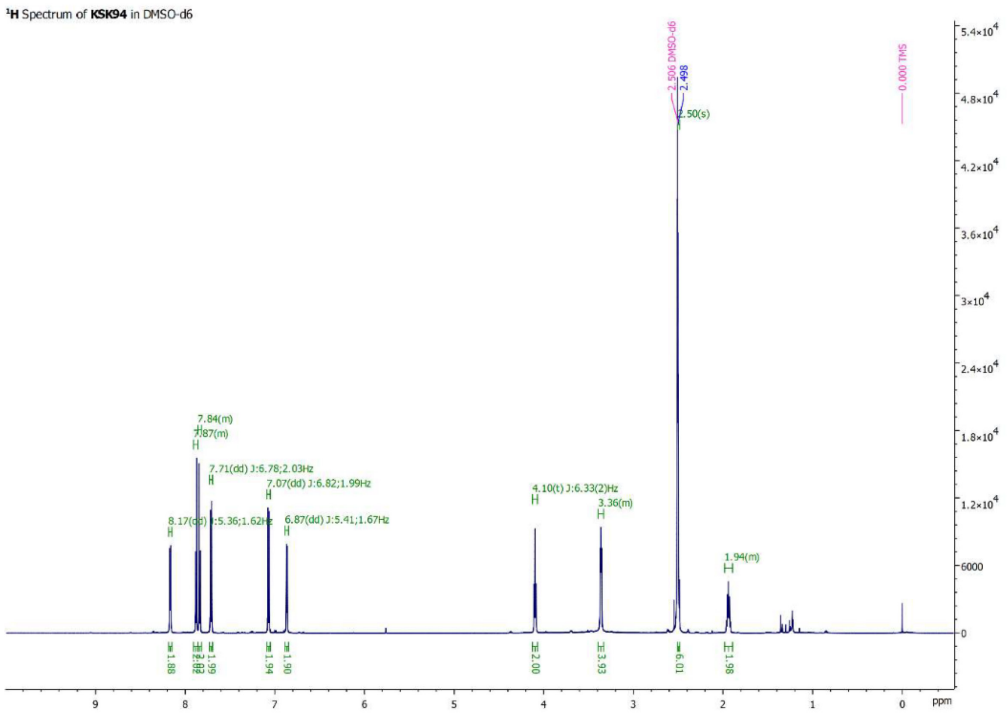
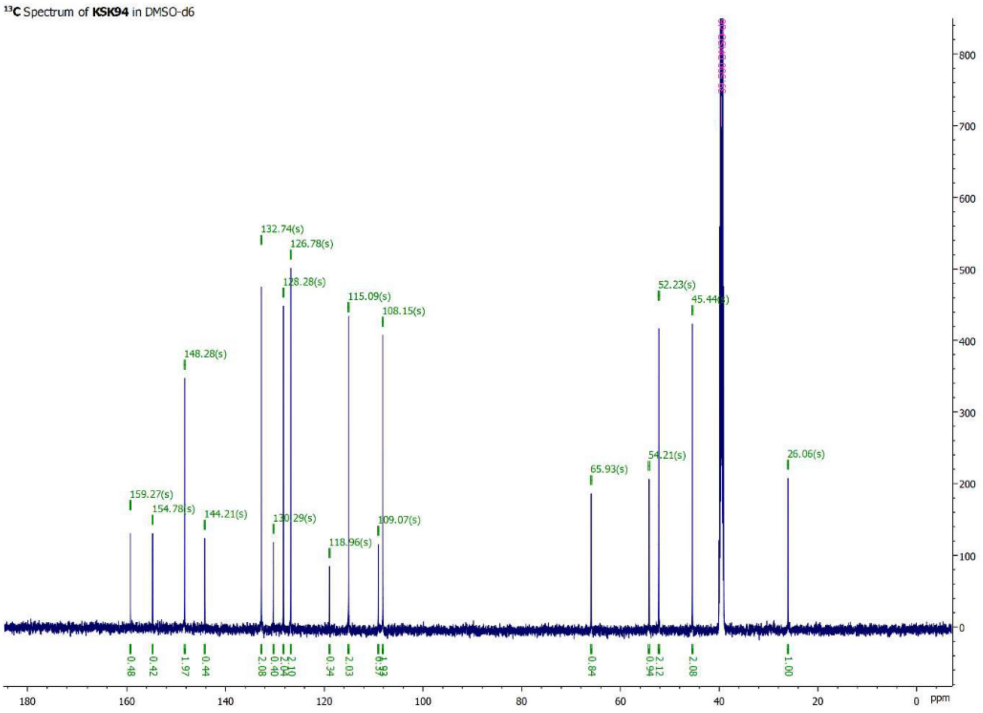
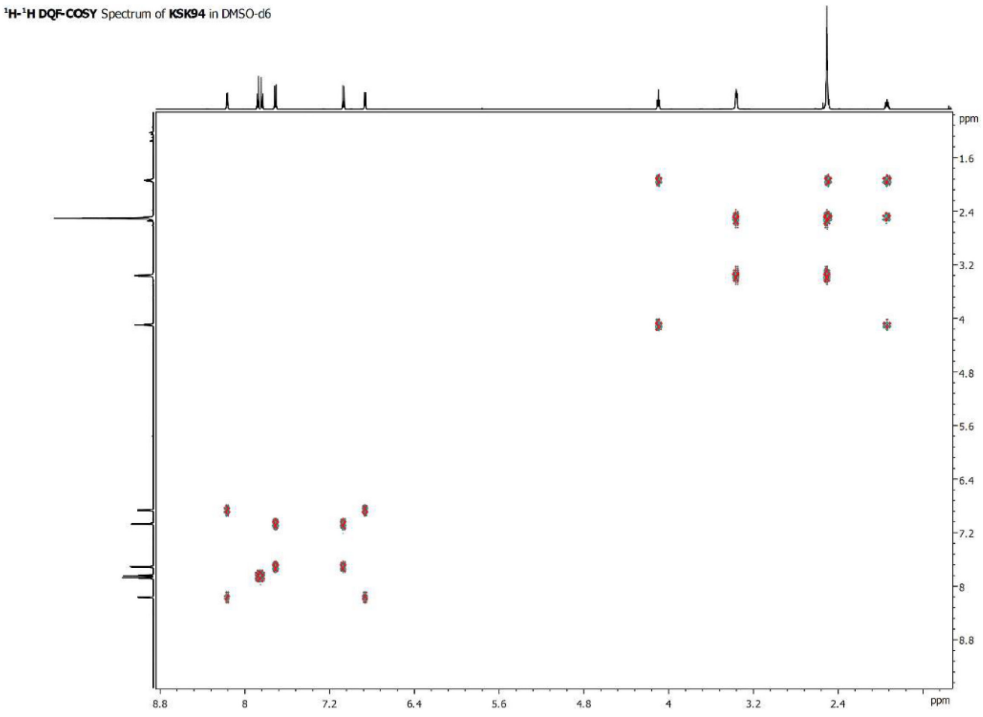


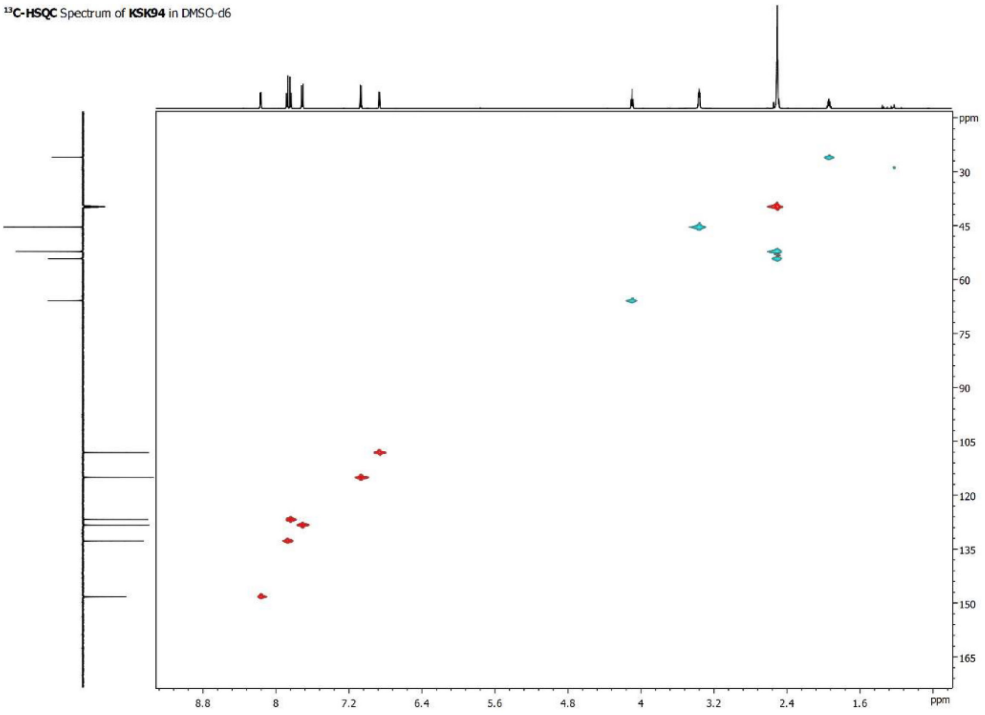
Figure S20. Structure of **KSK94** with ^{13}C chemical shifts applied on.

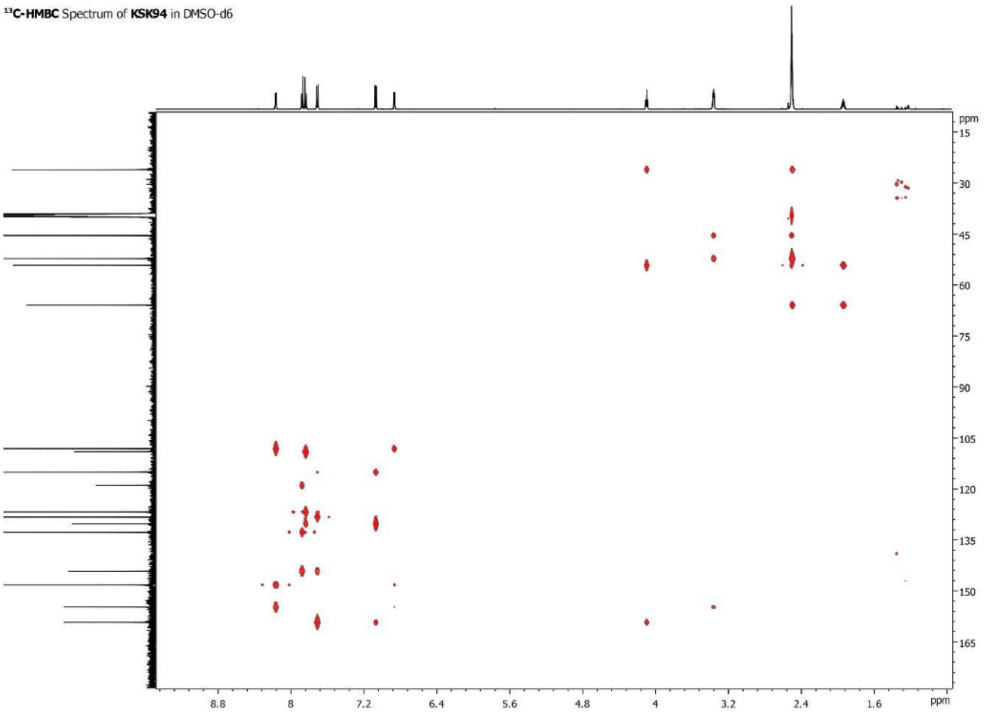



^{13}C Spectrum of KSK94 in DMSO-d6
132.74(s)
126.78(s)
128.28(s)
115.09(s)
108.15(s)
148.28(s)
52.23(s)
45.44(s)
65.93(s)
54.21(s)
26.06(s)
159.27(s)
154.78(s)
144.21(s)
130.29(s)
118.96(s)
109.07(s)
ppm

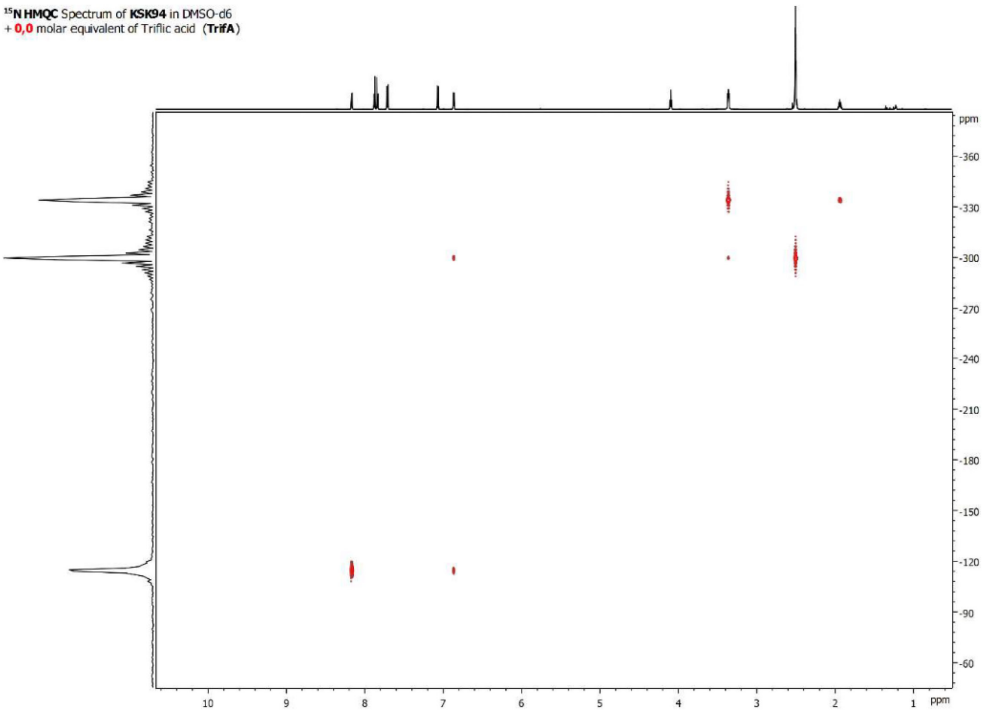

^{1}H-^{1}H DQF-COSY Spectrum of KSK94 in DMSO-d6
ppm

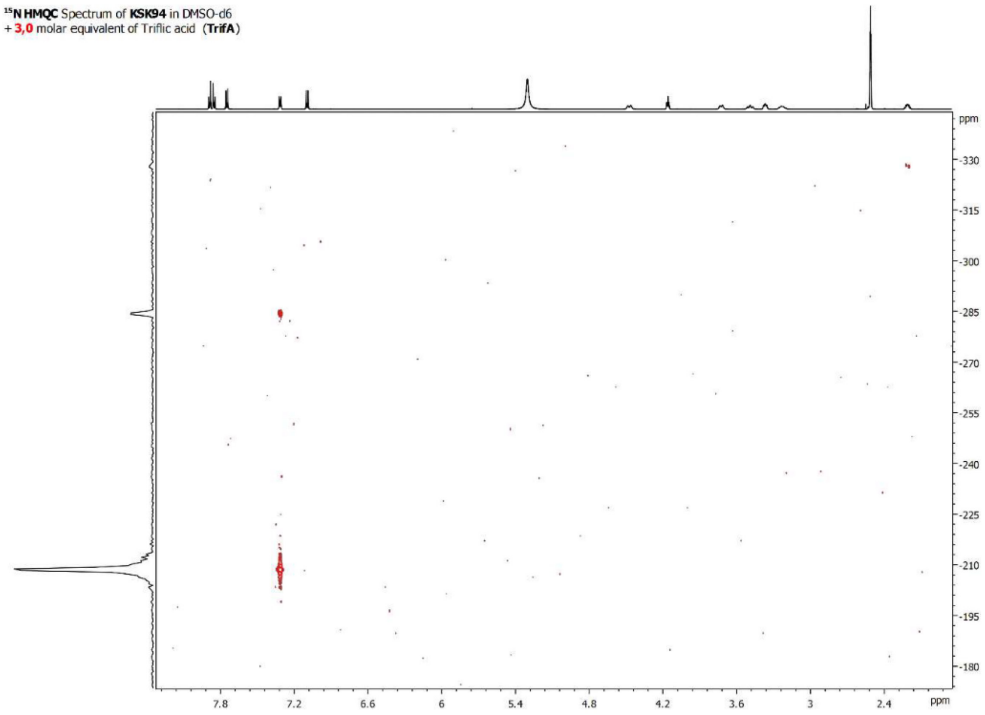
S21


13C-HSQC Spectrum of KSK94 in DMSO-d6
ppm
30
45
60
75
90
105
120
135
150
165
8.8
8
7.2
6.4
5.6
4.8
4
3.2
2.4
1.6
ppm


13C-HMBC Spectrum of KSK94 in DMSO-d6
ppm
15
30
45
60
75
90
105
120
135
150
165
8.8
8
7.2
6.4
5.6
4.8
4
3.2
2.4
1.6
ppm

S22


^{15}N HMQC Spectrum of KSK94 in DMSO-d6
+ 0,0 molar equivalent of Triflic acid (TrifA)
ppm
360
330
300
270
240
210
180
150
120
90
60
10
9
8
7
6
5
4
3
2
1
ppm


^{15}N HMQC Spectrum of KSK94 in DMSO-d6
+ 3,0 molar equivalent of Triflic acid (TrifA)
ppm
330
315
300
285
270
255
240
225
210
195
180
7.8
7.2
6.6
6
5.4
4.8
4.2
3.6
3
2.4
ppm

S23

KSK94

Titration experiment

Table S4. Proton chemical shifts of signals of compound **KSK94** with increasing TfOH concentration during titration.

	Chemical shifts [ppm] in reference to TMS in DMSO-d_6												
Atom label	1	2	3a	3b	4a	4b	5	6	7	8	9	10	11
Molarity of acid													
0.0	8.168	6.865	3.362	3.362	2.500	2.500	2.500	1.939	4.097	7.069	7.711	7.837	7.877
0.2	8.190	6.975	3.470	3.470	2.527	2.527	2.517	1.945	4.101	7.070	7.714	7.839	7.881
0.4	8.211	7.081	3.577	3.577	2.551	2.551	2.540	1.952	4.106	7.070	7.712	7.837	7.876
0.6	8.235	7.177	3.680	3.680	2.604	2.604	2.587	1.969	4.112	7.072	7.715	7.839	7.878
0.8	8.272	7.226	3.769	3.769	2.805	2.805	2.771	2.028	4.124	7.077	7.722	7.841	7.879
1.0	8.313	7.261	3.849	3.849	3.055	3.055	2.990	2.096	4.139	7.084	7.732	7.844	7.882
1.2	8.359	7.297	3.927	3.927	3.323	3.323	3.215	2.166	4.152	7.091	7.745	7.851	7.890
1.4	8.386	7.318	3.498	4.474	3.231	3.720	3.365	2.212	4.161	7.095	7.750	7.853	7.892
1.6	8.386	7.318	3.496	4.475	3.230	3.725	3.367	2.213	4.161	7.095	7.750	7.852	7.891
1.8	8.385	7.318	3.493	4.475	3.232	3.727	3.368	2.212	4.161	7.095	7.750	7.853	7.891
2.0	8.385	7.318	3.497	4.475	3.232	3.728	3.368	2.213	4.161	7.096	7.749	7.854	7.892
2.2	8.383	7.316	3.494	4.475	3.232	3.728	3.368	2.214	4.160	7.095	7.750	7.854	7.892
2.4	8.383	7.316	3.494	4.475	3.232	3.728	3.368	2.214	4.160	7.095	7.750	7.854	7.892
2.6	8.383	7.316	3.494	4.475	3.232	3.728	3.368	2.214	4.160	7.095	7.750	7.854	7.892
2.8	8.383	7.316	3.494	4.475	3.232	3.728	3.368	2.214	4.160	7.095	7.750	7.854	7.892
3.0	8.383	7.316	3.494	4.475	3.232	3.728	3.368	2.214	4.160	7.095	7.750	7.854	7.892

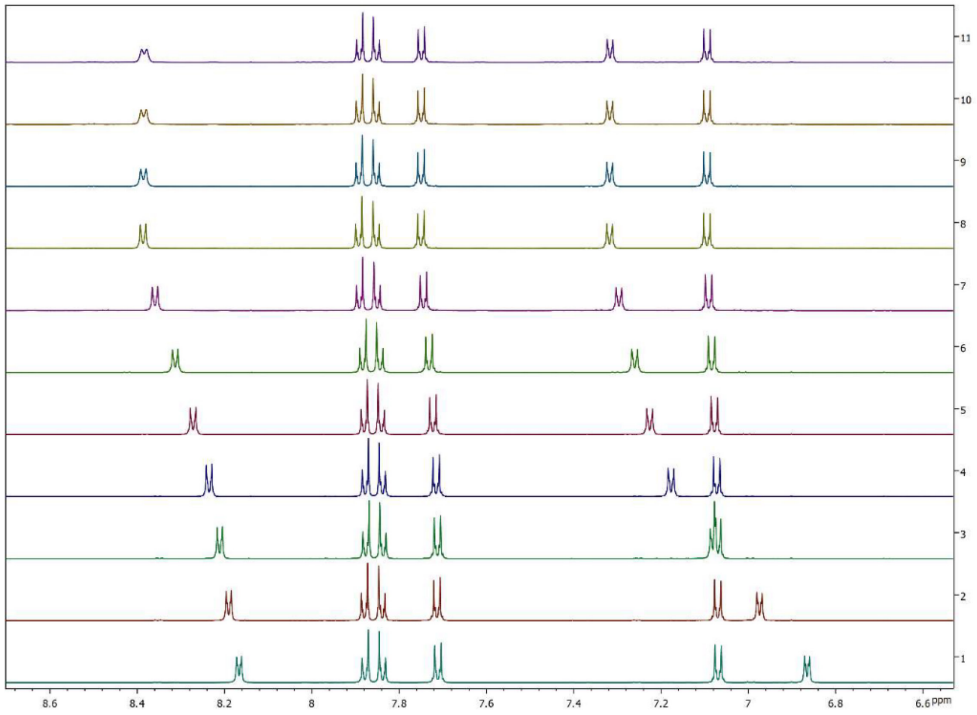


Figure S21. Stacked ^{1}H spectra of **KSK94** with increasing TfOH concentration. Aromatic region of spectrum. Acid concentration is increasing from the bottom spectrum (no acid) in steps of molar equivalents equal to 0.2.

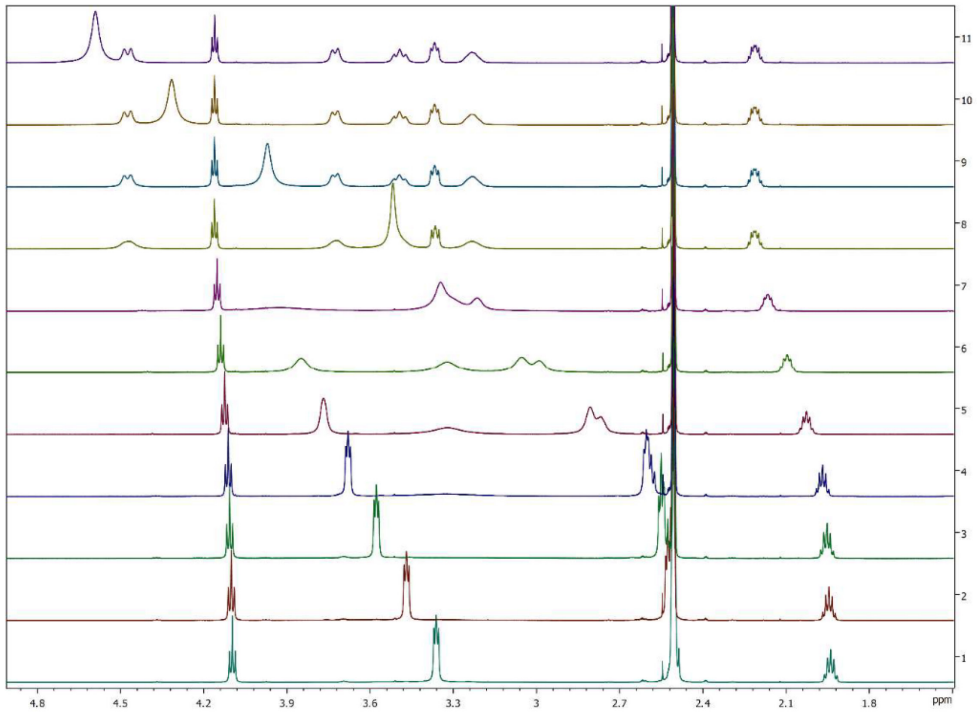


Figure S22. Stacked ^{1}H spectra of **KSK94** with increasing TfOH concentration. Aliphatic region of spectrum. Acid concentration is increasing from the bottom spectrum (no acid) in steps of molar equivalents equal to 0.2.

S25

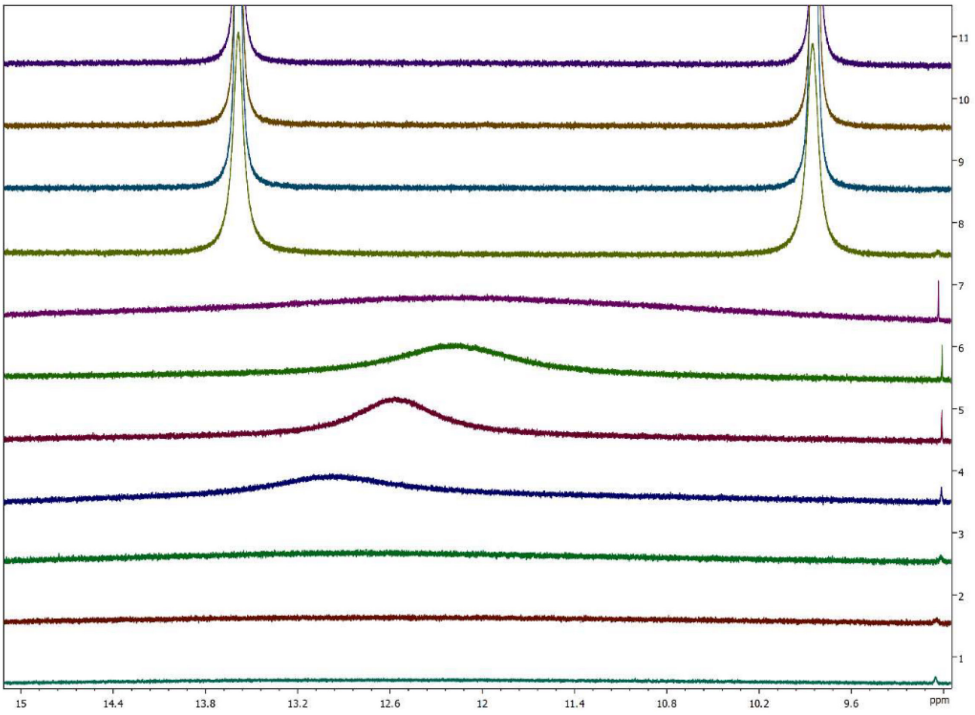


Figure S23. Stacked ^{1}H spectra of **KSK94** with increasing **TfOH** concentration. High frequency region of spectrum. Acid concentration is increasing from the bottom spectrum (no acid) in steps of molar equivalents equal to 0.2.

4. *In silico* studies. Molecular modeling: docking studies and molecular dynamics simulations

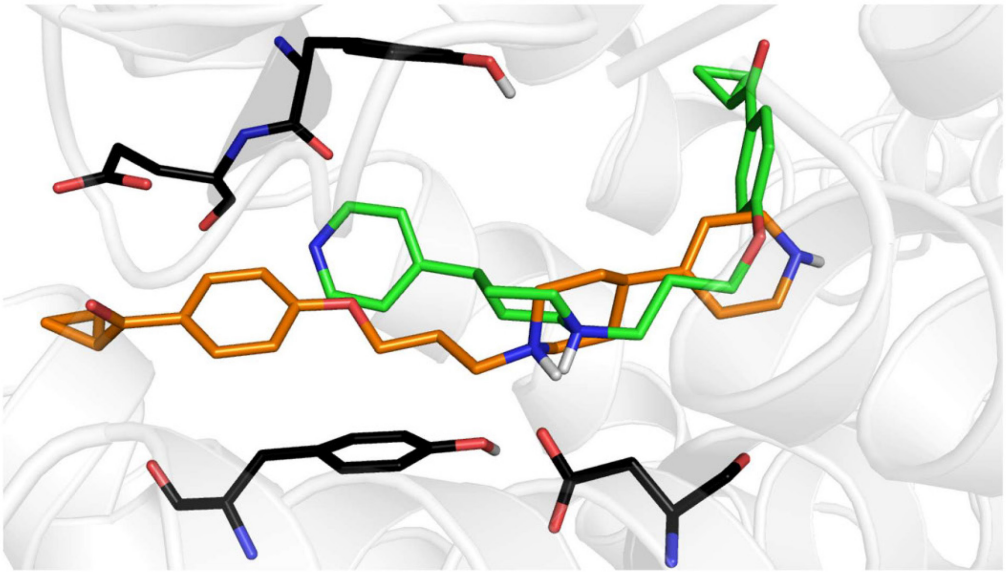


Figure S24. Comparison of the previously described **KSK68** binding mode (orange) and that obtained with induced-fit docking (green) at the H_3R binding site (homology model).

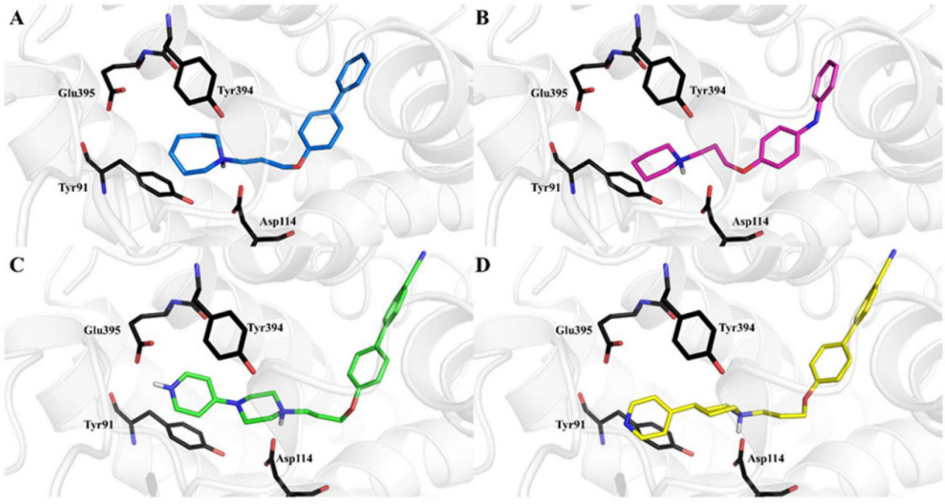


Figure S25. The binding mode of **3** (navy) (**A**), **7** (magenta) (**B**), **KSK94** (green) (**C**) in tautomeric monoprotonated state and **12** (yellow) (**D**) in the σ_1R (PDB ID: 6DJZ).

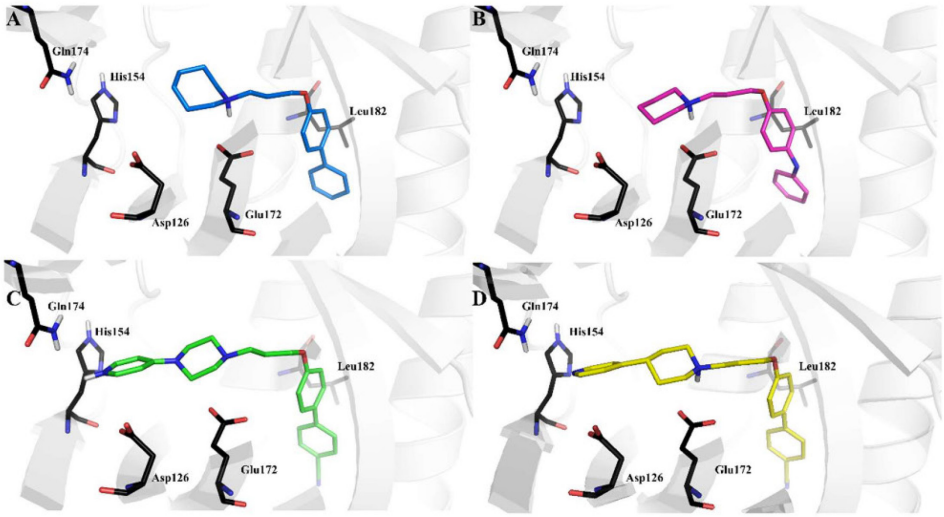


Figure S26. The binding mode of **3** (navy) (**A**), **7** (magenta) (**B**), **KSK94** (green) (**C**) in tautomeric monoprotonated state and **12** (yellow) (**D**) in H_3R binding site (homology model).

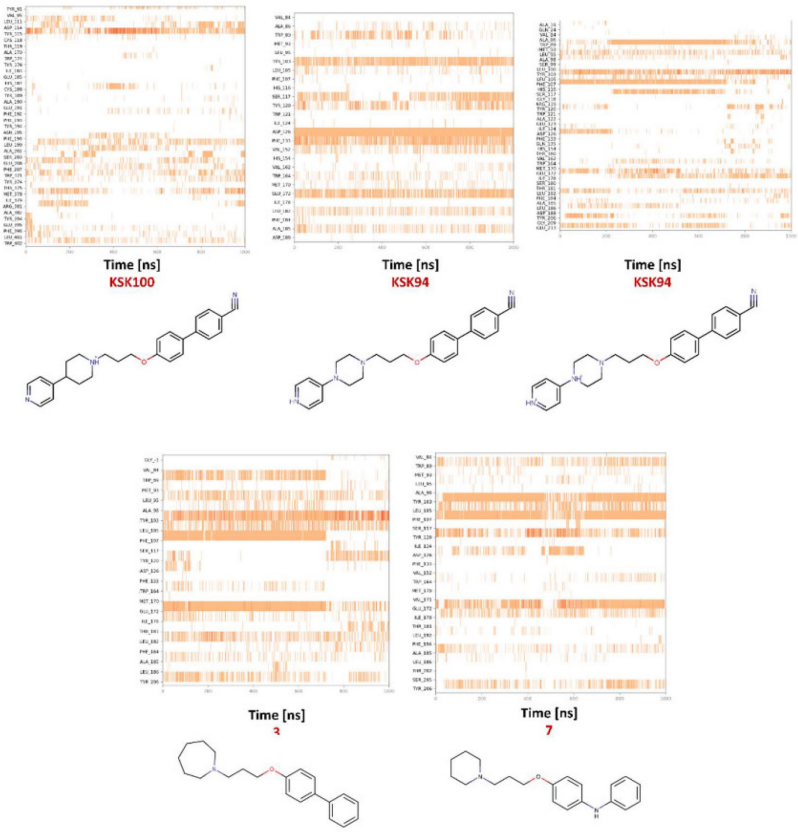


Figure S27. Ligand-protein interaction diagrams obtained during MD simulations studies for selected compounds in different protonation states docked to the σ_1R (PDB ID: 6DJZ).

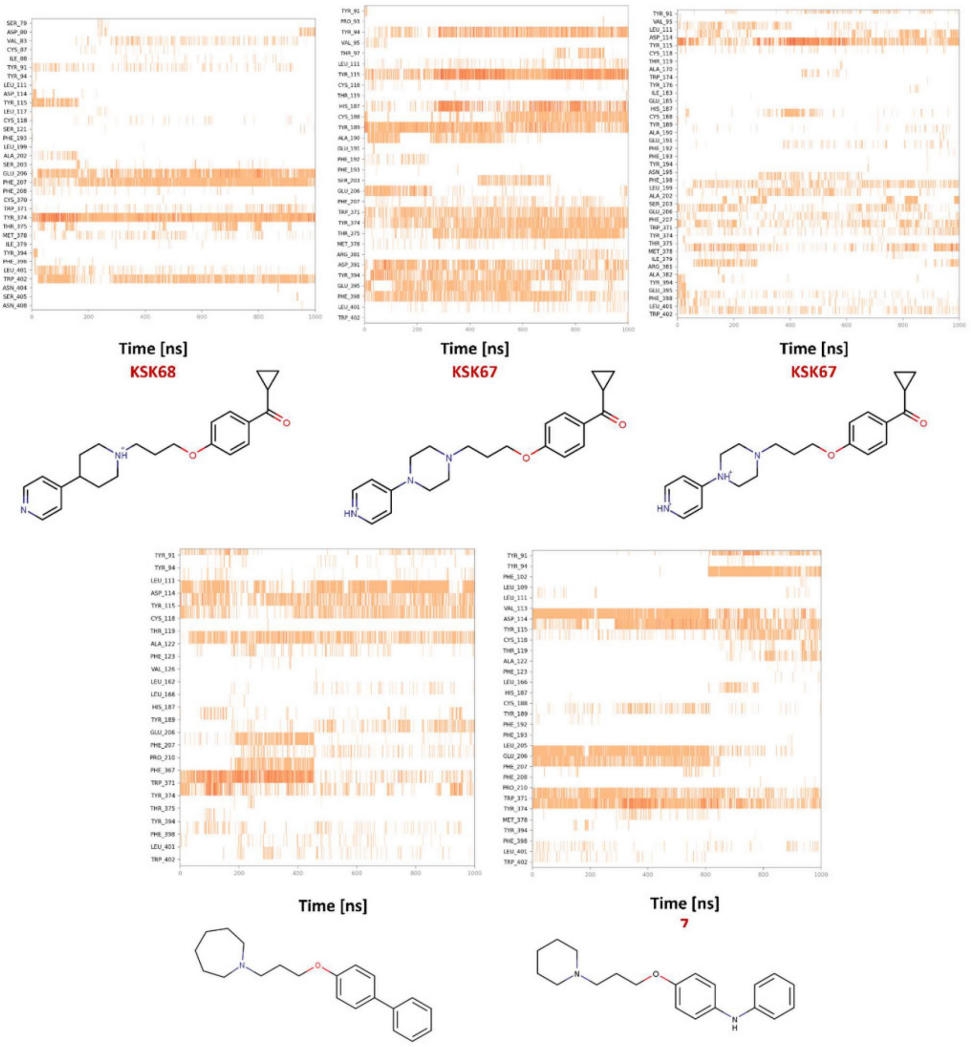


Figure S28. Ligand-protein interaction diagrams obtained during MD simulations studies for selected compounds in different protonation states docked to the H_3R binding site (homology model).

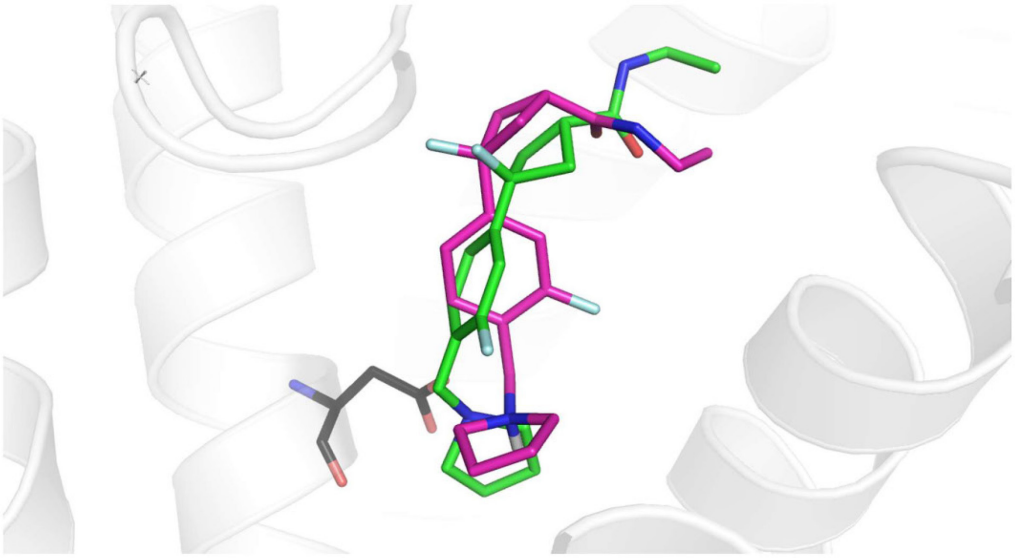
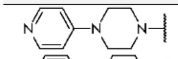
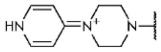
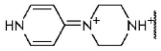
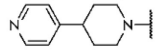
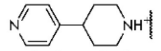
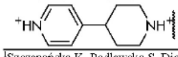


Figure S29. Superposition of the crystalized PF-03654746 (green) in crystal structure of H_3R (PDB ID: 7F61) with the binding mode (magenta) obtained with induced-fit docking to the described homology model.

Table S5. Comparison of binding free energies and docking scores (for all protonation states) with *in vitro* activity of **KSK67**, **KSK68**, **KSK94** and **12** with σ_1 and H_3 receptors. The calculated percentage of particular protonation state were published in our previous studies[1]. For the mono- and diprotonated tautomeric form of **KSK94** we couldn't estimate percentage of protonation state at physiological pH.

Form	Calc. % of protonation state	Compound	σ_1R			H$_3$R			Compound	σ_1R			H$_3$R		
			K_i [nM]	Docking score	ΔG [kcal/mol]	K_i [nM]	Docking score	ΔG [kcal/mol]		K_i [nM]	Docking score	ΔG [kcal/mol]	K_i [nM]	Docking score	ΔG [kcal/mol]
	2.08			-7.56	-34.23		-8.63	-57.97			-9.32	-71.32		-9.64	-71.2
		KSK67	1531	-8.04	-61.24	3.2	-9.67	-98.11	KSK94	2958	-10.45	-81.44	7.9	-10.22	-95.71
				-10.53	-78.88		-10.71	-96.25			-12.52	-113.23		-10.58	-99.18
	3.73			-7.66	-23.72		-8.65	-53.11			-9.31	-73.15		-9.58	-73.57
	95.69	KSK68	3.6	-9.56	-99.29	7.7	-10.79	-98.69	12	4.5	-11.514	-99.47	7.7	-10.47	-97.64
	0.52			-10.278	-99.75		-11.08	-109.89			-12.23	-111.48		-10.94	-101.99

[1]Szczepańska K, Podlewska S, Dichiara M, Gentile D, Patamia V, Rosier N, Mönnich D, Ruiz Cantero MC, Karcz T, Łażewska D, Siwek A, Pockes S, Cobos EJ, Marrazzo A, Stark H, Rescifina A, Bojarski AJ, Amata E, Kieć-Kononowicz K. Structural and Molecular Insight into Piperazine and Piperidine Derivatives as Histamine H_3 and Sigma-1 Receptor Antagonists with Promising Antinociceptive Properties. *ACS Chem Neurosci*. 2022;13(1):1-15.

5. *In vivo* pharmacological activity

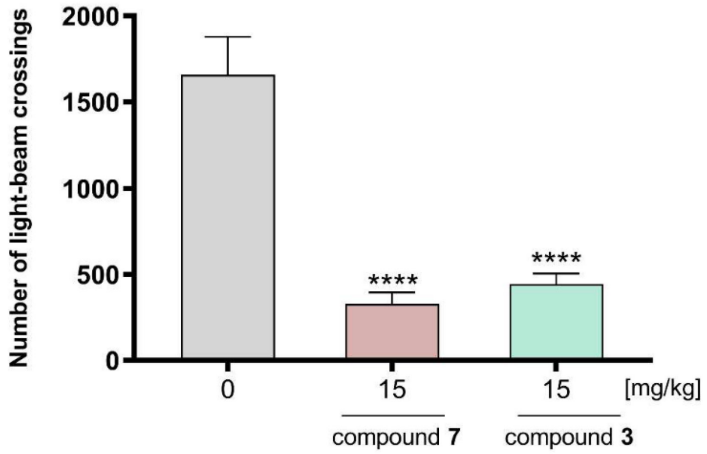


Figure S30. The influence of **3** and **7** on the spontaneous locomotor activity. Results are shown as number of light beam crossings during 30 min of observation beginning at 30 min after compound administration (i.p.). Each value represents the mean ± S.E.M. for 8-10 animals. 0 – vehicle (1% Tween 80). Statistical analysis: one-way ANOVA followed by post hoc Dunnett's test. Statistical significance compared to vehicle-treated animals: **** $p < 0.0001$.

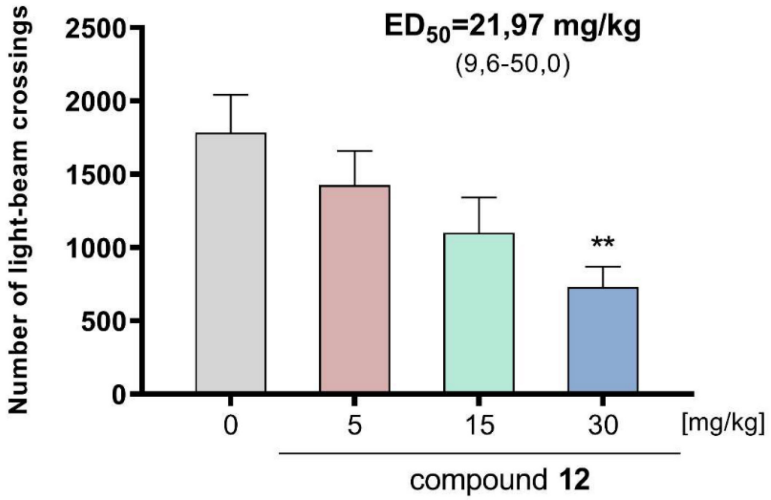


Figure S31. The influence of **12** on the spontaneous locomotor activity. Results are shown as number of light beam crossings during 30 min of observation beginning at 30 min after compound administration (i.p.). Each value represents the mean ± S.E.M. for 8-10 animals. 0 – vehicle (1% Tween 80). Statistical analysis: one-way ANOVA followed by post hoc Dunnett's test. Statistical significance compared to vehicle-treated animals: ** $p < 0.01$.

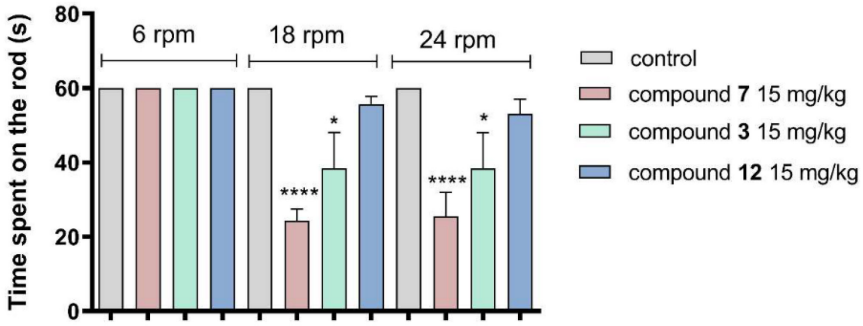


Figure S32. The influence of the test compounds **3**, **7** and **12** on rotarod test performance (measure of motor coordination). Bar graph plots the time (sec.) spent on the rotating rod when tested at different speed (6 rpm, 18 rpm and 24 rpm). Each value represents the mean ± S.E.M. for 6-8 animals. Control – mice treated with vehicle (1% Tween 80). Statistical analysis: one-way ANOVA followed by post hoc Dunnett's test. Statistical significance compared to vehicle-treated animals: * $p < 0.05$; **** $p < 0.0001$.

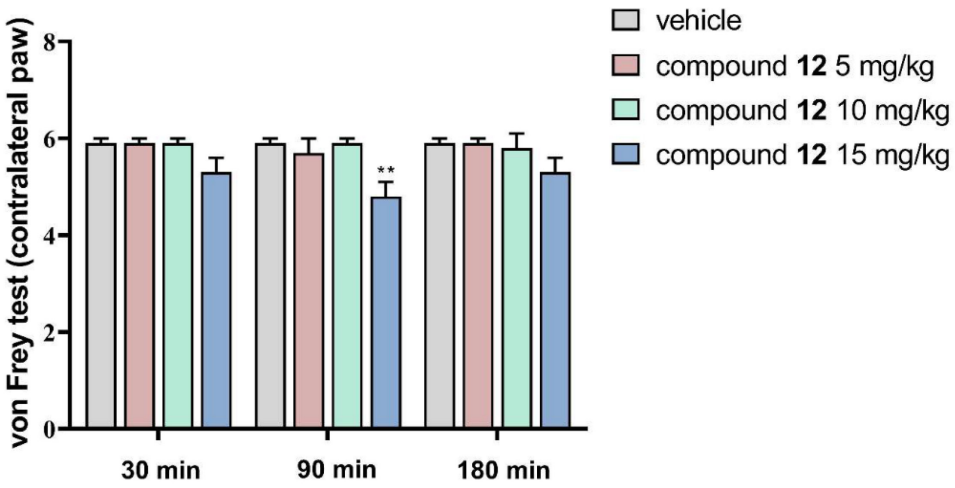


Figure S33. The effects of single i.p. administration of **12** (5, 10 and 15 mg/kg) on mechanical (von Frey test) stimulus on day 14 following CCI to the sciatic nerve, were evaluated (n = 7-8 animals per group). The results are presented as means ± SEM. Intergroup differences were analyzed by one-way ANOVA with Bonferroni's multiple comparison post-hoc test. $^{**}p < 0.01$ vs vehicle-treated group.

S33

6. ^{1}H-, ^{13}C-NMR spectra, HRMS analysis and HPLC traces

4 Conclusion and Perspectives

Histamine and its receptors have an underestimated therapeutic potential in neurological and neurodegenerative diseases. This cumulative dissertation describes the pharmacological evaluation of novel H_3R ligands contributing to the ongoing search for therapeutic strategies against neurological and neurodegenerative diseases. The first part focused on developing novel structural elements, while the second part of the dissertation aimed to design and evaluate multi-target directed ligands bearing an H_3R pharmacophore merged or linked to other targets. This reflects the increasing awareness that complex CNS diseases require multifaceted pharmacological concepts for therapeutic efficacy.

The scaffold hopping approach was applied for the structural optimization of previously identified ligands[362, 363], in terms of pharmacokinetic, physicochemical properties, and toxicity profile. This led to identifying the easily accessible compound **d2** (Figure 16) with favorable ADME and toxicity values, showing moderate affinity at H_3R (K_i = 2.61 µM) (Chapter 3.1). The affinity at H_3R was evaluated using a radioligand displacement assay to confirm the result of molecular docking studies and showed concordance with the obtained docking scores. In addition, the demethylated derivative of **d2** showed lower potency at the H_3R, underscoring the importance of subtle chemical modifications (e.g., methylation) in modulating receptor affinity. Molecular docking and dynamics simulations provide mechanistic insights into receptor-ligand interactions: ionic interaction of the nitrogen with Glu206 (TM5) and hydrogen bonds of the amide with Tyr115 (TM3) and Tyr374 (TM6). The 1,2,3,4-tetrahydroisochinoline scaffold may serve for optimization to obtain higher potency and retain the predicted safety profile.

In the second study, eight purine derivatives were designed by isosteric replacement of pyrrolo[2,3-d]pyrimidines [364, 365] with purine, resulting in compound **3d** (Figure 16) with low nanomolar binding affinity to the H_3R (K_i = 2.91 nM), in the range of the clinically approved drug Pitolisant (Chapter 3.2). The structure-activity relationship analysis indicates that 2,6-dichlorobenzyl derivatives have the lowest affinity, and ligand-receptor interaction is stabilized by the hydrogen bond of purine with Tyr374 (TM6). Importantly, predicted physicochemical properties, including blood-brain barrier permeability and *in vitro* cytotoxicity properties, are favorable.

Two approaches of structure-based drug design for H_3R ligands, namely isosteric replacement and scaffold-hopping, were applied, demonstrating their complementary strengths: scaffold-hopping for exploration of diverse chemical scaffolds and isosteric replacement for novel ligands that retain high potency. The integrative computational approaches are complemented by experimental *in vitro*

studies, presenting a valuable tool towards the development of novel CNS-targeted drugs. Since the crystal structure of H_3R was not available at the time of these studies, the computational calculations were conducted on a homology model of H_1R.

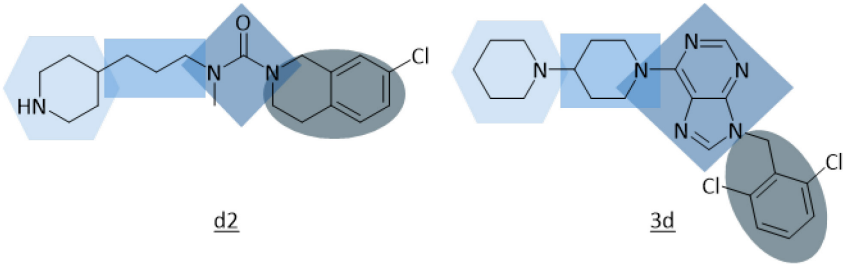


Figure 16: New compounds **d2** and **3d**.

Dopamine receptors are suitable co-targets due to their modulation of several CNS pathways involved in schizophrenia and PD, and the co-expression of H_3R on dopaminergic neurons. The third study investigated ligands with phenylmethyl and -ethyl linkers on dopamine D_2 and D_3 receptors. In the structure-based approach, the western part of Cariprazine and the eastern part of BP897 were linked by these two aromatic linkers, revealing the phenylethyl linker with low nanomolar binding affinities at both dopamine receptors. The affinities obtained in radioligand displacement assays led to compound **6c** ($pKi(D_2R)$ =7.83, $pKi(D_3R)$ = 8.04), comprising similar activity on both targets (Chapter 3.3). The electron-donating group (e.g., amide) and phenethyl spacer improve affinity to the receptors compared to the electron-withdrawing group.

The first MTDL study focused on a series of substituted piperazines linked to BP897 with the aim of simultaneous interaction of H_3R, D_3R, and cholinesterases. Lead compounds **LINS05006** and **LINS05015** (Figure 17) exhibited similar activity across the GPCR targets in the micromolar range (Chapter 3.4). Methylpiperazine moiety and longer alkyl linkers enhanced affinity and balanced properties. Balanced activity towards all targets is of great importance, as shown by a recent study of the MTDL AG-0029 with imbalanced dual target properties.[294] Different aspects of MTDLs were investigated with novel insights into binding modes and pharmacological properties of these ligands. However, the study is limited by the lack of information on functional properties at the dopamine receptors and the overall micromolar affinity or inhibition values. This study supports the utility of modular ligand design for investigating novel ligands for H_3R, D_3R, and cholinesterase inhibition, with the prospect of lead optimization.

Dual-acting ligands combining H_3R and ion channel inhibition present a class of MTDLs that has barely been studied. The investigation of this target combination at specific L-type calcium channels, $Ca_V1.2$ and $Ca_V1.3$, is novel, which was realized in fluorescence calcium assay. The lead compounds **3f** and **5b** (Figure 17) showed no cytotoxic effect, selectivity over other histamine receptors, and low, respectively, no frequency dependence in patch clamp experiments (Chapter 3.5). The study provides new insights into the binding properties and the mutual influences of this target combination, demonstrating the flexibility and suitability of the H_3 pharmacophore for MTDL, while balanced pharmacological properties and sufficient inhibition of LTCC are challenging. These results support previous studies of MTDLs with calcium channel blockers that could not attain balanced activity even with unspecific calcium channel assay.[340, 341] The slight preference of **5b** (Figure 17) for the $Ca_V1.3$ channel was found and might be helpful for further structural optimization towards $Ca_V1.3$ selective inhibitors.

The discovery that several H_3R antagonists also modulate σ receptors[359] raises questions of these ligands' mechanism of action and structure-activity relationships. Systematic analysis of protonation states comparing recently published piperazine and piperidine-based ligands[360] reveals that the 4-pyridylpiperazine fragment determines the basic character of pyridine nitrogen and therefore selectivity for H_3R over σ_1R (Chapter 3.6). Gained knowledge that piperidine forms a salt bridge with Glu172 in σ_1R was utilized to synthesize and evaluate novel dual target compounds. The *in vitro* evaluation of H_3R, σ_1R, and σ_2R affinity revealed three lead compounds, **3** and **7** (Figure 17), with the highest σ receptor selectivity values, and compound **12** (Figure 17) with balanced properties at all three targets. The pharmacological *in vitro* and *in vivo* activities are summarized in Table 4. Extensive *in vivo* evaluation in multiple neuropathic and inflammatory pain models demonstrates that compound **12** (Figure 17) is a promising lead with a broad analgesic effect. The combination of H_3R and σR is the most feasible with balanced activity and selectivity, and the *in vivo* properties emphasize their potential for future therapeutic application.

Table 4: Summary of the *in vitro* and *in vivo* properties of lead compounds 3, 7, and 12 from chapter 3.6.[366]

	3	**7**	**12**
H_3R K_i and IC_{50} [nM]	4.3 and 83.4	5.2 and 83.7	7.7 and 215
σ_1 K_i [nM]	1.9	4.8	4.5
σ_2 K_i [nM]	25	116	10
P_e (10^{-6} cm/s)	6.57	10.63	12.00
$t_{1/2}$ [h]	n.d.	n.d.	7.7 h
Sedative effect (rotarod test)	Sedative effect	Sedative effect	Decreased but not significant
Antinociceptive activity formalin test	Decrease of nociceptive response in acute and late phase	Duration of nociceptive response and late phase of test attenuated	High analgesic effect in acute and late phase
Capsaicin-induced nociception	n.d.	n.d.	Significant effect
Loperamide-induced antinociception	n.d.	n.d.	Dose-dependent increase of antinociceptive effect
Oxaliplatin induced neuropathy	n.d.	n.d.	Antiallodynic effect
CCI-exposed mice	n.d.	n.d.	Analgesic effect

Abbreviations: CCI – chronic constriction injury, n.d. – not determined

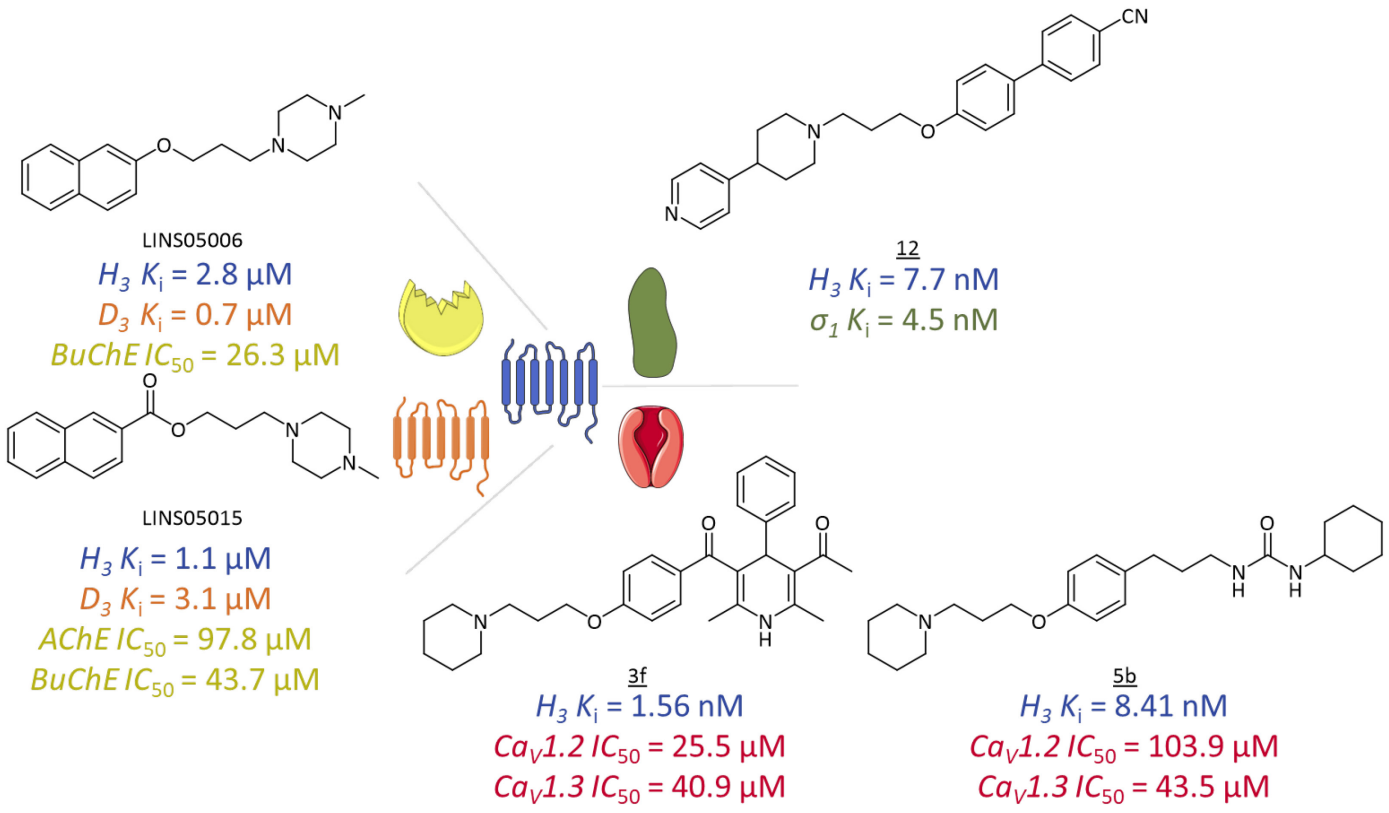


Figure 17: Lead structures of multi-target ligands and their pharmacological properties (Chapter 3.4 to 3.6).

In conclusion, rationally designed multitarget ligands integrating *in vitro* biological evaluation, medicinal chemistry principles, and computational modeling provide a solid foundation for MTDL development. The in-depth analysis led to a promising lead compound. However, the early tentative nature of the herein described MTDL should be augmented with further lead optimization and *in vivo* investigation of lead structures to confirm therapeutic relevance. This work offers valuable insights into pharmacological properties and mutual influence on the desired targets with potential application in neurological and neurodegenerative diseases. The large heterogeneity in H_3R elements and target combinations with different activities provides numerous rational approaches to new disease therapies.

5 References

(1) Calik, M. W. Update on the treatment of narcolepsy: clinical efficacy of pitolisant. *Nat Sci Sleep* **2017**, *9*, 127-133. DOI: 10.2147/NSS.S103462.

(2) Wager, T. T.; Pettersen, B. A.; Schmidt, A. W.; Spracklin, D. K.; Mente, S.; Butler, T. W.; Howard, H.; Lettiere, D. J.; Rubitski, D. M.; Wong, D. F.; et al. Discovery of two clinical histamine H_3 receptor antagonists: trans-N-ethyl-3-fluoro-3-[3-fluoro-4-(pyrrolidinylmethyl)phenyl]cyclobutanecarboxamide (PF-03654746) and trans-3-fluoro-3-[3-fluoro-4-(pyrrolidin-1-ylmethyl)phenyl]-N-(2-methylpropyl)cyclobutanecarboxamide (PF-03654764). *J Med Chem* **2011**, *54* (21), 7602-7620. DOI: 10.1021/jm200939b.

(3) Letavic, M. A.; Aluisio, L.; Apodaca, R.; Bajpai, M.; Barbier, A. J.; Bonneville, A.; Bonaventure, P.; Carruthers, N. I.; Dugovic, C.; Fraser, I. C.; et al. Novel benzamide-based histamine h3 receptor antagonists: the identification of two candidates for clinical development. *ACS Med Chem Lett* **2015**, *6* (4), 450-454. DOI: 10.1021/ml5005156.

(4) Wagner, G.; Mocking, T. A. M.; Arimont, M.; Provensi, G.; Rani, B.; Silva-Marques, B.; Latacz, G.; Da Costa Pereira, D.; Karatzidou, C.; Vischer, H. F.; et al. 4-(3-Aminoazetidin-1-yl)pyrimidin-2-amines as High-Affinity Non-imidazole Histamine H3 Receptor Agonists with in Vivo Central Nervous System Activity. *J Med Chem* **2019**, *62* (23), 10848-10866. DOI: 10.1021/acs.jmedchem.9b01462.

(5) Lim, H. D.; van Rijn, R. M.; Ling, P.; Bakker, R. A.; Thurmond, R. L.; Leurs, R. Evaluation of histamine H1-, H2-, and H3-receptor ligands at the human histamine H4 receptor: identification of 4-methylhistamine as the first potent and selective H4 receptor agonist. *J Pharmacol Exp Ther* **2005**, *314* (3), 1310-1321. DOI: 10.1124/jpet.105.087965.

(6) Nirogi, R.; Shinde, A.; Goyal, V. K.; Ravula, J.; Benade, V.; Jetta, S.; Pandey, S. K.; Subramanian, R.; Chowdary Palacharla, V. R.; Mohammed, A. R.; et al. Samelisant (SUVN-G3031), a histamine 3 receptor inverse agonist: Results from the phase 2 double-blind randomized placebo-controlled study for the treatment of excessive daytime sleepiness in adult patients with narcolepsy. *Sleep Med* **2024**, *124*, 618-626. DOI: 10.1016/j.sleep.2024.10.037.

(7) Obara, I.; Telezhkin, V.; Alrashdi, I.; Chazot, P. L. Histamine, histamine receptors, and neuropathic pain relief. *Br J Pharmacol* **2020**, *177* (3), 580-599. DOI: 10.1111/bph.14696.

(8) Lorente, J. S.; Sokolov, A. V.; Ferguson, G.; Schioth, H. B.; Hauser, A. S.; Gloriam, D. E. GPCR drug discovery: new agents, targets and indications. *Nat Rev Drug Discov* **2025**. DOI: 10.1038/s41573-025-01139-y.

(9) Hauser, A. S.; Attwood, M. M.; Rask-Andersen, M.; Schioth, H. B.; Gloriam, D. E. Trends in GPCR drug discovery: new agents, targets and indications. *Nat Rev Drug Discov* **2017**, *16* (12), 829-842. DOI: 10.1038/nrd.2017.178.

(10) Forneau, E.; Bovet, D. Recherches sur l'action sympathicolytique d'un nouveau dérivé du dioxane. *Arch Int Pharmacodyn Ther* **1933**, *46*, 178-191.

(11) Panula, P.; Chazot, P. L.; Cowart, M.; Gutzmer, R.; Leurs, R.; Liu, W. L.; Stark, H.; Thurmond, R. L.; Haas, H. L. International Union of Basic and Clinical Pharmacology. XCVIII. Histamine Receptors. *Pharmacol Rev* **2015**, *67* (3), 601-655. DOI: 10.1124/pr.114.010249.

(12) Emanuel, M. B. Histamine and the antiallergic antihistamines: a history of their discoveries. *Clin Exp Allergy* **1999**, *29 Suppl 3*, 1-11; discussion 12. DOI: 10.1046/j.1365-2222.1999.00004.x-i1.

(13) Panula, P.; Nuutinen, S. The histaminergic network in the brain: basic organization and role in disease. *Nat. Rev. Neurosci.* **2013**, *14* (7), 472-487. DOI: 10.1038/nrn3526.

(14) Barocelli, E.; Ballabeni, V. Histamine in the control of gastric acid secretion: a topic review. *Pharmacol Res* **2003**, *47* (4), 299-304. DOI: 10.1016/s1043-6618(03)00009-4.

(15) Ganellin, C. R. The tautomer ratio of histamine. *J Pharm Pharmacol* **1973**, *25* (10), 787-792. DOI: 10.1111/j.2042-7158.1973.tb09942.x.

(16) Haas, H. L.; Sergeeva, O. A.; Selbach, O. Histamine in the nervous system. *Physiol Rev* **2008**, *88* (3), 1183-1241. DOI: 10.1152/physrev.00043.2007.

(17) Parsons, M. E.; Ganellin, C. R. Histamine and its receptors. *Br J Pharmacol* **2006**, *147 Suppl 1* (Suppl 1), S127-135. DOI: 10.1038/sj.bjp.0706440.

(18) Schlicker, E. K., M. Role of the Histamine H3 Receptor in the Central Nervous System. In *Histamine and Histamine Receptors in Health and Disease*, Hattori, Y. S., R. Ed.; Vol. 241; Springer, 2016.

(19) Arrang, J. M.; Garbarg, M.; Schwartz, J. C. Auto-inhibition of brain histamine release mediated by a novel class (H3) of histamine receptor. *Nature* **1983**, *302* (5911), 832-837. DOI: 10.1038/302832a0.

(20) Panula, P.; Kaartinen, M.; Macklin, M.; Costa, E. Histamine-containing peripheral neuronal and endocrine systems. *J Histochem Cytochem* **1985**, *33* (9), 933-941. DOI: 10.1177/33.9.3894504.

(21) Hu, W.; Chen, Z. The roles of histamine and its receptor ligands in central nervous system disorders: An update. *Pharmacol Ther* **2017**, *175*, 116-132. DOI: 10.1016/j.pharmthera.2017.02.039.

(22) Borriello, F.; Iannone, R.; Marone, G. Histamine Release from Mast Cells and Basophils. *Handb Exp Pharmacol* **2017**, *241*, 121-139. DOI: 10.1007/164_2017_18.

(23) Thangam, E. B.; Jemima, E. A.; Singh, H.; Baig, M. S.; Khan, M.; Mathias, C. B.; Church, M. K.; Saluja, R. The Role of Histamine and Histamine Receptors in Mast Cell-Mediated Allergy and Inflammation: The Hunt for New Therapeutic Targets. *Front Immunol* **2018**, *9*, 1873. DOI: 10.3389/fimmu.2018.01873.

(24) Maintz, L.; Novak, N. Histamine and histamine intolerance. *Am J Clin Nutr* **2007**, *85* (5), 1185-1196. DOI: 10.1093/ajcn/85.5.1185.

(25) Akdis, C. A.; Blaser, K. Histamine in the immune regulation of allergic inflammation. *J Allergy Clin Immunol* **2003**, *112* (1), 15-22. DOI: 10.1067/mai.2003.1585.

(26) Shahid, M.; Tripathi, T.; Sobia, F.; Moin, S.; Siddiqui, M.; Khan, R. A. Histamine, Histamine Receptors, and their Role in Immunomodulation: An Updated Systematic Review. *The Open Immunology Journal* **2009**, *2* (1), 9-41. DOI: 10.2174/1874226200902010009.

(27) Giannoni, P.; Passani, M. B.; Nosi, D.; Chazot, P. L.; Shenton, F. C.; Medhurst, A. D.; Munari, L.; Blandina, P. Heterogeneity of histaminergic neurons in the tuberomammillary nucleus of the rat. *Eur J Neurosci* **2009**, *29* (12), 2363-2374. DOI: 10.1111/j.1460-9568.2009.06765.x.

(28) Yoshikawa, T.; Nakamura, T.; Yanai, K. Histaminergic neurons in the tuberomammillary nucleus as a control centre for wakefulness. *Br J Pharmacol* **2021**, *178* (4), 750-769. DOI: 10.1111/bph.15220.

(29) Panula, P.; Airaksinen, M. S.; Pirvola, U.; Kotilainen, E. A histamine-containing neuronal system in human brain. *Neuroscience* **1990**, *34* (1), 127-132. DOI: 10.1016/0306-4522(90)90307-p.

(30) Panula, P.; Nuutinen, S. The histaminergic network in the brain: basic organization and role in disease. *Nat Rev Neurosci* **2013**, *14* (7), 472-487. DOI: 10.1038/nrn3526.

(31) Takeshita, Y.; Watanabe, T.; Sakata, T.; Munakata, M.; Ishibashi, H.; Akaike, N. Histamine modulates high-voltage-activated calcium channels in neurons dissociated from the rat tuberomammillary nucleus. *Neuroscience* **1998**, *87* (4), 797-805. DOI: 10.1016/s0306-4522(98)00152-3.

(32) Haas, H.; Panula, P. The role of histamine and the tuberomamillary nucleus in the nervous system. *Nat Rev Neurosci* **2003**, *4* (2), 121-130. DOI: 10.1038/nrn1034.

(33) Sadek, B.; Saad, A.; Sadeq, A.; Jalal, F.; Stark, H. Histamine H3 receptor as a potential target for cognitive symptoms in neuropsychiatric diseases. *Behav Brain Res* **2016**, *312*, 415-430. DOI: 10.1016/j.bbr.2016.06.051.

(34) Benarroch, E. E. Histamine in the CNS: multiple functions and potential neurologic implications. *Neurology* **2010**, *75* (16), 1472-1479. DOI: 10.1212/WNL.0b013e3181f884b1 From NLM Medline.

(35) Yang, D.; Zhou, Q.; Labroska, V.; Qin, S.; Darbalaei, S.; Wu, Y.; Yuliantie, E.; Xie, L.; Tao, H.; Cheng, J.; et al. G protein-coupled receptors: structure- and function-based drug discovery. *Signal Transduct Target Ther* **2021**, *6* (1), 7. DOI: **10.1038/s41392-020-00435-w**.

(36) Gusach, A.; Garcia-Nafria, J.; Tate, C. G. New insights into GPCR coupling and dimerisation from cryo-EM structures. *Curr Opin Struct Biol* **2023**, *80*, 102574. DOI: 10.1016/j.sbi.2023.102574.

(37) Bond, R. A.; Ijzerman, A. P. Recent developments in constitutive receptor activity and inverse agonism, and their potential for GPCR drug discovery. *Trends Pharmacol Sci* **2006**, *27* (2), 92-96. DOI: 10.1016/j.tips.2005.12.007.

(38) Seifert, R.; Wenzel-Seifert, K. Constitutive activity of G-protein-coupled receptors: cause of disease and common property of wild-type receptors. *Naunyn Schmiedebergs Arch Pharmacol* **2002**, *366* (5), 381-416. DOI: 10.1007/s00210-002-0588-0.

(39) Latorraca, N. R.; Venkatakrishnan, A. J.; Dror, R. O. GPCR Dynamics: Structures in Motion. *Chem Rev* **2017**, *117* (1), 139-155. DOI: 10.1021/acs.chemrev.6b00177.

(40) Gao, M.; Ooms, J. F.; Leurs, R.; Vischer, H. F. Histamine H_3 Receptor Isoforms: Insights from Alternative Splicing to Functional Complexity. *Biomolecules* **2024**, *14* (7). DOI: 10.3390/biom14070761.

(41) Gupta, M. K.; Mohan, M. L.; Naga Prasad, S. V. G Protein-Coupled Receptor Resensitization Paradigms. *Int Rev Cell Mol Biol* **2018**, *339*, 63-91. DOI: 10.1016/bs.ircmb.2018.03.002 From NLM Medline.

(42) Ash, A. S.; Schild, H. O. Receptors mediating some actions of histamine. *Br J Pharmacol Chemother* **1966**, *27* (2), 427-439. DOI: 10.1111/j.1476-5381.1966.tb01674.x.

(43) Black, J. W.; Duncan, W. A.; Durant, C. J.; Ganellin, C. R.; Parsons, E. M. Definition and antagonism of histamine H 2 -receptors. *Nature* **1972**, *236* (5347), 385-390. DOI: 10.1038/236385a0.

(44) Oda, T.; Morikawa, N.; Saito, Y.; Masuho, Y.; Matsumoto, S. Molecular cloning and characterization of a novel type of histamine receptor preferentially expressed in leukocytes. *J Biol Chem* **2000**, *275* (47), 36781-36786. DOI: 10.1074/jbc.M006480200.

(45) Young, J. M.; Timmerman, H.; Thurmond, R.; Stark, H.; Shankley, N. P.; Seifert, R.; Schwartz, J.-C.; Schunack, W.; Panula, P.; Liu, S.; et al. Histamine receptors in GtoPdb v.2023.1. *IUPHAR/BPS Guide to Pharmacology CITE* **2023**, *2023* (1). DOI: 10.2218/gtopdb/F33/2023.1.

(46) Schwartz, J. C.; Arrang, J. M.; Garbarg, M.; Pollard, H.; Ruat, M. Histaminergic transmission in the mammalian brain. *Physiol Rev* **1991**, *71* (1), 1-51. DOI: 10.1152/physrev.1991.71.1.1.

(47) Hill, S. J.; Ganellin, C. R.; Timmerman, H.; Schwartz, J. C.; Shankley, N. P.; Young, J. M.; Schunack, W.; Levi, R.; Haas, H. L. International Union of Pharmacology. XIII. Classification of Histamine Receptors. *Pharmacological Reviews* **1997**, *49* (3), 253-278. DOI: 10.1016/s0031-6997(24)01328-0.

(48) Leurs, R.; Church, M. K.; Taglialatela, M. H1-antihistamines: inverse agonism, anti-inflammatory actions and cardiac effects. *Clin Exp Allergy* **2002**, *32* (4), 489-498. DOI: 10.1046/j.0954-7894.2002.01314.x.

(49) Simons, F. E.; Simons, K. J. H1 antihistamines: current status and future directions. *World Allergy Organ J* **2008**, *1* (9), 145-155. DOI: 10.1186/1939-4551-1-9-145.

(50) Shimamura, T.; Shiroishi, M.; Weyand, S.; Tsujimoto, H.; Winter, G.; Katritch, V.; Abagyan, R.; Cherezov, V.; Liu, W.; Han, G. W.; et al. Structure of the human histamine H1 receptor complex with doxepin. *Nature* **2011**, *475* (7354), 65-70. DOI: 10.1038/nature10236.

(51) Xia, R.; Wang, N.; Xu, Z.; Lu, Y.; Song, J.; Zhang, A.; Guo, C.; He, Y. Cryo-EM structure of the human histamine H_1 receptor/G(q) complex. *Nat Commun* **2021**, *12* (1), 2086. DOI: 10.1038/s41467-021-22427-2.

(52) Wang, D.; Guo, Q.; Wu, Z.; Li, M.; He, B.; Du, Y.; Zhang, K.; Tao, Y. Molecular mechanism of antihistamines recognition and regulation of the histamine H_1 receptor. *Nat Commun* **2024**, *15* (1), 84. DOI: 10.1038/s41467-023-44477-4.

(53) Meskanen, K.; Ekelund, H.; Laitinen, J.; Neuvonen, P. J.; Haukka, J.; Panula, P.; Ekelund, J. A randomized clinical trial of histamine 2 receptor antagonism in treatment-resistant schizophrenia. *J Clin Psychopharmacol* **2013**, *33* (4), 472-478. DOI: 10.1097/JCP.0b013e3182970490.

(54) Alonso, N.; Fernandez, N.; Notcovich, C.; Monczor, F.; Simaan, M.; Baldi, A.; Gutkind, J. S.; Davio, C.; Shayo, C. Cross-desensitization and cointernalization of H1 and H2 histamine receptors reveal new insights into histamine signal integration. *Mol Pharmacol* **2013**, *83* (5), 1087-1098. DOI: 10.1124/mol.112.083394.

(55) Kock, Z.; Schnelle, K.; Persechino, M.; Umbach, S.; Schihada, H.; Januliene, D.; Parey, K.; Pockes, S.; Kolb, P.; Dotsch, V.; et al. Cryo-EM structure of cell-free synthesized human histamine 2 receptor/G_s complex in nanodisc environment. *Nat Commun* **2024**, *15* (1), 1831. DOI: 10.1038/s41467-024-46096-z.

(56) Schneider, E. H.; Seifert, R. The histamine H4-receptor and the central and peripheral nervous system: A critical analysis of the literature. *Neuropharmacology* **2016**, *106*, 116-128. DOI: 10.1016/j.neuropharm.2015.05.004.

(57) Buckland, K. F.; Williams, T. J.; Conroy, D. M. Histamine induces cytoskeletal changes in human eosinophils via the H_4 receptor. *Br J Pharmacol* **2003**, *140* (6), 1117-1127. DOI: 10.1038/sj.bjp.0705530.

(58) Leurs, R.; Chazot, P. L.; Shenton, F. C.; Lim, H. D.; de Esch, I. J. Molecular and biochemical pharmacology of the histamine H4 receptor. *Br J Pharmacol* **2009**, *157* (1), 14-23. DOI: 10.1111/j.1476-5381.2009.00250.x.

(59) Neumann, D.; Seifert, R. The therapeutic potential of histamine receptor ligands in inflammatory bowel disease. *Biochem Pharmacol* **2014**, *91* (1), 12-17. DOI: 10.1016/j.bcp.2014.06.004.

(60) Hartwig, C.; Munder, A.; Glage, S.; Wedekind, D.; Schenk, H.; Seifert, R.; Neumann, D. The histamine H4 -receptor (H4 R) regulates eosinophilic inflammation in ovalbumin-induced

experimental allergic asthma in mice. *Eur J Immunol* **2015**, *45* (4), 1129-1140. DOI: 10.1002/eji.201445179.

(61) Werfel, T.; Lynch, V.; Asher, A.; Tsianakas, A.; Gupta, B.; Sarmiento, R.; Ploszczuk, A.; Majorek-Olechowska, B.; Cimoszko, B.; Nikkels, A.; et al. A phase 2a proof of concept clinical trial to evaluate ZPL-3893787 (ZPL-389) a potent, oral histamine H4, receptor antagonist for the treatment of moderate to severe atopic dermatitis (AD) in adults. *Journal der Deutschen Dermatologischen Gesellschaft* **2016**.

(62) Sanna, M. D.; Ghelardini, C.; Thurmond, R. L.; Masini, E.; Galeotti, N. Behavioural phenotype of histamine H_4 receptor knockout mice: Focus on central neuronal functions. *Neuropharmacology* **2017**, *114*, 48-57. DOI: 10.1016/j.neuropharm.2016.11.023.

(63) Gutzmer, R.; Mommert, S.; Gschwandtner, M.; Zwingmann, K.; Stark, H.; Werfel, T. The histamine H4 receptor is functionally expressed on T_H2 cells. *J Allergy Clin Immunol* **2009**, *123* (3), 619-625. DOI: 10.1016/j.jaci.2008.12.1110.

(64) Thurmond, R. L.; Desai, P. J.; Dunford, P. J.; Fung-Leung, W. P.; Hofstra, C. L.; Jiang, W.; Nguyen, S.; Riley, J. P.; Sun, S.; Williams, K. N.; et al. A potent and selective histamine H4 receptor antagonist with anti-inflammatory properties. *J Pharmacol Exp Ther* **2004**, *309* (1), 404-413. DOI: 10.1124/jpet.103.061754.

(65) Thurmond, R. L.; Venable, J.; Savall, B.; La, D.; Snook, S.; Dunford, P. J.; Edwards, J. P. Clinical Development of Histamine H_4 Receptor Antagonists. In *Handb Exp Pharmacol*, Vol. 241; 2017; pp 301-320.

(66) Beyer, L.; Kabatas, A. S.; Mommert, S.; Stark, H.; Werfel, T.; Gutzmer, R.; Schaper-Gerhardt, K. Histamine Activates Human Eosinophils via H_2R and H_4R Predominantly in Atopic Dermatitis Patients. *Int J Mol Sci* **2022**, *23* (18). DOI: 10.3390/ijms231810294.

(67) Xia, R.; Shi, S.; Xu, Z.; Vischer, H. F.; Windhorst, A. D.; Qian, Y.; Duan, Y.; Liang, J.; Chen, K.; Zhang, A.; et al. Structural basis of ligand recognition and design of antihistamines targeting histamine H_4 receptor. *Nat Commun* **2024**, *15* (1), 2493. DOI: 10.1038/s41467-024-46840-5.

(68) Im, D.; Kishikawa, J. I.; Shiimura, Y.; Hisano, H.; Ito, A.; Fujita-Fujiharu, Y.; Sugita, Y.; Noda, T.; Kato, T.; Asada, H.; et al. Structural insights into the agonists binding and receptor selectivity of human histamine H_4 receptor. *Nat Commun* **2023**, *14* (1), 6538. DOI: 10.1038/s41467-023-42260-z.

(69) Tardivel-Lacombe, J.; Morisset, S.; Gbahou, F.; Schwartz, J. C.; Arrang, J. M. Chromosomal mapping and organization of the human histamine H3 receptor gene. *Neuroreport* **2001**, *12* (2), 321-324. DOI: 10.1097/00001756-200102120-00028.

(70) Leurs, R.; Bakker, R. A.; Timmerman, H.; de Esch, I. J. The histamine H3 receptor: from gene cloning to H3 receptor drugs. *Nat Rev Drug Discov* **2005**, *4* (2), 107-120. DOI: 10.1038/nrd1631.

(71) Bongers, G.; Sallmen, T.; Passani, M. B.; Mariottini, C.; Wendelin, D.; Lozada, A.; Marle, A.; Navis, M.; Blandina, P.; Bakker, R. A.; et al. The Akt/GSK-3beta axis as a new signaling pathway of the histamine H_3 receptor. *J Neurochem* **2007**, *103* (1), 248-258. DOI: 10.1111/j.1471-4159.2007.04752.x.

(72) Lovenberg, T. W.; Roland, B. L.; Wilson, S. J.; Jiang, X.; Pyati, J.; Huvar, A.; Jackson, M. R.; Erlander, M. G. Cloning and Functional Expression of the Human Histamine H 3 Receptor. *Mol. Pharmacol.* **1999**, *55* (6), 1101-1107. DOI: 10.1124/mol.55.6.1101.

(73) Stevens, D. R.; Eriksson, K. S.; Brown, R. E.; Haas, H. L. The mechanism of spontaneous firing in histamine neurons. *Behav Brain Res* **2001**, *124* (2), 105-112. DOI: 10.1016/s0166-4328(01)00219-4.

(74) Lundius, E. G.; Sanchez-Alavez, M.; Ghochani, Y.; Klaus, J.; Tabarean, I. V. Histamine influences body temperature by acting at H1 and H3 receptors on distinct populations of preoptic neurons. *J Neurosci* **2010**, *30* (12), 4369-4381. DOI: 10.1523/JNEUROSCI.0378-10.2010.

(75) Sanchez-Lemus, E.; Arias-Montano, J. A. Histamine H3 receptor activation inhibits dopamine D1 receptor-induced cAMP accumulation in rat striatal slices. *Neurosci Lett* **2004**, *364* (3), 179-184. DOI: 10.1016/j.neulet.2004.04.045.

(76) Cogé, F.; Guénin, S. P.; Audinot, V.; Renouard-Try, A.; Beauverger, P.; Macia, C.; Ouvry, C.; Nagel, N.; Rique, H.; Boutin, J. A.; et al. Genomic organization and characterization of splice variants of the human histamine H3 receptor. *Biochemical Journal* **2001**, *355* (2), 279-288. DOI: 10.1042/bj3550279.

(77) Krueger, K. M.; Witte, D. G.; Ireland-Denny, L.; Miller, T. R.; Baranowski, J. L.; Buckner, S.; Milicic, I.; Esbenshade, T. A.; Hancock, A. A. G protein-dependent pharmacology of histamine H3 receptor ligands: evidence for heterogeneous active state receptor conformations. *J Pharmacol Exp Ther* **2005**, *314* (1), 271-281. DOI: 10.1124/jpet.104.078865.

(78) Sahlholm, K.; Nilsson, J.; Marcellino, D.; Fuxe, K.; Arhem, P. Voltage sensitivities and deactivation kinetics of histamine H_3 and H_4 receptors. *Biochim Biophys Acta* **2012**, *1818* (12), 3081-3089. DOI: 10.1016/j.bbamem.2012.07.027.

(79) Drutel, G.; Peitsaro, N.; Karlstedt, K.; Wieland, K.; Smit, M. J.; Timmerman, H.; Panula, P.; Leurs, R. Identification of Rat H3 Receptor Isoforms with Different Brain Expression and Signaling Properties. *Molecular Pharmacology* **2001**, *59* (1), 1-8. DOI: 10.1016/s0026-895x(24)12349-8.

(80) Giovannini, M. G.; Efoudebe, M.; Passani, M. B.; Baldi, E.; Bucherelli, C.; Giachi, F.; Corradetti, R.; Blandina, P. Improvement in fear memory by histamine-elicited ERK2 activation in hippocampal CA3 cells. *J Neurosci* **2003**, *23* (27), 9016-9023. DOI: 10.1523/JNEUROSCI.23-27-09016.2003.

(81) Silver, R. B.; Mackins, C. J.; Smith, N. C.; Koritchneva, I. L.; Lefkowitz, K.; Lovenberg, T. W.; Levi, R. Coupling of histamine H3 receptors to neuronal Na+/H+ exchange: a novel

protective mechanism in myocardial ischemia. *Proc Natl Acad Sci U S A* **2001**, *98* (5), 2855-2859. DOI: 10.1073/pnas.051599198.

(82) Silver, R. B.; Poonwasi, K. S.; Seyedi, N.; Wilson, S. J.; Lovenberg, T. W.; Levi, R. Decreased intracellular calcium mediates the histamine H3-receptor-induced attenuation of norepinephrine exocytosis from cardiac sympathetic nerve endings. *Proc Natl Acad Sci U S A* **2002**, *99* (1), 501-506. DOI: 10.1073/pnas.012506099.

(83) Schwartz, J. C.; Morisset, S.; Rouleau, A.; Tardivel-Lacombe, J.; Gbahou, F.; Ligneau, X.; Heron, A.; Sasse, A.; Stark, H.; Schunack, W.; et al. Application of genomics to drug design: the example of the histamine H3 receptor. *Eur Neuropsychopharmacol* **2001**, *11* (6), 441-448. DOI: 10.1016/s0924-977x(01)00121-3.

(84) Berlin, M.; Boyce, C. W.; Ruiz Mde, L. Histamine H3 receptor as a drug discovery target. *J Med Chem* **2011**, *54* (1), 26-53. DOI: 10.1021/jm100064d.

(85) Gao, M.; Dekker, M. E.; Leurs, R.; Vischer, H. F. Pharmacological characterization of seven human histamine H_3 receptor isoforms. *Eur J Pharmacol* **2024**, *968*, 176450. DOI: 10.1016/j.ejphar.2024.176450.

(86) Arrang, J. M.; Garbarg, M.; Schwartz, J. C. Autoinhibition of histamine synthesis mediated by presynaptic H3-receptors. *Neuroscience* **1987**, *23* (1), 149-157. DOI: 10.1016/0306-4522(87)90279-x.

(87) Peng, X.; Yang, L.; Liu, Z.; Lou, S.; Mei, S.; Li, M.; Chen, Z.; Zhang, H. Structural basis for recognition of antihistamine drug by human histamine receptor. *Nat. Commun.* **2022**, *13* (1). DOI: 10.1038/s41467-022-33880-y.

(88) Ferrada, C.; Ferre, S.; Casado, V.; Cortes, A.; Justinova, Z.; Barnes, C.; Canela, E. I.; Goldberg, S. R.; Leurs, R.; Lluis, C.; et al. Interactions between histamine H3 and dopamine D2 receptors and the implications for striatal function. *Neuropharmacology* **2008**, *55* (2), 190-197. DOI: 10.1016/j.neuropharm.2008.05.008.

(89) Ferrada, C.; Moreno, E.; Casado, V.; Bongers, G.; Cortes, A.; Mallol, J.; Canela, E. I.; Leurs, R.; Ferre, S.; Lluis, C.; et al. Marked changes in signal transduction upon heteromerization of dopamine D1 and histamine H3 receptors. *Br J Pharmacol* **2009**, *157* (1), 64-75. DOI: 10.1111/j.1476-5381.2009.00152.x.

(90) Bakker, R. A.; Schoonus, S. B. J.; Smit, M. J.; Timmerman, H.; Leurs, R. Histamine H1-Receptor Activation of Nuclear Factor-κB: Roles for Gβγ- and Gαq/11-Subunits in Constitutive and Agonist-Mediated Signaling. *Molecular Pharmacology* **2001**, *60* (5), 1133-1142. DOI: 10.1016/s0026-895x(24)12523-0.

(91) Arrang, J. M.; Garbarg, M.; Lancelot, J. C.; Lecomte, J. M.; Pollard, H.; Robba, M.; Schunack, W.; Schwartz, J. C. Highly potent and selective ligands for histamine H3-receptors. *Nature* **1987**, *327* (6118), 117-123. DOI: 10.1038/327117a0.

(92) Arrang, J. M.; Roy, J.; Morgat, J. L.; Schunack, W.; Schwartz, J. C. Histamine H3 receptor binding sites in rat brain membranes: modulations by guanine nucleotides and divalent cations. *Eur J Pharmacol* **1990**, *188* (4-5), 219-227. DOI: 10.1016/0922-4106(90)90005-i.

(93) Ligneau, X.; Lin, J.-S.; Vanni-Mercier, G.; Jouvet, M.; Muir, J. L.; Ganellin, C. R.; Stark, H.; Elz, S.; Schunack, W.; Schwartz, J.-C. Neurochemical and Behavioral Effects of Ciproxifan, A Potent Histamine H3-Receptor Antagonist. *The Journal of Pharmacology and Experimental Therapeutics* **1998**, *287*, 658–666.

(94) Stark, H.; Purand, K.; Huls, A.; Ligneau, X.; Garbarg, M.; Schwartz, J. C.; Schunack, W. [125I]iodoproxyfan and related compounds: a reversible radioligand and novel classes of antagonists with high affinity and selectivity for the histamine H3 receptor. *J Med Chem* **1996**, *39* (6), 1220-1226. DOI: 10.1021/jm9504767.

(95) van der Goot, H.; Schepers, M. J. P.; Sterk, G. J.; Timmerman, H. Isothiourea analogues of histamine as potent agonists or antagonists of the histamine H3-receptor. *European Journal of Medicinal Chemistry* **1992**, *27* (5), 511-517. DOI: 10.1016/0223-5234(92)90185-4.

(96) Sasse, A.; Sadek, B.; Ligneau, X.; Elz, S.; Pertz, H. H.; Luger, P.; Ganellin, C. R.; Arrang, J. M.; Schwartz, J. C.; Schunack, W.; et al. New histamine H_3-receptor ligands of the proxifan series: imoproxifan and other selective antagonists with high oral in vivo potency. *J Med Chem* **2000**, *43* (17), 3335-3343. DOI: 10.1021/jm000971p.

(97) Sasse, A.; Stark, H.; Reidemeister, S.; Huls, A.; Elz, S.; Ligneau, X.; Ganellin, C. R.; Schwartz, J. C.; Schunack, W. Novel partial agonists for the histamine H_3 receptor with high in vitro and in vivo activity. *J Med Chem* **1999**, *42* (20), 4269-4274. DOI: 10.1021/jm991068w.

(98) Sander, K.; Kottke, T.; Stark, H. Histamine H3 receptor antagonists go to clinics. *Biol Pharm Bull* **2008**, *31* (12), 2163-2181. DOI: 10.1248/bpb.31.2163.

(99) Monti, J. M.; Jantos, H.; Ponzoni, A.; Monti, D. Sleep and waking during acute histamine H3 agonist BP 2.94 or H3 antagonist carboperamide (MR 16155) administration in rats. *Neuropsychopharmacology* **1996**, *15* (1), 31-35. DOI: 10.1016/0893-133X(95)00151-3.

(100) Tedford, C. E.; Hoffmann, M.; Seyedi, N.; Maruyama, R.; Levi, R.; Yates, S. L.; Ali, S. M.; Phillips, J. G. High antagonist potency of GT-2227 and GT-2331, new histamine H3 receptor antagonists, in two functional models. *Eur J Pharmacol* **1998**, *351* (3), 307-311. DOI: 10.1016/s0014-2999(98)00396-3.

(101) Halpern, M. GT-2331. *Current Opinion in Central and Peripheral Nervous System Investigational Drugs* **1999**, *1*, 524-527.

(102) Ligneau, X.; Morisset, S.; Tardivel-Lacombe, J.; Gbahou, F.; Ganellin, C. R.; Stark, H.; Schunack, W.; Schwartz, J. C.; Arrang, J. M. Distinct pharmacology of rat and human histamine H(3) receptors: role of two amino acids in the third transmembrane domain. *Br J Pharmacol* **2000**, *131* (7), 1247-1250. DOI: 10.1038/sj.bjp.0703712.

(103) Celanire, S.; Wijtmans, M.; Talaga, P.; Leurs, R.; de Esch, I. J. Keynote review: histamine H3 receptor antagonists reach out for the clinic. *Drug Discov Today* **2005**, *10* (23-24), 1613-1627. DOI: 10.1016/S1359-6446(05)03625-1.

(104) Cowart, M.; Altenbach, R.; Black, L.; Faghih, R.; Zhao, C.; Hancock, A. A. Medicinal chemistry and biological properties of non-imidazole histamine H3 antagonists. *Mini Rev Med Chem* **2004**, *4* (9), 979-992. DOI: 10.2174/1389557043403215.

(105) Ganellin, C. R.; Leurquin, F.; Piripitsi, A.; Arrang, J.-M.; Garbarg, M.; Ligneau, X.; Schunack, W.; Schwartz, J.-C. Synthesis of Potent Non-imidazole Histamine H3-Receptor Antagonists. *Archiv der Pharmazie* **1998**, *331* (12), 395-404. DOI: 10.1002/(sici)1521-4184(199812)331:12<395::Aid-ardp395>3.0.Co;2-7.

(106) Hancock, A. A. The challenge of drug discovery of a GPCR target: analysis of preclinical pharmacology of histamine H3 antagonists/inverse agonists. *Biochem Pharmacol* **2006**, *71* (8), 1103-1113. DOI: 10.1016/j.bcp.2005.10.033.

(107) Schuster, D.; Laggner, C.; Langer, T. Why drugs fail--a study on side effects in new chemical entities. *Curr Pharm Des* **2005**, *11* (27), 3545-3559. DOI: 10.2174/138161205774414510.

(108) Garrido, A.; Lepailleur, A.; Mignani, S. M.; Dallemagne, P.; Rochais, C. hERG toxicity assessment: Useful guidelines for drug design. *Eur J Med Chem* **2020**, *195*, 112290. DOI: 10.1016/j.ejmech.2020.112290.

(109) Bautista-Aguilera, O. M.; Hagenow, S.; Palomino-Antolin, A.; Farre-Alins, V.; Ismaili, L.; Joffrin, P. L.; Jimeno, M. L.; Soukup, O.; Janockova, J.; Kalinowsky, L.; et al. Multitarget-Directed Ligands Combining Cholinesterase and Monoamine Oxidase Inhibition with Histamine H_3R Antagonism for Neurodegenerative Diseases. *Angew Chem Int Ed Engl* **2017**, *56* (41), 12765-12769. DOI: 10.1002/anie.201706072.

(110) Bicker, J.; Alves, G.; Fortuna, A.; Falcao, A. Blood-brain barrier models and their relevance for a successful development of CNS drug delivery systems: a review. *Eur J Pharm Biopharm* **2014**, *87* (3), 409-432. DOI: 10.1016/j.ejpb.2014.03.012.

(111) Banks, W. A. From blood-brain barrier to blood-brain interface: new opportunities for CNS drug delivery. *Nat Rev Drug Discov* **2016**, *15* (4), 275-292. DOI: 10.1038/nrd.2015.21.

(112) Fromm, M. F. Importance of P-glycoprotein at blood-tissue barriers. *Trends Pharmacol Sci* **2004**, *25* (8), 423-429. DOI: **10.1016/j.tips.2004.06.002**.

(113) *Wakix (pitolisant) NDA Approval*; NDA 211150; Food Drug Administration, 2019. https://www.accessdata.fda.gov/scripts/cder/daf/index.cfm?event=BasicSearch.process (accessed February 02, 2025).

(114) *Wakix -EPAR: summary public*; EMA/63272; European Medicines Agency, 2016. https://www.ema.europa.eu/en/medicines/human/EPAR/wakix (accessed Feb. 02, 2025).

(115) Ligneau, X.; Perrin, D.; Landais, L.; Camelin, J. C.; Calmels, T. P.; Berrebi-Bertrand, I.; Lecomte, J. M.; Parmentier, R.; Anaclet, C.; Lin, J. S.; et al. BF2.649 [1-3-[3-(4-Chlorophenyl)propoxy]propylpiperidine, hydrochloride], a nonimidazole inverse agonist/antagonist at the human histamine H3 receptor: Preclinical pharmacology. *J Pharmacol Exp Ther* **2007**, *320* (1), 365-375. DOI: 10.1124/jpet.106.111039.

(116) *Ozawade - EPAR: medicines overview*; EMA/371398; European Medicines Agency, 2021. https://www.ema.europa.eu/en/medicines/human/EPAR/ozawade (accessed Feb. 02, 2025).

(117) Meier, G.; Apelt, J.; Reichert, U.; Grassmann, S.; Ligneau, X.; Elz, S.; Leurquin, F.; Ganellin, C. R.; Schwartz, J. C.; Schunack, W.; et al. Influence of imidazole replacement in different structural classes of histamine H_3-receptor antagonists. *Eur J Pharm Sci* **2001**, *13* (3), 249-259. DOI: 10.1016/s0928-0987(01)00106-3.

(118) Petroianu, G.; Arafat, K.; Sasse, B.; Stark, H. Multiple enzyme inhibitions by histamine H3 receptor antagonists as potential procognitive agents. *Die Pharmazie-An International Journal of Pharmaceutical Sciences* **2006**, *61* (3), 179-182.

(119) Wingen, K.; Stark, H. Scaffold variations in amine warhead of histamine H_3 receptor antagonists. *Drug Discov. Today Technol.* **2013**, *10* (4), e483-489. DOI: 10.1016/j.ddtec.2013.07.001.

(120) Levoin, N.; Calmels, T.; Poupardin-Olivier, O.; Labeeuw, O.; Danvy, D.; Robert, P.; Berrebi-Bertrand, I.; Ganellin, C. R.; Schunack, W.; Stark, H.; et al. Refined docking as a valuable tool for lead optimization: application to histamine H3 receptor antagonists. *Arch Pharm (Weinheim)* **2008**, *341* (10), 610-623. DOI: 10.1002/ardp.200800042.

(121) Kooistra, A. J.; Kuhne, S.; de Esch, I. J.; Leurs, R.; de Graaf, C. A structural chemogenomics analysis of aminergic GPCRs: lessons for histamine receptor ligand design. *Br J Pharmacol* **2013**, *170* (1), 101-126. DOI: 10.1111/bph.12248.

(122) Zhang, X.; Liu, G.; Zhong, Y. N.; Zhang, R.; Yang, C. C.; Niu, C.; Pu, X.; Sun, J.; Zhang, T.; Yang, L.; et al. Structural basis of ligand recognition and activation of the histamine receptor family. *Nat Commun* **2024**, *15* (1), 8296. DOI: 10.1038/s41467-024-52585-y.

(123) Lazewska, D.; Kiec-Kononowicz, K. Histamine H_3 receptor antagonists/inverse agonists: a patent review (October 2017 - December 2023) documenting progress. *Expert Opin Ther Pat* **2025**, 1-25. DOI: 10.1080/13543776.2024.2446227.

(124) Bioprojet. *Proof of Concept Study on Pitolisant Effect on Autism Spectrum Disorders in Children and Adolescents*. https://clinicaltrials.gov/ (accessed October 07, 2025).

(125) Harmony Biosciences Managment, I. *A Study of Pitolisant in Patients with Prader-Willi Syndrome*. https://clinicaltrials.gov/ (accessed April 20, 2025).

(126) Revana, A.; Bhattacharjee, R.; Miller, J. L.; Chidekel, A.; Khanna, P.; Ratnam, S.; Runyan, G.; Bauer, E.; Rapchak, K. D.; Seiden, D.; et al. A proof-of-concept study of pitolisant for

excessive daytime sleepiness in patients with Prader-Willi syndrome. *J Clin Sleep Med* **2025**. DOI: 10.5664/jcsm.11800.

(127) Harmony Biosciences Management, I. *WAKIX® (Pitolisant) Pregnancy Registry*. https://clinicaltrials.gov/ (accessed April 20, 2025).

(128) Bioprojet. *Efficacy and Safety of Pitolisant in Pediatric Narcoleptic Patients With or Without Cataplexy, Double-blind Study Followed by a Prolonged Open-label Period*. https://clinicaltrials.gov/ (accessed April 20, 2025).

(129) Voysey, Z. J.; Barker, R. A.; Lazar, A. S. The Treatment of Sleep Dysfunction in Neurodegenerative Disorders. *Neurotherapeutics* **2021**, *18* (1), 202-216. DOI: 10.1007/s13311-020-00959-7.

(130) Liblau, R. S.; Latorre, D.; Kornum, B. R.; Dauvilliers, Y.; Mignot, E. J. The immunopathogenesis of narcolepsy type 1. *Nat Rev Immunol* **2024**, *24* (1), 33-48. DOI: 10.1038/s41577-023-00902-9.

(131) Chavda, V.; Chaurasia, B.; Umana, G. E.; Tomasi, S. O.; Lu, B.; Montemurro, N. Narcolepsy-A Neuropathological Obscure Sleep Disorder: A Narrative Review of Current Literature. *Brain Sci* **2022**, *12* (11). DOI: 10.3390/brainsci12111473.

(132) Nirogi, R.; Jayarajan, P.; Benade, V.; Abraham, R.; Goyal, V. K. Hits and misses with animal models of narcolepsy and the implications for drug discovery. *Expert Opin Drug Discov* **2024**, *19* (6), 755-768. DOI: 10.1080/17460441.2024.2354293.

(133) Dauvilliers, Y.; Mignot, E.; Del Rio Villegas, R.; Du, Y.; Hanson, E.; Inoue, Y.; Kadali, H.; Koundourakis, E.; Meyer, S.; Rogers, R.; et al. Oral Orexin Receptor 2 Agonist in Narcolepsy Type 1. *N Engl J Med* **2023**, *389* (4), 309-321. DOI: 10.1056/NEJMoa2301940.

(134) Alkermes, I. *A Long-Term Study of ALKS 2680 in Subjects With Narcolepsy and Idiopathic Hypersomnia*. https://clinicaltrials.gov/ (accessed April 20, 2025).

(135) Alkermes, I. *A Study to Evaluate the Safety and Effectiveness of ALKS 2680 in Subjects With Narcolepsy Type 2 (Vibrance-2)*. https://clinicaltrials.gov/ (accessed April 20, 2025).

(136) Takeda. *A Study of TAK-861 for the Treatment of Narcolepsy Type 1*. https://clinicaltrials.gov/ (accessed April 20, 2025).

(137) Takeda. *A Study of TAK-861 in People With Narcolepsy Type 1*. https://clinicaltrials.gov/ (accessed April 20, 2025).

(138) De la Herran-Arita, A. K.; Garcia-Garcia, F. Current and emerging options for the drug treatment of narcolepsy. *Drugs* **2013**, *73* (16), 1771-1781. DOI: 10.1007/s40265-013-0127-y.

(139) John, J.; Thannickal, T. C.; McGregor, R.; Ramanathan, L.; Ohtsu, H.; Nishino, S.; Sakai, N.; Yamanaka, A.; Stone, C.; Cornford, M.; et al. Greatly increased numbers of histamine cells in human narcolepsy with cataplexy. *Ann Neurol* **2013**, *74* (6), 786-793. DOI: 10.1002/ana.23968.

(140) Valko, P. O.; Gavrilov, Y. V.; Yamamoto, M.; Reddy, H.; Haybaeck, J.; Mignot, E.; Baumann, C. R.; Scammell, T. E. Increase of histaminergic tuberomammillary neurons in narcolepsy. *Ann Neurol* **2013**, *74* (6), 794-804. DOI: 10.1002/ana.24019.

(141) Pepin, J. L.; Georgiev, O.; Tiholov, R.; Attali, V.; Verbraecken, J.; Buyse, B.; Partinen, M.; Fietze, I.; Belev, G.; Dokic, D.; et al. Pitolisant for Residual Excessive Daytime Sleepiness in OSA Patients Adhering to CPAP: A Randomized Trial. *Chest* **2021**, *159* (4), 1598-1609. DOI: 10.1016/j.chest.2020.09.281.

(142) Anton, R. F.; O'Malley, S. S.; Ciraulo, D. A.; Cisler, R. A.; Couper, D.; Donovan, D. M.; Gastfriend, D. R.; Hosking, J. D.; Johnson, B. A.; LoCastro, J. S.; et al. Combined pharmacotherapies and behavioral interventions for alcohol dependence: the COMBINE study: a randomized controlled trial. *JAMA* **2006**, *295* (17), 2003-2017. DOI: 10.1001/jama.295.17.2003.

(143) Plosker, G. L. Acamprosate: A Review of Its Use in Alcohol Dependence. *Drugs* **2015**, *75* (11), 1255-1268. DOI: 10.1007/s40265-015-0423-9.

(144) Abrahao, K. P.; Salinas, A. G.; Lovinger, D. M. Alcohol and the Brain: Neuronal Molecular Targets, Synapses, and Circuits. *Neuron* **2017**, *96* (6), 1223-1238. DOI: 10.1016/j.neuron.2017.10.032.

(145) Korpi, E. R.; den Hollander, B.; Farooq, U.; Vashchinkina, E.; Rajkumar, R.; Nutt, D. J.; Hyytia, P.; Dawe, G. S. Mechanisms of Action and Persistent Neuroplasticity by Drugs of Abuse. *Pharmacol Rev* **2015**, *67* (4), 872-1004. DOI: 10.1124/pr.115.010967.

(146) Panula, P. Histamine, histamine H_3 receptor, and alcohol use disorder. *Br J Pharmacol* **2020**, *177* (3), 634-641. DOI: 10.1111/bph.14634.

(147) Center, B. M. *Pitolisant Effects on Alcohol Self-Administration in Heavy Drinkers*. https://clinicaltrials.gov/ (accessed April 20, 2025).

(148) Bioprojet. *Randomized Clinical Trial Evaluating BP1.3656 Versus Placebo For Alcohol Use Disorder Treatment*. https://clinicaltrials.gov/ (accessed April 20, 2025).

(149) PHARMA, B. *Bioprojet Research Pipeline*. https://pharma.bioprojet.com/en/research/pipeline/# (accessed April 20, 2025).

(150) PHARMA, B. *A Multisite Randomized Clinical Trial Evaluating BP1.3656 Versus Placebo For Alcohol Use Disorder Treatment* https://www.clinicaltrialsregister.eu/ (accessed April 20, 2025).

(151) Poveda, R.; Fernandez-Duenas, V.; Fernandez, A.; Sanchez, S.; Puig, M. M.; Planas, E. Synergistic interaction between fentanyl and the histamine H3 receptor agonist R-(alpha)-

methylhistamine, on the inhibition of nociception and plasma extravasation in mice. *Eur J Pharmacol* **2006**, *541* (1-2), 53-56. DOI: 10.1016/j.ejphar.2006.05.008.

(152) Colloca, L.; Ludman, T.; Bouhassira, D.; Baron, R.; Dickenson, A. H.; Yarnitsky, D.; Freeman, R.; Truini, A.; Attal, N.; Finnerup, N. B.; et al. Neuropathic pain. *Nat Rev Dis Primers* **2017**, *3*, 17002. DOI: 10.1038/nrdp.2017.2.

(153) van Velzen, M.; Dahan, A.; Niesters, M. Neuropathic Pain: Challenges and Opportunities. *Front Pain Res (Lausanne)* **2020**, *1*, 1. DOI: 10.3389/fpain.2020.00001.

(154) Treede, R. D.; Jensen, T. S.; Campbell, J. N.; Cruccu, G.; Dostrovsky, J. O.; Griffin, J. W.; Hansson, P.; Hughes, R.; Nurmikko, T.; Serra, J. Neuropathic pain: redefinition and a grading system for clinical and research purposes. *Neurology* **2008**, *70* (18), 1630-1635. DOI: 10.1212/01.wnl.0000282763.29778.59.

(155) Chaparro, L. E.; Wiffen, P. J.; Moore, R. A.; Gilron, I. Combination pharmacotherapy for the treatment of neuropathic pain in adults. *Cochrane Database Syst Rev* **2012**, *2012* (7), CD008943. DOI: 10.1002/14651858.CD008943.pub2.

(156) Ahmadi, R.; Kuner, R.; Weidner, N.; Kessler, J.; Bendszus, M.; Krieg, S. M. The Diagnosis and Treatment of Neuropathic Pain. *Dtsch Arztebl Int* **2024**, *121* (25), 825-832. DOI: 10.3238/arztebl.m2024.0215.

(157) Colleoni, M.; Sacerdote, P. Murine models of human neuropathic pain. *Biochim Biophys Acta* **2010**, *1802* (10), 924-933. DOI: 10.1016/j.bbadis.2009.10.012.

(158) Moore, R. A.; Derry, S.; Aldington, D.; Cole, P.; Wiffen, P. J. Amitriptyline for neuropathic pain and fibromyalgia in adults. *Cochrane Database Syst Rev* **2012**, *12*, CD008242. DOI: 10.1002/14651858.CD008242.pub2.

(159) Derry, S.; Rice, A. S.; Cole, P.; Tan, T.; Moore, R. A. Topical capsaicin (high concentration) for chronic neuropathic pain in adults. *Cochrane Database Syst Rev* **2017**, *1* (1), CD007393. DOI: 10.1002/14651858.CD007393.pub4.

(160) Aiyer, R.; Barkin, R. L.; Bhatia, A. Treatment of Neuropathic Pain with Venlafaxine: A Systematic Review. *Pain Med* **2017**, *18* (10), 1999-2012. DOI: 10.1093/pm/pnw261.

(161) Duehmke, R. M.; Derry, S.; Wiffen, P. J.; Bell, R. F.; Aldington, D.; Moore, R. A. Tramadol for neuropathic pain in adults. *Cochrane Database Syst Rev* **2017**, *6* (6), CD003726. DOI: 10.1002/14651858.CD003726.pub4.

(162) Pergolizzi, J. V., Jr.; Raffa, R. B.; Taylor, R., Jr.; Rodriguez, G.; Nalamachu, S.; Langley, P. A review of duloxetine 60 mg once-daily dosing for the management of diabetic peripheral neuropathic pain, fibromyalgia, and chronic musculoskeletal pain due to chronic osteoarthritis pain and low back pain. *Pain Pract* **2013**, *13* (3), 239-252. DOI: 10.1111/j.1533-2500.2012.00578.x.

(163) Lunn, M. P.; Hughes, R. A.; Wiffen, P. J. Duloxetine for treating painful neuropathy, chronic pain or fibromyalgia. *Cochrane Database Syst Rev* **2014**, *2014* (1), CD007115. DOI: 10.1002/14651858.CD007115.pub3.

(164) Medhurst, S. J.; Collins, S. D.; Billinton, A.; Bingham, S.; Dalziel, R. G.; Brass, A.; Roberts, J. C.; Medhurst, A. D.; Chessell, I. P. Novel histamine H3 receptor antagonists GSK189254 and GSK334429 are efficacious in surgically-induced and virally-induced rat models of neuropathic pain. *Pain* **2008**, *138* (1), 61-69. DOI: 10.1016/j.pain.2007.11.006.

(165) Cannon, K. E.; Chazot, P. L.; Hann, V.; Shenton, F.; Hough, L. B.; Rice, F. L. Immunohistochemical localization of histamine H3 receptors in rodent skin, dorsal root ganglia, superior cervical ganglia, and spinal cord: potential antinociceptive targets. *Pain* **2007**, *129* (1-2), 76-92. DOI: 10.1016/j.pain.2006.09.039.

(166) Cannon, K. E.; Hough, L. B. Inhibition of chemical and low-intensity mechanical nociception by activation of histamine H3 receptors. *J Pain* **2005**, *6* (3), 193-200. DOI: 10.1016/j.jpain.2004.12.003.

(167) Huang, L.; Adachi, N.; Nagaro, T.; Liu, K.; Arai, T. Histaminergic Involvement in Neuropathic Pain Produced by Partial Ligation of the Sciatic Nerve in Rats. *Regional Anesthesia and Pain Medicine* **2007**, *32* (2), 124-129. DOI: 10.1097/00115550-200703000-00006.

(168) Smith, F. M.; Haskelberg, H.; Tracey, D. J.; Moalem-Taylor, G. Role of histamine H3 and H4 receptors in mechanical hyperalgesia following peripheral nerve injury. *Neuroimmunomodulation* **2007**, *14* (6), 317-325. DOI: 10.1159/000125048.

(169) Chaumette, T.; Chapuy, E.; Berrocoso, E.; Llorca-Torralba, M.; Bravo, L.; Mico, J. A.; Chalus, M.; Eschalier, A.; Ardid, D.; Marchand, F.; et al. Effects of S 38093, an antagonist/inverse agonist of histamine H3 receptors, in models of neuropathic pain in rats. *Eur J Pain* **2018**, *22* (1), 127-141. DOI: 10.1002/ejp.1097.

(170) Cowart, M.; Hsieh, G.; Black, L. A.; Zhan, C.; Gomez, E. J.; Pai, M.; Strakhova, M.; Manelli, A.; Carr, T.; Wetter, J.; et al. Pharmacological characterization of A-960656, a histamine H(3) receptor antagonist with efficacy in animal models of osteoarthritis and neuropathic pain. *Eur J Pharmacol* **2012**, *684* (1-3), 87-94. DOI: 10.1016/j.ejphar.2012.03.048.

(171) Wei, H.; Jin, C. Y.; Viisanen, H.; You, H. J.; Pertovaara, A. Histamine in the locus coeruleus promotes descending noradrenergic inhibition of neuropathic hypersensitivity. *Pharmacol Res* **2014**, *90*, 58-66. DOI: 10.1016/j.phrs.2014.09.007.

(172) Wei, H.; Viisanen, H.; You, H. J.; Pertovaara, A. Spinal histamine in attenuation of mechanical hypersensitivity in the spinal nerve ligation-induced model of experimental neuropathy. *Eur J Pharmacol* **2016**, *772*, 1-10. DOI: 10.1016/j.ejphar.2015.12.039.

(173) Popiolek-Barczyk, K.; Lazewska, D.; Latacz, G.; Olejarz, A.; Makuch, W.; Stark, H.; Kiec-Kononowicz, K.; Mika, J. Antinociceptive effects of novel histamine H_3 and H_4 receptor antagonists and their influence on morphine analgesia of neuropathic pain in the mouse. *Br J Pharmacol* **2018**, *175* (14), 2897-2910. DOI: 10.1111/bph.14185.

(174) Medhurst, A. D.; Briggs, M. A.; Bruton, G.; Calver, A. R.; Chessell, I.; Crook, B.; Davis, J. B.; Davis, R. P.; Foley, A. G.; Heslop, T.; et al. Structurally novel histamine H3 receptor antagonists GSK207040 and GSK334429 improve scopolamine-induced memory impairment and capsaicin-induced secondary allodynia in rats. *Biochem Pharmacol* **2007**, *73* (8), 1182-1194. DOI: 10.1016/j.bcp.2007.01.007.

(175) Medhurst, A. D.; Atkins, A. R.; Beresford, I. J.; Brackenborough, K.; Briggs, M. A.; Calver, A. R.; Cilia, J.; Cluderay, J. E.; Crook, B.; Davis, J. B.; et al. GSK189254, a novel H3 receptor antagonist that binds to histamine H3 receptors in Alzheimer's disease brain and improves cognitive performance in preclinical models. *J Pharmacol Exp Ther* **2007**, *321* (3), 1032-1045. DOI: 10.1124/jpet.107.120311.

(176) Sors, A.; Panayi, F.; Bert, L.; Favale, D.; Nosjean, O.; Audinot, V.; Arrang, J. M.; Buisson, B.; Steidl, E.; Delbos, J. M.; et al. Mechanistic characterization of S 38093, a novel inverse agonist at histamine H3 receptors. *Eur J Pharmacol* **2017**, *803*, 11-23. DOI: 10.1016/j.ejphar.2017.03.013.

(177) Bloem, B. R.; Okun, M. S.; Klein, C. Parkinson's disease. *Lancet* **2021**, *397* (10291), 2284-2303. DOI: 10.1016/S0140-6736(21)00218-X.

(178) Vijiaratnam, N.; Simuni, T.; Bandmann, O.; Morris, H. R.; Foltynie, T. Progress towards therapies for disease modification in Parkinson's disease. *Lancet Neurol* **2021**, *20* (7), 559-572. DOI: 10.1016/S1474-4422(21)00061-2.

(179) de Bie, R. M. A.; Clarke, C. E.; Espay, A. J.; Fox, S. H.; Lang, A. E. Initiation of pharmacological therapy in Parkinson's disease: when, why, and how. *Lancet Neurol* **2020**, *19* (5), 452-461. DOI: 10.1016/S1474-4422(20)30036-3.

(180) Blair, H. A.; Dhillon, S. Safinamide: A Review in Parkinson's Disease. *CNS Drugs* **2017**, *31* (2), 169-176. DOI: 10.1007/s40263-017-0408-1.

(181) Foltynie, T.; Bruno, V.; Fox, S.; Kuhn, A. A.; Lindop, F.; Lees, A. J. Medical, surgical, and physical treatments for Parkinson's disease. *Lancet* **2024**, *403* (10423), 305-324. DOI: 10.1016/S0140-6736(23)01429-0.

(182) Church, F. C. Treatment Options for Motor and Non-Motor Symptoms of Parkinson's Disease. *Biomolecules* **2021**, *11* (4). DOI: 10.3390/biom11040612.

(183) Kambey, P. A.; Liu, W. Y.; Wu, J.; Tang, C.; Buberwa, W.; Saro, A.; Nyalali, A. M. K.; Gao, D. Amphiregulin blockade decreases the levodopa-induced dyskinesia in a 6-hydroxydopamine Parkinson's disease mouse model. *CNS Neurosci Ther* **2023**, *29* (10), 2925-2939. DOI: 10.1111/cns.14229.

(184) Espay, A. J.; Morgante, F.; Merola, A.; Fasano, A.; Marsili, L.; Fox, S. H.; Bezard, E.; Picconi, B.; Calabresi, P.; Lang, A. E. Levodopa-induced dyskinesia in Parkinson disease: Current and evolving concepts. *Ann Neurol* **2018**, *84* (6), 797-811. DOI: 10.1002/ana.25364.

(185) Fernandez, H. H.; Isaacson, S. H.; Hauser, R. A.; Agarwal, P.; Ondo, W.; Park, A.; Elmer, L.; Kremens, D.; Leoni, M.; Duvvuri, S.; et al. Tavapadon, an Orally Administered, Once-Daily, Selective D1/D5 Partial Dopamine Agonist for Adjunctive Treatment of Parkinson's Disease With Motor Fluctuations. *Parkinsonism & Related Disorders* **2025**, *134*. DOI: 10.1016/j.parkreldis.2025.107623.

(186) Bezard, E.; Gray, D.; Kozak, R.; Leoni, M.; Combs, C.; Duvvuri, S. Rationale and Development of Tavapadon, a D1/D5-Selective Partial Dopamine Agonist for the Treatment of Parkinson's Disease. *CNS Neurol Disord Drug Targets* **2024**, *23* (4), 476-487. DOI: 10.2174/1871527322666230331121028.

(187) González-Sepúlveda, M.; Rosell, S.; Hoffmann, H. M.; Castillo-Ruiz, M. d. M.; Mignon, V.; Moreno-Delgado, D.; Vignes, M.; Díaz, J.; Sabriá, J.; Ortiz, J. Cellular distribution of the histamine H3 receptor in the basal ganglia: Functional modulation of dopamine and glutamate neurotransmission. *Basal Ganglia* **2013**, *3* (2), 109-121. DOI: 10.1016/j.baga.2012.12.001.

(188) Yu, X.; Ye, Z.; Houston, C. M.; Zecharia, A. Y.; Ma, Y.; Zhang, Z.; Uygun, D. S.; Parker, S.; Vyssotski, A. L.; Yustos, R.; et al. Wakefulness Is Governed by GABA and Histamine Cotransmission. *Neuron* **2015**, *87* (1), 164-178. DOI: 10.1016/j.neuron.2015.06.003.

(189) Avila-Luna, A.; Verduzco-Mendoza, A.; Olmos-Hernandez, A.; Cortes-Altamirano, J. L.; Alfaro-Rodriguez, A.; Arias-Montano, J. A.; Bueno-Nava, A. The Interaction of Histamine H_3 and Dopamine D_1 Receptors on Hyperkinetic Alterations in Animal Models of Parkinson's Disease. *Pharmaceuticals (Basel)* **2024**, *17* (12). DOI: 10.3390/ph17121726.

(190) Rinne, J. O.; Anichtchik, O. V.; Eriksson, K. S.; Kaslin, J.; Tuomisto, L.; Kalimo, H.; Roytta, M.; Panula, P. Increased brain histamine levels in Parkinson's disease but not in multiple system atrophy. *J Neurochem* **2002**, *81* (5), 954-960. DOI: 10.1046/j.1471-4159.2002.00871.x.

(191) Anichtchik, O. V.; Peitsaro, N.; Rinne, J. O.; Kalimo, H.; Panula, P. Distribution and modulation of histamine H_3 receptors in basal ganglia and frontal cortex of healthy controls and patients with Parkinson's disease. *Neurobiol Dis* **2001**, *8* (4), 707-716. DOI: 10.1006/nbdi.2001.0413.

(192) Garbarg, M.; Javoy-Agid, F.; Schwartz, J. C.; Agid, Y. Brain histidine decarboxylase activity in Parkinson's disease. *Lancet* **1983**, *1* (8314-5), 74-75. DOI: 10.1016/s0140-6736(83)91613-6.

(193) Nakamura, S.; Ohnishi, K.; Nishimura, M.; Suenaga, T.; Akiguchi, I.; Kimura, J.; Kimura, T. Large neurons in the tuberomammillary nucleus in patients with Parkinson's disease and multiple system atrophy. *Neurology* **1996**, *46* (6), 1693-1696. DOI: 10.1212/wnl.46.6.1693.

(194) Liu, C. Q.; Chen, Z.; Liu, F. X.; Hu, D. N.; Luo, J. H. Involvement of brain endogenous histamine in the degeneration of dopaminergic neurons in 6-hydroxydopamine-lesioned rats. *Neuropharmacology* **2007**, *53* (7), 832-841. DOI: 10.1016/j.neuropharm.2007.08.014.

(195) Liu, L.; Zhang, S.; Zhu, Y.; Fu, Q.; Zhu, Y.; Gong, Y.; Ohtsu, H.; Luo, J.; Wei, E.; Chen, Z. Improved learning and memory of contextual fear conditioning and hippocampal CA1 long-term

potentiation in histidine decarboxylase knock-out mice. *Hippocampus* **2007**, *17* (8), 634-641. DOI: 10.1002/hipo.20305.

(196) Nowak, P.; Noras, L.; Jochem, J.; Szkilnik, R.; Brus, H.; Korossy, E.; Drab, J.; Kostrzewa, R. M.; Brus, R. Histaminergic activity in a rodent model of Parkinson's disease. *Neurotox Res* **2009**, *15* (3), 246-251. DOI: 10.1007/s12640-009-9025-1.

(197) Scheltens, P.; De Strooper, B.; Kivipelto, M.; Holstege, H.; Chetelat, G.; Teunissen, C. E.; Cummings, J.; van der Flier, W. M. Alzheimer's disease. *Lancet* **2021**, *397* (10284), 1577-1590. DOI: 10.1016/S0140-6736(20)32205-4.

(198) Kwon, K. J.; Kim, H. Y.; Han, S. H.; Shin, C. Y. Future Therapeutic Strategies for Alzheimer's Disease: Focus on Behavioral and Psychological Symptoms. *Int J Mol Sci* **2024**, *25* (21). DOI: 10.3390/ijms252111338.

(199) Bajda, M.; Lazewska, D.; Godyn, J.; Zareba, P.; Kuder, K.; Hagenow, S.; Latka, K.; Stawarska, E.; Stark, H.; Kiec-Kononowicz, K.; et al. Search for new multi-target compounds against Alzheimer's disease among histamine H_3 receptor ligands. *Eur J Med Chem* **2020**, *185*, 111785. DOI: 10.1016/j.ejmech.2019.111785.

(200) Knopman, D. S.; Amieva, H.; Petersen, R. C.; Chetelat, G.; Holtzman, D. M.; Hyman, B. T.; Nixon, R. A.; Jones, D. T. Alzheimer disease. *Nat Rev Dis Primers* **2021**, *7* (1), 33. DOI: 10.1038/s41572-021-00269-y.

(201) Korczyn, A. D.; Grinberg, L. T. Is Alzheimer disease a disease? *Nat Rev Neurol* **2024**, *20* (4), 245-251. DOI: 10.1038/s41582-024-00940-4.

(202) Schneider, L. A resurrection of aducanumab for Alzheimer's disease. *Lancet Neurol* **2020**, *19* (2), 111-112. DOI: 10.1016/S1474-4422(19)30480-6.

(203) Glymour, M. M.; Weuve, J.; Dufouil, C.; Mayeda, E. R. Aduhelm, the Newly Approved Medication for Alzheimer Disease: What Epidemiologists Can Learn and What Epidemiology Can Offer. *Am J Epidemiol* **2022**, *191* (8), 1347-1351. DOI: 10.1093/aje/kwac063.

(204) Kang, C. Donanemab: First Approval. *Drugs* **2024**, *84* (10), 1313-1318. DOI: 10.1007/s40265-024-02087-4.

(205) Hoy, S. M. Lecanemab: First Approval. *Drugs* **2023**, *83* (4), 359-365. DOI: 10.1007/s40265-023-01851-2.

(206) Agency, E. M. *Questions and answers on the refusal of marketing authorisation for Kisunla (donanemab)*; European Medicines Agency, 2025. https://www.ema.europa.eu/en/documents/smop-initial/questions-answers-refusal-marketing-authorisation-kisunla-donanemab_en.pdf (accessed April 01, 2025).

(207) Shan, L.; Bossers, K.; Unmehopa, U.; Bao, A. M.; Swaab, D. F. Alterations in the histaminergic system in Alzheimer's disease: a postmortem study. *Neurobiol Aging* **2012**, *33* (11), 2585-2598. DOI: 10.1016/j.neurobiolaging.2011.12.026.

(208) Medhurst, A. D.; Roberts, J. C.; Lee, J.; Chen, C. P.; Brown, S. H.; Roman, S.; Lai, M. K. Characterization of histamine H3 receptors in Alzheimer's Disease brain and amyloid over-expressing TASTPM mice. *Br J Pharmacol* **2009**, *157* (1), 130-138. DOI: 10.1111/j.1476-5381.2008.00075.x.

(209) Saper, C. B.; Scammell, T. E.; Lu, J. Hypothalamic regulation of sleep and circadian rhythms. *Nature* **2005**, *437* (7063), 1257-1263. DOI: 10.1038/nature04284.

(210) Rizk, A.; Curley, J.; Robertson, J.; Raber, J. Anxiety and cognition in histamine H3 receptor-/- mice. *Eur J Neurosci* **2004**, *19* (7), 1992-1996. DOI: 10.1111/j.1460-9568.2004.03251.x.

(211) Haig, G. M.; Pritchett, Y.; Meier, A.; Othman, A. A.; Hall, C.; Gault, L. M.; Lenz, R. A. A randomized study of H3 antagonist ABT-288 in mild-to-moderate Alzheimer's dementia. *J Alzheimers Dis* **2014**, *42* (3), 959-971. DOI: 10.3233/JAD-140291.

(212) Grove, R. A.; Harrington, C. M.; Mahler, A.; Beresford, I.; Maruff, P.; Lowy, M. T.; Nicholls, A. P.; Boardley, R. L.; Berges, A. C.; Nathan, P. J.; et al. A randomized, double-blind, placebo-controlled, 16-week study of the H3 receptor antagonist, GSK239512 as a monotherapy in subjects with mild-to-moderate Alzheimer's disease. *Curr Alzheimer Res* **2014**, *11* (1), 47-58. DOI: 10.2174/1567205010666131212110148.

(213) Servier. *Clinical Study Report: S38093*. 2012. http://clinicaltrials.servier.com/wp-content/uploads/CL2-38093-009_synopsis_report.pdf (accessed April 21, 2025).

(214) Delay-Goyet, P.; Blanchard, V.; Schussler, N.; Lopez-Grancha, M.; Menager, J.; Mary, V.; Sultan, E.; Buzy, A.; Guillemot, J. C.; Stemmelin, J.; et al. SAR110894, a potent histamine H3-receptor antagonist, displays disease-modifying activity in a transgenic mouse model of tauopathy. *Alzheimers Dement (N Y)* **2016**, *2* (4), 267-280. DOI: 10.1016/j.trci.2016.10.002.

(215) Wang, L.; Fang, J.; Jiang, H.; Wang, Q.; Xue, S.; Li, Z.; Liu, R. 7-Pyrrolidinethoxy-4'-Methoxyisoflavone Prevents Amyloid beta-Induced Injury by Regulating Histamine H3 Receptor-Mediated cAMP/CREB and AKT/GSK3beta Pathways. *Front Neurosci* **2019**, *13*, 334. DOI: 10.3389/fnins.2019.00334.

(216) Zou, Y.; Yang, L.; Zhu, J.; Fan, J.; Zheng, H.; Liao, X.; Yang, Z.; Zhang, K.; Jia, H.; Konnerth, A.; et al. Pitolisant alleviates brain network dysfunction and cognitive deficits in a mouse model of Alzheimer's disease. *Transl Psychiatry* **2025**, *15* (1), 126. DOI: 10.1038/s41398-025-03358-8.

(217) Miyamoto, S.; Jarskog, L. F.; Fleischhacker, W. W. New therapeutic approaches for treatment-resistant schizophrenia: a look to the future. *J Psychiatr Res* **2014**, *58*, 1-6. DOI: 10.1016/j.jpsychires.2014.07.001.

(218) Giordano, G. M.; Bucci, P.; Mucci, A.; Pezzella, P.; Galderisi, S. Gender Differences in Clinical and Psychosocial Features Among Persons With Schizophrenia: A Mini Review. *Front Psychiatry* **2021**, *12*, 789179. DOI: 10.3389/fpsyt.2021.789179.

(219) Krause, M.; Zhu, Y.; Huhn, M.; Schneider-Thoma, J.; Bighelli, I.; Nikolakopoulou, A.; Leucht, S. Antipsychotic drugs for patients with schizophrenia and predominant or prominent negative symptoms: a systematic review and meta-analysis. *Eur Arch Psychiatry Clin Neurosci* **2018**, *268* (7), 625-639. DOI: 10.1007/s00406-018-0869-3.

(220) Leucht, S.; Corves, C.; Arbter, D.; Engel, R. R.; Li, C.; Davis, J. M. Second-generation versus first-generation antipsychotic drugs for schizophrenia: a meta-analysis. *Lancet* **2009**, *373* (9657), 31-41. DOI: 10.1016/S0140-6736(08)61764-X.

(221) Kaar, S. J.; Natesan, S.; McCutcheon, R.; Howes, O. D. Antipsychotics: Mechanisms underlying clinical response and side-effects and novel treatment approaches based on pathophysiology. *Neuropharmacology* **2020**, *172*, 107704. DOI: 10.1016/j.neuropharm.2019.107704.

(222) Lobo, M. C.; Whitehurst, T. S.; Kaar, S. J.; Howes, O. D. New and emerging treatments for schizophrenia: a narrative review of their pharmacology, efficacy and side effect profile relative to established antipsychotics. *Neurosci Biobehav Rev* **2022**, *132*, 324-361. DOI: 10.1016/j.neubiorev.2021.11.032.

(223) Butini, S.; Nikolic, K.; Kassel, S.; Bruckmann, H.; Filipic, S.; Agbaba, D.; Gemma, S.; Brogi, S.; Brindisi, M.; Campiani, G.; et al. Polypharmacology of dopamine receptor ligands. *Prog Neurobiol* **2016**, *142*, 68-103. DOI: 10.1016/j.pneurobio.2016.03.011.

(224) Dean, B. IUPHAR Review on muscarinic M1 and M4 receptors as drug treatment targets relevant to the molecular pathology of schizophrenia. *Pharmacol Res* **2024**, *210*, 107510. DOI: 10.1016/j.phrs.2024.107510.

(225) Arrang, J. M. Histamine and schizophrenia. *Int Rev Neurobiol* **2007**, *78*, 247-287. DOI: 10.1016/S0074-7742(06)78009-6.

(226) Jin, C. Y.; Anichtchik, O.; Panula, P. Altered histamine H3 receptor radioligand binding in post-mortem brain samples from subjects with psychiatric diseases. *Br J Pharmacol* **2009**, *157* (1), 118-129. DOI: 10.1111/j.1476-5381.2009.00149.x.

(227) Weisler, R. H.; Pandina, G. J.; Daly, E. J.; Cooper, K.; Gassmann-Mayer, C.; Investigators, A. T. T. S. Randomized clinical study of a histamine H3 receptor antagonist for the treatment of adults with attention-deficit hyperactivity disorder. *CNS Drugs* **2012**, *26* (5), 421-434. DOI: 10.2165/11631990-000000000-00000.

(228) Arumuham, A.; Nour, M. M.; Veronese, M.; Onwordi, E. C.; Rabiner, E. A.; Howes, O. D. The histamine system and cognitive function: An in vivo H3 receptor PET imaging study in healthy volunteers and patients with schizophrenia. *J Psychopharmacol* **2023**, *37* (10), 1011-1022. DOI: 10.1177/02698811231177287.

(229) Hasin, D. S.; Sarvet, A. L.; Meyers, J. L.; Saha, T. D.; Ruan, W. J.; Stohl, M.; Grant, B. F. Epidemiology of Adult DSM-5 Major Depressive Disorder and Its Specifiers in the United States. *JAMA Psychiatry* **2018**, *75* (4), 336-346. DOI: 10.1001/jamapsychiatry.2017.4602.

(230) De Aquino, J. P.; Londono, A.; Carvalho, A. F. An Update on the Epidemiology of Major Depressive Disorder Across Cultures. In *Understanding Depression*, 2018; pp 309-315.

(231) Plana-Ripoll, O.; Pedersen, C. B.; Holtz, Y.; Benros, M. E.; Dalsgaard, S.; de Jonge, P.; Fan, C. C.; Degenhardt, L.; Ganna, A.; Greve, A. N.; et al. Exploring Comorbidity Within Mental Disorders Among a Danish National Population. *JAMA Psychiatry* **2019**, *76* (3), 259-270. DOI: 10.1001/jamapsychiatry.2018.3658.

(232) Perez-Caballero, L.; Torres-Sanchez, S.; Romero-Lopez-Alberca, C.; Gonzalez-Saiz, F.; Mico, J. A.; Berrocoso, E. Monoaminergic system and depression. *Cell Tissue Res* **2019**, *377* (1), 107-113. DOI: 10.1007/s00441-018-2978-8.

(233) Cui, L.; Li, S.; Wang, S.; Wu, X.; Liu, Y.; Yu, W.; Wang, Y.; Tang, Y.; Xia, M.; Li, B. Major depressive disorder: hypothesis, mechanism, prevention and treatment. *Signal Transduct Target Ther* **2024**, *9* (1), 30. DOI: 10.1038/s41392-024-01738-y.

(234) Burcusa, S. L.; Iacono, W. G. Risk for recurrence in depression. *Clin Psychol Rev* **2007**, *27* (8), 959-985. DOI: 10.1016/j.cpr.2007.02.005.

(235) Kendall, K. M.; Van Assche, E.; Andlauer, T. F. M.; Choi, K. W.; Luykx, J. J.; Schulte, E. C.; Lu, Y. The genetic basis of major depression. *Psychol Med* **2021**, *51* (13), 2217-2230. DOI: 10.1017/S0033291721000441.

(236) Fries, G. R.; Saldana, V. A.; Finnstein, J.; Rein, T. Molecular pathways of major depressive disorder converge on the synapse. *Mol Psychiatry* **2023**, *28* (1), 284-297. DOI: 10.1038/s41380-022-01806-1.

(237) Qian, H.; Shu, C.; Xiao, L.; Wang, G. Histamine and histamine receptors: Roles in major depressive disorder. *Front Psychiatry* **2022**, *13*, 825591. DOI: 10.3389/fpsyt.2022.825591.

(238) Casarotto, P. C.; Girych, M.; Fred, S. M.; Kovaleva, V.; Moliner, R.; Enkavi, G.; Biojone, C.; Cannarozzo, C.; Sahu, M. P.; Kaurinkoski, K.; et al. Antidepressant drugs act by directly binding to TRKB neurotrophin receptors. *Cell* **2021**, *184* (5), 1299-1313 e1219. DOI: 10.1016/j.cell.2021.01.034.

(239) Ye, N.; Qin, W.; Tian, S.; Xu, Q.; Wold, E. A.; Zhou, J.; Zhen, X. C. Small Molecules Selectively Targeting Sigma-1 Receptor for the Treatment of Neurological Diseases. *J Med Chem* **2020**, *63* (24), 15187-15217. DOI: 10.1021/acs.jmedchem.0c01192 From NLM Medline.

(240) Ren, P.; Wang, J.; Li, N.; Li, G.; Ma, H.; Zhao, Y.; Li, Y. Sigma-1 Receptors in Depression: Mechanism and Therapeutic Development. *Front Pharmacol* **2022**, *13*, 925879. DOI: 10.3389/fphar.2022.925879 From NLM PubMed-not-MEDLINE.

(241) Johnston, J. N.; Zarate, C. A., Jr.; Kvarta, M. D. Esketamine in depression: putative biomarkers from clinical research. *Eur Arch Psychiatry Clin Neurosci* **2024**. DOI: 10.1007/s00406-024-01865-1 From NLM Publisher.

(242) Vekhova, K. A.; Namiot, E. D.; Jonsson, J.; Schioth, H. B. Ketamine and Esketamine in Clinical Trials: FDA-Approved and Emerging Indications, Trial Trends With Putative Mechanistic Explanations. *Clin Pharmacol Ther* **2025**, *117* (2), 374-386. DOI: 10.1002/cpt.3478 From NLM Medline.

(243) Femenia, T.; Magara, S.; DuPont, C. M.; Lindskog, M. Hippocampal-Dependent Antidepressant Action of the H3 Receptor Antagonist Clobenpropit in a Rat Model of Depression. *Int J Neuropsychopharmacol* **2015**, *18* (9). DOI: 10.1093/ijnp/pyv032.

(244) Kumar, A.; Dogra, S.; Sona, C.; Umrao, D.; Rashid, M.; Singh, S. K.; Wahajuddin, M.; Yadav, P. N. Chronic histamine 3 receptor antagonism alleviates depression like conditions in mice via modulation of brain-derived neurotrophic factor and hypothalamus-pituitary adrenal axis. *Psychoneuroendocrinology* **2019**, *101*, 128-137. DOI: 10.1016/j.psyneuen.2018.11.007.

(245) Bahi, A.; Schwed, J. S.; Walter, M.; Stark, H.; Sadek, B. Anxiolytic and antidepressant-like activities of the novel and potent non-imidazole histamine H_3 receptor antagonist ST-1283. *Drug Des Devel Ther* **2014**, *8*, 627-637. DOI: 10.2147/DDDT.S63088.

(246) Iida, T.; Yoshikawa, T.; Karpati, A.; Matsuzawa, T.; Kitano, H.; Mogi, A.; Harada, R.; Naganuma, F.; Nakamura, T.; Yanai, K. JNJ10181457, a histamine H3 receptor inverse agonist, regulates in vivo microglial functions and improves depression-like behaviours in mice. *Biochem Biophys Res Commun* **2017**, *488* (3), 534-540. DOI: 10.1016/j.bbrc.2017.05.081.

(247) Gao, Z.; Hurst, W. J.; Czechtizky, W.; Hall, D.; Moindrot, N.; Nagorny, R.; Pichat, P.; Stefany, D.; Hendrix, J. A.; George, P. G. Identification and profiling of 3,5-dimethyl-isoxazole-4-carboxylic acid [2-methyl-4-((2S,3'S)-2-methyl-[1,3']bipyrrolidinyl-1'-yl)phenyl] amide as histamine H_3 receptor antagonist for the treatment of depression. *Bioorg Med Chem Lett* **2013**, *23* (23), 6269-6273. DOI: 10.1016/j.bmcl.2013.09.081.

(248) Alfageh, B. H.; Wang, Z.; Mongkhon, P.; Besag, F. M. C.; Alhawassi, T. M.; Brauer, R.; Wong, I. C. K. Safety and Tolerability of Antipsychotic Medication in Individuals with Autism Spectrum Disorder: A Systematic Review and Meta-Analysis. *Paediatr Drugs* **2019**, *21* (3), 153-167. DOI: 10.1007/s40272-019-00333-x.

(249) Lord, C.; Brugha, T. S.; Charman, T.; Cusack, J.; Dumas, G.; Frazier, T.; Jones, E. J. H.; Jones, R. M.; Pickles, A.; State, M. W.; et al. Autism spectrum disorder. *Nat Rev Dis Primers* **2020**, *6* (1), 5. DOI: 10.1038/s41572-019-0138-4.

(250) Lord, C.; Elsabbagh, M.; Baird, G.; Veenstra-Vanderweele, J. Autism spectrum disorder. *The Lancet* **2018**, *392* (10146), 508-520. DOI: 10.1016/S0140-6736(18)31129-2 (acccessed 2025/03/16).

(251) Canitano, R.; Vivanti, G. Tics and Tourette syndrome in autism spectrum disorders. *Autism* **2007**, *11* (1), 19-28. DOI: 10.1177/1362361307070992.

(252) Wright, C.; Shin, J. H.; Rajpurohit, A.; Deep-Soboslay, A.; Collado-Torres, L.; Brandon, N. J.; Hyde, T. M.; Kleinman, J. E.; Jaffe, A. E.; Cross, A. J.; et al. Altered expression of histamine signaling genes in autism spectrum disorder. *Transl Psychiatry* **2017**, *7* (5), e1126. DOI: 10.1038/tp.2017.87 From NLM Medline.

(253) Sztainberg, Y.; Zoghbi, H. Y. Lessons learned from studying syndromic autism spectrum disorders. *Nat Neurosci* **2016**, *19* (11), 1408-1417. DOI: 10.1038/nn.4420.

(254) Eissa, N.; Al-Houqani, M.; Sadeq, A.; Ojha, S. K.; Sasse, A.; Sadek, B. Current Enlightenment About Etiology and Pharmacological Treatment of Autism Spectrum Disorder. *Front Neurosci* **2018**, *12*, 304. DOI: 10.3389/fnins.2018.00304.

(255) Lacivita, E.; Perrone, R.; Margari, L.; Leopoldo, M. Targets for Drug Therapy for Autism Spectrum Disorder: Challenges and Future Directions. *J Med Chem* **2017**, *60* (22), 9114-9141. DOI: 10.1021/acs.jmedchem.7b00965.

(256) Eissa, N.; Venkatachalam, K.; Jayaprakash, P.; Falkenstein, M.; Dubiel, M.; Frank, A.; Reiner-Link, D.; Stark, H.; Sadek, B. The Multi-Targeting Ligand ST-2223 with Histamine H_3 Receptor and Dopamine D_2/D_3 Receptor Antagonist Properties Mitigates Autism-Like Repetitive Behaviors and Brain Oxidative Stress in Mice. *Int J Mol Sci* **2021**, *22* (4). DOI: 10.3390/ijms22041947.

(257) Griebel, G.; Pichat, P.; Pruniaux, M. P.; Beeske, S.; Lopez-Grancha, M.; Genet, E.; Terranova, J. P.; Castro, A.; Sanchez, J. A.; Black, M.; et al. SAR110894, a potent histamine H3-receptor antagonist, displays procognitive effects in rodents. *Pharmacol Biochem Behav* **2012**, *102* (2), 203-214. DOI: 10.1016/j.pbb.2012.04.004.

(258) Baronio, D.; Castro, K.; Gonchoroski, T.; de Melo, G. M.; Nunes, G. D.; Bambini-Junior, V.; Gottfried, C.; Riesgo, R. Effects of an H3R antagonist on the animal model of autism induced by prenatal exposure to valproic acid. *PLoS One* **2015**, *10* (1), e0116363. DOI: 10.1371/journal.pone.0116363.

(259) Eissa, N.; Jayaprakash, P.; Azimullah, S.; Ojha, S. K.; Al-Houqani, M.; Jalal, F. Y.; Lazewska, D.; Kiec-Kononowicz, K.; Sadek, B. The histamine H3R antagonist DL77 attenuates autistic behaviors in a prenatal valproic acid-induced mouse model of autism. *Sci Rep* **2018**, *8* (1), 13077. DOI: 10.1038/s41598-018-31385-7.

(260) Abdalla, S.; Eissa, N.; Jayaprakash, P.; Beiram, R.; Kuder, K. J.; Lazewska, D.; Kiec-Kononowicz, K.; Sadek, B. The Potent and Selective Histamine H3 Receptor Antagonist E169 Counteracts Cognitive Deficits and Mitigates Disturbances in the PI3K/AKT/GSK-3beta Signaling Pathway in MK801-Induced Amnesia in Mice. *Int J Mol Sci* **2023**, *24* (16). DOI: 10.3390/ijms241612719.

(261) Eissa, N.; Azimullah, S.; Jayaprakash, P.; Jayaraj, R. L.; Reiner, D.; Ojha, S. K.; Beiram, R.; Stark, H.; Lazewska, D.; Kiec-Kononowicz, K.; et al. The dual-active histamine H3 receptor antagonist and acetylcholine esterase inhibitor E100 ameliorates stereotyped repetitive behavior and neuroinflammmation in sodium valproate induced autism in mice. *Chem Biol Interact* **2019**, *312*, 108775. DOI: 10.1016/j.cbi.2019.108775.

(262) Proschak, E.; Stark, H.; Merk, D. Polypharmacology by Design: A Medicinal Chemist's Perspective on Multitargeting Compounds. *J. Med. Chem.* **2019**, *62* (2), 420-444. DOI: 10.1021/acs.jmedchem.8b00760.

(263) Gwee, K. A.; Goh, V.; Lima, G.; Setia, S. Coprescribing proton-pump inhibitors with nonsteroidal anti-inflammatory drugs: risks versus benefits. *J Pain Res* **2018**, *11*, 361-374. DOI: 10.2147/JPR.S156938.

(264) Walsh, C. A.; Cahir, C.; Tecklenborg, S.; Byrne, C.; Culbertson, M. A.; Bennett, K. E. The association between medication non-adherence and adverse health outcomes in ageing populations: A systematic review and meta-analysis. *Br J Clin Pharmacol* **2019**, *85* (11), 2464-2478. DOI: 10.1111/bcp.14075.

(265) Mao, J.; Gold, M. S.; Backonja, M. M. Combination drug therapy for chronic pain: a call for more clinical studies. *J Pain* **2011**, *12* (2), 157-166. DOI: 10.1016/j.jpain.2010.07.006.

(266) Kavanagh, O. N.; Albadarin, A. B.; Croker, D. M.; Healy, A. M.; Walker, G. M. Maximising success in multidrug formulation development: A review. *J Control Release* **2018**, *283*, 1-19. DOI: 10.1016/j.jconrel.2018.05.024.

(267) Zhou, J.; Jiang, X.; He, S.; Jiang, H.; Feng, F.; Liu, W.; Qu, W.; Sun, H. Rational Design of Multitarget-Directed Ligands: Strategies and Emerging Paradigms. *J Med Chem* **2019**, *62* (20), 8881-8914. DOI: 10.1021/acs.jmedchem.9b00017.

(268) Ban, T. A. The role of serendipity in drug discovery. *Dialogues Clin Neurosci* **2006**, *8* (3), 335-344. DOI: 10.31887/DCNS.2006.8.3/tban.

(269) Kiss, B.; Horvath, A.; Nemethy, Z.; Schmidt, E.; Laszlovszky, I.; Bugovics, G.; Fazekas, K.; Hornok, K.; Orosz, S.; Gyertyan, I.; et al. Cariprazine (RGH-188), a dopamine D_3 receptor-preferring, D_3/D_2 dopamine receptor antagonist-partial agonist antipsychotic candidate: in vitro and neurochemical profile. *J Pharmacol Exp Ther* **2010**, *333* (1), 328-340. DOI: 10.1124/jpet.109.160432.

(270) Garnock-Jones, K. P. Cariprazine: A Review in Schizophrenia. *CNS Drugs* **2017**, *31* (6), 513-525. DOI: 10.1007/s40263-017-0442-z.

(271) Anighoro, A.; Bajorath, J.; Rastelli, G. Polypharmacology: challenges and opportunities in drug discovery. *J. Med. Chem.* **2014**, *57* (19), 7874-7887. DOI: 10.1021/jm5006463.

(272) Rosier, N.; Gratz, L.; Schihada, H.; Moller, J.; Isbilir, A.; Humphrys, L. J.; Nagl, M.; Seibel, U.; Lohse, M. J.; Pockes, S. A Versatile Sub-Nanomolar Fluorescent Ligand Enables NanoBRET Binding Studies and Single-Molecule Microscopy at the Histamine H_3 Receptor. *J Med Chem* **2021**, *64* (15), 11695-11708. DOI: 10.1021/acs.jmedchem.1c01089 From NLM Medline.

(273) Stark, H. Recent advances in histamine H3/H4 receptor ligands. *Expert Opinion on Therapeutic Patents* **2005**, *13* (6), 851-865. DOI: 10.1517/13543776.13.6.851.

(274) Hagenow, S.; Affini, A.; Pioli, E. Y.; Hinz, S.; Zhao, Y.; Porras, G.; Namasivayam, V.; Muller, C. E.; Lin, J. S.; Bezard, E.; et al. Adenosine $A_{2A}R/A_1R$ Antagonists Enabling Additional H_3R Antagonism for the Treatment of Parkinson's Disease. *J Med Chem* **2021**, *64* (12), 8246-8262. DOI: 10.1021/acs.jmedchem.0c00914.

(275) Venkatachalam, K.; Zhong, S.; Dubiel, M.; Satala, G.; Sadek, B.; Stark, H. The Novel Pimavanserin Derivative ST-2300 with Histamine H_3 Receptor Affinity Shows Reduced 5-HT_{2A} Binding, but Maintains Antidepressant- and Anxiolytic-like Properties in Mice. *Biomolecules* **2022**, *12* (5). DOI: 10.3390/biom12050683.

(276) Khanfar, M. A.; Affini, A.; Lutsenko, K.; Nikolic, K.; Butini, S.; Stark, H. Multiple Targeting Approaches on Histamine H3 Receptor Antagonists. *Front. Neurosci.* **2016**, *10*, 201. DOI: 10.3389/fnins.2016.00201.

(277) Kebabian, J. W. Multiple classes of dopamine receptors in mammalian central nervous system: the involvement of dopamine-sensitive adenylyl cyclase. *Life Sci* **1978**, *23* (5), 479-483. DOI: 10.1016/0024-3205(78)90157-1.

(278) Andersen, P. H.; Gingrich, J. A.; Bates, M. D.; Dearry, A.; Falardeau, P.; Senogles, S. E.; Caron, M. G. Dopamine receptor subtypes: beyond the D1/D2 classification. *Trends Pharmacol Sci* **1990**, *11* (6), 231-236. DOI: 10.1016/0165-6147(90)90249-8.

(279) Spano, P. F.; Govoni, S.; Trabucchi, M. Studies on the pharmacological properties of dopamine receptors in various areas of the central nervous system. *Adv Biochem Psychopharmacol* **1978**, *19*, 155-165.

(280) Anden, N. E.; Carlsson, A.; Dahlstroem, A.; Fuxe, K.; Hillarp, N. A.; Larsson, K. Demonstration and Mapping out of Nigro-Neostriatal Dopamine Neurons. *Life Sci (1962)* **1964**, *3*, 523-530. DOI: 10.1016/0024-3205(64)90161-4.

(281) Dahlstroem, A.; Fuxe, K. Evidence for the Existence of Monoamine-Containing Neurons in the Central Nervous System. I. Demonstration of Monoamines in the Cell Bodies of Brain Stem Neurons. *Acta Physiol Scand Suppl* **1964**, SUPPL 232:231-255.

(282) Sokoloff, P.; Diaz, J.; Le Foll, B.; Guillin, O.; Leriche, L.; Bezard, E.; Gross, C. The dopamine D3 receptor: a therapeutic target for the treatment of neuropsychiatric disorders. *CNS Neurol Disord Drug Targets* **2006**, *5* (1), 25-43. DOI: 10.2174/187152706784111551.

(283) Beaulieu, J. M.; Gainetdinov, R. R. The physiology, signaling, and pharmacology of dopamine receptors. *Pharmacol Rev* **2011**, *63* (1), 182-217. DOI: 10.1124/pr.110.002642.

(284) Giros, B.; Sokoloff, P.; Martres, M. P.; Riou, J. F.; Emorine, L. J.; Schwartz, J. C. Alternative splicing directs the expression of two D2 dopamine receptor isoforms. *Nature* **1989**, *342* (6252), 923-926. DOI: 10.1038/342923a0.

(285) Monsma, F. J., Jr.; McVittie, L. D.; Gerfen, C. R.; Mahan, L. C.; Sibley, D. R. Multiple D2 dopamine receptors produced by alternative RNA splicing. *Nature* **1989**, *342* (6252), 926-929. DOI: 10.1038/342926a0.

(286) Usiello, A.; Baik, J. H.; Rouge-Pont, F.; Picetti, R.; Dierich, A.; LeMeur, M.; Piazza, P. V.; Borrelli, E. Distinct functions of the two isoforms of dopamine D2 receptors. *Nature* **2000**, *408* (6809), 199-203. DOI: 10.1038/35041572.

(287) De Mei, C.; Ramos, M.; Iitaka, C.; Borrelli, E. Getting specialized: presynaptic and postsynaptic dopamine D2 receptors. *Curr Opin Pharmacol* **2009**, *9* (1), 53-58. DOI: 10.1016/j.coph.2008.12.002.

(288) Giros, B.; Martres, M. P.; Pilon, C.; Sokoloff, P.; Schwartz, J. C. Shorter variants of the D3 dopamine receptor produced through various patterns of alternative splicing. *Biochem Biophys Res Commun* **1991**, *176* (3), 1584-1592. DOI: 10.1016/0006-291x(91)90469-n.

(289) Van Tol, H. H.; Wu, C. M.; Guan, H. C.; Ohara, K.; Bunzow, J. R.; Civelli, O.; Kennedy, J.; Seeman, P.; Niznik, H. B.; Jovanovic, V. Multiple dopamine D4 receptor variants in the human population. *Nature* **1992**, *358* (6382), 149-152. DOI: 10.1038/358149a0.

(290) Siafis, S.; Wu, H.; Wang, D.; Burschinski, A.; Nomura, N.; Takeuchi, H.; Schneider-Thoma, J.; Davis, J. M.; Leucht, S. Antipsychotic dose, dopamine D2 receptor occupancy and extrapyramidal side-effects: a systematic review and dose-response meta-analysis. *Mol Psychiatry* **2023**, *28* (8), 3267-3277. DOI: 10.1038/s41380-023-02203-y.

(291) Pytka, K.; Podkowa, K.; Rapacz, A.; Podkowa, A.; Zmudzka, E.; Olczyk, A.; Sapa, J.; Filipek, B. The role of serotonergic, adrenergic and dopaminergic receptors in antidepressant-like effect. *Pharmacol Rep* **2016**, *68* (2), 263-274. DOI: 10.1016/j.pharep.2015.08.007.

(292) Belujon, P.; Grace, A. A. Dopamine System Dysregulation in Major Depressive Disorders. *Int J Neuropsychopharmacol* **2017**, *20* (12), 1036-1046. DOI: 10.1093/ijnp/pyx056.

(293) Muller, T. What are the main considerations when prescribing pharmacotherapy for Parkinson's disease? *Expert Opin Pharmacother* **2022**, *23* (7), 745-750. DOI: 10.1080/14656566.2022.2045275.

(294) Ghazanfari, N.; van Waarde, A.; Doorduin, J.; Sijbesma, J. W. A.; Kominia, M.; Koelewijn, M.; Attia, K.; Vallez-Garcia, D.; Willemsen, A. T. M.; Heeres, A.; et al. Binding of the Dual-Action Anti-Parkinsonian Drug AG-0029 to Dopamine D_2 and Histamine H_3 Receptors: A PET Study in Healthy Rats. *Mol Pharm* **2022**, *19* (7), 2287-2298. DOI: 10.1021/acs.molpharmaceut.2c00121.

(295) Correa, M. F.; Barbosa, A. J. R.; Fernandes, G. A. B.; Baker, J. G.; Fernandes, J. Pharmacological and SAR analysis of the LINS01 compounds at the human histamine H_1, H_2, and H_3 receptors. *Chem Biol Drug Des* **2019**, *93* (1), 89-95. DOI: 10.1111/cbdd.13387.

(296) Corrêa, M., F.; Reiner, D.; Fernandes, G. A. B.; Varela, M. T.; Aranha, C. M. S. Q.; Stark, H.; Fernandes, J. P. S. Profiling of LINS01 compounds at human dopamine D2 and D3 receptors. *Journal of Chemical Sciences* **2019**, *132* (1). DOI: 10.1007/s12039-019-1694-6.

(297) Venkatachalam, K.; Eissa, N.; Awad, M. A.; Jayaprakash, P.; Zhong, S.; Stolting, F.; Stark, H.; Sadek, B. The histamine H3R and dopamine D2R/D3R antagonist ST-713 ameliorates autism-

like behavioral features in BTBR T+tf/J mice by multiple actions. *Biomed Pharmacother* **2021**, *138*, 111517. DOI: 10.1016/j.biopha.2021.111517.

(298) von Coburg, Y.; Kottke, T.; Weizel, L.; Ligneau, X.; Stark, H. Potential utility of histamine H3 receptor antagonist pharmacophore in antipsychotics. *Bioorg Med Chem Lett* **2009**, *19* (2), 538-542. DOI: 10.1016/j.bmcl.2008.09.012.

(299) Soreq, H.; Seidman, S. Acetylcholinesterase--new roles for an old actor. *Nat Rev Neurosci* **2001**, *2* (4), 294-302. DOI: 10.1038/35067589.

(300) Greig, N. H.; Utsuki, T.; Yu, Q.; Zhu, X.; Holloway, H. W.; Perry, T.; Lee, B.; Ingram, D. K.; Lahiri, D. K. A new therapeutic target in Alzheimer's disease treatment: attention to butyrylcholinesterase. *Curr Med Res Opin* **2001**, *17* (3), 159-165. DOI: 10.1185/0300799039117057.

(301) Sun, T.; Zhen, T.; Harakandi, C. H.; Wang, L.; Guo, H.; Chen, Y.; Sun, H. New insights into butyrylcholinesterase: Pharmaceutical applications, selective inhibitors and multitarget-directed ligands. *Eur J Med Chem* **2024**, *275*, 116569. DOI: 10.1016/j.ejmech.2024.116569.

(302) Boyko, K. M.; Baymukhametov, T. N.; Chesnokov, Y. M.; Hons, M.; Lushchekina, S. V.; Konarev, P. V.; Lipkin, A. V.; Vasiliev, A. L.; Masson, P.; Popov, V. O.; et al. 3D structure of the natural tetrameric form of human butyrylcholinesterase as revealed by cryoEM, SAXS and MD. *Biochimie* **2019**, *156*, 196-205. DOI: 10.1016/j.biochi.2018.10.017.

(303) Gotti, C.; Clementi, F.; Fornari, A.; Gaimarri, A.; Guiducci, S.; Manfredi, I.; Moretti, M.; Pedrazzi, P.; Pucci, L.; Zoli, M. Structural and functional diversity of native brain neuronal nicotinic receptors. *Biochemical Pharmacology* **2009**, *78* (7), 703-711. DOI: 10.1016/j.bcp.2009.05.024.

(304) Saxena, M.; Dubey, R. Target Enzyme in Alzheimer's Disease: Acetylcholinesterase Inhibitors. *Curr Top Med Chem* **2019**, *19* (4), 264-275. DOI: 10.2174/1568026619666190128125912.

(305) Thiele, A. Muscarinic signaling in the brain. *Annu Rev Neurosci* **2013**, *36*, 271-294. DOI: 10.1146/annurev-neuro-062012-170433.

(306) Pardo-Moreno, T.; Gonzalez-Acedo, A.; Rivas-Dominguez, A.; Garcia-Morales, V.; Garcia-Cozar, F. J.; Ramos-Rodriguez, J. J.; Melguizo-Rodriguez, L. Therapeutic Approach to Alzheimer's Disease: Current Treatments and New Perspectives. *Pharmaceutics* **2022**, *14* (6). DOI: 10.3390/pharmaceutics14061117.

(307) Zhou, S.; Huang, G. The biological activities of butyrylcholinesterase inhibitors. *Biomed Pharmacother* **2022**, *146*, 112556. DOI: 10.1016/j.biopha.2021.112556.

(308) Hoffmann, M.; Stiller, C.; Endres, E.; Scheiner, M.; Gunesch, S.; Sotriffer, C.; Maurice, T.; Decker, M. Highly Selective Butyrylcholinesterase Inhibitors with Tunable Duration of Action by Chemical Modification of Transferable Carbamate Units Exhibit Pronounced Neuroprotective

Effect in an Alzheimer's Disease Mouse Model. *J Med Chem* **2019**, *62* (20), 9116-9140. DOI: 10.1021/acs.jmedchem.9b01012.

(309) Bautista-Aguilera, O. M.; Budni, J.; Mina, F.; Medeiros, E. B.; Deuther-Conrad, W.; Entrena, J. M.; Moraleda, I.; Iriepa, I.; Lopez-Munoz, F.; Marco-Contelles, J. Contilisant, a Tetratarget Small Molecule for Alzheimer's Disease Therapy Combining Cholinesterase, Monoamine Oxidase Inhibition, and H3R Antagonism with S1R Agonism Profile. *J Med Chem* **2018**, *61* (15), 6937-6943. DOI: 10.1021/acs.jmedchem.8b00848.

(310) Wen, G.; Liu, Q.; Hu, H.; Wang, D.; Wu, S. Design, synthesis, biological evaluation, and molecular docking of novel flavones as H_3R inhibitors. *Chem Biol Drug Des* **2017**, *90* (4), 580-589. DOI: 10.1111/cbdd.12981.

(311) Feng, B.; Li, X.; Xia, J.; Wu, S. Discovery of novel isoflavone derivatives as AChE/BuChE dual-targeted inhibitors: synthesis, biological evaluation and molecular modelling. *J Enzyme Inhib Med Chem* **2017**, *32* (1), 968-977. DOI: 10.1080/14756366.2017.1347163.

(312) Darras, F. H.; Pockes, S.; Huang, G.; Wehle, S.; Strasser, A.; Wittmann, H. J.; Nimczick, M.; Sotriffer, C. A.; Decker, M. Synthesis, biological evaluation, and computational studies of Tri- and tetracyclic nitrogen-bridgehead compounds as potent dual-acting AChE inhibitors and hH3 receptor antagonists. *ACS Chem Neurosci* **2014**, *5* (3), 225-242. DOI: 10.1021/cn4002126.

(313) Lazewska, D.; Bajda, M.; Kaleta, M.; Zareba, P.; Doroz-Plonka, A.; Siwek, A.; Alachkar, A.; Mogilski, S.; Saad, A.; Kuder, K.; et al. Rational design of new multitarget histamine H_3 receptor ligands as potential candidates for treatment of Alzheimer's disease. *Eur J Med Chem* **2020**, *207*, 112743. DOI: 10.1016/j.ejmech.2020.112743.

(314) Striessnig, J. Voltage-Gated Ca(2+)-Channel alpha1-Subunit de novo Missense Mutations: Gain or Loss of Function - Implications for Potential Therapies. *Front. Synaptic Neurosci.* **2021**, *13*, 634760. DOI: 10.3389/fnsyn.2021.634760 From NLM PubMed-not-MEDLINE.

(315) Zamponi, G. W.; Striessnig, J.; Koschak, A.; Dolphin, A. C. The Physiology, Pathology, and Pharmacology of Voltage-Gated Calcium Channels and Their Future Therapeutic Potential. *Pharmacol Rev* **2015**, *67* (4), 821-870. DOI: 10.1124/pr.114.009654.

(316) Ertel, E. A.; Campbell, K. P.; Harpold, M. M.; Hofmann, F.; Mori, Y.; Perez-Reyes, E.; Schwartz, A.; Snutch, T. P.; Tanabe, T.; Birnbaumer, L.; et al. Nomenclature of voltage-gated calcium channels. *Neuron* **2000**, *25* (3), 533-535. DOI: 10.1016/s0896-6273(00)81057-0.

(317) Catterall, W. A.; Perez-Reyes, E.; Snutch, T. P.; Striessnig, J. International Union of Pharmacology. XLVIII. Nomenclature and structure-function relationships of voltage-gated calcium channels. *Pharmacol Rev* **2005**, *57* (4), 411-425. DOI: 10.1124/pr.57.4.5.

(318) Bech-Hansen, N. T.; Naylor, M. J.; Maybaum, T. A.; Pearce, W. G.; Koop, B.; Fishman, G. A.; Mets, M.; Musarella, M. A.; Boycott, K. M. Loss-of-function mutations in a calcium-channel alpha1-subunit gene in Xp11.23 cause incomplete X-linked congenital stationary night blindness. *Nat Genet* **1998**, *19* (3), 264-267. DOI: 10.1038/947.

(319) Strom, T. M.; Nyakatura, G.; Apfelstedt-Sylla, E.; Hellebrand, H.; Lorenz, B.; Weber, B. H.; Wutz, K.; Gutwillinger, N.; Ruther, K.; Drescher, B.; et al. An L-type calcium-channel gene mutated in incomplete X-linked congenital stationary night blindness. *Nat Genet* **1998**, *19* (3), 260-263. DOI: 10.1038/940.

(320) Casamassima, F.; Hay, A. C.; Benedetti, A.; Lattanzi, L.; Cassano, G. B.; Perlis, R. H. L-type calcium channels and psychiatric disorders: A brief review. *Am J Med Genet B Neuropsychiatr Genet* **2010**, *153B* (8), 1373-1390. DOI: 10.1002/ajmg.b.31122.

(321) Ortner, N. J.; Striessnig, J. L-type calcium channels as drug targets in CNS disorders. *Channels* **2016**, *10* (1), 7-13. DOI: 10.1080/19336950.2015.1048936.

(322) Filippini, L.; Ortner, N. J.; Kaserer, T.; Striessnig, J. $Ca_v1.3$-selective inhibitors of voltage-gated L-type Ca^{2+} channels: Fact or (still) fiction? *Br J Pharmacol* **2023**, *180* (10), 1289-1303. DOI: 10.1111/bph.16060.

(323) Striessnig, J.; Ortner, N. J.; Pinggera, A. Pharmacology of L-type Calcium Channels: Novel Drugs for Old Targets? *Curr Mol Pharmacol* **2015**, *8* (2), 110-122. DOI: 10.2174/1874467208666150507105845 From NLM Medline.

(324) Ortner, N. J.; Bock, G.; Dougalis, A.; Kharitonova, M.; Duda, J.; Hess, S.; Tuluc, P.; Pomberger, T.; Stefanova, N.; Pitterl, F.; et al. Lower Affinity of Isradipine for L-Type Ca2+ Channels during Substantia Nigra Dopamine Neuron-Like Activity: Implications for Neuroprotection in Parkinson's Disease. *J. Neurosci.* **2017**, *37* (28), 6761-6777. DOI: 10.1523/JNEUROSCI.2946-16.2017.

(325) Sinai, I. S. o. M. a. M. *Evaluating Isradipine for Cognitive Enhancement in Schizophrenia and Schizoaffective Disorder*. https://clinicaltrials.gov/ (accessed April 21, 2025).

(326) University, N. *Safety, Tolerability and Efficacy Assessment of Dynacirc CR in Parkinson Disease (STEADY-PD)*. https://clinicaltrials.gov/ (accessed April 21, 2025).

(327) Rochester, U. o. *Efficacy of Isradipine in Early Parkinson Disease*. https://clinicaltrials.gov/ (accessed April 21, 2025).

(328) University, N. *Parkinson's Disease Isradipine Safety Study*. https://clinicaltrials.gov/ (accessed April 21, 2025).

(329) Hospital, M. G. *Adjunctive Isradipine for the Treatment of Bipolar Depression (Isradipine)*. https://clinicaltrials.gov/ (accessed April 21, 2025).

(330) Parkinson Study Group, S.-P. D. I. I. I. I. Isradipine Versus Placebo in Early Parkinson Disease: A Randomized Trial. *Ann Intern Med* **2020**, *172* (9), 591-598. DOI: 10.7326/M19-2534 From NLM Medline.

(331) Wankerl, K.; Weise, D.; Gentner, R.; Rumpf, J. J.; Classen, J. L-type voltage-gated Ca2+ channels: a single molecular switch for long-term potentiation/long-term depression-like plasticity

and activity-dependent metaplasticity in humans. *J Neurosci* **2010**, *30* (18), 6197-6204. DOI: 10.1523/JNEUROSCI.4673-09.2010.

(332) Bader, P. L.; Faizi, M.; Kim, L. H.; Owen, S. F.; Tadross, M. R.; Alfa, R. W.; Bett, G. C.; Tsien, R. W.; Rasmusson, R. L.; Shamloo, M. Mouse model of Timothy syndrome recapitulates triad of autistic traits. *Proc Natl Acad Sci U S A* **2011**, *108* (37), 15432-15437. DOI: 10.1073/pnas.1112667108.

(333) Cross-Disorder Group of the Psychiatric Genomics, C. Identification of risk loci with shared effects on five major psychiatric disorders: a genome-wide analysis. *Lancet* **2013**, *381* (9875), 1371-1379. DOI: 10.1016/S0140-6736(12)62129-1.

(334) Cooper, G.; Kang, S.; Perez-Rosello, T.; Guzman, J. N.; Galtieri, D.; Xie, Z.; Kondapalli, J.; Mordell, J.; Silverman, R. B.; Surmeier, D. J. A Single Amino Acid Determines the Selectivity and Efficacy of Selective Negative Allosteric Modulators of CaV1.3 L-Type Calcium Channels. *ACS Chem. Biol.* **2020**, *15* (9), 2539-2550. DOI: 10.1021/acschembio.0c00577.

(335) Ortner, N. J.; Bock, G.; Vandael, D. H.; Mauersberger, R.; Draheim, H. J.; Gust, R.; Carbone, E.; Tuluc, P.; Striessnig, J. Pyrimidine-2,4,6-triones are a new class of voltage-gated L-type Ca2+ channel activators. *Nat. Commun.* **2014**, *5*, 3897. DOI: 10.1038/ncomms4897 From NLM Medline.

(336) Huang, H.; Ng, C. Y.; Yu, D.; Zhai, J.; Lam, Y.; Soong, T. W. Modest CaV1.342-selective inhibition by compound 8 is beta-subunit dependent. *Nat. Commun.* **2014**, *5*, 4481. DOI: 10.1038/ncomms5481 From NLM Medline.

(337) Caulfield, M. E.; Manfredsson, F. P.; Steece-Collier, K. The Role of Striatal Cav1.3 Calcium Channels in Therapeutics for Parkinson's Disease. In *Handb Exp Pharmacol*; Vol. 279; 2023; pp 107-137. DOI: 10.1007/164_2022_629.

(338) Steece-Collier, K.; Stancati, J. A.; Collier, N. J.; Sandoval, I. M.; Mercado, N. M.; Sortwell, C. E.; Collier, T. J.; Manfredsson, F. P. Genetic silencing of striatal CaV1.3 prevents and ameliorates levodopa dyskinesia. *Mov Disord* **2019**, *34* (5), 697-707. DOI: 10.1002/mds.27695 From NLM Medline.

(339) Caulfield, M. E.; Vander Werp, M. J.; Stancati, J. A.; Collier, T. J.; Sortwell, C. E.; Sandoval, I. M.; Manfredsson, F. P.; Steece-Collier, K. Downregulation of striatal $Ca_V1.3$ inhibits the escalation of levodopa-induced dyskinesia in male and female parkinsonian rats of advanced age. *Neurobiol Dis* **2023**, *181*, 106111. DOI: 10.1016/j.nbd.2023.106111 From NLM Medline.

(340) Malek, R.; Arribas, R. L.; Palomino-Antolin, A.; Totoson, P.; Demougeot, C.; Kobrlova, T.; Soukup, O.; Iriepa, I.; Moraleda, I.; Diez-Iriepa, D.; et al. New Dual Small Molecules for Alzheimer's Disease Therapy Combining Histamine H3 Receptor (H3R) Antagonism and Calcium Channels Blockade with Additional Cholinesterase Inhibition. *J. Med. Chem.* **2019**, *62* (24), 11416-11422. DOI: 10.1021/acs.jmedchem.9b00937.

(341) Malek, R.; Sałat, K.; Totoson, P.; Karcz, T.; Refouvelet, B.; Skrzypczak-Wiercioch, A.; Maj, M.; Simakov, A.; Martin, H.; Siwek, A.; et al. Discovery of New Highly Potent Histamine

H3 Receptor Antagonists, Calcium Channel Blockers, and Acetylcholinesterase Inhibitors. *ACS Chem. Neurosci.* **2024**, *15* (18), 3363-3383. DOI: 10.1021/acschemneuro.4c00341.

(342) Zamanillo, D.; Romero, L.; Merlos, M.; Vela, J. M. Sigma 1 receptor: a new therapeutic target for pain. *Eur J Pharmacol* **2013**, *716* (1-3), 78-93. DOI: 10.1016/j.ejphar.2013.01.068.

(343) Malar, D. S.; Thitilertdecha, P.; Ruckvongacheep, K. S.; Brimson, S.; Tencomnao, T.; Brimson, J. M. Targeting Sigma Receptors for the Treatment of Neurodegenerative and Neurodevelopmental Disorders. *CNS Drugs* **2023**, *37* (5), 399-440. DOI: 10.1007/s40263-023-01007-6.

(344) Maurice, T.; Su, T. P. The pharmacology of sigma-1 receptors. *Pharmacol Ther* **2009**, *124* (2), 195-206. DOI: 10.1016/j.pharmthera.2009.07.001.

(345) Ruiz-Cantero, M. C.; Gonzalez-Cano, R.; Tejada, M. A.; Santos-Caballero, M.; Perazzoli, G.; Nieto, F. R.; Cobos, E. J. Sigma-1 receptor: A drug target for the modulation of neuroimmune and neuroglial interactions during chronic pain. *Pharmacol Res* **2021**, *163*, 105339. DOI: 10.1016/j.phrs.2020.105339.

(346) Hong, V. M.; Rade, A.; Bhaskara, A.; Ehsan, T.; Tack, S. H.; Yousuf, M. S.; Martin, S. F.; Price, T. J.; Kolber, B. Sigma-2 Receptor/Transmembrane Protein 97 in Pain Modulation: Tracing Historical Roots and Current Research Directions. *ACS Pharmacol Transl Sci* **2025**, *8* (7), 1867-1890. DOI: 10.1021/acsptsci.5c00157.

(347) Mishina, M.; Ishiwata, K.; Ishii, K.; Kitamura, S.; Kimura, Y.; Kawamura, K.; Oda, K.; Sasaki, T.; Sakayori, O.; Hamamoto, M.; et al. Function of sigma1 receptors in Parkinson's disease. *Acta Neurol Scand* **2005**, *112* (2), 103-107. DOI: 10.1111/j.1600-0404.2005.00432.x.

(348) Francardo, V.; Bez, F.; Wieloch, T.; Nissbrandt, H.; Ruscher, K.; Cenci, M. A. Pharmacological stimulation of sigma-1 receptors has neurorestorative effects in experimental parkinsonism. *Brain* **2014**, *137* (Pt 7), 1998-2014. DOI: 10.1093/brain/awu107.

(349) Uchida, N.; Ujike, H.; Tanaka, Y.; Sakai, A.; Yamamoto, M.; Fujisawa, Y.; Kanzaki, A.; Kuroda, S. A Variant of the Sigma Receptor Type-1 Gene Is a Protective Factor for Alzheimer Disease. *The American Journal of Geriatric Psychiatry* **2005**, *13* (12), 1062-1066. DOI: 10.1097/00019442-200512000-00005.

(350) Minoshima, S.; Giordani, B.; Berent, S.; Frey, K. A.; Foster, N. L.; Kuhl, D. E. Metabolic reduction in the posterior cingulate cortex in very early Alzheimer's disease. *Ann Neurol* **1997**, *42* (1), 85-94. DOI: 10.1002/ana.410420114.

(351) Mishina, M.; Ohyama, M.; Ishii, K.; Kitamura, S.; Kimura, Y.; Oda, K.; Kawamura, K.; Sasaki, T.; Kobayashi, S.; Katayama, Y.; et al. Low density of sigma1 receptors in early Alzheimer's disease. *Ann Nucl Med* **2008**, *22* (3), 151-156. DOI: 10.1007/s12149-007-0094-z.

(352) Jin, J. L.; Fang, M.; Zhao, Y. X.; Liu, X. Y. Roles of sigma-1 receptors in Alzheimer's disease. *Int J Clin Exp Med* **2015**, *8* (4), 4808-4820.

(353) Tsai, S. Y.; Pokrass, M. J.; Klauer, N. R.; Nohara, H.; Su, T. P. Sigma-1 receptor regulates Tau phosphorylation and axon extension by shaping p35 turnover via myristic acid. *Proc Natl Acad Sci U S A* **2015**, *112* (21), 6742-6747. DOI: 10.1073/pnas.1422001112.

(354) Tsai, S. Y.; Hayashi, T.; Harvey, B. K.; Wang, Y.; Wu, W. W.; Shen, R. F.; Zhang, Y.; Becker, K. G.; Hoffer, B. J.; Su, T. P. Sigma-1 receptors regulate hippocampal dendritic spine formation via a free radical-sensitive mechanism involving Rac1xGTP pathway. *Proc Natl Acad Sci U S A* **2009**, *106* (52), 22468-22473. DOI: 10.1073/pnas.0909089106.

(355) Fisher, A.; Bezprozvanny, I.; Wu, L.; Ryskamp, A.; Bar-Ner, N.; Natan, N.; Brandeis, R.; Elkon, H.; Nahum, V.; Gershonov, E.; et al. AF710B, a Novel M1/σ1 Agonist with Therapeutic Efficacy in Animal Models of Alzheimer's Disease. *Neurodegenerative Diseases* **2016**, *16* (1-2), 95-110. DOI: 10.1159/000440864.

(356) Ryskamp, D.; Wu, L.; Wu, J.; Kim, D.; Rammes, G.; Geva, M.; Hayden, M.; Bezprozvanny, I. Pridopidine stabilizes mushroom spines in mouse models of Alzheimer's disease by acting on the sigma-1 receptor. *Neurobiol Dis* **2019**, *124*, 489-504. DOI: 10.1016/j.nbd.2018.12.022.

(357) Macfarlane, S.; Grimmer, T.; Teo, K.; O'Brien, T. J.; Woodward, M.; Grunfeld, J.; Mander, A.; Brodtmann, A.; Brew, B. J.; Morris, P.; et al. Blarcamesine for the treatment of Early Alzheimer's Disease: Results from the ANAVEX2-73-AD-004 Phase IIB/III trial. *J Prev Alzheimers Dis* **2025**, *12* (1), 100016. DOI: 10.1016/j.tjpad.2024.100016.

(358) Kaur, G.; Dar, Z. A.; Bajpai, A.; Singh, R.; Bansal, R. Clinical Update on an Anti-Alzheimer Drug Candidate CT1812: A Sigma-2 Receptor Antagonist. *Clin Ther* **2024**, *46* (11), e21-e28. DOI: 10.1016/j.clinthera.2024.08.013.

(359) Riddy, D. M.; Cook, A. E.; Shackleford, D. M.; Pierce, T. L.; Mocaer, E.; Mannoury la Cour, C.; Sors, A.; Charman, W. N.; Summers, R. J.; Sexton, P. M.; et al. Drug-receptor kinetics and sigma-1 receptor affinity differentiate clinically evaluated histamine H_3 receptor antagonists. *Neuropharmacology* **2019**, *144*, 244-255. DOI: 10.1016/j.neuropharm.2018.10.028.

(360) Szczepanska, K.; Podlewska, S.; Dichiara, M.; Gentile, D.; Patamia, V.; Rosier, N.; Monnich, D.; Ruiz Cantero, M. C.; Karcz, T.; Lazewska, D.; et al. Structural and Molecular Insight into Piperazine and Piperidine Derivatives as Histamine H_3 and Sigma-1 Receptor Antagonists with Promising Antinociceptive Properties. *ACS Chem Neurosci* **2022**, *13* (1), 1-15. DOI: 10.1021/acschemneuro.1c00435.

(361) Kotanska, M.; Zadrozna, M.; Kubacka, M.; Mika, K.; Szczepanska, K.; Nowak, B.; Alesci, A.; Miller, A.; Lauriano, E. R.; Kiec-Kononowicz, K. The Effect of KSK-94, a Dual Histamine H_3 and Sigma-2 Receptor Ligand, on Adipose Tissue in a Rat Model of Developing Obesity. *Pharmaceuticals (Basel)* **2024**, *17* (7). DOI: 10.3390/ph17070858.

(362) Ghamari, N.; Zarei, O.; Reiner, D.; Dastmalchi, S.; Stark, H.; Hamzeh-Mivehroud, M. Histamine H_3 receptor ligands by hybrid virtual screening, docking, molecular dynamics simulations, and investigation of their biological effects. *Chem Biol Drug Des* **2019**, *93* (5), 832-843. DOI: 10.1111/cbdd.13471.

(363) Ghamari, N.; Dastmalchi, S.; Zarei, O.; Arias-Montano, J. A.; Reiner, D.; Ustun-Alkan, F.; Stark, H.; Hamzeh-Mivehroud, M. In silico and in vitro studies of two non-imidazole multiple targeting agents at histamine H_3 receptors and cholinesterase enzymes. *Chem Biol Drug Des* **2020**, *95* (2), 279-290. DOI: 10.1111/cbdd.13642.

(364) Espinosa-Bustos, C.; Frank, A.; Arancibia-Opazo, S.; Salas, C. O.; Fierro, A.; Stark, H. New lead elements for histamine H_3 receptor ligands in the pyrrolo[2,3-d]pyrimidine class. *Bioorg Med Chem Lett* **2018**, *28* (17), 2890-2893. DOI: 10.1016/j.bmcl.2018.07.023.

(365) Frank, A.; Meza-Arriagada, F.; Salas, C. O.; Espinosa-Bustos, C.; Stark, H. Nature-inspired pyrrolo[2,3-d]pyrimidines targeting the histamine H(3) receptor. *Bioorg Med Chem* **2019**, *27* (14), 3194-3200. DOI: 10.1016/j.bmc.2019.05.042.

(366) Szczepanska, K.; Karcz, T.; Dichiara, M.; Mogilski, S.; Kalinowska-Tluscik, J.; Pilarski, B.; Leniak, A.; Pietrus, W.; Podlewska, S.; Popiolek-Barczyk, K.; et al. Dual Piperidine-Based Histamine H_3 and Sigma-1 Receptor Ligands in the Treatment of Nociceptive and Neuropathic Pain. *J Med Chem* **2023**, *66* (14), 9658-9683. DOI: 10.1021/acs.jmedchem.3c00430.

List of publications

Peer reviewed articles

[1] Brandao, P.; Lopez, O.; Leitzbach, L.; Stark, H.; Fernandez-Bolanos, J. G.; Burke, A. J.; Pineiro, M. Ugi Reaction Synthesis of Oxindole-Lactam Hybrids as Selective Butyrylcholinesterase Inhibitors. ACS Med Chem Lett 2021, 12 (11), 1718-1725. DOI: 10.1021/acsmedchemlett.1c00344.

[2] Ghamari, N.; Kouhi Hargelan, S.; Zivkovic, A.; Leitzbach, L.; Dastmalchi, S.; Stark, H.; Hamzeh-Mivehroud, M. Guided rational design with scaffold hopping leading to novel histamine H_3 receptor ligands. Bioorg Chem 2021, 117, 105411. DOI: 10.1016/j.bioorg.2021.105411.

[3] Gajic, M.; Knez, D.; Sosic, I.; Mravljak, J.; Meden, A.; Kosak, U.; Leitzbach, L.; George, S.; Hofmann, B.; Zivkovic, A.; et al. Repurposing of 8-Hydroxyquinoline-Based Butyrylcholinesterase and Cathepsin B Ligands as Potent Nonpeptidic Deoxyribonuclease I Inhibitors. ChemMedChem 2022, 17 (5), e202100694. DOI: 10.1002/cmdc.202100694.

[4] Espinosa-Bustos, C.; Leitzbach, L.; Anazco, T.; Silva, M. J.; Campo, A. D.; Castro-Alvarez, A.; Stark, H.; Salas, C. O. Substituted Purines as High-Affinity Histamine H_3 Receptor Ligands. Pharmaceuticals (Basel) 2022, 15 (5). DOI: 10.3390/ph15050573.

[5] Moutayakine, A.; Marques, C.; Lopez, O.; Bagetta, D.; Leitzbach, L.; Hagenow, S.; Carreiro, E. P.; Stark, H.; Alcaro, S.; Fernandez-Bolanos, J. G.; et al. Evaluation of chromane derivatives: Promising privileged scaffolds for lead discovery within Alzheimer's disease. Bioorg Med Chem 2022, 68, 116807. DOI: 10.1016/j.bmc.2022.116807.

[6] Marques, C. S.; López, Ó.; Leitzbach, L.; Fernández-Bolaños, J. G.; Stark, H.; Burke, A. J. Survey of New, Small-Molecule Isatin-Based Oxindole Hybrids as Multi-Targeted Drugs for the Treatment of Alzheimer's Disease. Synthesis 2022, 54 (19), 4304-4319. DOI: 10.1055/s-0041-1737343.

[7] Aranha, C. M. S. Q.; Reiner-Link, D.; Leitzbach, L. R.; Lopes, F. B.; Stark, H.; Fernandes, J. P. S. Multitargeting approaches to cognitive impairment: Synthesis of aryl-alkylpiperazines and assessment at cholinesterases, histamine H_3 and dopamine D_3 receptors. Bioorg Med Chem 2023, 78, 117132. DOI: 10.1016/j.bmc.2022.117132.

[8] Hofmanova, T.; Marques, C.; García-Sosa, A. T.; López, Ó.; Leitzbach, L.; Carreiro, E. P.; González-Bakker, A.; Puerta, A.; Stark, H.; Padrón, J. M.; Fernández-Bolaños, J. G.; Burke, A. J.; N-Substituted 3-Aminooxindoles and N-Propargyl Derivatives: Potential Biological Activities against Alzheimer's Disease. Results Chem. 2023, 6, 101032. DOI: 10.1016/j.rechem.2023.101032.

[9] Szczepanska, K.; Karcz, T.; Dichiara, M.; Mogilski, S.; Kalinowska-Tluscik, J.; Pilarski, B.; Leniak, A.; Pietrus, W.; Podlewska, S.; Popiolek-Barczyk, K.; Humphrys, L. J. Ruiz-Cantero, M. C.; Reiner-Link, D.; Leitzbach, L.; Lazewska, D.; Pockes, S.; Gorka, M.; Zmyslowski, A.; Calmels, T.; Cobos, E. J.; Marrazzo, A.; Stark, H.; Bojarski, A. J.; Amata, E.; Kiec-Kononowicz, K. Dual Piperidine-Based Histamine H_3 and Sigma-1 Receptor Ligands in the Treatment of Nociceptive and Neuropathic Pain. J Med Chem 2023, 66 (14), 9658-9683. DOI: 10.1021/acs.jmedchem.3c00430.

[10] Di Biase, C.; Leitzbach, L.; Frank, A.; Zivkovic, A.; Stark, H. Aromatic linker variations in novel dopamine D_2 and D_3 receptor ligands. Arch Pharm (Weinheim) 2024, 357 (8), e2400071. DOI: 10.1002/ardp.202400071.

[11] Tomovic Pavlovic, K.; Ilic, B. S.; Leitzbach, L.; Anichina, K. K.; Yancheva, D.; Zivkovic, A.; Mavrova, A. T.; Stark, H.; Smelcerovic, A. Bis(benzimidazol-2-yl)amine-Based DPP-4 Inhibitors Potentially Suitable for Combating Diabetes and Associated Nervous System Alterations. Chem Biodivers 2024, 21 (10), e202401227. DOI: 10.1002/cbdv.202401227.

[12] Zanetti, L.; Torok, F.; Leitzbach, L.; Stark, H.; Striessnig, J. Sclareol and cinnarizine are non-selective inhibitors of voltage-gated Cav1.3 L-type Ca^{2+} channels. Channels (Austin) 2025, 19 (1), 2556101. DOI: 10.1080/19336950.2025.2556101.

[13] Leitzbach, L.; Zhong, S.; Zivkovic, A.; Török, F.; Zanetti, L.; Ortner, N.J.; Sindi, M.; Albrecht, P.; Striessnig, J.; Stark, H. Design, synthesis and biological in vitro properties of dual acting ligands as histamine H_3 receptor and L-type Ca^{2+} channel inhibitors, In preparation.

Non-peer reviewed articles

L. Leitzbach and H. Stark, Memantin – Wie war das noch? Beratungswissen zu Wirkungen, Nebenwirkungen und Interaktionen. Deutsche Apotheker Zeitung 2021, 161, (18, pp.).

Poster/Presentations

[1] C.M.S.Q. Aranha, F.B. Lopes, L. Leitzbach, D. Reiner-Link, D. N. Okamato, H. Stark, J.P.S. Fernandes
Assessment of Multitargeting Compounds for Histamine/Dopamine Receptor Subtypes and Cholinesterases, 50th Annual Meeting of the European Histamine Research Society (EHRS), Hannover/Germany (Sept. 1-3, 2022), Abstract Book, p. 52 (O20).

[2] T. Anazco, L. Leitzbach, A. Castro-Alvarez, C. O. Salas, H. Stark, and C. Espinosa-Bustos.
Substituted Purines as High Affinity Histamine H3 Receptor Ligands. 10th BrazMedChem 2022, Poco de Caldas/Brazil (Sept. 25-28, 2022), poster.

[3] C. Aranha, D. Reiner-Link, L. Leitzbach, F. Barrio Lopes, D. Okamoto, H. Stark, and J.P. dos Santos Fernandes.
Heterocyclic Multitargeting Ligands of Cholinesterases, Hitamine and Dopamine Receptor Subtypes: Promising Agents for Cognitive Dysfunctions. 10th BrazMedChem 2022, Poco de Caldas/Brazil (Sept. 25-28, 2022), lecture and poster.

[4] C. Espinosa-Bustos, M. F. Hornos-Carneiro, C. O. Salas, L. Leitzbach, and H. Stark.
Aminoalkyloxichalcone Ligands Targeting Histamine H3 Receptor and MAO-B for Treatment of Parkinson's Disease.
The Brazilian Symposium on Medicinal Chemistry (BrazMedChem 23), Salvadore/Brazil (October 24-27, 2023).

[5] L. Lucarini, S. Villano, S. Sgambellone, S. Marri, E. Masini, A. Nocentini, C. T. Supuran, F. Iovane, M. Schultes, L. Leitzbach, T. Werner, H. Stark.
H_3R Antagonist-CA Inhibitor Hybrid Compounds in a Rabbit Model of Transient Ocular Hypertension. 1st Joint Meeting of the European Histamine Research Society (51st EHRS Meeting) and the Histamine Research Society Europe (1st HRSE Meeting), Turino/Italy (May 23-25, 2024).

[6] M. Stark, L. Leitzbach and H. Stark
Tetrazine-Building Blocks for Click Chemistry on Histamine H3 Receptor Ligands. 1st Joint Meeting of the European Histamine Research Society (51st EHRS Meeting) and the Histamine Research Society Europe (1st HRSE Meeting), Turino/Italy (May 23-25, 2024).

[7] M. Stark, L. Leitzbach, T. Werner, A. Zivkovic, H. Stark.
Tetrazine-Based Building Blocks for Click Chemistry on Histamine H3 Receptor Ligands. Online WebEx Lecture Histamine Research Society Europe (HRSE), May 6, 2025.

Curriculum Vitae

Personal Information	
Name	Luisa Rosa Leitzbach
Adress (academic)	Heinrich Heine University, Institute of Pharmaceutical and Medicinal Chemistry, Universitatsstr. 1, 40225 Duesseldorf
E-Mail	Luisa.Leitzbach@hhu.de
Phone (academic)	+ 49 (0) 211 81 13831
Nationality	German
Education	
2020 – 2024	PhD graduation Heinrich Heine University Duesseldorf, Germany
Since 01/2020	Licensed pharmacist
2014-2018	Studies of Pharmacy 2018: Second degree of pharmaceutical education 2016 First degree of pharmaceutical education Ruprecht Karls University Heidelberg
Work Experience	
2024 – now	Manager stability studies B. Braun Melsungen AG Berlin
2020-2024	PhD candidate Heinrich Heine University Duesseldorf
2019	Pre-registration year Analytical Development Merz Consumer Care
2018-2019	Pre-registration year Oskar Ziethen Apotheke Berlin
2016	Holiday assistant NCE Formulation Sciences Abbvie GmbH & Co. KG
Internships	
2017	School of Pharmacy Department of Practice and Policy University College London
2015	NCE Formulation Sciences Abbvie GmbH & Co. KG
Skills	
Languages	German (native language), English (fluent)
Practical Skills	GraphPad, instrumental analytic, *in vitro* assays, Biosafety level 1 tasks, cell culture

Acknowledgements

First and foremost, I am deeply thankful to Prof. Dr. Dr. h.c. Holger Stark, whose guidance, encouragement, and invaluable feedback were instrumental in shaping this work. Your expertise, insights and encouragement pushed me to think critically and to strive for excellence.

I would like to thank Prof. Dr. Rainer Kalscheuer for taking over my mentorship, constructive suggestions and for reading and evaluating this PhD thesis.

I am grateful to Dr. Aleksandra Zivkovic for her support, feedback and ideas. Your expertise and encouragement helped me during my time in the lab and also to finish this work.

I would like to acknowledge Prof. Dr. Jörg Striessnig, Dr. Nadine Ortner, Lucia Zanetti and Ferenc Török from University of Innsbruck for the collaboration, their support with the calcium assay and the calcium cells.

Thanks to my colleagues within the working group for the nice time and atmosphere at work. Special thanks to my colleagues in the lab Mariam Dubiel, Tobias Werner and Kathrin Grau, without your support, expertise and help, this time would have been more difficult. To all working group members during my PhD time, Milica Elek, Martin Stark, Markus Schultes, Lars Seiffert, Patrick Krolikowski, Mihajlo Gajic, Reham Waheed, Markus Falkenstein, Cristian di Biase and Sicheng Zhong. The skiing trips, hats crafting, cocktail nights, carnival, setting up the bar and switch game nights made the time even during the Corona pandemic great and enjoyable.

Special thanks go to my friends and family, whose love and belief in me provided the strength I needed during the challenging moments of this process. I am grateful for the support, your visits in Düsseldorf and that you are always there for me, to the friends Vicky, Mila, Malina, Marija and Sarah, Eva and Franzi.

My deepest gratitude goes to Hannes. All of this would not have been possible without your unlimited support and your patience with me. Your faith in me has always encouraged me to do my best and pushed me through this challenging time. Thank you for your unconditional love.

Eidesstaatliche Erklärung

Name: Luisa Rosa Leitzbach

Ich versichere an Eides Statt, dass die Dissertation „Pharmacological studies of aminergic scaffolds and the development of multi-target ligands with focus on the histamine H_3 receptor“ von mir selbstständig und ohne unzulässige fremde Hilfe unter Beachtung der „Grundsätze zur Sicherung guter wissenschaftlicher Praxis an der Heinrich-Heine-Universität Düsseldorf“ erstellt worden ist. Ich erkläre weiterhin, dass die vorliegende Arbeit noch nicht im Rahmen eines anderen Prüfungsverfahrens eingereicht wurde.

Düsseldorf, den Unterschrift: